DTIC
SELECTE
SEP 1 2 1985
A

1984 REVIEW

Naval Research Laboratory
Washington, DC

Cover:

    The Naval Research Laboratory has been involved in many aspects of fiber-optics research and development for several years. The work is centered in the Acoustics and Optical Sciences Divisions. This photograph is a visual representation of the separate coils of a prototype fiber-optic hydrophone sensor array illuminated with different colors. The sensor array will actually operate in the infrared (T. Hickman; photo by M. Savell and D. Boyd).

REVIEWED AND APPROVED
16 July 1985

James P. O'Donovan

Commanding Officer

NRL-0056-1000

1984

Naval Research Laboratory
Washington, DC 20375-5000

REVIEW

NRL presents in this Review *highlights of the unclassified research and development programs for calendar year 1984. This book fulfills a dual purpose: it provides an exchange of information among scientists, engineers, scholars, and managers; and it is used in recruiting science and engineering professionals. As you read this* Review, *you will become even more aware that the Laboratory is a dynamic team working together to promote the programs, progress, and innovations that will continue to foster discoveries, inventiveness, and scientific advances for the Navy of the future.*
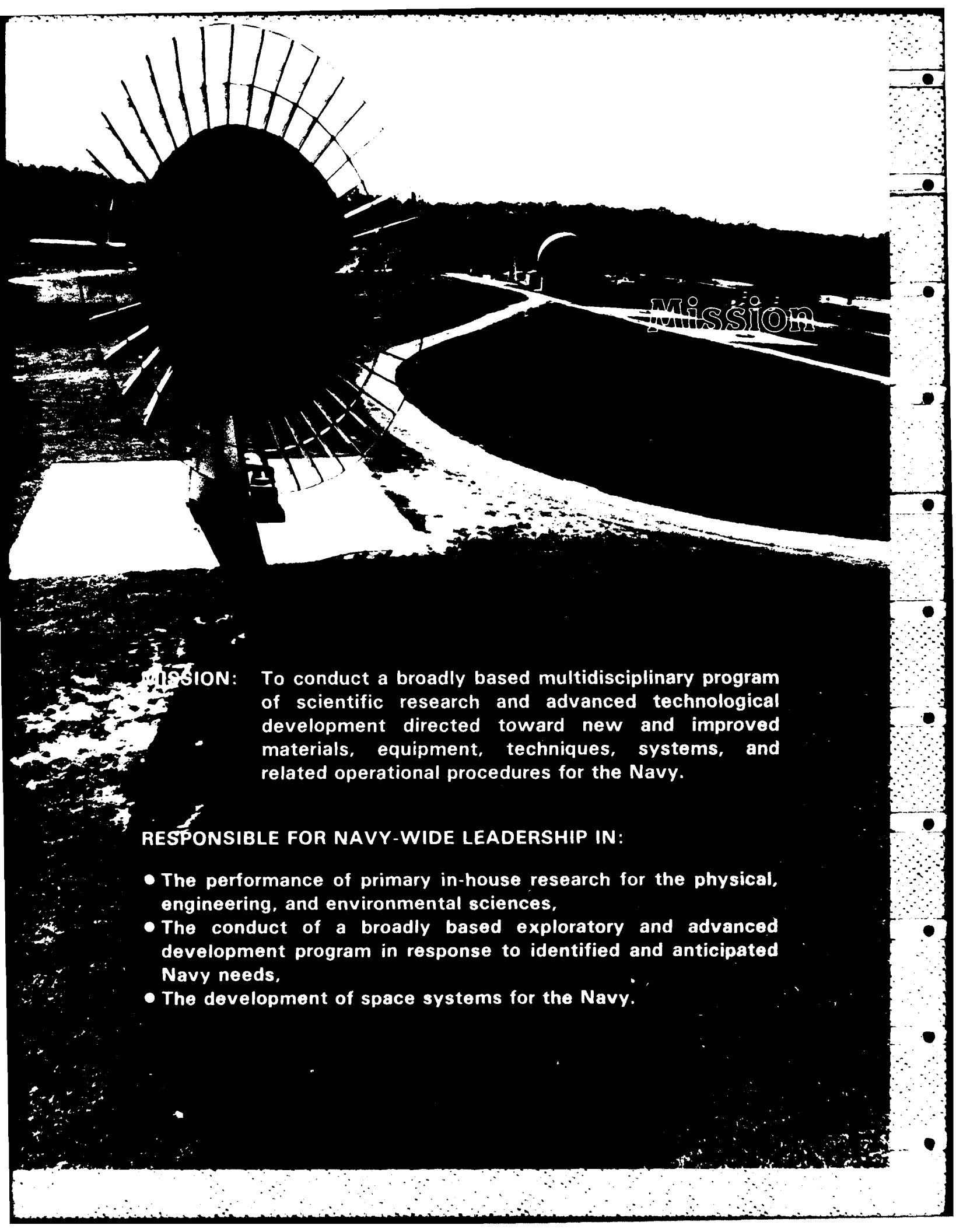
MISSION: To conduct a broadly based multidisciplinary program of scientific research and advanced technological development directed toward new and improved materials, equipment, techniques, systems, and related operational procedures for the Navy.

RESPONSIBLE FOR NAVY-WIDE LEADERSHIP IN:

- The performance of primary in-house research for the physical, engineering, and environmental sciences,
- The conduct of a broadly based exploratory and advanced development program in response to identified and anticipated Navy needs,
- The development of space systems for the Navy.

CONTENTS

The Naval Research Laboratory

The Naval Research Laboratory, located in southwest Washington, DC, has grown from the original five small buildings and a dozen or so scientists to today's approximately 150 buildings and 3200 researchers and support personnel

THE NAVAL RESEARCH LABORATORY

"I believe [that] the Government should maintain a great research laboratory, jointly under military and naval and civilian control. In this could be developed the continually increasing possibilities of ... all the technique of naval progression ....

"When the time came, if it ever did, we could take advantage of the knowledge gained through this research work and quickly produce the very latest and most efficient instruments ...."

Thomas A. Edison
The New York Times Magazine
May 30, 1915

NRL'S TOP MANAGEMENT DISCUSSES THE NAVY'S CORPORATE LABORATORY

*An Interview with the Commanding Officer
and the Director of Research*

As the corporate research laboratory of the Navy, NRL's mission is to devote its resources to a broad-spectrum approach to the basic technological research and development that will improve the overall effectiveness of tomorrow's Navy. The most precious resource that NRL has to accomplish this mission is its people whose diligence and devotion to science and engineering over the past 62 years have made NRL a respected laboratory possessing an enviable reputation. NRL is *people* engaged in creative enterprise. The Laboratory's success begins with a single scientist or a small group of researchers with ideas and goals fostered by the diverse scientific interactions that occur among our divisions. These ideas flourish with the backing of a well-managed scientific and support organization whose personnel put a premium on excellence and create a climate for inventiveness.

The *NRL Review* highlights this inventiveness. Published in its present form since 1967, the Reviews annually report NRL's unclassified research. Although not comprehensive in scope, the selected work described here demonstrates the broad technological base of research conducted at NRL.

Since one purpose of this publication is to provide an exchange of information among scientists, engineers, scholars, and scientific managers, the editors of this year's *Review* sought to foster that exchange by conducting an interview with Captain James O'Donovan, NRL's Commanding Officer, and Dr. Timothy Coffey, NRL's Director of Research. This interview highlights the Laboratory's unique qualities; NRL's R&D programs, its facilities, and their applications; the opportunities the Laboratory offers professionals; and some thoughts on the future of NRL.

NRL — An Overview

Review: NRL is the Navy's corporate research laboratory and a center of excellence in the areas of space research, tactical electronic warfare, microelectronics R&D, artificial intelligence, and fire suppression. How do you feel about NRL? What are some of its major qualities?

Dr. Coffey: NRL is a unique institution. To my knowledge, there is no other laboratory in the Western World with the breadth of programs that exist at NRL. One of the amazing attributes of the Laboratory is that it has been able to achieve technical excellence in most of the research areas we're involved in. Although I would like to claim that it has been management that has led to this success, I think in reality it is due to circumstances of history and a rather peculiar chemistry which is operative here. It is unlikely that you could start over again and create another NRL as we know it today.

Captain O'Donovan: I'd like to add that I think it's important you have singled out areas of excellence that are relevant to Navy interest. Certainly I feel NRL is a very fundamental key element in the Navy community. It is unique, and it is an excellent Navy resource. Since I've been here, I've observed a custom of everybody pulling together to create that excellence. The Navy is a demanding customer with a challenging mission, and this drives the kinds of research you see here. If we were a commercial activity, we would be very focused in a product line or in the base of the market that is trying to be reached. We don't do that here at NRL. We have to be broad enough in scope to meet the mission of the global Navy, and that drives the kinds of excellence you see here. NRL is excellent because it is a *naval* research laboratory.

Review: Captain O'Donovan, you've been here only a few months. What were your initial impressions, and have they changed since you came?

Captain O'Donovan: My initial impressions were somewhat narrow, driven by the viewpoint of where I sat at the time. As one of the customers looking at the Laboratory, I saw only that part of NRL that I was interested in. Because of its breadth, there's no way that someone external to NRL can ever understand all that goes on here. You have to be a part of this Laboratory to understand the magic that is NRL. So my first impressions were a constant exhilaration of finding all these wonderful things—and I'm still discovering.

Coming in at the top of this organization is a rare privilege that few people ever have. Most people external to NRL really don't understand the interdisciplinary aspect of the Lab either. The way we develop technical consortia at the principal investigator level among several research divisions is tremendously exciting to experience, and to see the enthusiasm that these scientists bring to the consortia conveys great confidence in the ability of NRL to successfully tackle tough multidisciplinary jobs effectively. You don't appreciate that unless you're here.

> *"The way NRL develops technical consortia at the principal investigator level among several research divisions is tremendously exciting to experience."*

R&D Programs, Facilities, and Applications

Review: Why does NRL pursue particular areas of research? Where could they lead in the future?

Dr. Coffey: There are, of course, various reasons why NRL undertakes particular areas of research. In some cases it is to push back the frontiers of understanding in areas that are of long-term interest to the Department of the Navy or DoD. In other cases we are pursuing research that is driven by immediate and identified naval needs. In still other cases we have a corporate responsibility to maintain com-petence in areas that the Navy or the nation may need to call on in times of need. The metric which is used to judge the products pro-duced is different for each of these types of research.

To push back the frontiers of science, for example, we are initiat-ing new programs in biomaterials technology—a rather new wrinkle on materials research, an area where NRL has been very active since the foundation of the Labora-tory. We believe that the physical sciences orientation of the Lab, combined with our outstanding analytical tools and the revolution-ary advances that have occurred in biomolecular engineering exter-nal to NRL, will make a marriage that leads to profound advances of interest to the Navy. Time, of course, will tell whether our judg-ment is correct.

An area where the Laboratory program is driven by the immediate requirements of naval systems is the NRL radar program. The Lab conducts an extensive program of advanced radar research in response to the ever-expanding requirements of naval radar, for air, sea, or space. Interestingly, radar has remained an active area at NRL to maintain the "corporate memory" for the Navy. Radar is also an area where the Lab has been and will be called on as a national resource in times of crisis.

Review: NRL receives about $60M a year from ONR [Office of Naval Research] to support basic research. What do you view the purpose of this money to be?

Dr. Coffey: The Lab obtains its funding through an annual proposal to ONR to support scientific and engineering research which is quite basic in nature. Once the proposal is approved by the ONR corporate board, we are bound to exercise the program; if we choose to modify it, we must go back to the board. To understand the purpose of the pro-gram, you have to look at the Lab's mission: we are chartered to act as the corporate research laboratory for the Navy. To fulfill this mis-sion, it is essential that NRL retain a cadre of outstanding scientific personnel in areas that are believed to be of long-term interest or potential interest to the Department of the Navy. The ONR basic research program at NRL is a major component in the preservation and maintenance of this cadre of scien-tific talent.
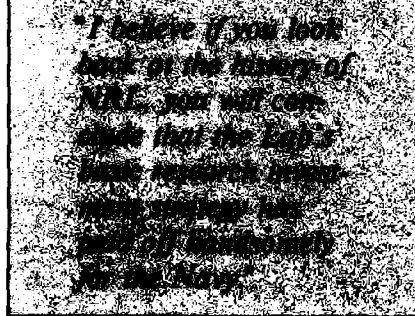
In the program which we an-nually propose to ONR, we strive for a balance of approximately 70% of the program in areas of long-term scientific endeavor, and about

30% addressing more near-term research topics. Our basic research program does not have an emphasis on the development of systems. It is, however, driven by what we perceive to be the future requirements of the Navy. The success of this aspect of our basic research program can, of course, be judged only in retrospect. I believe if you look back at the history of NRL, you will conclude that the Lab's basic research investment strategy has paid off handsomely for the Navy. The scientific quality of our basic research program can, of course, be judged on a more near-term basis. One need only examine the number of invited papers at scientific meetings, the papers published in refereed journals, and the election of NRL employees to fellowships and professional societies to conclude that the Lab is doing quite well in a peer review sense.

Captain O'Donovan: One thing that I must note is the rigor with which that annual ONR proposal is assembled and the integrity with which it is reviewed. I don't think there is a parallel anywhere else in the Department of the Navy. That speaks well for the payoff, and I think it's a handsome payoff.

Review: How do NRL's facilities support the Navy and the nation's science and engineering effort?

Dr. Coffey: It is difficult in the space available to list and comment on all of NRL's important facilities. There are, of course, a number of major facilities that come to mind. Among these are: the Cray X-MP supercomputer; the Spacecraft Checkout Facility; the Central Target Simulator; the Gamble II Electron Accelerator; the Fire I Fire Simulator; the Microelectronics Processing Facility; and the Laboratory's P-3 aircraft.

● The Cray X-MP supercomputer places NRL at the forefront of large-scale scientific computing. This computer represents the state of the art in general purpose supercomputers and will be a major vehicle for bringing the power of supercomputing to the Laboratory's research, technology, and engineering programs.

● The Spacecraft Checkout Facility is the only DoD in-house facility capable of fully qualifying spacecraft. This facility includes a number of clean rooms, vibration simulators, and a thermal vacuum chamber capable of housing a shuttle pallet for space-qualifying shuttle payloads.

● The Central Target Simulator is a very large anechoic chamber, fully instrumented with microwave sources, receivers, and necessary computers to simulate realistic electronic warfare environments and their effect on actual military hardware. It is a major component of the laboratory's electronic warfare simulation capabilities.

● Gamble II is a major high-current (MA), high-voltage (MV) accelerator that was developed under DNA [Defense Nuclear Agency] sponsorship to prove that low-impedance accelerators such as this were possible. This technology has since been transitioned to industry and picked up by a number of other government laboratories. The machine is now used to conduct research on high-current diodes and high-current electron and ion beams. We expect in the near future that DNA will construct another major facility at NRL to demonstrate the feasibility of a new generation of pulse-power devices.

● The Fire I Fire Simulator is a unique vehicle for studying the spread of fire and the suppression of fire in enclosed spaces. This facility has proved to be an extremely important vehicle for understanding fires and environments of interest to the U.S. Navy.

● The Microelectronics Processing Facility is a major tool in

"I believe if you look back at the history of NRL, you will conclude that the Lab's basic research investment strategy has paid off handsomely for the Navy."

the Laboratory's electronics technology program. It is capable of generating micron-scale electron devices and is used to test basic ideas in electron device technology, to demonstrate concepts, and to fabricate small quantities of devices used in the Laboratory's research and technology programs. Without this facility, we would have great difficulty discharging our responsibilities in the area of electronics technology.

• NRL's P-3 aircraft represent a major asset for conducting the Laboratory's field programs. The standard ASW [antisubmarine warfare] payload has been removed from these aircraft, and they have been reconfigured to allow the relatively rapid introduction of scientific and research instrumentation for a large number of applications from such areas as atmospheric physics to the testing of electronic warfare concepts.

There are, of course, numerous other facilities which are perhaps smaller in scale than those listed above but nevertheless are critical components of the Laboratory's research and technology program.

Review: What is NRL doing to support the Fleet directly? What can it continue to do?

Captain O'Donovan: One thing that is often overlooked is the capability that NRL brings to the Fleet test and evaluation environment to simulate and model the real world

of Fleet operation. For example, CBD [Chesapeake Bay Detachment] can perform, in microcosm and under controlled conditions, weapons and electronic warfare effectiveness demonstrations that just could not be performed repeatedly at sea with aircraft and ships. Without NRL's capabilities in testing and evaluation, these large-scale field demonstrations would tie up vast resources and present a tremendous expense—an expense the Navy can ill-afford. So in that sense, we perform very valuable direct Fleet support research that will be enhanced in the future with the renovation program and military construction initiative.

Dr. Coffey: I'd like to add that NRL is in the peculiar position of having dual responsibilities. On the one hand, it is expected to maintain the role of corporate research laboratory and thereby protect the Navy's long-term research interests, while on the other hand it is expected to respond as needed to near-term Navy needs. These

requirements can often be in conflict with each other. I believe the Lab has done a reasonable job over the years in balancing these requirements. Much of our activity in direct support of the Fleet occurs in the space systems area, the electronic warfare area, the radar area, and the fire suppression area. Our activities in support of the Fleet vary from participating in the actual operation of assets that support the Fleet, to providing technical experts on a quick reaction basis, to assisting the Fleet in resolving immediate critical technical problems. I expect this situation to continue in the future.
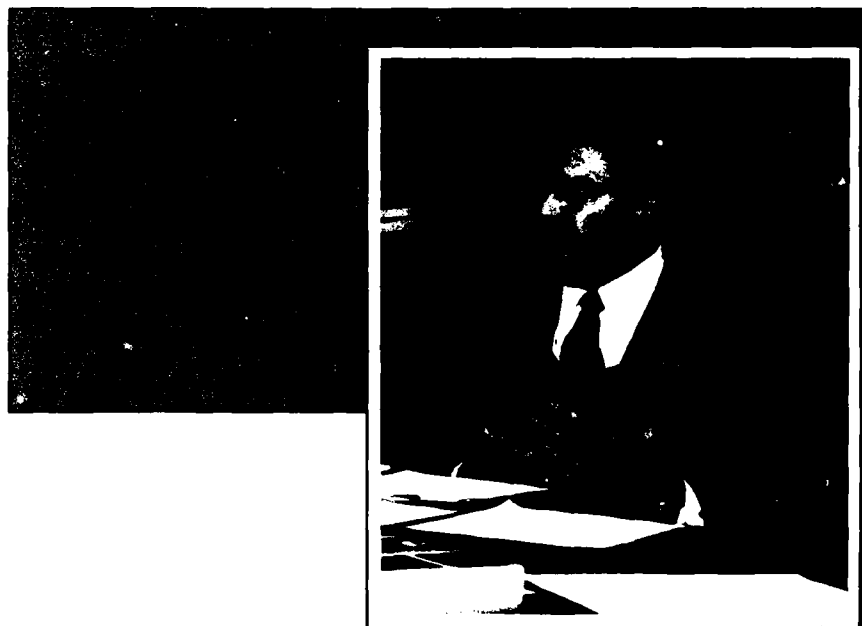
Professionals at NRL and Their Opportunities

Review: What are the short- and long-range impacts and benefits to NRL of hiring new professionals? Why would NRL be a good place for new professionals to begin a career?

Dr. Coffey: The Lab feels we need to populate the institution with a larger number of people who are recent recipients of bachelors degrees or masters degrees in the scientific or engineering disciplines—but not at the expense of the senior or the doctoral recruitment. It is not a tradeoff, but more like a balancing of the professional staff. What are the short-term impacts? On the negative side, the senior laboratory professionals are going to have to invest some time and effort in spinning these individuals up to a point where they can be a positive asset to our programs. On the positive side, there is nothing like the vitality and enthusiasm of young people to keep an organization alive. We in Civil Service must face up to the fact that we are going to have to invest a certain amount of energy into what I would call a "grow your own effort." It is unlikely that we will ever be one-on-one competitive with the private sector, and if we're going to have a process of growth within the Lab, some of that must occur with people moving into the junior positions and gradually gravitating into senior positions. We will make the necessary investments to allow our scientists and engineers to pursue higher degrees by upgrading our facilities and providing many opportunities for advanced training and education. In the long range, I think everybody wins. We wind up with a better balanced workforce and have a vehicle for keeping the place

young in spirit. In addition, professionals coming in have the ability to work with established scientists, and if they choose to leave, they leave more marketable than they would have been if they had not come to NRL.

Captain O'Donovan: Why would NRL be a ␣c␣d place for new professionals to pursue a career here? Well, where else could you interact professionally and rub elbows with some of the world-class physicists, chemists, computer scientists, and radar experts and work in preeminent facilities in some of these areas? I believe these features are very important, and we should use them to recruit top professionals.

Review: The Laboratory's ability to respond rapidly to R&D needs, its broad expertise, and an orientation toward more basic research make NRL important to the Navy. But how is NRL perceived by other research laboratories and scientific institutions?

Dr. Coffey: I think you need to answer that question on the inter-

national scale and then on the national level. On the international level, most major universities and other government laboratories view NRL as one of the great research institutions of the world. I personally observed this in foreign countries where I was asked what has made NRL such a good laboratory for such a long time. We're talking about a period that spans all of modern technology—the 62 years that the Lab has been in existence. During that time, its record has been consistently one of outstanding performance. The Eastern bloc countries are perhaps even more mystified by NRL's long-term success than are the Western bloc countries.

In the U.S., we're more competitive with other labs. Here, I believe most other research and scientific institutions view the Naval Research Laboratory with respect, just as NRL views with respect many of the other major research institutions in this country.

Captain O'Donovan: I might add, coming in from a systems command environment, that NRL is

8

viewed as the final authority in many disciplines—the underwriter's laboratory, if you will—in areas such as chemistry, materials, software engineering, fiber optics, and space systems, to mention a few. With the connotation we all have of an underwriter's laboratory, we know that when NRL speaks out on a particular issue, that statement is accepted as baseline fact. In any community, that's an enviable leadership position to be in. The Navy stands behind that preeminence right down to the principal investigator. I think it's important to note that the stability of this Lab derives from an organization that is not given to doing precipitous sorts of things. The Navy comprises a very deliberate, very conservative, very professional, and consistently effective group of men and women with a serious, challenging mission. NRL reflects that tradition. There's a lot of pride and professionalism at NRL and no wonder—it's part of an organization based on pride, professionalism, and performance.

Review: NRL has collaborated with other Navy and non-Navy laboratories. What are some of the results of these, and what about future collaborations?

Dr. Coffey: It would be next to impossible to discuss everything that has come out of collaboration with other labs and other industry or academia; there are classic examples, however. In the 1930s, NRL, working with industry, provided the U.S. Navy with radar. In the 1950s and 1960s, NRL's collaboration with other labs and industry was a major component in developing the satellite system that the Navy depends on for communications. In developing Navy space capabilities in general, there has been substantive interaction between NRL and industry. Our collaboration generally manifests itself in the publication of papers and the generation of ideas, and there's probably no way to quantify the impact of that relationship, but no doubt, it has major impact on the Navy and the nation. This situation will most certainly continue. NRL is in the business of generating ideas, seeing that appropriate ideas are carried to the demonstration phase, and ensuring that those ideas that are important enough are transitioned to organizations that will actually provide systems to the Fleet.

Review: How will NRL respond to future research requirements?

Captain O'Donovan: A practical answer to that is *in all ways.* Certainly we will take the time scale that we are presented here and respond according to what is expected of us. We have to look at the conditions of the environment that we're presented with—peace or war...what's the immediate need...what do we have to draw on in terms of resources at hand? My personal impression of the Lab and what makes it great is that the trend, if any, is toward allowing the system to address the challenge within its own resources. I think we're better off as a Navy in managing our material acquisition responsibilities to have not only the organic basic research capability, but also the exploratory, advanced engineering development and good, solid, hands-on, systems engineering experience to continue the Navy's reputation as a smart buyer.

Dr. Coffey: If the Laboratory is to fulfill its responsibilities, it must maintain its in-house technical competence. If this competence is lost, then there is no real reason for NRL to exist, and we will not be able to respond to future research requirements. The Laboratory will, therefore, do what is necessary to maintain the technical competence which puts it in a position to respond to future research and future naval requirements. To accomplish this, we must ensure that we have the research facilities to conduct the required research. This is a nontrivial problem since, in some areas, it involves military construction monies and the purchase of some rather expensive instrumentation. Nevertheless, I believe the Laboratory will continue to recruit top professionals and will maintain its research facilities; and we have the backing of Navy senior management to see that this happens.

9

THE NAVAL RESEARCH LABORATORY

Our Heritage

Today, when government and science seem inextricably linked, when virtually no one questions the dependence of national defense on the excellence of national technical capabilities, it is noteworthy that in-house defense research is relatively new in our Nation's history. The Naval Research Laboratory (NRL), the first modern research institution created within the United States Navy, began operations in 1923, just 62 years ago.

Thomas Edison's Vision: The first step came in May 1915, a time when Americans were deeply worried about the great European war. Thomas Edison, asked by a *New York Times* correspondent to comment on the conflict, argued that the Nation should look to science. "The Government," he proposed in a published interview, "should maintain a great research laboratory .... In this could be developed ... all the technique of military and naval progression without any vast expense." Secretary of the Navy Josephus Daniels seized the opportunity created by Edison's public comments to enlist Edison's support. He agreed to serve as the head of a new body of civilian experts—the Naval Consulting Board—to advise the Navy on science and technology. The Board's most ambitious plan was the creation of a modern research facility for the Navy. Congress allocated $1.5 million for the institution in 1916, but wartime delays and disagreements within the Naval Consulting Board postponed construction until 1920.

The Laboratory's two original divisions, Radio and Sound, pioneered in the fields of high-frequency radio and underwater sound propagation. They produced communications equipment, direction-finding devices, sonar sets, and, perhaps most significant of all, the first practical radar equipment built in this country. They also performed basic research, participating, for example, in the discovery and early exploration of the ionosphere. In addition, the Laboratory was able to work gradually toward its goal of becoming a broad-based research facility. By the beginning of World War II, five new divisions had been added: Physical Optics, Chemistry, Metallurgy, Mechanics and Electricity, and Internal Communications.

The War Years and Growth: Total employment at the Laboratory jumped from 396 in 1941 to 4400 in 1946, expenditures from $1.7 million to $13.7 million, the number of buildings from 23 to 67, and the number of projects from 200 to about 900. During the war, scientific activities necessarily were concentrated almost entirely on applied research. New electronics equipment—radio, radar, sonar—was developed. Countermeasures were devised. New lubricants were produced, as were antifouling paints, luminous identification tapes, and a sea marker to help save survivors of disasters at sea. A thermal diffusion process was conceived and used to supply some of the ^{235}U isotope needed for one of the first atomic bombs. Also, a host of new devices that developed from booming wartime industry were type-tested and then certified as reliable for the fleet.

NRL Reorganizes for Peace: After the war, scientific research was widely recognized as a vital national resource, and the Laboratory had a major and continuing role to play in providing such research. When the Office of Naval Research was created in 1946, NRL was transferred to this office; NRL thus became the *corporate research laboratory* of the Navy.

The demands of this new position required substantial reorganization. Rapid expansion had met wartime demands but had left NRL improperly structured to address long-term Navy requirements. One major task—neither easily nor

11

rapidly accomplished—was that of reshaping research. This was accomplished by transforming a group of largely autonomous scientific divisions into a unified institution with a clear mission and a fully coordinated research program. The first attempt at reorganization vested power in an executive committee composed of all the division superintendents. This committee was impracticably large, so in 1949 a civilian director of research was named and given full authority over the program. Positions for associate directors were added in 1954.

The Breadth of NRL: During the 39 years since the war, the areas of study at the Laboratory have included basic research concerning the Navy's environment of sea, sky, and space. Investigations have ranged widely from monitoring the sun's behavior, to analyzing marine atmospheric conditions, to measuring parameters of the deep oceans. Detection and communication capabilities have benefited by research that has exploited new portions of the electromagnetic spectrum, extended ranges to outer space, and provided means of transferring information reliably and securely, even through massive jamming. Submarine habitability, lubricants, shipbuilding materials, fire fighting, along with the study of sound in the sea, have also been steadfast concerns.

The Laboratory has pioneered naval research into space, from atmospheric probes with captured V-2 rockets, through direction of the Vanguard project—America's first satellite program—up to involvement in such projects as the Navy Global Positioning System. Today, NRL is the Navy's lead laboratory in space research, fire research, tactical electronic warfare, microelectronic devices, and artificial intelligence. NRL has also evaluated new issues, such as the effects of intense radiation and various forms of shock and vibration on aircraft, ships, and satellites. In 1977, NRL studied and identified the source of the mysterious sonic boom heard along the east coast of the United States. And in 1983, NRL helped identify the reason for the failure of the first artificial heart and then improved its design. NRL has made and continues to make important nonmilitary contributions to science and technology: development of better composite

materials, new numerical techniques, new and improved microelectronic devices, and high-energy sources.

One goal has guided NRL's diverse activities through the years—to conduct pioneering scientific research and development that will provide improved materials, equipment, techniques, systems, and operations for the Navy, for the Department of Defense, and for the U.S. Government.

NRL Today

ORGANIZATION AND ADMINISTRATION

The position of NRL within the Navy, illustrated on the organizational chart that appears on page 297 of this *Review*, is that of a field command under the Chief of Naval Research.

Heading the Laboratory with joint responsibilities are the naval commanding officer, Capt. James P. O'Donovan, and the civilian director of research, Dr. Timothy Coffey. Staff functions such as security and personnel management fall within their administration. Line authority passes from the commanding officer and the director of research to five associate directors of research in the following areas:

- Technical services
- General science and technology
- Systems research and technology
- Material science and component technology
- Space and communications technology

The first of these provides centralized technical support; the other four are the research directorates responsible for executing NRL's research and development program. Further details of the organization of the Laboratory are given on the organizational chart that appears on page 298 of this *Review*.

Financially, NRL operates as a Navy Industrial Fund activity. This requires that all costs, including overhead costs, be charged to various research projects. Funding for scientific projects

in 1984 came from the Chief of Naval Research, the Naval Systems Commands, the Naval Material Command, and other government agencies, such as the Defense Advanced Research Projects Agency, the Department of Energy, and the National Aeronautics and Space Administration. NRL's relationship to its sponsoring agencies, both inside and outside the Department of Defense, is defined by a comprehensive policy on interagency support agreements.

Besides funding for scientific work, NRL received Navy monies for general construction, maintenance, and operations. In fiscal year 1984, the Laboratory's budget totaled $391 million.

PERSONNEL DEVELOPMENT

At the end of 1984, NRL employed 3234 personnel—33 military officers, 99 enlisted, and 3102 civilians. The research staff of 1946 employees consists of 681 with doctorates, 319 with masters degrees, and 506 with bachelors degrees. The 1156-person support staff provides

to the research staff administrative, computer-aided designing, machining, fabrication, electronic construction, publication, personnel development, information retrieval, large mainframe computer services, and contracting and supply management services.

Opportunities for higher education and other professional training for NRL employees are available through several programs offered by the Employee Development Branch. These programs provide for graduate work leading to advanced degrees, advanced training, college course work, short courses, continuing education, and career counseling. Graduate students, in certain cases, may use their NRL research for thesis material.

For non-NRL employees, several postdoctoral research programs exist. There are also cooperative education agreements with several universities, summer and part-time employment programs, and various summer and interchange programs for college faculty members, professional consultants, and employees of other government agencies.

CAPT John McMorris II (left) and CAPT James O'Donovan join in cutting the cake at the Change of Command Ceremony on October 26, 1984

13

NRL has active chapters of Women In Science and Engineering, Sigma Xi, Toastmaster's International, and the Federal Executive and Professional Association. Three personal computer clubs meet regularly—Edison Atari, NRL IBM-PC, and Edison Commodore. An amateur radio club, a wives' club, a musical drama group—the Showboaters, and several sports clubs are also active. NRL has a recreation club which provides swimming, sauna, whirlpool bath, gymnasium, and weight-room facilities. The recreation club also offers classes in karate, aerobics, swimming, and cardiopulmonary resuscitation.

A community outreach program at NRL provides tutoring for local students, science fair judging, participation in high school and college career day programs, an art and essay contest during Black History Month, and a Christmas party with donated gifts for disadvantaged children.

NRL has an active, growing Credit Union with assets of $69 million. A day-care center is located near one of the gates to NRL, and public transportation to NRL is provided by Metrobus.

More information on these programs can be found in the *Review* chapter entitled "Programs for Professional Development," page 245.

SCIENTIFIC FACILITIES

In addition to its main campus of about 130 acres and 152 buildings, NRL maintains 12 other research sites and a Flight Support Detachment. The many diverse scientific and technological research and support facilities are described in the following paragraphs.

Research Facilities

- Space

NRL has been a major center for space research and technology since the late 1940s, providing technical expertise and guidance for the nation's civilian and military space programs. NRL's space science facilities include the E.O. Hulburt Center for Space Research, the 26-m (85
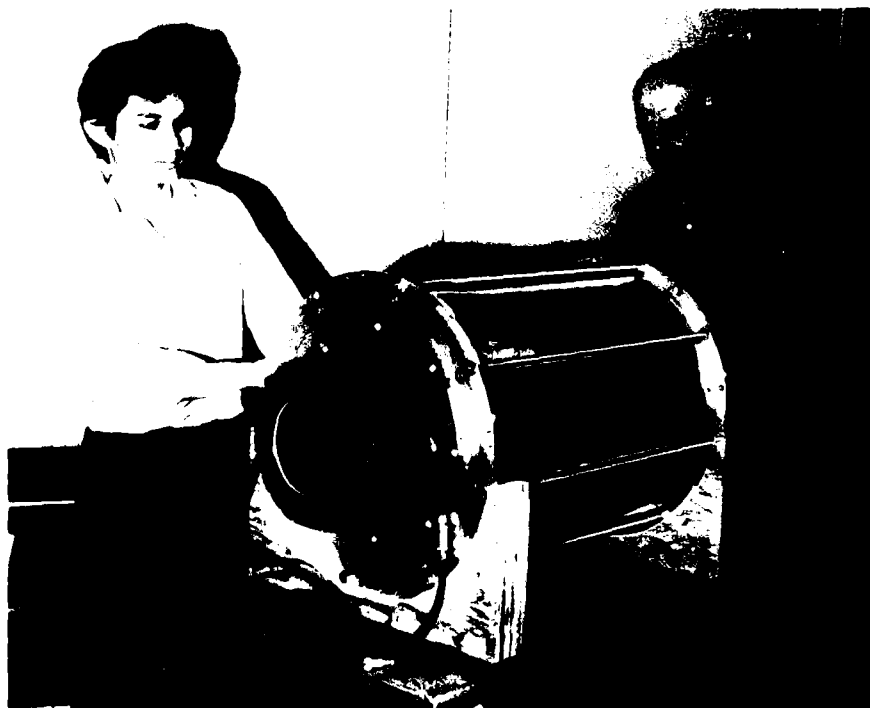
Kon Tran (left) and Darrell King of the Space Science Division make adjustments on the
Mark II far-ultraviolet camera planned for flight as NASA's Spartan-3 shuttle payload
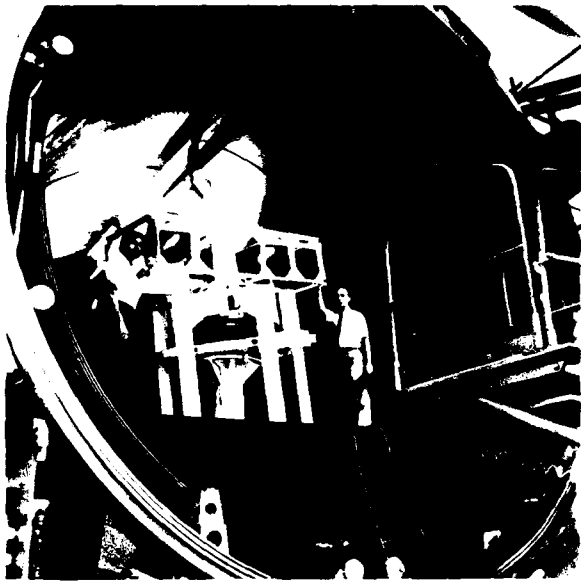
A Gyrodynamics Motion Simulator (GMS), believed to be the largest in the USA, is shown inside NRL's 16-foot-diameter vacuum chamber

ft), high-precision radio telescope at Maryland Point, and antennas for radio astronomy.

- Space Systems

In its role as a center of excellence for space research, NRL establishes and supports the development of spacecraft and systems that use these spacecraft. The Space Systems and Technology Division designs, builds, analyzes, tests, and operates spacecraft, as well as identifies and conducts promising research to improve spacecraft and their support systems. Division facilities that support this work include large and small anechoic electromagnetic chambers, clean rooms, shock and vibration facilities, an acoustic reverberation chamber, a spin balance facility, large and small thermal/vacuum test chambers, and modal analysis test facilities. These facilities provide NRL with the capability of testing and space-qualifying spacecraft payloads of any weight and size that can be launched by the space shuttle transportation system. This Division also has a 31-m, computer-controlled wind and wave tank

The Space Ultraviolet Radiation Environment (SURE) experiment, in its Get Away Special (GAS) canister, flies attached to the outside of the shuttle bay. SURE observes extreme and far ultraviolet spectroscopic emissions from constituents in the earth's ionosphere.

Mr. Peter G. Wilhelm, Superintendent of the Space Systems and Technology Division has been named Director, Naval Space Technology Center (NSTC). This center was established to preserve and enhance a strong technology base and to provide expert assistance in the development and acquisition of space systems which support naval missions. NRL was selected for this role because of its long and successful involvement in space-related activities, in which Mr. Wilhelm has been a key contributor and leader and also because of NRL's broadly based science and technology expertise. Seven other divisions at NRL, as well as other Navy and Government organizations, will participate in the NSTC.

15
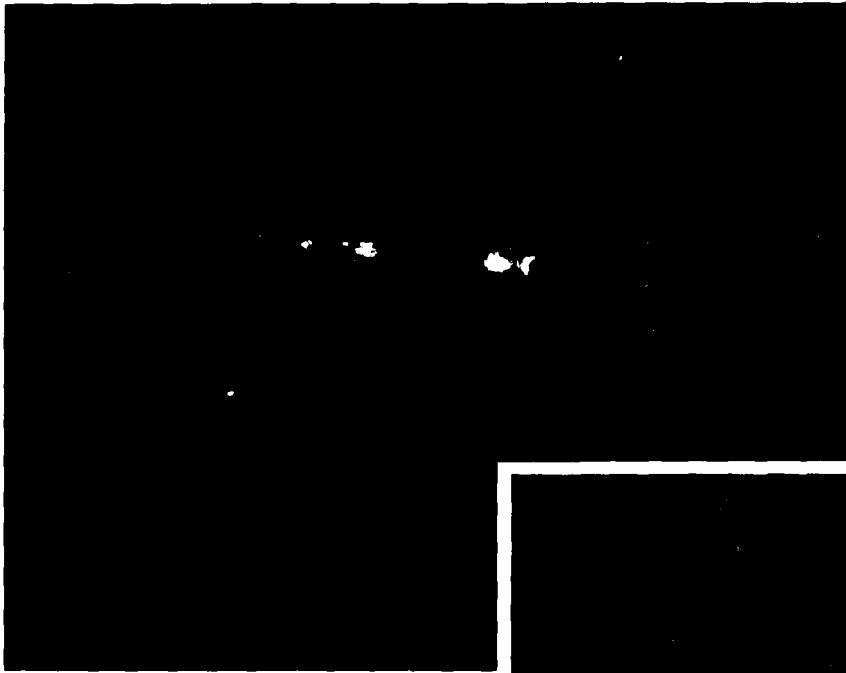
Blue (459 nm) laser beam produced by nonlinear mixing of yellow and infrared Raman laser beams generated in methane cells by using a solid-state neodymium pump laser. One application for this laser is underwater communication with submersibles (R. Burnham).
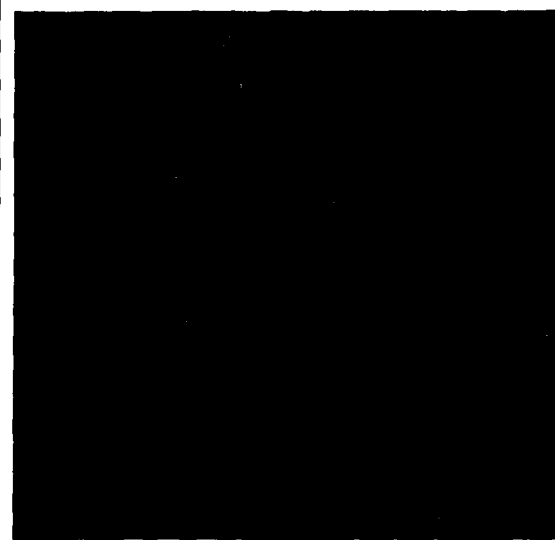
Thermal infrared image of clouds above mountains, taken looking straight down from a high-altitude aircraft. The pseudocolor treatment of the image shows the hottest parts of the mountain slopes in red and orange, the cooler slopes and stream beds in yellow and green, and the clouds, which are cold, in blue, purple, and black (N. Stone).
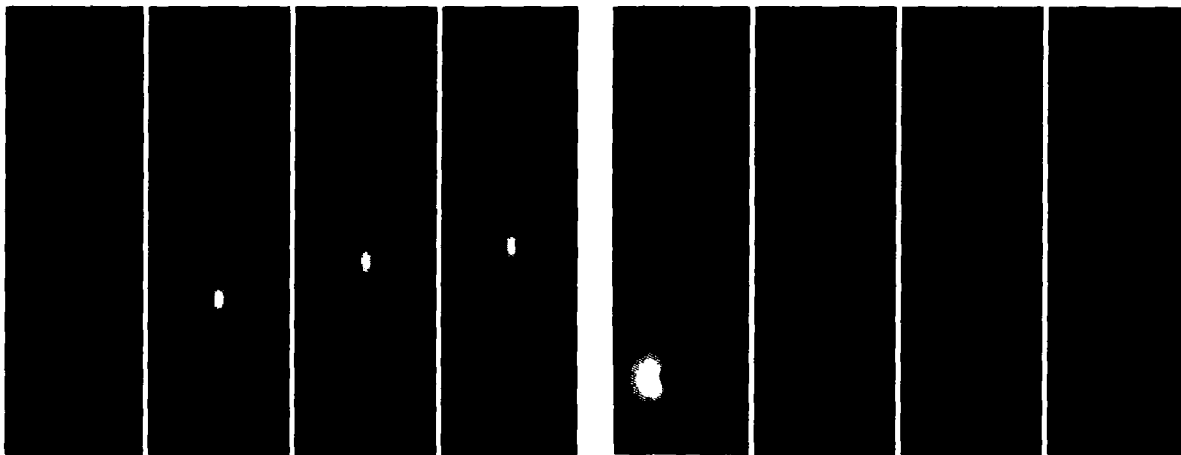
Gross evolution of a high-speed barium cloud injected across the geomagnetic field in the ionospheric F region. The red circles represent the position of the neutral barium vapor, and the colored contours of the left photo (from left to right) denote the integrated Pedersen conductivity at times $t = 1, 9, 17,$ and 25 s; the colored contours of the right photo denote the electrostatic potential at times $t = 1, 9, 17,$ and 25 s (H. Mitchell).

16

This pattern was computed by using a one-dimensional cellular automata rule which gives the next value (1 or 0) at a cell based on the sum of the previous values at that cell and the two adjacent cells. The initial conditions are shown as the top line, and the subsequent evolution develops downward. Cellular automata are important because they illuminate how nature can generate incredibly complex phenomena and global patterns from very simple local laws (J. Boris and E. Oran).

A geographical representation of a missile/ship engagement simulated in the NRL Central Target Simulator (CTS) is displayed in geometrically accurate real-time images. Electrical data from the simulation are superimposed onto a representation of the real-world coordinate system and scenario of seascape, ships, and chaff clouds. The single red line flanked by two blue lines indicates the boresight and 3 dB beam width of the seeker's antenna. The helical pattern of yellow to white spots represents a chaff cloud (A. DiMatessa).

Color-encoded contour plots of the gas density profiles from four successive snapshots of a cylindrical gas jet are shown from left to right. The axis of symmetry is on the left as the jet enters quiescent air at the bottom and moves upward. The transition to turbulence is indicated by the growing vortices (yellow and green) (J. Boris and E. Oran).

One anvil from a diamond-anvil, high-pressure cell. Using this device, NRL scientists have set world records both at very low temperatures (100,000 atm at 0.03K) and at very high temperatures (50,000 atm at 1500K). The blue laser beam emanating from the diamond is used to both align the cell and to measure the pressure (E. Skelton).

17

Reflections from crystalline defects and irregularities (the Nomarski effect) are much more visible in color. These defects are observed in a {100} oriented wafer of indium phosphide after etching in a hydrobromic and acetic acid solution. Dislocations on either side of the twin lamina produce rectangular etch pits whereas dislocations intersecting the twin lamina produce distorted etch pits (R. Henry and H. Lessoff).

Visual display of the progress (represented by white dots) of a parallel adaptive search algorithm developed by artificial intelligence researchers to find global optima in complex, multipeaked search spaces (represented by red surfaces) (K. DeJong).

Dr. Ken Levin, of the Optical Sciences Division, passes a laser beam through an optical fiber coil to evaluate a fluoropolymer coating on the fiber. This coating protects the fiber from water intrusion and has a low index of refraction that aids in light containment. The orange glow on the spool is the very small residual light leakage from the fiber coils (G. Sigel and J. Griffith).
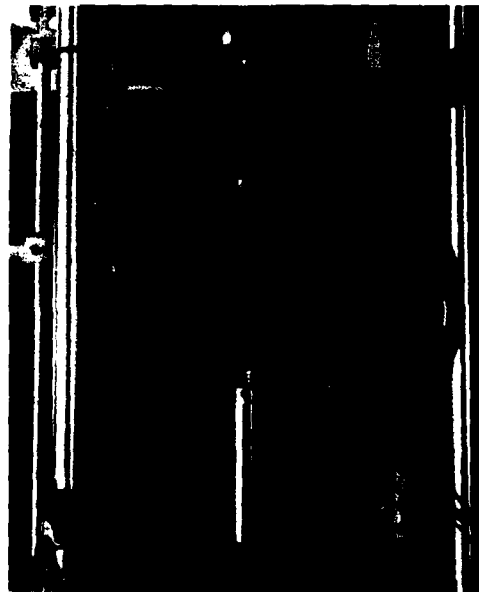
Experimental set-up simulating the high-temperature, fatigue damage conditions experienced by Navy engine turbine blades (K. Sadananda)

18

NRL's full sky X-ray map, produced by the HEAO A1 experiment, shows 842 sources displayed in galactic coordinates. Dot radius is proportional to logarithm of source intensity. Sources include active galactic nuclei (AGN), clusters of galaxies, supernova remnants (SNR), accreting objects in binary systems, and coronae of normal stars. Identification work continues (K. Wood).
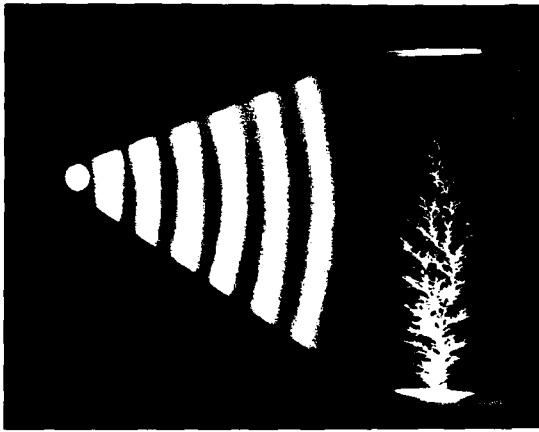
The orange-yellow structure in the lucite block, a Lichtenberg tree named after the physicist who first observed them, can quite properly be termed "frozen lightning." It occurs when the lucite is irradiated by an intense electron beam (depicted by gray waves generated by NRL's linear accelerator (LINAC)). During irradiation, the air around the lucite is ionized producing the blue-green glow (R. Farr).
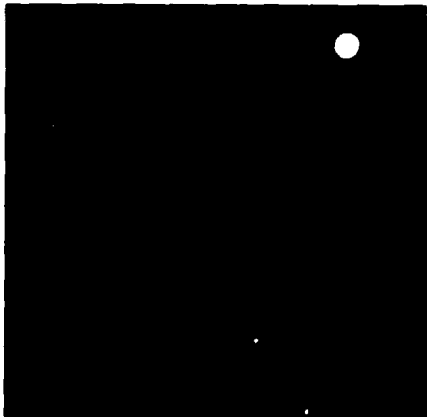
Computer-generated infrared image of a perfectly reflecting sphere floating in the ocean with the sun setting near the horizon. The model used for this image allows multiple scattering by a realistic distribution of ocean waves and includes the sun and sky infrared emission. The yellow speckles in the water are sun glint. This is a simple test case for a model to generate infrared ship signatures (D. Honn).

Two-dimensional axisymmetric flow from an explosion in a barrel. The axis is the left border of the figures, and the grey wall in the center is heavy and rigid, confining the explosion until it reaches the end of the barrel. Free of the barrel, the flow begins expanding as a roughly spherical blast wave. *Left and center:* Each color represents a different range of density values in the flow. The leading shock is followed by a rarefaction and a recompression. The shock is strongest moving along the axis and drops to zero just outside the barrel. *Right:* The same problem is shown to a different scale at a much later time. Each color now shows a range of axial (upward or downward) velocities (J. Boris and T. Young).

19
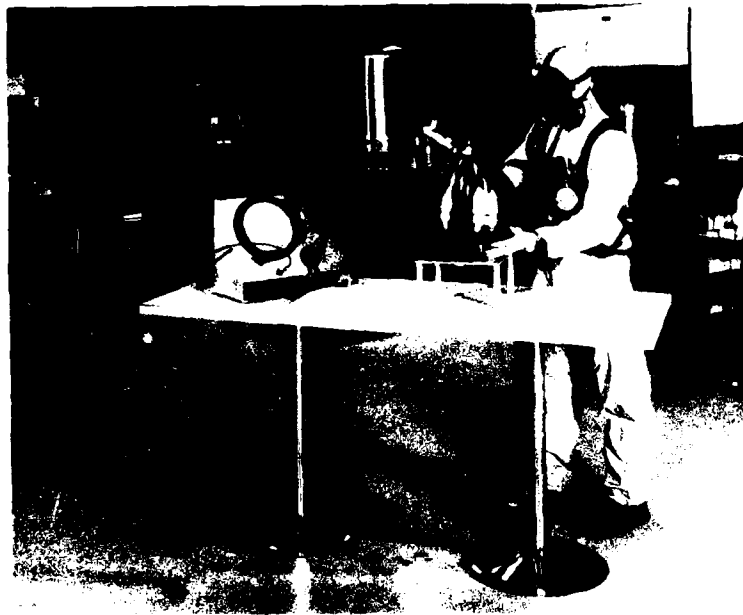
Technician prepares a propellant tank for materials compatibility testing
at the Materials Compatibility Test Facility located at Blossom Point, MD

and special airborne instrumentation for developing electromagnetic remote sensing systems; a facility for long-term testing of satellite clock time/frequency standards under thermal/vacuum conditions linked to the Naval Observatory; a computer-aided design/manufacture facility; a 5-m optical bench laser laboratory; a hologram research laboratory; and limited photographic processing facilities to conduct research in support of developing space systems. NRL also uses Patuxent River Naval Command P-3s to perform experiments in surveillance that may have satellite implications. Finally, the Space Systems and Technology Division possesses many specialized computer facilities of the most current design to perform the manifold functions required for space research programs.

● Electronic Warfare

The field of electronic warfare has been a growing concern at NRL since the 1940s. A major area of expansion is simulation studies, which not only eliminate many costly field measurements, but also permit rigorous and repeat-

Dr. Gerald Friedman, Head of the Advanced Techniques Branch of the Tactical Electronics Warfare Division, is a recognized expert in the field of electronic warfare technology, tactics, and simulation

20
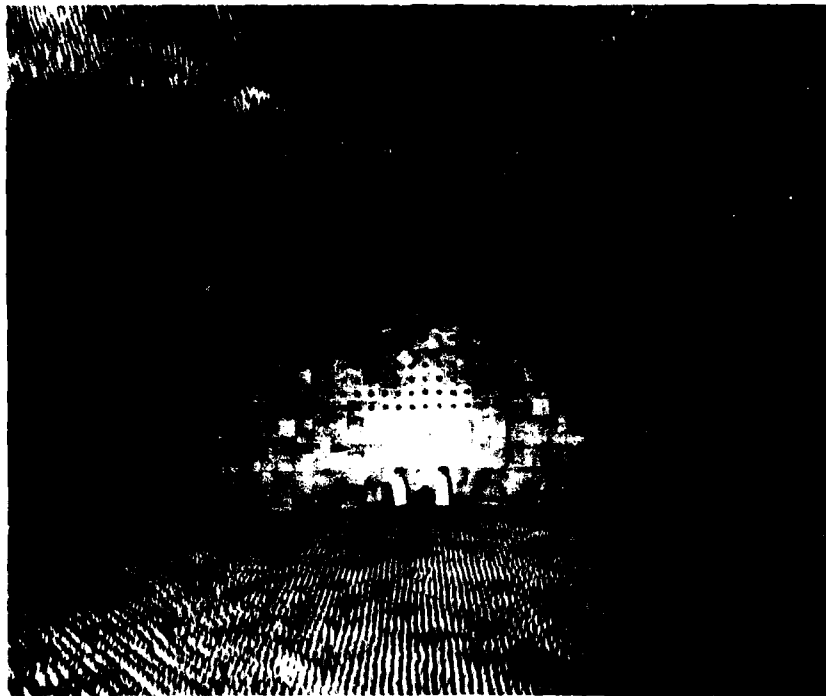
Interior view of a shielded anechoic chamber shows the microwave
absorber lining and matrix array of antennas

Fred Horner, of the Airborne Electronic
Warfare Systems Branch, adjusts the
antenna drift bias on the Hawk Missile
Seeker in the techniques development
chamber of the Electronic Warfare Divi-
sion
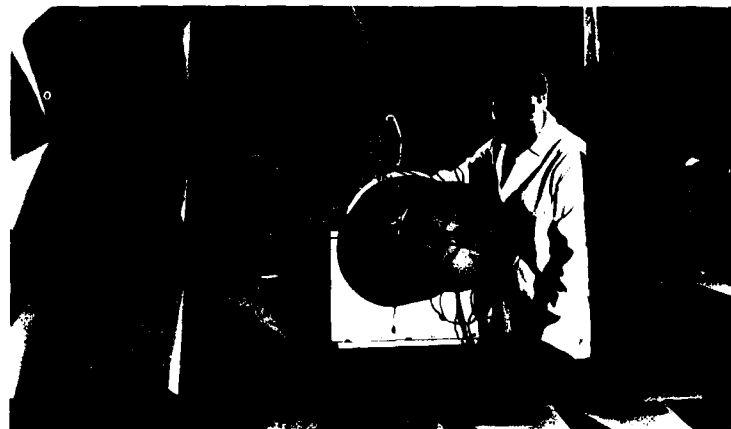
able analyses in controlled environments. A
complex, computer-supported central target simu-
lator is now operating with good results, and its
capabilities are being expanded to accommodate a
broader range of electronic warfare problems. As
research tools, NRL has a mobile infrared signa-
ture measurement and simulation facility and a
hybrid RF/IR missile seeker simulation facility.
A number of antenna measurement chambers, a
radar cross-section measurement facility, and

other advanced research facilities are also avail-
able.

• Information Technology

In recent years, NRL has become a leading
Navy center in information science and technol-
ogy. Much of this effort supports Navy require-
ments in space systems and in communication
and navigation. Major information technology

21

facilities include a microwave space research facility, a voice processing and analysis facility, the Navy Center for Applied Research in Artificial Intelligence, a computer architecture and evaluation facility, and facilities for high frequency (HF) and signal analysis.

● Electronic Sciences

In addition to specific equipment and facilities to support individual technology-base programs in electronics, NRL operates two major central facilities that provide services to electronics programs throughout the Laboratory and at external organizations. The latter two facilities are the microelectronics processing facility and the high magnetic field facility. Specific equipment and facilities include: a full range of crystal-growing equipment used to grow compound semiconductors and other materials of military interest; a molecular beam epitaxy (MBE) system used to grow GaAs-Ga$_x$Al$_{1-x}$As superlattice and quantum well heterostructures; an organometallic chemical vapor deposition (OMCVD) system used to grow various heterostructures; radiation sources for activities in radiation effects and hardening; several scanning electron microscopes and a scanning/transmission electron microscope; an ion implantation facility; a wide range of lasers to characterize materials, interfaces, and heterostructures, and to use in optical-biasing applications; ultrahigh vacuum systems incorporating various electron diffraction and scattering probes used primarily to investigate the properties of interfaces; a specialized processing capability for refractory superconducting devices; a wide range of spectrographic facilities, including electron spin resonance (ESR), nuclear magnetic resonance (NMR), Raman, and optically detected magnetic resonance (ODMR) instruments used to analyze defects in semiconductors; and a tube fabrication facility to support activities in microwave and mm-wave tube technology.

Microelectronics Processing Facility—This facility provides support for NRL programs in electronics R&D design and process technology which require microelectronics processing skills
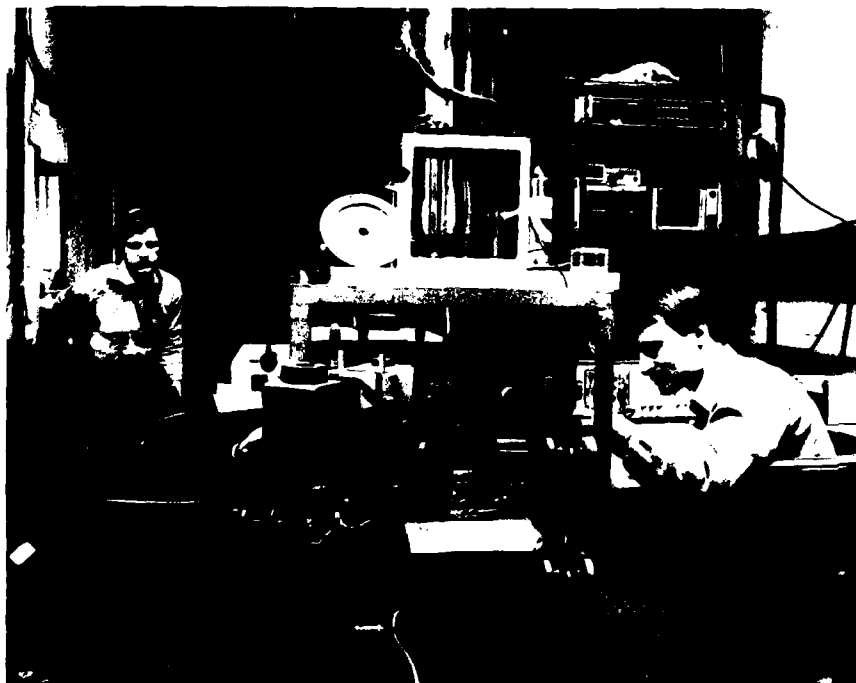
Drs. Stuart Wolf (left, front), Jim Culbertson (right), and Ulrich Strom adjust optical beams which are used in the time-resolved phonon studies

Dr. David Oleniewski of the Electronics Technology Division inspects a mask produced by electron beam writing system in the Microelectronics Processing Facility

and equipment. The facility has a computer-aided design capability; a submicrometer electron beam (e-beam) mask-making capability; and optical, e-beam direct write, and X-ray lithographic capabilities. It also has facilities for: oxidation and diffusion processes, dry and wet etching, metallization, chemical vapor deposition, hybrid bonding, integrated circuit (IC) packaging, process diagnostics, and other miscellaneous state-of-the-art microelectronics processing capabilities. The facility supplies NRL programs with a range of items from discrete structures and devices to complete integrated circuits with very large scale integration (VLSI) complexity based on silicon metal oxide semiconductors (MOS) submicrometer technology.

High Magnetic Field Facility—This facility is used to support research projects throughout NRL, DoD, and, to a limited extent, the local scientific community. The facility provides the capability to determine the response of materials and devices to high magnetic fields up to 17 tesla with a variety of electrical, optical, and magnetic probes. This capability is presently based on the use of both water-cooled, high-current solenoids and superconducting magnets in a variety of con-figurations. The superconducting magnets are served by an in-line helium liquifier, and the facility is being phased into all superconducting magnet operations. As an adjunct service, the facility serves as the central distributor for liquid helium used at NRL.

- Chemistry

NRL has been a major center for chemical research in support of Navy operational requirements since the late 1920s. The Chemistry Division continues its tradition with a broad spectrum of basic and applied research programs concerned with fuels and combustion, corrosion, advanced polymeric materials, ultrasensitive detection methods for chemical agents, and special materials for electronic warfare applications. Modern facilities for research include a wide range of the most modern optical, magnetic, and ion-based spectroscopic instruments, lasers, computers, electrochemical devices, a 325-m^3 ($11{,}400\text{-ft}^3$) fire research chamber (Fire I), multiple facilities for materials synthesis and physical/chemical characterization, high- and low-temperature equipment, and extensive surface-analytical instrumentation.

23

The Fire I Test Chamber is a 325-m^3 pressurizable test facility equipped for research on combustion and energy-transfer mechanics and continuous spectroscopic monitoring of certain gases. The chamber is ideally suited for fire simulation and testing fire suppression systems aboard submarines.

Interior of Fire I Test Chamber where the firepan is prepared for the next series of submarine hull insulation fire tests

24
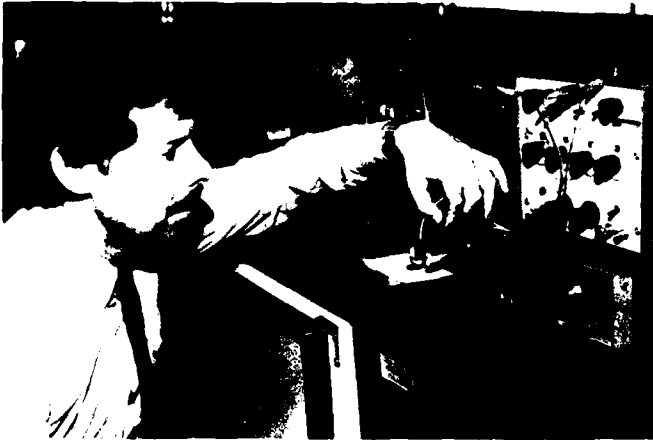
Dr. T.M. Keller of the Chemistry Division uses a four-point probe to measure the resistivity of a new, highly conductive, plastic material

To fabricate biosensors, NRL will take advantage of existing technology for studying membrane proteins such as patch-clamping the formation of Langmuir/Blodgett films. Here, scientists in the Chemistry Division use a Langmuir/Blodgett trough in a dust-free, class 100 clean room.

Dr. Joel Schnur, Head, Biotechnology Branch, in the lipid synthesis laboratory where novel lipids are synthesized for future potential applications in blood surrogates, ultrasensitive detection, hybrid sensors, and other biologically derived microstructures

Dr. Danh Tran of the Optical Sciences Division draws a rod of high-transparency fluoride glass for use in low-loss fiber-optic waveguide fabrication

Dr. John F. Reintjes, head of the Nonlinear Optics Section in the Laser Physics Branch of the Optical Science Division, is shown with a molecular selective microscope based on coherent anti-Stokes Raman scattering. Other research done in Dr. Reintjes' section includes studies of stimulated Raman scattering and phase conjugation for improvement and control of laser beam quality and optical frequency conversion for production of coherent vacuum ultraviolet light sources.

● Optics

Ultralow-Loss Fiber-Optic Waveguides—NRL has established facilities for the purification, synthesis, preform fabrication, fiber-drawing, and comprehensive characterization of ultrahigh transparency fluoride glasses and waveguides. This new class of optical materials offers the promise of both long-distance communications without the need for signal amplification or optical power transfer that uses visible and infrared laser sources. A new, tunable color-center laser facility has been placed into operation during the past year to establish the first operational laboratory data link employing the new fluoride glass waveguides.

Focal Plane Evaluation Facility—NRL has developed a comprehensive capability to measure the optical and electrical characteristics of infrared focal plane arrays being developed for advanced Navy sensors. The facility includes clocking and drive electronics to operate the arrays, calibrated continuous wave (CW) and pulsed infrared sources and electronics for video signal processing and digitization, and computer data reduction for the large volumes of data required to obtain statistical information on each detector in the array. The arrays that have been evaluated include monolithic and hybrid structures which use charge-coupled device (CCD), charge-injection device (CID), and charge-imaging matrix (C/M) technologies.

IR Missile Seeker Evaluation Facility—This facility performs open-loop measurements of the susceptibilities of infrared tracking sensors to optical countermeasures. The facility includes rate

26

tables to simulate target motion, infrared sources with optics and modulators, and electronic instrumentation and data-recording capabilities. The operation of the sources and rate table, as well as the data acquisition and reduction, is computer-controlled. Measurements are performed on modulation and image-based seekers.

Large-Optic, High-Precision Tracker—NRL has developed a tracker system with an 80-cm primary and an 8-mrad field of view designed to measure atmospheric transmittance on the open sea. The unique optical design sends incoming radiation down through the yoke of the tracker mount and presents it at an optical port inside the trailer. Conversely, radiation can be sent out through this port if desired. The optical bench in the trailer holds a high-resolution Fourier transform spectrometer to use in the receiving mode and several lasers to use in the transmitting mode. The tracking system control is through joystick, track ball, digital switches, or error input. By using a silicon quad cell detector, the servo system has been able to produce a 12-μrad tracking accuracy while locked onto a signal. An optical correlation tracking system is being added to facilitate automatic tracking of moving objects without the requirement of a beacon.

High-Energy Excimer Laser—An X-ray preionized discharge excimer laser has been constructed which has reliably produced 60 J of laser radiation at 308 nm in a 200-ns-long pulse, representing the highest output energy achieved to date in any discharge-pumped excimer laser device. This facility is used to investigate a variety of research areas including Raman beam cleanup and combining, nonlinear optical phase conjugation, high-energy laser-beam propagation, advanced optical resonator concepts, and ultraviolet optical damage mechanisms.

Fiber-Optic Sensors—The development and fabrication of fiber-optic sensor concepts, including acoustic, magnetic, electromagnetic, and rate-of-rotation sensors, are conducted in several facilities within the Laboratory's Optical Sciences and Acoustics Divisions. Specialized equipment used for this research includes an automated system for fabricating fiber-optic couplers, facilities for evaluating the properties of optical fiber coatings, single-mode fiber splicers, a high-pressure acoustic test cell, a three-axis magnetic sensor

test cell, and computer modeling of the acoustic response of individual fibers and of alternative sensor concepts.

Digital Processing Facility—This facility is used to collect, process, analyze, and manipulate infrared data and imagery from several sources. A Digital Equipment Corporation VAX 11/785 computer system aids the facility digital image and signal processing. This central processing unit (CPU) accesses 8 megabytes of memory and has a storage disk of 2 gigabytes, a floating point systems AP-120B array processor, a CSPI mini-MAP array processor, a RAMTEK image display, and a Gould Deanza three-color image display. In addition, the facility operates a video system consisting of visible and infrared television cameras, a high-quality video cassette recorder and display, and a digitizer to convert television raster images into digital image data.

● Plasma Physics

The Plasma Physics Division is the major center for in-house Navy and other DoD plasma physics research. It has first-rate facilities with unique capabilities to support this research. The Division has high-power pulsed sources to generate intense electron and ion beams, powerful discharges, and various types of radiation which span the spectrum from X rays to microwaves. The largest of these pulsers is Gamble II, used to study the production of megampere ion beams and their use for producing very hot, high-density plasmas. It is also used to develop inductive switching to allow its output to increase from 2 terawatts (TW) to substantially higher levels needed for new-generation weapon effects simulators. Smaller electron-beam pulsers are used to study the propagation of the electron beams through the atmosphere. A large propagation facility will soon be built where advanced, charged particle beam propagation concepts will be evaluated. Other particle beam generators are used to produce beams which are injected into structured magnetic fields and/or other cavities to generate microwave pulses sufficiently powerful to break down air at atmospheric pressure. Research in related areas involves the use of extremely high-power lasers. NRL's PHAROS III neodymium glass laser can generate powerful

27

Nicholas Nocerino checks the alignment of one of the three beams of the Pharos III laser system in the Plasma Physics Division
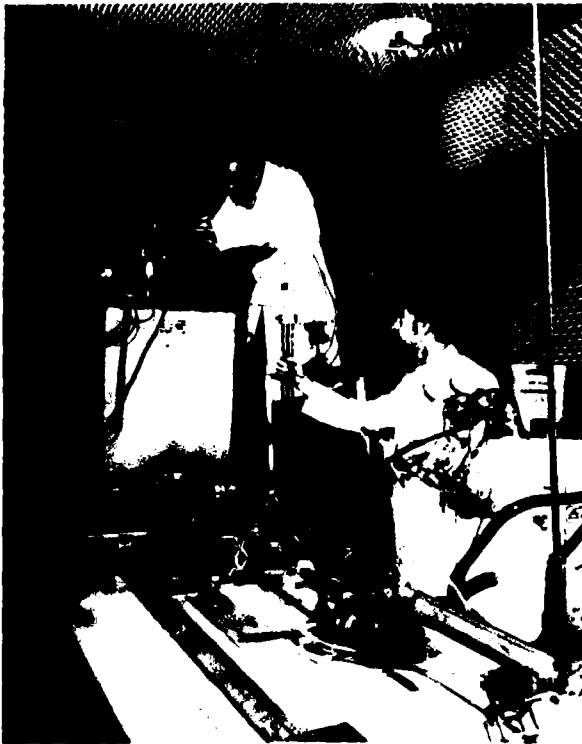
Sam Perry (left) and Jack Condon of the Plasma Physics Division, operate the gyrotron oscillator (200 kW, 356 Hz) developed at NRL. The output waveguide is in the foreground, and the larger vessel contains the superconducting magnet that produces the 13-kG magnetic field.

Robert Lanham inspects the rim of a flywheel for the
Plasma Technology Branch homopolar generator

beams to examine laser-matter interactions; applications presently include inertial fusion research and high-altitude nuclear explosions effects. Lasers are equally important in other parts of the research program. They are used in the atmosphere to guide long discharges that are being studied to find better propagation modes for electron beams, as instantaneous antennas that radiate RF signals, and for possible other military applications.

● Computational Physics

The Laboratory for Computational Physics has been developing a stand-alone Reactive Flow Modeling Facility on its VAX 11/780 computer. The host VAX system has been installed, and a virtual memory system (VMS) driven, general purpose reactive flow model (RFM) has been written, debugged, and applied to a number of fluid dynamics problems in the Laboratory. A Fortran vector version of this two-dimensional fluid dynamics model was used to benchmark

several modest array processors and array processor combinations. This system also serves as a centralized high-speed communications link to the DNA Cray 1 supercomputer system. at the Los Alamos National Laboratory.

● Radar

NRL has gained worldwide renown as the "birthplace of radar" and has maintained its reputation as a leading center for radar-related research and development for a half century. An impressive array of facilities managed by NRL's Radar Division continues to contribute to this reputation. These include an antenna measurement laboratory; a radar area measurement system; a radar research and development activity at the Chesapeake Bay Detachment (CBD), Chesapeake Beach, Maryland; an Identification Friend or Foe (IFF) ground station; and separate facilities for specific types of systems ranging from high-frequency, over-the-horizon radars to mm-wave radars.

29

The directed mirror antenna radar (DMAR) and the fixed array surveillance radar (FASR) are currently under test at CBD. The DMAR combines surveillance and weapons control for potential fleet air-defense, antiaircraft warfare application. This antenna is based on technology that allows radar beams to be scanned by movement of only one lightweight RF mirror. The FASR combines very low antenna sidelobes in a scanning phased array with distributed microprocessors to steer the beam and to monitor the state of active components in the array.

● Acoustics

NRL's facilities in support of acoustical investigations are located at the main Laboratory site and in Orlando, Florida—at the Underwater Sound Reference Detachment (USRD). At the main Laboratory site, there are three research tanks instrumented to study echo characteristics and to develop devices; the largest tank is 9 m deep, 12 m long, and 8 m wide. There is also an underwater acoustic holography facility for research in acoustic fields and a water tunnel having a large blow-down channel with a 15-m test section used for acoustic and flow-induced

vibration studies of towed line arrays and flexible cables. For acoustic surveillance array processing and acoustic data processing, researchers have access to the multichannel, programmable, digital data processing system—a system of DEC computers, high-speed array processors, and peripherals for up to 256 channels. The USRD facilities are described with NRL's field stations.

● Materials

The characteristics of materials also can be examined with a number of instruments. NRL has capabilities for X-ray and electron diffraction analysis and for electron and Auger spectroscopy. It has a high-performance, secondary ion mass spectrometer that represents a standard for surface analysis and significantly extends the diagnostic capability of the technique. A high-resolution, high-performance, reverse-geometry mass spectrometer is used to probe reactions between ions and molecules. The Laboratory has a variety of machines with capacity up to 272,000 kg to test fatigue and fracture of new materials.

NRL facilities for rapid solidification processing were expanded significantly when the ultrasonic gas atomization (UGA) system was
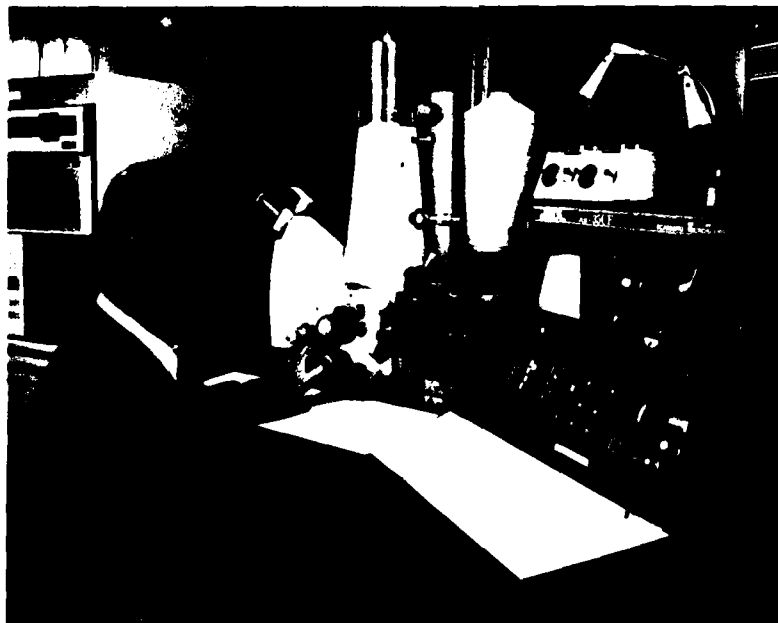
Lloyd Richards of the Material Science and Technology Division, operates the scanning electron microscope used to observe surface structures and components of metallic materials
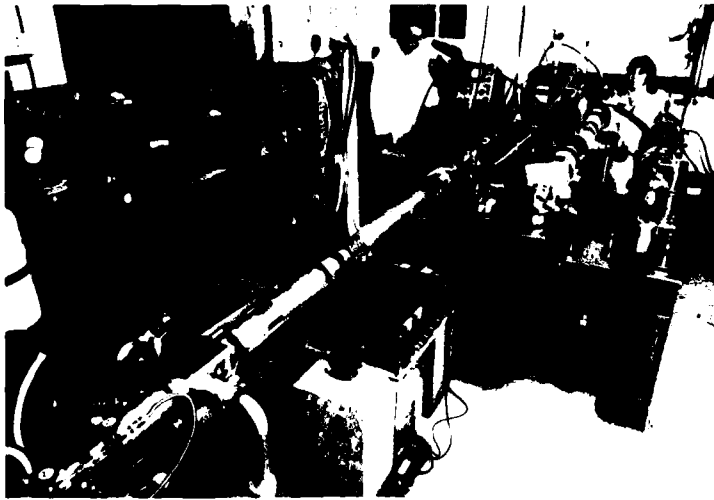
Shock tube used to diagnose the mechanisms and intermediate molecular fragments in gas-phase reactions. In current studies, this shock tube is used to trace the critical events and species involved in high-temperature combustion.

Dr. Kuntamaddi Sadananda of the Material Science and Technology Division operates a universal high-temperature machine that checks for signs of fatigue in specimens

completed. This atomizer includes a UGA nozzle, a molten alloy capacity of 1 to 5 kg, a gas inlet pressure capacity of up to 27.6 MPa, and a process controller for programmable actuation of the system components.

The Laser-Materials Application Center provides laser irradiation services in support of a wide range of laser material interaction and effects studies and material processing development. A high-energy, continuous wave (CW), CO_2 electrical discharge laser operating at 10.6 μm can provide 12 kW or more of optical power at a workpiece. Both highly focusable (unstable resonator) and spatially uniform (multimodal resonator) optics are available along with associated workpiece optics and fixtures. Laser output characteristic and workpiece transducer data-recording capabilities are also available.

- Condensed Matter and
  Radiation Sciences

Ion Implantation Facility—The facility consists of a 200-keV ion implanter with specialized ultrahigh vacuum chambers and associated instrumentation for *in situ* surface analysis of specimens undergoing implantation. The facility is used to develop advanced surface treatment methods for the modification of surface properties such as corrosion, oxidation, wear, index of refraction, and

31
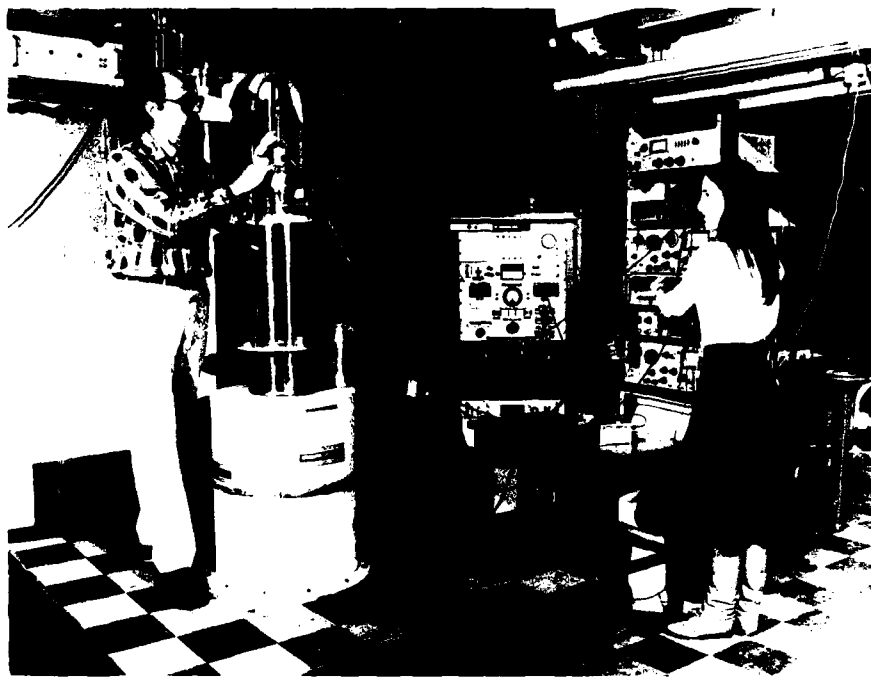
Dr. Robert Wagner (Electronics Technology Division) and Dr. Wendy Fuller (Condensed Matter and Radiation Sciences Division) adjust experimental apparatus in a study of the effect of high magnetic fields on thin films of single crystal iron

electrical conductivity. A recent addition to this facility is the capability to vapor deposit a thin film during ion bombardment. This approach provides the capability to fabricate highly adherent thin films of controlled composition.

5-MeV Van de Graaff—This facility is used in a variety of research projects ranging from the study of the effect of charged particle radiation damage, characteristic of the space environment on microelectronic circuits, to the performance of surface analysis such as Rutherford backscattering spectroscopy and nuclear reaction analysis for use in materials research problems requiring high-sensitivity composition depth profiles.

Radiation Facilities—A number of radiation facilities are operated to support research in radiation effects. The principal facility is the electron linear accelerator (Linac). The Linac can produce intense electron beams with energies that are selectable from 10 to 65 MeV. The pulse repetition rate per second can be varied from 1 to 360 pulses. Pulsewidths can be chosen in the range from 0.05 to 1.4 μs. The Linac group also operates a large Cobalt-60, gamma-ray source and a 2-MeV Van de Graaff accelerator.

Epitaxial Growth of Metallic Films—The fabrication of ultrathin, crystalline metallic films is of great interest both from a technology viewpoint (integrated circuitry) and from a purely scientific viewpoint (fundamental quantum limits). NRL has two facilities dedicated to this research. One is a molecular beam epitaxy system with *in situ* diagnostics for structurally monitoring the films as they are grown and a vacuum specification of 10^{-11} torr. This system is devoted to the study of magnetic films and magnetic multilayers. The second facility (new this year) is an electron beam epitaxy system, also with *in situ* diagnostics for structural monitoring and a vacuum specification of 10^{-11} torr. This system is devoted to the growth of refractory metals which require high synthesis temperatures. Specific interest is in superconducting and optical properties with an emphasis on periodically grown multilayers.

Hypervelocity Impact Facilities—Three facilities are used routinely for terminal ballistics

research at speeds up to 6 km/s. For unusual test conditions, the accelerators may be operated at speeds of over 9 km/s. A typical test would include measurements of projectile velocity, projectile orientation, and dynamic projectile-target interaction. The largest of the three test facilities may be used for impact tests with targets containing toxic or explosive materials.

● Marine Technology

The Marine Technology Division has several facilities for experimental studies in fluid dynamics. These include a 30-m-long wind/wave tank to study wave forces on ocean structures and the interaction of ship wakes with ambient waves; a 20-m, dual-carriage tow channel capable of vertical stratification to study geophysical flows and wakes; and a large, blow-down water tunnel with a 15-m-long test section to study noise associated with turbulent boundary layer flows around towed arrays. These facilities are equipped with state-of-the-art data acquisition and analysis systems. Other facilities include towed sensor arrays and related processors to acquire field information on upper ocean dynamic processes, a computer-controlled experimental stress analysis capability,

and extensive equipment for shock and vibration measurement.

With these and other research facilities, NRL scientists are able to undertake advanced research in the 9 broad fields highlighted in this *Review*. The high-quality instrumentation required to support such a diversity of research represents a capital investment of over $100 million.

Research Support Facilities

● Central Computing Services

In March 1985, NRL installed a computer system consisting of a Cray X-MP/12 Class VI supercomputer and three VAX 11/785 front-end computers. The Cray provides a high-speed computational facility especially suitable for scientific and engineering research and development programs. It is a balanced vector and very high-speed scalar processor. The peak processing speed of the Cray is 315 million floating point operations per second (MFLOPS) with a sustainable speed of 210 MFLOPS. A speed of 105 MFLOPS can be achieved by typical FORTRAN
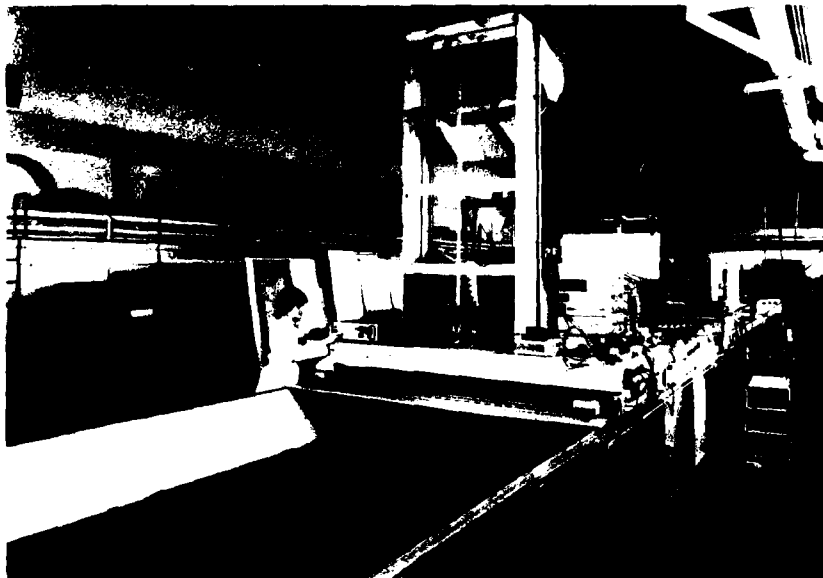
This 30-m-long wind/wave tank is used to study wave forces on ocean structures and the interaction of ship wakes with ambient waves

The Cray X-MP/12 computer serves NRL scientists and engineers as well as the Navy Laboratory Computing Committee and the Navy Lab Computing Network

application programs. The NRL Cray has a central memory capacity of 2 million 64-bit words and an I/O subsystem with three interconnected I/O processors. It runs the Cray operating system (COS) and has a FORTRAN 77 compiler with vectorizing capabilities.

Access to the Cray is provided by user-friendly, front-end machines at the central site. These consist of three, closely coupled VAX 11/785 processors with shared disk and tape units. Other remote machines are connected via local area networks and the Defense Data Network/Military Network (DDN/MILNET). The front-end systems recognize and exploit the features of typical modern terminals whether they are connected by dial-up, direct line, local area networks, or the DDN/MILNET. The front-end systems also provide such services as a data-base management system, a document processor, and graphics support. The primary programming language for the Cray is FORTRAN; PASCAL is also available. The front-end system offers FORTRAN, PASCAL, and C. A wide range of scientific, statistical, and mathematical software is available. The networking aspects of this new system provide the capability to link terminals, PCs, minicomputers, and other host systems to the front-end system and to the Cray by using RS232C connections and DECNET and TCP/IP protocols.

Significant plotting capabilities are available: both a high-performance, pen-plotting capability to reproduce quality plots and a high-speed, electrostatic plotter/printer that quickly produces inexpensive plots for preview purposes; plots can also be previewed on graphics terminals. Plotting software is available that provides data to produce DICOMED graphics. The DICOMED system, located in the Technical Information Division, provides off-line, enhanced graphics capability and produces color or black and white images on 16-mm movies, 35-mm slides, 8 by 10 in. viewgraphs, or microfiche.

● Technical Information Services

The Ruth H. Hooker Technical Library contains more than one million volumes, reports, and microforms along with 1700 current journal subscriptions. The library has access to 5 on-line computer search services accessing well over 100 data bases. These can search most of the open literature, classified and unclassified DoD publications, other technical report material, and chemical substances by structure and substructure. On-line computer access to the library's card catalog is also possible inside and outside of the library by using the Integrated Library System. The library also provides interlibrary loans, Library of Congress stack passes, translation services, foreign language tapes, college catalogs, published technical society standards, telephone books from major U.S. cities, and a map collection.

Publication services are offered by technical and nontechnical editors who arrange and format communications from author to audience into quality publications such as formal reports, brochures, handbooks, manuals, proceedings, or monographs. Illustrators and visual information specialists prepare camera-ready artwork, proceed-

The DICOMED System, located in the Technical Information Division, provides NRL with offline graphics. By using computer-generated data it produces either color or black and white images on film for viewgraphs, microfiche, slides, and movies.

ings, journals, bulletins, certificates, and plaques for composition and printing. These specialists also prepare interpretive art, brochures, flyers, displays, and cartoons and caricatures for special projects. The Computerized Technical Composition (CTC) Section prepares reports which may contain difficult formulas or mathematical equations. Some material is keyboarded in CTC, and other material is entered through an optical character recognition (OCR) scanner or magnetic media. The CTC Section generates double-spaced draft copy and single-spaced camera-ready copy through phototypesetters.

Motion-picture and still-camera photographers provide microphotography, aerial and high-speed photography, and other experimental data documentation for the R&D community at NRL, as well as in the field.

Information specialists develop press releases, feature articles, and written items on NRL technical programs for dissemination to the print and broadcast media. They also help researchers prepare visually effective materials to use in exhibitions and presentations at professional meetings and seminars. They assist scientists in planning and organizing major meetings and set up and operate projection and other equipment to support these meetings.

● Engineering Services

The Engineering Services Division (ESD) provides NRL and other Navy laboratories with engineers/technicians, highly skilled mechanics, and extensive production facilities to support research projects. The work is normally accomplished in one main building and several small shops located throughout the Laboratory.

ESD works with the researchers on state-of-the-art needs from briefings, freehand sketches, and detailed drawings according to MIL- and NASA standards to produce research/application hardware to scientists' specifications. ESD performs engineering analysis in support of research; fabrication of heavy structures; and design and fabrication of original electronic devices and instruments. A CAD/CAM (Computed Aided Design/Computer Aided Manufacture) Facility is now in operation in ESD. This system is used for designing mechanical parts and printed circuit boards; for plant design, architecture, and drafting; and for data preparation for manufacturing parts on numerically controlled machines.

ESD also has extensive capabilities for sheet metal fabrication; machining; plastic, laminate, polymer, and fiberglass fabrication, forming and

Across top:

Panorama (eastward) of building 210 (on the left-hand side), which houses the Tactical Electronic Warfare Division; and building 222, home of the Technical Information, Public Works, and Financial Management Divisions

Far left:

Bust of Thomas A. Edison facing the Laboratory's main entrance The Naval Research Laboratory originated from his suggestion for a national laboratory for defense-related research.
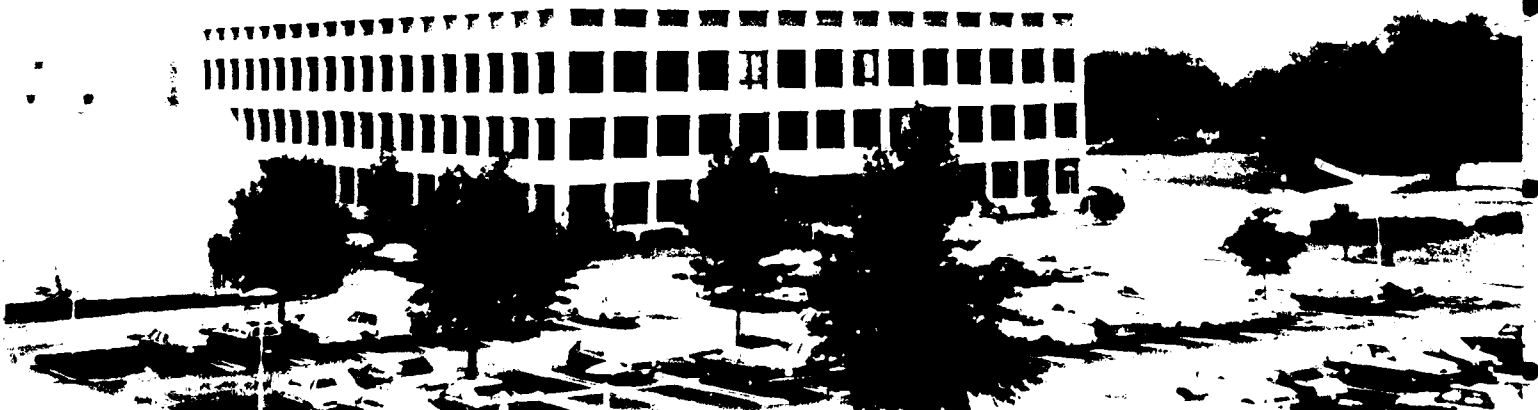
Center left:

Building 43 is the administrative head-
quarters and management information center
for NRL. Scientists called the 50-ft dish of
the radio telescope mounted atop this building
the first "accurately figured" radio telescope
in the world

Center right:

Building 12 (part of the original NRL)
on the North side of the mall

Across bottom:

Panorama (westward) of building 207,
which houses the Chemistry Division, building
208, home of the Electronics Technology Divi-
sion, building 226 a secure auditorium, and
building 209 which houses the Space Sci-
ence Division

Elaine Snider, of the Electronic Fabrication Branch, Engineering Services Division, designs a printed circuit board on a REDAC computer-aided-design station

Mike Lowery of the Mechanical Manufacturing Branch, Engineering Sciences Division, arc welds an instrument chassis for scientific calibration units

molding; electroplating; heat-treating of metals; limiting castings; and sand blasting.

FIELD STATIONS

NRL has acquired or made arrangements over the years to use a number of field sites or auxiliary facilities for research that cannot be conducted in Washington, DC. They are located in Maryland, Virginia, California, and Florida. The two largest facilities are the Chesapeake Bay Detachment (CBD) and the Underwater Sound Reference Detachment (USRD).

• CBD

CBD, which occupies 68.1 hectares near Chesapeake Beach, Maryland, provides facilities and services for research in radar, fire-control equipment, optical devices, materials, communications, and other subjects. Because of its location on the western shore of Chesapeake Bay, unique experiment ·) be performed. Radar antennas 50 to 60 m above the water overlook the bay. Another site, Tilghman Island, is 16 km across the bay from CBD and in a direct line of sight from CBD. This creates a unique environ-

38

The Chesapeake Bay Detachment (CBD) facility overlooks the Chesapeake Bay from 50-m cliff. The Tilghman Island site (*inset*) is 16 km across the Bay from CBD and in a direct line of sight from it, thus creating a pair of facilities for unique propagation studies.
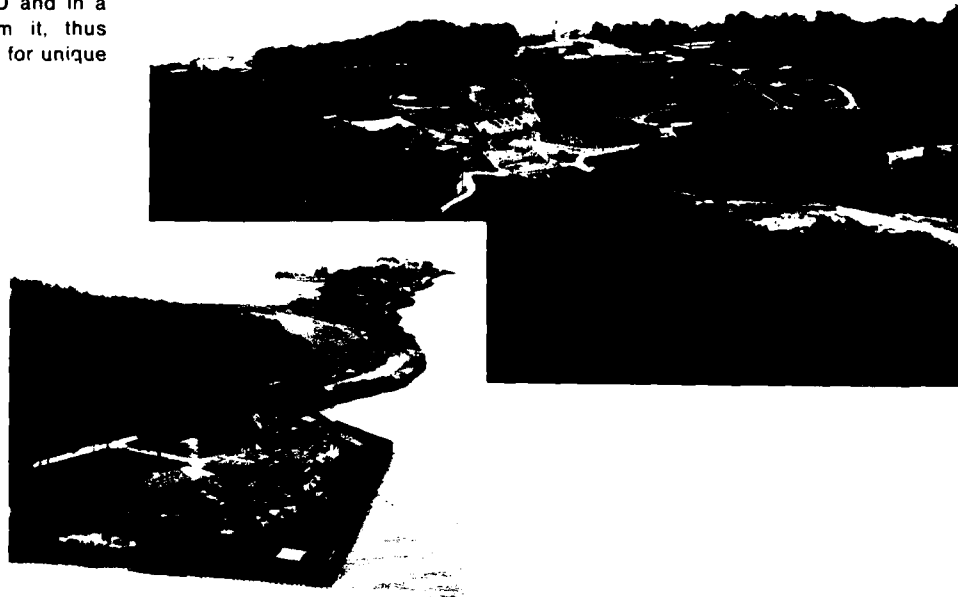
ment for low clutter and generally low background radar measurements. Experiments involving chaff dispensing overwater and radar target characterizations of aircraft and ships are examples of military-oriented research. Basic research in radar antenna properties, testing of radar remote sensing concepts, use of radar to sense ocean waves, and laser propagation is also conducted.

● USRD

Located at Orlando, Florida, USRD functions in many ways like a standards bureau of underwater sound. Its semitropical climate and two clear, quiet lakes (the larger is 50 m across, 11 m deep, and nearly circular) are distinct assets to its research and development on sonar transducers and underwater reference standards and to its improvement of techniques to calibrate, test, and evaluate underwater acoustic devices. USRD has an anechoic tank for simulating ocean depths to 700 m and smaller pressure tanks for simulating depths to 7000 m. A spring located in a remote area about 40 miles north of USRD, at

the Leesburg Facility, provides a natural anechoic tank for water depths to 52 m with ambient noise level 10 dB below that for sea state zero; larger objects can be calibrated here. The detachment has provided acoustic equipment and calibration services not only to hundreds of Navy activities and their contractors but also to allied governments.

● Marine Test Facilities

Located on Fleming Key at Key West, Florida, these facilities contain piers in an average water depth of 3 m and several flowing seawater test facilities capable of flow speeds to 70 knots (36 m/s). The site offers a clear, unpolluted seawater and atmospheric environment to study salt atmosphere weathering, stress corrosion, fouling resistance of coatings, cathodic protection, and electrochemical corrosion.

● Other Sites

Some field sites have been chosen primarily because they provide favorable conditions to
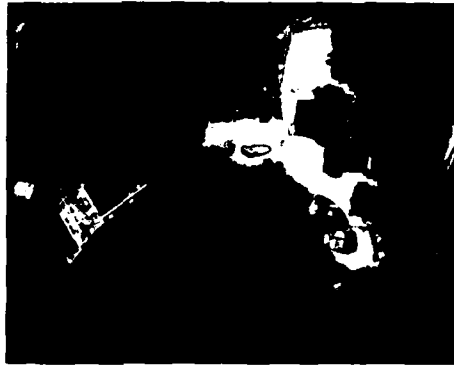
NRL is the principal Navy activity for acoustic calibration, tests, and evaluation. The Underwater Sound Reference Detachment, located near Orlando, Florida, carries out the majority of these tasks. The nearly circular 50-m diameter lake is ideal for these purposes. *Inset*: the Leesburg (Florida) Facility provides an extremely quiet, natural underwater anechoic environment for calibration.

Radio telescope site, Maryland Point, Maryland. Each telescope, about 25 m in diameter, is used for high-precision radio astronomy measurements.
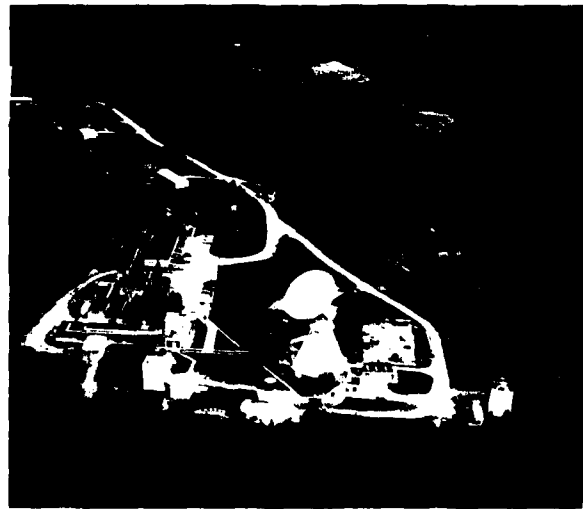
The Satellite Communication Facility, Waldorf, Maryland, is used as a transmit/receive site in the 2 to 20 GHz range
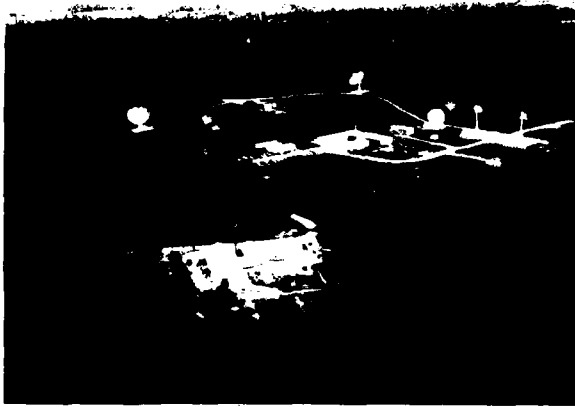
The satellite tracking station, Blossom Point, Maryland, is mainly used by the Space Systems Division

operate specific antennas and electronic subsystems. Maryland Point, Maryland, 80 miles south of NRL, operates two radio telescopes with antennas measuring 25.6 and 26 m in diameter for radio astronomy research. NRL's Waldorf facility, approximately 40 miles south of NRL, operates an 18.3-m, X-band antenna and an S-band antenna of the same size for space and communications research. Pomonkey, a third field site in Maryland, 40 miles south of NRL, has a free-space antenna range to develop and test a variety of antennas. Another facility used to improve communications is the antenna model measurement range in Brandywine, Maryland, 40 miles southeast of NRL. Here, scaled model ships can be set up and rotated in the center of a range 305 m in diameter to provide data to aid in theoretical and experimental antenna design. NRL has installations for satellite tracking at Blossom Point, Maryland, and at Vandenberg Air Force Base, California.

• Research Platforms

NRL uses ships and aircraft to conduct some of its research. Oceangoing research ships are obtained from a pool of vessels maintained by the Naval Oceanographic Office, Mississippi. For airborne research, NRL uses three four-engine turboprop P-3A Orions and one four-engine tur-

boprop P-3B Orion. These airplanes annually log about 1300 hours of flying time on projects ranging from magnetic bathymetry and electronic countermeasure research to studies of radar signal reflections.

NRL in the Future

To continue its growth and provide preeminent research for tomorrow's Navy, NRL must maintain and upgrade its scientific and technological facilities at the forefront. Its physical plant to house these facilities must also be adequate. NRL recently embarked on a Corporate Facilities Investment Plan (CFIP) to renew its physical plant. This plan and future facility plans are described below.

THE CFIP — NEW SCIENTIFIC FACILITIES

In 1983, NRL celebrated its 60th anniversary; some of its buildings date back to its beginning, 1923. In response to today's rapid growth and tomorrow's acceleration of science and technology, NRL has developed a comprehensive modernization plan (CFIP). It calls for the expenditure of nearly $250 million to provide 46,500 m² of either new or renovated floor space by 1995. The plan calls for the construction of 5 new buildings or facilities, major rehabilitation of 8 buildings, limited rehabilitation of 25 buildings,

A unique combination of a current photograph and an artist's concept of how NRL could look in the year 2000. Under the CFIP, certain buildings will be renovated and modernized while other temporary buildings will be torn down to make way for new construction.

and demolition of 34 very old or temporary buildings. Present and future research require, in addition to sound structures, more precise environmental (temperature, humidity, and dust) control and more reliable power sources. Collocated, secure laboratory, computation, and office space is needed for future involvement in highly sensitive research. Buildings must be easily adaptable to presently unknown future needs, and greater overhead space will be needed for the larger pieces of equipment that will be required.

The five new facilities to be constructed will contain specialized laboratories. These are:

- Electro-Optics Laboratory

This 3359-m^2 laboratory will provide unique facilities for research in ultrapure materials for low-loss, long-distance communication and surveillance links; fiber-optic sensors for undersea applications and weapons fusing; infrared technology for detection and surveillance schemes; and laser weaponry and related technologies for space applications. Construction, scheduled to begin in 1985, will include special soil preparation and development techniques to minimize building vibration and settling; structurally isolated laboratory rooms in the ground bays where the laboratory floors will hang free from the building structure; isolated foundation blocks and specialized mountings for mechanical equipment that will enter the building through special mechanical runways; class 100 clean suites; a 7.32-m, class 100, fiber draw tower; vaulted and shielded laboratories and computer facility; and 24-hr temperature, humidity, and pressure control.

- Plasma Physics Facility

Two separate laboratories will be constructed (in an existing building with a high overhead) to provide facilities for advances associated with the generation and propagation of very high-energy density plasmas and charged particle beams.

One of the laboratories will house an inductive energy storage and switch development facility. This facility will develop opening switches and power flow techniques to generate output

pulses at levels exceeding 10^{13} W. It will also provide intense sources of X-ray radiation to simulate nuclear weapon effects on military systems.

The other laboratory will be established to study the propagation of very intense charged particle beams. A 5-MV generator will inject short pulses of electron current into the atmosphere or other simulated environments. An optional laser beam will be available to preionize the propagating channel, and the properties and effects of such beams will be studied. The characteristics of more energetic beams should provide information for future military applications.

- Tactical Electronic Warfare (TEW) Laboratory

A current military construction project will provide the Navy with significant new capabilities to assess and optimize the coordinated use of distributed U.S. EW systems opposing multiple threat formations in battle group environments. Critical EW decision processes and EW system operator functions will be incorporated into real-time, closed-loop, simulated naval engagements. Broadband and fiber-optic local area networks will integrate new and existing R&D facilities into a centrally coordinated simulation environment. The addition of nearly 14,000 m^2 will almost double the size of the current EW facility. Along with extensive modeling and simulation capabilities, the new addition will also contain a number of new facilities including a radar cross-section model measurements facility, an off-board (remote) countermeasures facility—principally a subsonic wind tunnel, an EW-pod development laboratory, and an optical integration laboratory.

The total EW complex will permit a quicker and more effective response to Navy EW needs. Variations in operational conditions can be explored under controlled conditions leading to less expensive and quicker development of coordinated EW systems. These variations will focus on and support R&D and lead to a scale-down in the number of the very expensive at-sea and in-air tests and evaluations now required to quantify system effectiveness and to optimize utilization.

● Secure Laboratory Facility

This facility will address the continuing and expanding need for secure computational and laboratory spaces. The building will house more than 70% of the highly classified work now in progress at NRL.

● General Purpose Laboratory

This environmentally controlled facility will provide stringently clean laboratories with carefully controllable temperature, humidity, ambient dust, and power for investigations in the rapidly evolving fields of electronic technology and composite materials synthesis and exploitation.

REHABILITATION OF SCIENTIFIC FACILITIES

Several of the research facilities at NRL will be upgraded in the near future. These are highlighted below.

● Central Computing Facilities

An NRL integrated communications network (NICENET) is being installed that will provide access to the central site facilities from both terminals and other computers at NRL; other potential NICENET uses (for example, video conferencing) are also under consideration. The ultimate goal of this network is to provide universal access to common-shared computer resources, gateways to other networks and graphics peripherals, and other noncomputer communications services.

● Other Facilities

Specialized facilities are being installed or upgraded in several of the research and support divisions.

Information Services—The Artificial Intelligence (AI) Center will continue installation of the local area network for its eight computers. Additional computers planned are the Symbolics 3500 listing processing (LISP) machines to complete accessibility to all LISP and AI developments, plus SUN Microsystems, Inc. SUN® workstations for the multisensor integration project also will be installed.

Plasma Physics—Facilities (combining the established technology with new concepts) are being constructed to study methods of accelerating electrons to high energy at very high current levels. Such facilities will provide the technology needed to develop very compact (and economical) accelerators for advanced military systems. A large inductive store is being designed to provide a driver for an advanced plasma implosion facility to serve in a variety of applications, including X-ray laser development.

Electronic Warfare—The electronic warfare program includes plans to develop, as part of the CFIP, a major simulation capability—the coordinated electronic warfare simulation laboratory (CEWSL)—to explore electronic countermeasure applications in all stages of naval combat.

Computational Physics—Work is continuing on the Reactive Flow Modeling Facility, which the Laboratory for Computational Physics is developing on its VAX 11/780 computer. This facility couples multiple inexpensive array processors working asynchronously in parallel. It is now being installed and, when complete, will provide near-supercomputer performance for the cost of a minicomputer installation. This facility can be used for applied research on nuclear and environmental airblast effects; turbulence modeling for jets, wakes, and reactive flows; and for atmospheric turbulence predictions.

Materials—In 1985, a repetitively pulsed, high-energy CO_2 laser operating at 10.6 μm will join the existing Laser-Materials Application Center's 12-kW continuous-wave (CW) CO_2 laser. Energies up to 500 J will be available from 20 to 100 μs pulses at repetition rates to 100 Hz. New test cells and optics will permit CW, repetitively pulsed, or combined simultaneous irradiation of samples. The extension of state-of-the-art molecular beam epitaxy (MBE) technology to silicon and related materials is planned with the addition of new equipment.

Engineering Services—In the future, engineers will work with materials such as powdered metal-mixture fabrications, ion implantations, base metal claddings, boron and graphite fiber-reinforced plastics, and laser-activated machining of ceramics. An advanced technology and fabrication facility is being planned to pursue

43

investigations leading to fabrication techniques by using these new and/or unusual materials, processes, and techniques developed by NRL research divisions or other Navy Laboratories. Longer range plans call for new machines: both computer-controlled drives by our new computer-aided device/computer-aided manufacture (CAD/CAM) system, and human-controlled drives with enhanced precision capability using new and unusual material fabrication. Coupled with this modernization will be structural, thermal, and cost analysis capabilities as well as electronic engineering, design, analysis, and printed circuit board layouts.

Further Information: The *NRL Fact Book* gives more details about the Laboratory and its operations. It lists major equipment, current fields of research, field sites, and outlying facilities, and it also presents information about the responsibilities, organization, key personnel, and funding of the divisions, detachments, and other major organization units.

Information on the research described in this *Review* may be obtained by contacting Mr. Richard Fulper, Jr., Head, Technology Transfer and Special Programs, Code 1005.4, (202) 767-3744. General information about NRL may be obtained from the Public Affairs Office, Code 2610, or by phone (202) 767-2541. The sources of information on the various nonresearch programs at NRL are listed in the *Review* Chapter entitled "Programs for Professional Development."

HIGHLIGHTS OF NRL RESEARCH IN 1984

Artificial Intelligence and Signal Processing

A new, high-frequency (HF) channel prober provides the equivalent of an almost instantaneous multispectral analysis of the 1 MHz, HF channel. It provides information about the instantaneous bandwith of the propagating channel modes as well as information relating to fast and slow fluctuations of channel parameters. These measurements are essential for spread-spectrum communication.

***

The use of information theory has led to the development of a new approach to isolated-word speech recognition. Highly accurate speaker-independent recognition is achieved with substantially reduced computations and memory. It was also shown that words out of context can be more easily recognized than was previously assumed. See *1983 NRL Review*, p. 43.

***

A new methodology to develop software systems, especially real-time embedded systems commonly found in critical DoD applications, has been developed. The methodology will drastically reduce the time and cost to integrate, test, modify, and maintain software systems. All or part of the methodology is being used by the Naval Weapons Center, the U.S. Air Force, Bell Labs, Grumman Aerospace, and MIT Draper Labs, among others. See article on p. 79.

***

An expert system using artificial intelligence has been devised to help artillery officers to determine the effectiveness of their weapons against various targets and to optimize their weapons allocation. In the field, decisions must be made quickly. As a result, the expert system asks the most critical questions first so that if questioning ceases, time has been used optimally. This generic system was easily adapted to help radar officers classify targets. See *1983 NRL Review*, p. 39.

***

NRL has developed a multirate processor (MRP) that uses a single voice processing algorithm to generate digitized speech at 2.4, 9.6, and 16 kilobits/s. This system preserves end-to-end encryption by making it ideally suited for military communications. The MRP allows narrowband and wideband systems to be easily interconnected. MRP processors are being deployed, and MRP terminals are being fabricated for naval deployment. See *1983 NRL Review*, p. 45.

45

Electromagnetic Sensing and Systems

NRL has developed a new, three-frequency, microwave scatterometer (TRIFAR) from the parent dual-frequency scatterometer. TRIFAR promises significant improvement in signal quality and an increase in the accuracy of directional measurements of ocean wave spectra and surface winds. Field tests indicate that the new technique is practical and effective to use in an advanced ocean remote sensing system to support strategic and tactical Navy operations. See *1983 NRL Review*, p. 65.

***

A model to explain the observed emission enhancement of thermionic dispenser cathodes used for millimeter-wave tubes has shown that electron emission is maximized for certain cathode alloy percentages. This could increase the practicality of new tube designs having a 5-fold increase in current density and a 10-fold improvement in emission uniformity. These tubes are used in radar and electronic countermeasure systems.

Environmental Research

Mass ejections of plasma through the corona of the sun into the interplanetary medium are observed by the NRL Solwind Coronagraph. Analysis of these events has led to fundamental understanding that will enable scientists to predict whether the shock wave from a particular coronal mass ejection will reach the Earth, how long it will take to arrive, and ultimately, the effect it will have on the Earth's magnetosphere. See articles on pp. 133 and 135.

***

The entire sky was mapped in the 0.25 to 25 KeV X-ray region by NRL's large-area, sky survey instrument on NASA's HEAO-1 satellite. Scientists observed 842 sources including galaxies and galactic clusters, possible black holes, pulsars, and white dwarfs. These data will provide background for any system operating in the measured X-ray band. These sources provide plasma conditions far exceeding those accessible in laboratories. See article on p. 137.

***

A data processing technique has been developed to analyze the structure of small-scale temperature fluctuations in the ocean. Their frequency of occurrence and energy levels can be calculated. This is important to characterize the ocean background for nonacoustic antisubmarine warfare and for ship homing torpedo systems.

Optical Research

A process has been developed that uses stimulated Raman scattering to convert one or more beams of poor optical quality, ultraviolet laser radiation into a single ultraviolet laser beam of diffraction-limited optical quality. The process leads to a brightness enhancement of over 5,000 and has significance for large short-wavelength lasers.

***

A newly developed fiber-optic, towed cable system offers many advantages to submarine communications. The advantages include wider bandwidth, less external noise pickup, lower crosstalk, and absence of ground loops when compared to existing systems using conventional transmission lines. Endurance testing of the optic rotary joint in the laboratory to 310,000 revolutions at a 30 RPM rate resulted in no degradation to the 1.3 dB maximum throughout loss at 830 nm wavelength. The optical attenuation of the multimode fibers in the armored cables ranged from 3.6 to 5.6 dB/km. Tensile loading of the cable to 0.5% elongation resulted in an approximate 20 db/km increase in attenuation. Bandwidth-distance products of several hundred MHz-km are easily obtained.

Materials Research

A coating has been selected and successfully applied to ceramic fibers that can significantly improve both the strength and toughness of ceramic fiber composites while causing little or no degradation of fiber strengths. These improved composites are four times stronger and nearly 100 times tougher than those previously obtained. They have applications. to armor, heat engines, radomes, and antenna windows. See *1983 NRL Review*, p. 160.

***

The ion implantation process has been combined with vapor deposition of coatings to produce highly adherent, wear-resistant surface layers at room temperature. The combined process does not degrade the substrate. In contrast, chemical vapor deposition requires processing temperatures high enough to degrade many materials, and for ion implantation alone, the thickness of the affected layer is limited by the ion range. With this combined technique, the treated layer can be as thick as the deposited coating.

***

Optimum conditions have been determined for the use of hot isostatic pressing (HIP) to significantly improve the life of turbine blades. HIP not only eliminates casting porosity and creep-induced voids, but it can also alter the alloy microstructure. Analysis of variously HIP-heated alloys showed that their microstructure could be significantly improved under optimum conditions.

***

A 25 to 40% increase in ball-bearing life has been demonstrated by using a deuterated pentapolyol ester lubricant developed at NRL. Other deuterated lubricants produced similar increases. These lubricants have over 95% of their hydrogen replaced with deuterium. This process produces major cost savings because it reduces scheduled bearing maintenance.

***

A new method to produce high transverse-strength, metal matrix composites (MMCs) has been demonstrated. The method ion plates graphite fibers with metal matrix materials before consolidation of the plated fibers into MMCs. These composites have significantly higher strengths than have previously been achieved. They will be useful for space applications. See *1983 NRL Review*, p. 162.

***

47

The phonon spectrum of high superconducting-transition-temperature niobium nitride films was determined from electron tunneling measurements. The films were prepared by RF reactive sputtering in an ultrahigh vacuum. The phonon spectrum is necessary to fully understand the properties of these films. These films are used in a host of Josephson junction devices such as superconducting magnetometers and high frequency RF detectors. See article on p. 202 and *1983 NRL Review*, p. 176.

***

Single-crystal iron films have been grown on gallium arsenide by using the molecular beam epitaxy (MBE) technique. These crystals have excellent quality. This indicates that a new class of hybrid magnetic/semiconductor materials can be fabricated in one continuous process by employing the same MBE technology for the substrate and the film. See *1983 NRL Review*, p. 151.

***

NRL has developed a military specification for nonskid deck coatings which lists performance requirements and necessary tests and is developing improved nonskid deck coatings. Present coatings used on aircraft carriers last six months or less and then fragment so that pieces are drawn into jet engines damaging the turbine blades. The new coatings should not fragment as readily saving millions of dollars in jet-engine repair. See *1983 NRL Review*, p. 164.

Specialized Systems and Components

NRL has developed the first rare earth-iron-boron alloy to show real promise as a high-energy density permanent magnet. These new magnet materials are having tremendous impact. One of the most promising uses is in the design of new, compact, high-efficiency electric motors. In recent months, other laboratories have produced magnets with world-record energy densities based on these new materials.

***

A class of DC-to-RF converters, capable of significantly higher efficiencies than contending devices, has been demonstrated at 30 GHz and 82.5 GHz. The converters comprise self-oscillating frequency doublers using gallium arsenide field-effect transistors. This development is significant for efforts to develop on-chip, full-band receivers for high millimeter-wave frequencies. See *1983 NRL Review*, p. 191.

***

A high-power, low-frequency, underwater acoustic source using the principle of the Helmholtz resonator has been developed, evaluated, and is being implemented in Navy systems. This type of source is: used in a deep-towed geophysical array system (DTGAS); will increase the capability of the USS *Dolphin*, a deep, diesel-electric, research submersible; and is being considered for use as a source for ocean acoustic tomography.

High-Power Radiation Sources

A free electron laser (FEL) has successfully produced a 1- to 2-μs pulse of 30 GHz radiation at a power level of 4 MW. The cyclotron emission that has plagued

other FELs is absent. Furthermore, the pulse duration of this device is 50 to 100 times longer than other high-power FELs in this regime. Applications of this work include advanced radar, communications, countermeasures, and directed-energy devices. See *1983 NRL Review*, p. 142.

***

A compact, high-power (10^{10} to 10^{11} W), electron-beam controlled switch has been demonstrated. It can perform repetitive pulsing and may achieve voltage gains of 100 with nanosecond rise times. This switch could have applications in radar and directed beam devices and should enhance the applicability of inductive storage techniques to pulsed power applications.

***

NRL has designed, built, and is testing a first generation gyroklystron amplifier which delivers millimeter-wave (4.2 GHz) energy with an 18 to 36 db signal gain, 30% efficiency, and a peak power of 45 KW. This grew out of an NRL theoretical program to study and upgrade earlier gyroklystrons which had poorer performance because of spurious oscillations and mode competition. Gyroklystrons have applications in radar, millimeter-wave communications, RF heating, and linear accelerators. See article on p. 205.

Featured research at NRL

Three of NRL's several
research areas of
tradition and excellence
are featured in this
chapter. In one of
these areas—fire
research—new fire
protection measures and
fire-fighting agents
are tested on Navy and
commercial liquid
fuel fires.

FEATURED RESEARCH AT NRL

NRL, the Navy's corporate laboratory, has a tradition of national and international leadership in several areas of research and development relevant to the Navy. These areas include radar, artificial intelligence, numerical simulation, microelectronics, fire, tactical electronic warfare, acoustics, space research, and systems development. In this chapter, in-depth articles describe the recent history and accomplishments of NRL's contributions in three of these areas: numerical simulation, fire, and artificial intelligence.

Transition to Turbulence
in Free Shear Flows

E.S. Oran and J.P. Boris
Laboratory for Computational Physics

Elaine S. Oran

Jay P. Boris

Shear Flows in Nature: A shear flow occurs when adjacent elements of a fluid move past each other with different velocities or when a fluid moves past a rigid surface. These types of flows are extremely important because most natural flows have shear, and this is one way large amounts of distinct, initially separate materials can interpenetrate and rapidly mix. This shear-flow mixing is the main mechanism converting potential or directed kinetic energy to kinetic energy, instabilities and in small-scale fluid motions. Instabilities of shear flows are important in the transition from laminar to turbulent flows.

Shear flows are common in nature, and their effects are observed over space and time scales that differ by many orders of magnitude. Radio astronomers observe the effects of supersonic shear flows over distance of megaparsecs. These flows are generated by material thrown out from galaxies to form astrophysical jets. The effects of shear flows in Earth's atmosphere are seen in phenomena such as cloud formation, tropical cyclones, and radar signals returning from the ionosphere. Effects of shear flows are felt in clear-air turbulence. The ocean is sheared almost everywhere, both vertically and horizontally. Shear flows occur in engines when a stream of combustible material enters a region of slower or faster flow. They also occur in solid and plastic materials when uneven stresses are applied. An example of a large-scale terrestrial shear flow is

53

the tectonic movement of plates on Earth's surface; a small-scale example is the submillimeter vertical shear at the air-sea interface.

Studies at the Naval Research Laboratory of shear flows and the turbulence they drive include: solar, magnetospheric, atmospheric, and oceanic (both mesoscale and fine-scale) observations, analysis, and modeling; tactical aspects of naval weather forecasting; instabilities, jets, and wakes; fundamental computational investigations into turbulent structures and mixing; and shear flows and instabilities in combustion engines. Several of these computational and experimental efforts are described below and with the color graphics which follow.

Unstable Shear Flows and the Transition to Turbulence: There are a number of physical effects which influence the behavior of these varied shear flow systems. These include dissipative fluid properties (such as viscosity), variable fluid density, chemical energy release, the presence of multiple phases, various geometries and boundary conditions, and elastic-plastic effects in the fluids. A major change in the behavior of shear flows is observed when the flow speed is faster than the rate that viscosity diffuses momentum through the fluid. This variation is measured by the nondimensional Reynolds number for a given scale of flow structure, $R = LV/\mu$, where L is the physical length of interest, V is a velocity difference in the flow measured on that scale, and μ is the coefficient of kinematic viscosity.

When two adjacent fluids move relative to each other, different types of shear flows result depending on the Reynolds number. When the viscosity is large enough so that the Reynolds number is $\lesssim 100$, the shear flow is dynamically stable. This means that a finite-thickness shear layer develops between the two moving fluids. The fluid velocity parallel to the shear layer varies smoothly from one side of the shear layer to the other and is nearly steady. When the Reynolds number becomes larger, that is, when the velocity difference is large enough and the viscosity is small enough, the flow can be unstable. Then the flow fluctuates by itself without the need for an external driver. A small velocity perturbation perpendicular to the shear layer grows

exponentially following a growth pattern generally predicted by linear stability theory.

These high Reynolds number shear flows soon deviate from the linear theory and produce long-lived vortex structures which are often called coherent structures. Since the linear theories cannot describe the interactions among these structures, computational physics techniques capable of describing the nonlinear effects are used to simulate them numerically on large digital computers.

In idealized two-dimensional problems, the larger coherent structures tend to grow in size as they leave their point of formation. They grow by entraining fluid from the essentially laminar flow on either side of the shear layer and by merging with other structures. The growing structures may eventually break up into smaller ones by other fluid instabilities. This process is chaotic, and often but not always leads to turbulence. Understanding the evolution of coherent structures in terms of their size, pattern of formation, and fluid entrainment properties has been a major scientific thrust in the last few decades.

The Laboratory for Computational Physics at NRL has used numerical simulations to study the evolution of coherent structures in a number of shear flows. These studies involve computer-intensive calculations of multidimensional, compressible fluid dynamics that require large, fast computers such as an ASC (NRL's previous supercomputer) or the new CRAY X-MP. Physical systems containing shear flows have also been studied both theoretically and experimentally in other NRL divisions, such as Plasma Physics, Space Sciences, and Marine Technology. The specific systems studied have different geometries and boundary conditions. The research has considered both general elements of basic fluid dynamics common to many different shear flows as well as applications to very specific flows. Usually the more general fluid dynamics is coupled with specific physical processes to bring about the particular problem-dependent form of energy conversion which drives the flow.

The Use of Computer Graphics: To perform calculations of multidimensional flows, finite-difference techniques are used in which

time is divided into short but finite intervals called timesteps, and space is divided into finite volume elements called cells. In a typical two-dimensional calculation there might be 100×200 cells and 5000 to 10,000 timesteps. Three-dimensional flows have not been studied as extensively to date because the additional dimension increases the computational requirements by 2 orders of magnitude. At each timestep, we calculate the fluid density, velocity, energy, and individual chemical species densities as well as derived quantities such as temperature and pressure by solving a set of time-dependent, coupled, nonlinear, partial differential equations. The implementation of the equations on the computer is done through a set of coupled algebraic equations which approximate the partial differential equations. Experimental observations of shear flow systems similarly consist of spatially resolved and sometimes temporally resolved information. In both the computations and the experiments there is a plethora of data to be analyzed and displayed. Typical finite-difference resolution allows two or three hundred pixels in each direction, which is well-matched to the resolutions and recording power of most experimental systems.

Using graphical output to help display results from time-dependent multidimensional calculations and observations is crucial. Carefully thought out graphics can distill an enormous amount of data into a single frame. Studying these graphical displays plays an important part in helping to interpret results and to understand physical mechanisms. In general, contour plots of calculated quantities at selected times are the most useful displays of data. These contour plots can be generated as line or shadow plots from regular printers or in final display form by using special color graphics enhancement and recording systems such as the DICOMED. The judicious use of color in graphical displays permits encoding an image with extra information that might otherwise require additional graphics or greater dimensionality to represent. Soon it will be possible to record and replay high-resolution images by using laser disks.

Graphical Displays of Shear Flows: The various graphical outputs from NRL research projects in this article illustrate the universality of shear flows and turbulence and show how computer graphics and simulations are used to study these flows. These include:

- Figure 1. Calculation of the solar wind flowing past the Earth's magnetospheric boundary (J. Lyon and P. Palmadesso, Plasma Physics Division)

- Figure 2. Calculation of plasma bubbles, rising in the equatorial nighttime ionosphere (S. Zalesak, Plasma Physics Division)

- Figure 3. Calculation of the bifurcation of an ionized barium cloud driven by the neutral wind in the ionosphere (S. Zalesak, Plasma Physics Division)

- Figure 4. Mass transfer between anticyclonic ocean eddies (R. Mied and G. Lindemann, Marine Technology Division)

- Figure 5. Calculations of a cylindrical air jet injected into a slower air stream (J. Boris and E. Oran, Laboratory for Computational Physics)

- Figure 6. Calculations of a cylindrical air jet injected into a slower stream of freon (E. Oran and J. Boris, Laboratory for Computational Physics)

- Figure 7. Calculations of a hot cylindrical jet of hydrogen injected into air (K. Laskey, F. Grinstein, E. Oran, and J. Boris, Laboratory for Computational Physics)

- Figure 8. Calculations of unequal mixing in planar shear layers (F. Grinstein, E. Oran, and J. Boris, Laboratory for Computational Physics)

- Figure 9. Densitometer tracings of 90-cm radiation from what is probably a quasar-driven jet in another galaxy (R. Simon, Space Science Division)

- Figure 10. Observed and calculated Bartels diagrams showing the effect of differential rotation (shear) on the Sun's large-scale magnetic "weather" (N. Sheeley, Space Science Division; C. DeVore, Laboratory for Computational Physics)

55

Figure 1. Simulations of the
Earth's Magnetosphere
(J. Lyon and P. Palmadesso,
Plasma Physics Division)

This figure shows results from a two-dimensional simulation of the interaction of the solar wind with Earth's magnetosphere. The solid white lines are magnetic field lines. Earth's dipole field is located at $(X,Z) = (0,0)$. The solid colors indicate the magnitude of the plasma flow velocity in km/s. The solar wind is driven by the sun which is to the left. The solar wind interaction with the magnetosphere causes the bow shock. Note the sharp speed decrease to the left of Earth. Magnetic field convected in the solar wind reconnects to Earth's field at the nose of the magnetosphere and is convected around Earth to form the magnetotail (the nearly horizontal field lines to the right of Earth). The boundary between the tail and the shocked solar wind plasma, the magnetopause, is marked by a strong velocity shear in the tail. In this picture the magnetopause lies near the boundary between the green and large yellow areas. Note the wave structure on the boundary. Here, shear flows apparently drive Kelvin-Helmholtz instabilities on the magnetopause and thus can significantly affect the energy balance of the magnetosphere.

Figure 2. Plasma Bubbles in the
Equatorial Nighttime Ionosphere
(S. Zalesak, Plasma Physics Division)

This two-dimensional numerical simulation of the nighttime equatorial ionosphere shows the development of plasma "bubbles." Colors from blue to red correspond to electron densities from low values to high values. The center of the red region represents the F2 peak in electron density at approximately 930 km altitude. The figure shows a two-dimensional slice of the ionosphere (east-west, up-down) at Earth's magnetic equator. Open-ended bubbles of low-density plasma (green) from lower altitudes have buoyantly risen upwards, penetrating beyond the F2 peak. This behavior is due to the nonlinear evolution of the collisional Rayleigh-Taylor instability just below the F2 peak. Tilting of the bubbles is caused by an eastward neutral wind. The plasma flow has large shears at the lateral edges of the bubbles.
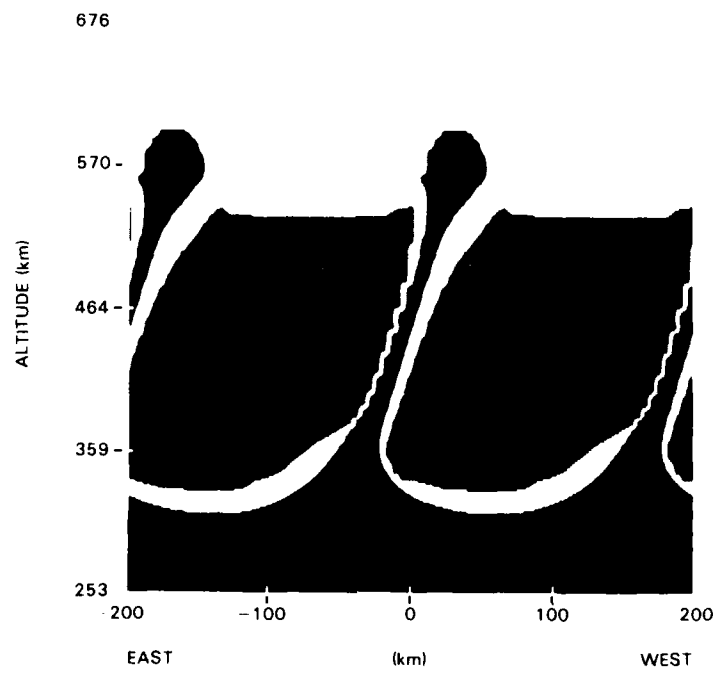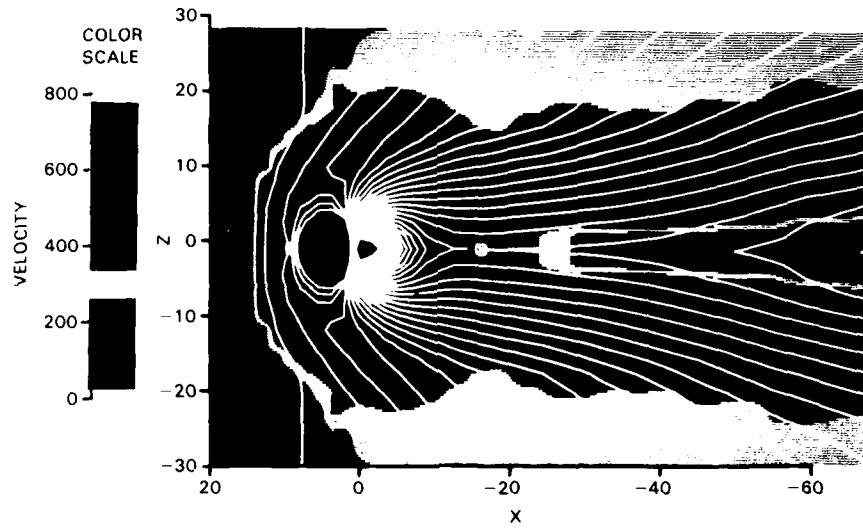
676

Figure 3. Bifurcation of a Barium Cloud
in the Ionosphere
(S. Zalesak, Plasma Physics Division)

This figure shows results from a numerical simulation of an ionospheric plasma cloud of barium ions looking upward from the ground plane perpendicular to the geomagnetic field. The barium ions were released at 180 km altitude and show steepening and bifurcation due to horizontal winds in the neutral atmosphere. Colors from blue to magenta correspond to ion densities from low to high values. In this coordinate system, the flow of the neutral atmosphere is in the $+y$ direction, and the magnetic field vector points toward the viewer. The steepening, bifurcation, and subsequent further structuring of the top of the cloud are due to the nonlinear evolution of the gradient-drift instability, an instability similar to the Rayleigh-Taylor instability. The equations describing the flow are strikingly similar to those describing the vorticity field of two-dimensional homogeneous turbulence. The plasma flow is incompressible, with large shears at the lateral edges of the cloud. Cloud evolution can be described as a cascade from large to small scales of plasma fluctuations and coherent structures. The cascade stops at some small scale due to dissipative mechanisms in the plasma.

Figure 4. Mass Transfer Between
Anticyclonic Ocean Eddies
(R. Mied and G. Lindemann,
Marine Technology Division)

This figure shows numerical simulations performed to study mass transfer between two anticyclonic eddies in the ocean. Experiments are conducted with a two-layer, primitive equation, beta-plane model (which allows the Coriolis force to increase with latitude) in a 1000-km square region. One eddy contains a tracer, and the other, located to the northeast of it, does not. The tracer distributions at day 20 are shown, as both the tracer diffusivity and kinematic viscosity are varied over a factor of 100.

When two adjacent eddies interact, material from one eddy is entrained into the other, and the material assumes a well-defined location in the second eddy, rather than being uniformly distributed in it. This is because the tracer largely follows contours of constant potential vorticity to its new position in the "undyed" (hence initially invisible) eddy. The vorticity fields inside these vortices are much larger than those due to the local ambient rotation and thus contribute most to the potential vorticity in the flow.

When tracer diffusivity and kinematic viscosity each equal 2.5×10^6 cm^2 s^{-1}, the tracer in the host eddy resembles satellite pictures of so-called streamers observed in warm core rings after they interact with the shelf front or the Gulf Stream.
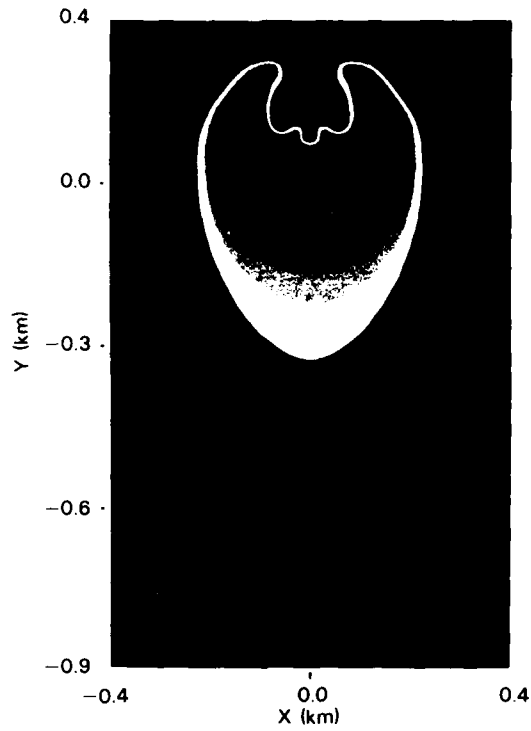
Figure 5. Cylindrical Air Jet Injected
into a Slow Air Stream
(J. Boris and E. Oran,
Laboratory for Computational Physics)

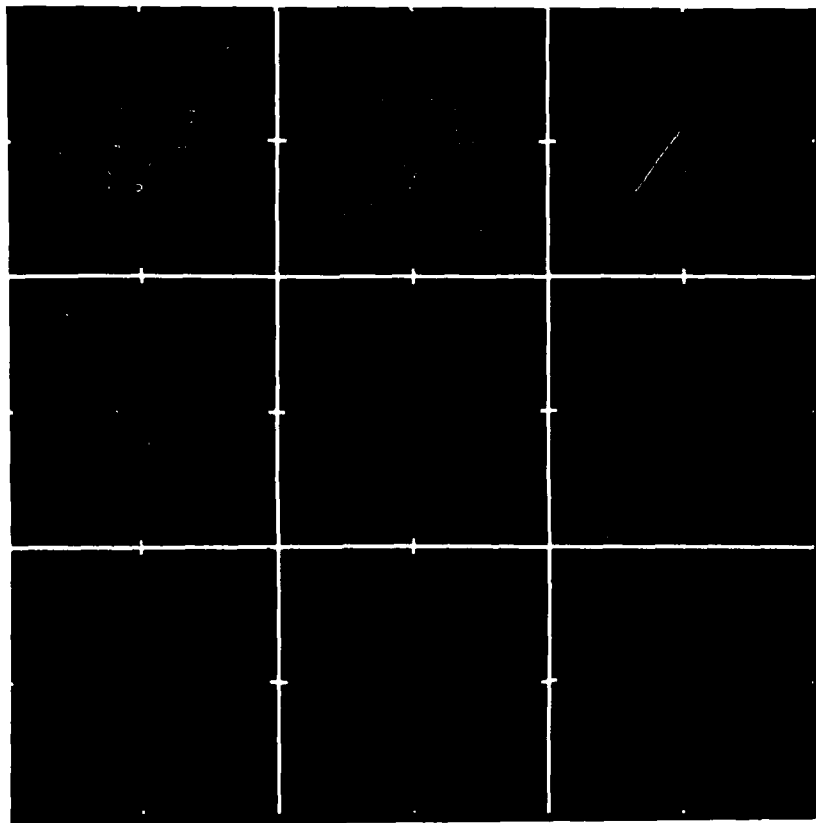This figure shows results from calculations of a high-speed (~100 m/s), axisymmetric air jet into a slower, coflowing air background. The high-speed jet enters the system from the bottom at the left. The central axis of the jet is the left border of the figure. The colors indicate the amount of mixing of the two fluids: red is pure high-speed air; magenta is pure background air; and violet, blue, green, and yellow indicate various intermediate levels of mixedness. The calculation was initiated with a laminar air jet having a sinusoidal perturbation along the interface. As the system evolves, coherent structures form because the interface is unstable to the Kelvin-Helmholtz mode. These structures at first form two or three nozzle radii downstream from the nozzle exit and then proceed to move downstream (up in the figures), entrain material from the slow air background, and grow by merging with other structures. The magenta patches within the multicolored structures indicate unmixed pockets of low-speed fluid entrained in the mixing layer.

Figure 6. Cylindrical Air Jet Injected
into Coflowing Freon
(E. Oran and J. Boris,
Laboratory for Computational Physics)

The figure shows the results of calculations of a high-speed (~100 m/s), axisymmetric air jet into a slow, high-density coflowing freon background. (In Fig. 5, both fluids were air, and so the density was the same.) The high-speed jet enters the system from the bottom left. The axis of symmetry is the left border of the figure. The colors indicate the amount of mixing of the two fluids: red is pure high-speed air, magenta is pure background freon, and the other colors indicate various levels of mixedness. The system instabil-ity and evolution are similar to the air-into-air background shown in Fig. 5. There are, however, some important qualitative differences. The air-into-freon structures form closer to the nozzle and then move more slowly downstream (upward in the figure) and grow by merging with other structures. In contrast to Fig. 5, note that pockets of the light jet gas (red within yellow) are entrained unmixed in the structures of the much greater density freon.
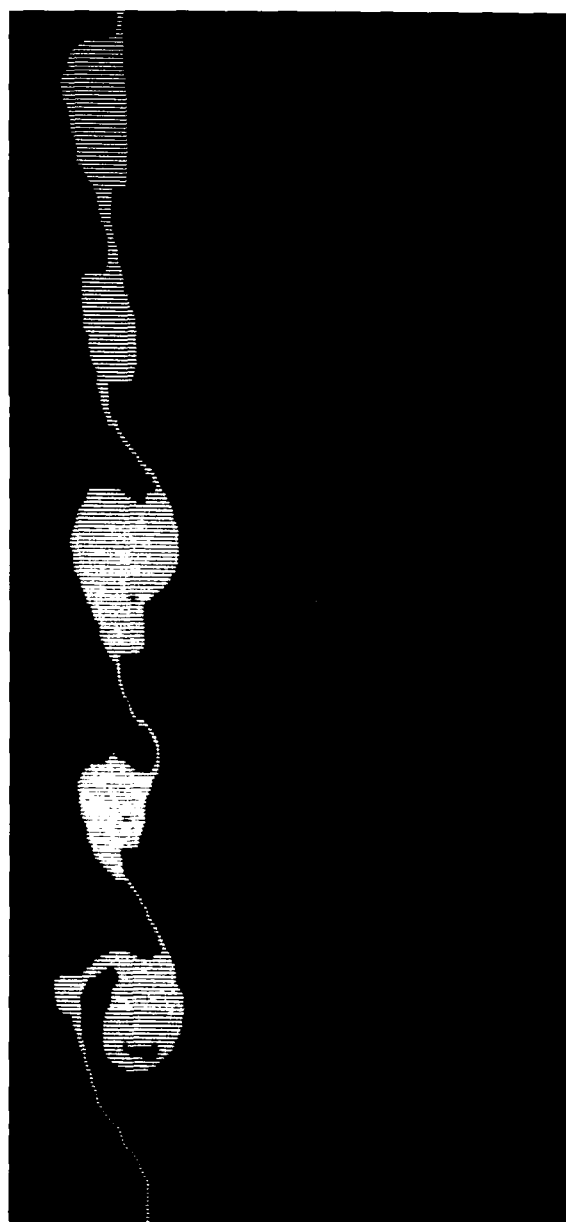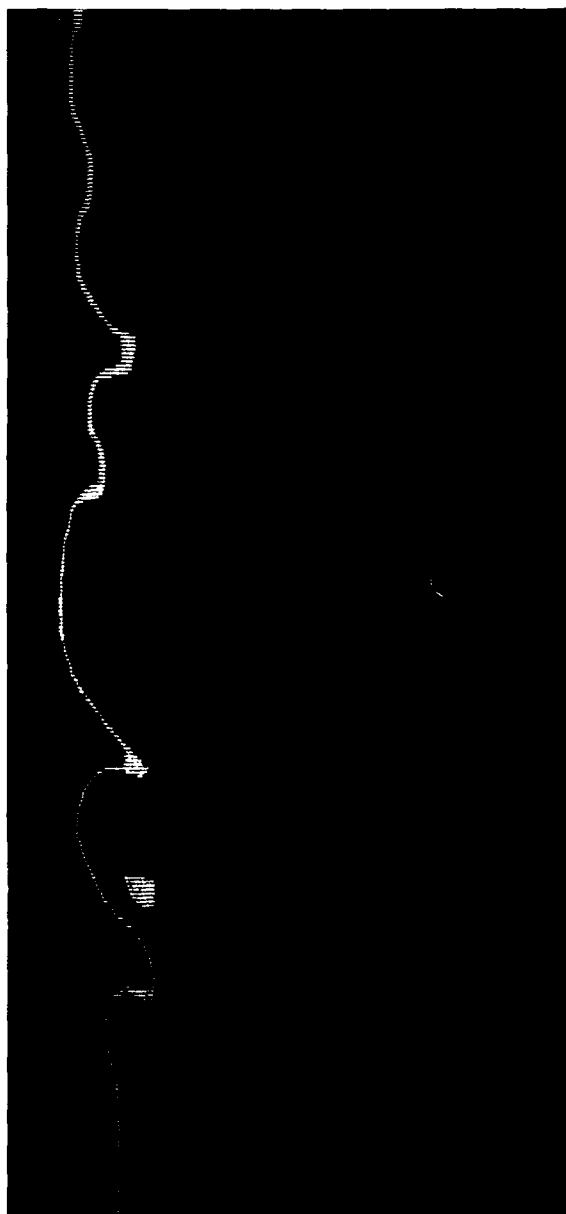
60

61

Figure 7. A Hot Cylindrical Jet of
Hydrogen Burning in Air
(K. Laskey, F. Grinstein, E. Oran, and J. Boris,
Laboratory for Computational Physics)

These two figures show results from a calculation of a hot axisymmetric jet of premixed hydrogen and nitrogen injected into a quiescent air background. The jet enters horizontally from the bottom left of each panel, and the symmetry axis is at the bottom. In the top picture, the colors indicate temperature, with yellow corresponding to the initial temperature of the jet—1200K and the black corresponding to the initial background temperature—298K. Red, green, and blue are intermediate temperatures in descending order. The contours (white lines) overlayed on the temperature field show the amount of water formed from the chemical reactions once the jet and background gases mix.

The white portions in the middle of the structures indicate very hot, fully reacted material; this is the region of maximum water vapor concentration. The bottom figure shows contours of the ratio of the amount of hydrogen to the amount of hydrogen plus oxygen. Blue indicates hydrogen but not oxygen is present, and black indicates that oxygen but not hydrogen is present. Intermediate colors are regions where hydrogen and oxygen are mixed. The white portions indicate the zones where chemical reactions are occurring. The blue zones surrounded by white are regions where all the oxygen has reacted and left unreacted hydrogen behind.

Figure 8. Unequal Shear Layer Mixing
Ahead of a Splitter Plate
(F. Grinstein, E. Oran, and J. Boris,
Laboratory for Computational Physics)

Asymmetries in mixing occur in coherent structures formed at the interface of two planar gas layers moving at different velocities. The two layers are initially separated by a flat plate, the splitter plate. The tip of the splitter plate is a point located at the center of the vertical axis; the actual splitter plate is to the left of the domain shown. The fluid enters from the left and moves to the right. The faster fluid enters below the splitter plate, while the slower fluid enters above. The figure shows the region in which the two fluid layers first slide past each other, then become unstable at the interface along the centerline, and finally mix and form coherent structures to the right. In the upper figure, it is assumed that the faster fluid is basic and the slower fluid is acidic; this is reversed in the lower figure. A pH-sensitive dye mixed with the acidic fluid allows us to monitor the extent of the mixing

process. This numerical simulation is of the experimental pH diagnostic used at the California Institute of Technology (by P. Dimotakis) to measure unequal mixing. The colored regions show where more basic fluid is present—the lighter the color, the higher the pH of the fluid. The comparison of the frames shows the amount of asymmetry in mixing of the two fluids within these structures. The chemical interaction between the the two streams does not influence the dynamics of the flow, since very dilute solutions are involved; thus, a single simulation interpreted two ways is enough to predict the results of the two different experiments, namely the faster fluid being first basic and then acidic. This asymmetry is very important for shear flows in combustion scenarios, since it could lead to the formation of pockets of fuel-rich or fuel-lean material in the mixing region.

TEMPERATURE AND PRODUCT

$3.24 \cdot 10^0$

X (cm)

$0.00 \cdot 10^0$

REACTION ZONE & DENSITY RATIO

$3.24 \cdot 10^0$

X (cm)

$0.00 \cdot 10^0$

$0.00 \cdot 10^0$ Y (cm) $6.48 \cdot 10^0$

FASTER FLUID IS BASIC

$5.64 \cdot 10^0$

X (cm)

$5.00 \cdot 10^{-1}$

FASTER FLUID IS ACIDIC

$5.64 \cdot 10^0$

X (cm)

$5.00 \cdot 10^{-1}$

$2.03 \cdot 10^0$ Y (cm) $1.23 \cdot 10^1$

63
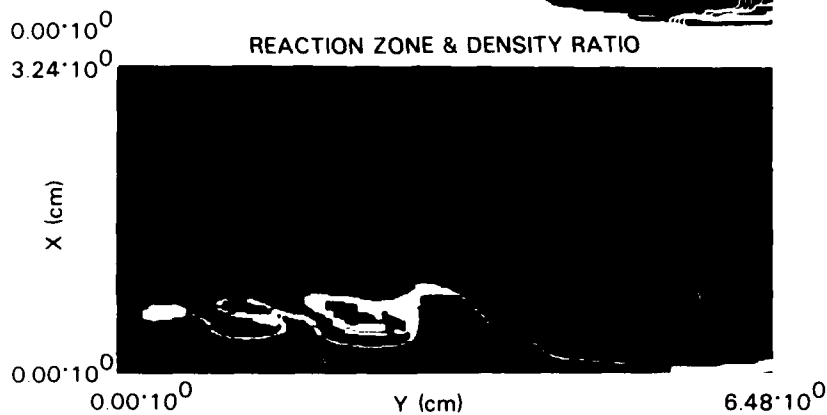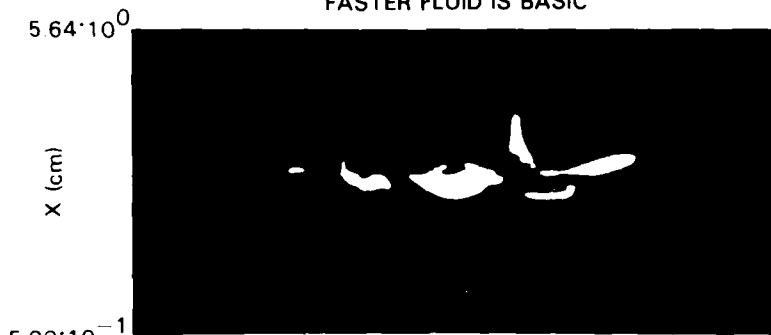
Figure 9. Densitometer Tracing of 90-cm
Radiation from Quasar-Driven Jet
(R. Simon, Space Science Division)

In this digitized, false-color image of the radio emission from the quasar 3C138, a long luminous jet can be seen extending to the east (right). The colors in this image are related to the radio brightness in 3C138, with red being the brightest features and blue the faintest. The probable center of activity, or core, of 3C138 is indicated with arrows. This core is the source of the energetic plasma which comprises the jet. With the radio wavelength used for this map, the core appears fainter (bluer) than the jet even though its luminosity is much greater at short wavelengths. The total length of the jet is about 10,000 light years (roughly 60,000 trillion miles). The complicated structure in the jet may be due to turbulent magnetohydrodynamic shear flows as observed in other radio jets or possibly due to angular scattering from the Milky Way.

The quasar 3C138 is approximately 10 billion light years distant, so extremely high resolution is needed to map such a radio source. This map was made by using the technique of very long baseline interferometry, in which radio telescopes in the United States, Europe, and Asia are used to make a composite synthetic aperture radio telescope as large as Earth. The smallest details in this radio image are less than 1/200,000th of a degree in angular size, roughly 50 times sharper than the best possible optical images.

Figure 10. Observed and Computed Bartels
Diagrams for Differential Rotation on the Sun
(N. Sheeley, Space Science Division; C. DeVore,
Laboratory for Computational Physics)

This figure displays daily values of the mean magnetic field of the Sun as seen from Earth in a Bartels format. The data observe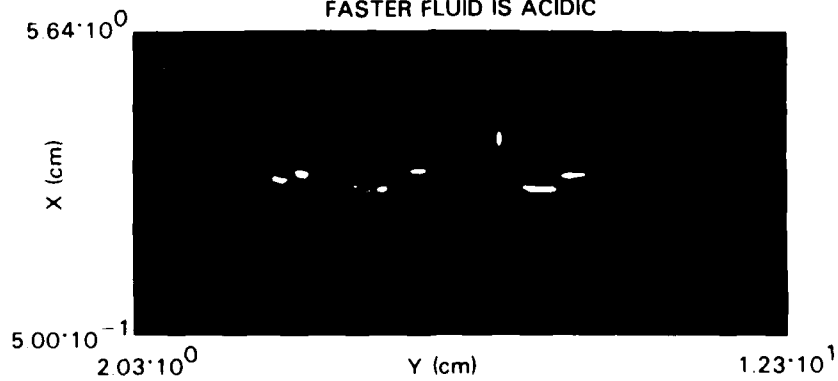d at the Stanford Solar Observatory are on the left, and the results of a numerical solar model calculated at NRL are on the right. A single simulation covers the eight-year period 1976 to 1984. The Bartels plot is a running calendar of 27-day "months," with each month plotted horizontally and the months progressing downward. The magnetic field polarities are coded in yellow (negative), red (neutral and small fields), and blue (positive). Black indicates absence of data. Note the substantial agreement in the large-scale organization of the patterns, particularly the location of the magnetic neutral line (red areas). In space, the magnetic neutral line usually reaches out to Earth and often signals when one can expect, after predictable delays, enhanced magnetospheric and ionospheric activity. This research has indicated that prediction of these field direction reversals for months in advance is possible, a potentially important result for scheduling space and communications activities.
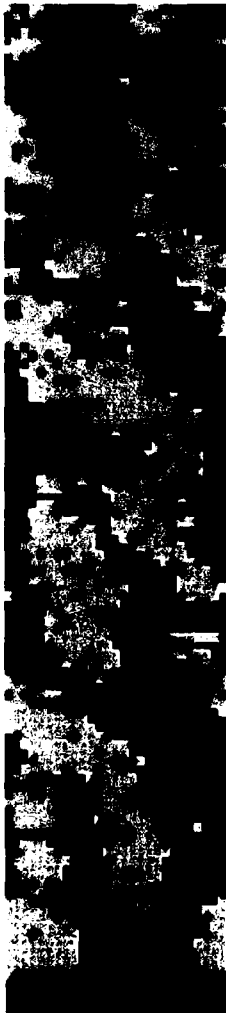
THE SUN   THE MODEL

65

FIRE !
(Fire Suppression Research at NRL)

Homer W. Carhart
Chemistry Division

At sea, the cry "FIRE !" is enough to instill a shudder of fear in even the staunchest soul. And well it should! Even in peacetime the Navy has suffered great losses of personnel and material in disastrous fires: 134 dead, $75 M plus in repairs on the U.S.S. *Forrestal* in 1967; a completely gutted ship, 7 dead, and $213 M rebuilding on the U.S.S. *Belknap* in 1975; and 7 dead, 3 F-14s lost in the crash on the U.S.S. *Nimitz* in 1981. What will it be like in wartime when the Navy most needs to be at its best? Most recently, the Falklands have shown that a single hit can cause total loss of a ship due to fire (the H.M.S. *Sheffield*). The tragedy of these disasters is that their losses could have been drastically reduced by both prevention and more effective fire fighting techniques and tactics, many of which have been developed at NRL during its course of fire research.

It is also unfortunate that in the Navy, as well as in the civil sector, we tend to respond to disasters and catastrophies after the fact. As a result, much of our R&D in fire follows a sawtooth pattern of support, with each peak right after a disaster, and with the effort concentrated on the causes and effects of that particular fire. That certain types of disasters will occur can be predicted with reasonable probability. What is more difficult to predict is their timing. For example, unless we take other action, we run the *high* risk that one of these days we will lose a submarine due to fire; a leak in the hydraulic system (and an ensuing fire/explosion) being a number one candidate. It is not a case of *if*, it is a case of *when* it will happen. All the makings are there—it's that simple! We must undo those makings. In R&D, we should not be fighting fires of the past, we should be fighting fires of the future; this is the R&D philosophy at NRL in its fire research program.

Homer W. Carhart

What follows is a partial picture of NRL's involvement in fire research and its accomplishments over the past 45 years. Many of our early developments are still in use today.

Early Accomplishments

Early in its being, NRL recognized the need for increased capability to "fight" fires in the Navy, and started R&D in this area before WW II. Fires, especially on shipboard, are complicated beasts and then, as today, civil fire fighting technology, based on overwhelming a fire by drowning it with water, needed greater sophistication. Ships that otherwise might have been saved have been lost by floundering because of the excessive weight of fire fighting water. Ships are floating arsenals which are densely packed with explosives, large volumes of fuel and other combustibles, and many men, who—in case of fire, have no place to run. The large volumes of liquid fuels used by the Navy could produce fires

67

that spread rapidly and are very difficult, if not impossible, to control. Because of this, NRL concentrated its early efforts on petroleum-based fuel fires. In those days, aviation gasoline, which is very volatile and highly flammable, was the only aircraft fuel being used. The less volatile NSFO (Navy Special Fuel Oil) was used for ship propulsion.

During WW II, NRL chose to study "foams" as a means of fighting fuel fires and to apply foam systems to naval use. The foam of choice in those days was "protein" foam, also known as "bean soup." It was made by partial catalyzed hydrolysis of waste proteins, feathers, fish scales, abattoir blood, and soy bean residue (hence its other name). A concentrate so prepared was mixed with water, and on aeration by special nozzles could be applied as a thick foam to blanket burning fuel. It was highly effective and, based on the NRL work, systems for its use were installed on Navy ships and at Navy air stations. But protein foam did have some drawbacks and a better "foam" was sought.

In the post-WW II years, NRL had become very interested in the effects of substitution of fluorine for hydrogen in organic molecules and the concomitant effect on properties, particularly in its behavior on surfaces. The main thrust was in lubrication, but as an offshoot, fluorinated surfactants were also prepared and studied. Several of these were evaluated for their foaming properties and, with the cooperation of industry, were developed into a new family of fire fighting materials used today and known as AFFF (Aqueous Film Forming Foam). Though today's AFFF is highly effective, research is still underway on an improved AFFF, and NRL is still responsible for qualifying new AFFF formulations for DoD purchase.

Following the flight deck disasters on the U.S.S. *Forrestal* (1967) and U.S.S. *Enterprise* (1969), NRL mounted a study program on flight deck fires and decided that the "wash-down" system—sprinkler nozzles embedded in the deck and elsewhere—originally installed for protection against NBC (nuclear, bacteriological, chemical agent) attack, might be converted to a fire fighting system. By incorporating AFFF into this system, NRL demonstrated, by essentially full-scale field demonstrations, the efficacy of such a

modification to extinguish flight deck fires rapidly. The concept was implemented quickly by the Navy and all carriers, and some other air-capable ships are now so protected.

PKP (Purple-K-Powder) is another NRL-developed fire-fighting agent also used worldwide today. It is a specially treated potassium bicarbonate. Because PKP is a "dry chemical," it is commonly found in hand-held extinguishers. Its ability to "knock down" a flame is much superior to earlier dry agents such as soda (which, interestingly, is also still in use).

Since NRL developed a superior foam to blanket a fire, and a superior dry chemical to knock a flame down, it was only natural that it should combine the two into a single system—the TAU, or twin-agent-unit. This NRL-developed device, either fixed or portable, is extensively applied in the Navy. Other agents were also developed for special uses, such as TMB (trimethyl borazine) and fritted glass for fighting magnesium fires (aircraft wheels and parts of the wings are magnesium alloys), but their use is much more limited than AFFF or PKP.

Later and Current NRL Research
in Fire Suppression

Fire research at NRL has expanded considerably in the last few years to include a much wider spectrum of topics in fire protection. Selected examples, in the fire suppression area only, will be discussed individually, followed by a description of NRL's fire research facilities and a look into the future. Other areas of fire research, such as spontaneous (autogenous) ignition and its relationship to molecular structure and to cetane and octane numbers of fuels, hazards of electrostatic ignition, oxidation mechanisms, cool flames and the role they play in combustion, and other related topics will not be discussed.

Control of the Atmosphere: Traditionally, most of us think of fire as needing air; also, that fires vitiate that air. However, fires can be controlled or exasperated by controlling the atmosphere, especially in a closed environment. A horrible example of the latter was the Apollo disaster of 1967. Being in a 100% oxygen environment, that fire was almost explosive (it

was estimated by the investigating team, of which the author was a member, that the fire ruptured the capsule in only 19 s). One can indeed do much to control fire by control of the atmosphere, as well as control vitiation of the atmospheres by the control of fire. Three related topics will be addressed: N_2 pressurization, low O_2, and toxicity.

N_2 *Pressurization*—Consider Table 1; we have three markedly different atmospheres in which human life has been sustained. The reason is that the partial pressure of O_2 is essentially the same in all three (last column). On the other hand, fire is dependent on the concentration of O_2, and in Table 1 these are very different. Fires in 100% O_2 are exceedingly violent, in 21% O_2 they occur normally, and in Sea Lab (4% O_2) the aquanauts could not even strike a match. Thus, sustaining fires and sustaining life are not the same, and we can take advantage of that fact.

Table 1 — Impact of O_2 on Fire and Life

Environment	Total Press. (atm)	Oxygen Conc. (%)	O_2 Press. (atm.)
Apollo (flight mode)	0.3	100	0.3
Submarine	~1.0	~21	0.2
Sea Lab	7.0	~4	0.3

Based on heat balances, NRL proposed in 1972 that overpressurization with N_2 in a closed environment to about 0.5 atm. should be able to extinguish a fire, but still allow life to be sustained. Extinguishment, even in large chambers, was later demonstrated, as seen in Fig. 1. This atmosphere can sustain life. Rats in an N_2 pressurization fire test were not fazed by the overpressurization. The application to submarines and other environments capable of being pressurized is obvious. Indeed, N_2 pressurization is now the backup extinguishing system for all experiments in NRL's 325-m^3 (11,400-ft^3) chamber, FIRE I (Fig. 2), and it has never failed even when experimental fires appeared to be getting out of hand.

Of concern in N_2 pressurization was that as the fire was being quenched, the production of carbon monoxide (CO) might be too high. But, as shown in Table 2, (which compares fire data for cellulose with and without N_2 pressurization) CO would be tolerable with N_2 pressurization, and lethal without. In Table 2, note that the final concentration of oxygen in both cases was the same at extinguishment; this had been predicted originally.

Low Oxygen—In a closed environment, one can choose an operating atmosphere to suit oneself. Table 1 shows that fact. It is also important to recognize that fires are much more sensitive to oxygen concentration than people are to partial pressure. To illustrate this, Fig. 3 shows that the
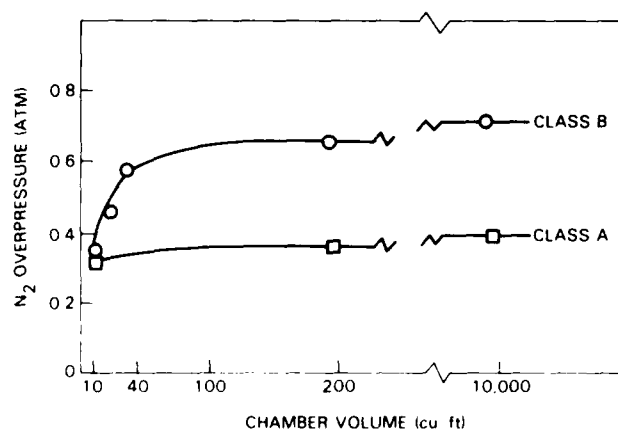
Fig. 1 — Extinguishment of fires by N_2 pressurization. Effect of chamber volume on N_2 required to extinguish Class A (solid) and Class B (liquid) fires.

Fig. 2 — FIRE I—NRL's 325-m^3 (11,400-ft^3) pressurizable chamber.
Control trailer is in right background; N$_2$ bottles are on top.

Table 2 — Typical Atmospheric Analyses Following Confined 100% Cotton Fires (Horizontal-Layered Specimens)

	N$_2$ Pressurization	
	With	Without
Final Pressure (atm.)	1.5	1.0
% O$_2$	14	14
P$_{O_2}$ (atm)	0.20	0.14
% CO$_2$	0.5	5
CO (ppm)	250	1750
Gas Phase Organics (ppm)	<25	50
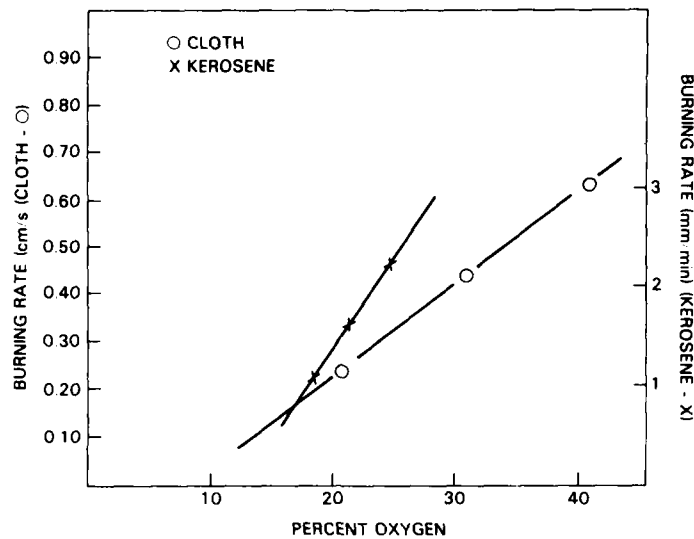
Fig. 3 — Burning rate of cotton cloth and kerosene
as a function of O_2 concentration

burning rate for cellulose and liquid fuels decrease markedly with even small decreases in O_2. On the other hand, people can tolerate a wide variation in O_2 partial pressure: from the 1.09 atm of the Apollo Capsule at takeoff to 0.21 atm (air at sea level); to 0.175 atm in Denver, and 0.12 atm on Pikes Peak, Colorado; and even lower partial pressures of O_2 at higher elevations.

It is proposed, therefore, that submarines be operated at some lower value of O_2, such as 19%. This might still allow people to smoke, but would cut down the rate of fire spread and intensity. In fighting fires, time is critical. As shown in Fig. 4, most fires have a relatively slow "induction" period before becoming violent and creating a disaster (as stated for the Apollo fire, 19 s; in the case of a cigarette dropped on the sofa, several hours). If one can react and fight the fire before the "knee" in the curve, the fire is more easily controlled. If we can "buy time" during the induction period, the knee can be postponed, maybe indefinitely, and we have no disaster. The use of 19% oxygen *would* buy time.

The effect of lowering O_2 concentration on fire behavior has not been fully quantified. The effect on people, though projected to be nil, also

Fig. 4 — Typical rate of fire growth with time

has not been quantified. Information on the latter could easily be obtained experimentally at the Navy's Submarine Medical Research Laboratory in Groton, CT.

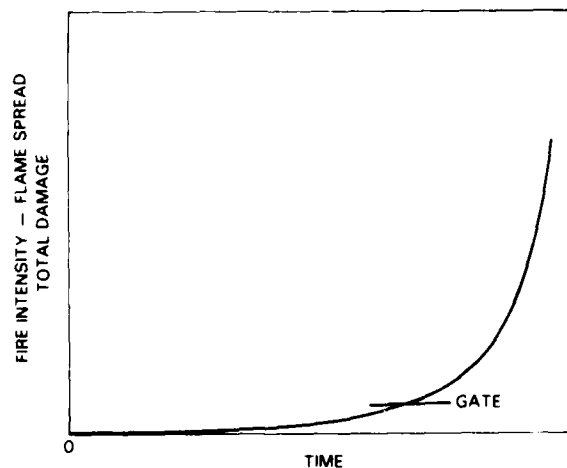One beauty of this suggested approach is that it could be done today with no retrofit or change of equipment of any kind. On "closing the boat," the O_2 can be "breathed down" to 19% and then maintained there with existing equipment. Indeed, examination of submarine atmosphere logs shows that a 19% value has occurred many times without the men being aware of it.

Toxicity — The most ubiquitous and dangerous toxicant from fires is CO. Most fire deaths are attributed to "asphyxiation," "smoke inhalation," and so forth. Autopsies in fire deaths have shown very high blood concentrations of carboxyhemoglobin due to CO. Thus, the major cause of fire deaths is CO poisoning.

In the Navy, however, we face a very different and insidious toxicological property of CO. In contrast to most poisons, CO affects the brain long before it affects motor function or other responses. Data obtained from the Toxicology Center at the National Academy of Sciences show that mental acuity is affected at 1/5 to 1/10 the lethal concentrations of carboxyhemoglobin in the blood. Under the duress of battle or damage, correct decisions must be made quickly and actions carried out correctly. Fuzzy-headedness could cause a wrong action that could even result in loss of a platform. A person is not aware when he is being poisoned by CO, and the phenomenon of people walking back into a burning building to their death can be attributed to fuzzy thinking. (Their motor ability is obviously still intact.) The six lives lost recently on the U.S.S. *Ranger* were attributed to CO poisoning; the men were found huddled within a few feet of an open deck, and apparently could easily have made it.

Most toxicological tests use death as the end point — the "kill-'em-and-count-'em" technique. From the Navy's standpoint, this is unacceptable as the only means for assessing a given material's contribution to toxic fire gases. What is needed is a measure of the potential impact of CO on mental acuity, and this cannot be done properly with animals; it is difficult to give a rat an IQ test. Therefore, chemical analyses and control

must also be used. As such, NRL is now deeply involved in developing technology to assess fire gases, and developing specification concepts and criteria to control not only this most insidious gas, CO, but other toxic and corrosive fire products as well, such as HCN, HCl, and HF.

The Smoke Problem: It is unconscionable that more action has not been taken to mitigate the smoke problem (by smoke we mean the particulate matter generated by a fire). Although also potentially toxic, its main impact is obscuration. Firefighters cannot see to find and quench the fire, and cannot stop it before the knee (shown in Fig. 4); also, people trapped cannot see to escape. There is evidence for considerable loss of life in the Navy because people "took the wrong turn."

The impact of smoke in the U.S.S. *Forrestal* arson fire of 1972 is shown in Table 3. As Table 3 shows, it took six hours to find the fire and two more hours to quench it just because of smoke obscuration. As a result, what should have been a trivial fire ended up putting a permanent bubble in the flight deck, and tying up the ship for months for repair.

Table 3 — Impact of Smoke Obscuration

USS *Forrestal*	
Sequence of Events — 10 July 1972 (All Times Approximate)	
0300	Fire Reported
0305	Firefighting Parties Arrive
0330	Firefighting Parties Pulled Back Because of "Smoke"
0330-0700	Fire "Contained," Portable Blowers Brought in
0900	Flame Visible — Started to "Attack" Fire Directly
1100	Fire Out

Following the U.S.S. *Forrestal* fire of 1972, NRL mounted a program to overcome, or at least mitigate the smoke problem. Three main thrusts were followed: using infrared to "see" through smoke, knockdown by wetting, and smoke re-

moval by electrostatic and dielectrophoretic means.

IR Imager—The most successful approach to date has been the development of an infrared imager for fleet use. Starting with a commercial device, NRL performed extensive studies in shipboard environments and has made a number of changes which have been incorporated into a hand-held device for Navy use. Operating at 8 to 14 μ, this device allows the user to see hot objects through the densest smoke. Its image of a man 9 m (30 ft) away in a totally obscured room is shown in Fig. 5. With this device a fire is even easier to find. This imager is so promising that the Navy has now started procurement for issue to the fleet.

Knockdown—NRL has also shown smoke knockdown by wetting to be effective. Where smoke is just allowed to "settle" it might take 20 min. or more to see 3 m (10 ft); wetting the smoke by sprinkling will allow visibility in as little as 20 s. It turns out that AFFF is an excellent wetting agent, and fortunately it is already on board our Navy ships.

Precipitation—Electrostatic precipitators (ESP) have long been used to remove airborne particulates. Fire smokes, however, are conductive and short out ESP units very quickly. NRL has developed and patented a "nonshorting" ESP by the simple expedient of markedly reducing the conductivity of the collecting plates. Thus the high voltages needed can still be maintained to remove large quantities of smoke, but current flow is markedly reduced. Placed inside a ventilation system (as now used in submarines), it could then be used as an adjunct for smoke removal. This new ESP is now being perfected in cooperation with industry.

Agents and Shipboard Application: The Navy has a special need for fast and highly effective means for extinguishment of fires. Ships are floating arsenals, loaded with liquid fuels, and crammed with people. As such, it is important

Fig. 5 — Infrared imager picture of man groping his way through zero visibility dense smoke in chamber at Norfolk, VA, fire school

73

that efforts continue to develop better fire-fighting agents, and means for their application. NRL is doing just that.

Foam—AFFF has been improved markedly in the last decade, not only in performance but in reduced cost. However, it is time to develop an even better agent, and based on recent experiments and tests, NRL is now reexamining requirements for AFFF-type agents and is working on a completely new specification.

Dry chemicals—NRL is also reexamining dry chemicals. A systematic study has revealed that for a given powder, particles above a critical size contribute little to fire extinguishment. The particle must be small enough so that the whole particle becomes involved in the quenching process. This is because the residence times of particles in a fire are short enough so that bigger particles go through the flame front too rapidly to be effective.

It has also been postulated that powders are effective primarily because they absorb heat. This theory would make prediction of quenching by new chemicals possible, thus opening the door for potential new agents *and* how they should be used.

Applications—Following the U.S.S. *Nimitz* crash and fire of 1981, NRL was requested to determine experimentally why the ensuing fire (which lasted so long that ordnance cooked off with lethal results) could not be controlled better. It was suggested that a wing of one or more of the F-14s was slit allowing fuel to cascade into the burning debris. AFFF was originally designed to fight a pool of burning liquid (that is, a 2-dimensional (2-D) fire), and its efficacy for 3-D (cascading fuel) fires had never been established. To get quantitative comparative data, a reproducible debris pile with cascading fuel was developed at NRL's Chesapeake Bay Detachment (CBD). This was coupled to a washdown system on a simulated deck, and technology was developed for fighting the combined pool and cascading debris pile fires. Figure 6 shows several pictures of such a fire. The first frame of the figure shows the initial stages of the 2-D deck fire. Note the wind machines (converted swamp buggies) used to generate 30 knots across the simulated deck. Also note that radiation from this quiescent fire is relatively low, as seen by the

darker red color. Such a fire can therefore be approached more clearly by unprotected personnel. The wash-down system quickly controls the deck fire (upper right), but note that in a 30-knot wind, the fire is much more radiant (brighter red/orange color), and close approach by unprotected personnel is not possible. As can be seen (lower left), the AFFF wash-down system, creating a 2-D blanket, extinguishes the pool fire readily, but the 3-D fire remains in full fury and must now be attacked by hand. In the last frame, it is evident that the firefighters must be very aggressive in attacking this 3-D fire, and because of thermal radiation, must be protected. However, with this type of attack they are successful in less than 60 s. If ordnance were present in the debris fire, potential cook off would put such men in a very high-risk situation. The fuel used here is the Navy's jet fuel, JP-5 (flash point of 60°C (140°F) min). Tests on fires with more volatile fuels (gasoline and JP-4) could not be extinguished even with the best efforts of the firefighters. The debris pile was purposefully designed to make fire fighting difficult so that development of successful fire-fighting capability would give the Navy high-confidence means to control truly difficult crash and other types of fuel fires on carriers.

In an expansion of this program, conducted at the Naval Weapons Center (NWC), China Lake, CA, instrumented dummy ordnance was included in the debris pile, and there were occasions, depending on experimental fire-fighting tactics used, when cook off would have occurred. As a result of these large scale experiments, a number of important conclusions have been reached:

(1) In a debris pile fire, ordnance cook-off could occur in less than a minute.

(2) It is very important to quench the fire as soon as possible to keep thermal insult to the ordnance to an absolute minimum. Up until these tests it had been Navy practice to try to cool ordnance in a fire with seawater. But this dilutes any AFFF being used and makes it much less effective, thereby increasing the potential for longer exposure of the ordnance to the fire and increasing the risk.

(3) AFFF is about equal to the seawater in cooling, and should be used in place of seawater
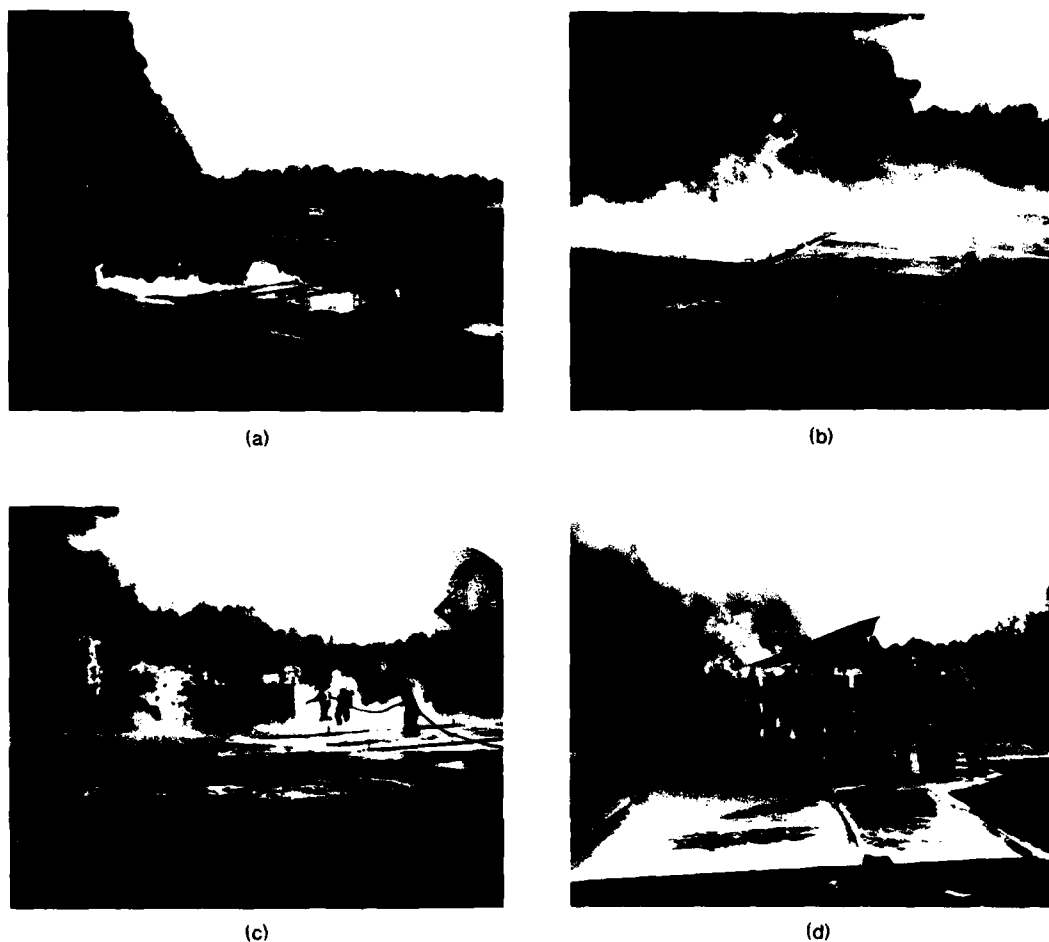
(a)

(b)

(c)

(d)

Fig 6 — Suppression of deck fire at CBD facility. A. Start of test (note wind machines at right, for generating up to 30-kn winds across deck). B. Wash-down system getting control of pool fires. C. Debris pile fire not extinguished by wash-down system. D. Firefighters must use hand lines to extinguish cascading fuel fire in debris pile.

for cooling ordnance; it also helps quench the fuel fire.

4) Crosswinds impede fire fighting with hoses (or monitors) because they reduce "reach" markedly. The stream gets blown away and reach can be less than half that in still air.

5) Winds help fire extinguishment if AFF (from the wash-down system) is also delivered upwind from the fire. The wind helps spread the AFFF blanket over the fire.

6) The AFFF wash-down system alone was sufficient to extinguish pool (2-D) fires on the deck, even with volatile fuels.

7) To fight a debris pile fire successfully, firefighters must be practically "on top" of the fire. Therefore, a need exists for fighting debris pile fires aggressively without undue exposure of

the firefighters. Preliminary tests with mobile remote-controlled devices (robots) and hose tie-downs were very promising, and they are being pursued vigorously.

Modeling and Scaling: Large-scale experiments are costly in time and money. But we are still too ignorant of fire behavior to be able to extrapolate from the laboratory to the real world. Therefore, NRL is now emphasizing the development of models to understand and predict fire behavior. The main thrust is for fires in closed environments (for example, submarines) because experimental work in FIRE I (Fig. 2) has demonstrated that fires with the hatches closed develop must faster in spread and intensity than when the hatches are open. Preliminary models are already

75

giving very encouraging results, but much more needs to be done.

Models must be properly scaled. Thus, in verifying the N_2 pressurization concept first espoused in 1972, NRL began with a 3-m³ (10-ft³) chamber. Suppression was achieved with an overpressure of only 0.3 atm, but the original calculations indicated that it should be 0.5 atm or more. It was quite apparent that even though small pan fires were used, wall effects and convection were interfering markedly. The need to settle scaling effects finally led to building FIRE I. Figure 1 shows clearly that not only is scaling very important, but also that essentially an asymptote has been reached. Data of these kinds will be very important in developing predictive models.

The final proofs of pudding, of course, are full-scale tests; hence, NRL performs large outdoor tests and demonstrations at CBD. NRL is also planning more tests in a full-sized ship cooperatively with the U.S. Coast Guard at a facility they now have at Mobile, AL (see Facilities).

Detection and Damage Control Central: The chance for successful suppression of a fire is much better if it is detected early. Even though most fire detectors respond in an analog fashion, they are forced to give an alarm in a digital, go-no-go, mode. Setting the "gate" for this digital response (Fig. 4) becomes critical. If too low, too many false alarms result; if too high, it might be too late. Would it not make more sense to use fire detectors in an analog mode and furnish that information, as it develops, to the central fire-fighting control point? NRL has developed such a detector and preliminary tests show it performs as planned.

Part of the original concept for this low-false-alarming analog detector is a hardened communication link between detector and Damage Control Central. Wires will burn (as shown repeatedly in Navy fires), fiber optics will melt, the stringing of emergency wires is clumsy and takes too long, and walkie-talkies are still too limited aboard ship. Accordingly, NRL has developed the concept of using the ship's hull as the message conductor employing pseudorandom noise (high-frequency sound) as the carrier.

Preliminary tests with devices designed and built to use this concept have been carried out at NRL's Underwater Sound Reference Detachment at Orlando, FL, and on the U.S.S. *Forrestal.* They show great promise as a totally fireproof communication link.

Having gathered the information, what is needed now is a Damage Control Center that can process lots of information rapidly (microprocessor), couple it with stored information, and give guidance to the bridge and Damage Control Assistant (DCA) by predicting the course of the fire, avenues of attack, escape, and actions to be taken. The Forest Service in the Department of Agriculture has a hand-held device of this type used by the line bosses in fighting forest fires. They have been very successful and the Navy should develop its own system. It would greatly mitigate fire losses, including personnel, in both peace and war. NRL is working on this.

Facilities

NRL has developed some of the finest fire research facilities anywhere. Most notable is FIRE I (Fig. 2), which is a highly instrumented 325-m³ (11,400-ft³) pressurizable chamber. It was built to boiler codes for strength. Immediately adjacent is a large trailer housing all the sensing, recording, and control equipment. It includes computer facilities for processing data in real time—a necessary feature for immediate decision making during the course of an experiment and for safety control. If an experiment is becoming too violent, the N_2 system is triggered to quench the fire. Other chambers are also available: a 5.66-m³ (200-ft³) converted decompression tank, and a 0.28-m³ (10-ft³) one for small experiments; both are highly instrumented.

A smoke chamber with a sampling and return duct system that allows removal of smoke to a laboratory test area and return is used for characterization of smokes and for removal techniques (such as ESP and dielectrophoresis).

A large, 9 × 9 × 9-m (30 × 30 × 30-ft) chamber for experiments in a protected environment is used for experiments with dry chemicals, hydraulic fluid fire suppression, and qualification

testing. It is coupled to a control room with a heat resistant window.

A large engineering space is used for work on proportioning AFFF concentrate into the fire mains in which full-scale shipboard proportioners and edductors are developed and evaluated.

Sophisticated laboratory equipment has also been developed and/or obtained, including a wide spectrum of analytical apparatus, fast-flow reactors, vertical tube reactors (for study of cool flames), shock tubes (for kinetic studies), lasers, spectroscopic equipment, mass spectrometers, chromatographs, computers, and other devices.

All of the above are at the main campus of NRL. In addition, NRL has a large field facility for fire suppression research at CBD (Fig. 6). This includes a minideck (simulating the flight deck of a carrier), a 7.6 × 7.6 × 7.6-m (25 × 25 × 25-ft) chamber for fire-fighting agent qualification studies, a smoke chamber for studying smoke knockdown and visibility, a large staging building, and an open pit for study of dangerous experiments (such as liquid oxygen hazards).

NRL has also cooperatively built a test bed in the range area at NWC to simulate a flight deck. Most of the final large-scale work has been performed there. We are also working cooperatively with the U.S. Coast Guard and using their Mobile, AL, facility (two ships, instrumented barge, plus a land-based staging area). It is planned that that facility will be expanded in the near future with a Navy ship under NRL control.

Future Impacts

Our main thrust in future work will be in passive fire protection. The concept of the "nonfire," (that is, a fire that did not happen), achieved through control of materials, geometry, specifications, and understanding through modeling and other research will be pursued. Active fire suppression will continue, and of special concern in this area are new agents, automation, and the concept of Damage Control Central.

Active Firefighting: NRL continues in the forefront in the development of new agents and concepts in fire protection. Of special note are the following.

New agents—New dry chemicals will be evolved using NRL's developing hypothesis on how they work. This should lead not only to more effective agents, but also to mixtures of agents for multiple action, for example, knockdown of the flame and also suppression of smoldering by depositing a "glassy" coat on the embers.

AFFF needs improvement. Particularly, the specification needs a complete overhaul to make AFFF more stable, more available, and more effective; use of a "stronger" concentrate should be evolved for Navy application.

Automation—We are still forcing firefighters into too high-risk situations. Controlling fires offers great applications of today's exploding technology in automation and artificial intelligence. Current work with the Naval Surface Weapons Center at White Oak on a mobile firefighting platform is an excellent start.

Damage control central—Again, the exploding technologies in computers, communications, and information processing lend themselves beautifully to the concept of a Damage Control Central System. It would automatically gather information (fire growth and other damage) as it happens and, with previously stored knowledge, process it to give the DCA and the bridge the "best" alternative for fire fighting, smoke control, and escape.

Passive Fire Protection (The nonfire): Obviously the best protection against unwanted fires is at their source—better yet, not to have them at all. Utopia will be reached when we achieve the concept of the nonfire, that is, a fire that would have happened but did not because we were smart enough to prevent it. At that point, research in fire at NRL will have happily worked itself out of a job. Proceeding in that direction NRL continues work on:

Materials—A "crying" need is for a nonflammable hydraulic fluid, especially for submarines. The explosions on the U.S.S. *Bennington* in 1954, with a loss of 103 lives, due to ignition of atomized fluid from a high-pressure leak, and other similar accidents, are bound to be repeated with disastrous results. Research in this area must be pursued aggressively.

There are many other flammable materials whose potential contributions to fire, smoke, and

77

toxicity can be minimized by changes in composition and structure. NRL is vigorously pursuing this concept in such materials as electrical cabling, hull insulation, composites, and acoustic damping.

Geometry—Fire spread can be controlled by geometry-spacing and shape. The old aphorism that it takes three logs to keep a fire going in a fireplace is true. It is also well known that excelsior burns much faster than a board, even though both come from the same tree. Current basic studies in modeling and scaling will help predict such effects and will be applied in this area to develop guidelines for designers, builders, and operators.

Specifications—An excellent control of fire, smoke, toxicity, and corrosivity is at the source, by proper specifications. "Fireproofness" or greater "fire resistance" can be incorporated into specifications. The key, however, is the use of the "correct" test methods in the specification. Fire test methods are supposed to be predictive, and are usually developed to simulate the real world, but this is very difficult to do. Scaling becomes critical here, and again, current work in modeling and scaling will have an important impact in developing these predictive "tools."

Software Cost Reduction
Through Disciplined Design

Paul C. Clements
Information Technology Division

The computer revolution that has occurred over the last twenty years or so has been especially intense within the Department of Defense. DoD currently spends about 3 to 4% ($10 billion per year) of its budget on software. That number is expected to grow quickly in the next few years. In the words of one senior DoD official, "DoD sees software as a key underlying technology, the functional driver of virtually all of its future defense systems."

Software in the DoD, then, is both critical and expensive. If there were a way to lower the cost of developing software—even a little, the potential savings would be enormous.

The process of specifying, designing, documenting, coding, testing, and fielding software is not at all well-defined. Today's systems can be far more complex than any one person can understand, and there is no generally practiced methodology for making the development task manageable. The state of software engineering practice is, unfortunately, quite *ad hoc*. In particular: (a) Projects are often begun without a clear, unambiguous, complete statement of what is supposed to be built. (b) The task is usually broken down in an arbitrary fashion so that the parts have strong interdependencies; therefore, workers have to know intricate details about all parts of the system. (c) Documentation that is supposed to be written to explain what the system does, what its parts are, and how the parts fit together is many times not written. If it is written, it is usually of poor quality, of undecipherable organization, full of undefined terms and rampant vagueness, and not of any practical use. (d) Little, if any, effort is invested in reusing software that already exists (perhaps previously developed as part of a similar system). (e) The search to find available software—if an attempt is made—is almost guaranteed to fail; virtually no software
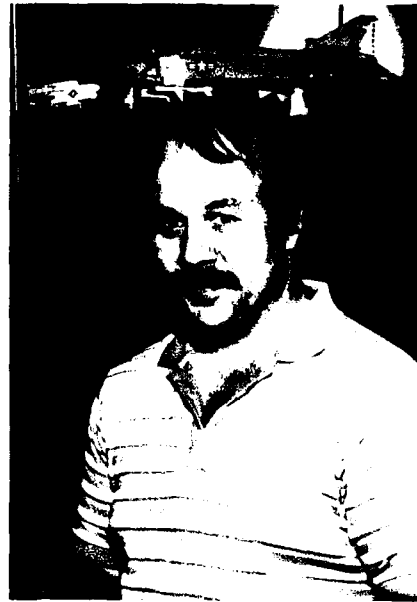
Paul C. Clements

exists that can be lifted from the system that spawned it and inserted into another. (f) No attention is paid to make the software easy to test, maintain, and change.

The last point is particularly important because, although software development costs are high, the costs of the software maintenance phase of the software life-cycle are even higher. Typically, a software system incurs the largest part of its expense after it has been deployed. Software maintenance occurs when software needs to be modified to account for changes in the environment or changes in the desired behavior over the life of the system. The same factors that inhibited orderly development (such as poor structure or poor documentation) also inhibit maintenance, with the added penalty that the people who change a system are more than likely not the

79

ones who built it. Thus, the problems are compounded.

In fact, techniques to solve these problems exist; many have existed for several years. Why aren't they used? The reasons include the following: (a) Some ideas are impractical for DoD systems because they may lead to programs that use too much memory or take too long to execute. For example, a missile program must reside in a very limited memory space, and the calculations must be made fast enough so that the missile will not miss its target. (b) Some ideas work fine for the small, experimental systems that one might find in an academic or laboratory environment, but fail when applied to large, complex systems that typify DoD software applications. For instance, techniques exist for mathematically proving whether or not a program is correct. However, the techniques are so complex that applying them to programs over a few lines long can take several weeks. (c) Managers are reluctant to bet their projects on techniques that haven't been tried before; this is a classic technology transfer problem, known to most engineering disciplines. In software engineering, it has been estimated that it takes up to 20 years

for a truly innovative development to achieve widespread use.

The Software Cost Reduction Project: A clear need existed for a software engineering project that would choose a set of principles and methods, apply them rigorously to an actual DoD system, refine them (or discard them) where necessary, faithfully report the results in the open literature, and (if successful) provide a working model of the software development process for others to follow. This is the charter of the Software Cost Reduction (SCR) project.

In 1978 an application was chosen to serve as the testbed for what has come to be known as the SCR methodology. The application was the onboard flight software for the Navy's A-7E attack aircraft (Fig. 1). This system was an ideal test for several reasons. First, the system is real time and embedded, meaning that it is always racing the clock and that it must interface with complicated peripheral devices such as atmospheric sensors and unusual cockpit displays. This is the most difficult kind of system to build correctly, and thus the most difficult test of the SCR methodology. Second, the system is an
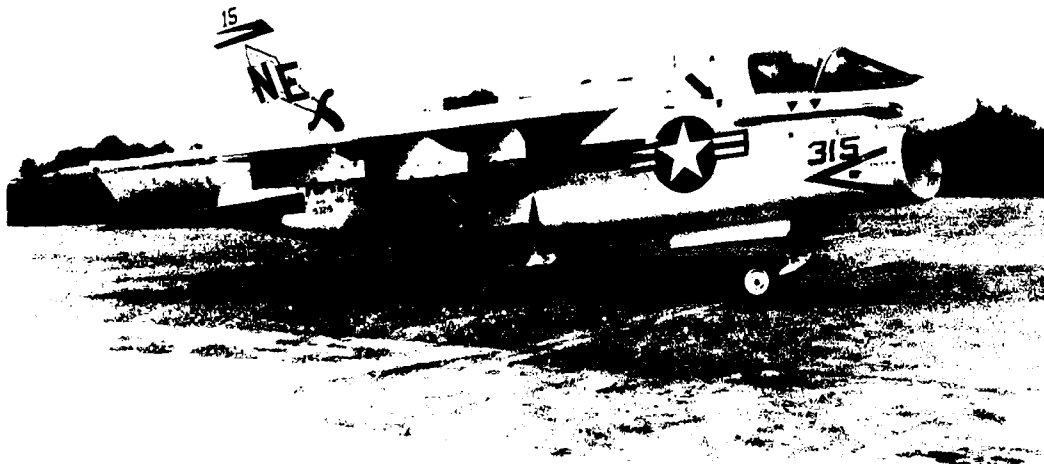

Fig. 1 — The A-7E aircraft software is the demonstration medium for the SCR mthododlogy

authentic and not a contrived example; its behavior is often not what a naive programmer would expect, and he cannot tailor it or simplify it to make his job easier; thus, it is a convincing test case. Third, the A-7E system, although developed via traditional *ad hoc* practices, is considered one of the Navy's best programs because of its sophistication and high reliability. Producing a better program than this one will be a more convincing demonstration. Finally, the program barely fits into the memory of its rather old computer, and it barely meets its timing requirements. Producing a program that is bigger or slower, will be immediately obvious.

The goal of SCR, then, is to produce a program that is behaviorally equivalent to the A-7E software by using state-of-the-art software engineering principles and techniques. The project is an **experiment**, because its result is to discover if the chosen methodology works. It is a **demonstration** because, assuming that the experiment is successful, it furnishes to the software community a fully worked-out example of applying the SCR methodology to a real system. It is a **research project** because some of the techniques still need refinement. It is a **development project** because the final product is an operational avionics program. Finally, it is a **technology transfer project** because it teaches the methodology via publications and seminars.

What is the SCR Methodology? This section describes the SCR software development methodology by describing the work products that it calls for. These steps are to: establish and document requirements, design and document the module structure, design and document the module interfaces, design and document the module internal structures, perform formal reviews, design and document the "uses" hierarchy, write programs, and integrate and test software.

Establish and document requirements—The first step of any software project must be to write down exactly what the software is supposed to do, that is, prepare a requirements document. As sensible as this sounds, it is rarely done. It isn't as easy as it sounds, and for large systems, specifying the thousands of necessary details can be an extremely expensive undertaking. However, a completely specified set of requirements is well worth producing for the following reasons:

- It is a record of the desired behavior of the system as described to the programmers by the user. This document is a product that the user or his representative can review.
- It prevents programmers from having to make requirements decisions accidentally while designing the program. Programmers are very often not familiar with the application area. Having a complete reference on externally visible behavior relieves them of any need to decide what is best for the user.
- It helps to avoid duplication and inconsistency. Without a requirements document, many of the questions it answers would be asked repeatedly throughout the development by designers, programmers, and reviewers. This duplication of effort is expensive and can result in inconsistent answers.
- It is necessary (but not sufficient) for making good estimates of the amount of work and money that it will take to build the system.
- It is valuable insurance against the liabilities of personnel turnover. The knowledge gained about the requirements will not be lost when someone leaves the project.
- It provides a good basis for test plan development. Software cannot be tested for correct behavior unless correct behavior is precisely defined.
- It can be used to to settle arguments; once they have a requirements document, programmers no longer need to consult, or be application experts.
- It can be used long after the system is in place to define changes.

The definition of the ideal requirements document is simple. It should contain everything one needs to know to write software that is acceptable to the customer, and no more. The SCR requirements document is divided into well-defined sections, each of which fully defines one aspect of the requirements. An example is the section that specifies the value at all times of each output of the system in terms of measurable   81

quantities in the system's environment. Another is the section that specifies for each output how often or how quickly the software is required to recompute it. A section unique to SCR requirements documents is one that defines likely changes to the system. Since software developed by using SCR methodology is designed to be easy to change, the requirements must contain a definition of the areas that are considered likely to change. One cannot design a system so that everything is equally easy to change, and programmers should not have to decide which changes are most likely.

The organization of the SCR requirements document into well-defined sections is one that can be easily followed and helps assure completeness. Consistency and precision are achieved by eschewing prose wherever possible in favor of tables and mathematical forms which are precise and whose correctness can be easily checked. Table 1 is an example of a specification; it shows under what conditions the modes of the system change to new modes.

A requirements document embodying these principles was one of the first publications of the SCR project [1,2], and over 800 requests for copies have since been received.

Design and document the module structure— Unless the product is small enough to be produced by a single programmer, one must consider how the work will be divided into work assignments, which we call modules. The document that should be produced at this stage is called a module guide; it defines the responsibilities of each of the modules. A module may consist of submodules, or it may be a single work assignment.

A module guide helps to assure that all work is assigned to exactly one person or team. After the system is in place, it helps a maintainer unfamiliar with the system find out which modules are affected by a problem report or change request.

The idea of modules is not new, but the principle by which SCR creates them is not widely used. Since the major cost of software occurs in the maintenance phase, it seems reasonable that software should be designed to be easily changed. One way to do that is to make sure that each change only affects one isolated well-defined part of the system, rather than causing unpredictable changes in many different parts. For instance, if an aircraft altitude sensor is likely to change or be replaced over the life of an avionics program, then it is reasonable to design the system so that one and only one module will have to change with it, leaving the rest of the software unaffected.

The way to do this is to decree that modules can only interact with each other via public facilities (interfaces) and keep other aspects hidden from each other (secrets). It should then be possible to design interfaces that remain the same even when the secrets change. If a module's secret changes but its interface does not, then no other module need change at all since they were never privy to the first module's secrets. The interface to the aircraft altitude sensor module, for example, might include a program that returned the aircraft's current altitude above sea level in feet as measured by that device. The secret of the module might be the scaling and units and format of the bitstring returned by the actual sensor, because those things are likely to change when the device is replaced.

The way to design software for ease of change, then, is to create exactly one module to encapsulate each likely change and to carefully design its interface to remain the same over all likely changes to its secret. This method is known as information hiding and was first described in 1972. The technique is widely known in academia, but SCR is proving the value of information hiding to DoD systems.

If one diligently applies information hiding to a large system, one is certain to end up with a great many modules. A guide that is simply a list of those modules, with no other structure, helps only those who are already familiar with the system. The SCR module guide has a tree structure, dividing the system into a small number of modules and treating each such module in the same way until all of the modules are quite small. This tree structure allows one to locate a module of interest very quickly. We continue the decomposition into submodules and design of their interfaces until each work assignment is small enough that we could afford to discard it and begin again if the programmer assigned to do it left the project. This is an example of a good

Table 1—Formal Tables and Notation Help to Achieve Precision in SCR Specifications

Current Mode	!Station selected!	!ACAIRB!=Yes	!MODEROT!=$PRESPOS$	/PRESPOS/=$UPDATE$	/UPDATTW/=$FLYOVER$	/UPDATTW/=HUD	/UPDATTW/=$RADAR$	/UPDATTW/=STAC L-L$	/GUNSEL/=Yes	!WD MFS!	!Data 23!=!Sea!	!Weapon model!=•BOC•	/MFSW/=$None$	/MFSW/=TF	!non-zero digit entered!	/ENTERSW/=On	!FLY-TO changed!	New Mode
FlyUpd	-	-	-	-	-	-	-	-	-	@T	-	-	-	-	-	-	-	*None*
	-	-	-	-	-	-	-	-	@T	-	-	-	-	-	-	-	-	
	@T	-	-	-	-	-	-	-	-	-	-	-	-	-	-	-	-	
	-	-	@F	-	-	-	-	-	-	-	-	-	-	-	-	-	-	
	-	-	-	@F	-	-	-	-	-	-	-	-	-	-	-	-	-	
	-	-	-	-	@F	-	-	-	-	-	-	-	-	-	-	-	-	
	-	-	-	-	-	-	-	-	-	-	-	-	-	-	-	@T	-	
	-	-	-	-	-	-	-	-	-	-	-	-	-	-	@T	-	-	*MapUpd*
	-	-	-	-	-	-	-	-	-	-	-	-	-	-	-	-	@T	
AflyUpd	-	@F	-	-	-	-	-	-	-	-	-	-	-	-	-	-	-	*None*
	-	-	-	-	-	-	-	-	@T	-	-	@F	-	-	-	-	-	
	@T	-	-	-	-	-	-	-	-	-	-	-	-	-	-	-	-	
	-	-	@F	-	-	-	-	-	-	-	-	-	-	-	-	-	-	
	-	-	-	@F	-	-	-	-	-	-	-	-	-	-	-	-	-	
	-	-	-	-	@F	-	-	-	-	-	-	-	-	-	-	-	-	
	-	-	-	-	-	-	-	-	-	-	-	-	-	-	-	@T	-	
	-	-	-	-	-	-	-	-	-	-	-	-	-	-	-	-	@T	
MayUpd	-	-	-	-	-	-	-	-	-	@T	-	-	-	-	-	-	-	*None*
	-	-	-	-	-	-	-	-	@T	-	-	-	-	-	-	-	-	
	@T	-	-	-	-	-	-	-	-	-	-	-	-	-	-	-	-	
	-	-	@F	-	-	-	-	-	-	-	-	-	-	-	-	-	-	
	-	-	-	@F	-	-	-	-	-	-	-	-	-	-	-	-	-	
	-	-	-	-	@F	-	-	-	-	-	-	-	-	-	-	-	-	
	-	-	-	-	-	-	-	-	-	-	-	-	-	-	-	@T	-	*FlyUpd*
	-	-	-	-	-	-	-	-	-	-	-	-	-	-	-	-	@T	*MapUpd*
	-	-	-	-	-	-	-	-	-	-	-	-	-	-	-	@T	-	
TacUpd	-	-	-	-	-	-	-	-	-	@T	-	-	-	-	-	-	-	*None*
	-	-	-	-	-	-	-	-	@T	-	-	-	-	-	-	-	-	
	@T	-	-	-	-	-	-	-	-	-	-	-	-	-	-	-	-	
	-	-	@F	-	-	-	-	-	-	-	-	-	-	-	-	-	-	
	-	-	-	@F	-	-	-	-	-	-	-	-	-	-	-	-	-	
	-	-	-	-	f	-	-	@F	-	-	-	-	-	-	-	-	-	
	-	-	-	-	-	-	-	-	-	-	-	-	-	-	-	@T	-	
	-	@T	-	-	-	-	-	-	-	-	-	-	-	-	-	-	-	*MapUpd*

idea (modules) needing a refinement (tree-structured organization) to make it practical. For a complete example of such a document, see Ref. 3 For a discussion of this approach and its benefits, see Refs. 4,5.

Design and document the module interfaces—For information hiding to work, each module's interface must be carefully designed to hide the secrets assigned to that module as specified by the module guide. Since a module's interface is all that other modules are allowed to interact with, it must be specified precisely. A module interface specification is written for each module. An interface specification for a module contains just enough information for the programmer of another module to use its facilities, and no more. The main content of these specifications [6] consists of:

- a list of the modules invokable by other modules, called access programs;
- the parameters for these access programs;
- the externally visible effects of these access programs;

- timing and accuracy constraints, where necessary; and
- a definition of undesired events (errors resulting from incorrect use of the module's facilities).

Designing interfaces that truly encapsulate a module's secrets is often difficult. However, by providing complete examples of information-hiding interfaces for various kinds of modules, SCR provides a model for others to follow. Published designs include Refs. 7,8,9,10.

Design and document the module internal structures—Once a module interface has been specified, it can be implemented as an independent task except for formal reviews (these are described below). However, before coding, the major design decisions are recorded in a document called the module design document [11]. This document is designed to allow an efficient review of the internal design before the coding begins and to explain the purpose of the code to a future maintenance programmer. For each of the access programs, it includes a mathematical function [12] that describes how inputs are mapped onto the internal data structures within the module. For each value returned by the module to its caller, it provides another mathematical function that maps the values of the data structure into the values that are returned. For each of the undesired events, it describes how we check for it. Finally, it provides a verification. This is a logical or mathematical formulation of the operations the module performs on the inputs to produce outputs. Its purpose is to provide a proof or convincing argument that the programs meet their specifications.

Perform formal reviews—A rigorous, formal review accompanies each of the steps mentioned so far. SCR review procedures are different from most in that they check not only for adherence to fact but also for adherence to principle. Reviewers who are knowledgeable about the application area are asked about likely changes to the system and to help assure that the interfaces are designed so that those changes can be accommodated. Other reviewers are asked to make sure that the document meets SCR organization rules, that all the terms are clearly defined, etc. Still other reviewers are asked to make sure that

the information in the documents is factually correct. Only if a document passes all of these tests is it considered correct. The reviews are hard work, but by finding errors in the requirements and design before code is written, they more than justify the effort. Design reviews are one of the most important parts of the SCR methodology, and are more fully discussed in Ref. 13.

Design and document the "uses" hierarchy—One of the traditional problems that is common during system development is that no part of the system performs correctly unless all the parts are present. This prevents developing system subsets, which can be useful during development to aid testing or to supply a fallback position when schedules slip. However, in the SCR methodology, we control and keep track of the programs that require the presence of other programs to work correctly. Because of this we can easily create mutually dependent sets of programs that form distinct subsets of the entire system. The relation "requires the presence of" is what we mean by uses [14], and the specification of the uses relation for the system allows SCR to define subsets easily and quickly.

The uses hierarchy can be designed once we know all of the modules and their access programs. It is conveniently documented as a binary matrix where the entry in position (A,B) is true if and only if the correctness of program A depends on the presence in the system of a correct program B. The uses hierarchy defines the set of subsets that can be obtained by implementing a subset of the programs of each module.

Write programs—After all of the design and documentation has been carried out, actual executable code is written. Experience shows that this goes quickly and smoothly as a result of the investment in carefully crafted specifications and separation of module concerns.

Integrate and test software—Once all of the modules are coded they must be tested separately and together. This is an area where SCR methodology has yielded another benefit. Testing and integration take much less time than with conventionally developed software for some of the following reasons:

- By carefully documenting and checking for undesired events in each module, a very large class of errors has effectively already been tested for.

- The precise interfaces between modules allow for rapid identification of the source of an error; a module either meets its specification or it does not, and it is straightforward to tell which is the case.

- The stringent review procedures applied to each module design and implementation weed out mistakes before code is written.

- The precise requirements specification provides a strict definition of correct behavior; its formalisms (such as tables) also lend themselves to the quick generation of systematic and complete tests.

- Dividing a module up into public and private parts (interfaces and secrets) leads to a notion of black-box behavior; that is, the correctness of a module is determined completely by whether or not it meets its specification. This makes testing for correctness quite simple because correct behavior is explicitly and completely defined.

Project Status: The SCR project recently provided a demonstration of all of its principles by completing the implementation of a small subset of the A-7E software. Although the program was quite small compared to the full program, it was carefully chosen to include part of every major module. The successful completion of that subset provided convincing evidence that modules written only in terms of each other's interfaces can be integrated to form a single, functionally correct program. It also provided a convincing test of the accompanying support software. This software helped translate the calls to programs through interfaces into low-level instructions that executed directly on the computer.

Armed with a working preliminary subset and a validated support environment, the next step is to build a much larger subset of the program. Called the useful subset, this program will represent over half of the full functionality and could pass for an actual (albeit lean) avionics pro-gram. Besides continuing to test the principle of implementing incremental subsets, this program will provide experience with some of the more difficult areas of applications such as navigation and weapon delivery. The useful subset will be implemented in the fall of 1985.

After the useful subset is implemented, the full A-7E program will be completed. At that time, measurements will be taken on the amount of time and storage required by the new program. These figures will be compared with those of the old program, thus giving the first indication of how big a performance penalty (if any) the methodology entails. Other experiments are also planned, such as making changes to the new program that were made to the old program and comparing the expense and effort required.

At the same time, software tools to help with SCR design and documentation methods will be developed. Ongoing technology transfer efforts will be continued and expanded. Currently, SCR project personnel routinely consult with software engineers on other large DoD systems under development. This is part of our ongoing technology transfer effort.

SCR's Contributions: The SCR project has already made the following contributions to the software engineering state of the art: (a) a requirements specification methodology for real-time embedded systems; (b) a modularization technique that applies to all software systems, and a sample modularization that applies to a large class of systems; (c) a specification technique for information-hiding module interfaces; (d) a new technique to synchronize parallel processes and to schedule the execution of the processes before run time [15]; (e) sample designs for several typical modules found in real-time embedded systems; (f) a new technique to ensure that a system can be implemented in incremental subsets and a technique to specify those subsets; (g) a set of general-purpose software tools used to build translators (such as compilers); and (h) a solution to the problem of avionics program portability; namely, a module that encapsulates the differences between avionics computers so that application software can be written for any of them.

In addition, there are strong indications of the following payoffs:

- The methodology leads to a significant reduction in integration and testing time. The experience with the preliminary subset indicates that an order of magnitude improvement over conventional techniques is likely.

- The methodology leads to a significant reduction in the amount of coding time necessary.

- The SCR approach to documentation leads to the amelioration of the "Mythical Man Month" effect [16] which holds that adding personnel to a project generally slows a project down because of the time it takes to bring the new people up to speed. When new programmers join an SCR-style project they do not have to depend completely on the old staff for their information. They will have an up-to-date and rational set of documents available. Further, because of separation of concerns, new people need not learn about all aspects of the project, but only their small part of it.

- The SCR modularization scheme can lead to a standard taxonomy for software that is necessary before libraries of reusable software can be developed.

- Management for an SCR-style project is easier because the formal interaction between work assignments (modules) and their relative independence leads to greater accountability.

- Management is also made easier because there is greater flexibility in scheduling tasks. For instance, once a module interface is designed, it need not actually be implemented before other modules can make effective use of it. Thus, design and implementation can occur simultaneously.

- The formal specifications make excellent task assignments for contractors.

- The loss of a person is never critical because there are no critical people.

Other organizations are discovering the benefits as well. Through publications and atten-

dance at software engineering conferences, the project staff has become aware of several companies and DoD organizations using SCR techniques. One large telecommunications company, which uses information hiding to design their switching systems, has been able to market systems for much less than their competitors because they can change it so easily to meet new customers' needs. Another claims that the SCR methodology is the most widely used within their company. At least two other government contractors have proposed using SCR techniques because they are the most cost-effective. At the present time, the project staff knows of over 50 large software engineering projects in government and industry that make use of all or part of the SCR methodology, and there is no way of telling how many more there ac.ually are.

Perhaps the best indication of the project's continued success is the large number of requests for information received. Literally thousands of documents have been distributed in response to inquiries. One request resulted in teaching SCR methodology in a software engineering course at a Texas university. Perhaps one day the methodology will be taught not as a new and innovative way to solve the problems of software development, but rather as standard practice.

References

1. K.L. Heninger, "Specifying Software Requirements for Complex Systems: New Techniques and Their Application," *IEEE Transactions on Software Engineering*, **SE-6**, 2-13 (Jan. 1980).

2. K. Heninger, J. Kallander, D.L. Parnas, and J. Shore, "Software Requirements for the A-7E Aircraft," NRL Memorandum Report 3876, Nov. 1978.

3. K.H. Britton and D.L. Parnas, "A-7E Software Module Guide," NRL Memorandum Report 4702, Dec. 1981.

4. D.L. Parnas, P. Clements, and D. Weiss, "The Modular Structure of Complex Systems," Proceedings of the Seventh International Conference on Software Engineering, Mar. 1984, pp. 408-417.

5. P. Clements, D. Parnas, and D. Weiss, "Enhancing Reusability with Information Hiding," Proceedings of a Workshop on Reusability in Programming, Sept. 1983, pp. 240-247.

6. P. Clements, A. Parker, D.L. Parnas, J. Shore, and K. Britton, "A Standard Organization for Specifying Abstract Interfaces," NRL Report 8815, June 1984.

7. D.L. Parnas, D.M. Weiss, P.C. Clements, and K.H. Britton, "Interface Specifications for the SCR (A-7E) Extended Computer Module," NRL Memorandum Report 5502, Dec. 1984.

8. K.H. Britton, R.A. Parker, and D.L. Parnas, "A Procedure for Designing Abstract Interfaces for Device Interface Modules," Proceedings of the Fifth International Conference on Software Engineering, 1981.

9. P. Clements, S. Faulk, and D. Parnas, "Interface Specifications for the SCR (A-7E) Application Data Types Module," NRL Report 8734, Aug. 1983.

10. A. Parker, K. Heninger, D. Parnas, and J. Shore, "Abstract Interface Specifications for the A-7E Device Interface Module," NRL Memorandum Report 4385, Nov. 1980.

11. S. Faulk, B. Labaw, and D. Parnas, "SCR Module Implementation Documentation Guidelines," NRL Technical Memorandum 7590-072:SF:BL:DP, April 1983.

12. R.C. Linger, H.D. Mills, and B.I. Witt, Structured Programming: Theory and Practice, (Addison-Wesley Publishing Company, 1979).

13. D. Parnas and D. Weiss, "Active Design Reviews: Principles and Practices," NRL internal report, in preparation.

14. D.L. Parnas, "Designing Software for Ease of Extension and Contraction," Proceedings of the Third International Conference on Software Engineering, May 1978, pp. 264-277.

15. S. Faulk and D. Parnas, "On the Uses of Synchronization in Hard-Real-Time Systems," Proceedings, 1983 Real-Time Systems Symposium, Dec. 1983.

16. F.P. Brooks, Jr., The Mythical Man Month: Essays on Software Engineering (Addison-Wesley Publishing Company, 1975).

Artificial intelligence, information processing, and signal transmission

NRL's Center for Applied Research in Artificial Intelligence is the leading AI research center in the Department of Defense

ARTIFICIAL INTELLIGENCE

A tremendous amount of information in many forms—precise quantitative through subjective verbal assessments—must be evaluated and assimilated to arrive at best possible decisions. Most of this information is transmitted in some form, many times through hostile environments. Systems to accomplish the data acquisition, interpretation, and management are being developed and can frequently be evaluated through simulations that are very economical compared to a full-scale test. NRL is active in all these areas. The articles in this chapter were contributed by the Information Technology Division (Code 7500) and the Tactical Electronic Warfare Division (Code 5700).

NRL has many research projects in artificial intelligence, information processing, and signal transmission. These include:

- expert systems for battle management
- target recognition and identification
- force level modeling and simulation
- advanced electronic warfare systems
- airborne dual-mode jamming
- Arctic communications concepts

Multisensor Integration—An AI Approach

Y.T. Chien and L.C. Davis
Information Technology Division

Introduction: A recent development in Artificial Intelligence (AI) is the deliberate representation and utilization of human expertise in computer-assisted problem solving in a complicated domain. Problem solving systems of this type rely heavily on knowledge, as opposed to mathematical algorithms and generalized problem solving strategies, as a principal tool for obtaining solutions. This approach is being applied successfully to a variety of well-defined problems, and NRL is investigating its utility for a number of Navy applications such as multisensor integration (MSI). Currently, we are developing a knowledge-based system to demonstrate how AI can improve the integration of sensor information from disparate sources, varying in completeness, timeliness, and accuracy, to provide effective decision support for naval Command, Control, Communication, and Intelligence (C^3I) operations.

As in most AI system research and development, we focus on a well-defined application domain which exploits AI but still maintains the generic nature of the research, so that results obtained can be readily applied to other environments. We have chosen the tactical operations of the P-3, a Navy aircraft engaging in antisubmarine warfare (ASW) and antisurface warfare (ASuW) as the application domain. In a typical P-3 mission, data from multiple sensors (such as SONAR, RADAR, and ESM (electronic support measures)) and other sources (visual, intelligence) with diverse characteristics must be integrated and assessed to guide time-critical tactical decisions. However, experience in the past indicates that techniques based only on mathematical algorithms to combine sensor data have major limitations in their ability to produce the necessary results. An AI-based MSI system can remove some of these limitations.

Knowledge vs Algorithms: Figure 1 depicts the functional organization of a knowledge-based MSI system. Besides the sensor environment, two of the key components in this system are the knowledge base(s) and the control and inference mechanism(s). Knowledge, in the context of AI systems, is composed of all the symbolic, relational, and physical information related to the problem domain. This should include not only facts, processes, and objects of interest, but
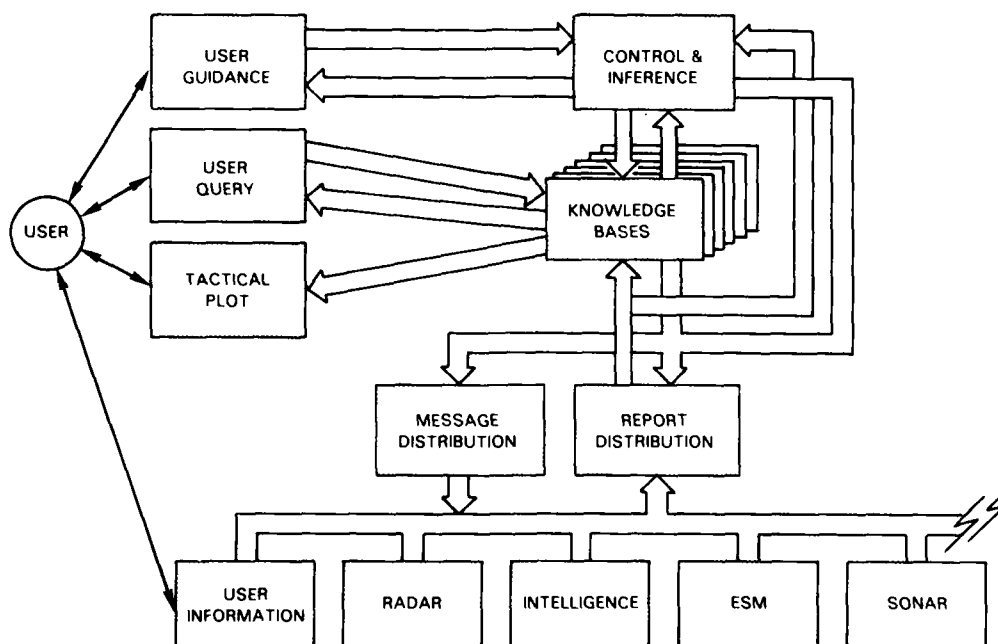
Fig. 1 — Functional organization of a knowledged-based MSI system

also heuristics, judgments, and other human expertise pertinent to the decision processes involved. Knowledge of this kind often cannot be easily described in a precise mathematical algorithm or formula and thus requires a representation or a combination of representations that is more convenient for symbolic manipulation. Indeed, a great deal of the effort in designing our MSI system is concerned with capturing, characterizing, and organizing the different kinds of knowledge for computer representation.

The domain knowledge used in P-3 ASW/ASuW tactical operations can be organized in a hierarchy of subareas. Figure 2 illustrates a simplified hierarchy. At the top level, the knowledge is divided into several groups, each representing a broad area of expertise. Each of these groups can be successively divided into smaller, more focused areas at lower levels. The category of tactics/actions, for instance, can be further divided into specific knowledge groups according to mission (ASW and ASuW, as shown here); for each mission, a finer division into mission phase (for example, search or attack) is pos-

sible. This hierarchical representation of knowledge permits efficient access and manipulation by the computer, especially when the knowledge base is large, as is likely the case in most military applications. It also facilitates corrections and additions to the knowledge base. If the knowledge required is extremely complex, as is the case in the P-3 domain, a separate knowledge category, called control knowledge or metalevel knowledge, may be needed. Control knowledge is used to manipulate the other types of knowledge, considered object-level knowledge, for more efficient and effective processing. Two examples of the kinds of knowledge used in P-3 operations, represented by IF-THEN rules, are shown in Table 1. To capture the necessary domain knowledge, hundreds or potentially thousands of rules along with other types of representations may be needed. In the P-3 environment, the attack segment alone of the knowledge base may need 50 to 200 rules to describe the required tactics and actions.

Inference and Control: To use the knowledge effectively, the MSI system must have
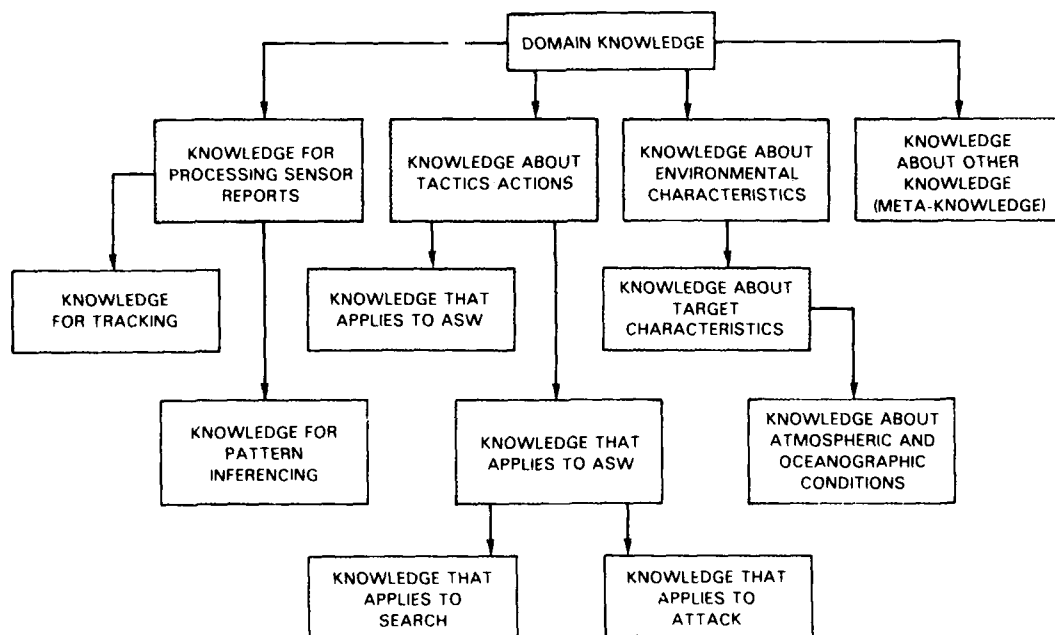
Fig. 2 — Knowledge and its representation in the computer. A typical hierarchy of domain knowledge in the P-3 environment.

Table 1 — Examples of IF-THEN Rules to
Represent P-3 Domain Knowledge

Example of a Report Processing Rule - To infer the existence of a task force (friendly or hostile) from patterns of tracks, based on sensor reports and knowledge of enemy's tactical intentions
IF (1) ESM and RADAR contacts provide tracks of at least 3 targets, (2) the tracks are following a course of movement which corresponds to an anticipated enemy convoy, and (3) ESM and RADAR contacts have determined that they are not friendly ships, THEN   (1) it is likely that these tracks are part of a hostile force (2) post a report to the tactical coordinator to that effect.
Example of a Metalevel Rule - To control the use of two different groups of object-level rules in the knowledge base
IF (1) the number of target tracks in the group is three or more, (2) there are rules which refer to **Immediate Threat**, and (3) there are rules which refer to **Potential Threat**, THEN   it is recommended that the rules in (2) should be used before those in (3).

proper computational mechanisms to transform the input data into appropriate conclusions or solutions. In principle, these mechanisms are not totally different from those typically used in other, non-AI systems—they involve searching for an optimal solution path and making logical inferences at various points along the solution path. However, since the data used in our system is primarily symbolic and knowledge intensive, there are additional requirements that must be met. First, the inference mechanism must be able to reason with uncertain and possibly errone-ous data, and must be capable of forming tenta-tive hypotheses. Second, there must be a way of combining and weighting information from dif-ferent sources to draw conclusions within time constraints. Third, the system should be both data-driven and goal-directed so that a combina-tion of inference mechanisms can come into play in searching for the best solution path possible.

Figure 3 illustrates some of the key features of the inference mechanisms being implemented in the MSI system. This figure shows the rela-tionship between the knowledge base(s) and the inference processes, with the user of the system (for example, tactical coordinator or mission
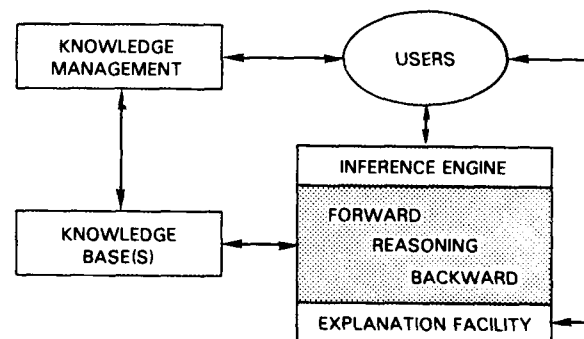
Fig. 3 — Relationship between knowledge, inference,
and the user

commander) having access to both components. The example in Table 2 indicates how two dif-ferent inference techniques can be used in combi-nation to provide decision support in the P-3 environment. The data-driven or forward-chaining mechanism is used to combine sensor reports for determining position, course, and speed of a target. At the same time, a goal-directed or backward-chaining mechanism is used to make inferences in regard to the assessment of

93

Table 2 — Examples Showing Typical Input/Output
Functions of Inference Mechanisms

Forward Chaining - Work from known facts and observed data to new, deduced facts or conclusions
Example: Tracking of targets in a P3 Mission INPUT - Sensor reports; environmental data OUTPUT - Position, course, and speed of target(s)
Backward Chaining - Hypothesize a conclusion and work backward toward an enumeration of facts and data that would support the hypothesis.
Example: Decision aid in threat assessment INPUT - Hypothesize a threat condition OUTPUT - (1) confirm or deny the hypothesis based on facts and data in knowledge base (2) provide line of reasoning to support conclusion

that target's threat. Through proper control, both inference mechanisms can be activated either automatically or at the command of the user.

Summary: By effectively using knowledge and inference, information fusion can take place at several levels in this MSI decision support system. Sensor information, for example, can be part of the rules comprising the knowledge in tactics and actions. On a different level, sensor data may be integrated with environmental data and intelligence reports to hypothesize about target threat and enemy tactics. In general, decision support functions ranging from situation description and threat assessment to resource management and fire control solution development can eventually be within the system's capability. The research described here is a first step towards designing this new class of decision support systems for future naval C^{3}I needs.

Reference

1. L. Davis and J. Aldrich, "A Knowledge-Based Approach to Naval Multisensor Information Integration." Proceedings of the IEEE Computer Society Conference on Trends and Applications, 1983. Gaithersburg, MD, May 25-26, 1983, pp. 216-223. ■

Automatic Processing of Military Messages for Dissemination and Summarization

E. Marsh
Information Technology Division

The natural language processing group at the Navy Center for Applied Research in Artificial Intelligence has built an experimental system that uses techniques of computational linguistics and artificial intelligence to extract information from Navy operational reports. These are typically written reports, and while they obey strict formatting conventions, they also contain important narrative descriptions. We have implemented a prototype system for extracting the informational content from the narrative descriptions contained in a class of operational messages about shipboard equipment failure (casualty reports or CASREPs); an example is shown in Fig. 4. The narrative information is contained in the sections labeled *AMPN* and *RMKS*. From the information in these reports, the system assigns a distribution list for each message and generates a summary of the equipment failure.

In constructing the system, we have adapted an approach developed by Sager et al. [1] at New York University. This approach, called *information formatting*, uses an explicit grammar of English and a classification of the semantic rela-
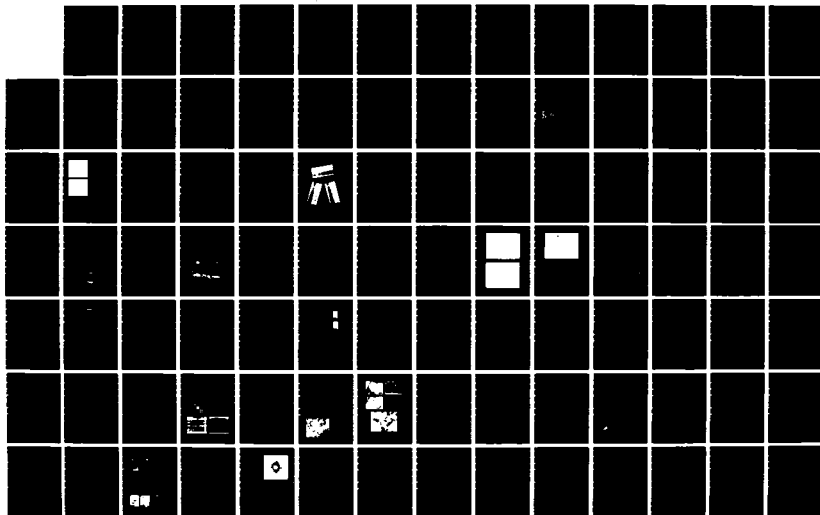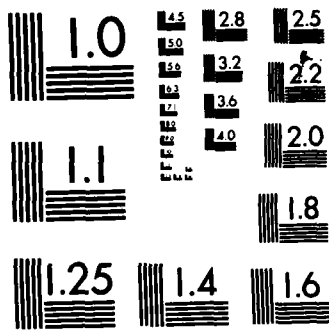
MICROCOPY RESOLUTION TEST CHART
NATIONAL BUREAU OF STANDARDS-1963-A

```
P 162305Z AUG 82
FM USS FIDELITY
TO RUCLBDA/COMINEGRU TWO
RUCBSAA/COMNAVSURFLANT NORFOLK VA
RUCBSAA/CINCLANTFLT NORFOLK VA
RUENAAA/CNO WASHINGTON DC
RUEOALA/NAVSAFECEN NORFOLK VA
RULSSAA/COMNAVSEASYSCOM WASHINGTON DC
RULSSAA/CHNAVMAT WASHINGTON DC
RUEBBSA/NSC NORFOLK VA
RUEDNAA/SPCC MECHANICSBURG PA
RUCLFEA/MOTU TWELVE
INFO RULSSAA/COMNAVELEXSYSCOM WASHINGTON DC
BT
MSGID/CASREP/MSO443FIDELITY/4//
POSIT/8204W4-2443N3/161500ZAUG82//
CASUALTY/INITIAL-82004/AN-URT-23V HF TRANSMITTER/EIC:QEIN/CAT:2//
ESTIMATE/252359ZAUG82/RECEIPT OF PARTS NLT 24AUG82//
ASSIST/TECHNICAL/PORT EVERGLADES FL//
AMPN/REQUEST ASSISTANCE FROM MOTU TWELVE MAYPORT//
RMKS/SHIPS SCHEDULE: 16AUG-19AUG OPEVAL KEYWEST OPAREA. 20AUG-23SEP
OPEVAL FT. LAUDERDALE FL//
RMKS/SHIP WILL BE IN PORT EVERGLADES IN THE EVENINGS AND ON
WEEKENDS UNTIL 23SEP.//
PARTSID/APL:58557823CL/CID:1A1A3/JCN:N07973-OE06-7545//
TECHPU/NAVELEX 0967-LP-879-50X10//
1PARTS
/DL NATIONAL STOCK NO.   RQD   COSAL   ONBD   CIRCUIT
/8$&1H5820-00-988-8033   001   000     000    1A1A3
/02 1H5820-00-988-3043   001   000     000    1A1A6//
AMPN/REASON ITEM NOT ONBOARD - NO ALLOWANCE. ALL PARTS LISTED
IN PARTSID APL//
1STRIP
/DL DOCUMENT ID   QTY  PRI  RDD  ACTIVITY REQUISITION STATUS
/01 V07973-2228-W542  001   06   236   NNZ 162300Z AUG82
/02 V07973-2228-W543  001   06   236   NNZ 162300Z AUG82
RMKS/APC-PPC CIRCUIT IS INHIBITING EXCITER AND PA DRIVER IN ALL
OPERATE MODES. RADIO SET WILL TUNE USING TUNE KEY, LOCAL KEY
AND REMOTE KEY. DRIVER AND PA CURRENTS GOOD DURING TUNING.
IN OPERATE MODES DRIVER CURRENT AND RF POWER OUT ARE ZERO,
AS IS INPUT TO PA. APC-PPC VOLTAGES TO T-827 IF STAGE IS
IN EXCESS OF 10 VOLTS. PPC IS NOT ADJUSTABLE. APC CAN BE
ADJUSTED TO 8 VOLTS MIN. WHICH ALLOWS EXCITER TO OVERDRIVE
IN TUNE. SYSTEM KEYLINE APPEARS GOOD IN THAT ALL ESSENTIAL
RELAYS SWITCH WHEN KEYED AND COUPLER CONTROLLER STANDBY
LIGHT GOES OUT. PA CURRENT OK WHEN SYSTEM IS KEYED IN
OPERATE MODE.//
```

Fig. 4 — An example CASREP

COMM	ASSIST	FUNC	INVEST	ORG	PART	PROCESS	REPAIR	SIGNAL	STATUS
REQUEST									
	ASSISTANCE			MOTU					
					CIRCUIT				
INHIBIT					DRIVER				
AND					CIRCUIT				
INHIBIT					DRIVER				
					SET	TUNE			
WHILE		USE			KEY				
		USE			KEY				
AND		USE			KEY				
								CURRENT	GOOD
AND									
								CURRENT	GOOD
								CURRENT	UNITS
AS								INPUT	UNITS
AND								POWER-OUT	UNITS
AS								INPUT	UNITS
								VOLTAGE	
								PPC	ADJUSTABLE
					KEYLINE				GOOD
IN-THAT					RELAY	SWITCH			
WHEN					RELAY	KEY			
AND					STANDBY-LI				GO
								CURRENT	OK
WHEN					SYSTEM	KEY			

Fig. 5 — An information format table

tionships generally used within the equipment failures domain to derive a tabular representation of the information in the message narrative. The automatic information formatting procedure involves three stages of processing: parsing, syntactic regularization, and mapping into the information format which is in tabular form. The configuration of the table is initially determined by performing a distributional analysis of the language used in a sample set of CASREPs. The rows of the table correspond to the clauses or assertions in the message, and the columns of the table correspond to the semantic classes associated with the words in the assertions. Figure 5 shows an information format table that was automatically derived from our example message in the last stage of processing. To illustrate the procedure, the last sentence of Fig. 4, *PA CURRENT OK WHEN SYSTEM IS KEYED IN OPERATE MODE*, appears in the last three lines of the table. A production rule system, written in the OPS5 programming language, then interprets the information in the tables and performs dissemination and summary generation.

Natural Language Analysis: In the information formatting procedure, the text sentences are first parsed using the broad-coverage Linguistic String Project English grammar [2], extended to handle sentence fragments and other constructions that are common in the Navy equipment failures domain (for example, date expressions *NLT 292300 Z SEP 82*). The output of parsing the sentence *DRIVER CURRENT AND RF POWER OUT ARE ZERO, AS IS INPUT TO PA* is a sentence tree, shown in Fig. 6. This tree is input to a syntactic regularization component, which regularizes the parse tree by a series of transformations to simplify the subsequent mapping into the information format table. For example, various types of clauses—such as passives, sentence fragments, and relative clauses— are transformed into simple active assertions, and variant spellings and abbreviations are replaced by their standard forms. The regularized version of our example sentence would be a tree corresponding to *DRIVER CURRENT BE ZERO AS INPUT TO PA BE ZERO AND RF POWER OUT BE ZERO AS INPUT TO PA BE ZERO.*

The regularized parse trees serve as input to a procedure that strips off connectives and prefixes them to their clausal arguments. Each argument is mapped into a separate format row, and the phrases of the argument are mapped into the format columns associated with their semantic category. For example, in Fig. 5, *AS* and *AND* are mapped into the connective column. *CURRENT* is a signal word, so the phrase *DRIVER CURRENT* is mapped into the signal column. The word *DRIVER* does not show up in Fig. 5, although it is available in the table, because it did not fit on our display screen. *ZERO* has become *ZERO UNITS*, and the phrase with its head *UNIT* is mapped into the status column because numerical values of signals indicate a status.

Distribution: The dissemination system derives the information needed for its decisions from both the *pro forma* fields of the CASREP (such as MSO443FIDELITY from the MSGID line) and the information table derived from the narrative fields. Dissemination decisions depend primarily on the particular type of equipment that failed (for example, propulsion systems and radar), on data about the ship that filed the CASREP (for example, name, class, and fuel type), and on data specifying the type of assistance that is necessary to correct a problem. This last data set may include narrative amplification.

Summary Procedure: The second application program generates a one-line summary describing the equipment malfunction from the narrative content of the CASREP. In summarizing a message, it is necessary to gain knowledge about linguistic relations, about the domain of discourse, and about the user's goals for the summary. For our example message, the summary is *APC-PPC CIRCUIT BAD.*

A comparison of computer-generated summaries with those obtained manually showed good agreement, indicating that it is possible to process message narrative automatically and to generate appropriate, and ultimately useful, summaries.

```
SENTENCE
   |
CENTER------ENDMARK
   |          |
ASSERTION
   |
SA---SUBJECT---VERB---OBJECT-----SA
   |    |        |       |         |
PN   NSTG     VVAR    OBJECTBE   CSSTG
   |    |        |       |         |
     LNR       TV     OBJBE     SUB8
   |    |        |       |         |
            ARE    NSTG     CS8---Q-INVERT
   |    |                |       |    |
                        *1*     AS   VERB1---SUBJECT
   |    |                                |       |       |
     LN-----NVAR---ANDSTG          LTVR   NSTG
   |    |     |        |                |       |
     NPOS   N    'AND'---Q-CONJ    TV    LNR
   |    |     |                |        |       |
     NNN   CURRENT       LN-----NVAR IS   NVAR---RN
   |    |                   |     |        |       |
     N                    NPOS  N       N     RNP
   |    |                   |     |        |       |
     DRIVER               NNN  POWER---OUT INPUT  PN
P----NSTGO                 |                        |
   |    |                   N                P----NSTGO
IN   NSTG                  |                   |       |
   |    |                   RF               TO    NSTG
     LNR                                              |
   |                                                LNR
     LN-----NVAR                                      |
   |    |     |                                     NVAR
     VPOS   N                                         |
   |    |                                            N
     V    MODES                                       |
   |                                                 PA
     OPERATE
```

Fig. 6 — A parse tree

References

1. N. Sager, "Natural Language Information Formatting: The Automatic Conversion of Texts to a Structured Data Base," in *Advances in Computers*, M.C. Yovits, ed. (Academic Press, NY, 1978), Vol. 17, pp. 89-162.

2. N. Sager, *Natural Language Information Processing* (Addison-Wesley, Reading, MA, 1981). ∎

How to Specify Software

J. McLean
Information Technology Division

Computer software is too expensive and too often incorrect. Even correct software produced at a reasonable cost is expensive to change. These problems often are caused by software specifications that are ambiguous, impossible to rigorously reason, or overly implementation-oriented. To reduce these problems, the software specification project has produced a formal, abstract specification language and has applied it to the specification of a submarine communication system, a military message system, and several communication protocols.

Specification Language: The specification language is an extension of first-order logic, a language originally developed to formalize mathematics. This extension has a rigorous syntax, semantics, and computer-checkable derivation system that is both sound and complete. Hence, an assertion about program behavior is

derivable from a specification if and only if the assertion is true in every implementation that models the specification.

Example — Consider a procedure, MAXREM, that takes an array as a parameter and returns the same array with a maximal element deleted. Letting V give the return value of a procedure call, a specification of MAXREM would contain the following assertion:

$$V(MAXREM(a)) = b \rightarrow (Ei)(j)(a[i] \geqslant a[j] \ \&$$

$$b[i] = 0 \ \& \ (i \neq j \rightarrow a[j] = b[j])).$$

By using the formal semantics and derivation system developed by the specification project, this specification can be interpreted unambiguously and can be subjected to rigorous validation techniques to prove such properties as specification consistency and completeness. Because such specifications are unambiguous, they reduce programming errors that are caused by misunderstanding. The programmer sees exactly what is meant by the word "delete" in this particular case, *viz.* change to 0. Hence, MAXREM([1,2,3,4,5]) would return [1,2,3,4,0] and not [1,2,3,4]. Because our specification language detects errors such as inconsistency and incompleteness early in the software development process, we can correct them more cheaply, in fact for roughly 1.3% of the cost to correct them after the software development is complete.

Implementation Independence: Being abstract, the specification language relieves programmers from gleaning specification essentials from a mass of extraneous implementation clutter. This reduces unnecessary module coupling in which one program's correct operation depends on the implementation details of another program—details which are likely to change over time. The result should be software that is more likely to be correct and that has independent modules which are relatively easy to understand and change.

Dependent Example — Consider a different formal specification of MAXREM that uses programming pseudocode instead of the specification language we advocate.

```
index := 1
do i = 2 to 5
```

if array[i] > array[index] then index := i
array[index] := 0
return([array])

This specification is formal, but it is too implementation oriented. In the original specification, it is clear that when presented with the array [1,2,5,4,5] a program can correctly return either [1,2,0,4,5] or [1,2,5,4,0]. However, the pseudocode program returns only the former. A programmer presented with this specification must decide for himself whether an implementation that returns the latter is correct as well. If he decides that it is, and a programmer writing a module that uses MAXREM decides that it isn't, the resulting software system won't work. It would be even worse if the original system were based on the assumption that only [1,2,0,4,5] were correct, and subsequently a system maintainer changed the system in a way that violated this assumption years hence. The software would suddenly fail to work, and it would be extremely difficult to determine why.

Independent Example — If such problems plague the specification of a software procedure as trivial as MAXREM, one can imagine the problems faced in specifying a system containing hundreds of complicated procedures that must interact with each other. What makes matters even worse is that not all procedures in such a system return values that allow them to be specified directly. In such cases, the specification method described here maintains formality and abstractness by specifying the procedures' behavior in terms of each other.

As an example, consider two programs, ADD and RETURN, such that ADD takes an integer and adds it to a bag, and RETURN returns the maximum integer from the bag. We would specify the two programs by describing the return values of all legal sequences of procedure calls that end with a call to RETURN. By using dots to form sequences of procedure calls and L to denote those sequences that are legal, the specification would contain the following assertions:

1. L(T) → (L(T.ADD(x)) & L(T.ADD(x).RETURN))
2. V(ADD(x).RETURN) = x
3. V(T.RETURN)>x → V(T.ADD(x).RETURN)
= V(T.RETURN)

99

4. $V(T.RETURN) \leqslant x \rightarrow V(T.ADD(x).RETURN) = x$
5. $L(T.ADD(x).RETURN) \rightarrow V(T.ADD(x).RETURN)$
$= V(T.ADD(x).RETURN.RETURN)$

Since ADD does not return any parameters, it is specified indirectly by describing how it interacts with RETURN. This allows us to specify ADD completely without having to give the type of implementation details that plagued the pseudocode specification of MAXREM.

Program Verification: We are extending the language's syntax, semantics, and derivation system to express and derive local effects of individual program statements. The extended language will be used to specify program language semantics and to prove programs correct in a computer-checkable way. The result will be a unified, formal framework into which software specification, programming language semantics, and program correctness proofs all fit. Hence, software development can be rigorously tracked from specification through implementation. Applications for such a framework include computer security and defense software whose correctness is vital to national interest.

Automatic Implementation: The specification language also serves as a foundation for a software support system that will contain a query system to enable programmers to clarify specification requirements, a rapid prototyping system to automatically generate software from specifications, and software to automatically prove specifications complete and consistent. This project uses artificial intelligence, theorem-proving techniques to derive program behavior from specifications. Hence, the computer will appear to the user as an inference-making machine rather than a machine that merely carries out detailed instructions. Eventually, automatic generation of software from an abstract specification may replace traditional programming completely, freeing humans to decide what computer programs should do and not how they must do it.

[Sponsored by ONR]

Reference

1. J. McLean, "A Formal Method for the Abstract Specification of Software," *Journal of the ACM* 31, 600-627 (1984). ∎

Tracker/Correlator Algorithm Testing

K. Askin
Information Technology Division

Introduction: NRL is testing and evaluating tracker/correlator (T/C) algorithms to provide technical guidelines to developers and to study trends in T/C requirements and related technology. Operating on sensor reports that are usually unidentified, T/C algorithms generate target tracks for many types of users, ranging from manual or automated weapon systems to various intelligence communities. In ocean surveillance systems that consist of sensors, communication lines, controls, resource management systems, and users, the T/C algorithms provide an essential service.

Tracking refers to the process of generating a picture of target movement in space, while taking into account sensor errors, dynamics governing target motion, and assumptions about the motion intended, such as straight course and maneuvering. Using the theory of stochastic processes in the modeling of target motion, one obtains stochastic differential equations. The solutions of these equations give good estimates of past and future motion and statistical confidence levels of these estimates.

The Major Problem: The major problem currently with T/C algorithms is the large number of them. In early 1970 there were around 300 algorithms. The current number is probably much greater; however, the number of different approaches used in these algorithms is believed to be much smaller. To stop costly duplication of effort and to guide research, NAVELEX established the Naval Tracker Correlator Technology Base (NTCTB) program at NRL in the late 1970s.

NRL's Contributions: One of the first accomplishments of the NTCTB program was to publish the 1978 and 1979 editions of the *Naval Ocean Surveillance Handbook.* Subsequently, NRL efforts, jointly with the Naval Ocean Systems Center (NOSC), concentrated on developing a test-bed capability to quantitatively test and

evaluate algorithms. The test bed, called the Ocean Surveillance Tracker Correlator (OSTC), depicts the operation of an Ocean Surveillance Information System (OSIS) node with and without an operator. In 1982, NRL evaluated two electronic intelligence (ELINT) algorithms: the Naval ELINT Analyst Tool (NEAT) and the Target Evaluation and Recognition by Extraction of Statistical Attributes (TERESA). NRL recommended that the best features of both T/C algorithms be combined resulting in the present Developmental Unified ELINT Tracker (DUET) project which has an implementation date of mid-1985.

Researchers at NRL stress-tested TERESA by varying its operator-set parameters over a wide range of values. During these tests, NRL suggested corrections to the algorithm along with recommendations on how the corrections might be accomplished [1]. NRL has been asked recently to test the improved version of TERESA being installed in DUET.

NRL scientists have also been involved in soft decision and distribution-free algorithms and have constructed a common test data base.

Soft Decision Algorithm—Most T/C algorithms are "hard" decision algorithms; that is, once a decision to associate a report to a particular track is made, this decision cannot be changed based on subsequent information. "Soft" decision algorithms have the flexibility to create alternate outcomes and to continue updating these outcomes with new reports (within resource limitations of the computer). A valuable feature of such algorithms is the ability to use all the information available for a commander by creating and maintaining all alternate outcomes. NRL tested a proprietary algorithm of the latter type, called Integrated Sensor And Tracking System (ISATS), developed by Science Applications Inc. Initially, this algorithm required excessively long runtimes, but subsequently this problem was corrected [2].

Distribution-free Algorithms—Since most statistical algorithms—for example, TERESA—make strong assumptions regarding the statistical distributions of data, an evaluation of distribution-free algorithms led to the investigation of cluster techniques. Cluster techniques are used in detecting separations between subsets (cluster) of a given point set in a metric space governed by a distance function $\rho(x,y)$. Promising approaches using decision-free and pattern recognition techniques were uncovered at NRL for algorithms with or without an operator in the decision loop.

Common Test Data Base—Scientists at NRL identified the need to have a common test data base for evaluating T/C algorithms early in their development cycle. The data base constructed for the ELINT Capability Analysis Project (ECAP) effort was a hybrid, made up of real ELINT parameters and simulated ground-truth tracks. This data-base capability is now being expanded to include Electromagnetic Control (EMCON) policies, decoy-deception practices, and multiple-emitter platforms. This new capability will be used in testing the DUET algorithm.

Future: Since T/C algorithms are critical components of any surveillance system, they need to be tested properly and evaluated to determine if they meet operational needs. Testing and evaluation of these algorithms requires multidisciplinary research skills, primarily in mathematics, statistics, and computer science and also requires an in-depth understanding of the operational needs and constraints of present and future naval surveillance systems. NRL is in a unique position to supply these skills and understanding to advance successfully the Navy's T/C program.

[Sponsored by NAVELEX]

References

1. K. Askin et al., "Measures of Performance as Applied to NEAT and TERESA Algorithms," NRL Report 8826, June 1984.

2. K. Askin et al., "ISATS Testing Using ECAP II Data," (NRL Report, in progress). ∎

Full Engagement Decoy Simulator

H.R. Bryant and G.H. Galloway
Tactical Electronic Warfare Division

The Full Engagement Decoy Simulation (FEDS), a digital software package, is an analytic

101

tool for determining decoy effectiveness, for setting performance specifications for decoy design, and for developing tactics for decoy deployment. This program has been developed on the VAX-11/780 in Fortran 77, and uses a proprietary graphics package, DISSPLA, to aid in analyzing output. NRL has developed FEDS under the Effectiveness of Navy Electronic Warfare Systems (ENEWS) Program to model the electronic countermeasure (ECM) effects during a missile attack against ECM-responsive ships.

Scope of FEDS Simulation: FEDS allows for a broad range of simulation situations. The missile models developed for FEDS allow simultaneous simulation of as many as 300 missiles, primarily for probabilisitic (Monte Carlo) studies of the effects of variations in the active environment. These missiles may all be the same type or a mixture of types. Several missile models are available: sea skimmers (cruise); midrange, midaltitude; and long-range, high-altitude missiles. Missile models either represent real missiles or generic types. FEDS can simulate missiles with markedly different acquisition and tracking logic in the same simulated engagement. FEDS also allows variation in parameters such as turn-on time, turn-on range, and attack angle.

Similarly, FEDS can simulate a variety of different decoys and ECM systems. FEDS can simulate all U.S. Navy chaff decoys used for ship defense for which the launching characteristics and radar cross sections are well-known. Several foreign systems as well as active decoys have also been simulated. Barrage jammers (jammers covering a broad frequency spectrum), ship-launched electronic decoys (SLED), and counter-ARM (antiradiation missile) decoys (CADS) are examples of active decoys that have been or are to be simulated. A total of 100 targets can be simulated at one time. Thus, FEDS can be used to analyze both offensive and defensive systems.

Environment Definition: The engagement situation which is simulated by FEDS can be developed by either of two methods. The first method is through the run-time generation. A collection of missiles with different attack axes, turn-on times, and turn-on ranges can be generated from a single prototype for each missile

type. The combination of missiles simulated varies from simulation to simulation and allows for simulation of future missile types with different logic and parameters. This method is ideal for the development of decoy deployment tactics and performance specifications. The second method is by selection of specific missiles from an existing set of complex engagement scenarios developed by the Evaluation of Navy Electronic Warfare Systems (ENEWS) group using the Simulation of Total Electronic Warfare Systems (STEWS) techniques. Scenarios covering the mid-East, the Baltic, and other geographical regions are available. The simulation model can also be used to determine the effectiveness of electronic countermeasures (ECM) in a complex engagement as well as the secondary effects on the electronic environment.

General Purpose of Decoy Simulation: FEDS simulation allows for the determination of the decoy effectiveness against the defined missile attack configuration. Initially, all missiles are determined to impact the primary target without ECM, then with ECM. As a result, effectiveness of the particular decoy deployment against the missiles is measured as the percentage of missiles which do not impact this target when ECM is employed. Relative effectiveness against a range of different missiles can be determined for a given decoy deployment strategy. Alternatively, the comparative effectiveness for a series of decoy deployment strategies against a single missile can be determined. Analysis generally involves a large number of separate simulations in which several decoy deployment strategies are evaluated against several missile types.

Uses: FEDS has been used in several instances to further the development of the Navy's decoy capability. The model was used to develop deployment strategies for the SEA GNAT hybrid distraction round—a shell containing both infrared and radar-frequency materials. Also, performance specifications have been developed through FEDS simulation for the SEA GNAT RF distraction decoy. Comparison simulations have been made using Super Rapid Bloom Offboard Chaff (SRBOC), DAGAIE (French chaff system), and seduction and distraction SEA

GNAT. Additional simulations have been made for air-launched chaff (AIRBOC), barrage jammers, and active repeaters (SLED). Future systems development of U. S. Navy decoys will be supported by this simulation tool.

[Sponsored by NAVELEX]   ∎

Acoustic systems and technology

Ice roughness as depicted at this location (30 miles from the North Pole) is present both above and below the ice and causes sound attenuation in long-range underwater propagation

ACOUSTIC SYSTEMS

Acoustics in the ocean environment has been of crucial importance to the Navy for many years. The advanced research at NRL described here covers propagation, scattering, transducer development and testing, acoustic properties of matter, and improved test methods. The work described here was performed by the Acoustics Division (Code 5100) and the Underwater Sound Reference Detachment at Orlando, Florida (Code 5900).

Many other basic and applied research projects in acoustics are being performed by the Laboratory. A few of these concern:

- basic propagation theory
- environmental assessments of large ocean areas and of the Arctic
- active sonar technology
- acoustic target physics
- rough surface scattering
- advanced spectral estimation
- acoustooptic technology

Modeling Long-range Arctic Acoustic Propagation

S.C. Wales and O.I. Diachok
Acoustics Division

The Under-Ice Model: Long-range sound propagation in the Arctic is characterized by upward refraction (a consequence of the oceanic vertical sound velocity profile) and repeated reflection from the ice canopy. One of the significant features of the ice canopy is the presence of randomly distributed, randomly oriented ice-pressure ridges. These ridges have keels that extend down to 50 m, but more typically, extend to about 5 m. Their mean spacing (about 100 m) and depth cause virtually the entire ice surface to lie in the geometrical shadow region of the keels for grazing angles less than about 4°. Figure 1 illustrates an idealization of the under-ice surface, proposed by Diachok [1] who reduced the under-ice surface to a pressure-released plane punctuated with randomly spaced, identical, parallel elliptic half-cylinders that have a constant spatial density of ridges. The depth and half-width of the cylinders are given respectively by the variables d and w. Together with the number of ridges per meter, n, these variables define the reflection characteristics of the surface.
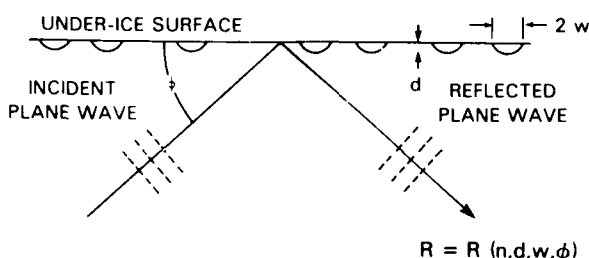
Fig. 1 — Geometry of under-ice reflectivity

A theory by Burke and Twersky (BT) [2] provides a means for calculating reflectivity and scattering from a surface of randomly placed protuberances such as the simplified Diachok surface. This basic theory requires the scattering function of an individual (arbitrarily shaped) protuberance. Its principal limitation is that it neglects interaction between scatterers, implying that scatterers must be far apart. BT provide solutions for a number of cases including randomly spaced, elliptically striated surfaces for which they developed both the exact and approximate, low- and high-frequency expressions. A plane acoustic wave incident on this surface suffers a reflection loss that is a function of n, w, d, ϕ (grazing angle), and k (wave number). This theory also permits calculation of the incoherently scattered energy.

Data Results and Analysis: We incorporated the asymptotic BT predictions into a wave-theoretical, long-range propagation model, the FFP, as an impedance at the ocean surface. This enables computation of under-ice transmission loss at high and low frequencies. In Fig. 2 we compare transmission-loss data with calculations that include BT reflection loss, but no scattered energy, at 20 and 200 Hz. The comparison between the predictions (curves) and the data (solid circles) is excellent. Independent calculations indicate that the incoherent scattering predicted by the model at low frequencies is essentially dipolar in nature and only slightly skewed in the forward direction, suggesting that negligible incoherent energy is scattered into the small grazing angle region (< 15°) required for long-range propagation of coherent waves. At high frequencies, however, this radiation pattern evolves into a narrow peak centered along the propagation direction implying that high-frequency incoherently scattered energy should be included in theoretical computations. Such computations, however, are consistent with data if the incoherent energy is disregarded. Incorporation of randomly oriented ridges and out-of-plane scattering is expected to resolve this inconsistency.

Measurements of the spatial coherence at a range of 220 km between two hydrophones
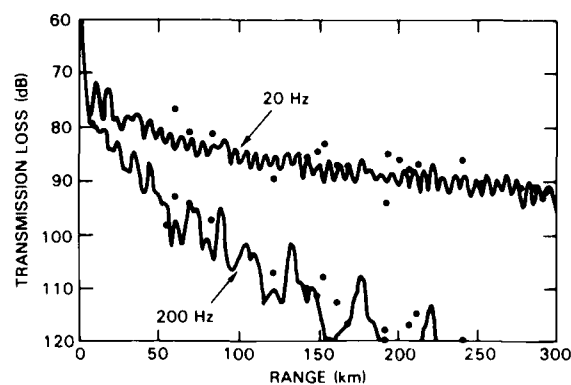
Fig. 2 — Predicted (curves) and measured (solid circles) transmission loss

separated by 1000 m, made by DiNapoli et al. [3], are shown in Fig. 3 as solid circles. The solid curve is a calculation of the coherence loss for a hydrophone spacing of 1000 m, C(1000), direction due to scattering by random inhomogeneities in the ocean volume according to an experimentally validated theory developed by Beran and McCoy [4]. The excellent fit to the data suggests that ice-induced coherence loss at low frequencies must be small.
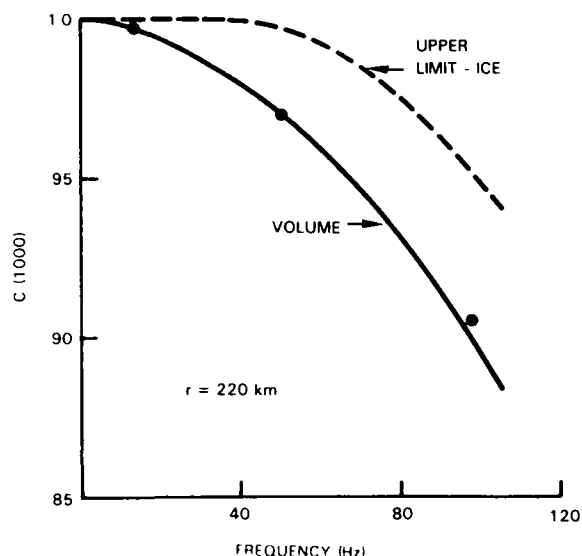
Fig. 3 — Measured (solid circles) and predicted horizontal coherence at a 220-km range. The agreement with the volume-induced prediction implies no ice-induced coherence loss at low frequencies.

Predictions based on the propagation model incorporating the Diachok-Burke-Twersky theory of under-ice scattering (parallel ridges, no out of plane scattering) are, despite its simplifying assumptions, in accord with this hypothesis. The dashed curve represents the upper bound on ice-induced coherence loss in this frequency range.

Ongoing Work: At low frequencies, we feel that the sound-ice interaction problem is reasonably well understood. The model is consistent with both propagation and spatial coherence-loss data. Ice-ridge scattered low-frequency energy is redirected to higher angles and into the bottom, away from the forward propagation direction; the neglect of this scattering by the model appears to be appropriate. At high frequencies, our propaga-

tion model is consistent with transmission-loss data only if the incoherent forward scattered energy is assumed negligible. The BT model's prediction that substantial incoherent energy is scattered into the direction of propagation, however, suggests that this assumption may not be appropriate. Present work is centered on resolving this inconsistency through theoretical refinements that include out-of-plane scattering from randomly oriented depth-distributed ridges using the exact theory, laboratory scale ultrasonic model investigations, and Arctic field experiments.

[Sponsored by ONR]

References

1. O.I. Diachok, "Sound Propagation Under Ice Ridges," *J. Acoust. Soc. Am.* **59**(5), 1110-1120 (1976).

2. J.E. Burke and V. Twersky, "Scattering and Reflection by Elliptically Striated Surfaces," *J. Acoust. Soc. Am.* **40**(4), 883-895 (1966).

3. F.R. DiNapoli, R. Nielson, D. Potter, and P.L. Stocklin, "TRISTEN/FRAM IV CW Spatial Coherence and Temporal Stability," NUSC Technical Document 7095, Naval Underwater Systems Center, New London, Conn., 1983.

4. M.J. Beran and J.J. McCoy, "Propagation Through An Anisotropic Random Medium," *J. Math. Phys.* **15**(11), 1901-1912 (1974). ■

Frequency Dependent Modal Excitation and Attenuation in Shallow Water

D.A. Gershfeld
Acoustics Division

Broadband acoustic propagation loss measurements in shallow water with a fixed source-receiver geometry frequently show that a certain frequency will propagate with less attenuation than others in a frequency band. Thus, for a given set of fixed physical and environmental parameters, an optimum frequency of propagation usually exists. There are three competing frequency dependent effects that govern the signal field: the modal excitation, the acoustic absorption mechanisms in the ocean and sediment

layers, and the degree of modal interaction within each layer. While the existence of an optimum propagation frequency in shallow water has been known for some time, a general characterization of the effect has been difficult due to the multiplicity of environmental variables that must be considered. In addition, measurements of the optimum frequency appear to vary widely even in similar environments.

Model: At NRL, we developed a normal-mode acoustic propagation model to study this optimum frequency effect. The model is analytical; this keeps the large number of calculations manageable and allows the scientists to isolate and evaluate the importance of the physical mechanisms responsible for the occurrence of the optimum frequency. The model consists of a semi-infinite half-space of two fluid layers to represent a three-dimensional shallow water acoustic duct with azimuthal symmetry. The upper layer represents the ocean and is characterized by a constant density and sound-speed. The ocean layer is bounded above by a pressure release (free) surface and contains a high-frequency acoustic absorption mechanism (primarily due to the ionic relaxation of oceanic magnesium sulfate) which is proportional to the square of the source frequency f^2. The lower layer models a homogeneous sediment and is also characterized by a constant density and sound-speed. In the sediment layer, compressional and shear acoustic waves are absorbed at a rate proportional to f, while the degree of modal interaction within this layer is proportional to $1/f^3$ which combine to yield a modal attenuation proportional to $1/f^2$. Hence, the sediment layer contains the primary low-frequency acoustic attenuation mechanisms.

The combined low- and high-frequency attenuation mechanisms then produce a minimum in the modal attenuation which increases with sediment absorption and mode number. The acoustic signal field is represented by a sum over the allowed normal modes in the duct. Each term in the sum has an excitation factor proportional to $1/f$ and is multiplied by an attenuating exponential which is uniquely determined by the receiver range, mode number, sediment type, water depth, and source frequency.

Results: The calculations show that the optimum frequency is strongly dependent upon the depths and separation distance of the source-receiver pair. The high spatial variability in the optimum frequency of propagation is due to the competing mechanisms of the preferential excitation and reception of certain waveguide modes as a function of the source-receiver geometry, and the modal attenuation rates as a function of range, mode number, sediment type, and frequency. Two sample calculations illustrate these effects.

Middepth Transducers — Figure 4 illustrates the typical behavior of the optimum frequency when both source and receiver are located near the central portion of the water column. Then the first waveguide mode dominates the acoustic field at all ranges because both the source and receiver are located near the antinode of the first mode. The optimum frequency increases with range until it finally approaches an asymptotic value. This effect was also found in the experimental data and is the result of the competition between a $1/f$ modal excitation factor and the frequency-range dependent modal attenuation. Near the source, the modal excitation is important. As the separation distance between the
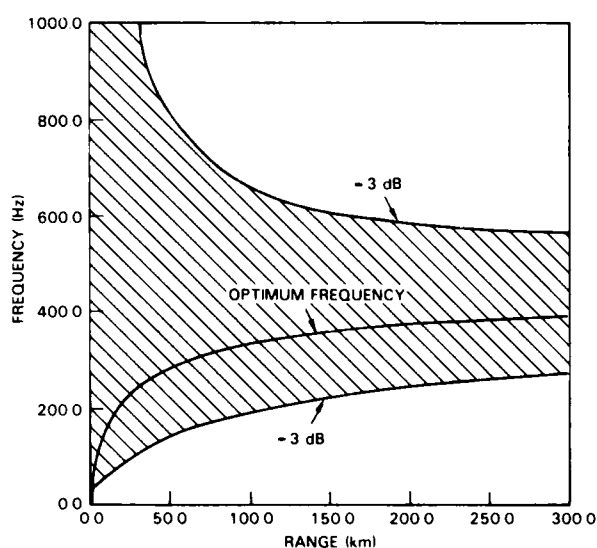
Fig. 4 — The optimum frequency and 3 dB frequency bandwidth curves above and below it for silt sediment with both source and receiver at middepth (50 m). This illustrates the asymptotic behavior of the optimum frequency, a single-mode effect.

source and receiver increases, the modal attenuation becomes dominant, until at long ranges the optimum frequency is determined solely by the minimum in the modal attenuation. An asymptotic expression for calculating the optimum frequency at long ranges was derived which is a function of the water depth and the sediment type.

Non-middepth Transducers — When the experimental geometry is such that either the source or receiver (or both) are located away from the central portion of the water column, then higher order modes dominate the acoustic field near the source. For these conditions, the typical range-dependent behavior of the optimum frequency is illustrated in Fig. 5. Close to the source, the optimum frequency increases with range due to the competition between the higher order modal excitation factors and the minima in the modal attenuations (which increase with mode number). As the range continues to increase past 50 km, the lower order modes begin to dominate the acoustic field (the minima in their modal attenuations occur at lower frequencies) and the optimum frequency decreases until only the first mode is left.
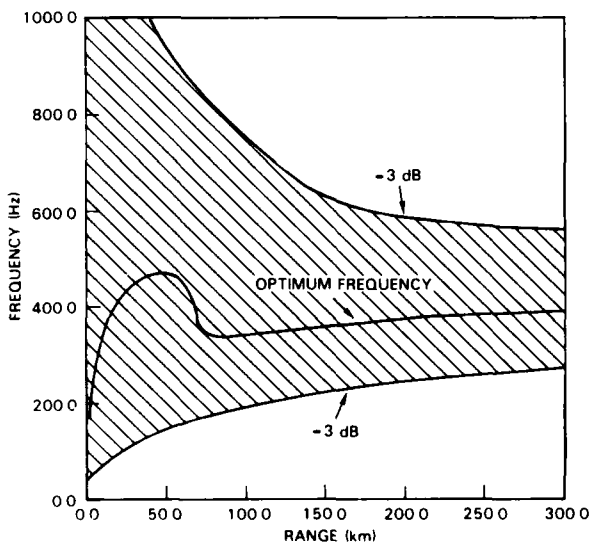
The results of this work are of interest in studying broadband propagation in continental shelf waters. The optimum frequency effect can be exploited to optimize the design of low-frequency underwater acoustic communication systems. In addition, this work suggests a remote sensing method for characterizing bottom properties by making broadband propagation loss measurements.

[Sponsored by ONR] ∎

Scattering from Rigid Bodies of Arbitrary Shape

C.F. Gaumond and A.G. Dallas
Acoustics Division

Solutions to acoustic scattering problems are computed by many methods. For special geometric shapes, such as spheres and infinite cylinders, the solution can be easily expanded in an infinite series of normal modes. Such infinite series solutions can be manipulated algebraically to provide approximate formulas to examine their functional dependence on various parameters. For example, if the scattered field is desired in the long wavelength limit, the terms in the series expansion can be approximated, and the resulting series summed to any specified degree of accuracy. This kind of solution is different from those obtained via implicit methods which are given as algorithms, such as iterative or discretization techniques for solving integral equations, Galerkin procedures, and direct methods in the calculus of variations [1]. These latter procedures yield the approximate numerical solution after a sequence of operations. However, it is not always possible to derive approximate qualitative formulas or examine parametric behavior from these implicit solutions. The solution described in this article—valid for any body of smooth shape—is not an implicit one, but rather one that can be written as an infinite series of terms, each term being computable independently of higher order terms, thus allowing the examination of parametric behavior of the solution. It is anticipated that this solution will prove to be as adaptable and useful as the separation-of-variable solutions available for simple geometric shapes. This

Fig. 5 — The optimum frequency as a function of range for a source at 20-m depth and a receiver at 50-m depth in 100-m-deep ocean. The multi-modal effect occurs at ranges less than 75 km. Beyond 75 km, only the first mode is left, and the familiar single-mode effect occurs.

new result also has desirable properties for direct computations: neither integrals with singular integrands nor potentially ill-behaved matrix inversions are required.

The Method: This new "orthonormalization method" has been developed for scattering from rigid, elastic, and shell-like bodies. An outline of the rigid body solution will show the differences between this technique and other methods.

In nearly all scattering problems, the total acoustic field is written as the sum of a known incident wave and an unknown scattered wave. The scattered field can be represented by a Helmholtz integral which relates the pressure on the surface, p, and the normal gradient of the pressure, $p_{,\nu}$, to the scattered pressure field everywhere. The rigid-body boundary condition requires that the fluid not move normally to the surface S of the scatterer, yielding the value of the normal pressure gradient on the surface in terms of the known normal gradient of the incident field $p_{\text{inc},\nu}$:

$$p_{,\nu}(y) = -p_{\text{inc},\nu}(y), \quad y \text{ on } S. \qquad (1)$$

With the normal gradient determined in Eq. (1), the pressure on the surface must be determined to compute the scattered pressure everywhere using the Helmholtz integral. This orthonormalization method uses elementary Hilbert space techniques to find the pressure on the surface. Taking the usual integral over the surface S as the inner product, the collection of functions which are square integrable over the surface defines the Hilbert space. The outgoing spherical wave functions span this space and can therefore be used to describe any function in the space. The outgoing spherical wave functions are usually written with double subscripts:

$$v_{lm}(r,\theta,\phi) = h_l(kr)P_l^m(\cos\theta)e^{im\phi}, \qquad (2)$$

where h_l is the spherical Hankel function of the first kind and order l and P_l^m is the associated Legendre function of degree l and order m. These doubly subscripted functions can be ordered into a singly indexed sequence in any convenient manner, and their conjugated normal derivatives orthonormalized using the Gram-Schmidt method, producing an orthonormal basis $(w_{n,\nu})$. Since each of the outgoing spherical wave

functions satisfies the wave equation outside the scattering body as well as the Sommerfeld radiation condition, the following integral relations can be used to determine the coefficients in the generalized Fourier series expansion of the scattered pressure field:

$$\int_S \{p\bar{w}_{n,\nu} + p_{\text{inc},\nu}\bar{w}_n\}dS = 0, \quad n = 1,2,\dots. \quad (3)$$

The use of orthonormalization and Eq. (3) is the central feature of the present method. When actual computations are carried out, the infinite series expansion must be truncated, creating an error in the computed value of the scattered field. However, this error can be estimated by taking the normal derivative of the series expansion on the surface of the scatterer and comparing the approximate normal gradient with the known value in Eq. (1).

Comparison with Other Methods: We first implemented this method with a rigid prolate ellipsoid, since its shape can be varied from that of a sphere to a slender finite body. This same scattering problem has also been solved using the separation-of-variables technique, allowing us to compare our computed results with published values. When the ellipsoid degenerates to a sphere, the resulting series expansion is identical to the separation-of-variables solution, since the set of spherical wave functions is already orthogonal over that surface. When the prolate ellipsoid is elongated, the computations become more involved. The integrals required for the Gram-Schmidt process and in Eq. (2) contain integrands which oscillate, the oscillations increasing as the expansion subscript increases; this makes higher-order terms more difficult to compute. In spite of this difficulty, computations for the normalized cross section were carried out. Figure 6 shows the agreement of our computations (points) with a published separation-of-variables solution (curve) [2].

In the future we shall investigate the behavior of this method in scattering from elastic shapes and shell structures. We expect that computationally beneficial approximations and acceleration techniques can be developed for this method as they have been for the separation-of-variables method.

111
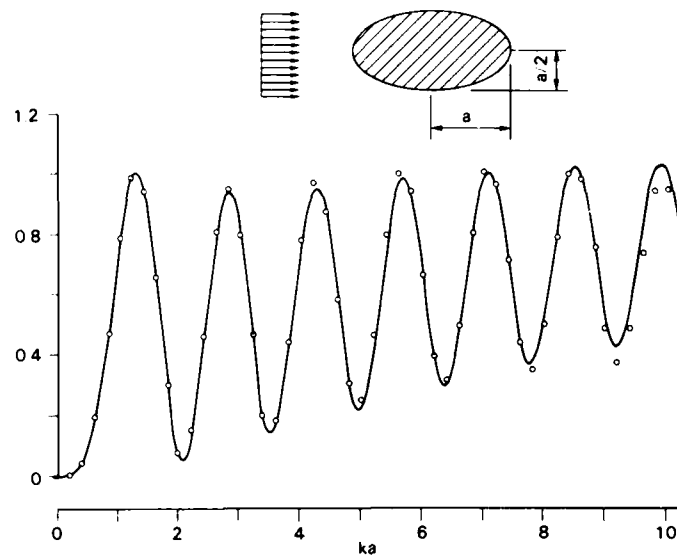
Fig. 6 — The backscattering cross section of a rigid 2:1 prolate ellipsoid under axial incidence. This cross section is normalized relative to the geometrical acoustics cross section. It is graphed as a function of the frequency parameter ka, and is computed by two methods: the curve is taken from [2], while the points were found by our orthonormalization method.

The work described was carried out at NRL while the second-named author (A.G.D.) was employed by Sachs/Freeman Associates, Bowie, MD.

[Sponsored by ONR]

References

1. H. Huang, "Submarine Acoustic Scattering and Radiation," *1982 NRL Review*, p. 64.

2. T.B.A. Senior, "The Scattering from Acoustically Hard and Soft Prolate Spheriods for Axial Incidence," *Can. J. Phys.* **44**, 655 (1966). ∎

Porous Ceramic Loss Mechanism

K.M. Rittenmyer and R.Y. Ting
Underwater Sound Reference Detachment

One of the important properties required of a transduction material for underwater acoustic applications is its piezoelectric response in the hydrostatic mode. This quality of the material may be characterized by a parameter called the hydrostatic piezoelectric voltage coefficient g_h. This coefficient is defined as the electric field in a piezoelectric material when exposed to a unit hydrostatic pressure.

Solid vs Porous PZT: Materials such as barium titanate and lead-zirconate-titanate (PZT) are used for conventional transducers even though they exhibit rather low values of g_h and therefore are not the most ideal materials for use in Navy's electroacoustic transducers. Recent studies [1,2] sponsored by the Office of Naval Research have shown that the introduction of a high degree of porosity in the PZT ceramic greatly increases its g_h-value, potentially improving it as a transduction material (also see p. 167). This increase in g_h-value is achieved by both lowering the material's dielectric constant and by reducing its Poisson's ratio to mechanically decouple the lateral strain. Commercial porous-PZT samples have recently become available for hydrophone development. Since this material's g_h-value is more than an order of magnitude greater than that of a conventional PZT, we designed and tested the free-field voltage sensitivity of a prototype hydrophone (Fig. 7) made of
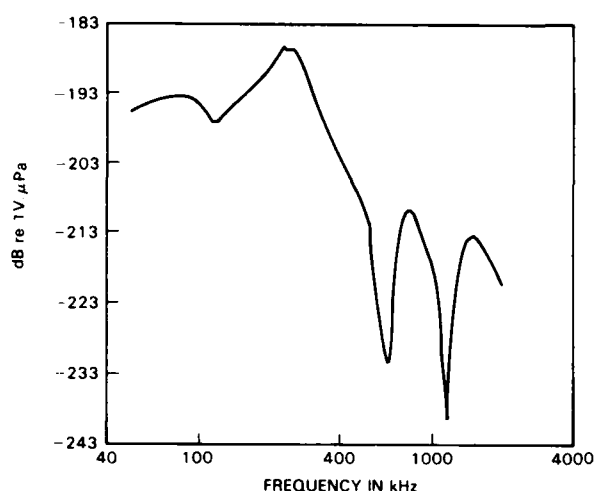
Fig. 7 — Free-field voltage sensitivity of a porous ceramic hydrophone showing sharp decrease in sensitivity above 200 kHz

Fig. 8 — Calculated strain amplitude of a ceramic disk in water under the influence of an acoustically generated stress (porous PZT, ————; solid PZT, - - - - -)

porous PZT. Below the frequency of 200 kHz, the sensitivity of porous PZT is much higher than that of a similar design with solid PZT and is quite constant up to this frequency. As the frequency increases above 200 kHz, however, the sensitivity decreases sharply.

Model of Porous PZT: This behavior of the porous ceramic hydrophone was modeled by considering the amplitude of strain of a ceramic disk in water. The strain in the disk was calculated as a function of the frequency of the stress wave in the ceramic produced by an acoustic wave impinging on the disk at normal incidence. The result showed that the calculated strain-vs-frequency relationship for porous PZT (solid curve, Fig. 8) was similar to that shown in Fig. 7 in terms of the resonant frequencies and the magnitude of amplitude reduction above the initial resonance. This agreement is considered a validation of the model. Since the model is characterized by the density and the elastic moduli of the ceramic, the loss in the sensitivity of a porous ceramic hydrophone at high frequencies may be explained by the reduced elastic moduli of the porous PZT. To extend the bandwidth of porous ceramic hydrophones, it is therefore necessary to modify the ceramic formulation with a different ceramic mix and processing such that the improved material will exhibit both a high elastic stiffness and a high percentage of

porosity to obtain a very high g_h over the extended bandwidth.

[Sponsored by ONR]

References

1. R.E. Newnham, D.P. Skinner, and L.E. Cross, "Conductivity in Piezoelectric-Pyroelectric Composites," *Materials Res. Bull.* **13**, 525 (1978).

2. K.M. Rittenmyer, T. Shrout, W.A. Schutze, and R.E. Newnham, "Piezoelectric 3-3 Composites," *Ferroelectrics* **41**, 189 (1982).

Glass Ceramics for Sonar Transducers

R.Y. Ting
Underwater Sound Reference Detachment

Lead-zirconate-titanate (PZT) ceramics are used almost exclusively in Navy sonar transducers. These conventional transducer ceramics suffer several shortcomings. The values of their hydrostatic piezoelectric constants are relatively low, and the dielectric constants are very high, thus producing less than ideal sensitivities. The PZT also exhibits serious depoling or aging problems. It is therefore desirable to develop new transduction materials that offer improved sensitivity and aging characteristics. Recent   113

approaches include PZT-polymer composites, porous PZT, optical fibers, and most notably piezoelectric polymers.

Polar Glass Ceramic Transducers: A new family of materials called polar glass ceramics has been studied for pyroelectric applications at Pennsylvania State University under the support of the Office of Naval Research. Glass ceramics containing the crystalline phases of Li_2 Si O_3, Li_2 Si_2 O_5, Ba_2 Ti Si_2 O_8, Ba_2 Ti Ge_2 O_8, and Li_2 B_4 O_7 were shown to exhibit large pyroelectric sensitivities comparable to those of respective single crystals, yet large pieces of the materials can be made much more easily and at a much lower cost. These characteristics, combined with a low dielectric constant (in the range of 10 to 20), make polar glass ceramics very attractive for piezoelectric application in sonar transducers. Furthermore, since the crystalline phase is permanently developed in the recrystallization process during sample preparation, the material will not dipole, therefore will not age. Potentially, this property can completely alleviate the problems of PZT aging in sonar transducers.

Polar Ceramic Properties: The piezoelectric and dielectric properties of glass ceramic samples with grain-oriented Ba_2 Ti Si_2 O_8 crystallites were measured at the Underwater Sound Reference Detachment (USRD). The samples were fabricated at Penn State University by preparing the glasses of compositions in the BaO-TiO_2-SiO_2 system. The glass specimen was carefully polished and then placed in a well-controlled temperature gradient for recrystallization. The amount of crystalline phase in the samples was controlled by the exposure time in the temperature field. Figure 9 compares the electric field generated per unit applied pressure for several samples. The glass ceramic sample (BST composite) has a nearly constant g_h value of 83 × 10^{-3} Vm/N (volt/meter per Newton/meter^2), which is an improvement by nearly two orders of magnitude over that of a PZT-5 (a conventional PZT) sample. It is also comparable to those values for the state-of-the-art vinylidene fluoride polymers (PVF$_2$). Most interestingly, the g_h value of glass ceramics was found to be independent of pressure up to 35 MPa, whereas PVF$_2$ samples showed a reduction of about 0.5 dB over such a pressure range.

Hydrophone Performance: The hydrophone characteristics of the BST glass ceramics were also investigated by using them as a single element in a standard USRD H23 oil-filled hydrophone assembly. Figure 10 shows the free-field voltage sensitivity of this prototype design. A sensitivity of −207 dB referenced to 1 V/μPa was measured over the frequency range of 100 Hz to 40 kHz; the response was constant. This fre-
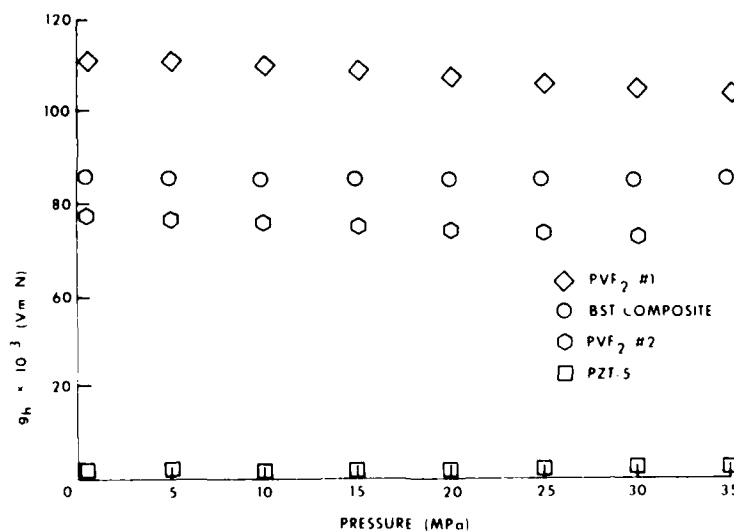
Fig. 9 — Hydrostatic g-constant of glass ceramic compared with PVF$_2$ and PZT-5 as a function of pressure
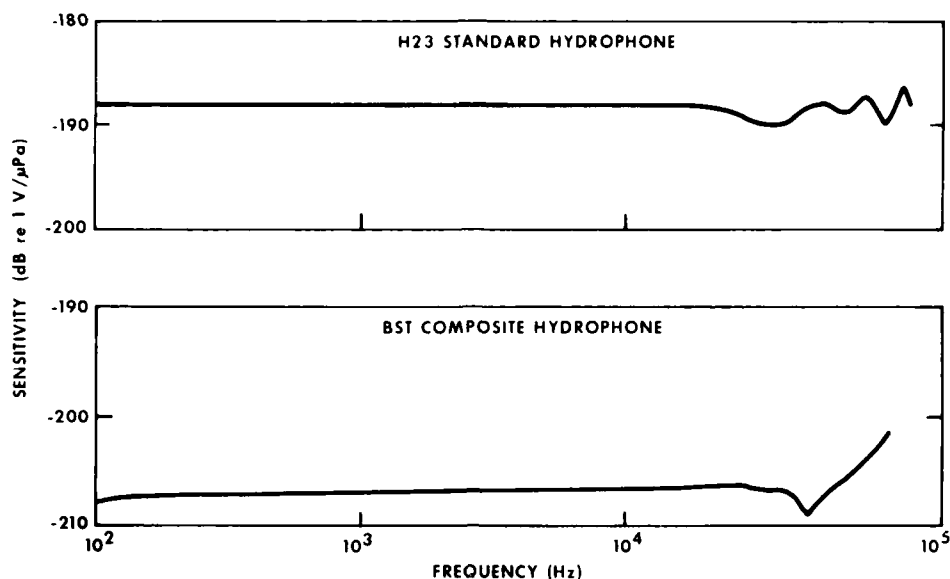
Fig. 10 — Comparison of sensitivity response of glass ceramic hydrophone
with standard H23 hydrophone

quency response is compared with that of a standard H23 hydrophone containing eight lithium sulfate elements. The comparison is quite favorable. In terms of the g_h value, the glass ceramics (83×10^{-3} Vm/N) are approaching the lithium sulfate crystal (148×10^{-3} Vm/N). This crystal has been used in underwater transducers and remains the favorite piezoelectric material for use in many of the Navy's standard transducers.

The availability of lithium sulfate from commercial sources has declined rapidly in recent years; however, the glass ceramics would be an excellent candidate as a replacement.

[Sponsored by ONR] ■

Dynamic Bulk Modulus Measurement

P.S. Dubbelday and Jean C. Piquette
Underwater Sound Reference Detachment

Relevance: The proper operation of equipment designed for production and reception of sound in the sea is intimately tied to the acoustic properties of the materials used in the construction of these devices. The concern with acousti-

cal properties does not stop there; shielding of the equipment against seawater should not interfere with sound propagation, whereas other coverings are used to increase "inaudibility" of the vessel, either by absorbing incoming sound or by muffling the noise produced by engines and motion through the water.

The speed of sound is a function of the elasticity and density of the acoustic medium; in liquids the elasticity is measured by the compressibility, defined as the volume decrease of a unit volume relative to the pressure increase of the surrounding medium. The bulk modulus is the inverse of the compressibility. In solids a second elastic modulus, the shear modulus, is a measure of the resistance of the material to a shearing force. In this article, dynamic applies to the measurement of the modulus for a periodic pressure variation; this is appropriate for acoustic measurements. Rubber-like materials, or elastomers, convert part of the acoustic energy into heat. This acoustic loss is part of the measured dynamic modulus. For sound absorption one wants to maximize this effect, but for acoustic transparency the acoustic loss is deleterious.

There is relatively little work done on bulk modulus measurement; usually one infers its value from other acoustic or mechanical methods, 115

such as in the *1984 NRL Review*, p. 117. Two methods used at the Underwater Sound Reference Detachment (USRD) will be described.

First Measurement Method: In the first method of measuring the bulk modulus the sample is enclosed inside an acoustic coupler (Fig. 11) filled with castor oil, together with two spherical piezoelectric transducers. One transducer acts as an acoustic driver under an impressed voltage; the other, acting as a hydrophone, senses the varying pressure field and generates a voltage. The lock-in analyzer isolates the proper signal against a noise background. The ratio of the impressed voltage on the driver to the hydrophone voltage is a function of the dynamic bulk modulus of the sample. The magnitude and phase of the hydrophone voltage signal are shown on the x-y plotter as a function of the frequency sweep produced by the oscillator. This method is an adaptation of the one developed at the National Bureau of Standards. It is applied to materials considered for use in Navy systems.
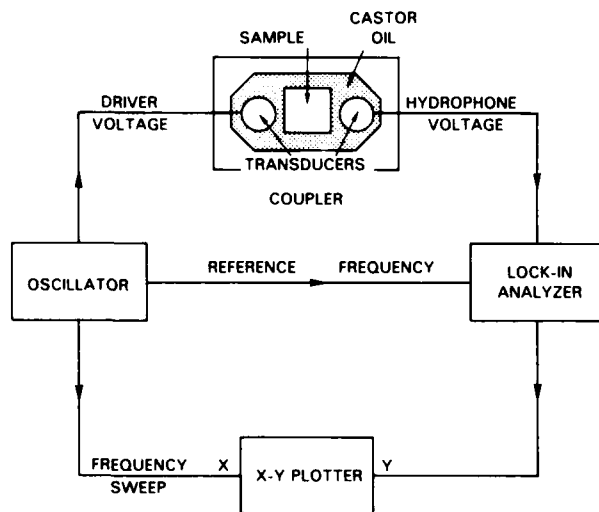
Fig. 11 — Experimental arrangement of acoustic coupler

The coupler can be pressurized and cooled to simulate the environmental conditions of the deep ocean. The samples are also soaked in seawater for prolonged periods, and their properties are measured at regular intervals to study the effect of aging in the presence of seawater.

A dozen elastomers are involved in the measurement program. The bulk moduli are determined in the frequency range from 100 to 3000 Hz and at temperatures varying from 0° to 30°C. The bulk moduli are comparable to those of liquids, varying from 2 to 5 MPa.

Second Method: This method, conceived and developed at the USRD, is quite different in principle and appearance from the first. An obstacle placed in a plane sound wave scatters part of the sound in all directions. The angular distribution of the intensity of these scattered waves for a given shape of an obstacle is a function of the elastic properties of the obstacle material. By the so-called inverse scattering technique [1] the value of the dynamic bulk modulus is deduced from the measured angular distribution. We have performed the measurements in the USRD Lake Facility at frequencies of 5, 10, and 15 kHz. Figure 12 shows how the receiving hydrophone may be rotated about the spherical scatterer to obtain the angular distribution of intensity. The sound speed derived from this method is in good agree- *ment with that obtained from the more tradi-* tional impedance-tube measurements, which were done at NRL-USRD.

Fluid-Saturated Foamed Aluminum: The coupler filled with castor oil has been used to measure the properties of foamed aluminum as a damping material in a liquid. The damping effect of porous materials on sound in air is well known and widely applied; it is due to the friction between the acoustically driven airflow in the pores and the solid material. Foamed materials in liquids behave in a similar manner, but for liquid immersion they must be more rigid than those used in air. One particularly interesting material is foamed aluminum (Fig. 13), which promises to be a good damping material for liquids. We used the coupler method to measure the apparent dynamic bulk modulus of two foamed aluminum cylinders, one with pore size of 0.64 mm and relative density of 14%, the other with pore size of 1.3 mm and relative density of 10% [2]. The castor oil of the coupler fills the open-pore structure. We performed the measurements as a function of frequency, pressure, and temperature— the latter strongly influences the viscosity of the

116
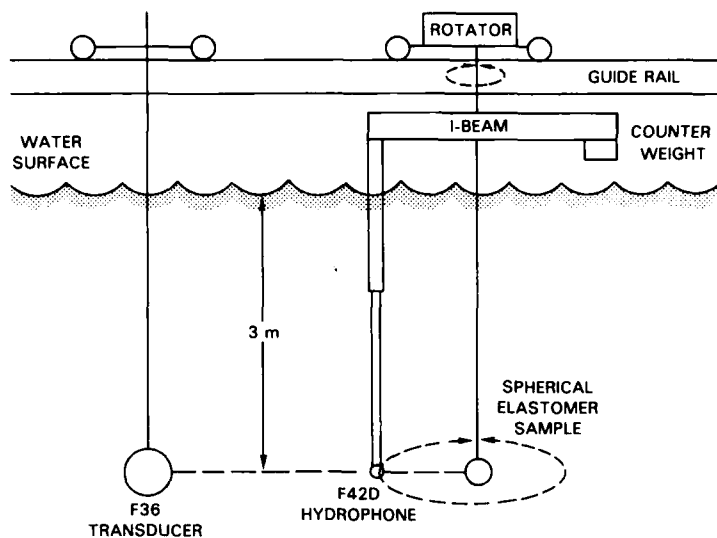
Fig. 12 — Implementation of inverse scattering technique
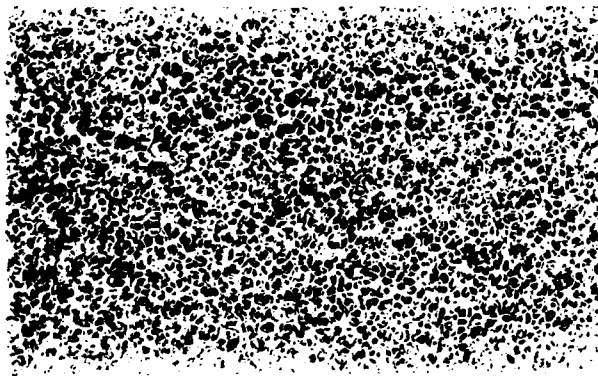
Fig. 13 — Foamed aluminum

oil. Since a detailed description of the liquid flow through the random pores is difficult, a model of a sample consisting of parallel capillaries is considered to understand the dynamics of the castor-oil-filled foam. The foamed aluminum's damping effect is an order of magnitude larger than the theoretical results for the capillary sample. It will be attempted in the future to explain this observation theoretically. Saturated foamed aluminum shows potential for use in hydrophones because it combines large mechanical strength with good sound absorption.

Future Work: This measurement program continues for existing elastomers and others synthesized to satisfy special requirements in fleet applications. The data base of measurements made at the USRD is the basis for theoretical analysis, which in turn will guide the development of new materials. We intend to expand the measurements on saturated foamed aluminum and start applying it to acoustic devices.

[Sponsored by ONR]

References

1. J.C. Piquette, "Determination of the Complex Dynamic Bulk Modulus of Elastomers by Inverse Scattering," *J. Acoust. Soc. Am.* (in press).

2. P.S. Dubbelday, "Complex Bulk Modulus Measurement of Fluid-Saturated Porous Aluminum," *J. Acoust. Soc. Am.* **76** Supplement 1, 1984, S83. ■

Extrapolation of Thick-Panel Reflection Measurements

Jean C. Piquette
Underwater Sound Reference Detachment

The underwater acoustic behavior of elastomeric coating materials as a function of frequency, temperature, and pressure is often evaluated in the Anechoic Tank Facility in Orlando, Florida, by performing a reflection 117

Fig. 14 — Typical multiple-layer panel showing incident and reflected waveforms. The reflected waveform measured with interference present (————) is schematically compared to the interference-free reflected waveform obtained by extrapolation of leading "clean" portion of the measured waveform (- - -).

MULTIPLE-LAYER PANEL OF COATING MATERIAL

INCIDENT WAVEFORM

REFLECTED WAVEFORM
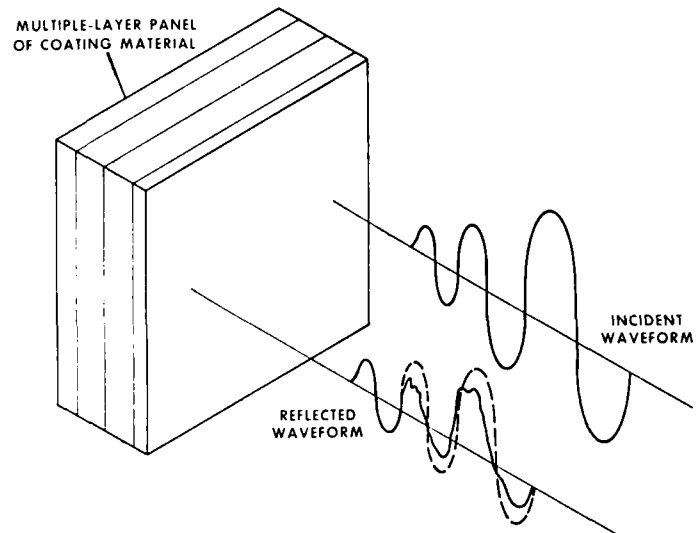
measurement on a finite rectangular sample panel (Fig. 14), even though the acoustic behavior of a sample of infinite area is desired. In practice, finite can mean sample dimensions less than one acoustic wavelength in the surrounding fluid. The primary difficulty associated with using a panel of finite size is the interfering influence of the diffracted wave originating at the sample edges that "contaminates" the reflected signal.

Traditional Method: The traditional approach to eliminate the interfering effects of edge diffraction is to transmit a short acoustic pulse to the test sample. This pulse is reflected by the front, back, and internal surfaces in the sample and is diffracted by its edges. Because the reflected wave travels a shorter path length than the edge-diffracted wave, the initial contributions to the experimentally observed return signal contain no information from the sample edges. As the frequency is lowered and the sample thickness is increased, however, the uncontaminated portion of the reflected waveform decreases (relative to a steady-state wavelength) and may not accurately represent the steady-state reflected wave (Fig. 14).

New Technique: I developed a procedure to extrapolate the early uncontaminated portion of the reflected signal from the total return. The extrapolation is achieved by an iterative technique that requires a least-squares fitting of the experimental data to a multiple-layer model of the test

panel. The multiple-layer theory, including loss, was developed by Shau and Bugl [1]. The model I selected to represent a typical acoustic panel treats the sound speed in each layer as constant, but treats the loss in each layer as frequency dependent.

To initiate the extrapolation technique, only the thickness and density of each panel layer need be accurately known. In addition, an approximate (within a factor of two) sound speed for each layer is all that is required. This information about the physical properties of each panel layer is used to divide the experimental reflection data into "arrival epochs." Each epoch contains information about an individual panel layer. The time boundaries of each epoch are established based on the thickness and approximate sound speed required *a priori*. The reflection data contained in each epoch can be used to determine starting values for the sound speed and the loss of each layer that are sufficiently accurate to allow convergence of the iterative least-squares process. The least-squares algorithm yields material properties that are most consistent (in a least-squares sense) with the experimental data. These material properties are then substituted into the multiple-layer theory to predict steady-state sample performance.

Demonstration of New Technique: I demonstrated the technique experimentally by extrapolating measurements made on a simple multiple-layer panel. The sample consisted of a

118
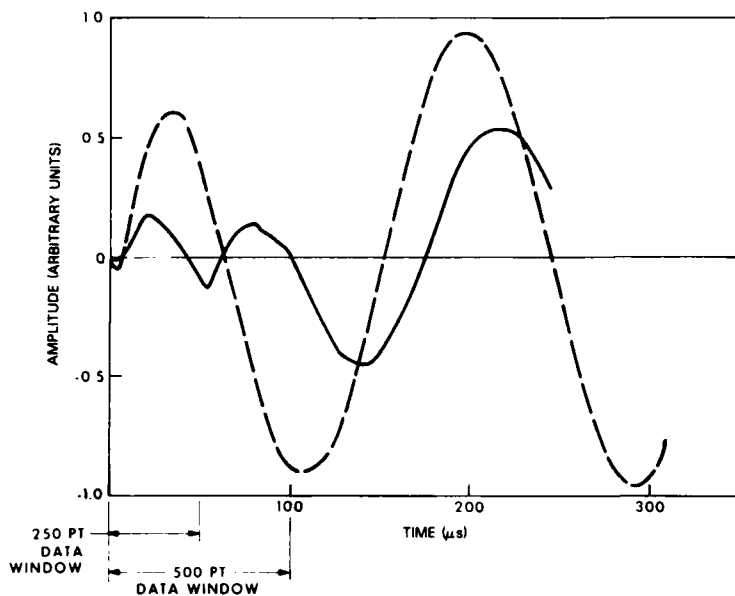
Fig. 15 — Experimental waveforms obtained for a simple three-layer panel. The measured incident waveform (- - -) is compared to the measured reflected waveform (———).

0.025-m-thick plexiglass layer, backed by a 0.013-m-thick steel plate. The steel plate was offset from the plexiglass by 0.025 m. When the panel was immersed in water, the offset region flooded freely and effectively created a three-layer panel. The sample was square, 0.76 m on a side. The acoustic evaluation was performed using a 5-kHz test pulse of approximately 300-μs duration.

Figure 15 presents experimental waveforms. The dashed line represents the incident pulse, and the solid line represents the reflected pulse. In this test, I chose the pulse length to avoid edge diffraction. Note that extrapolation would not actually be required if the amount of data presented in Fig. 2 were available in a measurement of interest. However, the effectiveness of the procedure can be evaluated with this data by performing an extrapolation on a short portion of the initial return signal and by comparing this extrapolation with the directly observed latter portion of the return signal. The significance of this comparison is that one sees directly how well the extrapolation would work if the early portion of the return signal were all that were experimentally measurable under interference-free conditions. Such would be the case for a sample with a smaller cross section than that used here, or for the same sample at a lower frequency. Figure 15 shows that two "data windows" were applied to the data: One window had a time width of 100

μs and contained 500 data points; the second had a time width of 50 μs and contained 250 data points. The extrapolation procedure was applied to the reflection data contained in each of these data windows, and the extrapolated steady-state performance was compared to the observed reflected signal at a time late in the reflected pulse (corresponding to approximately 210 μs. From this, I determined the panel's reflection coefficient. The predicted reflection coefficient based on the 500-point data window was in error by approximately 1.6%; that based on the 250-point data window was in error by approximately 7.1%.

Future measurements are anticipated on panels of more complicated design. I expect that this technique will extend the panel measurement capability of the Anechoic Tank Facility to a considerably lower frequency than is presently possible. In addition, the maximum panel thickness for which the acoustic behavior can be accurately determined will be substantially increased.

[Sponsored by NAVSEA]

Reference

1. R.P.S. Shau and P. Bugl, "Transmission of Plane Waves Through Layered Viscoelastic Media," *J. Acoust. Soc. Am.* **46**, 649-654 (1968).

■ 119

Electromagnetic sensing and systems

NRL's 85-foot
radio telescope,
located at Maryland
Point, Maryland,
is used to conduct
basic research in
radio astronomy

ELECTROMAGNETIC SENSING

Virtually all remote sensing relies on the detection, measurement, and processing of the emission or reflection of electromagnetic radiation. This chapter describes studies of radar and infrared signatures of ships and natural sources and a specialized radar technology developed at NRL. The divisions involved in this research are Radar (Code 5300) and Space Systems and Technology (Code 7700).

NRL has many other radar and electromagnetic sensing projects. Some of these are:

- shipboard and air surveillance radar
- target and cluster scattering
- electronic counter countermeasures (ECCM)
- intermodulation sideband suppression
- Navy remote ocean sensing system (NROSS)

Time-Domain Radar Interference Rejection

B.R. Jarrett
Radar Division

Radars on surface ships in close proximity can encounter serious mutual-interference problems, particularly when operating in the same frequency band where frequency-domain filtering is not effective. NRL has developed a time-domain technique which enables a radar to reject interference at all frequencies by discriminating against other signals that have different pulse repetition frequencies (PRFs).

Background: Any scheme to reject interference must discriminate on the basis of some parameter such as frequency, time of arrival, direction of arrival, signal strength, waveform, or polarization and degrades when the interfering signal begins to assume the dimension of the return signal in the discrimination parameter. For example, a system that eliminates interference on the basis of direction of arrival is not able to reject interference that arrives in the same direction as the main beam, a system that uses frequency is not able to block out interference at the radar's frequency, and a system that uses time of arrival is not able to suppress interference occurring at the radar's PRF. Nevertheless, these limitations can be overcome in some cases. For example, the frequency or the PRF of the radar to be protected from interference by frequency or PRF discrimination can be "jittered" to ensure that another emitter does not have the same frequency or PRF. However, from a systems standpoint, it is relatively easy to jitter the PRF, but quite difficult to jitter the frequency. Radars of the same (or different) type seldom operate at exactly the same PRF. Hence, PRF discrimination systems naturally work very well without PRF jittering.

Time-Domain Signal Processor (TDSP): The TDSP is a new technique, developed for the AN/SPS-10 radar, which eliminates pulsed interference from other radars or other sources. For consecutive radar sweeps, it selects the smaller of two returns from the same spatial location. The PRF of the transmitting radar is used to align return signals from the same location in consecutive sweeps. If another radar with an identical PRF to the transmitting radar is operating in the same frequency band, interference occurs which the TDSP cannot reject, since their PRF synchronization produces signals indistinguishable as a function of PRF. To overcome this situation, the transmitting radar's PRF is jittered.

To implement the TDSP, fast, large-capacity random access memory is essential. Many radars have pulsewidths of about 1 μs or less with corresponding video bandwidths of several megahertz. The AN/SPS-10 radar with selectable pulsewidths of 1.25 μs and 0.25 μs, is typical. A memory capacity large enough to store an entire sweep of digitized video is required (all returns from each pulse emitted). Only very recently have large-capacity, random-access memory chips fast enough for this application (<100 ns read/modify write) become available. Small, economical analog-to-digital converters, capable of the required conversion rate ($\sim$ 10 MHz), are also recent introductions. Thus, from an implementation standpoint, what would have been considered totally impractical just a few years ago has become reality.

Advantages: The TDSP can be modularly retrofitted to eliminate pulsed interference in existing radars. In fact, a TDSP is being developed for the AN/SPS-40 radar.

The technique can be incorporated quite easily in new radar developments, which invariably use digital time-domain signal processing. The development is particularly attractive because of the absence of any requirement for signal detection and because of the simplicity of the rejection algorithm. Previous time-of-arrival rejection systems used some form of signal detection and blanking-on-anticoincidence or electrical path-length matching at the radar or intermediate frequencies. The operational principle of PRF discrimination systems is that consecutive returns from the same spatial location occur at the PRF rate; that is, they are coincident at the PRF rate. It follows, then, that a signal from another emitter at a different PRF will not be coincident at the radar's PRF. Choosing the smaller of consecutive returns from the same spatial location **123**

(a)

(b)

Fig. 1 — Plan Position Indicator showing (a) interference and (b) completely suppressed interference

provides equivalent rejection to blanking-on-anticoincidence and tends to reduce the noise level.

Prototype Performance: We tested the breadboarded TDSP for the AN/SPS-10 radar at the Chesapeake Bay Division (CBD) of NRL and at sea on the USS *HENRY B. WILSON*, DDG-7. At CBD, we ran two different sets of interference tests. The first tests used another AN/SP-10 radar mounted on the roof of the same building as the interference source. The second used a Hewlett-Packard RF signal generator, Model HP-618c. The generator PRF was varied from about 2 to 16 KHz; the pulsewidth from about 2 to 13

μs. In all of these tests, including those at maximum PRF and pulsewidth, the TDSP removed the interference from the radar display. Figure 1 shows photographs of the radar display representative of the CBD tests. Figure 1(a) shows the interference created by the second AN/SPS-10; in Fig. 1(b), the TDSP rejects the interference.

The DDG-7 was selected as a test platform because its two AN/SPG-51 radars, part of the Tarter/Terrier Missile Fire Control System, operate in the same frequency band as the AN/SPS-10 and are known to present an interference problem for AN/SPS-10 operation. In all of the DDG-7 tests, TDSP performance was very impressive. In one case, the crew conducted a 3-hr gun-firing exercise in which the AN/SPG-51 was used. Although the AN/SPS-10 radar was tuned to the AN/SPG-51 frequency, the operators at the AN/SPS-10 display consoles did not see any interference because of the effectivenss of the TDSP. Without the TDSP, an interference problem would have existed.

Our experience is that the TDSP provides a quality of filtering that would be difficult to obtain in any other way, and has these important advantages:

- It is relatively easy to jitter the PRF of the radar, which essentially eliminates the possibility of degradation of the discrimination mechanism.
- It is a digital implementation, which is economical and achieves repeatability and precision.
- A signal detection is not required.

Modeling Radar Scattering From Ships

D.Y. Northam
Tactical Electronic Warfare Division

The Tactical Electronic Warfare Division is developing systems that help protect ships from attack by antiship missiles. Such missiles often employ radar to continuously determine the location of (track) the ship that is the intended target. The radar performs this tracking by transmitting a pulse of electromagnetic (EM) energy that is then scattered by the ship back to the radar. This scattered energy (or scattered EM field) is then

measured and processed by the radar to estimate the ship's location. One of the roles of electronic countermeasures (ECM) is to deny this location information to the radar.

The design and evaluation of such ECM systems requires knowledge of what ships "look like" to radars; that is, what properties of the scattered EM field are perceived by the radar. This knowledge is most usefully expressed as a mathematical model. Ships are structurally very complex and thus produce scattered EM fields that are complex and difficult to describe mathematically. This complexity is analogous to the tremendous amount of information needed to accurately draw a picture of a person's face as opposed to the small amount of information necessary to accurately draw a picture of a ping-pong ball. Because of the complexity of ship structures, an exact mathematical model of the scattering from it is not presently feasible. Fortunately, the performance of many tracking radars can be predicted from knowledge of only two parameters of the complex backscattered EM field. These parameters are radar cross section (RCS) and glint. RCS represents the apparent size of the target, and glint represents the apparent angular location of the target, as sensed by the radar.

Prior Models: Prior models of ship scattering are approximations that range from extremely complex models that describe many aspects of the scattered field, and are difficult and/or expensive to use, to simple models that ignore many aspects, but are easy and/or inexpensive to use. Each model has been developed subject to constraints imposed by specific application requirements. Most of the simple models describe only RCS. This new model was developed to evaluate the performance of continuous tracking, monostatic, pulse radars that operate at microwave frequencies and track only in range and angle (azimuth and elevation).

Scattering from objects is commonly represented as scattering from a point source even though physical objects are three-dimensional and produce scattering from various locations distributed in space. However, a point source is often a good approximation. The existing models were of two basic types. The first type represented the ship as a single point source and assigned to that source appropriate statistical properties (such as density type, mean, variance, and spectrum) that are determined from measured data. The second type represented the ship as a large collection of point sources each representing a specific physical part of the ship. The first type requires measured data on the ships of interest, yields simulations that efficiently generate time series of data, but is not based directly on specific physical parameters of the ship's structure. The second type does require detailed structural data on the ship, is based on physical parameters of the structure, but does not yield simulations that efficiently generate time series of data. The new model we developed is based directly on physical parameters and yields simulations that efficiently generate time series of scattered pulses.

New Model: The new model is based on the observations that complex radar targets appear to most tracking radars as a collection of a few, large, point-source scatterers, which we refer to as unit scatterers (USs). A small, fundamental set of USs have been identified as the generators of the dominant scattering characteristics of ships. To model a given ship, an appropriate subset of these USs is chosen and located to represent the desired ship (analogous to a caricature of a face rather than a photograph). By combining the scattering from each US, the total scattered EM field is obtained. The ship is assumed to be a rigid-body object whose motion is determined by maneuvering and the random motion of the sea surface.

In summary, the model requires, as input, a representation of the desired ship in terms of a few USs (ship structure), information about maneuvering of the ship, and a simple characterization of the surface of the sea (sea state and direction) in which the ship is sailing. The model predicts pulse-to-pulse RCS and glint simultaneously. Simulations based on this model have been run, and the resulting RCS and glint time series have been shown to have statistical properties that are good approximations to those properties of measured data.

[Sponsored by NAVELEX]

Studies of Ship Infrared Signatures

S. Moroz and D. Taylor
Tactical Electronic Warfare Division

The design of systems to protect ships from infrared-guided missile attack requires realistic electronic warfare simulations of tactical combat situations. An important ingredient in these simulations is a series of infrared (IR) images of a ship at sea. NRL is responding to this Navy requirement by applying computer image processing techniques to the IR characteristics of U.S. Navy ships. We start from close-in IR images, where all the features of the ship are evident, and reconstruct ship images at longer ranges, where the ship blends with the background and is not discernable. To do this accurately we must include oceanic and atmospheric effects in the IR image.

Ship and Background Signatures: Unlike a ship viewed with the naked eye, the IR ship signature is dominated by emission from "hot spots" which produce high intensity regions. IR radiation from the sea surface and sky background are also an integral part of the IR image and have their own special characteristics. The sea-surface radiation is a combination of emission from the water and reflection of sky radiation. In addition, wave action creates a random noise-like clutter in the sea-surface background. Atmospheric absorption and emission along the line of sight tend to mask the ship, making it blend with the background. This is especially true at long distances or when viewed against the horizon.

Simulation Technique: Simulating the ship IR signature, and the sea and sky backgrounds, would allow great flexibility in generating image data for the tactical simulations. Unfortunately, the difficulty, complexity, and uncertainties resulting from a pure simulation currently rule out this type of approach. We developed an alternate semiempirical method at NRL to provide IR image data for these simulations. It uses ship signature data collected with an IR imager mounted on one of the NRL P-3 Orion research aircraft. We then perform image processing on the basic data set collected in the field to suit the

scenarios to be studied. The background signatures are separated out, the instrument noise is removed, and the ship signature is modified as we describe below. The final images are all derived from the IR imagery collected in the field.

Image Processing: The images collected in the field are decomposed into segments which represent the actual ship signature, the sea-sky background and data from which atmospheric effects can be extracted. The infrared imager contributes its own unique resolution and noise to the data. These effects have been characterized and incorporated into the image processing techniques applied to the data.

Atmospheric effects are characterized by two parameters; an exponential scale factor describing absorption with path length, and the emission of the atmosphere from an optically thick path length. Ship signatures viewed through this atmospheric model will decrease in contrast with the sky emission until finally blending in completely with the horizon at very long path length.

The IR ship signature is extracted from a selected image which contains the greatest detail of the ship; generally this image is obtained at close range. In this image, and others obtained at greater range, the sea-sky background contribution is separated from the ship signature by applying a simple local threshold to the ship area in the image. Pixels with intensity levels above the threshold are considered ship, and pixels below the threshold are considered part of the background. Although simple, this method is very effective because the ship is almost always a high-intensity, highly localized area in the image.

Measurements of ship signature strength, at various ranges, and IR emission from the sky at the horizon provide enough information to characterize atmospheric absorption and emission present in the data. Once the atmospheric contributions are removed, the basic elements of the imagery can be altered, then reassembled to form realistic IR images of ships at sea.

Ship Image Reconstruction: Recently, we have concentrated on modifying the close range ship signature, by either reducing the intensity of

all or part of the ship, and then projecting that data to long range by applying suitable transformations. We transform the close-range ship signature by scaling the size of the ship to match observed size at long range, perform spatial filtering to blur the detail in the ship signature to the same degree that would occur because of the imager system resolution, and reduce the contrast with the background to account for atmospheric absorption and emission. This new ship signature is finally combined with a background segment containing appropriate noise and clutter. This then constitutes an accurate image of a ship which has been reconstructed from the original data. A series of these reconstructed images representing the ship at various distances are used as input to tactical electronic warfare simulations.

[Sponsored by NAVSEA and NAVELEX] ∎

Microwave Sensing of Sea-Floor Topography

G.R. Valenzuela, W.J. Plant, D.L. Schuler, D.T. Chen, and W.C. Keller
Space Systems and Technology Division

Radar imagery of side-looking airborne radar (SLAR) and synthetic aperture radar (SAR) over shallow water, usually <40 m deep but in some cases deeper than that, contain patterns correlating with the bottom topography (*1982 NRL Review*, p. 43). Since the penetration of microwaves into seawater is negligible, these patterns in radar imagery are caused by processes which relate surface features to the bottom topography. The presence of such surface features is potentially important to a number of Navy programs—ocean surveillance, antisubmarine warfare, and mapping, charting and geodesy—so it is important to understand the processes involved.

Electromagnetic Scattering: The mechanisms responsible for the microwave backscatter from the ocean surface which contribute to radar image formation are well known and have been covered extensively in the literature. They include Bragg and specular scattering, multiple scattering, and wedge diffraction. In effect, the ocean surface behaves very much like an optical grating. The short gravity-capillary waves of length proportional to the radar wavelength (one-half the radar wavelength at grazing incidence) traveling along the line of sight— advected by orbital motion of long waves and currents—are the main backscatterers of the microwave backscatter power (Bragg scattering). For angles of incidence close to nadir, local wave facets, which have large radii of curvature compared to the radar wavelength and which are normal to the radar look, also contribute significant microwave backscatter power (specular scattering). Ocean surface features of horizontal scales much larger than the Bragg wavelength, such as mesoscale eddies and macroscale phenomena, are detectable by radar because they influence the Bragg resonant waves or other scattering elements such as specular points, breaking waves, and turbulent fluid.

Ocean Hydrodynamics: In principle, radar imagery of the ocean due only to surface waves may be predicted with available scattering theory *and hydrodynamics*. However, the physical processes responsible for the generation of surface features related to complex bottom topography in shallow water are not well understood. Therefore, a remote sensing experiment was carried out in July 1982 under the leadership of NRL in collaboration with other laboratories from the U.S. and England. The experiment involved coordinated and near-simultaneous microwave (L- and X-band) and *in situ* measurements which were performed to examine the nature of the microwave backscatter surface signatures generated by topographic features on the sea floor and by current fronts [1]. Subsequent analysis of the data has suggested a mechanism for the generation of surface features related to the bottom topography [2], and work is in progress for its quantitative validation. According to this mechanism, the two-dimensional nonuniform surface current field caused by the interaction of tides with bottom topography modulates the amplitude and wave number of Bragg resonant waves on the surface into distinct surface patterns resembling the bottom features. To first order, the spatial modulation of the energy of the Bragg resonant waves is proportional to bottom slopes **127**
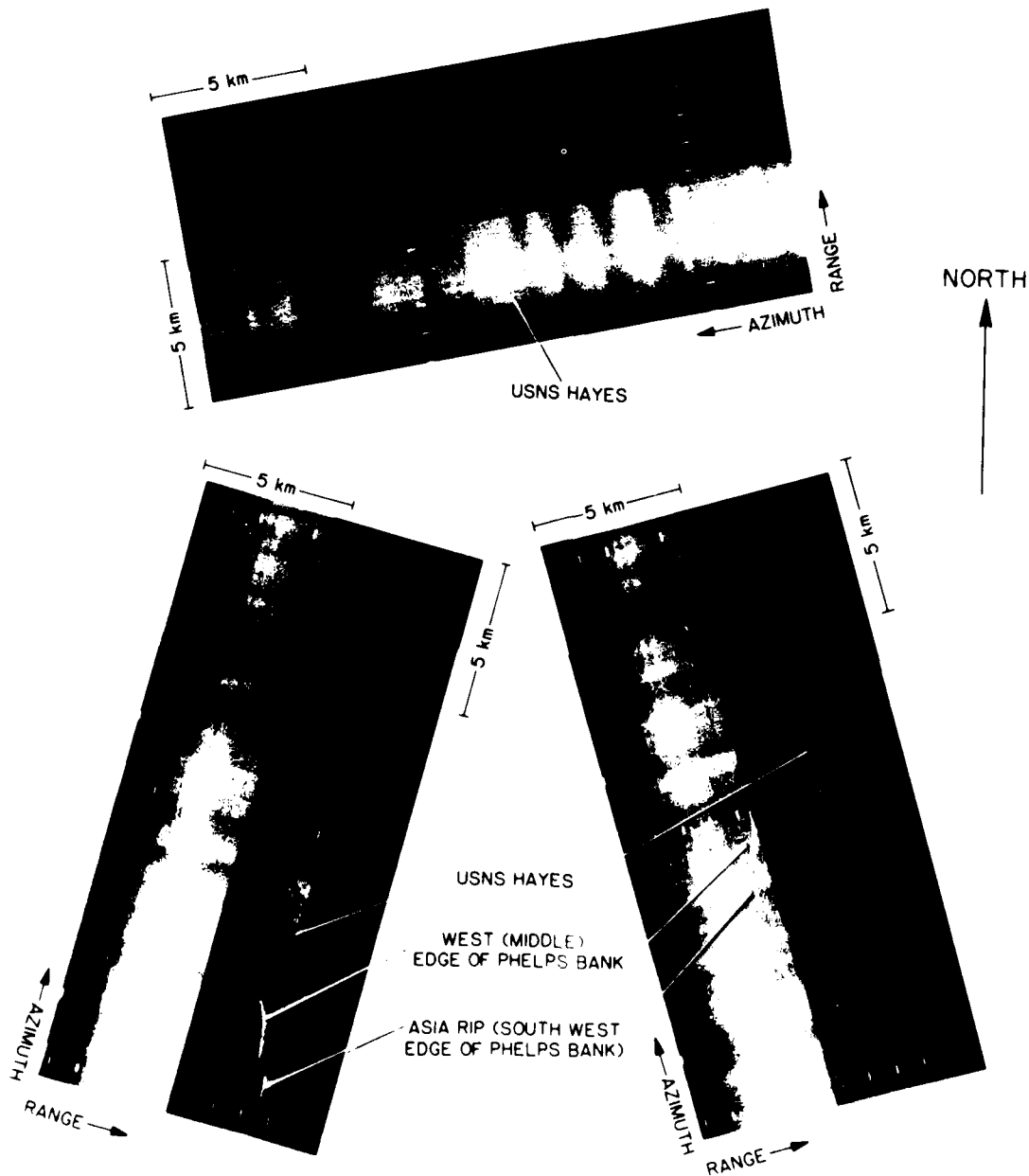
Fig. 2 — X-band APD-10 SAR imagery (portions of subswaths A and B) of Phelps Bank taken within 24 min during July 11, 1982. Phelps Bank is imaged from three different directions at almost constant environmental conditions. USNS Hayes is located at (40° 49.85′N, 69° 19.30′W), and the wind speed was 1.2 to 1.7 m/s from 47° to 93° true.

and inversely proportional to the mean square depth. However, other factors such as wind vector, dominant wave height, stability of the air-sea interface, and current fronts also enhance, mask, or destroy the surface patterns related to the bottom topography.

Experimental Results: Microwave measurements with an X-band APD-10 SAR from U.S. Marine RF-4 aircraft, an X-band radar onboard NRL/RP-3A aircraft, and a shipboard L-band coherent radar show variations in backscatter power >20 dB for winds <7 m/s (meters/second) in locations with pronounced topographic features. Figure 2 shows portions of two subswaths of SAR imagery containing Phelps Bank for three RF-4 passes within 24 min during July 11, 1982. The imagery has been placed in the approximate direction of radar look in relation to true north. Note the strong signatures of the west edge of Phelps Bank (white in the imagery means large backscatter, and darker means less backscatter). Generally, regions of strong backscatter cluster near large bottom slopes, suggesting their generation by bottom topography. For winds >7 m/s, the variations of microwave backscatter power decrease to 2 to 3 dB for both frequency bands and seemingly become decorrelated from the bottom topography. Figure 3 shows X-band microwave backscattered power while crossing Phelps Bank for two wind conditions. The upper record was obtained during 4.7 to 5.5-m/s winds while for the lower record the wind was 10.4 to 12.2 m/s. In principle, the large variations in microwave backscatter power encountered in the Phelps Bank region for light winds can be explained in terms of the unusually stable atmospheric conditions prevailing during the experiment (the water was up to 8°C colder than the air in this upwelling region).

A current gradient (front) not related to bottom topography also produced 20 dB variations in the power backscattered to the L-band radar (Fig. 4). The large backscatter occurs where the surface current changes from 80 to 120 cm/s, the upper record is the output from the amplitude-demodulated channel, and the lower record is the output from the phase-demodulated channel of the radar.
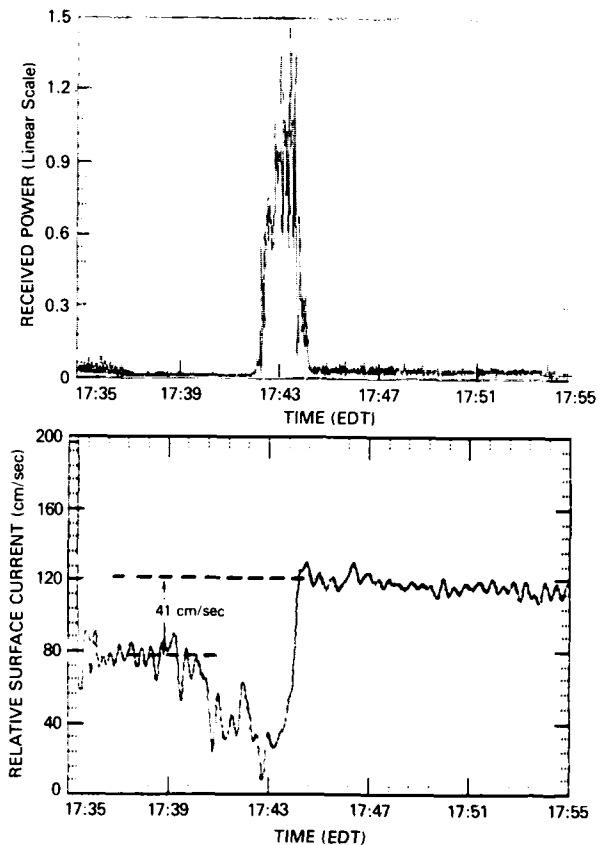
Fig. 3 — Time record of received power for X-band radar. Top: July 12, 1982 (1314 to 1319 EDT); heading, 350°T; track center, 40° 50' N, 69° 20' W; and wind speed, 4.7 to 5.5 m/s. Bottom: July 21, 1982 (1952 to 1055 EDT); heading, 270°T; track center, 40° 50'N, 69° 20'W; and wind speed, 10.4 to 12.2 m/s.
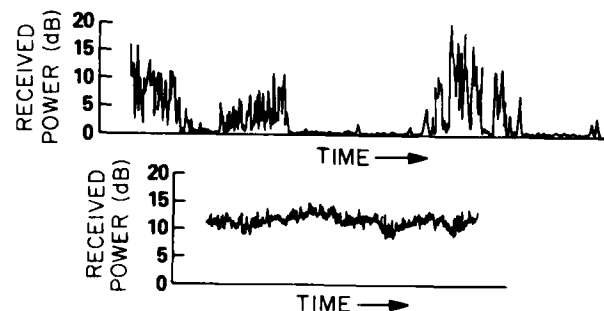
Fig. 4 — L-band measurements of the surface effects of a surface current gradient located to the west of Phelps Bank (40° 48.05' N, 69° 16.42' W). Top: backscattered power vs time; depression angle, 2.58°; range, 600 m; radar cell size, 7.5 m × 149 m; wind speed, 1.5 m/s; and wind direction, 60°. Bottom: relative ocean surface current vs time. Ship was on a constant heading and speed run, and the L-band antenna was aligned with the ship's bow. Current values during 1735 to 1740 EDT and 1744 to 1755 EDT are accurate. Signal fading due to calm water caused the apparent current decrease from 1739 to 1743 EDT.

In future work *in situ* data collected in the 1982 NRL remote sensing experiment will be used as input to a barotropic circulation model for the computation of the perturbed tidal field. The computed current field will then be used together with available wave measurements in a current-wave interaction model for the description of the perturbed/modulated wave field in the Phelps Bank region. The resultant wave field will be used to predict the intensity of SAR imagery using Bragg scattering; these predictions will be compared to the X-band SAR images taken during the 1982 experiment.

[Sponsored by ONR]

References

1. G.R. Valenzuela, D.T. Chen, W.D. Garrett, and J.A.C. Kaiser, "NRL Remote Sensing Experiment," EOS (The Oceanography Report) *Trans. Am. Geophys. Un.* **64**, 618 (1983).

2. G.R. Valenzuela, D.T. Chen, W.D. Garrett, and J.A.C. Kaiser, "Shallow Water Bottom Topography for Radar Imagery," *Nature* **303**, 687 (1983). ∎

Space and environmental research

Great helium eruptions of the sun such as this one periodically bombard the earth with intense ion fluxes. The Space Science Division is studying the threat of these ion fluxes to astronauts and electronics in space.

SPACE AND ENVIRONMENTAL RESEARCH

NRL has been a pioneer in X-ray astronomy and the space program, and the Laboratory continues to contribute to the national space program in several capacities, such as the study of solar flares and the harmful space environment they create. The naval environment also includes the ocean. Physical features produced by surface ships and submarines are of interest because they may be detectable or detected. This chapter summarizes some selected research into space and certain aspects of the ocean. The Space Science Division (Code 4100) and the Marine Technology Division (Code 5800) contributed articles.

Some of the other projects at NRL in space and environmental research include:

- Combined Release and Radiation Effects Satellite Microelectronics package (CRRES)
- Navy Remote Ocean Sensing Satellite (NROSS)
- High Resolution Telescope and Spectrograph (HRTS) and Solar Ultraviolet Spectral Irradiance Monitor (SUSIM) on Spacelab and other shuttle flights
- SPARTAN I & II--X-ray and ultraviolet experiments thrown overboard from the shuttle for 40 hours and then retrieved
- payload data management system
- radio and infrared interferometry and source investigations
- the solar corona and its extended influence towards Earth
- very low frequency ionospheric effects
- the development of severe storms

Solar Flare Effects in the Atmosphere

R. Silberberg and C.H. Tsao
Space Science Division

The high-energy, penetrating radiation in space consists of atomic nuclei and elementary particles. Without adequate shielding, long-duration (multiyear) exposures to this radiation would generate serious radiation damage in humans, for example, leukemia, other cancers, and eye-lens cataracts. This radiation also causes single-event upsets in microelectronic computer components on satellites and high-flying aircraft as it would on future space stations. These upsets alter information stored on the components. For these reasons it is important to know the nature of this radiation, its interaction with materials, and of procedures to reduce the radiation damage.

There are three primary components to radiation in space, each with different distributions in space, energy, and time. The three are (1) cosmic radiation, which permeates the whole galaxy; (2) the solar-flare particles within the solar system; and (3) the radiation-belt particles trapped in the earth's magnetic field.

In the *1983 NRL Review*, p. 124, we explored the effects of the atomic nuclei of cosmic-ray particles on microelectronic components. Now we shall consider the solar-flare particles. First, however, we point out essential differences between cosmic rays and solar-flare particles. These differences result in differing forms of radiation damage and suggest different shielding for these respective radiations.

Protons, Neutrons, and Shielding: Figure 1 shows a comparison of the energy spectra of cosmic-ray protons from periods of maximum and minimum solar activity and of solar-flare protons from the large flare of August 1972. The flux of solar-flare protons can be much higher than that of cosmic rays. However, the energy spectrum is much steeper, so that at energies above a few hundred MeV (million electron volts) the cosmic rays are more abundant. While the flux of cosmic rays is nearly steady with time, the solar-flare particle bombardment lasts about two days. A very large flare like the one depicted occurs only about once during the 11-year sunspot cycle.

Because the energy of solar-flare protons and nuclei is relatively low, as seen in Fig. 1,
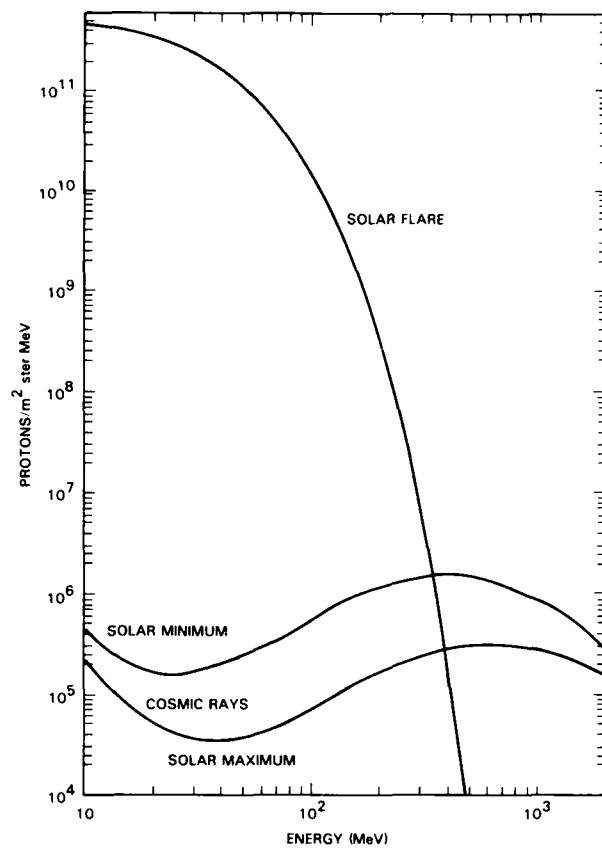
Fig. 1 — A comparison of the energy spectrum of protons for the solar flare of August 4-7, 1972, and of the spectra of cosmic-ray protons. These curves represent 1-week accumulations.

they can be brought to rest in shielding material more readily than cosmic-ray particles that also are mainly protons, with some contribution of heavier nuclei. Thus, one might conclude that less shielding is needed for solar-flare protons; however, this is not so. The flux of protons from a very large flare is so high that their nuclear interactions within shielding material generate numerous secondary neutrons and protons. These neutrons are highly penetrating and generate highly ionizing nuclear recoils through nuclear interactions.

Even below heavy shielding, or at relatively large depths in the atmosphere, the nuclear interactions of these flare-particle-generated secondary neutrons pose a significant radiation hazard to both personnel and the operation of microelectronic computer components. For this reason, the cosmic ray research group at NRL has been investigating solar-flare effects in the atmosphere.

133

Radiation Dosages: Figure 2 illustrates the absorbed dose per hour of exposure at high latitudes as a function of atmospheric depth at high altitude at the time of the very large solar flare of February 1956. The doses of the flares in 1949 and August 1972 were, respectively, about 50% and 20% of that in 1956. The primary flare-particle dose rate is shown as well as those due to secondary protons and neutrons. The dose is given in units of rad and the dose rate is given in units of rad/hour. One rad corresponds to an energy deposition of 100 ergs per cm^3. The radiation dose of rad can be converted to the unit rem, which is equal to the radiation unit rad times the radiation quality factor, defined so that the various radiations for a given dosage in units of rem generate equal biological damage. This type of dose is defined as the dose equivalent. For example, the quality factor of neutrons is 10, hence a neutron dose of 1 rad corresponds to a dose equivalent of 10 rem.

We see from Fig. 2, that even at an altitude of of 55,000 ft (16.76 km), the dose rate of a very large flare is 0.2 rad/h (of which 0.2 rad/h is due to neutrons), or 2 rem/h. Thus in a 2 1/2-h period, a person on board an aircraft at 55,000 ft and at a high latitude receives 5 rem, or about 1/2 the dose permitted for radiation workers in a one-year period. About 2/3 of this dose equivalent comes from the secondary neutrons

generated by interactions and not from the direct flux or secondary protons.

Upset Rate: Binary information is stored on microelectronic chips in the form of electrical charges in small subvolumes of the chip (in bits). This charge (in picocoulombs) is typically stored in a 10- by 10-μm-wide by 5-μm-thick volume of the bit. Energetic particles passing through such a volume can deposit a charge above the critical level to change or upset the information stored there. Figure 3 shows the single-event upset rate per day as a function of the component's critical charge. The upset rate for unshielded components at high latitudes and at an altitude of 55,000 ft was calculated for a very large flare like that of 1956. Curve *a* in Fig. 3 represents the upset rate due to slow protons from flare particle interactions and neutron interactions, and curve *b* shows the upset rate due to neutron-generated nuclear recoils. Curve *e* shows the total upset rate at 55,000 ft. For comparison, the upset rates for unshielded components at solar quiet times due to the galactic cosmic rays are shown: curve *c* is for 150,000 ft (45.72 km) near the top of the atmosphere; and curve *d* is for 55,000 ft. We note that even at 55,000 ft, a very large solar flare generates about 10 upsets per kilobit-day in components that can be upset by a charge deposition of 0.01 picocoulombs. This exceeds by 2
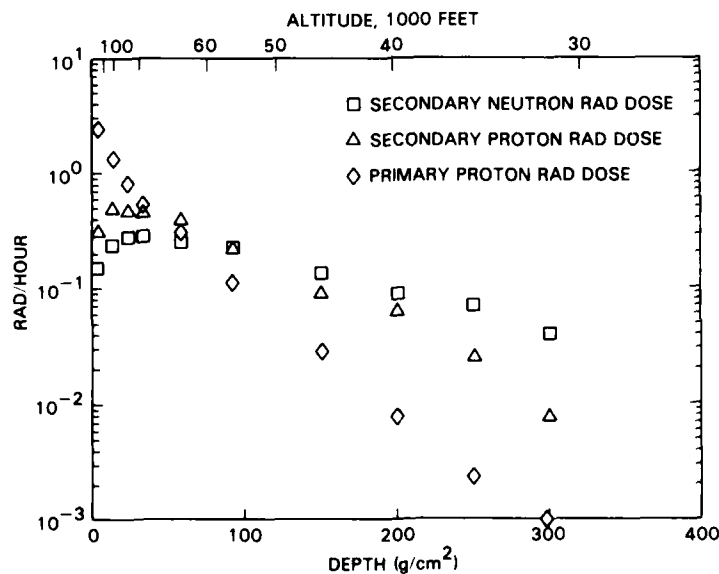
Fig. 2 — The absorbed dose per hour at various atmospheric depths of primary protons, and secondary protons and neutrons during the very large flare of February 23, 1956
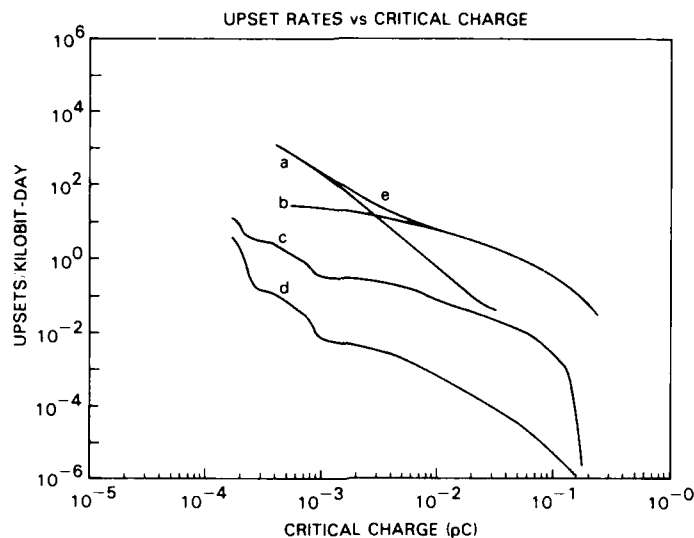
Fig. 3 — The single-event upset rate for unshielded components at high latitudes and at 55,000 ft altitude at the time of a very large flare. The curves a and b show the upset rates due to slow protons and neutron interactions. For comparison, the upset rates for unshielded components due to cosmic-ray nuclei are shown at 150,000 ft by curve c, and at 55,000 ft, by curve d. The total upset rate at 55,000 ft is indicated by curve e.

orders of magnitude the upset rate due to galactic cosmic rays at the top of the atmosphere — 150,000 ft, curve c.

Since cosmic-ray-generated upsets have been found to be troublesome, those at high latitudes due to solar-flare particles and their secondary progeny are a hundred times more troublesome. Shielding has to be extremely thick to suppress the deeply penetrating secondary neutrons; the shielding due to the atmosphere above 55,000 ft corresponds to the shielding of about 1 ft of aluminum.

[Sponsored by DNA/DARPA] ∎

Periodic Occurrence of Solar Flares?

G.H. Share
Space Science Division

Predicting the occurrence of solar flares is becoming more important as we use space for increasing civilian and military applications. Intense X-ray and particle emissions pose a hazard to astronauts and can be responsible for failures of electronic components on communications, weather, and surveillance satellites. These flares also precede intense geomagnetic storms which disrupt radio communications. Recent measurements from 1980 to 1983 by the gamma-ray spectrometer on board NASA's Solar Maximum Mission (SMM) satellite indicate flares had a tendency to occur in groups with a mean spacing of about 154 days. The same regularity was also observed in other monitors of solar activity.

Identifying Flares: SMM was launched in February 1980 with a complement of instruments primarily designed to study solar flares. The work reported here from the gamma-ray spectrometer experiment on SMM is a collaborative effort with E. Rieger of the Max Planck Institute for Extraterrestrial Physics (MPE), the Federal Republic of Germany, and E.L. Chupp and D.J. Forrest of the University of New Hampshire. From the 1980 launch to September 1983 we have identified 139 solar flares emitting continuum radiation above 300 keV. These flares were identified at NRL by a computer algorithm which searches for significant fluctuations in the background gamma radiation and at MPE by visual screening. Their solar origin was confirmed by ground-based and satellite observations at other

135
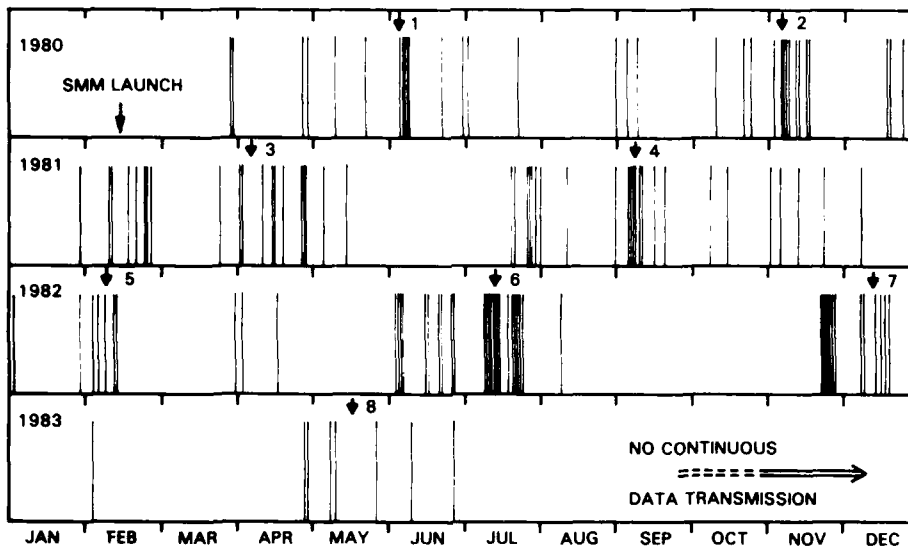
Fig. 4 — Solar flares detected above 300 keV by the SMM gamma-ray spectrometer are represented by the vertical lines plotted against time for 1980 to 1983. The numbered arrows designate the groupings of flares which contribute to the apparent 154-day period.

electromagnetic wavelengths. Figure 4 shows the temporal distribution of these flares. Each vertical line represents a solar flare with emission above 300 keV. It is of interest to note that the interval of greatest flare activity occurred in June/July and November/December 1982, 2 to 3 years after the maximum rate in sunspots was reported for this solar activity cycle (11 years). A similar delay was observed in the previous solar cycle.

Flare Groups Occur Periodically: Closer inspection of Fig. 4 reveals that the flares tend to occur in groups which are about 5 months apart. The eight groupings are identified by the numbered arrows. A Fourier power spectrum analysis was performed and revealed a significant peak at a period of 154 days. We estimate that the probability of this type of periodic effect being mimicked by a random distribution of flares is $< 10^{-6}$. To prove that this result was not due to some systematic effect in the operation of SMM, we analyzed a sample of 532 relatively intense flares observed in the soft X-ray band by NOAA's Geostationary Operational Environmental Satellites (GOES) over the same 1980 to 1983 time interval; similar evidence for periodic behavior was observed in this larger sample, which included the flares observed by SMM.

Another way to illustrate this regularity in the occurrence of flares is to overlay every contiguous 154-day segment of data. The phase histogram obtained in this manner, with a bin size of 15.4 days, is shown in Fig. 5. Thirty-five percent (48) of all the flares occurred during the same 15.4-day phase bin (that is, in only 10% of the observing time).

Other Periodic Data: This observed regularity in the occurrence of X-ray flares from 1980 to 1983 is also apparent in other indicators of solar activity, such as the monthly mean sunspot number and the 10.7-cm radio flux (tabulated along with the GOES X-ray data in NOAA's monthly Solar-Geophysical Data). Other investigations of the solar activity by using the mean sunspot number also have indicated that solar activity varies with some regularity every 5 months. The most extensive analysis covered measurements of the mean sunspot number from 1749 to 1979. The most prominent period less than 200 days found in this analysis was 155.4 days; that is close to what we have found for energetic solar flares. The cause of such periodic behavior in solar activity is not known; however, one suggestion is that it may be the result of oscillations believed to occur in the interior of stars.
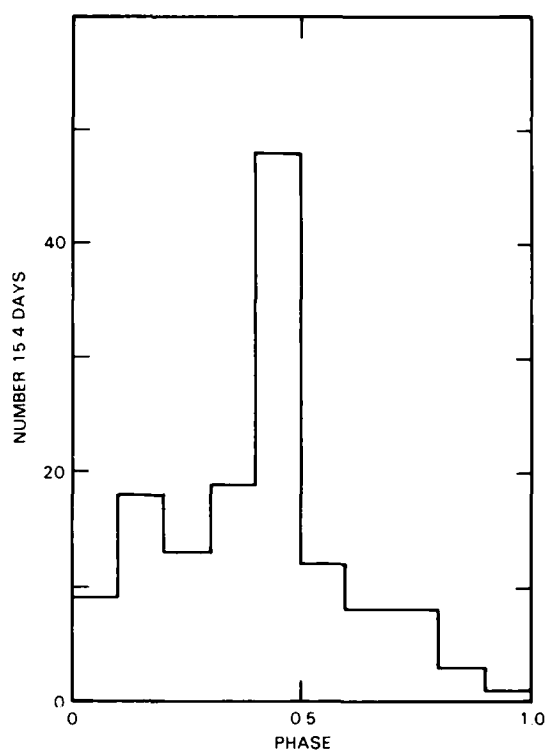
Fig. 5 — Number of flares detected by SMM per 15.4-day phase bin after overlaying every 154-day segment of the SMM observations

Studies of this kind may ultimately lead to a relatively reliable prediction of the occurrence of solar flares and provide a means of alert to protect astronauts and space instrumentation from the intense radiation accompanying the most energetic flares.

[Sponsored by NASA]

Reference

1. E. Rieger, G.H. Share, D.J. Forrest, G. Kanbach, C. Reppin, and E.L. Chupp, "A 154-Day Periodicity in the Occurrence of Hard Solar Flares?" *Nature* 312, 623 (1984). ∎

HEAO A-1 Discovers X-ray Eclipses

K.S. Wood
Space Science Division

The NRL Large Area Sky Survey Experiment (HEAO A-1) on NASA's HEAO-1 satellite

surveyed the sky for bright X-ray sources and collected data which are important for characterizing the extreme physical conditions encountered in these objects, including densities exceeding 10^{15} g cm^{-3} and magnetic fields exceeding 10^{12} G.

Burst Sources: For several years prior to the launch of HEAO-1 in 1977, it had been known that some X-ray sources produce dramatic bursts in which the luminosity rises abruptly (in tens of milliseconds) by several orders of magnitude, then decays slowly over tens of seconds. About 20 such burst sources are known in our galaxy.

Theories: Prolonged study of these objects by many researchers had uncovered important clues to the physical basis for bursting. A persistent emission detected between bursts accounts for 99% of the emitted energy, and bursts account for the remaining 1%. The pervasive occurrence of this division of energy in many sources can be explained if the bursts are thermonuclear explosions occurring on neutron stars *using material being gathered by accretion as fuel.* Then, the division of energy would be the ratio of nuclear energy in a given mass of accreted matter to the gravitational energy released when that same mass falls onto the neutron star surface. The gravitational energy is released as a continuous, persistent emission while the nuclear energy is released in bursts.

This picture of the bursting required, among other things, a source for the accreted material. If the neutron star were receiving the accreted material from a companion star, the need would be met, but then every burst source would necessarily be a binary source. In other kinds of binary X-ray sources, binary companions can manifest themselves by eclipsing the neutron star at regular, periodic intervals. Considerable searching had failed to detect any eclipses in burst sources. Then, the missing piece of the burst model was given in an ingenious suggestion, by M. Milgrom [1]: no eclipses were seen among burst sources because of a simple selection effect that made any eclipsing sources undetectable. If the binary system were viewed from a vantage point well out of the orbital plane of the binary system, there would be no difficulty seeing the

137

X-ray source. But there would also be no eclipses because, seen from such a vantage point, the two stars could never be coaligned so as to produce eclipses. If instead the observer were in or near the orbital plane, eclipses would be possible geometrically. However, such systems would not be detected, according to Milgrom, because the neutron star would always be hidden from view by the accretion disk of material spiraling onto the star surface. Figure 6 shows such a binary system drawn from a vantage point slightly out of its orbital plane. The large companion star is on the left and the neutron star is in the center of the disk on the right. Here the disk does not quite eclipse the neutron star. The picture shows how the disk around the neutron star can be an important third component in these systems in terms of its effect on observations, although its mass is many orders of magnitude smaller than the mass of either of the stars.

Observations: Milgrom's model did not stop the search for eclipses. One system, designated as MXB 1659-29, was regarded as a particularly apt candidate, because in 1978, researchers had seen it undergo sudden changes in its *persistent* flux that were possibly eclipses. A systematic study of the source was carried out collaboratively by L. Cominsky of University of California, Berkeley, and K. Wood of NRL. We obtained an intensity for the source every time HEAO-1 scanned through it, roughly once every half hour for several days. Such a sampling of measurements was too sparse to detect bursts, but we found patterns in the variation of the persistent flux. In particular, during the spring of 1978, the source was unusually bright in most measurements, but occasionally was completely missing. By folding the intensity data (i.e., overlaying contiguous equal periods of data) to determine mean intensity as a function of orbit phase,

III Unobstructed view of neutron star — no eclipse or disk occultations

II True eclipses of neutron star by its companion.

I Neutron star intermittently occulted by turbulent flow on trailing side of the disk, where gas stream hits it.
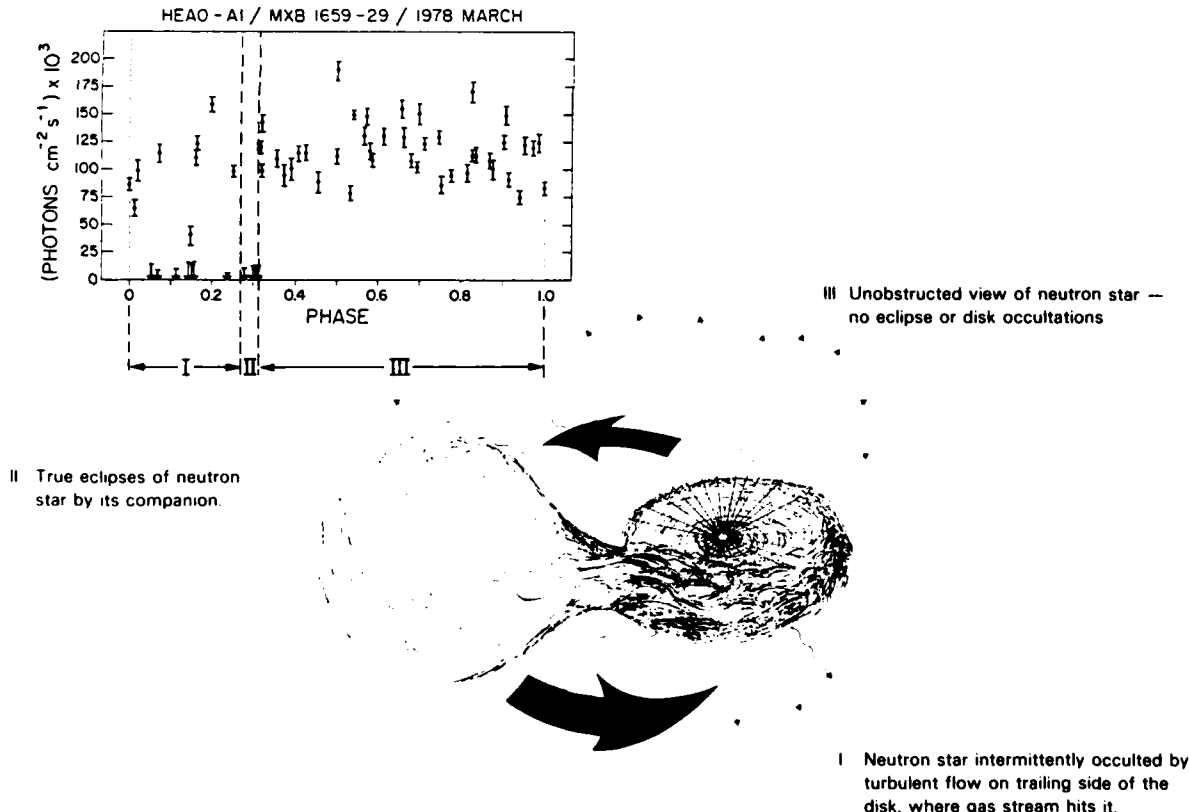
Fig. 6 — Observations of the first true eclipses in any X-ray burst source. The system is MXB 1659-29. The three vantage points indicated — I, II, and III — correspond to different binary orbit phases. The observed photon fluxes at these phases are plotted in the insert (upper left). Roman numerals on this insert indicate which orbit cycle phases correspond to which vantage points.

and by using many trial orbital periods, the actual orbital period of 7.1 hr was discovered [2]. (This technique had to be developed to cope with the irregular monitoring caused by scanning.)

Modulation Pattern: Knowing the orbital period made it possible to display the intensities (photon fluxes) as a function of orbital phase and gave the pattern shown at the upper left in Fig. 6. If the photon flux was zero within an error limit while HEAO-1 was observing MXB 1659-29, this was a nondetection. We then observed that the full cycle was divided into three parts. In part III, the source was always present, and there were no nondetections. In part I, both detections and nondetections were found, while in a small portion of the cycle there were only nondetections (part II). Statistical analysis indicated that the cluster of nondetections in part II very probably represented true eclipses, because a chance clustering of so many nondetections in a small interval was unlikely.

By using the orbital period established from HEAO A-1, it was possible to search other data bases for MXB 1659-29 at the appropriate times for eclipses. The data from three other satellites have now been searched and the pattern in Fig. 6 has been confirmed with no detections having been found in part II of the cycle. The occasional nondetections in part I of the cycle are now explained as eclipses of the neutron star by its own accretion disk. Thus we find the picture proposed by Milgrom is essentially correct, even though the unusual vantage point in the MXB 6659-29 system permits detection of true eclipses. In Fig. 1, the observer's vantage point at part I of the cycle is indicated by I on the drawing, and similarly for parts II and III, showing how the three conditions of eclipse, unobstructed view, and intermittent occultation by the accretion disk arise.

Companion Star: Knowing the orbital period (7.1 hr) and the mass of the acreting neutron star (roughly 1.4 times the mass of the sun), it is possible to solve for the mass of the companion star. This mass lies in the range 0.3 to 0.8 solar masses, where the range reflects uncertainty in the angle between the line of sight and the orbital plane. This confirms the idea that the

companions of burst sources must have comparatively low masses.

Research on this source is expected to continue in the future. It should be possible to use the high-quality timing information provided by eclipses to refine models of the binary system and to study the transfer of matter between the components.

References

1. M. Milgrom, *Astron. Astrophys,* **275**, 278 (1978).

2. L.R. Cominsky and K.S. Wood, "Discovery of a 7.1-Hour Period and Eclipses from MXB 1659-29," *Astrophys. J.* **283**, 765 (1984). ∎

Mixing Within an Ocean Front

G.O. Marmorino
Marine Technology Division

To detect man-made disturbances in the ocean, it is necessary to know the characteristics of naturally occurring mixing processes and how they affect the temperature structure of the ocean. In a field exercise conducted in the vicinity of an ocean frontal zone, we observed a mixing event and have inferred some information about its source.

Mixing is part of the process in which the ocean transfers heat from near the surface downward through the thermocline (where temperature changes rapidly with depth) to the deeper, cooler, denser water below. In a motionless ocean, the thermocline is horizontal; but, in the presence of a major current, the thermocline develops a large-scale slope, changing its depth by 40 m over a horizontal distance of 10 km. An ocean region containing a sloped thermocline and associated current is called an ocean front in analogy with an atmr ., . ic front. Across the frontal surface, the vertical shear of the horizontal currents is large; this is one situation where intense mixing events are thought to occur as a result of dynamic instabilities in the flow. The **139**

parameter controlling the onset of the shear instabilities appears to be a form of the Richardson number—the ratio of the stabilizing effect of the vertical stratification to the destabilizing effect of the vertical shear. Where low values (about 0.25) of the Richardson number occur, instability develops rapidly, resulting in a "patch" of turbulent, actively mixing fluid. As oceanographic instruments have improved, patches have been increasingly observed in temperature data by various researchers.

A Frontal Patch: NRL conducted a shipborne experiment to simultaneously measure the current field and detailed temperature structure within a front in the Sargasso Sea (located approximately midway between Bermuda and Jacksonville, Florida). Currents were measured by observing the Doppler shifting of backscattered acoustic signals from a transponder mounted on the ship's hull (see article by Trump on p. 142); temperatures were measured by towing a vertical array ("chain") of thermistors behind the ship. The array of 180 thermistors extended from near the surface to a depth of about 90 meters.

Lowest values (<1) of the Richardson number occurred within the front, as expected [1]. A large patch was found there, too, and is shown in Fig. 7. The patch appears in the upper panel (a plot of about 70 simultaneous temperature records) as an area of high-frequency fluctuations extending for about 3 km along the tow. To accentuate the variability within the patch, the difference between successive measurements is plotted in the lower panel. Where the tempera-
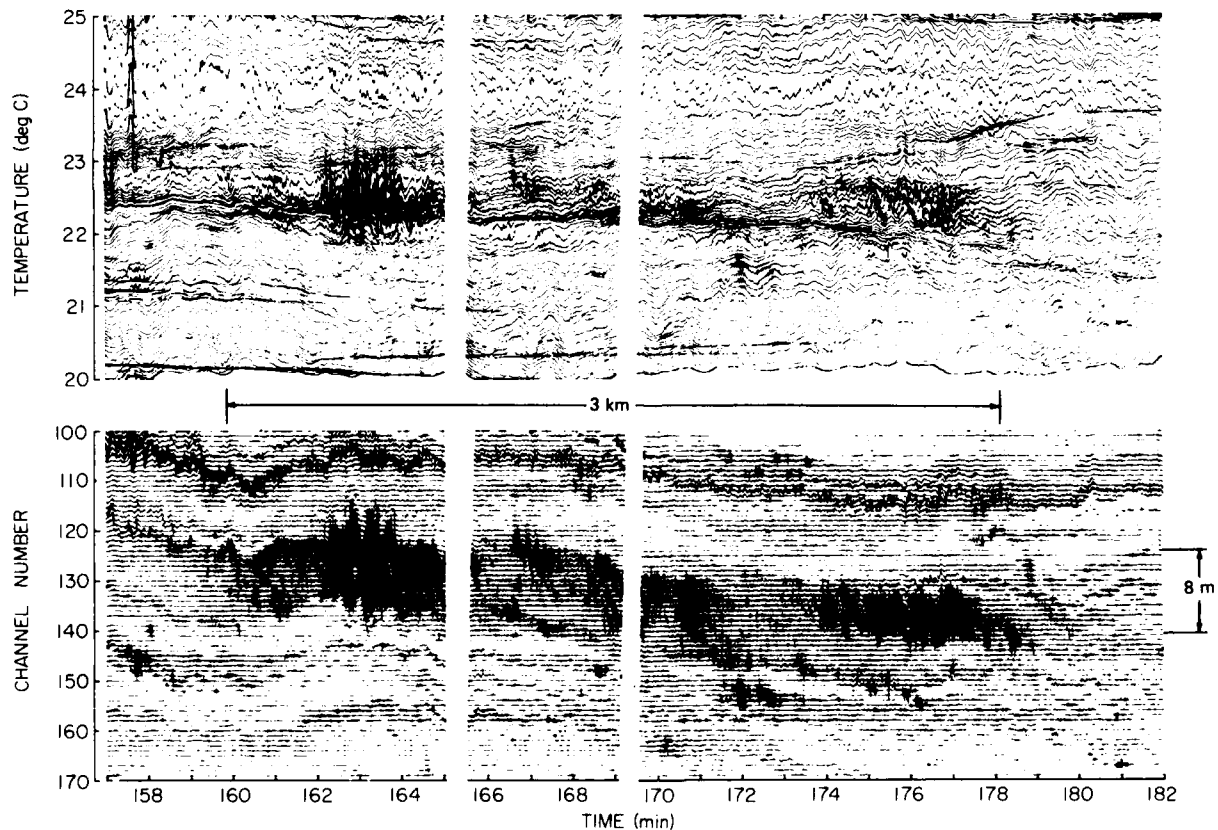
Fig. 7 — Time series of temperature (top panel) and corresponding temperature time-differences (bottom panel) as measured by the NRL thermistor chain during a tow through an ocean front in the Sargasso Sea. The thermistor recorded on channel 100 was at a depth of 45 m, and each successive thermistor was about 0.5 m deeper. The 25-min period corresponds to a horizontal tow of over 4 km. The mixing patch, lying between 22° and 23°C, appears after minute 160 near channel 130 then deepens as the tow proceeds through the deepening frontal surface. (The two blank areas are gaps in the data.)
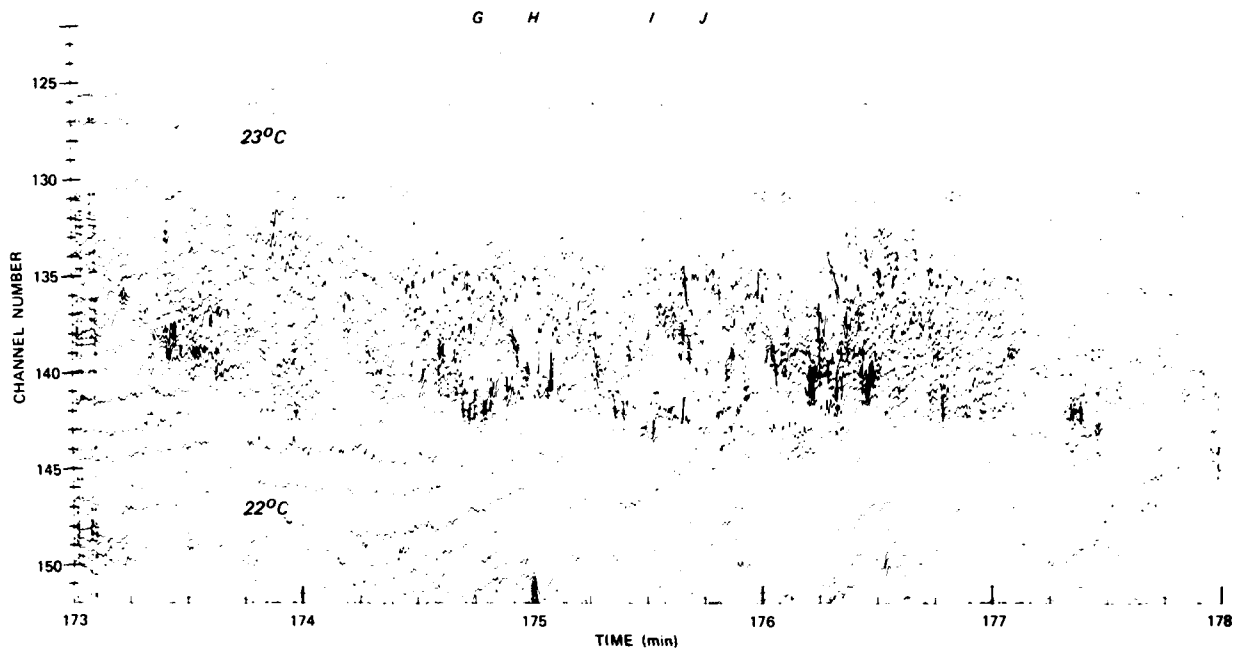
Fig. 8 — An isotherm plot of part of the Fig. 7 patch.
Temperature is contoured at intervals of 0.040°C.

ture is fairly constant, a straight line results on the plot; the patch appears as the darker region where horizontal temperature fluctuations are greatest.

Detailed Structure: A detailed look (Fig. 8) at one of the more energetic areas within the patch reveals some interesting structures, previously unreported for the ocean. In Fig. 8, the patch appears between channels 132 and 143 with relatively smooth isotherms above and below it. Embedded within the patch, a fairly regular series of roll-like structures are seen. These are found under the letters G, H, I, and J (top of figure). Regions of high temperature gradient (sloped from upper-left to lower-right) give the series of structures a "braided" appearance. Between the braids are regions of weak vertical temperature gradient which indicate vertically mixed water. This characteristic structure, the surrounding small-scale variability, and its location in a zone of low Richardson number suggest the patch is a naturally produced mixing event.

Discussion: We conjecture that mixing events similar to the one examined occur intermittently in the thermocline wherever the Richardson number is low enough. In this way, each event acting in turn causes a gradual downward transport of heat. The precise physical mechanisms responsible for the structures in the patch are not yet understood, but it is likely that the background shear and internal waves are involved. (Internal waves are the vertically coherent oscillations seen throughout Fig. 7 (upper panel) and in Fig. 8 away from the patch.) Shear enhances the "breaking" of internal waves, and internal waves enhance the shear, providing more favorable locations for mixing [2].

To determine the precise mechanisms at work, the Richardson number will have to be measured on a finer space scale. Also, it has been difficult to sample the ocean adequately to witness the evolution of a particular patch. We are planning new experiments with adequate sampling to more precisely address the physical mechanisms of patch growth, maintenance, and decay.

[Sponsored by ONR]

References

1. S.A. Thorpe, "Breaking Internal Waves in Shear Flow," in *Twelfth Symposium of Naval*

Hydrodynamics (National Academy of Sciences, Wash., DC, 1979), pp. 623-628.

2. C.L. Trump, B.S. Okawa, and R.H. Hill, "The Characterization of a Mid-Ocean Front with a Doppler Shear Profiler and a Thermistor Chain," *J. Atm. and Oceanic Tech.* (in press). ■

Acoustic Measurement of Ocean Water Velocities

C.L. Trump
Marine Technology Division

The formation and character of small, high kinetic energy, turbulent patches in the upper ocean depends on the vertical gradient of horizontal velocities, or shear. Natural oceanic motion, such as internal waves, in the presence of high shear can lead to instabilities producing patches (see p. 139); after a patch is formed, the shear field shapes a patch through differential advection. Understanding these processes is a critical part of nonacoustic antisubmarine warfare research.

Oceanographers usually measure ocean velocities with moored current meter arrays that produce estimates continuous in time, discrete in depth, and fixed in geographical location. Within the last decade, oceanographers have developed profiling systems, either by lowering current meters or by dropping electromagnetic sensors, that produce estimates continuous in depth but still discrete in time and geographical location. For the last four years, NRL has been using a ship-mounted Doppler current measurement system in which acoustic energy produces remote measurements continuous in time, depth, and location. To understand the dynamics of the velocity field and its relation to patches of turbulent water, the space and time continuity of the data makes this system superior to the others.

Characteristics: The system uses four transmitter/receiver heads mounted at 30° to the vertical and directed toward the bow, stern, and both sides of the ship. Each head emits a 300 kHz signal and range-gate samples the return sig-

nal from passive scatters embedded in the water. The frequency of the backscattered return signal is Doppler-shifted from 300 kHz because of the difference in speed between the ship and volumes of water at various depths. Each beam's Doppler shift is proportional to the component of the velocity difference along the beam. The signals from the four beams are combined with the ship's pitch, roll, and heading data to calculate the velocity components—in earth coordinates— of the water relative to the ship as a function of depth. The vertical derivative of the horizontal velocity components (shear) can be calculated directly, and the absolute velocities can be estimated by using some independent measure of ship's motion, typically Loran-C navigation. NRL's system measures velocities in 3.2-m depth bins from 15 m to 130 m. A data sample is taken every 0.6 s. Though the velocities from individual samples are quite variable, 1-min averages are accurate to 1.0 cm/s.

Data Example: Figure 9(a) indicates the ability of a Doppler system to characterize the velocity field in a portion of the ocean. This section shows velocity contours across a near-surface front encountered in the Sargasso Sea, about 500 miles east of Florida, during the summer of 1981. An oceanic front is similar to an atmospheric front in that two fluid masses with different temperatures are separated by a thin, slanting, interfacial zone that is associated with a strong velocity shear. In this case, the water to the north of the front (right side of the figure) is warmer, and the component of velocity shown is much stronger. A velocity difference of about 30 to 50 cm/s is apparent across this front over a horizontal distance of about 8 km and a vertical distance of about 20 m.

When the velocity data is combined with temperature data taken by NRL's towed thermistor chain (Fig. 9(b)), estimates of the vertical stability can be made. The estimator used is the Richardson number which is basically the nonnegative ratio of the stabilizing effect of the vertical temperature gradient to the destabilizing effect of the vertical shear of velocity. The smaller the Richardson number, the less stable the water, and the greater the likelihood of fluid
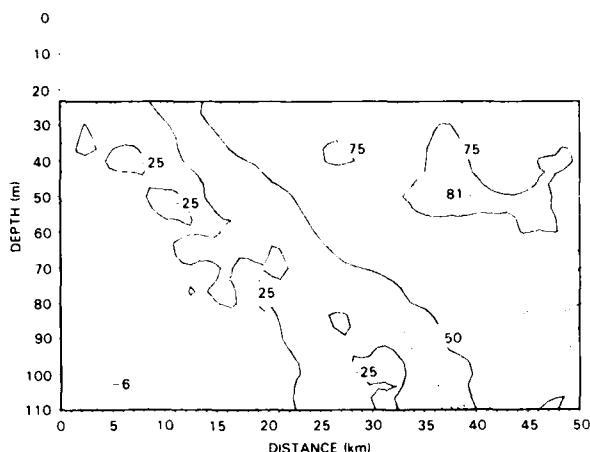
Fig. 9(a) — Contour plot of the velocity component parallel to front in 5-cm/s increments. Positive components are towards the North.
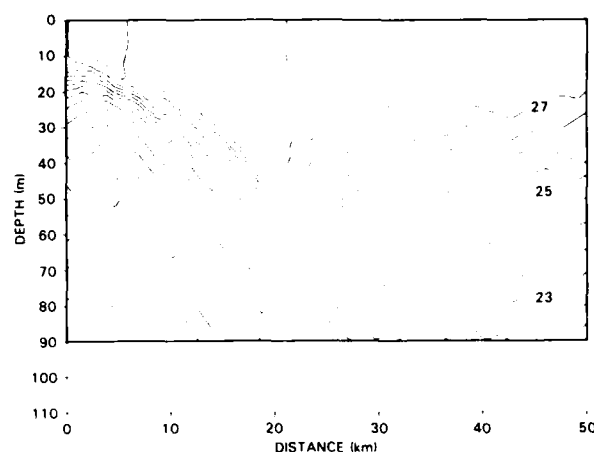
Fig. 9(b) — Contour plot of temperature in 0.5°C increments
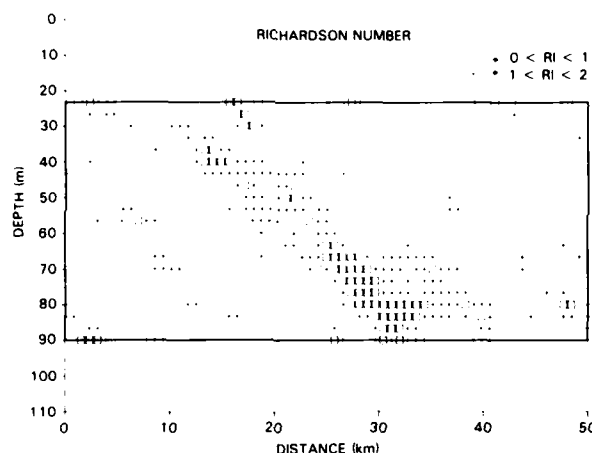
Fig. 9(c) — Plot of Richardson number RI estimates across the front. Only those estimates between 0 and 1 (□'s) and between 1 and 2 (+'s) are displayed. In all other locations, RI > 2.

motion overturning the density structure and forming a turbulent patch. Generally, values of the Richardson number < 1 are considered marginally stable.

Figure 9(c) shows the estimates of the Richardson number across the front. Here, discrete estimates were made by combining the Doppler data with the towed-thermistor-chain temperature data; only those values between 0 and 1 (□'s) and between 1 and 2 (+'s) are shown. This figure shows that the frontal interface and particularly the deeper portion of the frontal interface is associated with low Richardson

numbers that indicate a greater tendency towards overturning and hence vertical mixing. This is an area where patch production is felt to occur and indeed where a relatively great amount of patchiness was measured (see p. 139).

[Sponsored by ONR and NORDA]

References

1. R.H. Hill and C.L. Trump, "An Interim Doppler Shear Profiler: Experimental Results," NRL Memorandum Report 4920 (1982).

2. C.L. Trump, B.S. Okawa, and R.H. Hill, "The Characterization of a Mid-Ocean Front with a Doppler Shear Profiler and a Thermistor Chain," *J. Atm. and Oceanic Tech.* (in press). ∎

Imaging the Upper Ocean Temperature Variance Field

L.J. Rosenblum
Acoustics Division

G.O. Marmorino
Marine Technology Division

When a vertical array of temperature sensors (thermistors) [1] is towed through the ocean's upper thermocline, patches of large temperature variance of considerable horizontal length may be observed. Many different physical processes can produce such temperature fluctuations. These include shear instabilities, small-scale internal waves, interleaving, and double-diffusive convection. An algorithm has been developed [2] which provides an analytical tool to study these patches. Briefly, the algorithm detrends the temperature data from each sensor and then computes the fast Fourier transform (FFT) of the cosine-windowed data for 16-s (40-m) data blocks. The FFT provides an estimate of the variance within a user-selected wavelength band, typically 1 to 3 m. For each channel, the variance is normalized by dividing by the square of the local vertical temperature gradient. This normalized variance then should be independent of the changing vertical gradient.

More recently, the authors have applied imaging techniques to the patch algorithm output to obtain a picture of the ocean temperature variance field. Such pictures should help us understand both the mechanisms which create fine-scale patches and the distribution of these patches within the upper ocean. By using false color to display the temperature variance level and performing smoothing operations in the image space, we have produced pictures of the upper ocean temperature variance field. These pictures have provided new insight into the interpretation of the physical processes involved in temperature fluctuations and have also provided an effective and appealing means of comparing patch algorithm results with results from other researchers on the same data sets.

The data for the figures were obtained from tows of the thermistor array through a front in the Sargasso Sea in the summer. The tows were through part of an east/west-oriented front that lies north of the subtropical convergence zone. Figure 10 displays 48 km of temperature variance data; the front is approximately the middle third of the figure. Vertical interpolation was performed in image space to obtain values for points between the sensors, which were approximately 0.5 m apart. In Fig. 11 the color lookup table was used to blacken out variance levels below 5×10^{-4}. A Richardson number Ri plot for the same data set, computed by C. Trump [3], was converted to a set of verticies and overlayed on the imaged variance plot. The bounded polygons are those regions within which Ri $\leqslant$ 2. Theory predicts that where Ri is small, there is the likelihood of high variance patches due to fluid instabilities. Figure 12 shows the section of the data from Fig. 10 between 18 km and 24 km. Each variance is for a 0.5-m-vertical by 40-m-horizontal rectangle and is displayed as an 8-pixel by 6-pixel rectangle on the raster color device. Smoothing is performed in image space to obtain the final picture. Near the bottom right is the start of a 3-km-long patch, which was the largest patch observed during the experiment. The very quiet (low temperature variance) regions in the upper left are also of interest.

References

1. W.D. Morris et al., "Towed Thermistor System for Marine Research," IEEE Proc. of the Third Workshop Symposium on Oceanographic Data Systems, Sept. 1983, pp. 147-153.

2. L.J. Rosenblum, G.O. Marmorino, and J.P. Dugan, "A Processor for the Study of Ocean Fine-Scale Patches," NRL Memo Report 5573, in press.

3. C. Trump, "Acoustic Measurement of Ocean Water Velocities," NRL 1984 Review. ∎
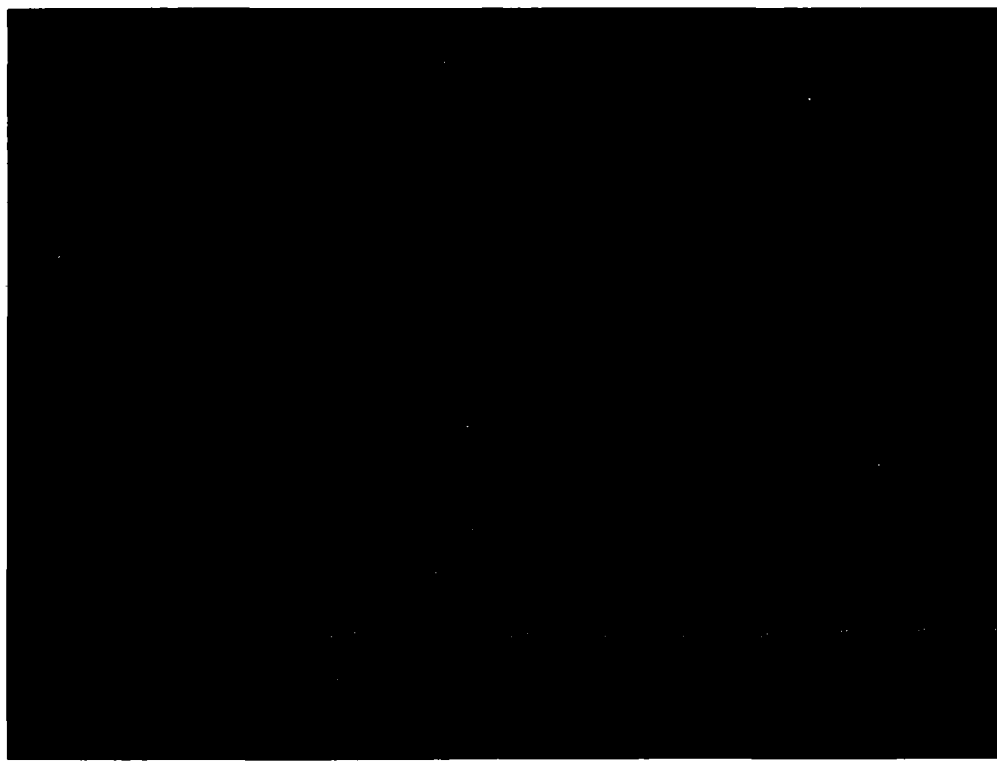
Fig. 10 — False-color, temperature variance data for the upper ocean obtained by
using data from an Atlantic Ocean experiment near the Sargasso Sea
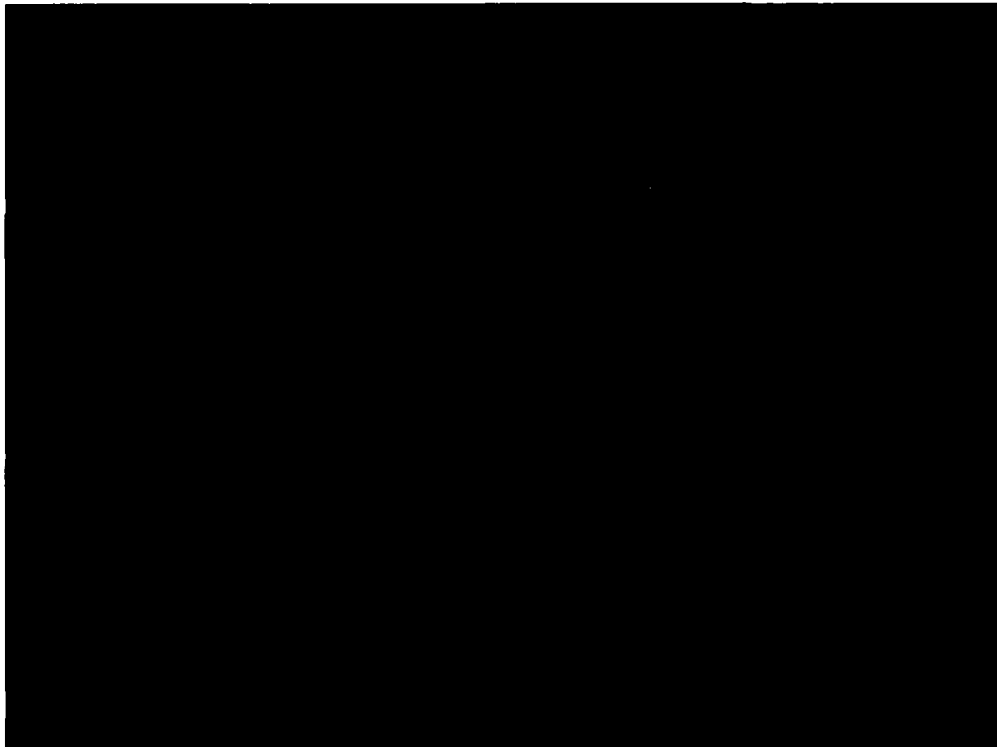
Fig. 11 — Imaged data from Fig. 10 with an overlay of polygonal regions
within which Ri $\leqslant$ 2; Ri denotes the Richardson number

145
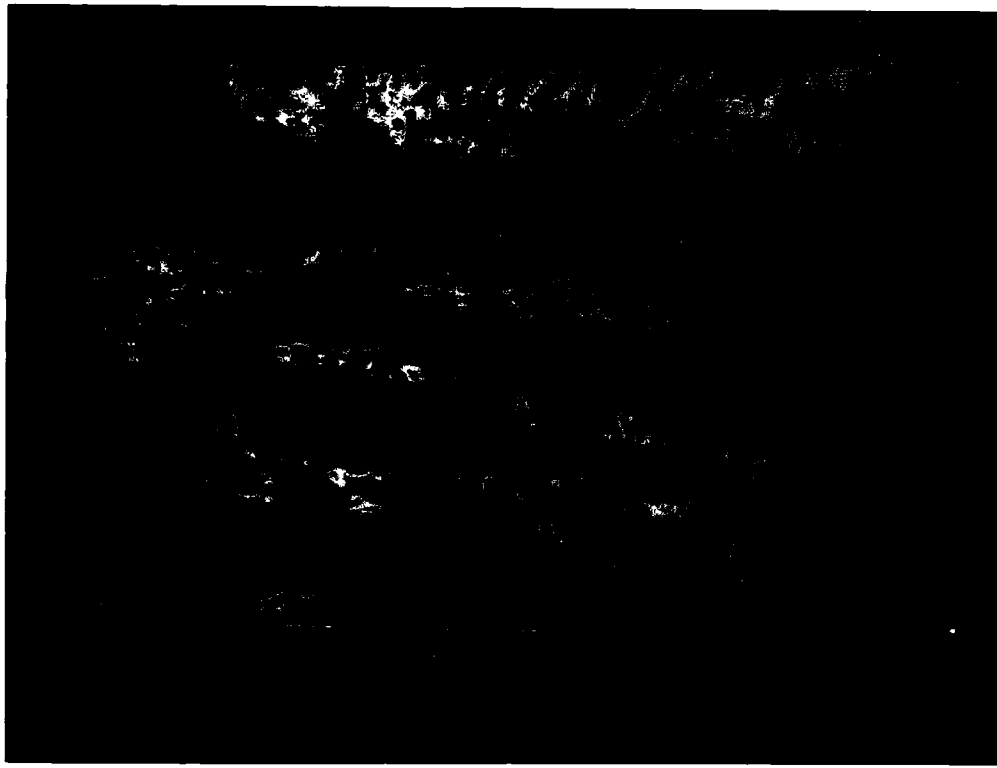
Fig. 12 — A section of data from Fig. 10 consisting of the data between 18 km and 24 km
expanded and smoothed in image space

Optical research and systems technology

Artist's concept of NRL's new 110,000-square-foot electro-optics laboratory. The building is scheduled to be completed in 1983.

OPTICAL RESEARCH

Light is finding ever more applications in modern technology. Laser research continues to be important at NRL, but the use of optics for gyroscopes and ultrabroadband communication systems in space continues to command more attention. The articles in this chapter describe some of NRL's research in these areas. The work was performed in the Optical Sciences (Code 6500) and the Space Systems (Code 7700) Divisions.

These articles present a small portion of the optics research at NRL. Some of the other areas of research are

- fiber-optic sensors and communications
- acoustooptic technology
- ultralow-loss fiber technology
- infrared focal plane arrays and surveillance
- optical, infrared, and ultraviolet target recognition
- high-energy laser development and beam combining technology
- solid-state laser development
- X-ray lasers

Tunable High-Power, Color-Center Laser

I. Schneider and C.L. Marquardt
Optical Sciences Division

In recent years, certain defects in alkali halide crystals called color centers have been used to produce efficient, stable sources of laser radiation which can be tuned within the infrared spectrum (0.8 to 4.0 μm). These lasers are very appealing for a wide range of applications, including the study of fundamental vibrational modes of molecules, chemical purification, fiber-optic communications, and infrared countermeasures.

To extend the usefulness of these color-center lasers to applications that require pulses with high peak powers, such as chemical dynamics and nonlinear spectroscopy, we have constructed a two-stage oscillator-amplifier system, each stage pumped with a 1.41-μm laser. This two-stage system delivers peak powers in excess of 0.4 MW, with a tuning range from 2.02 to 2.42 μm. Each pulse contains an adequate number of photons to produce macroscopic chemical reactions. In addition, we estimate the pulse energy to be within a factor of 3 of that required for single-pass Raman shifting in liquid nitrogen. This is important because when this threshold is surpassed, the range for high-energy continuous tunability could for the first time be extended to the 5 to 6-μm spectral region.

Laser-Amplifier System: The lasing medium used for both oscillator and amplifier is a potassium chloride crystal doped with lithium and containing defects called $(F_2^+)_A$ centers. Each $(F_2^+)_A$ center consists of an electron trapped by an aggregate of two neighboring halide vacancies and a lithium impurity substituting for a potassium ion. In 1981, NRL scientists discovered these centers and showed that they provided stable, efficient, continuous-wave laser action across the 2.0 to 2.5-μm band at low-power levels.

Figure 1 shows the oscillator-amplifier configuration used to achieve high-power pulsed laser action. The oscillator is a KCl:Li crystal at 77K located between a high-reflectivity dielectric mirror and diffraction grating which serves as the tuning element and output coupler. The amplifier contains a nearly identical crystal-cryostat arrangement but without the mirror and grating. Each crystal is pumped transversely with a 1.41-μm laser beam. This beam is produced from the 1.06-μm line of a pulsed neodymium:yttrium-aluminum-garnet (Nd:YAG) laser. Each 1.06-μm pulse is divided into two equal parts and then passed through dual liquid nitrogen Raman cells to shift the wavelength to 1.41 μm.

Performance: Figure 2 shows the tuning characteristics of the oscillator-amplifier combina-
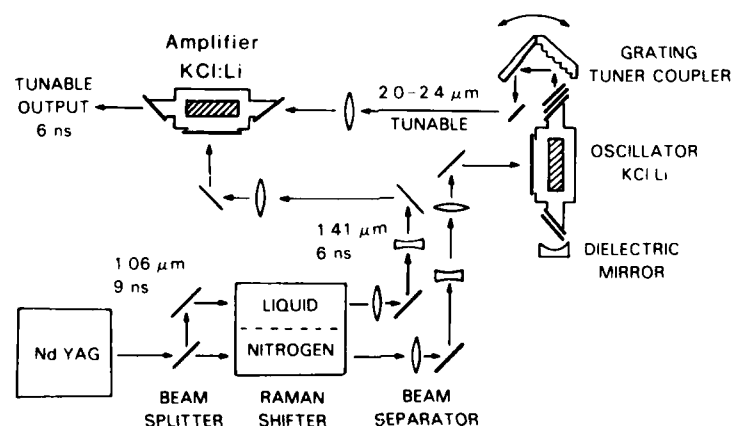
Fig. 1 — Schematic representation of the pump and color-center oscillator-amplifier configuration. Each section was pumped transversely with a 1.41 μm light generated by Raman shifting a Nd:YAG 1.06-μm laser line in liquid nitrogen.

Fig. 2 — Tuning curves of the pulsed lithium $(F_2^+)_A$ center KCl laser pumping the oscillator alone (▲) and the oscillator-amplifier combination (●)
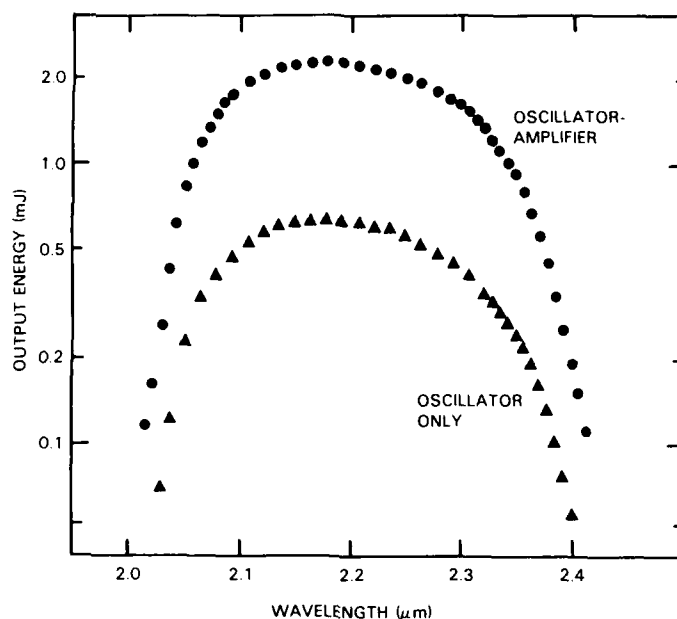
tion. The system has about a 6-ns pulsewidth, produces a maximum pulse energy of 2.3 mJ, and can be tuned from 2.02 to 2.42 μm. The oscillator alone can tune over approximately the same spectral range with a maximum energy of about 0.6 mJ. The amplifier gain is about 4 at maximum output.

If we can increase the output power of the system sufficiently to achieve single-pass Raman shifting in liquid nitrogen, we can extend the continuous high-power tuning range to approximately 6-μm wavelengths. This laser would then provide a unique source of high power pulses for experiments in infrared spectroscopy.

[Sponsored by ONR] ■

Fiber-Optic Gyroscope

W.K. Burns
Optical Sciences Division

The use of fiber-optic coils to sense their own rotation is attracting increasing commercial and military interest because of their potential for use in low-cost, compact instruments without moving parts. Commercial development of prototype devices is proceeding rapidly. Possible applications include oil-well logging, missile guidance, aircraft flight control, and high-precision air and shipboard inertial navigation. Since 1976, when Vali and Shorthill of the University of Utah first reported the application of fiber optics in a Sagnac interferometer [1], NRL's fiber-optic research has indicated the potential of fiber gyroscopes for inertial navigation applications. Gyroscope research and development at NRL has addressed sensitivity, linearity, dynamic range, and sensor mounting and packaging.

Basic Physics: The basic fiber-optic interferometer was demonstrated by G. Sagnac in a crude form (Fig. 3) in 1913. Light from a laser is incident on a beamsplitter, which divides the beam into two equal parts. The beams are coupled into each end of a fiber-optic coil of length L and radius R. The optical beams traverse the coil in clockwise and counterclockwise directions. Upon exiting the fiber ends, they are recombined by the beamsplitter to form an interference pattern at the output due to the relative phase shift of the two beams. If the interferometer is rotating with an angular velocity Ω, then the (Sagnac) phase shift is

$$\phi_s = \frac{4\pi\,RL\,\Omega}{\lambda_0 c}$$

where λ_0 is the wavelength of the exciting laser light in a vacuum, and c is the velocity of light.

Fig. 3 — Single coil (radius *R*) fiber-optic Sagnac interferometer that rotates with angular velocity Ω
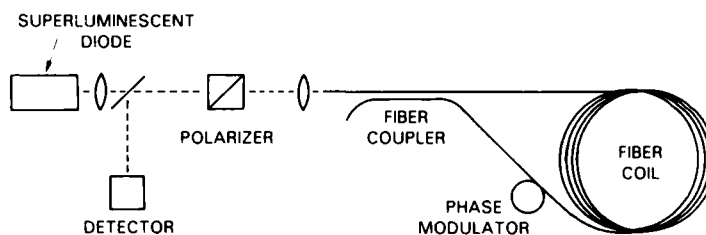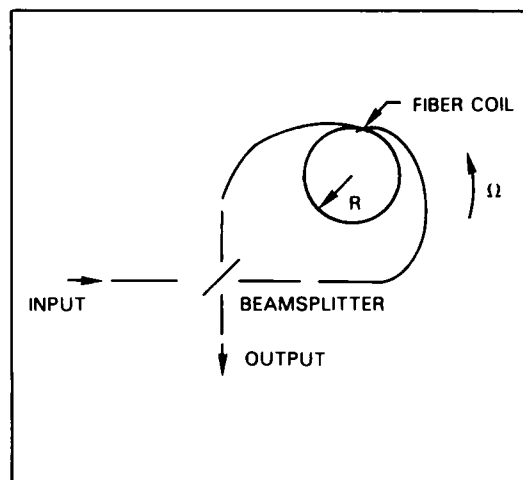
Fig. 4 — NRL gyro using a polarization-holding fiber and a superluminescent diode

Thus, for a fiber length of 500 m, wound on a 10-cm-radius coil with a laser wavelength of 1 μm, a rotation rate of 0.1°/hr (4.8 μrad/s) provides a Sagnac phase shift of 1 μrad. Even though this is a very small effect, it is about equal to those encountered in other fiber-optic sensing applications such as acoustic and magnetic field measurements, and it is readily measurable. Obviously longer fibers would give higher rotation sensitivity.

Demonstration System: We have designed, fabricated, and demonstrated a fiber gyroscope that detects rotation with high sensitivity. The gyroscope (Fig. 4) uses fibers which maintain an input polarization state in the coil and the fiber (Sagnac) coupler. The 430-m-long fiber is wound on a 16-cm radius drum. A phase modulator in the optical circuit provides an AC signal outpu..

The gyroscope noise level at zero rotation is shown in Fig. 5 for signal averaging times *TC*s of

1.25 and 40 s. The root-mean-square (rms) noise in these traces is plotted vs averaging time in Fig. 6 showing the inverse square root dependence on *T* that is characteristic of white noise. This figure also shows the experimentally determined noise of the detector only (□) at *T* = 1.25 s, which is within a factor of two of the gyro noise. This demonstrates that fiber-gyro baseline stability is very close to the fundamental limits imposed by thermal and shot noise in the detector. Rotation rates larger than the gyro noise limit can then be measured. This and other experiments have shown, at least in a laboratory environment, that the fiber-optical gyro can operate at the level required for navigational-quality strapdown inertial guidance systems.

Advantages: There are many reasons why fiber-optic gyros are attracting substantial interest. Fiber gyros are all solid-state with no moving parts; hence, they should have reduced maintenance schedules as compared to present spinning

TC = 1 25 sec

0 1 hr

| | | | |
| 0 | 2 | 4 | 6 | 8 | 10 |

TIME (min)

TC = 40 sec

0.02°/hr

| | | | |
| 0 | 2 | 4 | 6 | 8 | 10 |

TIME (h)
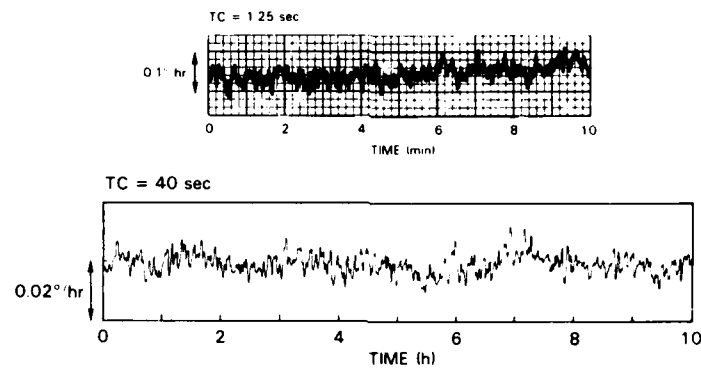
Fig. 5 — Noise levels (with no rotation) for the NRL gyro
for signal averaging times TCs of 1.25 and 40 s
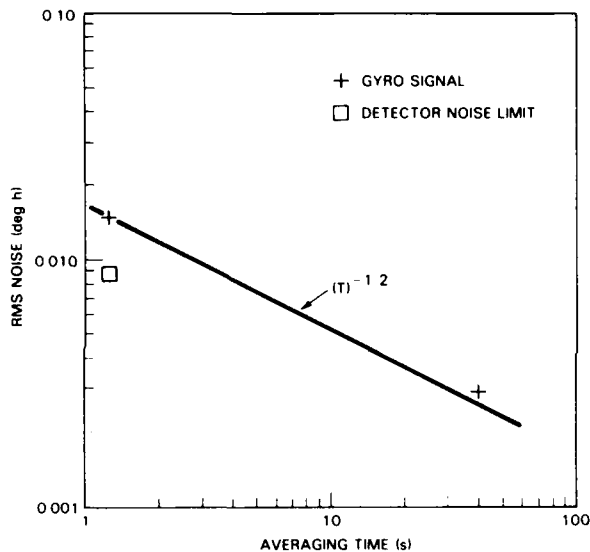
Fig. 6 — An rms noise against signal averaging time for
the NRL gyro at zero rotation conditions. The gyro noise
is within a factor of two of the experimentally determined
detector noise. Rotation rates above this noise floor can
be measured by the fiber gyro.

mass gyros. Fiber gyros have sensitivities equal to ring-laser gyros. They also lack the problems that have plagued ring-laser development, such as optical lock-in, which requires mechanical dithering, and requirements for precision block and high-quality mirror fabrication. Therefore, the ultimate advantage of fiber gyros for many applications is that they can be constructed from inexpensive components and should therefore be less expensive than other types of gyros.

Of course the fiber-optic and ring-laser gyros are simply different engineering implemen-

tations of the same physical phenomena—the Sagnac effect—to measure rotation. The ring-laser gyro, after two decades of development, is now commercially successful. The fiber-optic implementation is much newer, but the rapid improvement in fiber components will ensure that further improvements will be more rapidly realized.

[Sponsored by NAVAIR]

Reference

1. V. Vali and R.W. Shorthill, *Appl. Opt.* 15, 1099 (1976). ∎

A Hologram Wavefront Corrector for Laser Diode Beams

G.C. Gilbreath-Frandsen and W. H. Carter
Space Systems and Technology Division

Diode lasers have several outstanding features which make them well-suited for multi-gigabit data rate spacecraft communications. They are lightweight, compact, and provide surprisingly high output power relative to their size. Laser diodes are easily modulated by direct current injection, produce small beam divergences, and can be used as coherent light sources.

The emitting aperture of a laser diode is confined to a very small area (microns). Consequently, the beam divergence and angular spread is quite large compared to that of other lasers. Additionally, due to the architecture of the diode, the aspect ratio of the cavity is typically on the order of 3:1. As a result of the divergence and

the rectangular cavity, a fan-shaped output characterizes the diode, and its far field is elliptical (see Fig. 7).

Optical Link in Space: Conventional optics have been employed to correct and collimate the outputs beams of these diodes. However, such systems do not totally correct for the aspheric and asymmetric output. For spacecraft applications, they have the additional disadvantage of being heavy and bulky relative to the diode. A solution not only to the problem of bulk and weight but also to that of more completely correcting the output of the beam may lie in the use of holographic optical elements. A holographic optical element can not only perform the function of almost any conventional optical element but can also perform as an aspheric optical system. A hologram is formed by interfering two coherent beams of light and recording the resultant interference fringes in a thin photosensitive emulsion coating on a glass plate. When such a hologram is illuminated by either one of the original beams, it reproduces a beam similar to the other. Thus, it can be used as an optical element to transform laser beams. A complex conventional optical system can be replaced by a single hologram. Furthermore, a hologram can change a laser beam in ways a conventional optical system cannot. In the case of the laser diode, a hologram is made by interfering a beam having

the desired output with the output from the diode. Then the optical system is configured such that the diode illuminates the hologram and the resulting corrected beam is focused onto the detector or through an optical fiber. Figure 8 illustrates a typical system configuration for such an optical link.

Dichromated Gelatin Holograms: To be used in space, a hologram must be durable and efficient. Dichromated gelatin appears to be the best available photosensitive emulsion for this application. This material has nearly 100% diffraction efficiency, and the emulsion thickness can be modified, or "tuned," to adjust the spectral sensitivity. Emulsions made from this material have a generally flat spatial frequency response from 100 to 5000 lines per mm as well as low noise from scattering and stability when sealed properly. There are, however, some problems associated with this material. Dichromated gelatin is only sensitive in the blue-green (488 nm). A hologram made at this wavelength must therefore be tuned to the infrared to be useful with available laser diodes. Additionally, these types of holograms can only be made successfully with very careful laboratory technique and very good environmental control.

Prototype Holograms: Recently, we successfully made prototype holograms at NRL by
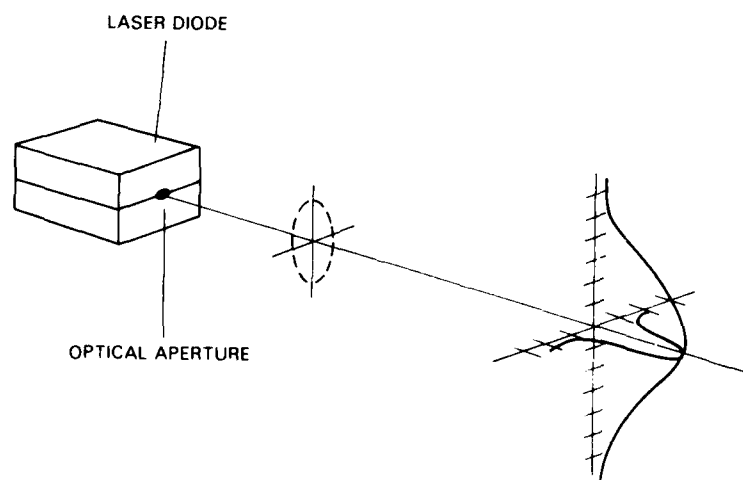
Fig. 7 — Elliptical output characteristic of a laser diode
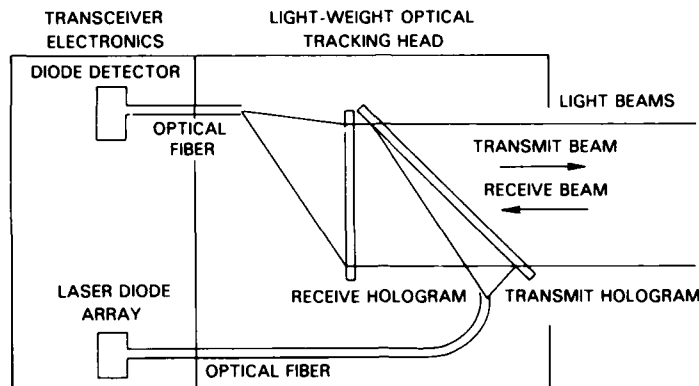
Fig. 8 — Optical communications system configuration using holographic optical elements to correct and collimate the output of a laser diode used as the coherent light source
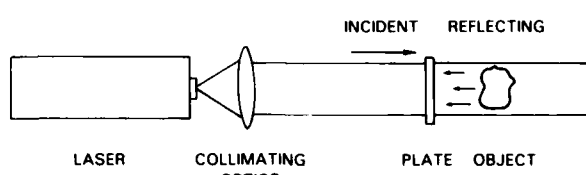
Fig. 9 — Hologram constructed by using Lippman geometry

using Lippman geometry, as illustrated in Fig. 9. The holograms were made by using conventional 649F photographic plates and a He-Ne laser (632.8 nm). Lippman geometry constructs reflection holograms which modify laser beams with reflected light. One major advantage to this type of hologram is that the emulsion can be swelled with water during processing to tune the hologram to respond at a desired wavelength. Thus, this geometry offers a possible solution to the problem of matching the hologram to the wavelength of the diode. The major disadvantage is that this type of hologram must be made in a virtually vibration-free environment which is isolated from air currents; otherwise the hologram will not provide the proper output.

Future work will build upon this preliminary investigation. We will derive a mathematical solution to correct the elliptical beam characterizing the output of the diode, convert the experiments from 649F plates to dichromated gelatin, and tune the hologram to operate at the required frequency. We will also investigate the possibility

of using the technique to correct the severe aspheric and asymmetric output of laser diode arrays for similar applications.

[Sponsored by ONR]

References

1. W.H. Carter and H.J. Caulfield, "Hologram Laser Beam Corrector and Combiner for a Satellite Data Link," *Appl. Opt.* (in press).

2. G. Evans, J. Leary, and J. Wilcox, "Applications of Semiconductor Lasers in Space Communications," *Opt. Eng.* **22**, 247-255 (1983). ∎

Optical Control of a Phased Laser Diode Array

L. Goldberg, H. F. Taylor, and J. F. Weller
Optical Sciences Division

Many military communication systems and signal processors require laser sources with the following characteristics: (a) optical power levels >100 mW, (b) diffraction-limited beam sizes, (c) a single frequency spectral line, (d) compactness, and (e) operation near room temperature. Conventional optics can efficiently focus such sources and are used in optical processors because they increase the signal-to-noise ratio. Semiconductor lasers are small and reliable, but state-of-the-art devices can generate power levels only up

154

to 15 mW. Generation of continuous or pulsed, high optical output power from semiconductor lasers with the above properties would greatly benefit several Navy communication systems.

An experimental approach has succeeded in obtaining more than one watt of optical power by coherently combining the power of many laser diodes that operate on the same chip [1]. The lasers are fabricated close enough to each other to interact and couple energy from one laser to another. The optical phase of each laser is locked (that is, fixed) to every other one in the array resulting in an optical system analogous to a one-dimensional microwave phased array. However, laser arrays generally have not exhibited single frequency output and diffraction-limited profiles. The array outputs have multiple spectral lines and a far-field pattern that is broader than expected for a diffraction limited beam. Furthermore, the far-field intensity pattern has two lobes (or spots) instead of one. At NRL, scientists have developed a technique to control the frequency spectrum of the laser array as well as the far-field intensity pattern which makes the array more useful for a variety of Navy applications. The technique is based on injecting light from a discrete laser (the master laser) into the laser array (the slave laser). Previous work at NRL [2-4] used this technique to control the phase and frequency of individual lasers, but never before had an array been locked by a master laser.

Experimental Setup: Figure 10 shows the experimental arrangement. The commercially obtained laser diode array consists of 10 gallium-aluminum-arsenide (GaAlAs) lasers spaced on 10-μm centers. Each laser is a proton-implanted, gain-guided, 5.0-μm-wide stripe device with a 250-μm cavity length. The master laser is a standard single-frequency GaAlAs laser that is mounted on a thermoelectric cooler that controls temperature. A combination of cylindrical and spherical lenses produces an injecting field distribution at the array facet that is <5μm wide perpendicular to the plane of the laser array and approximately 100 μm parallel to it. One facet of the array is a mirror that reflects nearly all the light from that side. Thus, the injecting beam is incident on one side only. A beam splitter (BS) between the master and slave array extracts a portion of the beam for characterization. Little optical feedback enters the master laser or the array.

Array Performance: Figure 11 provides the far-field intensity distribution and spectral intensity distribution for both unlocked and locked
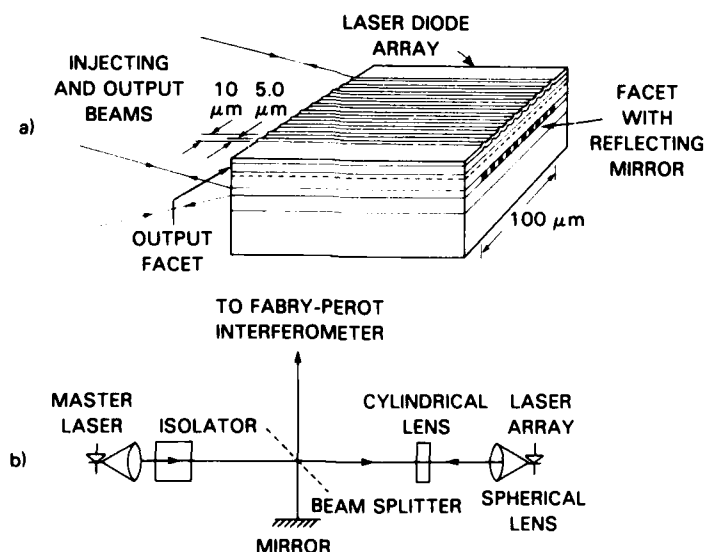
Fig. 10 — Optical injection locking of a laser diode array; (a) a 10-element laser diode array with one facet being a reflecting mirror opposite the output facet and (b) the experimental arrangement for optical characterization of the master and slave laser array

FAR FIELD INTENSITY DISTRIBUTION

SPECTRAL INTENSITY
DISTRIBUTION
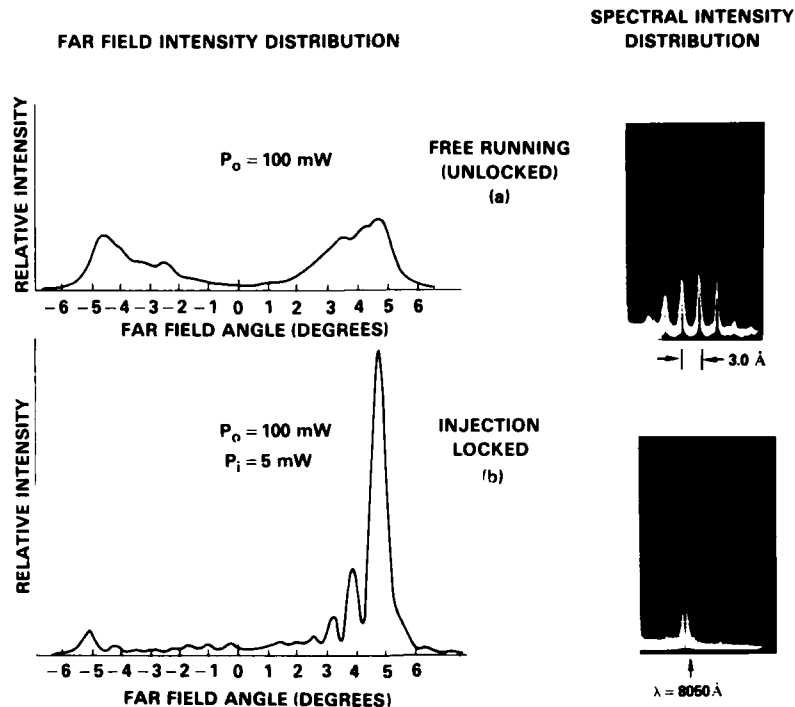
Fig. 11 — Properties of a laser diode array in (a) an unlocked condition and (b) a locked condition. Injection locking changes the spatial pattern (left) from a broad, double peak to a narrow signal peak. Injection locking changes the spectral output of the array from six broad lines to a single narrow line near 8050 Å (right).

conditions. The far-field intensity distribution of a free-running (unlocked) array (upper left) consists of two broad peaks with an angular separation of approximately 9.0°. When injection-locked with 5.0 mW of optical power, the far field changes to a single narrow lobe (lower left) with a half-width of 0.5°, that is centered at 4.5° away from the normal to the array facet. The measured half-width (0.5°) agrees well with the calculated half-width of a diffraction pattern from a 100-μm-wide aperture illuminated by a plane wave. Under injection-locked conditions, the main lobe contains 60 to 70% of the total laser array output power of 100 mW.

The spectral output of the unlocked array (Fig. 11, upper right) consists of five modes of comparable intensity, separated by 3.0 Å. Each mode has a spectral width of approximately 40 GHz, and the spectral envelope is centered at 8050 Å. Compare this with injection locking which results in single mode emission at 8050 Å (Fig. 11, lower right). The locking results in the

suppression of the subsidiary spectral lines by a factor of more than 200. The spectral width takes on the characteristics of the master laser with a linewidth less than the 100 MHz resolution of the Fabry-Perot interferometer used.

The overall stability of injection locking is determined by the locking bandwidth, which is defined as the master laser frequency range with the single lobe height >50% of its maximum value. The locking stability is in turn determined by the temperature stability of the master laser. For locking conditions such as Fig. 11b, a locking bandwidth of 16 GHz is measured. That means that a temperature stability of only 0.1° is required for the master laser and is easily achieved.

The NRL experiments in optical injection locking of laser diode arrays have produced a source that meets all criteria of successful military communication systems. This includes power levels in excess of 100 mW, diffraction limited

beam sizes, single frequency emission, narrow linewidth, and stable output. Future work will address higher power arrays (20 laser elements), modulation of the slave array as it is injection-locked, and improved coupling schemes to obtain the full beam output from the array.

[Sponsored by ONR and NAVELEX]

References

1. D.R. Scifres, R.D. Burnham, and W. Streifer, "High Power Coupled Multiple Stripe Quantum Well Injection Lasers," *Appl. Phys. Lett.*, **41** (2), (July 1982).

2. L. Goldberg, H.F. Taylor, and J.F. Weller, "FM Sideband Injection Locking of Diode Lasers," *Electron. Lett.*, **18** (23) 1019-1020 (Nov. 1982).

3. L. Goldberg, H.F. Taylor, J.F. Weller, and D.M. Bloom, "Microwave Signal Generation with Injection-Locked Laser Diodes," *Electron, Lett.*, **19** (13) 491-493 (1983).

4. L. Goldberg, C. Rauscher, J.F. Weller, and H.F. Taylor, "Optical Injection Locking of X-Band FET Oscillator Using Coherent Mixing of GaAlAs Lasers," *Electron. Lett.*, **19** (20) 848-850 (Sept 1983). ∎

Characterization of Detector Sensitivity Using Heterodyne Detection

G.C. Gilbreath-Frandsen
Space Systems and Technology Division

Optical heterodyning is a well-known technique for enhancing the signal-to-noise ratio in optical systems. The specific sensitivity of different types of photodiodes when used with this type of configuration however, was not clear. In 1984, as part of an effort to configure an optical system for beam steering a phased-array antenna, scientists at NRL examined and quantified the sensitivity of two types of standard photodiodes utilizing heterodyne detection.

Optical heterodyning is achieved by splitting a light beam into two separate beams and then recombining them. If both beams are the same frequency, stationary fringes will be observed in the recombined beam as in an interferometer. If one beam is frequency-shifted, then the fringes move at the beat, or difference, frequency which is equal to the amount of the frequency shift. The ratio of intensities between the modulated beam, known as the signal beam, and the unmodulated beam, known as the local oscillator (LO) beam, determines how quickly a given detector reaches a shot noise-limited condition.

Noise Sources: The ultimate sensitivity of a back-biased photodiode is limited by three types of noise: dark noise, Johnson noise, and shot noise. Dark noise is generated by the random action of primarily thermally excited electrons when no light impinges upon the active area of the detector as well as by excitation by cosmic rays and radioactive bombardment. This contribution is nominal for positive/negative (PN) and positive intrinsic negative (PIN) detectors. Dark noise can be a factor in characterizing the sensitivity of an avalanche photodiode (APD) but its contribution is usually very small.

Johnson noise, also called Nyquist noise, is the noise generated by the thermal motion of charge carriers in dissipative circuit elements, and its contribution is characterized by its mean square current:

$$<i_J>^2 = \frac{4kTB}{R_l}, \qquad (1)$$

where k is Boltzmann's constant, T is temperature in degrees Kelvin, B is bandwidth, and R_L is load resistance. Johnson noise includes contributions not only from the detector circuit but from the amplifier(s) as well. Shot noise, or quantum noise, refers to the noise generated by random quantum events in the detector. This noise is a direct result of discrete photo electron events and cannot be eliminated. Both dark noise and Johnson noise are independent of the optical input to the detector, but shot noise increases with increasing optical input. Because of this, the detector's signal-to-noise ratio (SNR) increases with increasing optical input until it reaches the shot-noise limit. To achieve a response which is shot-noise limited, the shot noise contributions must be made large enough to overshadow the contributions from the other noise sources.
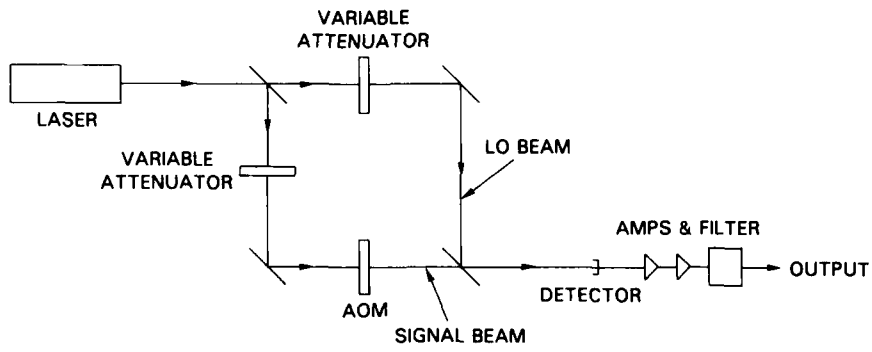
Fig. 12 — Optical heterodyne detection configuration employing a Mach-Zehnder
interferometer with an acoustooptic modulator
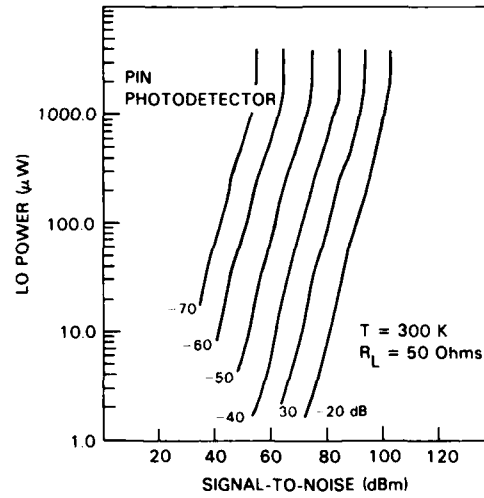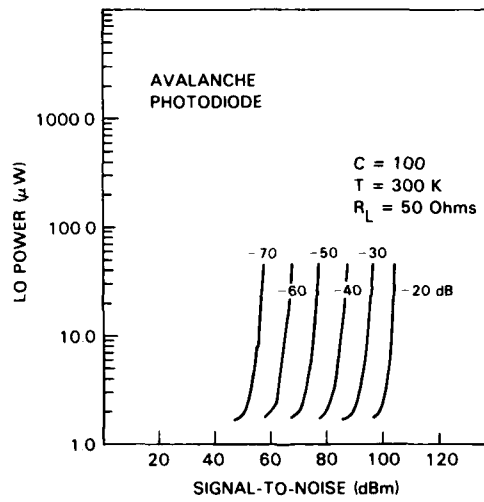
Fig. 13 — Detector sensitivity curves for
APD and PIN photodetectors

Shot-Noise Limit: There are a number of ways to enable the shot noise contribution to dominate the overall noise figure. One way is to increase the load resistance until the contribution from the shot noise is significantly greater than that from Johnson noise. However, the larger the load resistance, the slower the detector response. Another way is to increase the overall power impinging on the detector. The greater the light intensity, the greater the quantum noise level.

Once a shot-noise-limited condition is reached, the S/N for semiconductor photodiodes is defined as:

$$\frac{<i_S>^2}{<i_N>^2} = \frac{\eta P_S P_L}{h\nu B(P_S + P_L)}, \qquad (2)$$

where η is the efficiency, h is Planck's constant, ν is the optical frequency, B is the bandwidth, and P_S and P_L are the incident signal and local oscillator powers, respectively.

Measurements and Results: The apparatus used in this investigation, as shown in Fig. 12, employs a Mach-Zehnder interferometer. The beam in one leg is modulated by using an acousto-optic modulator (AOM) which is driven at 47 MHz. The signal and LO beams are combined and focused onto the detector with a microscopic objective. The signal from the detector is amplified and passed through a narrow bandpass filter. The S/N is then measured by using a Hewlett-Packard 8566B Spectrum Analyzer.

The detectors under consideration were a standard Hewlett Packard PIN and an RCA APD which are photodiodes that are sensitve in the red and infrared. Intensities in the signal leg were varied, thereby varying the total amount of power

in P_S. When the intensity of P_L is much greater than the intensity of P_S, Eq. (2) simplifies to:

$$\frac{<i_S>^2}{<i_N>^2} = \frac{\eta P_S}{h\nu B}. \qquad (3)$$

Both the PIN and APD achieved shot-noise-limited performance using this system configuration when $P_L/P_S \gg 1$. In fact, both detectors reached the calculated limit when $P_L = 2\,\mu W$ for the APD and $P_L = 2$ mW for the PIN. Figure 13 presents families of curves for the LO power vs signal-to-noise for each detector used in the configuration shown in Fig. 12. Each curve represents a different level of attenuation in the signal beam.

Photodiode Operation: PIN and APD detectors employ wide depletion regions in their architecture. When light impinges on a doped layer, electrons and "holes" are freed into the intermediate region. When this region is biased, the electrons and holes drift in the direction of the applied field thereby contributing to the current. However, the APD is back-biased with a relatively high voltage (230 to 500 V). Consequently, the carriers are accelerated across the depletion layer and acquire enough kinetic energy to enable new electrons to "jump" from the valence to the conduction band. The result is a dramatic increase in junction current, or current gain. In this case, the APD exhibits a 30 dB gain with respect to the PIN using heterodyne detection and the Mach-Zehnder configuration.

[Sponsored by ONR]

Reference

1. A. Yariv, *Introduction to Optical Electronics* (Holt, Rinehart, and Winston, Inc., New York, 1971). ∎

Materials modification and behavior

Among the new materials developed in the Biomolecular Engineering Branch are synthetic red blood cells, expected to be used for emergency transfusions. Here an NRL scientist prepares these cells for testing.

MATERIALS MODIFICATION

NRL conducts a broad spectrum of research into materials modification and behavior. These articles highlight some of this diverse research. The first two articles describe work in biotechnology, a relatively new endeavor for NRL, while the other articles describe more traditional work. The work in this chapter was performed in four NRL divisions. They are Plasma Physics (Code 4700), Chemistry (Code 6100), Material Science and Technology (Code 6300), and Optical Sciences (Code 6500).

A few of the many research projects at NRL in materials modification and behavior, other than those described in this chapter, are:

- energetic materials
- advanced joining science
- rapid solidification techniques
- development of structural and electronic ceramics and ceramic composites
- biophysical properties of liposomes
- advanced aircraft fuel development

- carbon as an absorbent and catalyst support
- high-temperature alloys and coatings
- ion implantation
- optoelectronic materials development
- molecular beam epitaxy growth
- microelectronics

High Pressure Nervous Syndrome

E.L. Chang and P. Yager
Chemistry Division

High pressure nervous syndrome (HPNS) is a set of life-threatening symptoms exhibited by divers at depths greater than 600 m where the pressure is about 60 bars (~60 atm). These symptoms—tremors, and in extreme cases, convulsions—prevent humans from free-diving in a nonrigid suit below these depths and would theoretically lower the survival chances of sailors escaping from disabled submarines. Research by other laboratories has studied the effects of pressure on whole neural systems, on live animals, or on the intriguing connection between pressure and the anesthetic effect. At NRL, we are exploring the molecular basis of this pressure-induced syndrome by examining the effects of pressure on various models of the neural synapse—the most exposed feature of the nervous system.

The synapse is the region where one nerve cell communicates with others through molecules (such as acetylcholine) called neurotransmitters (Fig. 1). These chemical neurotransmitters are stored inside synaptic vesicles in the presynaptic region of the junction. Release of the neurotransmitters occurs when the vesicles fuse with the presynaptic membrane and the molecules diffuse across the synaptic gap binding the protein receptors in the postsynaptic region. The binding event causes an ion channel in the receptor to open. Any distortion or destruction of these synaptic systems by pressure would have severe physiological implications. Our research has focused on the effects of pressure on the conformation of the receptors as well as on the process of synaptic vesicle fusion.

Receptor Structure: The opening and closing of receptor ion channels in the postsynaptic membrane involves structural changes in the proteins. Does pressure affect the structure of these receptor proteins and cause synaptic malfunction? Since membrane proteins are extremely hard to crystallize, very few are candidates for structural determination by X-ray crystallography; thus other methods are needed to study their
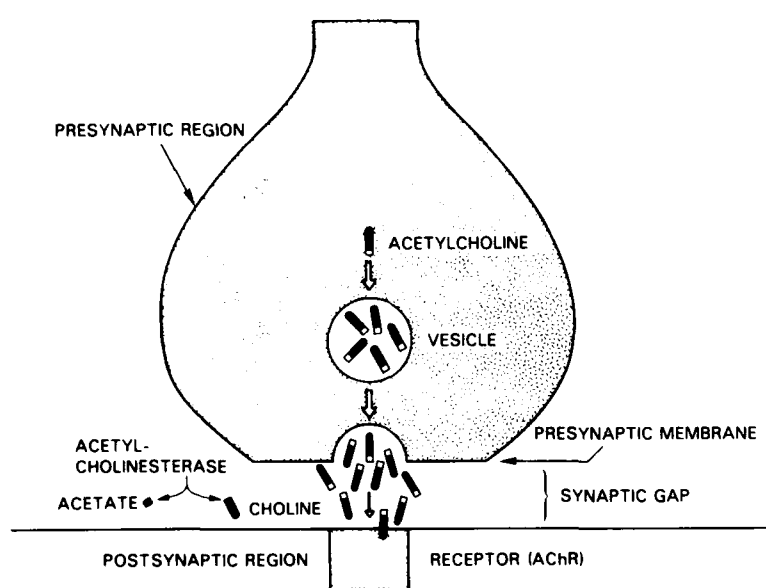
Fig. 1 — The synaptic region. The neurotransmitter (in this case, acetylcholine) is assembled in the presynaptic bulb and packaged in vesicles. Fusion of vesicles occurs on demand causing emptying of contents into the synaptic gap (cleft) region. Diffusion of the neurotransmitters across the gap is followed by binding of the acetylcholine molecules to AChR, the receptor specific for acetylcholine. Channels inside the receptors then open, allowing ion flow.

Fig. 2 — A vesicle fusing to a flat membrane. Note in the center that the bilayer structure is transiently disrupted in the process.
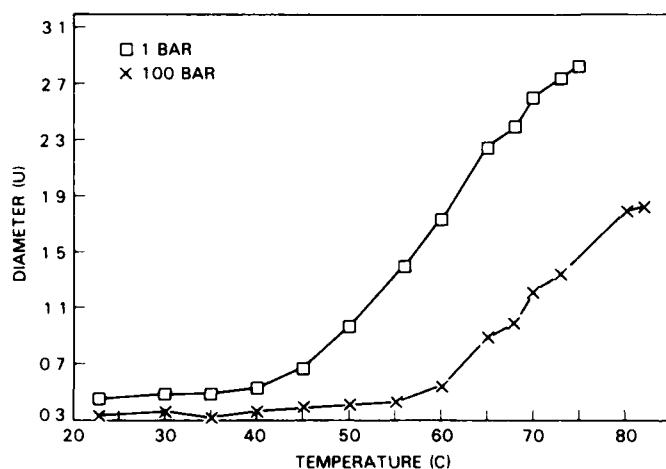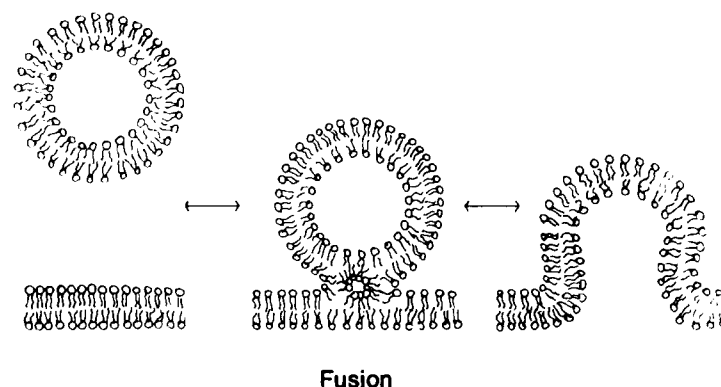
Fusion

Fig. 3 — Plot of the increases in average size of vesicles as a function of temperature at two different pressures. Fusion of vesicles decreases the total number of vesicles but increases the average size of individual vesicles (more lipids per vesicle); therefore, monitoring average vesicle size increase is equivalent to following the progress of vesicle fusion. Note that at 100 bars, the onset of size increase (i.e. fusion) has been delayed from about 45° to 60° C.

structure. We have taken the Raman spectra of the reconstituted membrane protein, acetylcholine receptor (AChR). Using an algorithm previously developed at NRL by Dr. R. W. Williams, we have analyzed the Raman spectra and determined the percentages of various secondary structures of AChR such as alpha helices, beta-sheets, and beta-turns. After characterizing the secondary structure of AChR at atmospheric pressure, the protein will be pressurized and examined for structural changes. Since this receptor depends on conformational changes to open and close its ion channel, any structural changes under pressure would imply that the AChR is not functioning. This type of abnormality constitutes a possible molecular mechanism for HPNS.

Synaptic Vesicle Fusion: Fusion of two lipid bilayers occurs when they come into contact, comingle, and meld into one integral membrane. This process is a very important one for many

cellular functions—in particular, the fusion of the vesicles to the presynaptic membrane. This fusion is one of the major steps in neurotransmission, yet the mechanism of vesicle fusion itself is not well understood and requires exploratory research. Figure 2 illustrates the possible mechanism of vesicle fusion with the presynaptic membrane. As fusion begins, a transient nonbilayer structure forms where the vesicle and membrane meet (center of Fig. 2). One possible transient structure that may be involved in this fusion is the inverted hexagonal phase, H_{II}. Our previous research has shown that the transition temperature from the bilayer phase to the H_{II} phase is very sensitive to changes in pressure and that pressure increases the temperature at which the H_{II} phase is stable. Recently, we have obtained data showing that the fusion of vesicles made up of lipids that undergo a H_{II} transition is inhibited by pressure (Fig. 3). The fusion of vesicles increases the size of individual vesicles in a sam-

ple while decreasing their number. So the increase in average vesicle size with temperature is equivalent to increased fusion with temperature. At a pressure of 100 bars (~100 atm)—the range where HPNS occurs—the rate of vesicle size increase with temperature does not occur until much higher temperatures are reached, indicating that pressure inhibits fusion. Thus, we have shown that pressure inhibits vesicle fusion in model systems and that the H_{II} phase may well play a role in vesicle fusion. In the future, we will characterize how actual synaptic vesicles fuse with the presynaptic membrane.

[Sponsored by ONR]

Synthetic Red Blood Cells

M.C. Farmer and B.P. Gaber
Chemistry Division

There is a recognized national need for an oxygen-carrying blood surrogate for emergency resuscitation of trauma victims. Blood surrogate research at NRL has led to the development of liposome encapsulated hemoglobin (LEH). This material resembles a synthetic red blood cell, but it lacks the surface blood-type antigen (the substance which stimulates the production of antibodies that cause rejection if blood is mismatched). An acceptable blood surrogate must meet certain criteria. These include high oxygen capacity, an oxygen affinity low enough to ensure adequate release of oxygen to the tissues and comparable

CO_2 release at the lungs, functional circulatory persistence of at least 12 h, lack of toxicity, universal transfusability, prolonged shelf life, and large-scale fabrication feasibility. We have had considerable success in meeting many of these criteria. Further evaluation, however, will be necessary before preclinical trials are begun. These trials will be performed in collaboration with the Department of Surgical Research at Michael Reese Hospital and the University of Chicago.

Method: The liposomes are produced by extruding a suspension of lipids in a buffered hemoglobin solution through a size-graded series of porous membranes. The hemoglobin is prepared from outdated human blood, carefully separated from the membrane fragments of red blood cells. The extrusion procedure produces a nearly uniform suspension of vesicles averaging 0.5 μm in diameter as determined by photon correlation spectroscopy (PCS).

Oxygen Binding: The encapsulated hemoglobin binds oxygen reversibly and cooperatively, with binding parameters comparable to those of the original hemoglobin solution. Cooperativity is indicated by the S-shaped oxygen-binding curve in Fig. 4. The inset Hill plot, replotted from the oxygen-binding curve, is a means of quantifying the cooperativity. A Hill coefficient n_{50} of 2.8 indicates that, for a given drop in oxygen partial pressure as the blood passes through the tissues, 2.8 times as much oxygen will be released from
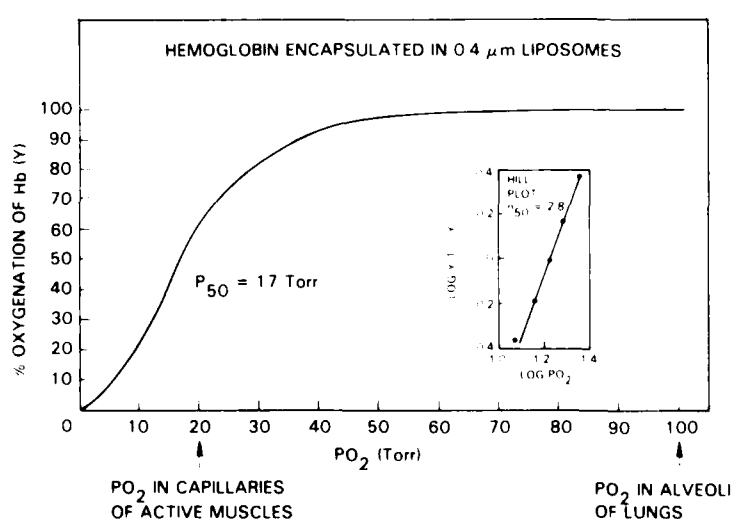
Fig. 4 — The oxygenation curve for 0.4 μm vesicles at 37°C. The partial pressure of oxygen required for 50% saturation of the LEH is 17 Torr, and the Hill coefficient n_{50} is 2.8.

165

Fig. 5 — Ca^{++}-induced changes in particle size are measured by PCS. The changes are reversible by gentle agitation and by chelation of Ca^{++} with EDTA, indicating aggregation rather than fusion.
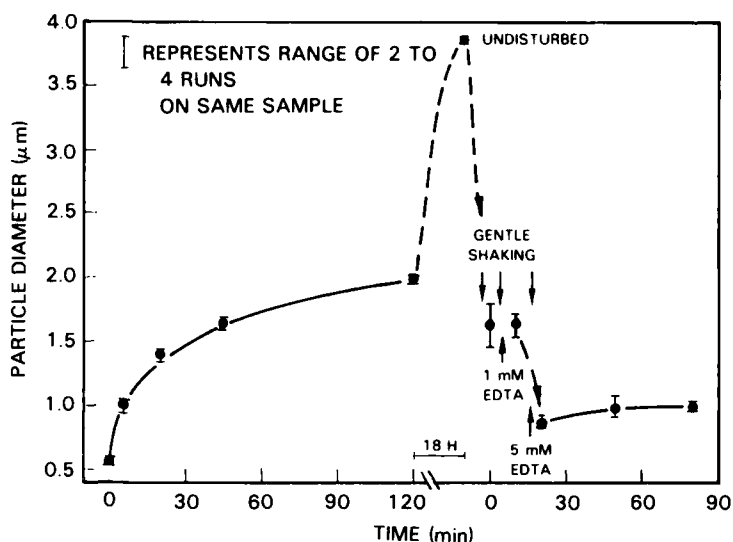
the blood as would have been the case in the absence of cooperativity. This property of hemoglobin makes it a much better oxygen carrier for use as a blood surrogate than an oxygen-binding material which is noncooperative, such as myoglobin (found in the muscles) or the perfluorinated hydrocarbon-based blood surrogate under investigation elsewhere. In addition, oxidation of the encapsulated hemoglobin proceeds very slowly, and the LEH binds oxygen reversibly for many months when stored at 4°C [1].

Interactions of LEH and Red Cells: Incubation of LEH with red cells in serum at 37°C for 8 ı results in neither red cell breakdown nor clotting. Surface repulsion due to the presence of negatively charged lipids permits prolonged storage without fusion or pronounced aggregation. Some aggregation of the LEH in serum due to Ca^{++} is expected and does, in fact, occur. As shown in Fig. 5, adding of Ca^{++} (as CaCl at time = 0) to a suspension of LEH results in a rapid increase in average particle size; however, the aggregates are easily dispersed by gentle agitation even after 18 h. A chelate (EDTA) which binds Ca^{++} strongly was added after gentle agitation. It further reverses the aggregation, verifying that fusion does not occur [2].

Viscosity: The viscosity of LEH and red blood cell suspensions decreases as the flow rate, and therefore the shearing, increases within a blood vessel. The two materials exhibit similar
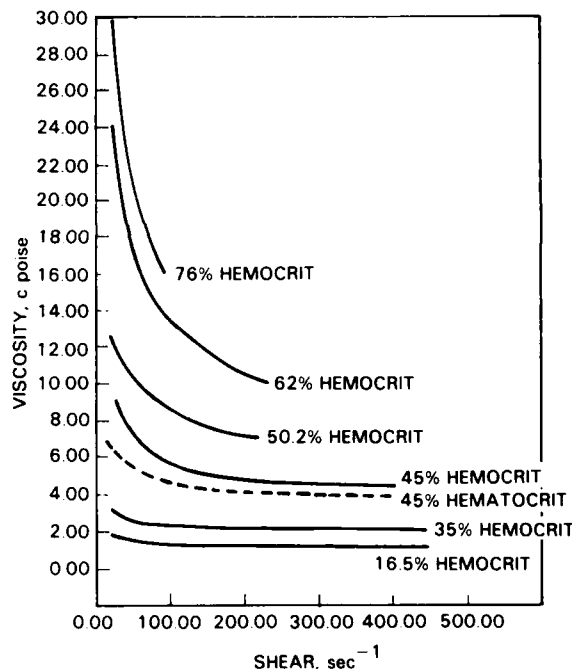
Fig. 6 — The viscosity of LEH and red blood cell suspensions decreases as the shear rate increases, exhibiting non-Newtonian behavior. The viscosity of blood also increases as the hematocrit increases. At a hematocrit of 45%, a suspension of red blood cells (dashed line) has a slightly lower viscosity than the LEH of a similar hemocrit.

patterns of nonlinear (non-Newtonian) behavior for a wide range of percentage cell concentrations by volume (hematocrit) (Fig. 6). The viscosity of the LEH at 45% "hemocrit" (the percent of

166

blood volume occupied by LEH) is similar to that of whole blood at the same red blood cell hematocrit (dashed line), as measured by standard techniques. The low shears at which the curves markedly change slope indicate that dispersal of aggregates is occurring. These shears are well below those encountered in blood vessels.

Circulation Persistence: We have developed a simple, accurate method for measuring circulation persistence by using small samples of blood drawn into a 50 μl centrifuge or hematocrit tube. The LEH fraction is less dense than the red blood cells because of its somewhat lower hemoglobin content; consequently, the LEH component in the sample sediments as a discrete layer above the red blood cells.

An injection of LEH into a mouse disappears from its bloodstream within hours. Using the hematocrit tubes, this disappearance can be readily observed without the use of radioactive tracers. A volume of LEH, equivalent to 30% of the total blood volume of a mouse, was injected into 25 mice. The half-life of the LEH varied from 5 to 15 h, depending on the lipid composition. This has also been predicted from other liposome studies [3]. All mice survived without noticeable adverse side effects. This circulation persistence is considered adequate for an emergency temporary blood replacement.

We have been able to produce synthetic red cells which have the appropriate oxygen-binding characteristics and prolonged shelf life that are required for successful blood surrogates. They lack acute toxicity and are blood-type free which should permit universal transfusability. The LEH circulation persistence in mice is adequate, but modifications in liposome composition may permit us to attain longer circulation half-lives. Large-scale fabrication procedures are feasible and are being developed. Animal testing to verify the efficacy of this blood surrogate is in progress.

References

1. B.P. Gaber, P. Yager, J.P. Sheridan, and E.L. Chang, "Encapsulation of Hemoglobin in Phospholipid Vesicles," *FEBS Ltr* **153**, 285-289 (1983).

2. M.C. Farmer and B.P. Gaber, "Encapsulation of Hemoglobin in Phospholipid Vesicles: Preparation and Properties of a Red Cell Surrograte," Proceedings of the 6th International Symposium on Red Blood Cell Metabolism and Function, G.J. Brewer, ed., (Alan R. Liss, Inc., New York, 1984) pp. 179-190.

3. J. Senior and G. Gregoriadis, "Stability of Small Unilamellar Liposomes in Serum and Clearance From the Circulation: the Effect of the Phospholipid and Cholesterol Components," *Life Sciences* **30**, 2123 (1982). ∎

Ceramics With Ordered Pore Structures

M. Kahn
Material Science and Technology Division

Ceramics are usually prepared from fine powders. These powders are often pressed into pellets or suspended in a slurry and cast and dried. High temperature sintering then fuses the compacted powder into a hard and often quite strong ceramic.

Dense ceramics are incompressible; they are similar to silly putty in that if the faces of a disk are compressed, its rim will expand. A rigid constraint around the rim makes it more difficult to depress the face. Such a material is said to have a high Poisson ratio, that is, a relatively large ratio of transverse to compressive strain.

Dense PZT Behavior: Lead zirconate titanate (PZT) is a piezoelectric ceramic. In disk form, it can generate a substantial amount of charge on its electroded faces when it is deformed by a uniaxial force on these electrodes; this response is designated "d_{33}." Because of this property, PZT is useful for sensing underwater sound pressure, that is, as a listening device or hydrophone. The design and performance of hydrophones made from conventional (dense) **167**

PZT is limited, because the application of hydro-static pressure (equal pressure from all directions) gives a response that is only 10% to 20% of that under uniaxial pressure. Recent work at NRL has shown that the hydrostatic response d_h of PZT and of many other piezoelectric materials is strongly related to its Poisson ratio γ by

$$d_h = d_{33}(1 - 2\gamma).$$

The Poisson ratio of dense PZT is usually more than 0.40.

Porous PZT Behavior: Porous ceramics under pressure compress more than dense material. This causes them to have a lower Poisson ratio than dense ceramics. Conventional, round, and randomly distributed pores enhance the hydrostatic sensitivity of PZT. For example, 55% of equiaxed porosity raises the hydrostatic response of PZT to 38% of the uniaxial response, but the strength is reduced 88% from that of dense ceramic. This is inadequate for practical applications.

We extended the theory for dense PZT to porous PZT, and this led to a pore-structure model which maximizes the hydrostatic response. This model suggests modifications to the elastic properties of the hydrophone material so as to minimize its Poisson ratio by incorporating flat (anisotropic), aligned, and ordered pores (Fig. 7). Such a structure then becomes an air-ceramic composite. The pores are highly compressible normal to their major plane but are relatively stiff in a direction parallel to this plane. These pores, therefore, convey to the composite only a small reduction of the elastic modulus in the direction of their major plane. Such a composite can have a significantly enhanced hydrostatic response with more than adequate mechanical strength.

Porous PZT Manufacture: Such a composite was made by using photolithographic masks as developed for silicon-based semiconductor manufacture. This was combined with screen-pattern deposition used in the preparation
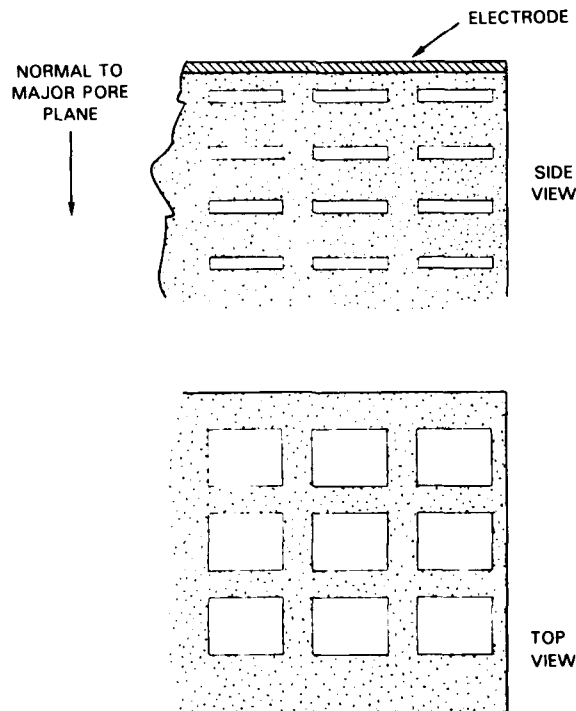
Fig. 7 — Side and top views of the rectangular pore model. Because of the ordered pore structure, the ceramic is quite stiff along the major pore plane but relatively compressible in the direction normal to the major pore plane.

of ceramic-based hybrid microcircuits. These screening techniques are used here to deposit a carbon-containing printing ink pattern onto ceramic tapes that are then stacked and laminated. The ink burns off during firing, leaving flat voids in the ceramic that replicate the ink pattern. The ink and the laminating techniques were adapted from multilayer capacitor manufacture, specifically those in which liquid electrodes fill internal voids formed during sintering.

Figure 8 shows computer-generated test patterns that were used to prepare and evaluate a variety of pore geometries. Figure 9 shows photomicrographs of a top view (a) and of cross sections (b) of pores made in PZT ceramic by using these techniques. These figures are an implementation of the model shown in Fig. 7.

Porous PZT Performance: With 15% of anisotropic and ordered pores, the hydrostatic charge response d_h of PZT was raised from 20% to 60% of the uniaxial response, with no noticeable reduction in strength as compared to dense PZT.

The dielectric constant ϵ of these porous samples, measured normal to the major pore plane, was less than half of that of dense ceramic. The hydrostatic voltage coefficient is $g_h = d_h/\epsilon$, and its value in the PZT with anisotropic and ordered pores often exceeds that of dense PZT by 600% or more.

Modeling and Further Developments: Refinements of the pore structure are expected to lead to performance improvements significantly

Fig. 8 — Computer generated experimental pore patterns for ceramics with ordered pore structures. The patterns represent the top view of the pores; the black areas are the pores or voids.
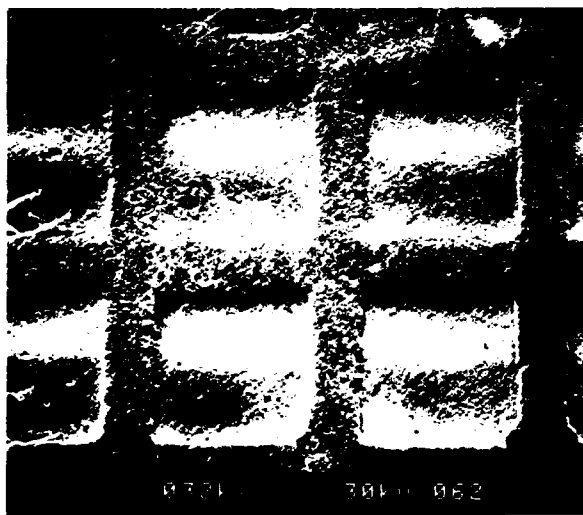
(a)
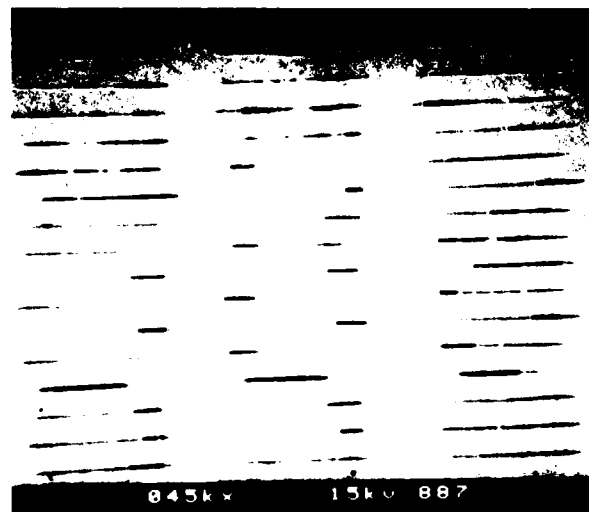
(b)

Fig. 9 — Microphotographs of the manufactured ceramics showing the top (a) and side views (b) of the pores

beyond those already achieved. This is being explored further, both by experiments as well as by finite element analysis of model structures. In this analysis, a calculated stress distribution in model pore structure is used to derive the piezoelectric output under hydrostatic pressure. The stress distribution is also used to find pore configurations that minimize stress peaks under loading or that shift the stress peaks into regions of highest strength. This is expected to also lead to an improved strength-weight ratio of the material. The reduction in dielectric constant mentioned previously may also find application in support members of very high frequency components, where minimization of stray capacitance to ground is important.

It should finally be noted that, during the preparation of ceramic-air composites, there are no two-phase diffusion and contamination problems, as there are during sintering of ceramic composites that contain two different compounds. The intermingling of two phases tends to degrade the performance of conventional composites, in particular when they are made for electronic applications where the materials are very sensitive to impurities and impurity gradients.

[Sponsored by ONR] ∎

The Mechanism of Void Formation and Ductile Fracture of Dispersion-Strengthened Copper-Aluminum Alloy

V. Provenzano and J.A. Sprague
Material Science and Technology Division

Internally oxidized copper-aluminum is a prototype of an important class of two-phase alloys known as the dispersion-strengthened alloys (DSAs). These DSAs contain small, hard, dispersed particles that are randomly distributed in a continuous ductile metal matrix. Usually, the metal matrix of these DSAs is either pure nickel, aluminum, or copper, while the common dispersoid particles are oxides of either silicon, aluminum, or thorium. The dispersoid particles strengthen the matrix giving it a significantly higher strength than the pure matrix alone. These DSAs are quite stable at elevated temperatures

because the size, shape, and spacing of the dispersoid particles are not affected by heat treatments. In addition, the creep resistance of these DSAs is quite high because the dispersoid particles straddle the grain boundaries preventing grain boundary sliding. The high strength, the creep resistance, and the structural and thermal stability make DSAs particularly appropriate for use at elevated temperatures.

Theories of Fracture: The mechanical properties of DSAs, such as tensile strength fracture toughness and ductility are determined by the size, the distribution, and the bonding of the particles to the metal matrix. These same variables profoundly affect the fracture properties of these DSAs because fracture is initiated as void formation and growth, and this always begins either by the fracturing of the particles or by the separation of the matrix at the particle-matrix interface. Thus, the knowledge of void formation is crucial to understand the fracture properties of DSAs. Previous studies of DSAs indicate that in almost all cases, void formation at the particle-matrix interface is preceded by plastic yielding of the metal matrix. A model of void formation (first formulated by Ashby [1]) consists of the following sequence of events. When an external stress is applied to a DSA and the matrix is plastically deformed, the stresses normal to the particle-matrix interface along the tensile direction increase with increasing strain. These normal stresses are the result of the mismatch of the strains at the particle-matrix interface. Voids should form at the interfaces when the normal stress exceeds the interfacial strength between the particle and the matrix. This condition is known as the "stress criterion" for void formation. Argon et al. [2], who later elaborated Ashby's model, pointed out that the stress criterion was a necessary but *not* a sufficient condition for void formation. According to Argon, for void nucleation to occur, a stress criterion as well as an energy criterion must be satisfied. During the plastic deformation stage, the elastic strain energy stored in the matrix material around the particle must exceed the energy required to separate the matrix from the particle. This added requirement is known as the "energy criterion" of void formation. Because of this energy criterion, it follows

that voids can form only around particles that are larger than a minimum particle size.

NRL has been studying the effects of dispersoid particles on the mechanisms of cavity formation and ductile fracture of DSAs. The initial research studied an internally-oxidized copper-aluminum alloy containing approximately 0.5% by volume of alumina (Al_2O_3) particles. Copper-aluminum is easily prepared by internal oxidation that produces well-defined spherical alumina particles in a pure copper matrix. The internally oxidized copper-aluminum DSA was produced by using powder metallurgy techniques and was then consolidated by hot extrusion.

Tensile Fracture Study: We performed room temperature tensile tests on the copper-aluminum alloy by using 0.25-in.-diameter rod-shaped smooth tensile specimens of uniform gauge section. Prior to the tensile tests, the as-extruded material was vacuum annealed for 1 hr at 850°C. We analyzed both the annealed and tensile-tested material with scanning electron microscopy (SEM) and energy dispersive X rays to study the microstructure and fractographic features. Analytical electron microscopy was used to relate the void formation to the spatial and size distribution of the alumina particles. The microstructure of the annealed material before stress testing is shown by the transmission electron micrograph (TEM) presented in Fig. 10.
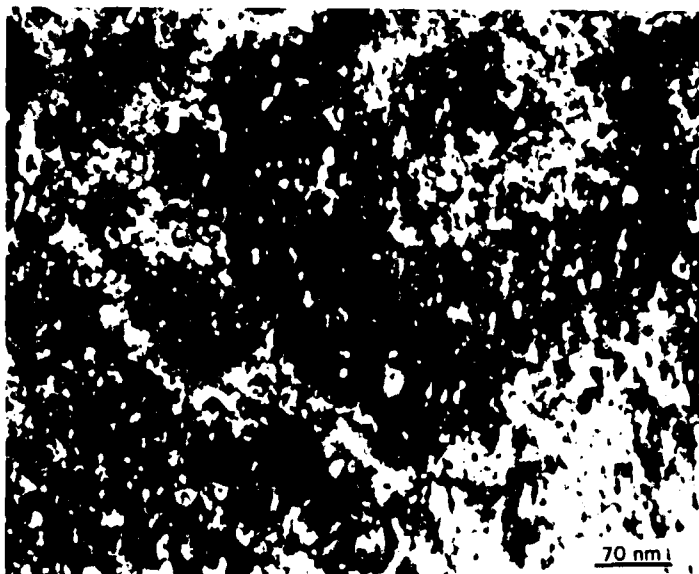
The micrograph shows the presence of many light-colored alumina particles of 3 to 5 nm in diameter. The small size prevented clear identification of the particles by electron diffraction or by composition analyses. Most of these particles, because of their small size, strengthen the alloy but do not form voids when the material is plastically strained during the tensile test.

When a tensile specimen of ductile material fails, it forms a "cup-cone" fracture. The cup side of the fracture is shown in Fig. 11(a). The failure occurred because the microvoids which formed around the particles grew and coalesced. Figure 11(b) is an SEM looking down on the fracture surface which contained void coalescence. X-ray analysis identified the precipitate particles at the bottom of the larger voids of Fig. 11(b) as alumina. A thin foil was cut from the longitudinal section of the failed specimen of Fig. 11(a)(b). Figure 11(c) is a scanning/transmission electron micrograph (STEM) of a portion of the foil about 4 mm from the fracture surface where the strain was about 25%. (Strain = $2 \ln (d_0/d)$, where d_0 is the diameter of the unstrained rod and d is the diameter of the rod at the point of analysis.) The STEM clearly shows that at this strain value only alumina particles larger than about 50 nm in diameter formed voids (bright crescents) while the smaller particles did not. Figure 12 shows that the TEM was taken from the foil cut from the longitudinal sec-

Fig. 10 — Microstructure of internally oxidized copper-aluminum alloy in the annealed condition. The light colored features on the TEM are believed to be alumina particles that strengthened the copper matrix but did not form voids when strained during tensile tests.
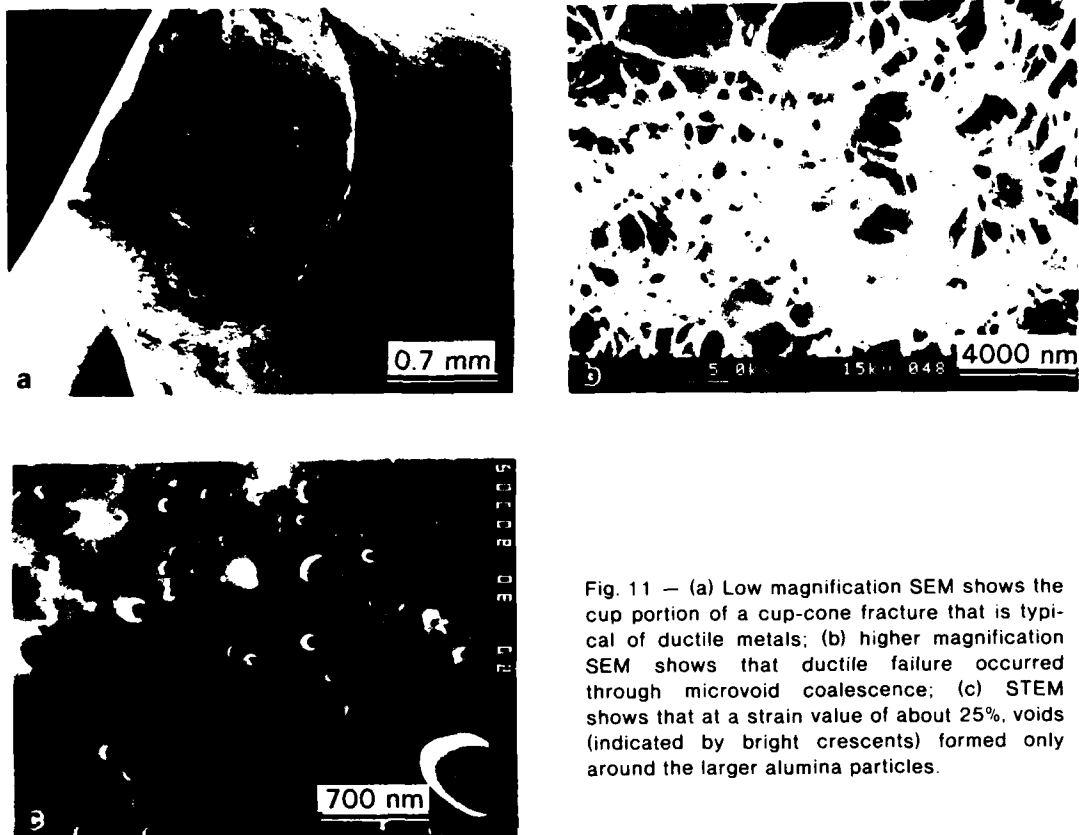
171

Fig. 11 — (a) Low magnification SEM shows the cup portion of a cup-cone fracture that is typical of ductile metals; (b) higher magnification SEM shows that ductile failure occurred through microvoid coalescence; (c) STEM shows that at a strain value of about 25%, voids (indicated by bright crescents) formed only around the larger alumina particles.
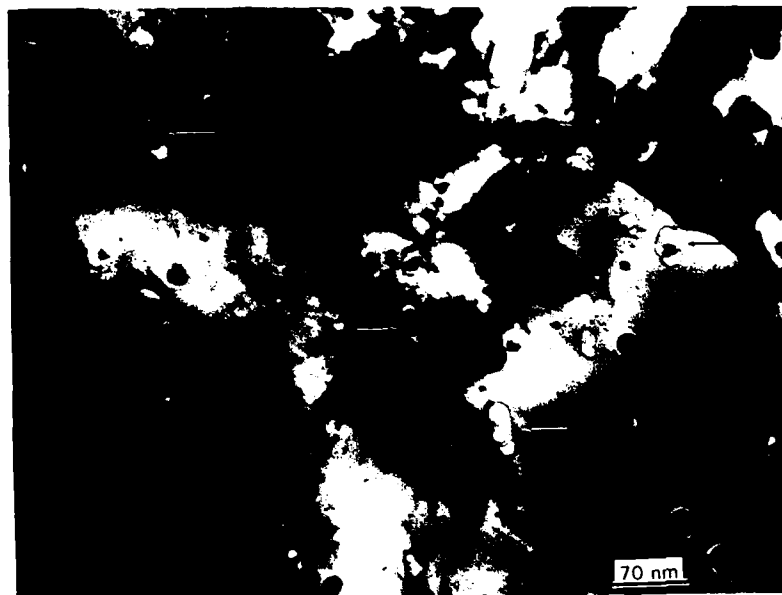

Fig. 12 — TEM of the same failed specimen shown in Fig. 11(a)(b). The micrograph shows that at a strain value in excess of 100% voids (indicated by arrows) formed both on larger and smaller size particles above a minimum diameter of about 5 nm. However, some large size particles (copper oxide) did not form voids, probably because they bond more strongly to the copper matrix than do the alumina particles.

tion of the failed specimen close to the fracture surface where the strain value was over 100%. At these higher strains and above a particle diameter of 5 to 6 nm, voids (indicated by arrows) formed both at the smaller and larger alumina particles. The TEM also shows that some larger particles from 50 to 100 nm did not form voids. These larger particles are probably copper oxide particles that appear to be more strongly bonded to the copper matrix than the alumina particles.

Interpretation of Study: The significant result of this NRL study on internally oxidized copper-aluminum is the following: there is a size dependence void formation which *is a function of strain level.* This is not consistent with Argon's energy criterion theory. For low concentrations of dispersoid particles, Argon's model predicts that when a critical strain value is reached and above a minimum particles diameter, void formation is independent of particle size. Instead, the NRL study showed that above a minimum particle diameter, void formation was independent of particle size *only* in high strain regions; in lower strain regions, voids formed only around *larger* diameter particles. Further, Argon's theory predicts a minimum particle size of about 20 nm for the present copper-aluminum alloy, whereas the experimental data yielded a minimum size of about 5 nm.

In the future, we will attempt to modify existing theories or develop new models of void formation and ductile fracture that are more consistent with the experimental results. We will investigate why voids are absent around some larger size particles even at high strain levels. We will also conduct mechanical tests and pertinent microstructural analyses on other copper-aluminum DSAs with larger concentrations of dispersoid particles to establish relationships between dispersoid particle interaction, void formation, and the growth and failure of dispersion-strengthened alloys.

References

1. M.F. Ashby, "Work Hardening of Dispersion Hardened Crystals," *Phil. Mag.* **14**, 1157-1172 (1966).

2. A.S. Argon, J. Im, and R. Safoglu, "Cavity Formation from Inclusions in Ductile Fracture," *Metall. Trans.* **A 6**, 825-837 (1975). ∎

Cure Monitoring of Polymeric Materials

B.S. Holmes
Chemistry Division

Polymers are being used increasingly in Navy combat platforms. This has generated an urgent requirement for a method to assure the uniformity and reliability of their mechanical properties which are governed by the cure state of the polymer. NRL scientists are using a newly developed technology called microdielectrometry to monitor and control the cure state of acoustical tiles, elastomeric repair systems for sonar dome rubber windows (see *1983 NRL Review*, p. 87), and adhesively bonded aircraft composite repair. Automated microdielectrometer systems are being adapted for production line process control and as field deployable units for battle damage repair.

Microdielectrometry: This measurement technology, developed under an Office of Naval Research contract at the Massachusetts Institute of Technology, measures changes in the dielectric properties of polymeric materials as they cure. The instrument measures the dielectric permittivity ϵ', the dielectric loss factor ϵ'', and the dielectric loss tangent ϵ''/ϵ' as a function of time and temperature during the cure cycle. The sensing electrodes are a pair of very small, planar, interdigitated electrodes with a 12.5 μm gap fabricated as part of a silicon integrated circuit sensor [1,2]. The miniature sensor has an active area of 0.1 in. × 0.2 in. and can be used with milligram samples or can be embedded in full-scale parts. The changes in dielectric properties observed with microdielectrometry reflect both chemical changes and thermal effects of the polymeric cure.

Dielectric Cure Monitoring: In dielectric cure monitoring, the polymeric material is placed on the sensor or the sensor is embedded in the material. Upon application of an alternating **173**

Fig. 13 — The change in dielectric loss factor
ϵ'' during a typical polymer cure cycle
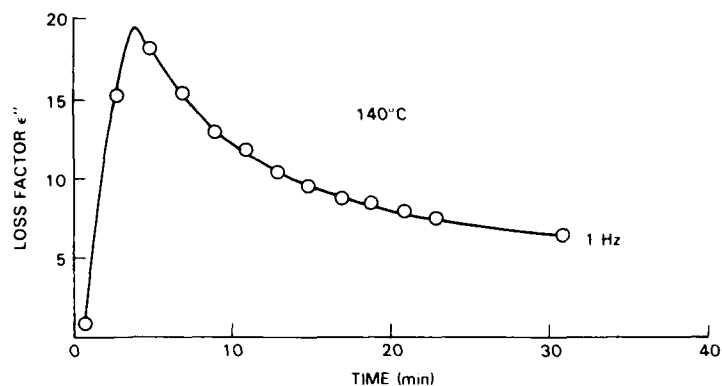
electrical field, the polar groups within the material attempt to align with the imposed field. In the initial solid state of the uncured material, it is difficult for the polar groups to align with the field due to restricted mobility. This results in a low loss factor ϵ'' at the beginning of the cure [3] as shown in a loss factor curve (Fig. 13). As the material heats up during cure, its viscosity decreases, and the mobility of the polar groups increases. This corresponds to the initial steep rise in the loss factor curve and is caused by increased alignment of the polar groups with the field. As the sample continues to heat, the chemical cure process increases the viscosity of the material, and the loss factor decreases as the mobility of the polar groups decreases due to network formation or solidification.

During a typical isothermal polymeric cure cycle as described above, microdielectrometry monitors the dielectric changes in the material as it goes from a solid to a liquid and back to a solid. The cure cycles for polymeric materials often involve heating cycles with thermal ramps, step holds and pressure application for adhesive materials. A manufacturer's typically recommended cure cycle for an adhesive is: (1) ramp the temperature up to 121°C (250°F) for 30 min, (2) hold the temperature at 121°C for 60 min, and (3) apply 40 psi to the system. Microdielectrometry allows us to monitor the cure cycle *in situ*, to determine the most effective time to apply the pressure, and to determine how long to hold the temperature constant.

Applications: Scientists at NRL have monitored *in situ* polymer cures for the production of

acoustical tile, for sonar dome repair elastomers, and for aerospace adhesives.

Acoustical Tile—We have monitored the *in situ* cure of elastomers in a mold which simulates acoustical tile production. In conjunction with mechanical and acoustical data, we determined an optimum processing window for the elastomer we studied. The ultimate use of the acoustical tile determines the optimum parameters. With this information, the correlated microdielectric response is used to reproducibly control the elastomeric cure to the desired state.

Sonar Dome Repair Elastomers—In another project, microdielectrometer techniques are being used to determine minimum cure times at various temperatures for the elastomers used in underwater and drydock repair of sonar dome rubber windows. The manufacturer recommends the same cure times for underwater as drydock repairs, but microdielectrometry indicates changes in the cure mechanism underwater which are not present in the drydock repair. Mechanical tests show that the underwater cure does not reach the same mechanical strengths in the same amount of time as the drydock cure. We are presently determining minimum times for the underwater cure of the elastomeric material. Underwater repairs will eliminate the need to dock a ship to repair its sonar dome rubber window, a very costly procedure.

Aerospace Adhesives—Scientists at NRL have also studied the curing characteristics of aerospace adhesives with microdielectrometry. The adhesives which are currently being studied must cure at 121°C in very short periods of time to be acceptable for the project. By monitoring

174

the cure *in situ*, we can determine the effectiveness of the thermal ramps, step holds, and pressure applications which the manufacturers recommend. Microdielectrometry data and correlated mechanical data on the adhesives will aid in the development of field-deployable, microdielectric, cure-monitoring instrumentation for aircraft composite repair.

[Sponsored by NAVAIR and NAVSEA]

References

1. S.D. Senturia, N.F. Sheppard, S.Y. Poh, and H.R. Appelman, "The Feasibility of Electrical Monitoring of Resin Cure with the Charge-Flow Transistor," *Polym. Eng. Sci.*, **21**, 113 (1981).

2. S.D. Senturia, N.F. Sheppard, H.L. Lee, and D.R. Day, "*In Situ* Measurement of the Properties of Curing Systems with Microdielectrometry," *J. Adhesion*, **15**, 69 (1982).

3. J.A. Hinkley, "Monitoring of Rubber Cure by Microdielectrometry," NRL Memo Report 5300, 1984. ∎

NRL is developing failure criteria for composites that will permit more efficient use of these materials in naval structures. We are developing an extensive experimental data base characterizing the failure behavior of composites under a range of loading conditions. These data, in conjunction with realistic mechanical modeling procedures, will be used to predict the structural response of composite components. The alternative to this is to base failure predictions on complex analytical procedures that have severe limitations.

In-Plane Loader: We have developed a unique loading machine that permits the application of a broad range of in-plane loads to small composite test coupons (Fig. 14). The in-plane loader applies shear, tension or compression, and rotational loads to specimens as illustrated in Fig. 15. A combination of translational and rotational loads are applied by three computer-controlled hydraulic actuators to notched coupons, 2.5 cm × 3.7 cm, clamped in the fixed and movable heads. Notched specimens are used so that failure will start away from the grips in an area that can be characterized reproducibly.

Prediction of the Failure Behavior of Fiber-Reinforced Composites

P.W. Mast, G.E. Nash, R.W. Thomas, I. Wolock, and B.B. Rath
Material Science and Technology Division

Fiber-reinforced composites are being used increasingly in naval applications, such as missile chambers, aircraft wings, small boats, and large sonar domes. Promising applications include minesweeper hulls. These composites have high strength, adequate modulus, lower density, good corrosion resistance, good fabricability and maintainability, favorable electromagnetic properties, and lower cost. Because of their complex physical structure, however, composites exhibit complex failure modes and require more complex failure criteria compared to conventional structural materials such as metals.

Fig. 14 — The in-plane loader. The displacement of three independent computer-controlled hydraulic actuators is programmed to apply, through the movable head, translation and rotation motions. This results in the application of a broad range of in-plane loads to the test specimens. The components of the in-plane loader are: A. Hydraulic actuators; B. Movable head; C. Fixed head; D. Specimen grips; E. Specimen loader/unloader; F. Test specimen; and G. Video camera.

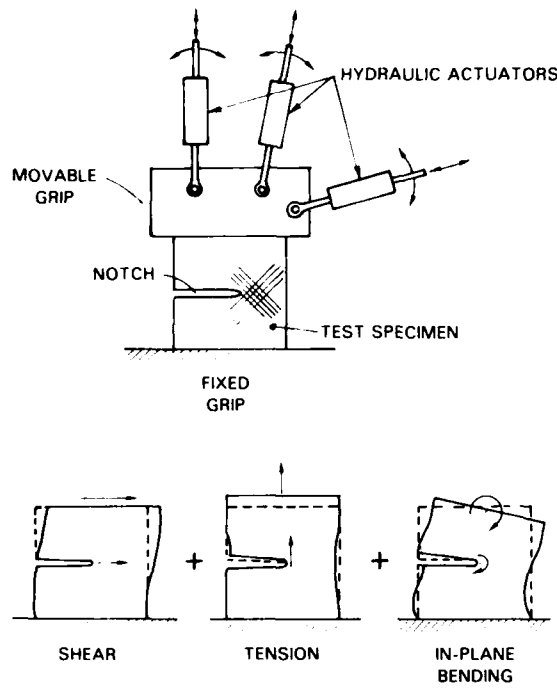SHEAR   TENSION   IN-PLANE BENDING

Fig. 15 — Forces produced by the in-plane loader. The shortening or lengthening of the hydraulic actuators in various combinations causes the movable head to apply shear, tensile/compressive and rotational forces to the specimen, leading to failure.

As a result, an extensive data base that characterizes the failure behavior of composite materials is being developed relatively inexpensively. During a single computer-controlled test in the in-plane loader, which lasts approximately 5 s, three loads and three displacements are measured 50 times and recorded and stored in a computer. The tests are repeated for a range of in-plane loading conditions, and a "failure surface" for the composite is developed. Figure 16 shows such a surface developed for a graphite fiber/epoxy resin. Above this surface the test specimen would fail. In Fig. 16, Θ_1 is the ratio of the shear displacement at the specimen boundary to the tension or compression displacement at the boundary, and Θ_2 is rotational angular displacement (in-plane bending) at the boundary. These displacements are demonstrated in Fig. 15(b)(c)(d). These data subsequently can be used to characterize the structural response of the material.

Verification of Tests: A unique triaxial loader (TAL) has also been developed at NRL as a part of the composite materials characterization capability. It applies loads in the plane of the specimen as well as perpendicular to the specimen, whereas the in-plane loader applies loads in the plane of the specimen only. Fifteen-inch square test sections of structural components are used in the TAL. This loader is used to demonstrate the validity of failure predictions made by using data obtained with the in-plane loader. So far, our measurements with both loaders show that we can predict quite accurately the initiation of failure of composites used in various naval applications. This capability is being developed further, using newly available hardware and software, to permit the graphical representation of
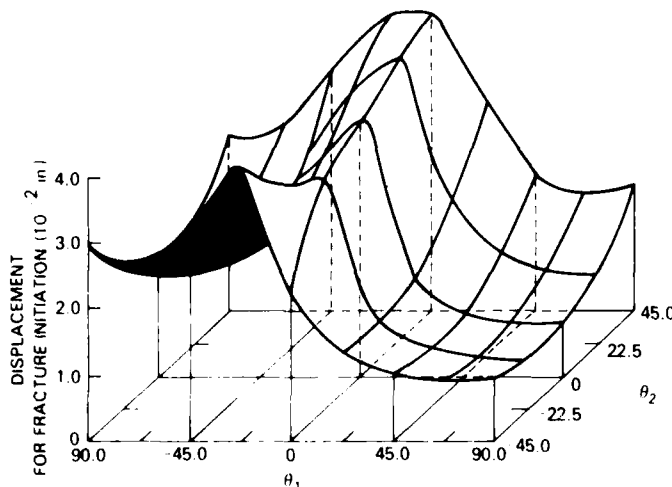
Fig. 16 — Typical failure surface for a composite based on critical displacement. Each point of the surface represents the displacement required to initiate failure in the specimen for the given in-plane loading condition. The surface describes the failure parameters for a graphite fiber/epoxy resin composite in which the crossply graphite reinforcement has an included angle of 60°. Θ_1 is the ratio of the shear displacements at the specimen boundary to the tensile or compressive displacements; Θ_2 is the angular displacement at the boundary.

structural components of interest and the structural response of these components containing defects or damage.

The in-plane loader system presents the Navy with an advanced capability to characterize the complex failure behavior of fiber-reinforced composites and to predict their behavior in structural components.

Vibrational Energy Relaxation in Nitrogen

A.W. Ali and S. Slinker
Plasma Physics Division

Electric, laser, microwave, and electron beam discharges in nitrogen-rich gases such as air store a fair portion of the released energy in nitrogen vibrational mode. The storage and relaxation of this energy affect the electron velocity distribution and the heating and cooling rates of the molecules along the discharge channel (such as a lightning stroke). These channel properties control the conductivity, the channel expansion, and various chemical reactions that determine the composition of the discharge. The vibrational relaxation studies coupled with appropriate chemistry models, therefore, enhance our understanding of discharge phenomena, such as lightning, laser and electron beam propagation in air with pulse-power switching, and other applications. These models, furthermore, provide the tools and capabilities for interpreting and scaling laboratory experiments.

Vibrational Models: Two models have been developed for the vibrational relaxation in nitrogen. These are the harmonic (HO) and the anharmonic (AHO) ocillator models. The HO model [1] assumes equal spacing between the vibrational levels (33 bound states) while the AHO model considers the actual nonequal energy spacings of the levels (46 bound states); the spacings become smaller as the levels reach the dissociation limit. For either case, a "master equation" is solved numerically (by computer). The master equation describes electron-molecule and molecule-molecule interactions. These are: the electron impact excitation and subsequent deexcitation of the vibrational levels (e-v), the vibrational-translational energy transfer collisions between a molecule in a vibrational state and the rest of the molecules (v-t), and the vibrational-vibrational energy exchange collisions between a pair of molecules (v-v). For the HO model, no energy is transferred in the v-v collisions between the vibrational and the translational modes because of the equal spacing between the vibrational levels. This is not the case for the AHO model, where the energy exchanges depend on the energy defect between the vibrational energies of the initial and final states of the colliding particles. Furthermore, the rate coefficients for v-v and v-t processes in the case of the AHO model do incorporate the anharmonicity effect. This makes the corresponding rates different from those of the harmonic model because the AHO interactions are nonresonant in nature.

The vibrational relaxation studies [1] usually solve the master equation under steady-state conditions and obtain analytic expressions by using various approximations which were valid for the limited cases only. Furthermore, no energy exchange between the vibrational and translational modes and their effects on the gas temperature (and consequently on the rates) were ever considered. Additionally, no study has been performed with a time-dependent model that includes all three processes: e-v, v-t, and v-v, with an *ab initio* description of the other discharge temperatures, i.e., the electron and gas temperatures and various other species (such as N_2^+, N^+, and N) densities. Therefore, our vibrational model is unique since it describes the discharge chemistry in a global manner with the vibrational relaxation and dissociation as an integral part of the model, thereby eliminating the deficiencies of previous studies!

Chemistry Model: The chemistry model describes the energy deposition into the gas, the ionization and dissociation, the recombination, and the time histories of various species other than the vibrationally excited molecules. The electron temperature is calculated by considering energy gain from the external source (photon or
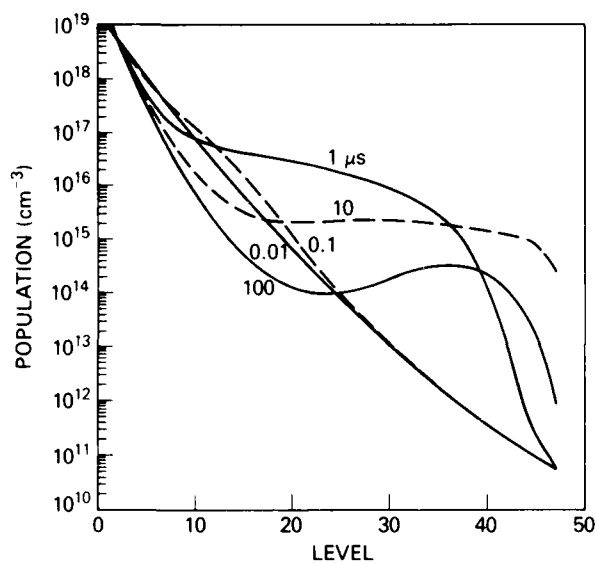
Fig. 17 — The vibrational level density as a function of the vibrational quantum number at different times in the relaxation process
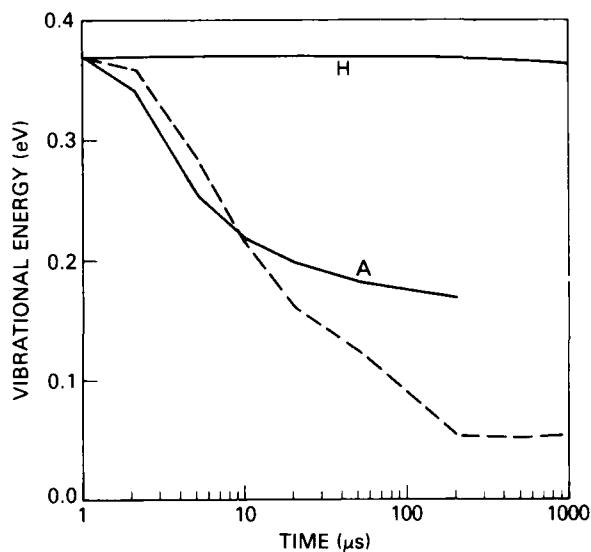

Fig. 18 — Vibrational energy relaxation—curve H for the HO model, curves A and dashed for the AHO model with varying and fixed gas temperature, respectively

particale beam) and superelastic collisions and loss to various inelastic processes. On the other hand, the gas temperature is calculated principally from electron-molecule collisions, dissociative recombination of the molecular ions, and charge exchange processes.

Results and Conclusions: Detailed results of the HO model can be found elsewhere [1]. Here, however, we compare some results from our AHO model to the HO model.

In Fig. 17 we show the time development of the vibrational levels in one atmosphere of nitrogen with a low degree of ionization, a vibrational temperature of 0.5 eV, and a gas temperature of 0.025 eV ($\sim$300K). The population inversion with time, particularly at 1 μs, at the higher vibrational levels (above 30) in the AHO model relative to midlevels can be seen easily. This phenomenon is most pronounced when the vibrational temperature is high and the gas temperature is low. However, such a phenomenon is never predicted by the HO model where the vibrational distribution is Boltzmann. Figure 18

shows the vibrational energy relaxation for the HO and the AHO models for the same initial conditions as above. Here one observes very little relaxation in the HO model (curve H), compared to the rapid relaxation for AHO case (curve A). Furthermore, the relaxation is more rapid when the temperature is fixed in the AHO model (dashed curve) compared to the more realistic AHO case (curve A) where energy flow between the vibrational and kinetic modes is included; that is, temperature is allowed to vary.

The global model (AHO) with hydrodynamics will be applied to electron beam propagation and laboratory discharge channel experiments to better understand details of the physics involved in nitrogen discharges.

[Sponsored by DARPA]

Reference

1. A.W. Ali and S. Slinker "Vibrational Relaxation and Dissociation in N2," NRL Memorandum Report No. 5347 (1984).　■

Materials analysis and properties

Crack growth along grain boundaries in a zig-zag fashion causes failure in a high-strength, high-temperature turbine blade alloy

MATERIALS ANALYSIS

Many new techniques are being developed at NRL to analyze and determine the properties of new exotic as well as traditional materials. The researchers study volumes of matter from molecular aggregates a few Å across up to submarine hull scales. A few of these projects and their findings are described here. The work in this section was performed in five NRL divisions: Marine Technology (5800), Laboratory for Structure of Matter (Code 6030), Chemistry (Code 6100), Material Science and Technology (Code 6300), and Electronics Technology (Code 6800).

Some other NRL research in materials analysis and properties not described in this section includes:

- structure determination of macromolecules by using anomalous X-ray dispersion
- nondestructive evaluation of high-performance structural materials
- continuum theory and structural mechanics
- antimalarial agents

- structure of peptides for drug design
- biomolecular assemblies for naval applications
- fluoropolymer applications
- detection and analysis of propellant vapors
- laser-induced shock physics

Structure Features in GaAs Substrates as Revealed by a Eutectic Chemical Etching

H. Lessoff, W.F. Tseng, and R.J. Gorman
Electronics Technology Division

NRL has developed a new eutectic chemical etchant that reveals significantly more information in semiconductors than other previously available etchants. In addition to dislocations, this new etchant reveals other crystalline structure and defects in the semiconductors which in many cases can be correlated with electronic device performance.

Etching and Dislocations: Chemical etching has been used since the early 19th century to study crystal symmetry in naturally occurring minerals. Since then the use of etching has expanded so that the etch patterns now can disclose information concerning dislocation arrays that are present in imperfect crystals. Etch techniques have become a powerful tool for the characterization of single crystals used in electronic and optoelectronic devices.

Dislocation arrays are imperfections in the orderly array of atoms that make up a crystal structure. These dislocations affect the optical and electronic properties of devices that are located on or near an imperfect area of the crystal whereas a similar device located on a perfect crystalline area is unaffected. Gallium arsenide (GaAs) and other III-V semiconductors have both a direct band gap and a high electron mobility. These properties allow the preparation of electronic and electro-optic devices that cannot be prepared with silicon. Such devices as light-emitting diodes, semiconductor lasers, and infrared detectors are the key to optical communications which use fiber optics. High-speed devices used in digital circuits as well as microwave and millimeter wave technology are based on the III-V semiconductors, especially GaAs. To achieve device uniformity and reproducibility, the semiconductor crystalline perfection is critical. Chemical etching is a valuable technique to determine crystal perfection and to analyze the causes of nonperfect areas of crystals.

Standard Etches: For {100} GaAs, the etchants have been limited to those developed by Abrahams and Buiocchi (A/B etch) and Grabmaier and Watson (potassium hydroxide, KOH). Both types of etchants have severe limitations. For example the A/B etch preferentially removes good crystalline material thus making it difficult to interpret the etch patterns. There are also problems in interpretation of the etch features developed by the A/B etch because of a memory defect inherent in this technique.

The KOH etch is based on the reaction of a GaAs wafer in molten KOH at temperatures between 300° to 450°C. Pure KOH melts at 360°C, and its use below this temperature depends on the residual moisture in the KOH pellets (or flakes). The KOH moisture content varies, and KOH continuously loses moisture until the 360°C melting point is reached. Therefore, the KOH etch is not reproducible. The KOH etchant (and the A/B etchant as well) is too fast-acting and unreliable to allow for the easy study of the very thin GaAs layers which are grown by molecular beam epitaxy (see *1983 NRL Review*, p. 151). These epitaxial layers are the electronically active regions for microwave, millimeter wave, and digital devices.

Improved Eutectic Etch: NRL has developed an improved eutectic etch that consists of equal mole percents of NaOH and KOH and has a melting point of 180°C. This etchant not only solves the reproducibility problems inherent in the KOH etch but also has a much slower rate of etching (by an order of magnitude) than either the KOH or the A/B etchants. Using the eutectic etch, thin epitaxial films of 3 μm or less in thickness can be studied.

Eutectic Etch Patterns: Typical patterns resulting from the eutectic etch are shown in Figs. 1 and 2. Not only are the normal dislocation structures shown, but new structures are also revealed which give important clues to the crystallographic homogeneity and hence, the electrical properties of GaAs. In thin samples analyzed by transmission electron microscopy the open arrows in Figs. 1(a), (c), and (d) and the rectangular-like features in Fig. 2(b) have been correlated with tangled dislocation networks that exhibit dislocation movement or that glide upon heating. The series of geometric structures seen in Figs. 1(d) and 2(c) are probably caused by defects in
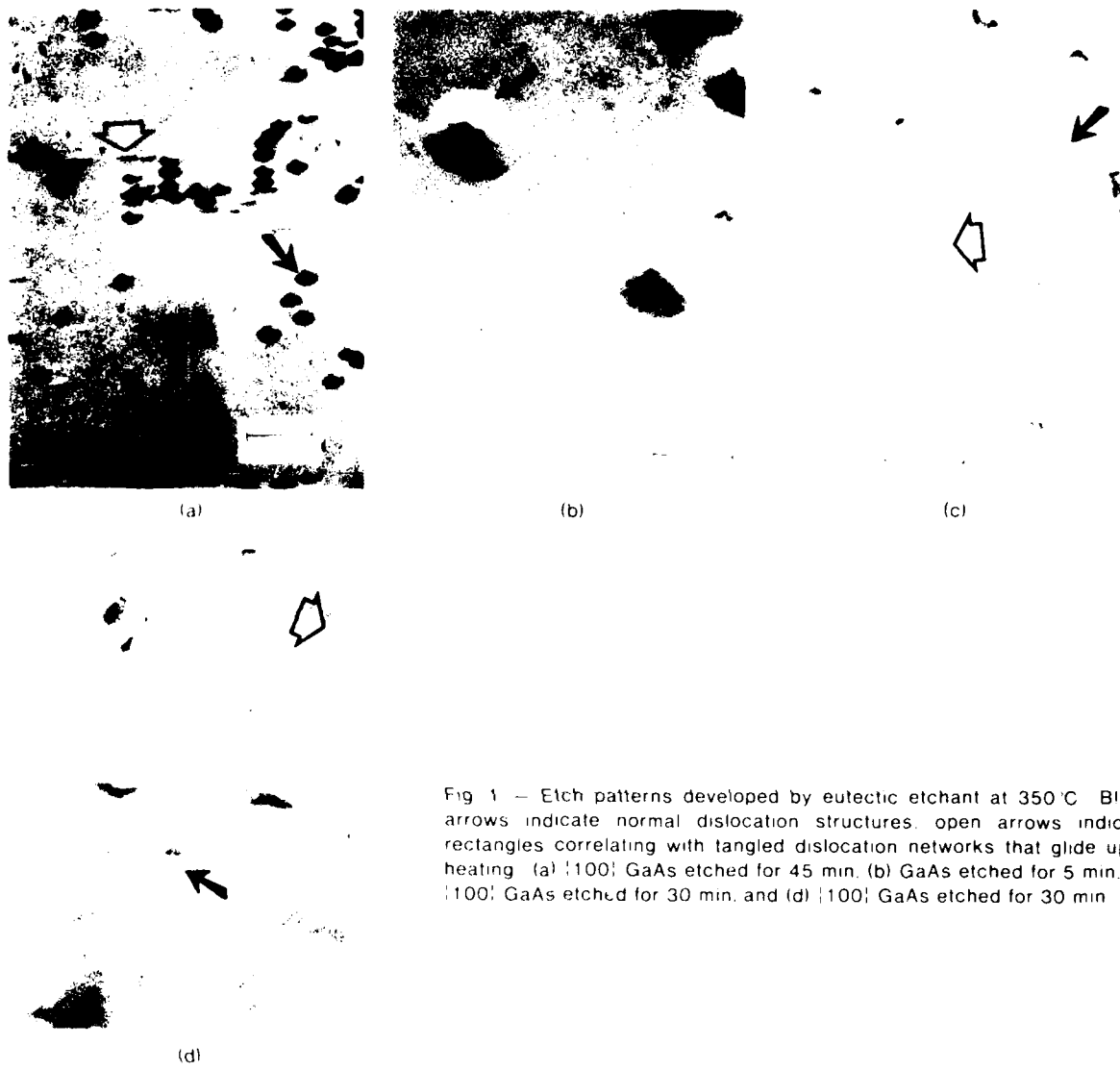
(a)　　　　　　　　　　(b)　　　　　　　　　　(c)

Fig 1 — Etch patterns developed by eutectic etchant at 350°C. Black arrows indicate normal dislocation structures, open arrows indicate rectangles correlating with tangled dislocation networks that glide upon heating. (a) |100| GaAs etched for 45 min. (b) GaAs etched for 5 min. (c) |100| GaAs etched for 30 min. and (d) |100| GaAs etched for 30 min
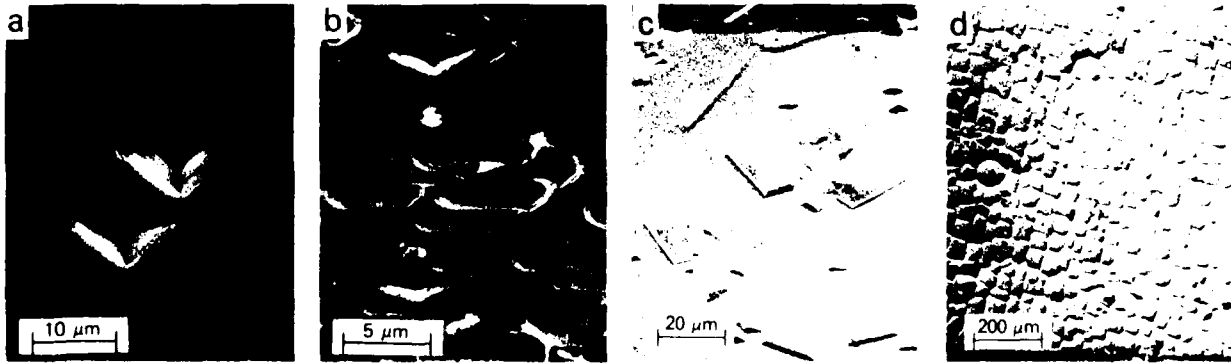
(d)

Fig 2 — The |100| GaAs surface etched by NRL's eutectic etchant showing (a) pyramidal dislocation etch pits, (b) dislocation glide pattern (c) raised defect, and (d) mosaic cellular patterns possibly related to thermal stress developed during crystal growth

atomic ordering. In Fig. 2(d), the mosaic pattern observed by the eutectic etch is possibly related to thermal stress developed during crystal growth, when large temperature gradients occur between the molten and crystallized GaAs.

The NRL-developed etch is useful on {100}, {111}, and {110} oriented crystalline GaAs. The etch rate is relatively slow and can be used on both bulk GaAs substrates as well as very thin GaAs layers. The KOH/NaOH etch not only is slow enough to allow the observation of the normal dislocation structures observable with other etchants but also gives much additional and necessary information concerning defect motion, order imperfections, and thermal stress. A number of industrial and university laboratories are using this NRL etching technique to correlate crystal properties with electronic device parameters.

[Sponsored by NAVELEX] ∎

Structural Information from Regions 6 to 20 Å in Diameter

J.H. Konnert
Laboratory for Structure of Matter

Recent advances in electron microscopy permit diffraction patterns to be obtained from extremely small volumes, thus providing an ultrahigh resolution probe of structure not previously available. Information now can be obtained from volumes containing several hundred atoms or less. NRL, in collaboration with the High Resolution Electron Microscope Facility at Arizona State University, has developed analytical techniques that yield interatomic distances from these small volumes that are critical to deducing the atomic arrangements. The new techniques are potentially important for studying the structures of amorphous materials, defects in crystals, interfaces, and catalytic materials.

Crystal Diffraction: Much of the knowledge concerning atomic structure has been obtained from studies of diffraction patterns of single crystals. These patterns consist of regular lattices of diffraction intensity maxima. The spacings between the maxima define the dimensions of the periodic building block of the crystal, the unit cell; the intensities are determined by the positions of the atoms within the cell. The positions of the atoms may be derived from the diffraction pattern by using certain theoretical and experimental techniques. With these crystallographic techniques, we can determine the structures of metals, minerals, proteins, and even viruses.

Amorphous Diffraction: Usually, single crystal investigations yield only the average structure of the thousands of unit cells within the scattering volume of the incident beam. However, these investigations generally are not useful for studying defects or interfaces because these atoms lack crystalline periodicity. Also many materials, such as glasses, are not crystalline. Diffraction patterns obtained from noncrystalline materials with conventional radiation sources are characterized by a limited number of diffuse, low-intensity maxima and not by the high-intensity maxima of crystalline materials. Fourier transform analyses of these diffuse patterns give the distribution of interatomic distances present in the sample. This distribution, one dimensional in nature, does not indicate the relative positions and orientations of the interatomic vectors that are necessary to completely describe the structure. For this reason, conventional diffraction patterns obtained from amorphous materials almost never contain sufficient information to uniquely characterize the material; additional information is necessary.

Small Beam Amorphous Diffraction: Quite different diffraction patterns may be obtained from amorphous materials by using a much smaller beam than that used in conventional diffraction work. A scanning/transmission electron microscope has been used to obtain diffraction patterns from volumes that contain several hundred atoms. This microscope, located at Arizona State University, incorporates a field emission electron gun and a special optical system. Figure 3 is a diffraction pattern obtained from a silicate glass, $NaAlSi_3O_8$. The structure of

183

Fig. 3 — Diffraction pattern obtained from a silicate glass with an electron beam 15 Å in diameter. The bright spots arise from the nonrandom atomic structure in a small volume. The parallel lines are the raster sweeps of a video monitor system.
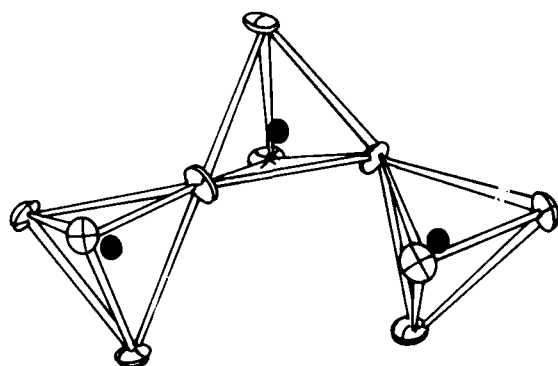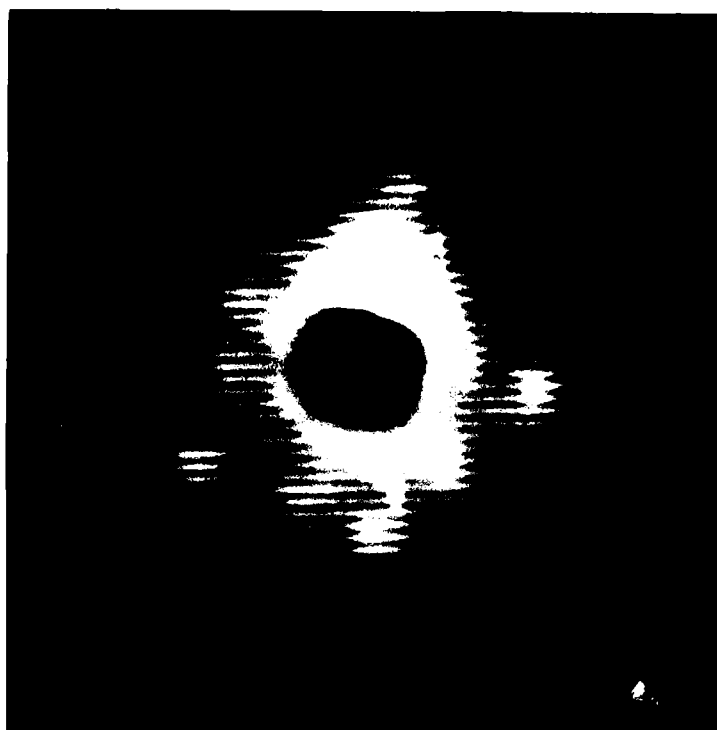

Fig. 4 — Linked tetrahedra present in $NaAlSi_3O_8$ glass. The Si and Al atoms are the dark circles at the tetrahedra centers. The oxygen atoms—open circles at the vertices—are shared by two tetrahedra to form an extended framework. The Na atoms are disorderly distributed within the framework.

$NaAlSi_3O_8$ glass consists of tetrahedra, of SiO_4 and AlO_4 atomic groups with the Al and Si atoms at the centers and the oxygen atoms at the vertices (Fig. 4). Each oxygen atom is shared by two tetrahedra forming a three-dimensional framework of linked tetrahedra. A primary goal of structural studies is to determine the topology of this framework.

The diffraction pattern of $NaAlSi_3O_8$ (Fig. 3) is characterized by bright spots, even though the material is a glass. The spots arise because the few hundred atoms in the irradiated volume have only a limited number of the atomic configurations found in a macroscopic sample. Thus, the bright spots are the interference patterns caused by reinforcement due to the local order of the atoms in the irradiated volume. Hence, it provides direct information on local crystallinity and may be analyzed with Fourier transforms to determine the orientation of the interatomic vectors present in the beam.

The potential power of this technique arises because diffraction patterns contain information on a much finer scale (0.3 to 0.6-Å resolution) than the dimensions of the beam (15 Å in diameter). For comparison, conventional scanning microscopy permits resolution equal to the beam diameter, usually greater than 50 Å; high resolution transmission microscopy has attained a resolution of 1.6 Å.

Figure 5 compares an interatomic distance distribution obtained with the 15-Å electron beam to the distribution calculated from data collected with a 1-mm X-ray beam. The similar peaks at
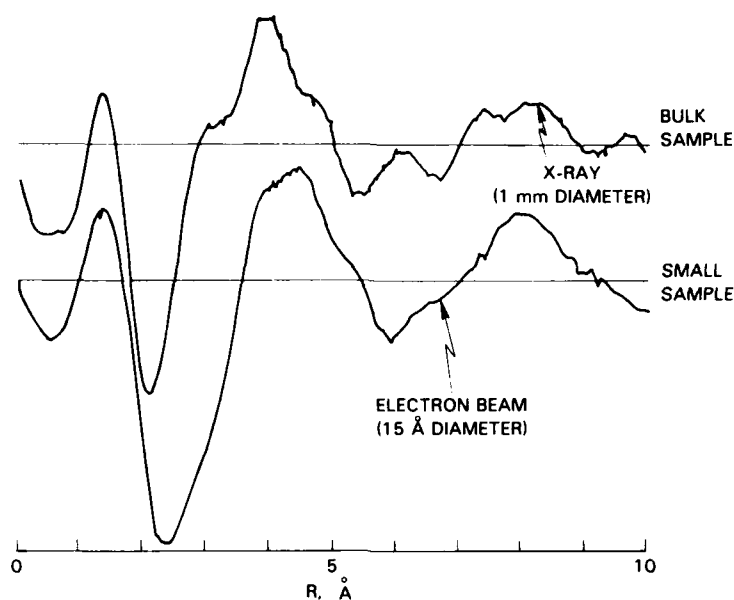
184

Fig. 5 — Comparison of interatomic distance distributions calculated from diffraction patterns obtained with a 15-Å-diameter electron beam and a 1-mm-diameter X-ray beam.

1.3 Å represent the average, projected Si(Al)-O interatomic distances whereas the peaks (at 4 Å) and valleys (at 6 Å) are noticeably different in shape. These differences are due to a sampling volume so small that it lacks many of the configuration types present in the bulk sample. If all the different types were present, they would average out, producing a curve similar to that of the bulk sample (as seen at 1.3 Å).

Theoretical calculations will evaluate the accuracy of the distance distributions obtained for microdiffraction patterns. If accuracy is confirmed, the method will be a powerful tool for identifying bond types, bond orientations, and atomic groupings in very small volumes.

[Sponsored by ONR] ∎

Hydrogenic Donors in Quantum Wells

B.V. Shanabrook, R.J. Wagner,
J.E. Furneaux, and J. Comas
Electronics Technology Division

The development of the molecular beam epitaxy growth technique (see *1983 NRL Review*,

p. 151) has resulted in an ever-growing class of new semiconductor materials with novel properties. These artificially structured semiconductors are being intensively studied both as model systems to test fundamental physical concepts and as starting material for new electronic devices. As with conventional semiconductor devices, these new devices depend on the controlled introduction of various types of impurity atoms (either donors or acceptors) that are necessary for n- and p-type doping. NRL scientists have recently made significant advances in understanding the properties of donor atoms intentionally introduced into artificially structured semiconductors.

Quantum Wells and Impurities: Previous studies have shown that when a layer of gallium arsenide (GaAs) is sandwiched between layers of aluminum-gallium-arsenide ($Al_xGa_{1-x}As$), the lowest energy state for electrons occurs in the GaAs layer. The cause of this phenomenon is the difference in the fundamental electron energy gaps of the two semiconductor materials. Figure 6(a) is a diagram of the spatial dependence of the lowest energy state for electrons in such a structure. An electron that is created in this structure with energy E_e must be localized in or confined
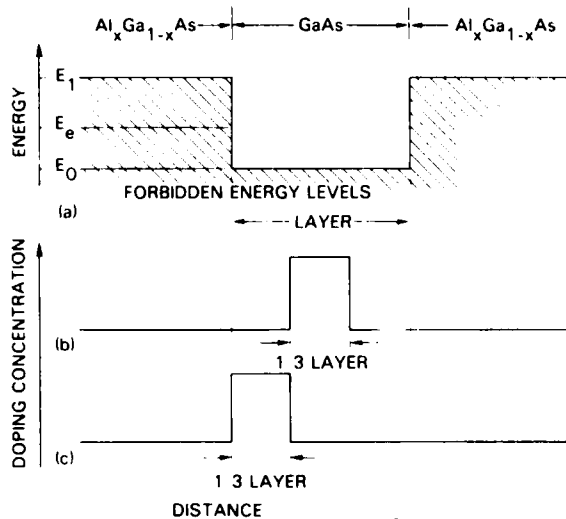
185

Fig. 6 — (a) The spatial dependence of the lowest energy state for electrons; (b) the concentration of donors selectively doped at the center of the well; (c) the concentration of donors selectively doped at the edge of the well

to the GaAs layer. This effect is described as the localization of an electron in a GaAs-$Al_xGa_{1-x}As$ quantum well.

When donor impurities are placed in this quantum well, there is an additional localization of the electron that arises from the coulomb interaction between the electron and the positively charged impurity ion. This additional localization results in the introduction of new electron energy levels into the quantum well. In bulk GaAs, these new levels are analogous to those of a hydrogen atom. Because the functional form of the distribution of electronic charge surrounding the donor ion and hydrogen ion are identical, the

donors are referred to as hydrogen-like or "hydrogenic." Thus, the notation from atomic spectroscopy has been borrowed, and the energy levels of the impurity are labeled as $1s$, for the ground state and $2s$, $2p$, $3s$, ... for the excited states. In quantum wells, the interaction between the electron and the quantum well causes the distribution of the electronic charge about the hydrogenic center to be different than that observed for donors in bulk GaAs. Furthermore, the functional forms for these charge distributions will depend on the width of the quantum well and the location of the impurity center within the quantum well. These important aspects are explored in this article. NRL scientists have employed photoluminescence [1], electronic Raman scattering [2], and far-infrared Zeeman spectroscopy to investigate the properties of hydrogenic donors in GaAs-$Al_xGa_{1-x}As$ quantum wells grown by molecular beam epitaxy. Only the far-infrared Zeeman measurements are described here.

Far-infrared Zeeman Results: Far-infrared Zeeman spectroscopy is the measurement of the transmission of far-infrared light (about 100 cm^{-1} or 100 μm wavelength) through a sample as a function of the intensity of an applied magnetic field. The minima in the transmission curve (as in Fig. 7(a)) indicate the magnitude of the magnetic field for which the $1s$ to $2p$ transition energy is equal to the energy of the far-infrared laser light. The binding energy, which is the amount of energy that is necessary to remove the electron from the impurity ion, is directly related to these transition energies.
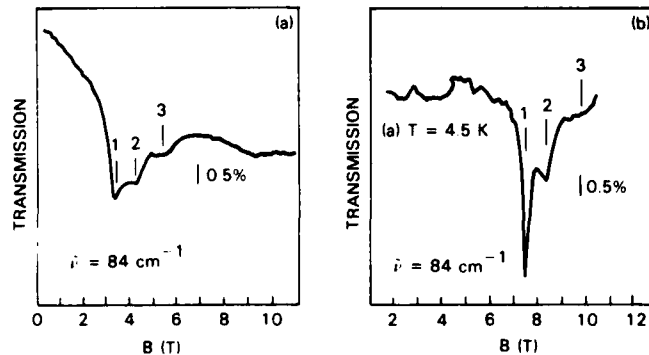

Fig. 7 — The magnetotransmission for a quantum well of width 450 Å that has been doped at the center of the well for (a) 84 cm^{-1} and (b) 142 cm^{-1} far infrared radiation

NRL scientists have performed far-infrared Zeeman spectroscopy on a variety of quantum wells with different widths that have been selectively doped—spike-doped—with donor atoms at the center or edge of the quantum wells. These doping profiles are represented schematically in Fig. 6(b)(c). The width of the doping spike was typically 1/3 the GaAs layer width. It is, however, important to realize that any movement of the impurity atoms during layer growth alters the actual doping profiles from those indicated in Fig. 6.

Typical transmission data are shown in Fig. 7. We characterize these curves by three valleys labeled 1, 2 and 3. Then the values of the magnetic field at these valleys are related to the transition energies of the electrons bound to the donor ions. These transition energies are denoted by the points in Fig. 8 as a function of quantum well width L_z for samples that were spike doped with donor impurities at the center of the well. Because the theoretically predicted transition energies for donors located at the center of the quantum well [3], indicated by the
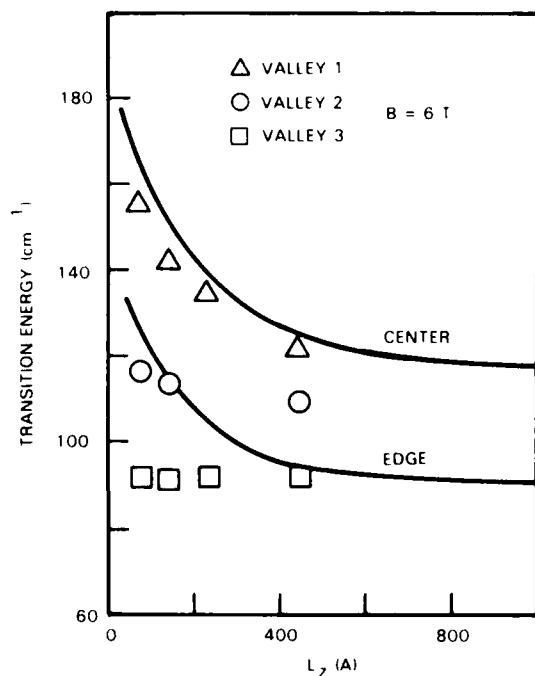
Fig. 8 — The transition energies for valleys labeled 1, 2 and 3 at a magnetic field of 6 T vs quantum well width. The theoretically determined $1s$ to $2p$ transitions for donors at the center and edge of the quantum well are indicated with solid lines.

upper curve of Fig. 8, are in excellent agreement with the transition energies of valley 1, we associate valley 1 with donors at the center of the well. In addition, we have performed Zeeman measurements on samples that have been selectively doped with donors at the edge of the quantum well. Again we find good agreement between experiment and theory.

These measurements have shown that the binding energies of hydrogenic impurities confined in quantum wells become larger as the width of the quantum well is reduced, and that the binding energy of these donors is sensitive to their location in the quantum well. Although we are still investigating valleys 2 and 3, the excellent agreement between the energy of valley 2 shown in Fig. 8 for the quantum wells with widths < 200 Å and the theoretically determined $1s$ to $2p$ transition energy for donors at the edge of the well suggests that a certain fraction of the donors may be moving toward the edge of the quantum well during growth. However, because the position of valley 2 is not in good agreement with this theoretical calculation for quantum wells with widths > 200 Å, we place an upper limit of 50 Å on the motion of donors during growth.

Summary: NRL scientists have shown that hydrogenic impurities in quantum wells exhibit a position-dependent binding energy. The electrons bound to donors at the center of the quantum well are the most strongly bound. Furthermore, as the width of the quantum well is reduced, the binding energy for donors located at the center or at the edge of the quantum well increases. We have also presented evidence that suggests that donors are moving about 50 Å during growth. This observation implies that "spike doping" as achieved with molecular beam epitaxy is rather effective. Because many novel device concepts are based upon abrupt doping profiles, these measurements are important for device design and future studies of materials growth.

[Sponsored by ONR]

References

1. B.V. Shanabrook and J. Comas, "Photoluminescence from 'Spike-Doped' Hydrogenic Donors in $Al_xGa_{1-x}As$-GaAs Quantum Wells," *Surface Science* **142**, 504 (1984).

2. B.V. Shanabrook, J. Comas, T.A. Perry, and R. Merlin, "Raman Scattering from Electrons Bound to Shallow Donors in GaAs-Al$_x$Ga$_{1-x}$As Quantum Well Structures," *Phys. Rev.* B **29**, 7096 (1984).

3. R.L. Greene and K.K. Bajaj, "Effect of Magnetic Field on the Energy Levels of a Hydrogenic Impurity Center in GaAs-Ga$_x$Al$_{1-x}$As Quantum Well Structures," *Phys. Rev* B **31**, 913 (1985). ■

Thermomechanical Response of Laser-Irradiated Composite Structural Elements

C.I. Chang, C.A. Griffis, F.R. Stonesifer, and L.A. Beaubien
Marine Technology Division

Numerous military and space applications of fiber-reinforced organic matrix composites have been successful due to the high strength-to-density ratios of these materials at moderate temperature. However, intense heating produced by fire or laser irradiation can adversely affect the integrity of composite structures due to the rapid degradation of their mechanical properties at temperatures above 200°C. Severe laser irradiation may also induce undesirable changes in structural geometry through ablation of critical load-carrying members or by the generation of high stress concentrations due to localized burn-through. Over the past several years, NRL has been developing an analysis methodology to predict the response of advanced composite aerospace structures subjected to simultaneous laser heating and applied service loads. In the present study, the behavior of simple composite panels is examined both experimentally and analytically to assess the validity of a new predictive model.

Experimentation: Graphite/epoxy (AS1/3501-6) laminated specimens containing 24, 48, and 96 plies were preloaded to a longitudinal tensile strain of 3300 μcm/cm which corresponds to approximately 25% of the room temperature fracture stress. Each ply (lamina) was approximately 0.13-mm thick and represents a single layer of orthotropic (different properties in each of three perpendicular directions) material which consists of graphite fibers embedded in an epoxy resin matrix. The ply-stacking sequences of the three laminate configurations were symmetric about the midthickness and incorporated lamina oriented at 0°, 90°, and ±45° to the longitudinal axis of the specimen. As indicated in the left portion of Fig. 9, the 38-mm wide coupons were spot-irradiated using a 25-mm diameter, 10.6 μ CO_2 laser beam having average intensities in the range 0.5 to 2.5

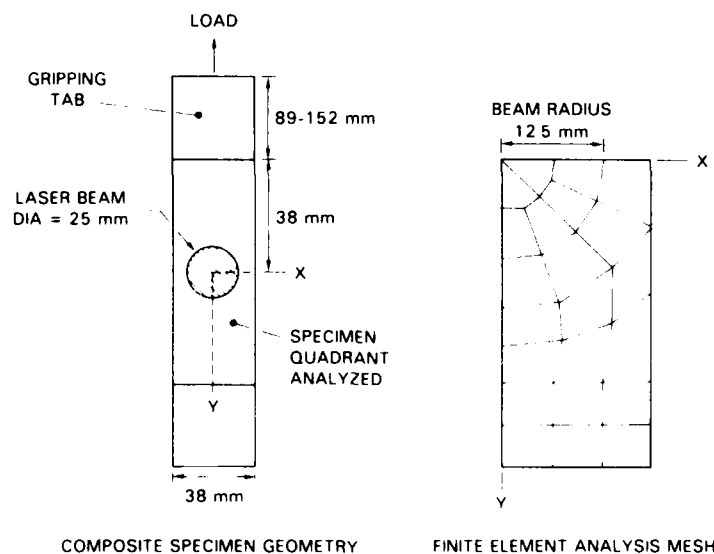COMPOSITE SPECIMEN GEOMETRY   FINITE ELEMENT ANALYSIS MESH

Fig. 9 — Physical geometry and corresponding finite element stress analysis model of laser-irradiated panel

kW/cm^2. The initial load was maintained constantly on the specimens throughout the laser tests by using a closed-loop mechanical testing device. For subsequent comparison with an analysis model, the laser exposure time required to produce failure in each test coupon, as well as the temperature history of the irradiated surface, was recorded.

Numerical Modeling: The development of a computational model to predict the response of loaded, laser-irradiated structures requires integration of both thermal and stress/fracture analyses. Temperature distributions and the characterization of the ablation resulting from the heat transfer calculations serve as the primary input to the subsequent mechanical analysis.

Thermal Analysis — An axisymmetric thermal analysis incorporating a lumped-mass, finite difference method was employed by using an orthogonal network of model points in the radial and thickness directions. Since an axisymmetric model was adopted, the computational grid did not include the circumferential direction. An insulation boundary condition was applied to the test coupons at the edge parallel to their axis and near the beam, but the coupon temperature at the far ends equalled the room temperature. To further simplify the computation, a mean radial conductivity for each laminate was defined by suitable averaging of the conductivities of the component plies. An incremental, forward time-difference equation of the form

$$\alpha_i \Delta T_i = \left[\sum_{j=1}^{3} A_{ij} + B_i + C_i + D_1 \right] \Delta t$$

was employed for each element (lumped mass) in the network. This expression represents a simple energy balance in which the four terms on the right hand side denote the energy fluxes into a typical surface element by conduction, incident laser irradiation, blackbody radiation, and convection. (The i-index represents the numerical value assigned to a generic surface element, and the j-index indicates the relative location of adjacent elements.) The term on the left-hand side of the equation represents the associated net heat acquired by the element and is a function of incremental temperature rise ΔT_i, which is calcu-

lated at each computational time step Δt. (α_i depends on the material specific heat and geometrical factors.) To account for ablation phenomena, surface elements are removed from the model upon accumulation of enough sublimation energy, and the incident flux is subsequently transmitted to an appropriate sideways or deeper element.

Stress/Fracture Analysis — The stress and fracture analysis in this study incorporated a finite element method in which the Mindlin laminated-plate theory was used. Thermal stress effects, temperature-dependent elastic moduli and fracture stresses, and a sequential ply-by-ply failure process were all accounted for in the nonlinear analysis. Since the failure of laminated composites occurs gradually in a step-like fashion, the finite element analysis was conducted in incremental time-temperature steps. At the end of each increment, the stress in each ply is computed and compared with prescribed critical values. If local fracture is indicated, the failed ply is assigned a zero stiffness and the solution is recalculated to ascertain that subsequent load redistribution does not include further fracture. The process is then repeated for another load step by application of a new spatial temperature distribution. Complete collapse of the structure occurs when a sufficient number of plys have failed such that the overall stiffness matrix becomes singular. The right-hand side of Fig. 9 indicates the particular finite element mesh employed in the analysis of the laser-irradiated coupons. It should be noted that owing to symmetry of both the specimen geometry and laser heat source, only a single quadrant of the panel was analyzed.

Comparison of Experimental and Computational Results: Figure 10 indicates the experimental results obtained from the three thicknesses of laminates investigated. It is apparent that for a given laminate thickness an inverse relationship exists between average intensity and time-to-failure as would be expected; that is, higher applied intensities induce failure after shorter exposure times. Additionally for a given level of irradiance, rupture occurs more quickly for the thinner laminates. Also shown in Fig. 10 are selected analytical predictions of failure time for both the 24- and 48-ply material. **189**
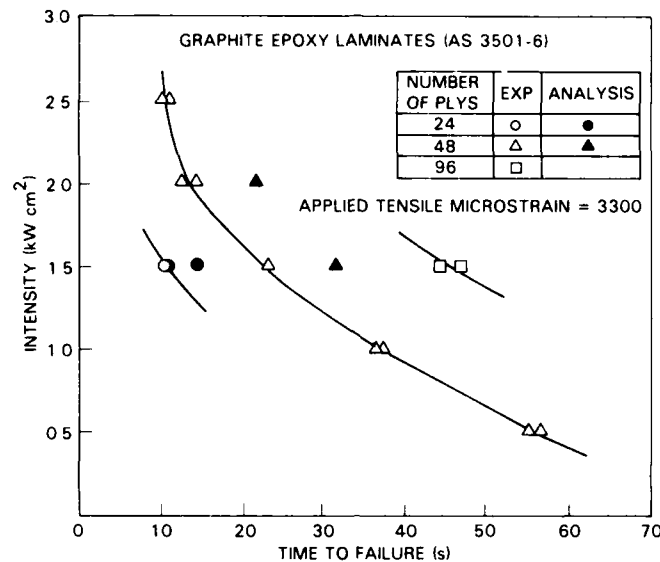
Fig. 10 — Comparison of experimental and analytical results for spot-irradiated laminated graphite/epoxy subjected to uniaxial tensile load

In general the agreement between theory and experimental results is reasonable, although there is a consistent tendency for the computational model to overestimate the measure failure time by about 35%. This disparity is due largely to the use of an approximate laser beam intensity profile in the thermal computations, as well as to the lack of detailed knowledge regarding the transverse and shear strength vs temperature relationships for the graphite/epoxy laminate. The numerical calculations provided considerable insight regarding the nature of the failure mechanism in the panels. Material directly within the beam path loses its load-carrying capability due to both ablation phenomena and thermal degradation of mechanical properties; whereas, the unirradiated flanks of the specimens suffer strength reduction solely due to their thermal degradation caused by the relatively slow conduction of heat away from the beam impingement zone.

Efforts are currently underway to obtain more accurate elevated temperature thermal and mechanical properties for input into the stress/fracture analysis, and to extend the computational model to include doubly curved shells.

190 [Sponsored by NAVAIR] ∎

Fatigue Crack Growth Process

K. Sadananda
Material Science and Technology Division

Fatigue, the predominant mode of failure of many structural components, is caused by cyclic loading during service. NRL has concentrated on understanding the mechanisms of fatigue failure to provide a better scientific basis for the selection and fabrication of materials for Navy applications and to reliably predict the life of components. When applied, this knowledge will decrease the probability of catastrophic failure in components, particularly aircraft structures and engine components.

Processes: Fatigue failure begins with the initiation of cracks either from weld defects or from localized stress concentrations. Fatigue is caused by plastic deformation that locally is only partially reversible during the loading and unloading of each stress cycle. This partial irreversibility leads to crack extension by mechanisms not yet clearly determined. However, careful analysis of the results of many fatigue crack growth studies, both at NRL and elsewhere, has permitted NRL scientists to develop a partial understanding of

these mechanisms and the two processes that cause fatigue failure: the plastic blunting process and the cumulative damage process.

Plastic Blunting Process — In this process (originally proposed by Laird in 1967) crack length incrementally increases in each load cycle. The increment a is related to the net residual plastic strain at the crack tip for each cycle. Application of continuum mechanics to the problem shows that the crack increment per cycle da/dN is related to the second power of the stress intensity factor and can be expressed as

$$\frac{da}{dN} = \frac{(\Delta K)^2}{4\sigma E}$$

where σ and E are material constants. The stress intensity factor ΔK is a measure of the applied stress field ahead of the crack tip. The plastic blunting process occurs in relatively ductile materials, particularly in the intermediate ΔK-range (10 to 40 MPa $\sqrt{m}$).

Cumulative Damage Process — In many high-strength, high-temperature structural materials crack growth does not occur in each cycle but rather in discrete jumps; each increment results from damage accumulating during several cycles. This mechanism results in the cumulative damage process—distinct from the plastic blunting process which causes cycle-by-cycle growth. In cumulative damage, plastic strain does not lead directly to crack length increment but rather to the accumulation of damage in the form of nucleation of microcracks, cleavage facets, cavities, or intergranular separation. Figure 11 illustrates the various cumulative damage processes. Dashed lines are slip planes, and the Ts are dislocations gliding on the slip planes because of plastic deformation. In Fig. 11a, as the crack widens because of dislocation emission, stresses get accentuated ahead of the crack tip; this opens up a microcrack, and the process repeats. Figures 11b, 11c, and 11d illustrate alternate mechanisms of crack growth. Each process has been analyzed at NRL. For the cumulative damage, a simple energy balance has been deduced [1] that relates the crack increment per cycle da/dN to ΔK:

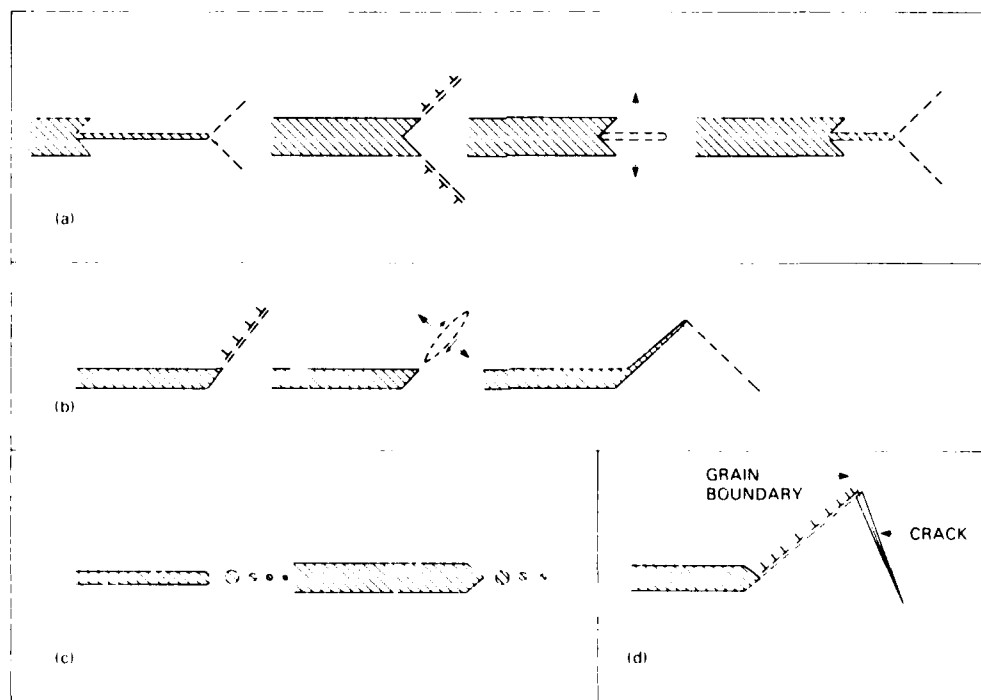$$\frac{da}{dN} = \frac{\Delta K^4}{8\pi^2\mu\sigma^2 U} \, .$$

Fig. 11 — Fatigue crack growth by cumulative damage. Such growth is caused by nucleating microcracks ahead of the main crack (a, b), by cavity nucleation (c), or by grain boundary cracking (d). The inverted Ts represent dislocations on slip planes indicating plastic flow from the crack tip; the dashed lines represent slip planes.

In this equation, μ and σ are material constants, and U is the measure of input energy stored in each cycle. U is determined experimentally from the load load-vs-displacement hysteresis loop.

Measurements: Fatigue crack growth rates were measured for a high-temperature gas turbine alloy, MA 956, at 25° and 1000°C. Figure 12 compares the results with theoretical predictions based on the plastic blunting and cumulative damage processes [2]. At the high temperature, theoretical predictions based on the cumulative damage process agreed well with experimental results. However, at the low temperature, the experimental data fell between the predicted curves for the cumulation damage and the plastic blunting processes. Microscopic examination of fracture surfaces revealed that, at the high temperature, crack growth occurred because of nucleation and coalescence of voids (Fig. 11c), a type of cumulative damage. However, at the low temperature, the crack growth occurred because of microcrack formation in some regions of the crack front and by plastic blunting process in other regions. In the plastic blunting process, predicted crack growth rates are the same at both temperatures. Thus, at the low temperature, experimental data corresponds to some weighted average of the two processes.

The application of these models allows the more accurate predictions of fatigue crack growth rates in high-temperature alloys and thus of the service life of structural components, especially high-temperature gas turbine components. Future efforts at NRL will involve the analysis of material variables and loading factors that control each of the mechanisms of fatigue crack growth
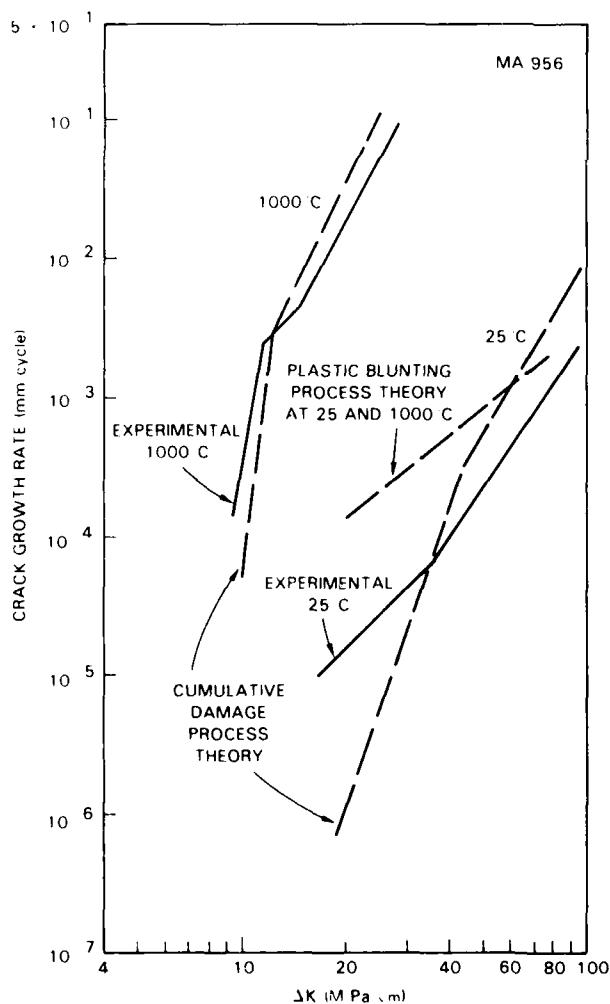
Fig. 12 — The theoretically predicted curve based on the cumulative damage mechanism agrees reasonably well with the experimentally observed growth rate curve at high temperatures (1000°C). The agreement is poor at room temperature (25°C) because both plastic blunting and cumulative damage occur simultaneously at different parts of the crack front.

as well as the estimation of thresholds for crack growth. These efforts will eventually lead to the development of better materials and improved manufacturing techniques that will minimize fatigue failures and extend the life of Navy components.

[Sponsored by ONR]

References

1. K. Sadananda, "Theoretical Aspects of Fatigue and Creep Crack Growth," in *Avances in Fracture Research*, S. R. Valluri et al., eds. (Pergamon Press, Oxford, 1984), Vol. 1, p. 211.

2. K. Sadananda and P. Shahinian, *Metal. Trans. A*, **15A** 527 (1984). ∎

Advanced Mass Spectrometry of Complex Lubricants

R.B. Freas and J.E. Campana
Chemistry Division

High-performance, high-temperature, oxidatively stable lubricants have been developed in the past decade to meet the needs of technological advances in mechanics, propulsion systems, and materials. A lubricant consists of a base stock and one or more additives. To provide fundamental lubrication characteristics, base stocks may consist of a mixture of chemicals of similar structure (homologs) or blends of different base stocks. Additives perform several functions. They modify the lubricant's properties such as oxidation inhibition (antioxidants), metal surface deactivation (metal passivator), and metal surface protection (rust inhibitors). Two or more additives may give synergistic effects. These new, complex, high-performance lubricants require novel analytical techniques to rapidly characterize them. We describe new techniques we have developed at NRL.

New Mass Spectrometric Technique: Mass spectrometric techniques are useful to analyze complex environmental and biological samples. We have applied a new technique—fast-atom bombardment (FAB) mass spectrometry—to characterize lubricants [1]. This technique is especially useful to analyze intractable chemical species that are dispersed in liquid matrices. In the FAB technique, we first bombard a droplet of the lubricant sample with a beam of fast atoms in a vacuum. These fast atoms sputter secondary ions (charged organic species) and neutral species from the droplet. The desorbed secondary ions, which are characteristic of the base stock and additives, are then analyzed by using conventional mass spectrometric techniques.

Figure 13 shows a FAB mass spectrum of a commercial lubricant base stock. This sample is representative of an important class of synthetic base stocks, the pentaerythritol tetraalkanoates, which are used extensively to lubricate the propulsion systems of aircraft, ships, and other vehicles. Figure 13 also shows the general structure of these tetraesters. The alkyl groups R_1, R_2, R_3, and R_4 in these tetraesters may have identical or different chemical structures. Different alkyl groups are used to control the physical properties of the base stock such as viscosity or pour point.

A FAB mass spectrum of the pentaerythritol tetraesters contains sample information on molecular structure because of the abundance of structurally informative fragment ions. A major fragmentation produces acylium ions RCO^+ and ions that correspond to the loss of an acid moiety from the tetraester molecule $[M - RCOO]^+$. However, the protonated molecules $[M + H]^+$ which can provide molecular weight and isomer information, occur in relatively low abundances ($<0.1\%$ of the most abundant ion). Pentaerythritol triester impurities, produced in the chemical manufacturing process of the tetraester base stocks, also yield analogous fragment ions that are seen in the FAB mass spectrum in Fig. 13.

The acid profile ($RCOO$ distribution for the various R groups as shown in Fig. 13) of a pentaerythritol tetraester mixture can be deduced from the abundance of the different acylium ion fragments RCO^+. The direct FAB chemical analysis of commercial base stocks provides quantitative results for the acid profile that agrees with results obtained by a slower, classical two-step analytical approach which requires (1) the hydrolysis of the ester linkage, followed by (2) the
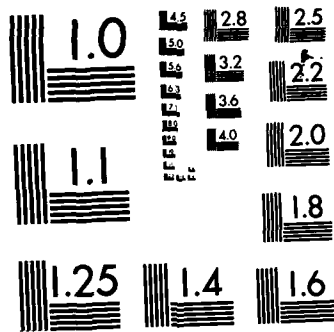
MICROCOPY RESOLUTION TEST CHART

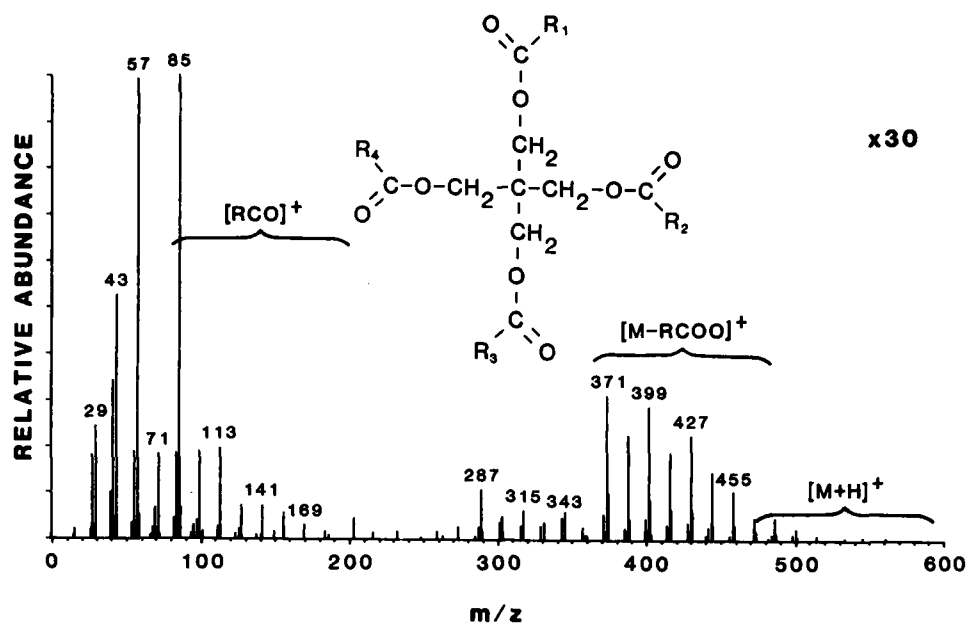NATIONAL BUREAU OF STANDARDS-1963-A

Fig. 13 — Fast-atom bombardment mass spectrum of a commerical lubricant base stock, pentaerythritol tetraalkanoates (inset). The quantity m/z is the mass-to-charge ratio of the ions and is also indicated on each species line. The acylium fragment ions RCO^+ can be used to profile the acid moieties of the tetraesters. The protonated molecules $[M + H]^+$ are not visible in this mass spectrum because of their relatively low abundance.

analysis of the resultant acids by gas chromatography.

The FAB technique also provides the direct analysis of additives present in a lubricant. Normally in FAB, a sample is analyzed by dissolving it in a drop of liquid that is then bombarded, sputtering the sample molecules from the surface of the drop. For lubricants, we can consider the base stock to be the liquid matrix and additives to be the analytes. Thus, we have detected and identified antioxidants and metal passivators in lubricants.

FAB Enhancements: During FAB, the number of sputtered or desorbed neutral organic species is considerably greater than the number of desorbed molecular ions. Therefore, a method to ionize the abundant sputtered neutral species increases the abundance of molecular and fragment ions available for mass spectrometric analysis. We have developed such a novel technique—chemical ionization/fast atom bombardment (CI/FAB) [2]. In this technique, the neutral species react with an ionized gas to pro-

duce ions of these species. To implement the CI/FAB technique, we constructed a high-pressure FAB ion source in which ion/molecule reactions of sputtered ions and neutrals can be studied. (These ion/molecule reactions include collisional stabilization, charge exchange, proton transfer, association, and condensation reactions.) This technique increases the numbers of molecular ions by two to three orders of magnitude and decreases the relative fragmentation of the molecules. Figure 14 displays the CI/FAB mass spectrum of a commercial base stock using isobutane as a ion/molecule reactant gas. The protonated molecules $[M + H]^+$ of the pentaerythritol tetraesters are almost 1000 times more abundant than in the FAB mass spectrum of Fig. 13. This increase results because of a proton transfer from the reactant-gas ion to the desorbed neutral lubricant molecules. The enhanced tetraester ion abundance permits the direct analysis of the different isomer compositions of each tetraester species using tandem mass spectrometric techniques, such as mass-analyzed ion kinetic energy (MIKE) spectrometry.
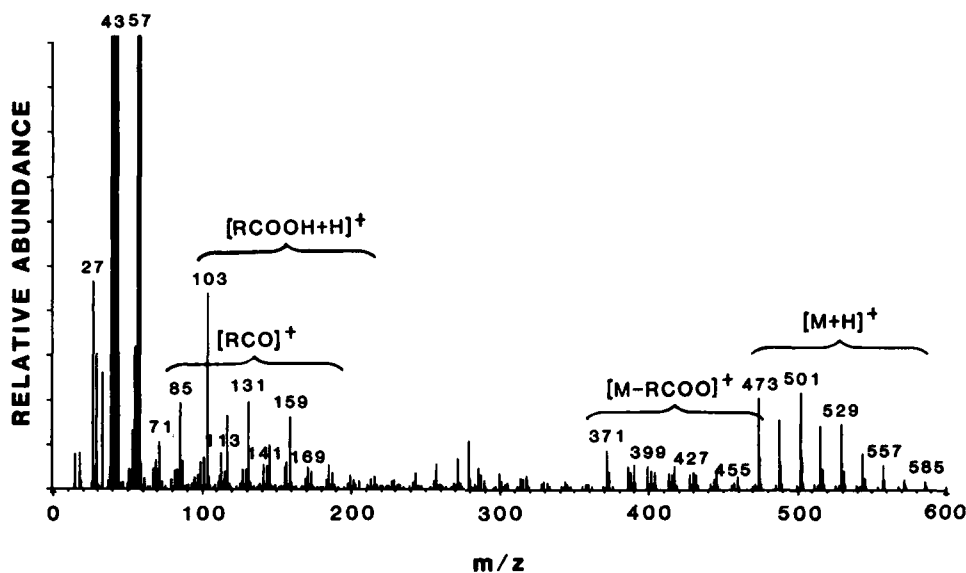
Fig. 14 — Chemical ionization/fast-atom bombardment mass spectrum of the same commercial lubricant base stock as in Fig. 13 showing an almost 1000 times enhancement of the protonated molecules $[M + H]^+$. This large abundance of the protonated molecules enables state-of-the-art mass spectrometric methods to be used to characterize the molecular isomers.

Advantages: Thus, state-of-the-art mass spectrometric techniques, such as CI/FAB used and developed at NRL, provide the lubrication chemist and engineer with invaluable tools to characterize lubricants. Fast-atom bombardment mass spectrometry is a direct, rapid, qualitative, and semiquantitative method to determine the complex base stock compositions of lubricants. Also, FAB mass spectrometry can provide direct screening of additives and other components or reaction products in lubricants. The CI/FAB mass spectrometric technique enhances the sensitivity, by ion/molecule reactions, to detect the various lubricant components. These techniques have immediate applications in quality control, trend analysis, failure analysis, and the fundamental studies of lubricants.

[Sponsored by NAVSEA and NAVAIR]

References

1. "Advanced Mass Spectrometry of Lubricants," presented at the Annual Meeting of the American Society of Lubrication Engineers, Las Vegas, NV, 1985 (to be published in ASLE Trans.).

2. J.E. Campana and R.B. Freas, "Chemical Ionization/Fast Atom Bombardment Mass Spectrometry: A Novel Ionization Method," *J. Chem. Soc., Chem. Commun.* 1414 (1984). ■

Damage Predictions for Torpedo-Submarine Collisions

E.W. Clements and R.S. Schechter
Marine Technology Division

During at-sea ASW maneuvers with unarmed torpedoes and submarines, the risk of a high-speed collision between the two exists. It is essential to understand the factors involved in the damage so that the safety of these maneuvers can be improved. NRL has developed a new technique for calculating the time history of the force exerted on the submarine during such a collision. This force-time curve is the fundamental datum used to predict and evaluate many of the effects of the collision on the safety and operability of the submarine. From these predictions, more damage-resistant design and/or a change in maneuvers should lessen the chance of crippling damage.

195

Damage Assessment Procedures: The most vulnerable classes of components critical to the safety and operability of the submarine are internal equipment, control surfaces, the hull, ballast tanks, and air flasks. Internal equipment is not hit during a collision but can be loaded inertially by the motion of the submarine's hull in the vicinity of the collision point. The other items could be struck directly. Earlier work in the field of torpedo-submarine collisions involved an experimental program in which torpedoes were fired against a dry-docked submarine or dropped on submarine components. The vulnerability of some critical components was assessed directly by these tests; motions that were measured during the impacts provided data which guided development of the Impact Dynamic Design Analysis Method (IDDAM).

Old Procedure: IDDAM is a procedure developed by NRL for assessing the vulnerability of internal equipment by predicting and evaluating their responses to a nearby collision. Theoretical assessment of the vulnerability of the other categories of critical components requires the impact force-time curve, which could not be measured. Previously, estimates were made by considering motion-time histories measured within the torpedo and on the submarine hull at various points in the vicinity of the impact. Then, trial-and-error adjustments of a hypothetical force-time polygon were made until motions computed from a finite-element model of the torpedo and the local structure of the submarine agreed reasonably well with measured motions. Since it is virtually impossible to build sufficient fine detail into the finite-element model and still have a tractable problem, the resulting force-time polygon was regarded with reservations, and the predictions calculated by using it were regarded with some skepticism.

New Procedure: The new method for calculating the impact force-time curve has a more solid scientific basis. It uses motion-time data measured within a floating test target structure upon which the torpedo is dropped. The target structure now used is a large cylinder resembling a submarine compartment in size and construction, although differing from any existing submarine in details such as plating thickness and frame spacing. This structure has been made sufficiently simple so that it can be modeled with a high degree of confidence by a finite-element model. It is fitted with a "simulated equipment" (an internal structure of precisely known dynamic characteristics) and an extensive array of motion and strain transducers. In applications, the mass lump of the finite-element model of the target structure corresponding to the impact point is forced to perform the same motion that is measured at that point of the target structure during the experiment. The structural reaction forces exerted on this mass lump as a result of its motion are then calculated from the finite-element model. The external force history, which is the desired force-time curve due to the impact of the torpedo on the target structure, is then the difference between the mass times acceleration history of the mass lump and the sum of the structural reaction forces acting upon it. The torpedo kinetic energy, impact velocity, momentum change, and rebound are used to verify the impact force-time curve.

Next, the force-time function is applied as a forcing function to the finite-element model, and its motions calculated at each point which corresponds to a measurement point of the target structure. The shock spectrum and time history of these calculated motions are compared to the measured motions. Adequate agreement then implies that the estimated impact force-time curve is reasonably valid. From the force-time curve, the force-stroke curve is calculated—this is the curve of force as a function of the distance the torpedo has crushed and is (within broad limits) a characteristic of the torpedo itself. The force-stroke curve can then be applied to computer models of *different* structural characteristics, and corresponding force-time curves can be calculated. This allows evaluation of the sensitivity of the original force-time curve to variations in target structure and gives guidance on which classes of submarine could produce different force-time curves. The estimated impact force-time curve may be applied to a finite-element model of a submarine compartment to generate tables of coefficients for IDDAM calculations and may be used as a starting point to assess the vulnerability of critical components in the other

(external) categories of critical submarine components.

Conclusion: The impact force-time curve associated with torpedo-submarine collision is an essential datum for finding ways to improve the safety of at-sea ASW exercises. The procedure developed by NRL to estimate this curve is relatively simple and straightforward and rests on a sounder technical basis than the semi-intuitive procedure previously used. It may be expected that refinements will be made to the procedure, and modifications may be necessary as new types of torpedo and classes of submarines appear. It would be expected, however, that the basic principle will remain the same.

The principal Navy agency collaborating with NRL in this project is the David Taylor Naval Ship Research and Development Center, which performed the experimental measurements and furnished data to NRL.

[Sponsored by NAVSEA]   ■

197

Component technology and specialized devices

When fluoropolymers synthesized at NRL are cured, the resins become strong, rigid plastics that have a permanently lubricated surface making them ideal for use in artificial joints for humans

COMPONENT TECHNOLOGY

Specialized devices based on modern technology have provided new and better ways to perform tasks. These devices have also provided a means to achieve new capabilities by combining more traditional research disciplines. The four articles in this chapter describe a small portion of the specialized devices and systems research at NRL. This research was performed in the Acoustics Division (Code 5100), the Condensed Matter and Radiation Sciences Division (Code 6600), and the Electronics Technology Division (Code 6800).

In addition to the work described in these articles, NRL has many other projects in component technology and specialized devices. A few of these are:

- charged particle beam propagation
- compact high-current accelerator
- free-electron laser
- inertial confinement fusion
- electronic warfare system improvement
- active and offboard decoys
- vacuum electronics
- NAVSTAR clock technology

NRL MOS Dosimeter for Space

L.S. August and J.C. Ritter
Condensed Matter and Radiation Sciences Division

R.R. Circle
Space Systems and Technology Division

Energetic electrons and protons are an important part of the Earth's space radiation environment known as the Van Allen belts. Frequently, these charged particles penetrate to the interior of a satellite and cause significant damage to its microelectronic circuitry. To assess the damage and evaluate the reliability of the information and data collected and transmitted from the satellite, NRL scientists have designed and fabricated a metal-oxide semiconductor (MOS), satellite-borne dosimeter [1,2] to make real-time, integrated dose measurements as a function of depth in aluminum. Aluminum is used extensively in satellites, and even when another material is employed for some components, the equivalent aluminum thickness is given since it serves as a reference. The dose measurements will permit an assessment of the radiation damage sustained by the microelectronics at various depths within the satellite. The data will also reveal any significant short-term change in the amount and kind of ambient space radiation encountered by the satellite. The dosimeter has been tested, calibrated, and space-qualified to fly aboard the Combined Release and Radiation Effects Satellite (CRRES), a joint research effort of the Air Force, Navy, and NASA. CRRES is scheduled to be launched in July 1987.

The Dosimeter: Figure 1 shows the NRL dosimeter with its thin protective cover removed. Four radiation-soft, MOS field-effect transistors (MOSFETs) are employed as radiation sensors. These transistors are the p-channel, enhancement-mode type; that is, the source to drain current consists of holes. The gate of the transistor must be biased negatively with respect to the source in order for the device to conduct. The dose is measured by the shift in negative gate bias voltage that produces a source-to-drain current of 50 μA. A constant current circuit is built into the dosimeter, so any voltage change results from the ionizing radiation that produces electron-hole pairs in the gate oxide. Under a positive gate bias during radiation exposure, holes are driven toward the silicon-silicon dioxide interface in the MOSFET and are trapped. These holes require a *larger negative* gate voltage to produce the constant source-to-drain current; hence, the increase in negative voltage measures the dose absorbed by the gate oxide. Each sensor is calibrated with a cobalt-60 gamma-ray reference

Fig. 1 — NRL MOS dosimeter with its cover removed, showing the electronic circuit board (left) and the four radiation sensors (right). The sensors are shielded by different thicknesses of aluminum ranging from 0.6 mm to 9.0 mm. This dosimeter will be mounted at the surface of the CRRES satellite and will measure radiation doses to compare it with other types of dosimeters and instruments on the satellite. The dosimeter is 7 cm × 7 cm × 4 cm, weighs 187 g, and requires less than 1/4 W of power to operate.

80564(2)

source. The relationship between the shift in gate voltage and dose is nearly linear under the conditions expected in space.

An ideal dosimeter measures the energy absorbed per unit mass (dose) independently of the type of radiation employed. To approach this ideal condition, the NRL dosimeter, in the EXPOSE (positive gate bias) mode, is operated with an electric field strength of 1 MV/cm across the gate oxide which is 0.12 μm thick. The large field eliminates errors in the dosimetry caused by charge recombination effects in the oxide for different radiations, and the response per unit dose is nearly the same for gamma rays, electrons, and protons. The READ mode of operation simply determines the negative gate voltage that gives the constant source-to-drain current after some exposure interval giving the dosage accumulated since the previous READ. The dosimeter is to be read approximately once a day for a 5-min interval. The EXPOSE and the READ modes are selected by telemetry signals from the ground. Note that during most of the time in orbit (99.7%), the dosimeter will be in the EXPOSE mode.

The four sensors are shielded by cylinders of different wall thicknesses. The thickest aluminum shield (9.0 mm) permits essentially only the most energetic protons to reach the transistor. The thinnest shield consists only of the TO-5 kovar container (0.6 mm aluminum equivalent) in which the transistor is mounted. This sensor responds to both electrons and protons. The other shields, of intermediate thickness, control the electron-proton ratios that reach the sensors and provide intermediate points on the dose-depth curve. The negative gate voltages obtained in the READ mode will be telemetered to Earth each day. The changes in these voltages will be calculated, and the individual sensor calibrations will yield the doses received by each of the four sensors. By using the shield thicknesses for each sensor, points on the depth-dose curve can be calculated. Such a curve can then provide data on the doses at various depths within the satellite. The results can also be compared to the predictions of space radiation models.

CRRES Advantages: The CRRES experiment will provide a large number of instruments to measure the near-Earth radiation environment in various ways. Data from other instruments such as particle counters and spectrometers will be compared with those of the NRL dosimeter. Previously, only limited space dosimetry measurements have been available, and these have not had the marked advantage of different instruments to provide intercomparisons. The CRRES data will be used to resolve large discrepancies among existing space radiation models and should provide a more accurate assessment of the near-Earth radiation environment and its hazards. This is an important objective of the CRRES mission.

[Sponsored by NAVELEX]

References

1. L.S. August, "Estimating and Reducing Errors in MOS Dosimeters Caused by Exposures to Different Radiations," *IEEE Transactions in Nuclear Science* **NS-29**, 2000 (1982).

2. L.S. August, R.R. Circle, J.C. Ritter, and J.S. Tobin, "An MOS Dosimeter for Use in Space," *IEEE Transactions in Nuclear Science* **NS-30**, 508 (1983). ∎

Niobium Nitride for Josephson Tunnel Junctions

E.J. Cukauskas, W.L. Carter, and M. Nisenoff
Electronics Technology Division

Completely refractory superconducting electronic devices have a variety of applications including low-noise, highly sensitive magnetometers, millimeter-wave mixers, and digital and analog signal processing systems. A thorough understanding of the properties of the materials used to fabricate superconducting devices such as Josephson tunnel junctions is critical to their development, performance, and applications. Recently, by using niobium nitride as the electrode material, NRL scientists have helped to solve many problems which occur in the conventional fabrication of superconducting devices at high temperatures.

A Josephson tunnel junction consists of two superconducting electrodes separated by a thin, 20 to 100-Å oxide or semiconducting film. These junctions are tested in the laboratory at about 4K, a temperature achieved by cooling with liquid helium. In field applications Josephson junctions should be operated at one-half the superconducting transition temperature Tc of the electrode materials. At this temperature, all the superconducting properties of the electrode material are stable. However, the use of superconducting material with higher transition temperatures ($Tc > 16K$) would allow the cooling of these devices by small, cryogenic refrigerators instead of cumbersome liquid helium systems.

Refractory superconducting materials usually require elevated substrate temperatures Ts (700° to 800°C) during deposition to obtain stoichiometric (with well-defined composition) films with maximum values of Tc. However, the use of such high temperatures during the fabrication of multilayer integrated circuit (IC) structures may drastically alter the material properties of the underlying layers and interfaces. Thus, one needs either superconducting electrode thin films, which can be deposited at reduced Ts or interface (barrier) materials which can withstand elevated temperatures.

At NRL we have been studying the use of niobium nitride (NbN) as electrodes in high-Tc Josephson junctions that incorporate semiconducting barriers. As we show, NbN can be deposited at temperatures as low as 200°C and still produce effective Josephson tunnel junctions. NbN displays a wide range of superconducting properties that can be obtained by altering the conditions under which the films are deposited. The specific application governs which properties we desire to control. For example, for electronic circuit applications, it is important to have high-Tc and low-residual resistivity to obtain a very short magnetic penetration length, which is proportional to the square root of Tc divided by the resistivity. A short penetration length is crucial in preventing external magnetic fields from penetrating into the junction region, thereby degrading the device performance.

We are studying the material properties of NbN films prepared under various conditions to fabricate high-Tc, low-resistivity materials at low Ts to reduce both the penetration depth and the degradation of the barrier properties. The films are characterized by their Tc, room temperature resistivity, residual resistance ratio, and crystal structure [1].

Sputtering in Methane: The NbN films were deposited in an ultrahigh vacuum RF magnetron sputtering system at different Ts. The system used a power density of 4 W/cm^2, a total pressure of 1.4 Pa (1 Pa = 10^{-5}), and a premixed sputtering gas consisting of argon, nitrogen, and methane. The films were all deposited at a nitrogen partial pressure of 0.15 Pa and a methane partial pressure as high as 0.12 Pa. The methane provides carbon that is incorporated into the films and that enhances the growth of a single crystallographic structure of NbN. This structure provides a high-quality material for Josephson tunnel junctions. Figure 2 illustrates the Tc as a function of the partial pressure of methane for several Ts during film deposition. The best films, those with the highest Tc, were prepared at the higher Ts under lower methane partial pressures. But even at a Ts as low as 200°C, high-quality films with a Tc above 13K were produced.
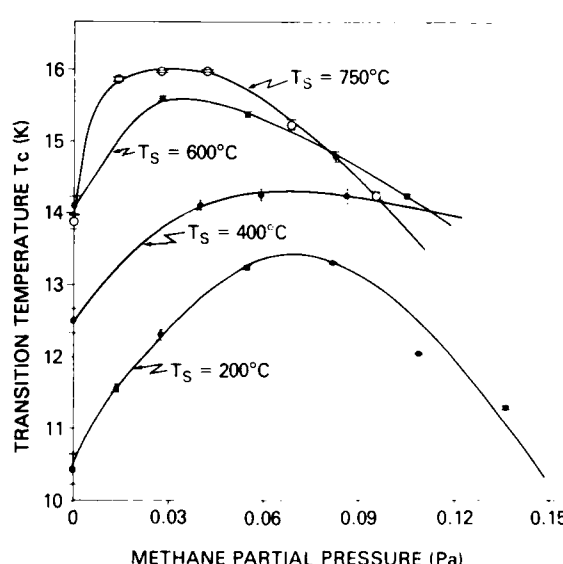

Fig. 2 — Tc as a function of methane partial pressure for rf magnetron sputtered niobium nitride (NbN) films prepared at different Ts in the presence of methane. The best films were prepared at the higher Ts at relatively low methane partial pressures.

Fig. 3 — Penetration depth, λ(0) cal, calculated from measured Tc and resistivity data, as a function of methane partial pressure present during fabrication. The diagonal line connects the maximum Tc obtained for each Ts. The performance of Josephson junctions is degraded as the magnetic field penetration of the films increases.
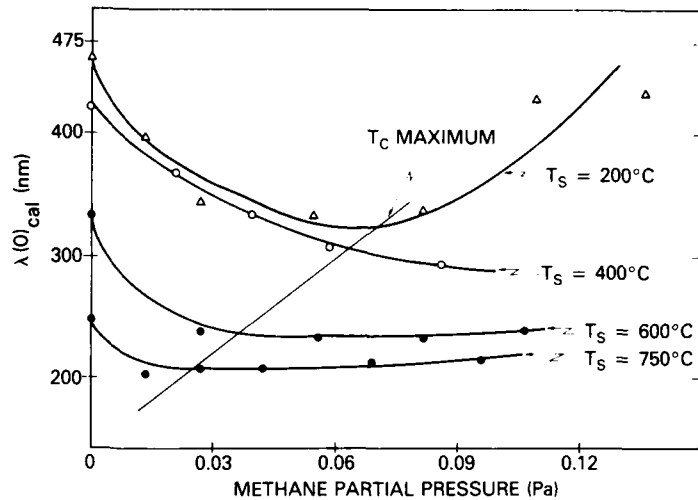
Figure 3 illustrates the magnetic penetration, $\lambda(0)$ cal (as calculated from the measured Tc and resistivity), vs methane partial pressure for the films in Fig. 2. The maximum Tc is also indicated for each curve. Here again, the best films, that is, those with the shallowest magnetic penetration, were prepared at the highest Ts in low-methane partial pressures. These films are good candidates to use as base electrodes for Josephson tunnel junctions [2] because their performance is least degraded by magnetic field penetration.

Josephson Junction: We have been using these materials to study barrier/electrode interfaces for NbN/Si/Nb Josephson tunnel junctions. A typical junction consists of a base electrode (NbN film) deposited at 750°C with the silicon barrier and a niobium counter electrode sputtered at room temperature. This approach optimizes the base electrode/barrier interface at room tem-

perature before addressing the problems associated with counter electrode deposition at higher Ts. Figure 4 illustrates the current-vs-voltage characteristics of such a device measured at 4.2K. This device has a base electrode $Tc > 16K$ and shows good tunneling characteristics at 4.2K where all superconducting properties are stable. In the future we will investigate such devices made with both electrodes of NbN.

We have shown that high-quality NbN suitable for the fabrication of Josephson junctions can be obtained by incorporating small amounts of carbon during film preparation. This is achieved by sputtering in a low partial methane pressure. These films have been successful in the fabrication of high-quality, completely refractory Josephson tunnel junctions which incorporate silicon barriers prepared at ambient substrate temperature. We are extending our Josephson junction research to include the use of
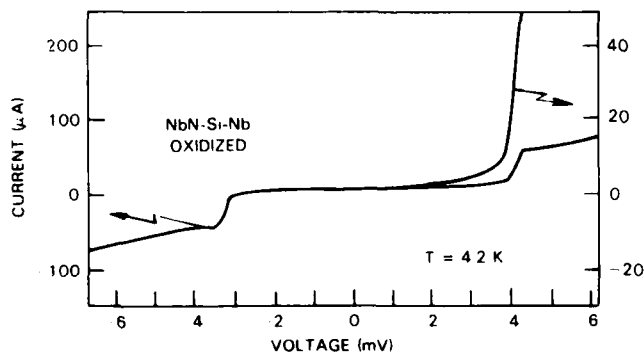

Fig. 4 — The current I vs voltage V characterization, measured at 4.2K, for a NbN-Si-Nb Josephson junction using a high-Tc NbN-film base electrode. The second curve was traced at an expanded (5X) current scale and illustrates the Josephson junction leakage below the sharp current rise at about 4 mV, the region of operation of a Josephson junction when used as a millimeter wave detector or mixer.

NbN counter electrodes, which will result in superconductive devices capable of operating at temperatures approaching 16K.

[Sponsored by NAVELEX and ONR]

References

1. E.J. Cukauskas, M. Nisenoff, H. Kroges, D.W. Jillie, and L.R. Smith, "All Refractory, High Tc Josephson Device Technology," *Advances in Cryogenics Engineering* **30**, 547 (1984).

2. E.J. Cukauskas, W.L. Carter, and S.B. Qadri, "Superconducting and Structure Properties of Niobium Nitride Prepared by rf Magnetron Sputtering, *J. Appl. Physics* **57**, 2538 (April, 1985). ∎

The Gyroklystron—An Efficient, High-Gain, Fast-Wave Amplifier

R.K. Parker and A.K. Ganguly
Electronics Technology Division

The millimeter wavelength region of the electromagnetic spectrum has long been recognized as offering the electromagnetic system designer numerous advantages relative to either longer or shorter wavelengths. The narrow beam widths and high gain that are readily available at these wavelengths result in good target resolution, elimination of multipath effects, improved clutter rejection, and resistance to jamming. Moreover, at the optimum frequencies for atmospheric transmission, the penetration during adverse conditions (such as clouds, fog, or smoke) is substantially better than that of electro-optical systems and is only moderately worse than that at microwave frequencies. Conversely, the attenuation coefficient of air generally increases with frequency requiring increased power for millimeter-wave operation in the atmosphere. In the past, the lack of transmitter power sufficient to overcome the attenuative losses has limited attempts to exploit the millimeter-wave region.

Power Tube Limitations: With power tubes, the primary constraints on power production at high frequency have been establishing and maintaining a strong interaction between an electron beam and the electromagnetic wave which is being generated. In conventional power tubes, a slow-wave circuit is used to reduce the phase velocity of the electromagnetic wave within the interaction space so that beam-wave synchronism can be maintained. Operation near synchronism is a necessary condition for energy exchange. To perform this function, the transverse dimensions of the slow-wave circuit must be small compared to the free-space electromagnetic wavelength. The power limitations imposed by scaling down the size of slow-wave tubes for smaller wavelengths result from the problem associated with power dissipation from the delicate, thermally isolated structures of the slow-wave circuit and from vacuum breakdown between closely spaced circuit elements.

Within the past decade, experimental progress with the electron cyclotron resonance maser (ECRM), a class of fast-wave amplifiers, has demonstrated their advantages for millimeter-wave power production. Recent studies have focused on the gyrotraveling wave tube (TWT) and the gyroklystron as specific embodiments of the ECRM. These devices eliminate the conventional slow-wave circuit by using the periodic motion of the electrons, induced by external fields applied in the interaction region, to couple (RKP) a natural beam resonance to a selected waveguide mode. With the gyrodevices, an axial magnetic field is used to couple the fast cyclotron wave on the beam to an appropriate transverse electric (TE) waveguide mode. The fast-wave amplifiers generate increased power because their coupling mechanism does not require the small transverse dimensions of the slow-wave circuit; indeed, large-scale cavities or lengths of simple waveguide can be used for gyrodevices.

Gyroklystron: For radar applications, the gyroklystron is a particularly interesting variant of the ECRM because it should be an efficient (>40%), high-gain (>40 dB) amplifier capable of generating high millimeter wavelength power over a narrow bandwidth (<5%). The gyroklystron, shown schematically in Fig. 5, illustrates the properties of the ECRM. A magnetron injection gun (MIG) is used to launch an annular
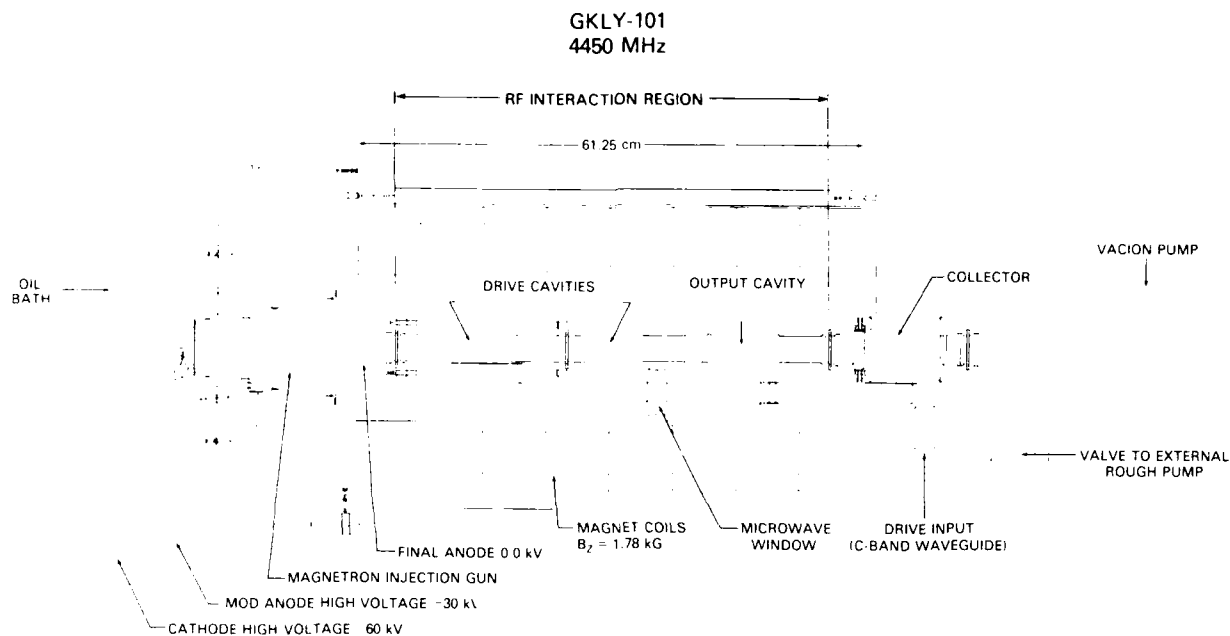
GKLY-101
4450 MHz

|◄──── RF INTERACTION REGION ────►|

──── 61 25 cm ────

VACION PUMP

OIL
BATH

DRIVE CAVITIES   OUTPUT CAVITY   ┌─ COLLECTOR

VALVE TO EXTERNAL
ROUGH PUMP

└─ MAGNET COILS   └─ MICROWAVE   DRIVE INPUT
   B_z = 1.78 kG   WINDOW   (C-BAND WAVEGUIDE)

└─ FINAL ANODE 0 0 kV

└─ MAGNETRON INJECTION GUN

└─ MOD ANODE HIGH VOLTAGE -30 k\

└─ CATHODE HIGH VOLTAGE   60 kV

Fig. 5 — Schematic of gyroklystron

electron beam into the rf interaction region which, in this design, consists of two drive cavities and one output cavity separated by radiation-free drift spaces. Unlike the usual electron gun, the MIG requires an intermediate electrode to optimize the ratio (α) of transverse ($v_\perp$) to axial velocity ($v_\|$) in the electron beam and operates with a temperature-limited electron flow from the cathode to minimize the axial velocity spread. In the interaction region, the transverse kinetic energy of the electrons is coupled to a selected TE cavity mode by an instability that has its origin in the energy dependence of the relativistic electron cyclotron frequency. Through this instability, the electrons become phase bunched in their cyclotron orbits thereby giving rise to a coherent interaction. To achieve positive gain, the instability requires that the radiation frequency slightly exceed the cyclotron frequency. For operation at the fundamental cyclotron frequency, this condition leads to a requirement for a high axial magnetic field in the interaction region. For example, a 35 GHz amplifier would need a magnetic field of approximately 13 kG; our device which operates at 4.5 GHz requires about 2 kG. Since the gyrodevices extract energy from the transverse or rotational motion of the

electrons, a large ratio of transverse to axial electron velocity, typically from 1 to 3, is required to obtain high efficiency operation.

In the gyroklystron, the first drive cavity is used to give the electrons a sinusoidal energy modulation, which sets up transverse drifts. Intermediate cavities are used to enhance the transverse velocity modulation. In the drive cavities, the external magnetic field and the cavity parameters are selected so that the electrons are bunched at low wave power with little beam-wave energy exchange. The last (output) cavity is located at the axial position which maximizes the energy extraction from the transversely bunched beam.

Through proper selection of the interaction parameters, this cavity system can be operated either as an amplifier or as an oscillator. Amplifier operation requires that the electrons either gain energy from the electromagnetic fields in the drive cavities or lose energy to the electromagnetic fields insufficient to compensate for wall losses. Alternatively, the system operates as a self-sustained oscillator if the electron energy given up to the electromagnetic fields in the bunching cavities is just sufficient to compensate for all radiative losses. Unlike the conventional

klystron, the interaction in the gyroklystron is distributed with energy modulation and extraction occurring over many cyclotron periods in the cavities.

The experimental configuration shown in Fig. 5 has been assembled at NRL to assess gyroklystron operation at the fundamental cyclotron frequency. For convenience, the frequency for this experiment, 4.45 GHz, was chosen to take advantage of an existing magnetron injection gun; however, subsequent efforts will use other guns to extend these studies to millimeter wavelengths. This tube was designed, based on a nonlinear analysis, to operate with a conversion efficiency of 40% and a small signal gain of 40 dB. For the design calculations, the electron gun was assumed to provide a 5-A beam with $\alpha = 2$ when operating at 60 kV. To avoid possible mode competition, the tunable rectangular cavities were designed to operate in the TE_{101} (fundamental) mode, and the cylindrical drift spaces are cut off to all radiation at the operating frequency.

The gyroklystron has been tested with an applied voltage of ~35 kV, currents ranging from 5 to 8 A, and a beam α of ~1.1. The basic operational characteristics such as power, efficiency, gain (linear and saturated), and bandwidth have been measured for both uniform and tapered magnetic field profiles in the interaction region. By tapering the magnetic field profile, the power, efficiency, and bandwidth can be significantly enhanced. As shown in Fig. 6, a peak power output of 54 kW was obtained while using a 30% linearly tapered magnetic field profile. Under optimum conditions, the maximum observed efficiency was 30% which corresponds to an orbital efficiency (efficiency of extraction of transverse energy) of ~60%. A large orbital efficiency implies that a higher overall efficiency is possible if the transverse kinetic energy of the electron beam were to be increased (for example, $\alpha = 2$). Similarly, the highest observed values for linear and saturated gain were 36 dB and 18 dB, respectively. As shown in Fig. 7, a
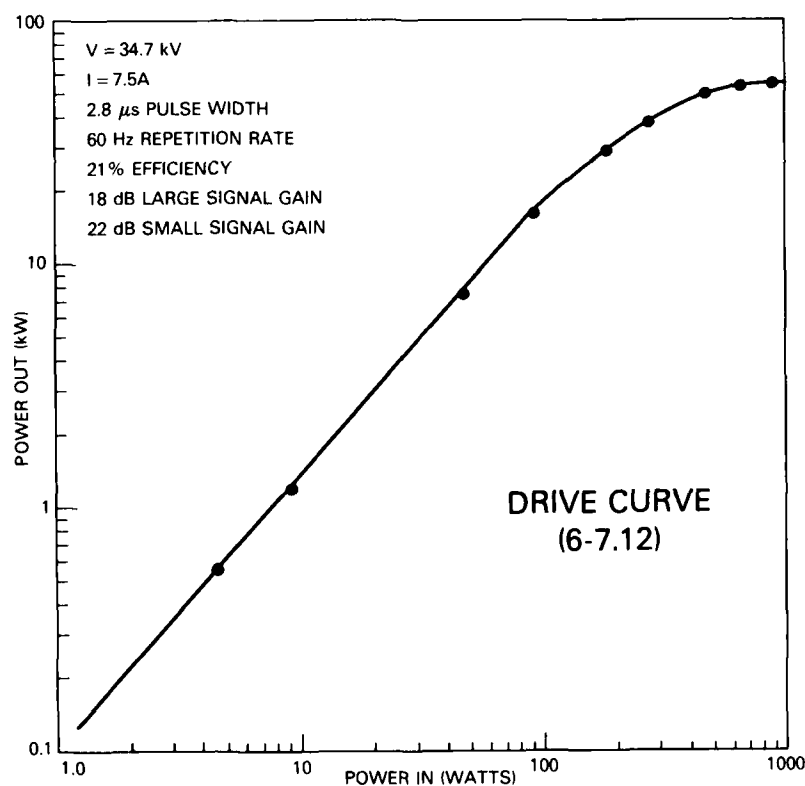
Fig. 6 — Experimental drive curve of three-cavity device

V = 33kV
I = 6.8 A

OUTPUT

INPUT

FREQUENCY (10 MHz/Div)
CF = 4.473 GHz
0.134% BANDWIDTH (FWHM)

POWER (LINEAR)
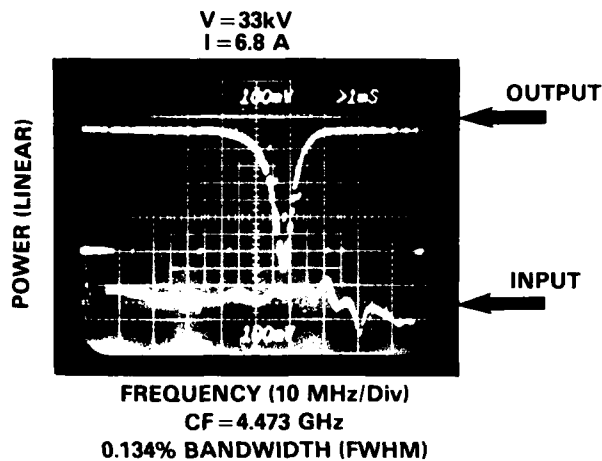
Fig. 7 — Bandwidth with uniform magnetic field profile

bandwidth of 0.13% was measured for a uniform magnetic field profile. This compares to a theoretically predicted value of 0.25%. By using both staggered tuning and a tapered magnetic field, the measured bandwidth was increased to 0.43%.

These preliminary NRL studies have contributed significantly to establishing the viability of the gyroklystron concept. The high gain and high orbital efficiency observed in the experiments look promising and show reasonable agreement with theory. Most importantly, this device has provided the first successful demonstration of stable gyroklystron operation.

W.M. Bollen of Mission Research Corp., Alexandria, VA and B. Arfin, previously with NRL, collaborated in this research.

[Sponsored by ONR and NAVELEX] ■

High-Precision Airborne Gravity System Demonstration

J.M. Brozena
Acoustics Division

Several Navy requirements depend on precise knowledge of the detailed structure of the Earth's gravity field. NRL scientists have developed and tested an airborne gravimetry system which approaches the accuracy of existing shipboard systems; however it is at least ten times faster and much less costly to operate than shipboard systems. To attain shipboard accuracy with the airborne system, many additional signal processing techniques were applied to the data. The system, the processing techniques, and the test of the system are described.

Gravity measurements are required to determine geoid height and deflection of the vertical, to develop gravitational models for satellite orbital prediction, to correct inertial guidance systems, to estimate underwater topography (or bathymetry) in poorly surveyed regions, and to remote sense the density structure deep beneath the Earth. The last application is important for research into the composition and structure of the Earth's core, mantle and crust, including the determination of mineral resources. Of the above, the primary Navy interests are to provide corrections to inertial guidance systems and to estimate bathymetry; hence the need for gravity measurements over the oceans.

Stationary Measurements: The technology of stationary gravity measurements is relatively simple. It consists of determining the amount of spring tension or magnetic force needed to support a known test mass at rest. These measurements can be reliably made to nearly one part in one hundred million. However, stationary measurements are very time consuming and expensive over land and impossible in deep water due to the lack of an ultrastable platform.

Complications of Moving Platforms: Gravity measurements from a moving platform or dynamic gravimetry adds several difficulties to the stationary problem. The gravimeter must be oriented with respect to the local vertical at all times. This is readily accomplished by gyro stabilization. Moreover, the test mass can no longer be brought to rest for the measurement due to the irregular motions of the platform. Instead, the vertical motions of the mass are averaged over some time interval and the supporting forces are varied as required to keep the mass within some limits of travel. This averaging changes the gravity field measurement from a point measurement to some spatial average along the track of the vehicle which depends on the averaging period and the velocity of the platform.

The dynamic measurement resulting from the above procedure is the sum of the gravitational acceleration plus the vertical accelerations of the platform. These vertical accelerations of the vehicle consist of two components: first, the changes in altitude with respect to the center of the earth; and second, the centripetal acceleration which results when the platform travels horizontally over a curved earth at a constant altitude. In the case of shipboard measurements, the first type of acceleration is primarily due to waves and is close to zero when averaged over several minutes. At typical research ship velocities (5 m/s) a spatial average of less than 5 km will nearly eliminate vertical motion from the gravity measurement. Shipboard accuracy is generally limited by the determination of the second type of vertical acceleration. This is computed from the course and speed of the ship and is termed the Eotvos correction. Under ideal conditions and with excellent navigation, shipboard measurements are accurate to within 1 to 2 mGals (1 mGal $= 10^{-5}$ m/s^2; $g \approx 9.8$ m/s^2).

While shipboard measurements are accurate compared to aircraft ships, they are slow and expensive per track km. So, scientists at NRL began developing an airborne gravity measurement system several years ago. However, the use of aircraft for gravity measurements introduces more complications. In addition to adequately determining the Eotvos correction (the error increases with velocity), the first type of vertical acceleration may no longer be simply averaged out. An aircraft usually cannot move along a relatively constant average surface as a ship does. The acceleration this induces must be determined from an altimetry profile which must be accurate to within a few cm.

Prototype System and Test: Scientists at NRL have recently completed a demonstration of a prototype airborne gravity measurement system which competes in precision with shipboard measurements. The demonstration was conducted as a blind test over the Outer Banks of North Carolina. Ground truth data, held by the Defense Mapping Agency (DMA), was not released to NRL until the completion of the experiment. The experiment was flown by the NRL Flight Detachment aboard one of the Laboratory's modified P-3 Orion research aircraft. Nominal altitude and speed were 600 m and 265 kn/hr.

System — The prototype system consists of a LaCoste-Romberg gravity meter, a Global Positioning System (GPS) for navigation and determination of the Eotvos correction, and highly precise pressure and radar altimeters. Data from all sources are acquired and stored by on-board computer systems. The radar altimeter was designed and built at NRL and measures the aircraft height above the ocean to a few cm. The pressure sensor, a Rosemount 1201FG, was mounted on a 3.8-m boom extending forward from the aircraft nose (Fig. 8) to reduce the effects of wake turbulence and bow shock on the measurements. Both altimeters are required since many tracks flown in the test area (Fig. 9) are over land and water; the radar provides altitudes over water, and the pressure is used over land. (Radar cannot be used over land due to uncertainties and changes in land elevation.) The slopes of the isobaric surfaces are determined along each track by comparing the radar altitudes to the pressure heights while over water. These slopes are used *to correct the pressure* altitudes over land. After the two altitude time series are merged and smoothed, the vertical accelerations are computed and subtracted from the gravimeter data. The data from each track is then low-pass filtered to remove noise caused by altimetry and navigation errors. The final step in data reduction is to perform a least squares adjustment of the individual gravity profiles to minimize differences at track crossings. The error in each profile is modeled as linear along the track with the slope and bias adjusted to obtain the least squares minimization.

Test — NRL's airborne measurements were compared by DMA to the ground truth in their terrestrial library. The results of the comparison show an rms difference between the gridded data sets of 2.5 mGals. This is very close to the accuracy achieved in shipboard measurement; however, the airborne results are at least an order of magnitude faster and less expensive to obtain!

Improvements: Now that the concept has been successfully demonstrated, the next step is to redesign the prototype as an operational surveying tool. The goals are to make the system simpler, lighter, and easier to operate. We are

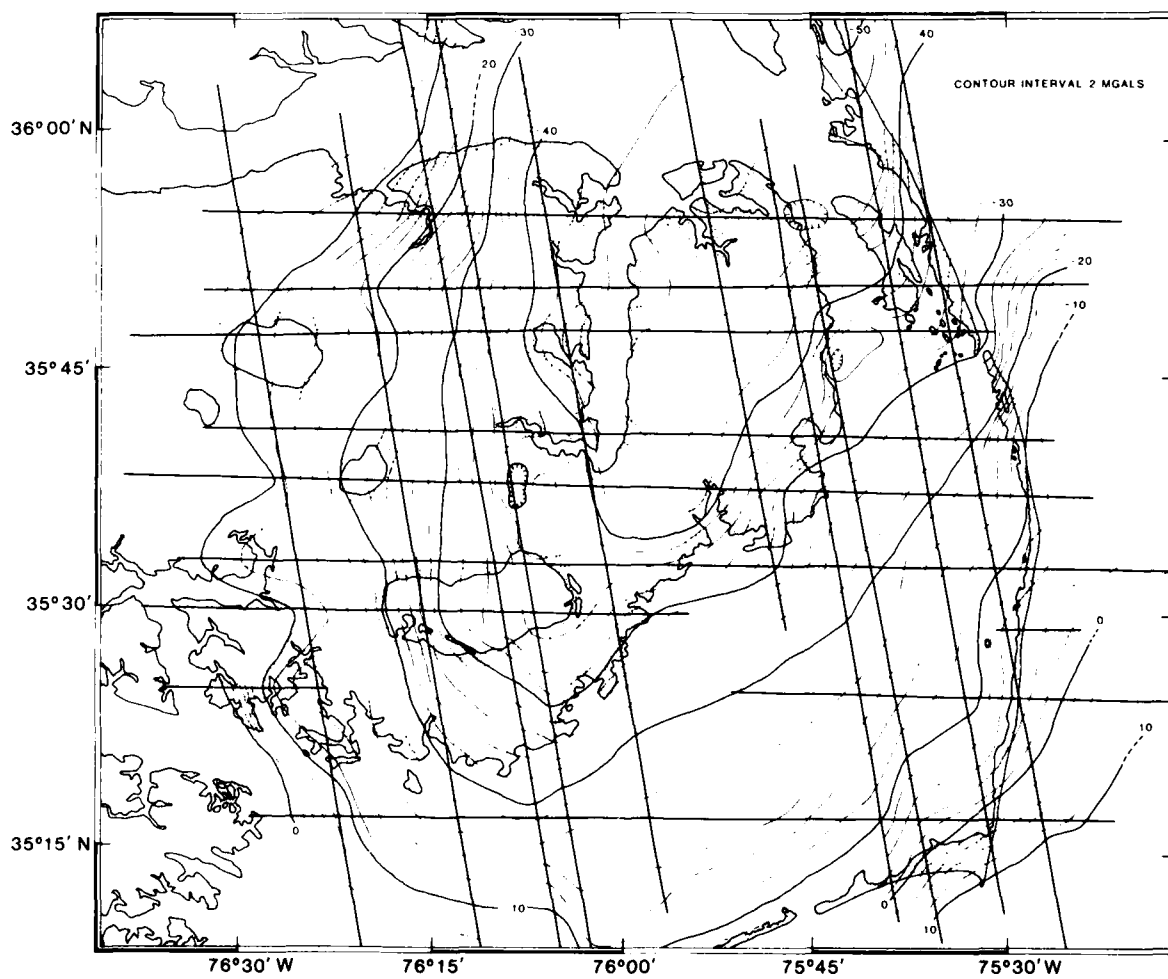Fig. 8 — NRL P-3A research aircraft with pressure altimeter probe mounted on the nose

Fig. 9 — Gravity contours (2-mGal increments) over the North Carolina test area.
Aircraft tracks are indicated by the heavy lines.

also investigating alternative sensors and signal processing methods to improve system accuracy and extend its use to the largely unsurveyed polar regions, where the year-round ice cover makes conventional shipboard measurements impossible. Interferometric navigation using the GPS satellites should provide three-dimensional positioning within a few cm and replace the current altimetry and navigation scheme. This will improve the accuracy of the vertical acceleration correction which is now the limiting factor on the accuracy of the airborne measurements.

[Sponsored by ONR and DMA]

Reference

1. J.M. Brozena, "A Preliminary Analysis of the NRL Airborne Gravimetry System," *Geophysics* **49**, 1060-1069 (1984). ∎

Fluid mechanics and applications

High-speed planing hulls generate extensive wakes which interact with the ocean surface waves

FLUID MECHANICS

Fluid mechanics research at NRL spans many divisions and disciplines, but this research serves two purposes. One is to gain new insights into the fluid physics important to the Navy; here articles discuss the behavior of ocean waves and ionospheric turbulence. The other purpose is to develop and test sophisticated numeric computational techniques. Fluid systems are ideal for this since they provide the necessary highly complex, nonlinear, coupled problems for meaningful tests; the article on detonation modeling illustrates this. This work was performed in the Laboratory for Computational Physics (Code 4040), the Plasma Physics Division (Code 4700), and the Marine Technology Division (Code 5800).

Other fluid mechanics research at NRL includes:

- reactive flow modeling
- boundary layer hydrodynamics
- towed array noise generation
- modeling of tropical storms

The Structure of a Propagating Detonation

K. Kailasanath and E. Oran
Laboratory for Computational Physics

What is a Detonation?: A detonation is a supersonic compression wave driven by the rapid release of chemical energy behind it. A simple way to picture a detonation is as a shock wave, followed by an exothermic chemical reaction zone, and finally a region of fully reacted, hot material behind the reaction zone. In most detonations, the configuration of the leading shock and reaction zones are complicated. As shown in Fig. 1, they consist of interactions of Mach stem shocks (MS), incident shock waves (IS), and transverse shock waves (TS).
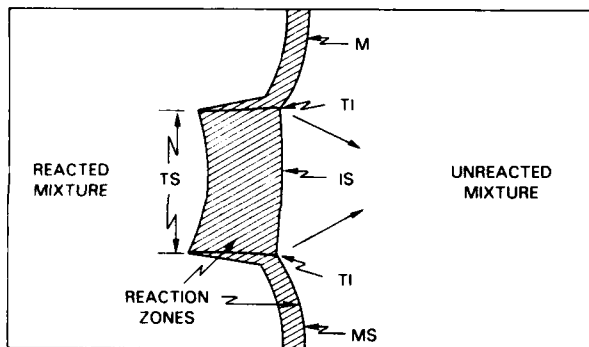
Fig. 1 — A schematic showing the main features of a detonation propagating from left to right: Mach stem shocks (MS), Incident shocks waves (IS), and Transverse shock waves (TS). The unlabelled arrows show the direction of propagation of the triple shock intersection points (TI).

Detonation Cells: Experiments at various laboratories show that a propagating detonation leaves a cell-like pattern on the sidewalls of a confining chamber. These patterns are etched by the triple shock intersection point (TI in Fig. 1) formed at the front of the detonation by the intersection of the transverse shock wave with the incident shock wave and the Mach stem shock. Thus the cell patterns are histories of the location of the triple intersection point. The size and regularity of the cell structure of a detonation is a function of the specific energetic material, its phase and dilution, and the nature of its confinement. The initiation and failure of detonations are related to the cell size and structure. There-fore, understanding the detonation structure and how it varies with geometry and material provides important information on the use and safety of explosives and propellants.

Numerical Simulations: During the past several years the Laboratory for Computational Physics has been studying these structures by using multidimensional numerical simulations. The models used for the simulations combine a time-dependent, compressible fluid model with a model for energy release. The numerical simulations have been used to develop a computational method for determining detonation cell sizes. The calculated cell sizes agree with experimental measurements. More interestingly, the calculations provide insight into the basic mechanisms of detonation cell formation, the formation of unreacted pockets behind detonations, and the role played by the transverse shock (TS) waves in the propagation of detonations. In particular, the simulations show that the evolution of the curvature of the transverse shock wave is very important in the propagation of detonations. The curvature of the transverse shock wave at the time of its reflection from either a neighboring transverse wave or a wall determines whether the cell is flattened, or whether pockets of unreacted gas can be formed. Examples of these phenomena are shown in Figs. 2 and 3.

Examples: In Fig. 2 we show the calculated paths of the triple shock intersection points for detonation propagation in channels of three different widths. In the top part of the figure, which is for detonation propagation in a 5-cm-wide channel, we see gaps in the paths of the triple points at the walls. When the channel width is increased to 7 cm, the gap decreases and by further increasing the channel width to 9 cm, we obtain complete detonation cells within the channel. These effects are due to the curvature of the transverse shock wave at the time of its interaction with the walls of the channel. If the channel width is slightly larger than the detonation cell size, we see pockets of unburned gas form behind the detonation front. This phenomenon has also been observed in experiments.

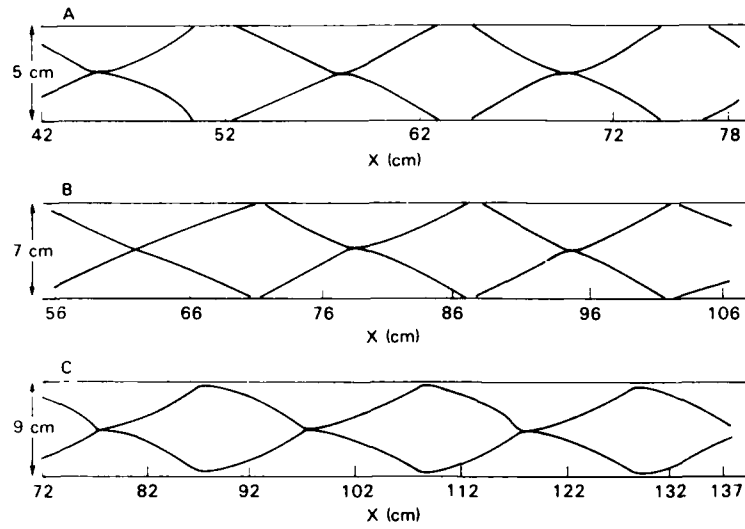The formation of unburned pockets is shown in Fig. 3 which is a composite of **215**

Fig. 2 — Calculated paths of triple shock intersection points for detonation propagation in channels of widths (A) 5 cm, (B) 7 cm, and (C) 9 cm. Complete detonation cells are observed in the 9-cm-wide channel.
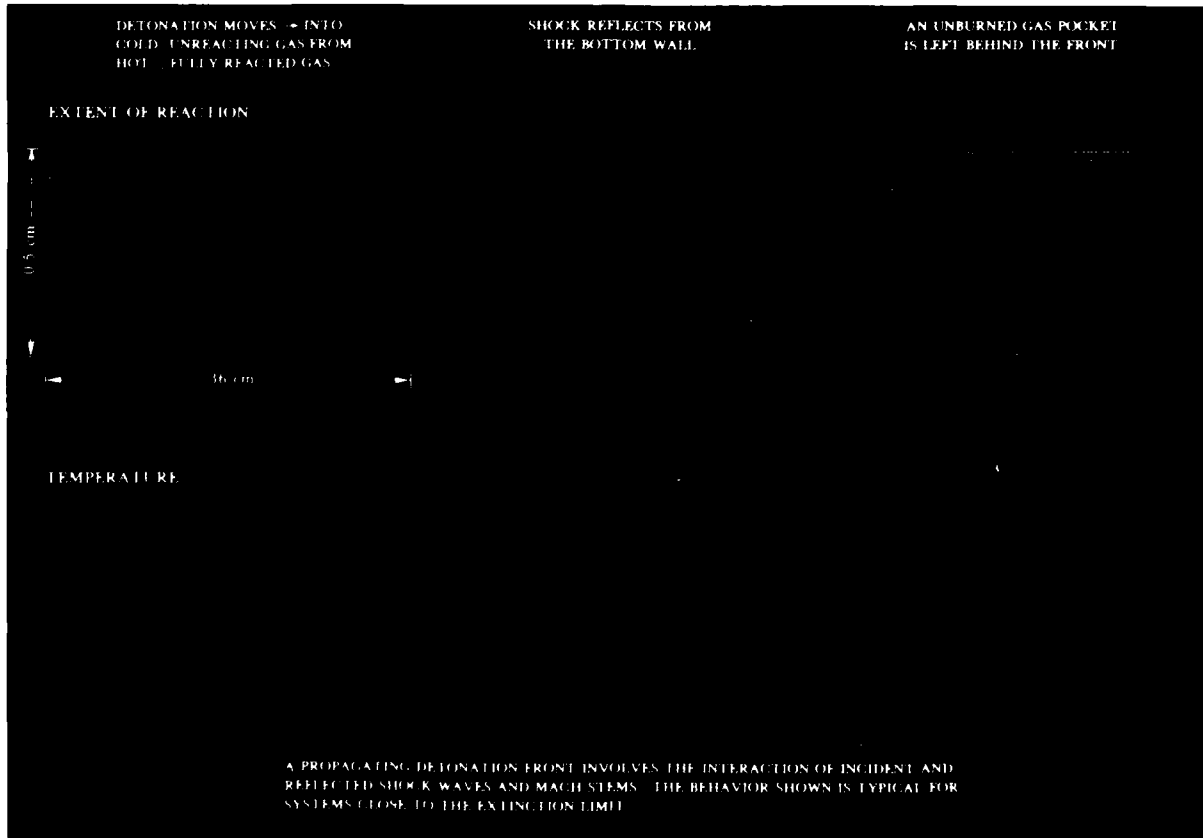

Fig. 3 — Extent of reaction and temperature contours showing the formation of an unburned gas pocket during detonation propagation

"snapshots" from numerical simulations. Only the portion of the channel containing the triple shock intersections is shown. In the top three panels of the figure, we show the extent of completion of the reactions. The detonation is propagating to the right into the unreacted gas mixture (shown in light blue). The fully reacted gas is on the left-hand side and is shown in yellow. The various shades in between represent different degrees of reactedness and together comprise the detonation front. In the third frame, we see a detached pocket of unburnt gas (red) behind the detonation front. The corresponding temperature of the gases in the various regions is shown in the bottom three panels of the figure. The dark blue region to the right is unreacted cool mixture and the red region on the left side of the figures is the hottest region. These unburnt gas pockets have important implications for detonation cell generation and the behavior of detonations near the extinction limits.

A better understanding of detonations is important both for the development of better propellants and explosives as well as to control the damage caused by accidental explosions. These detailed numerical simulations have been very useful in delineating features of the detonation structure in the gas phase. The simulations have also helped explain and provide insight into many experimental observations. New calculations are looking at detonation structure in the liquid phase.

[Sponsored by ONR]

References

1. E.S. Oran, T.R. Young, J.P. Boris, J.M. Picone, and D.H. Edwards, "A Study of Detonation Structure: The Formation of Unreacted Gas Pockets," Nineteenth Symposium (International) on Combustion, p. 573, The Combustion Institute, 1982.

2. K. Kailasanath, E.S. Oran, J.P. Boris, and T.R. Young, "Numerical Simulations of the Structure and Propagation of Self-Sustained Detonations," NRL Memorandum Report 5380, June 1984. (Also to be published in *Combust. Flame.*) ■

Laboratory Studies of Steep and Breaking Deep Water Waves

S.E. Ramberg and O.M. Griffin
Marine Technology Division

For more than a century, hydrodynamicists have been exploring the nonlinear behavior of ocean surface waves, with one special goal: a rationale for, and a description of, the catastrophic nonlinearity commonly known as wave breaking. The breaking of ocean waves is a common occurrence and an important element of many oceanographic, coastal and ocean engineering problems. Wave breaking is also an important consideraton in surface ship hydrodynamics. The wave resistance of a ship is increased by the breaking of the ship's bow wave and may influence both the wake energy balance and the ensuing white-water production.

Several significant advances toward an understanding of wave breaking have been made in recent years. These include the experimental and mathematical characterization of instability mechanisms which can lead to wave breaking and numerical simulations of wave overturning and incipient breaking. Much is still unknown, however, including such simple information as a general criterion for the onset of breaking. The causes of wave breaking are varied and often are reflected in the manner in which a wave breaks, from gentle spilling at the crest to sometimes spectacular curling and plunging of the forward face of the wave. In deep water, the most common breakers are spilling, or, in the presence of sufficient wind, white-capping.

Recent studies of deep water breaking have focused on the growth of subharmonic instabilities of steep, initially regular waves that lead to two- and three-dimensional spilling breakers. A summary and discussion of this material is given by Griffin [1]. In these studies an initially uniform train of steep waves evolves to breaking. The present work examines the onset of breaking for deep-water waves which grow as they travel along a laterally converging channel in NRL's Marine and Environmental Hydrodynamics Laboratory. Here, the channel convergence forces the wave growth.

217

Laboratory Studies: The growth of the steep waves in the NRL channel is akin to events at sea in the sense that wave reflections, wave instabilities, and mean currents in the experimental facility combine to yield conditions approaching the complexity of the open ocean. Yet, the slowly converging channel provides a well-defined input condition on the waves to permit study of the fundamental processes that lead to breaking.

Spilling breakers (Fig. 4a) were most commonly observed during the experiments although curling breakers (Fig. 4b) were occasionally recorded at the larger rates of wave growth. The curling or mildly plunging breakers had the largest wave asymmetries; the forward face of the wave crest became much steeper than the rear. This asymmetry appeared to result from very large local rates of wave growth caused not only by channel convergence but also by wave reflection patterns and other channel effects.

Breaking Criterion: Regardless of the type of breaking, the wave period, the growth rate, or any other experimental variable, the waves were found to break at or near to the same value of mean limiting steepness (ratio of wave height to wave length) which was significantly below the classical analytical limit of Stokes. The Stokes limit, derived nearly a century ago, corresponds to fluid velocities at the wave crest equaling the wave phase speed and, in that way, suggests the impending breakup of the wave form. The results from the NRL experiments are compared to the Stokes limit and the data of Ochi and Tsai

(a)

(b)

Fig. 4 — Typical photographs of a) spilling breaker and b) curling breaker in NRL's wave channel. Horizontal white line is the mean water level.
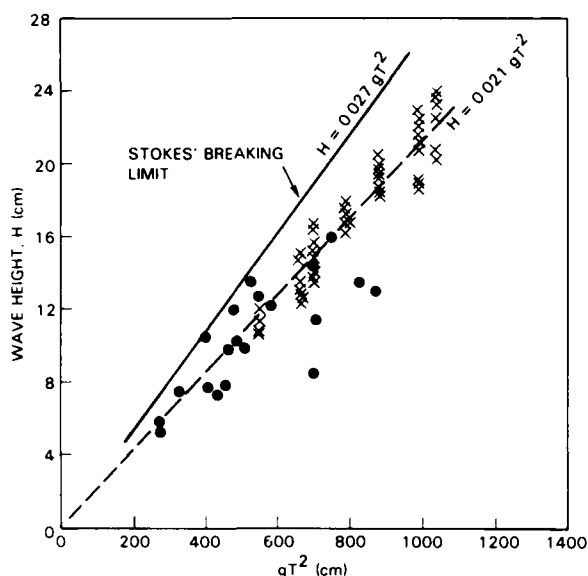
Fig. 5 — Deep water waveheight at breaking H_b, vs a wave period parameter gT^2: x—NRL experiments; ● —data from Ochi and Tsai [2].

[2] in Fig. 5. The data of Ochi and Tsai were obtained from laboratory studies of breakers formed during interactions of several different wavelengths. Limited observations of breaking waves over submerged objects and three-dimensional spilling waves yield similar results [3]. Taken together these results indicate a simple but universal criterion to describe the onset of wave breaking in deep water appropriate to many Navy problems:

$$H_b = 0.21gT^2$$

where H_b, is the waveheight at breaking, g is the gravitational acceleration, and T is the wave period.

Energy Balance: In addition to the above onset criterion, the NRL studies have examined the energy balances in the converging channel to determine the initial and cumulative wave energy losses due to wave breaking. Here the type of breaking becomes important with nearly a doubling of potential energy loss for curling breakers as opposed to spilling waves. In both instances, however, the bulk of the potential energy loss is apparently dissipated locally in turbulence rather than converted to any significant increase in kinetic energy possessed by the mean flow. This

process has not been previously reported and should be an important simplifying element in various models.

The results of the NRL experiments have provided valuable guidance for futher basic studies of breaking waves while yielding results for both steep and breaking waves of immediate utility in a number of areas of interest to the Navy and others.

[Sponsored by ONR]

References

1. O.M. Griffin, "The Breaking of Ocean Surface Waves," NRL Memorandum Report 5337 (1984).

2. M.K. Ochi and C.H. Tsai, "Prediction of Occurrence of Breaking Waves in Deep Water," *J. Physical Oceanography*, **13**, 2008-2019 (1983).

3. S.E. Ramberg, M.E. Barber, and O.M. Griffin, "Laboratory Studies of Steep and Breaking Deep Water Waves in a Convergent Channel," NRL Memorandum Report, in press. ■

A Doubly Asymptotic Approximation for the Interaction of Water Waves and Ship Wake Currents

R.A. Skop
Marine Technology Division

To better characterize the observability of ship wakes, an improved description of the ship-induced modifications to the ambient ocean wave field is needed. In particular, the ability to remotely sense a ship wake signature often depends on the modifications of the ambient wave background caused by the currents set up in the ship wake. A typical example is the long, narrow, calm region of water extending aft of the ship. This region is visually apparent in Fig. 6. It is also observed by radars operating in a Bragg backscatter mode as shown in Fig. 7; the dark region in this figure corresponds to the calm water region extending aft of the ship.

Fig. 6 — A typical visual (photographic) observation of ship wakes. Note the absence of the shorter ambient waves (visible mostly in the foreground) in the wake regions.
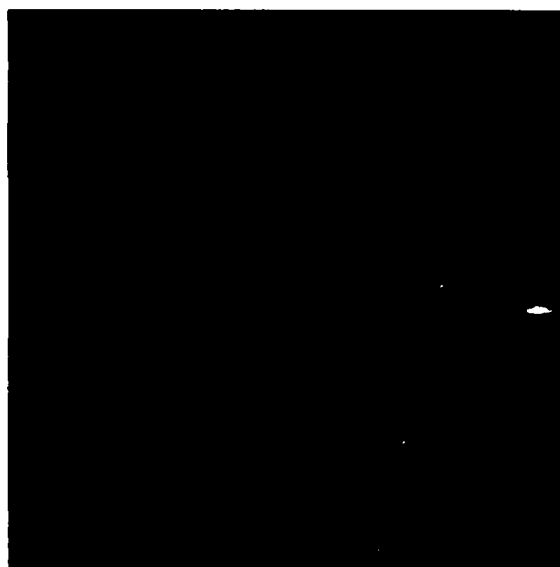

Fig. 7 — A satellite synthetic aperture radar image of a ship wake. The dark streak behind the ship is caused by an absence of short wavelength surface waves in the ship wake.

Physics of Ship Wake: Both the visual and radar observations can be explained by postulating an absence of diffuse, short surface waves in the region aft of the ship as compared to the ambient background. The absence of the short surface waves in this region is closely related, conceptually, to the stopping action of a hydraulic breakwater in which a current opposed to an incoming wave field effectively stops the penetration of all waves shorter than a certain wavelength. We can envision that the currents set up outward from and along the wake axis by the passage of the ship do function as stopping currents for the shorter ambient waves.

The latter situation is, however, decidedly more complex than the hydraulic breakwater problem. First, the velocity field set-up in the ship wake has three components of current each of which varies in the horizontal and with depth. Second, the direction of the incident wave field with respect to the wake axis is in general arbi-
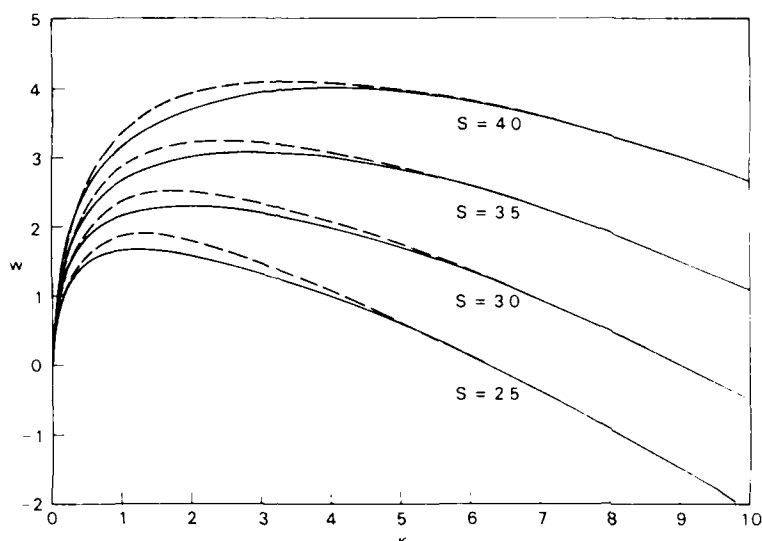
Fig. 8 — A comparison between the exact dispersion relation (solid line) and the doubly asymptotic approximate dispersion relation (dashed line) developed at NRL for a water wave propagating into a current which is uniform to some depth d and zero thereafter. In this figure, w is a dimensionless frequency, κ is a dimensionless wavenumber (inverse wavelength), and S = $(gd)^{1/2}/U$ where U is the velocity of the current and g is the gravitational acceleration.

trary. To simplify the situation, while still maintaining its physical meaningfulness, NRL investigators have developed a doubly asymptotic approximation for the interaction of water waves and depth-dependent currents. This approximation allows an accurate elimination of the depth coordinate from the problem and hence provides a significant reduction in modeling complexity.

Asymptotic Approximation: The approximation is based on the use of a depth averaged current in the dispersion relation which relates wave frequency, wavelength, and current. Specifically, we write the dispersion relation as $\omega = \Omega + k_x \tilde{U}_x + k_y \tilde{U}_y$ where ω is the observed wave frequency, Ω is the intrinsic (still water) wave frequency, $k_{x,y}$ are the two components of the wavenumber along the horizontal x and y directions, and $\tilde{U}_{x,y}$ are the two components of the averaged current along the horizontal directions. The latter is given by

$$\tilde{U}_{x,y} = k \int_{-\infty}^{0} U_{x,y}(z) \exp{(kz)}\,dz,$$

where k is the absolute value of the wavenumber and $U_{x,y}$ is the actual profile of the current components with depth. In addition to being asymptotic to the exact dispersion relation at long and short wavelengths, the approximate dispersion relation provides a highly satisfactory representation to the exact dispersion relation throughout wavelength space.

Several different current profiles have been studied. One of interest is for a water wave propagating into a current field which is uniform down to some depth d and zero below. This problem can be solved exactly and with the doubly asymptotic method. Figure 8 compares the exact and asymptotically derived dispersion relations. It is clear the dispersion relations agree at short $(K \rightarrow \infty)$ and long $(K \rightarrow 0)$ wavelengths.

Now that this doubly asymptotic theory has been validated for several cases, we plan to apply it to surface ship wakes by using realistic vertical profiles of ship-generated currents.

[Sponsored by ONR] ∎

Ionospheric Turbulence and Chaotic Fluid Behavior

J.D. Huba and M.J. Keskinen
Plasma Physics Division

I.B. Schwartz
Optical Sciences Division

Ionospheric research has been an active area of study at NRL over the past two decades. The Navy and other DoD agencies are concerned with the impact of ionospheric turbulence (that is, **221**

electron density irregularities) on command, control, communications, and intelligence systems because it can degrade communication and radar signals. One physical process likely to generate ionospheric turbulence is an interchange instability. This instability requires a density gradient and is analogous to gravitational fluid instabilities in which denser fluid sinks and lighter fluid rises in plumes creating density irregularities. Two forms of this instability, the Rayleigh-Taylor (see *1980 NRL Review*, p. 109) and the gradient drift, are believed to be active in the equatorial and high-latitude ionospheric F regions, and may produce the observed turbulence on length scales of 10^2 to 10^4 m. The difference between these instabilities is the external driving mechanism. The Rayleigh-Taylor is driven by a gravitational force, while the gradient drift is driven by an electric field or neutral wind.

In applying these instabilities to the ionosphere, they can be divided into two categories, collisional and inertial. The collisional limit occurs when $\nu \gg \omega$ while the inertial limit occurs when $\omega \gg \nu$ (ν is the ion-neutral collision frequency and ω denotes the frequency associated with plasma fluctuations). In the ionosphere, the collisional limit transitions to the inertial limit above 500 km altitude. The bulk of ionospheric research on the nonlinear phase of these instabilities has been restricted to the collisional regime. The present research is developing a nonlinear theory of these instabilities for *both* the collisional and inertial regimes.

Chaotic Behavior: We have, in collaboration with Dr. A. Hassam of the University of Maryland, derived a set of nonlinear, mode-coupling equations based on the magnetized two-fluid (that is, electrons and ions) electrostatic equations. The theory is restricted to two-dimensional turbulence in the xy plane transverse to the magnetic field, and only modes short compared to the scale length of the density gradient are considered. We find that for a three-mode system, the mode coupling equations for the Rayleigh-Taylor and gradient drift instabilities can be written as [1]

$$dX/dt = -\sigma X + \sigma Y \qquad (1)$$

$$dY/dt = -Y + rX - XZ \qquad (2)$$

$$dZ/dt = -2Z + XY. \qquad (3)$$

In the above, X is related to the electostatic potential fluctuations while Y and Z are related to the density fluctuations. The quantities r and σ are functions of the physical parameters of the plasma. The significance of this result is that Eqs. (1) to (3) correspond exactly to the equations studied by Lorenz [2] for the Rayleigh-Benard instability, which is the seminal work on chaotic behavior in deterministic systems.

Analysis of Eqs. (1) to (3) reveals a rich and complex nonlinear behavior of the system. Three fixed, limiting states can be shown to exist which are determined by setting $d/dt = 0$ in Eqs. (1) to (3). In one state, $X = Y = Z = 0$ and no motion occurs. In the other two states, which are determined by the values of r and σ, convection cells can develop having either positive or negative vorticity (as illustrated in Fig. 9). For certain values of r and σ, these convection states are stable and fixed; that is, the fluid approaches one of these convection states and remains in this state. However, a more interesting and fascinating phenomenon can occur for special values of r and σ. In this situation, the convection states are
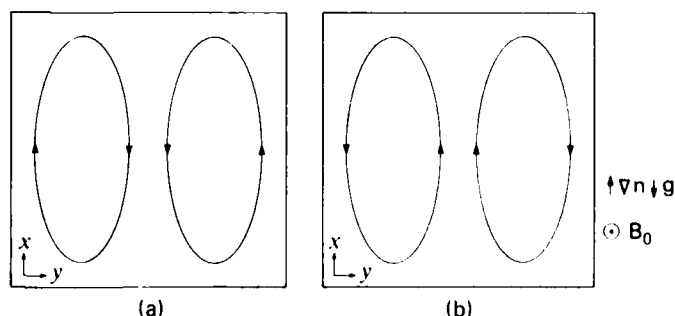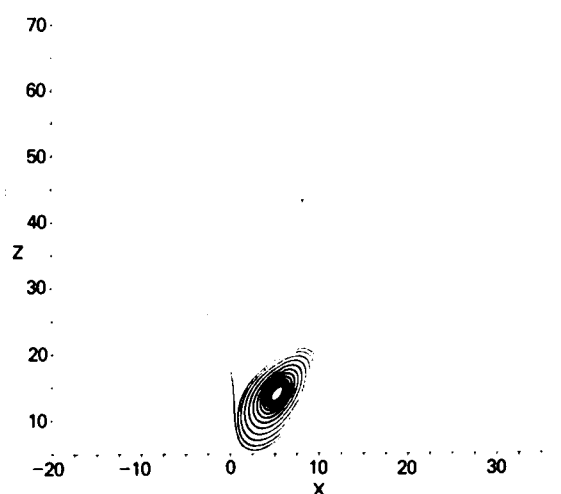

Fig. 9 — Convection cell patterns permitted in a three-mode system. In this example, the density gradient ∇n and gravitational force g are in the $+x$ and $-x$ directions, and the magnetic field B_0 is in the $-z$ direction; (a) Positive vorticity and (b) Negative vorticity.

(a)   (b)

themselves unstable, the fluid can approach one of two states in the limit as $d/dt = 0$, but in reality the fluid alternates from one convection cell to the other in a seemingly random manner. The behavior of the fluid as it approaches these two situations is contrasted in Figs. 10 and 11 by plotting the projection of the orbit on the X,Z plane. Figure 10 shows the approach to a "stable" attractor centered at $X \sim 6$ and $Y \sim 14$, while Fig. 11 shows the approach to a "strange" attractor. In the latter situation, the system is oscillating randomly between the two convection states shown in Fig. 9 in an apparently chaotic manner even though the system is deterministic.

An important point in applying chaotic fluid theory to ionospheric turbulence is the following. As noted earlier, we can consider two limits for interchange instabilities in the ionosphere: collisional and inertial. In the collisional limit $(\nu \gg \omega)$ it can be shown that the convection states are always stable for the three-mode system; that is, there is no chaotic behavior. Thus, only in the inertial regime $(\nu \ll \omega)$ can chaotic fluid behavior occur for a three-mode system.

Fig. 10 — An approach to the nontrivial, steady-state attractor to Eqs. (1) to (3) projected onto the $X-Z$ plane. The parameters used are $\sigma = 10$ and $r = 15$.

Fig. 11 — A strange attractor for Eqs. (1) to (3) is illustrated as a projection onto the $X-Z$ plane. The parameters used are $\sigma = 10$ and $r = 30$.
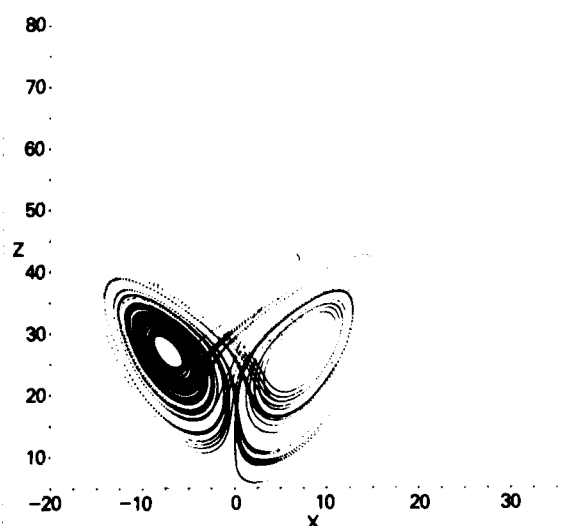
This result suggests there may be an altitude dependence concerning the nature of ionospheric turbulence since ν and ω cross at about 500 km.

Recapitulaton: We have shown that interchange instabilities relevant to ionospheric turbulence (Rayleigh-Taylor and gradient drift) can be studied in the context of modern nonlinear dynamics and chaos. In particular, we demonstrate that for a simple system (three modes), the equations governing these instabilities are exactly the same as those that govern the Rayleigh-Benard instability [2]. The physical analogy between our system and that considered by Lorenz is the following. The Rayleigh-Benard instability is driven by a temperature gradient and convects "hot and cold" fluid elements; the temperature gradient is maintained by a heat source at one end and a heat sink at the other. The Rayleigh-Taylor and gradient drift instabilities are driven by a density gradient and convect "heavy and light" fluid elements; in the case of the ionosphere, the density gradient could be maintained by photoionization at one end and recombination at the other.

Implications and Extensions: This work provides new insight into the relationship between ionospheric turbulence and nonlinear fluid behavior. Moreover, the theory developed is relatively general and has potential applications to a wide variety of other plasma interchange instabilities (such as the curvature drift instability). Finally, we note that the results presented are for a very simple system (that is, three modes), which could be argued to be unrealistic for most physical applications. However, we have recently developed a simulation code which follows the evolution of a many-mode system (100s of modes), and are in the process of studying chaotic fluid behavior of such a system.

References

1. J.D. Huba, A.B. Hassam, I.B. Schwartz, and M.J. Keskinen, "Ionospheric Turbulence: Interchange Instabilities and Chaotic Fluid Behavior," NRL Memorandum Report 5474, 1984; *Geophys Res. Lett.* **12**, 65, 1985.
2. E.N. Lorenz, "Deterministic Nonperiodic Flow," *J. Atmos. Sci.* **20**, 130, 1963. ∎

Excellence in research for tomorrow's Navy

NRL honors its many
distinguished scientists
and engineers for superior
accomplishments in the
fields of naval research
and in its documentation.
Here Judith L. Flippen-
Anderson of the Laboratory
for Structure of Matter
accepts a research publi-
cation award from Captain
James O'Donovan

AWARDS AND RECOGNITION

"We should ask ourselves, 'Are we, as an in-house laboratory, performing our job as Mr. Edison thought we should?' I believe the answer is that we are doing considerably better than he ever imagined we would. We have been responsive to Navy problems, we have maintained sustained technical competence over the many fields of Navy interest, and we have managed to maintain our intellectual independence.

"In the final analysis, [these awards recognize exceptional] commitment to continued productivity, intellectual integrity, and forefront work in science and technology."

Dr. Alan Berman, former Director of Research
10th Annual Research Publication Awards Presentation

SPECIAL AWARDS AND RECOGNITION

NRL is proud of its many distinguished scientists and engineers. A few of these have received exceptional honors for their achievements.

Albert I. Schindler
Material Science and Component
 Technology Directorate

1984 SENIOR EXECUTIVE SERVICE PERFORMANCE AWARD

George H. Sigel, Jr.
Optical Sciences Division

**1984 E. O. HULBURT ANNUAL SCIENCE
AND ENGINEERING AWARD**

"For his outstanding contributions to the understanding of optical materials and development of fiber optic technology."

Guenter E. Brueckner
Space Science Division

**DEPARTMENT OF THE NAVY
SUPERIOR CIVILIAN SERVICE AWARD**

"For world leadership at the Naval Research Laboratory in development of optical systems, technology, and their application for scientific observations from space. For development of a whole new class of universally acclaimed space-qualified optical ultraviolet telescopes and spectrographs of improved spatial and spectral resolution which have established a new standard of technology for observation of the sun and its atmosphere from space. For discovery of many dynamic solar phenomena, especially including tightly constrained fast-moving streams of charged plasma, and plasma regions. For development and flight of an ultraviolet instrument to establish with absolute precision the degree of variability of the sun's ultraviolet irradiation so important to terrestrial atmospheric processes."

227

William F. Gabriel
Radar Division

DEPARTMENT OF THE NAVY
MERITORIOUS CIVILIAN SERVICE AWARD

"... in recognition of his outstanding technical contributions in the field of adaptive radar antennas and superresolution."

Henry A. Resing
Chemistry Division

NRL—SIGMA XI
PURE SCIENCE AWARD FOR 1984

"... for bringing order and understanding to complex problems in surface chemistry through the development of powerful experimental and theoretical magnetic resonance techniques which elucidate the orientation of adsorbed molecules, the chemistry and dynamics of electrically active dopants in low dimensional systems, and the nature of bound water in heterogeneous catalysts, proteins, and muscle fibers."

Bruce P. Gaber
Optical Sciences Division

NRL—SIGMA XI
APPLIED SCIENCE AWARD FOR 1984

"For pioneering research on the properties of artificial biological membranes in the form of liposomes and for the development and demonstration of liposome-based encapsulation techniques for making artificial blood and for ultrasensitive detection of biochemical agents in the environment."

Isabella L. Karle
Laboratory for Structure of Matter

CHEMICAL PIONEER AWARD, 1984
THE AMERICAN INSTITUTE OF CHEMISTS

"For her pioneering development and application of the Symbolic Addition Procedure for crystal determination that has led to an exponential increase in the speed and facility with which identity and structural configuration can be determined."

Jerome Karle
Laboratory for Structure of Matter

PATTERSON AWARD IN X-RAY CRYSTALLOGRAPHY, 1984
THE AMERICAN CRYSTALLOGRAPHIC ASSOCIATION

"... for outstanding research in the theory and application of direct methods of structure solution."

Ben J. Lamb
Space Systems and Technology
  Division

IEEE CENTENNIAL MEDAL, 1984

"Is honored for extraordinary achievement and is deserving of special recognition by The Institute of Electrical and Electronic Engineers, Inc. and is hereby awarded The Centennial Medal presented during the Centennial Year, 1984."

Merrill I. Skolnik
Radar Division

IEEE CENTENNIAL MEDAL, 1984

"Is honored for extraordinary achievement and is deserving of special recognition by The Institute of Electrical and Electronics Engineers, Inc. and is hereby awarded The Centennial Medal presented during the Centennial Year, 1984."

Emanuel L. Brancato
Condensed Matter and
  Radiation Sciences Division

IEEE CENTENNIAL MEDAL, 1984

"Is honored for extraordinary achievement and is deserving of special recognition by The Institute of Electrical and Electronic Engineers, Inc. and is hereby awarded The Centennial Medal presented during the Centennial Year, 1984."

229

William D. Garrett
Space Systems and Technology
  Division

SPECIAL AWARD FOR EXCELLENCE IN TECHNOLOGY TRANSFER, FEDERAL LABORATORY CONSORTIUM, 1984

"For leadership in the development and transfer, both nationally and internationally, of a nontoxic mosquito control methodology."

James R. Griffith
Chemistry Division

SPECIAL AWARD FOR EXCELLENCE IN TECHNOLOGY TRANSFER, FEDERAL LABORATORY CONSORTIUM, 1984

"For Transfer of Fluoropolymers Technology"
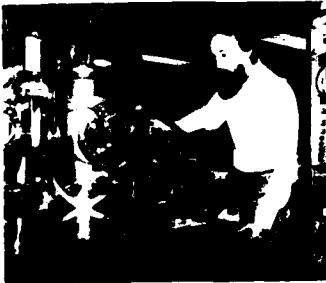
Gary A. Prinz
Condensed Matter and
  Radiation Sciences Division

ELECTED FELLOW, AMERICAN PHYSICAL SOCIETY

"For spectroscopic studies which clarified the roles of magnetic ions in insulators and the introduction of molecular beam epitaxy as a technique for growth of magnetic materials."

Carmine Vittoria
Condensed Matter and
230   Radiation Sciences Division

ELECTED FELLOW, AMERICAN PHYSICAL SOCIETY

"For the development of new microwave magnetic materials and discovery of surface spinwave excitations at magnetic-nonmagnetic material interface."

ELECTED FELLOW, AMERICAN PHYSICAL SOCIETY

"For substantial contributions to the basic understanding of superconductivity, and to applications of superconducting materials."
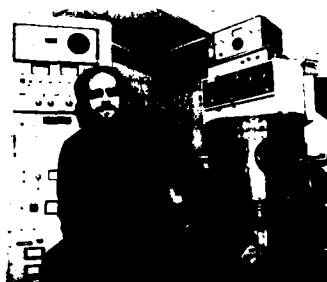
Stuart A. Wolf
Condensed Matter and
  Radiation Sciences Division

ELECTED FELLOW, AMERICAN ASSOCIATION
FOR THE ADVANCEMENT OF SCIENCE

"For investigations of crystal structures of the oxygen carriers found in animal bloods and for contributions to the methods of macromolecular crystallography."

Wayne A. Hendrickson
Laboratory for
  Structure of Matter

DEPARTMENT OF THE NAVY
MERITORIOUS CIVILIAN SERVICE AWARD

"... in recognition of your outstanding technical leadership and management initiatives during your tenure as Superintendent, Condensed Matter and Radiation Sciences Division."

J. Thomas Schriempf
Condensed Matter and
  Radiation Sciences Division

WILLIAM BLUM AWARD, NATIONAL CAPITAL SECTION,
THE ELECTROCHEMICAL SOCIETY

"In recognition of his contributions to corrosion science, particularly in advancing the understanding of the molten salt corrosion processes of complex alloys."

Robert L. Jones
Chemistry Division

231

ELECTED FELLOW, THE INSTITUTE OF ELECTRICAL AND ELECTRONICS ENGINEERS, INC.

"for contributions to the theory and application of guided wave optical devices."

Henry F. Taylor
Optical Sciences Division

INDIVIDUAL HONORS

During 1984 NRL staff members earned 1,953 awards under the Federal Incentive Awards program. These awards are summarized in the following table.

Distribution of Federal Incentive Awards During 1984

NRL E.O. Hulburt Annual Science Award	1
SES Performance Award	1
Navy Superior Civilian Service Award	1
Navy Meritorious Civilian Service Award	2
Outstanding Performance Ratings	471
Special Achievement Awards	79
Quality Step Increases	161
Research Publication Awards	88
Invention and Patent Awards	142
Sustained Superior Performance Awards	234
Employee Suggestions	16
Length of Service	651
Safety Certificates	96
Blood Donor Certificates	10
TOTAL	1953

In addition, Laboratory employees received numerous scientific medals, military service awards, academic honors, and other forms of recognition, including election and appointment to offices in technical societies. The following is an alphabetical list of persons receiving such recognition in 1984.

Aberg, R.L., *Cochairperson, Counter-Communications Panel for the Joint Logistics Commanders, Joint Technical Coordination Group for Electronic Warfare*

Ascher, H.E., *Coauthor, "Repairable Systems Reliability: Modeling, Inference, Misconceptions and Their Causes," Marcel Dekker, Inc., New York*

August. L.S., *Coauthor, Distinguished Poster Paper Award, 1983 Institute of Electrical and Electronics Engineers (IEEE) Conference on Nuclear and Space Radiation Effects*

Bartoli, F.J., *Chairperson, Optical Sensor Session, 1985 American Institute of Aeronautics and Astronautics (AIAA) Laser Effects and Target Response Meeting*

Beach, L.A., *President, NRL Chapter, Federal Executive and Professional Association*

Beal, R.T., *Member, AIAA, Space Systems Technical Committee*

NRL Chapter President of Sigma Xi, Loren Bearce (right), presents outgoing president Norman Koon with Certificate of Appreciation

Bishop, S.G., *Adjunct Professor, Dept. of Physics, State University of New York at Buffalo; Member, Organizing Committee, 3rd Conference on Semi-Insulating III-V Materials;* 233

Member, Organizing Committee, Topical Conference on Optical Effects in Amorphous Semiconductors; Cochairperson, Materials Research Society Symposium on Microscopic Identification of Electronic Defects in Semiconductors; Member, Program Committee, 13th Intl. Conference on Defects in Semiconductors; Member, Navy Technical Review Committee, Joint Services Electronics Program

Brady, R.F., Chairperson, Admissions Committee, American Chemical Society (ACS)

Brancato, E., IEEE Centennial Medal Award, 1984

Guenter E. Brueckner receives the coveted Navy Superior Civilian Service Award from then-NRL Commanding Officer, Capt. John McMorris, as wife Dorthea looks on. Brueckner was cited for his contributions to the development and application of optical systems to obtain space observations.

Brueckner, G.E., Navy Superior Civilian Service Award; Member, National Academy of Science, Space Science Board, Study Group: "Major Directions for Space Science"; Executive Member, Committee on Space Research (COSPAR) ISC-E "Research in Astrophysics From Space"

Buisson, J.A., Member, Executive Committee, Precise Time and Time Interval Planning Meeting; Session Chairperson, Sixteenth

Annual Precise Time and Time Interval Applications and Planning Meeting

Campana, J.E., Chairperson, Committee on Ion Physics and Instrumentation, American Society for Mass Spectrometry; Member, Organizing Committee, Fifth International Conference on Secondary Ion Mass Spectrometry; Cochairperson, Greater Washington Area Mass Spectrometry Discussion Group

Campillo, A.J., Fellow, American Physical Society (APS)

Carter, W.H., Member, Fellows Committee, Society of Photo-Optical Instrumentation Engineers (SPIE) — The International Society for Optical Engineering; General Chairperson, 1984 Washington Meeting of SPIE; Editorial Advisor, Journal of Optical Society of American; Guest Editor, Journal of Optical Society of America

Colton, R.J., Chairperson, American Society for Testing and Materials (ASTM) Subcommittee E42.06 on Secondary Ion Mass Spectrometry (SIMS); Chairperson, American Society for Mass Spectrometry (ASMS) Committee on Surface and Solid Analysis; Chairperson, Local Organizing Committee, Fifth International Conference on Secondary Ion Mass Spectrometry (SIMS V); Member, Editorial Board, International Journal of Mass Spectrometry and Ion Processes

Crepeau, P.J., Senior Member, IEEE

Crowe, C.R., Member, Tri-Service Manufacturing Committee (Munitions); Member, Association of Mining Engineers (AIME) Titanium and Composites Committees; Member, American Society for Metals (ASM) Surface Science Committee

Davis, G., Section Chairperson, 1984 Silicon-on-Insulator/Silicon-on-Sapphire (SOI/SOS) IEEE Workshop; Panel Member, International Electron Device Meeting (IEDM), 1983 SOI Discussion; Member, Technical Committee for 84/85 SOI/SOS IEEE Workshop

Diachok, O.I., Member, International Congress of Acoustics Committee for Organizing Special Session on Arctic Acoustics

Dicus, R.L., Member, Naval Underwater Systems Center (NUSC)/Naval Ocean Research Development Activity (NORDA)-sponsored Under-ice Scattering Loss Model Committee

NRL Research Director, Dr. Timothy Coffey, presents Lynwood A. Cosby (left), Head of NRL's Tactical Electronic Warfare Division, a Certificate of Merit upon his retirement

Doolittle, R.D., *Coordinator, SURTASS Workshop*

Elam, W.T., *Member, External Advisory Committee, Beamline X9, National Synchrotron Light Source*

Farmer, M.C., *Chairperson, Committee for Professional Opportunities for Women, Biophysical Society; Member, Executive Board, Association for Women in Science*

Faust, W.L., *Fellow, APS; Member, Technical Advisory Committee, Joint Services Electronics Program*

Fitzgerald, J.W., *Member, Committee on Nucleation of the International Commission on Cloud Physics; Member, Committee on Cloud Physics, American Meteorological Society*

Flippen-Anderson, J.L., *Superior Service Award, United States Department of Agriculture*

Fox, R.B., *Regional Director and Ex-Officio Councilor, ACS; Chairperson, ACS Board Committee on Public Affairs and Public Relations; Member, ACS Board Committees on Grants and Awards, on Planning, and on Regulations and Policy; Secretary, Interdivisional Committee on Nomenclature and Symbols, Intl. Union of Pure and Applied Chemistry; Program Chair, Chemical Society of Washington Centennial Celebration*

Gaber, B.P., *NRL Sigma Xi Applied Science Award, 1984*

Gabriel, W.F., *Navy Meritorious Civilian Service Award*

Gardner, R.E., *Member, Tri-Service Non-Cooperative Target Recognition Working Group*

Garrett, W.D., *Special Award for Excellence in Technology Transfer, Federal Laboratory Consortium, 1984; Chairperson, Working Group on Interchange of Pollutants Between Atmosphere and Oceans (World Meteorological Organization); Member, Joint Group of Experts on the Scientific Aspects of Marine Pollution (United Nations)*

Garroway, A.N., *Participant, NRL Advanced Research Program at University of California, Berkeley, 1983-1984*

Giallorenzi, T.G., *Editor, IEEE/Optical Society of America (OSA) Journal of Lightwave Technology; Chairperson, IEEE Optical Fiber Sensor Conference, 1985; U.S. Representative to International Management Committee, International Fiber Optics/Integrated Optics Conference; Member, Technical Program Committee, International Integrated Optics and Optical Communications Conference, 1985; Member, Technical Program Committee, NATO Advisory Group for Aerospace Research and Development (AGARD) Conference on Electromagnetic Wave Propagating, 1985*

Greene, R.F., *Chairperson, 1984 Tri-Service Cathode Workshop; Member, Editorial Board, Applications of Surface Science*

Griffin, O.M., *Associate Editor, Transactions of American Society of Mechanical Engineers (ASME), Journal of Energy Resources Technology; Member, Scientific Committee, International Symposium on Separated Flow Around*

William F. Gabriel is "pinned" by wife Evelyn as he receives the prestigious Navy Meritorious Civilian Service Award. Gabriel was cited for his outstanding technical contributions in the field of adaptive radar antennas and superresolution.

235

The 1984 Federal Laboratory Consortium Award for Excellence in Technology Transfer goes to William Garrett (left) and James Griffith, as the founder of NRL, Thomas Edison, "looks on"

Marine Structures, Norwegian Institute of Technology

Griffith, J.R., *Special Award for Excellence in Technology Transfer, Federal Laboratory Consortium, 1984*

Gubser, D.U., *Cochairperson, Electrical, Magnetic, and Optical Properties of Matter Subcommittee, Metallurgical Society of America*

Haas, G.A., *Navy Representative, Tri-Service Blue Ribbon Panel on Advanced Medium Range Anti-Aircraft Missile TWTs*

Hansen, R.J., *Chairperson, ASME Technical Committee on Flow Induced Noise and Vibration; Assistant Editor, ASME Symposium on Turbulence, Proceedings*

Health Physics Department Staff, *Certificate of Accreditation for providing specific Personnel Radiation Dosimetry Processing Services. National Voluntary Laboratory Accreditation Program, U.S. Dept. of Commerce, in cooperation with the National Bureau of Standards*

Hendrickson, W.A., *Elected Fellow, American Association for the Advancement of Science*

Hoppel, W.A., *Associate Editor, Journal of Geophysical Research; Member, Advisor Board,*

Chemical Rubber Company (CRC) Handbook on Air Ions

Huba, J.D., *Associate Editor, Space Physics, Journal of Geophysical Research*

Hubler, G.K., *Editor, Ion Implantation and Ion Beam Processing of Materials Symposium, Materials Research Society, Proceedings; Member, International Organizing Committee, Surface Modifications of Metals by Ion Beams Conference Series*

Hurdle, B.G., *Working Group Chairperson, Chief of Naval Operations (CNO) Antisubmarine Warfare (ASW) Review*

Johnston, K.J., *Member, National Radio Astronomy Observatory Visitors' Committee; Member, Organizing Committee; International Astronomical Union Commission 8: Reference Frames Discussion*

Jolles, M.I., *Chairperson, ASTM Task Group on Surface Crack Testing; Secretary, ASTM Subcommittee on Fracture Mechanics Test Methods; International Who's Who of Contemporary Achievement; Men of Achievement; Personalities of America*

Jones, R.L., *William Blum Award, National Capital Section, The Electrochemical Society*

Jordan, A.K., *Coeditor, NATO Advanced Research Workshop on Inverse Methods for Electromagnetic Imaging, Proceedings*

Kabler, M.N., *Fellow, APS; Member, Domestic Advisory Committee, International Conference on Defects in Insulating Crystals, 1984*

Kapetanakos, C.A., *Fellow, APS; Fellow, Washington Academy of Sciences; Chairperson, International Advisory Committee for the 2nd Christophilos Conference, 1984*

Karle, I.L., *Chemical Pioneer Award, 1984, American Institute of Chemists; Honorary Doctorate of Humane Letters, Georgetown University, Washington, D.C.; Who's Who in Frontier Science and Technology, 1st ed; Who's Who in America, 43rd ed; Who's Who in the East, 20th ed; Who's Who of American Women, 13th ed; Member, National Institutes of Health (NIH) Review Panel on Biophysics; Member, Advisory Board, Biopolymers; Member, Editorial Board, International Journal of Peptide and Protein Research; Member, Advisory Board, Chemistry Department, Massachusetts Institute of Technology*

Karle, J., *Patterson Award, American Crystallographic Association; Honorary Doctorate of Humane Letters, Georgetown University, Washington, D.C.; President, International Union of Crystallography; Representative, International Union of Crystallography to International Council of Scientific Unions (ICSU); Member, ICSU Committee on Science and Technology in Developing Countries; Chairperson, Auditing Committee, National Academy of Sciences*

Kaufman, B.N., *Associate Fellow, AIAA; Member, Astrodynamics Technical Committee, AIAA; Committee Member, Space Flight Mechanics, American Astronautical Society*

Killiany, J.M., *Deputy Navy Member, Subgroup B of Advisory Group on Electron Devices; Associate Navy Member, Subgroup C of Advisory Group on Electron Devices*

Kim, C., *Executive Director, Korean Scientists and Engineers Association in America; Keynote Speaker, 1984 Science and Technology Symposium, Seoul, Korea*

Klein, P.H., *Program Chairperson, Workshop on Purification of Materials for Crystal Growth and Glass Processing, 1985*

Kline, E.L., *Senior Member, IEEE; Member, Acoustics, Speech, and Signal Processing Society Technical Committee on Speech Processing, IEEE*

Knudson, A.R., *Member, Program Committee, Atomic Collisions in Solids Conference; Member, Organizing Committee, Eight Accelerator Conference Research Session*

Kraft, L.W., *Member, Executive Board, Washington Paint Technical Group*

Krowne, C., *Member, Technical Program Committee, 1984 IEEE International Microwave Theory and Techniques Symposium; Member, Technical Program Committee, 1984 International Antennas and Propagation Symposium*

Kruer, M.R., *Chairperson, Focal Plane Array (FPA) Session, 1984 Infrared Information Symposium (IRIS) Specialty Meeting on Infrared Detectors*

Lamb, B.J., *IEEE Centennial Medal, 1984*

Landwehr, C., *Vice Chairperson, IEEE Technical Committee on Security and Privacy, 1984; Member, Program Committee, IEEE Symposium on Privacy and Security, 1984; Invited Panelist, National Bureau of Standards Workshop on Security in Personal Computers, 1984*

Layman, G.E., *Graduate, Naval War College, with "highest distinction"*

Leroy, S.S., *U.S. Navy Member and Chairman, The Technical Cooperation Program (TTCP) Subgroup Q, Q Technical Panel (QTP)-13 Panel on Validation of Electronic Warfare (EW) Digital Modeling*

Lessoff, H., *Secretary/Treasurer, III Metal Organic Chemical Vapor Deposition (MOCVD) International Conference, 1986*

Lindberg, R.E., *Associate Editor, Journal of the Astronautical Sciences; Member, AIAA Astrodynamics Technical Committee*

Lister, M.J., *Member, Editorial Committee, Sixteenth Annual Precise Time and Time Interval Applications and Planning Meeting*

Mack, I.A., *Member, Program Committee, 1985 International Solid State Circuits Conference*

Markley, F.L., *Associate Fellow, AIAA, Associate Editor, Journal of Guidance, Control, and Dynamics, AIAA*

McCafferty, E., *Chairperson, Corrosion Division of the Electrochemical Society; Divisional Editor, Journal of the Electrochemical Society; Member, Honors and Awards Committee, the Electrochemical Society*

Michel, D.J., *Member, Operations Subcommittee of the Technical Program Committee, The Metallurgical Society of AIME*
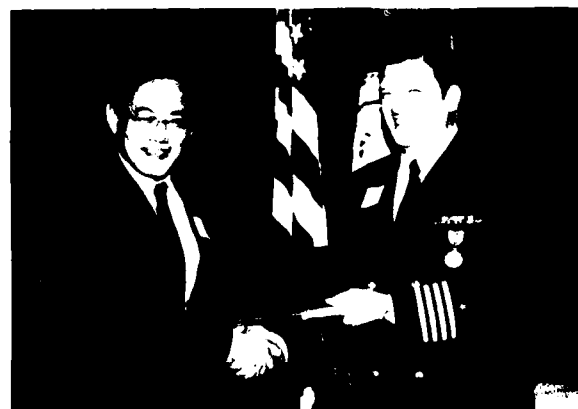
George S. Kang receives his publication award and congratulations from NRL's Commanding Officer, Capt. James P. O'Donovan

237

Murday, J.S., *Coeditor, Applied Surface Analysis Symposium, Proceedings; Associate Editor, Journal of Vacuum Science and Technology; Chairperson, Scholarships and Awards Committee, American Vacuum Society; Executive Committee Member, Division of Colloid and Surface Chemistry, ACS*

Murray, J.A., *Member, Executive Committee, Precise Time and Time Interval Planning Meeting; Member MIL-STD-188-115 (Timing and Synchronization) Working Group*

Nagel, D.J., *Member, U.S. Department of Energy Planning Study for Advanced Synchrotron Radiation Facilities*

Nisenoff, M., *Member, Board of Directors, Applied Superconductivity Conference; Advisory Editor, Cryogenics Journal; Member, Organizing Committee of International Conference on Small Cryocoolers for Electronic Devices and Systems; Chairperson, Program Committee, Fifth Josephson Electronics Workshop*

Oaks, O.J., *Vice Chairperson, Washington Section, IEEE Instrumentation and Measurement Society*

Ossakow, S.L., *Member, Nominating Committee for Officers, APS, Plasma Physics Division; Advisor, Office of Naval Research (ONR) Ionospheric Research; Member, U.S. Delegation, Union of Radio Science International (URSI) XXIst General Assembly, Florence, Italy*

Ozimina, C.D., *Chairperson, IEEE Control Systems Chapter, Northern Virginia Section*

Palik, E.D., *Editor, Handbook of Optical Constants of Solids; Member, Organizing Committee, Basic Properties of Optical Materials Meeting, National Bureau of Standards*

Palma, R.E., *Chairperson, Systems Working Group, Interagency Advanced Power Group*

Pande, C.S., *Chairperson, Electrical, Magnetic, and Optical Phenomena Committee of American Society of Metals; Member, Program Committee, Electron Microscopy Society of America*

Parker, R.K., *Member, Executive Committee, IEEE Plasma Science Technical Committee; Chairperson, Subcommittee on Electron Tubes, 1985 International Electron Devices Meeting*

Pattnaik, A., *Member, AIME-ASM Composites Committee; 'Key Reader' for Metallurgical Transactions (A)*

Peyser, P., *Invited Author, Chapter on Glass Transition for 3rd Edition of Polymer Handbook*

Phillips, G.W., *Member, Air Force Crew Light Advisory Panel; Chairperson, Particle Analysis Group, an interlaboratory working group reporting to OP-009V*

Plant, W.J., *Associate Editor, The Journal of Geophysical Research; Guest Associate Editor, IEEE Journal of Oceanic Engineering Special Issue on Remote Sensing*

Prinz, G.A., *Elected Fellow, APS*

Rao, J.B.L., *Elected Program Chairperson, IEEE Washington/Northern Virginia Chapter, Antennas and Propagation Society*

Rath, B.B., *Elected Fellow, Washington Academy of Sciences; Chairperson, Surface and Interface of Committee of ASM; Member, Board of Directors of the Metallurgical Society of AIME; Member, Joint Commission of the Metallurgical Transaction; Member, National Materials Advisory Board*

Reinecke, T.L., *Secretary, Steering Committee, Greater Washington Solid State Physics Colloquia; Member, Committee on Artifically Structured Materials of the National Academy of Sciences; Member, Virginia Selection Committee of the American Association of Rhodes Scholars*

Resing, H.A., *NRL Sigma Xi Pure Science Award, 1984; Member, Editorial Board, Langmuir; Member, Organizing Committee, 19th Biennial Conference on Carbon, 1985*

Richmond, E.D., *Member, Technical Committee, IEEE SOI/SOS Technical Workshop*

Rudgers, A.J., *Chairperson, Acoustical Society of America Technical Committee on Physical Acoustics*

Sadananda, K., *Cochairperson, Organizing Committee, ASM-AIME Symposium; Member, American Institute of Mining and Metallurgy Structural Materials and Mechanical Metallurgy Committees; Member, ASM, Flow and Fracture Committee*

Sartwell, B.D., *North American Editor, Surface Technology; Program Committee, International Conference on Metallurgical Coatings*

Schindler, A.I., *1984 Senior Executive Service (SES) Performance Award*

Schnur, J.M., *Full Professor, University of Paris VI, Dept. of Condensed Matter*

Schriempf, J.T., *Navy Meritorious Civilian Service Award*

Schuler, D.L., *Session Chairperson: "Navy Remote Ocean Sensor System (N-ROSS)," Oceans '84 Conference*

Shapiro, P., *Coauthor, Distinguished Poster Paper Award, 1983 IEEE Conference on Nuclear and Space Radiation Effects*

Sheinson, R.S., *Treasurer, Eastern States Section of the Combustion Institute*

Sigel, G.H., Jr., *1984 E.O. Hulburt Annual Science and Engineering Award*

Dr. George H. Sigel, Jr. receives the 1984 E.O. Hulburt Award from NRL Research Director Dr. Timothy Coffey

Skelton, E.F., *Invited Speaker, International Symposium, "Solid State Physics Under Pressure," Izu-Nagaoka, Japan, 1984; Invited Speaker, XIIIth International Union of Crystallography, Hamburg, Federal Republic of Germany, 1984; Invited Speaker, 11th Annual Federation of Analytical Chem. and Spectroscopy Societies, 1984; Invited Speaker, Annual User Conference, Stanford University, 1984; Award as coauthor for best paper, 31st National Symposium, American Vacuum Society, 1984*

Skolnik, M.I., *IEEE Centennial Medal, 1984*

Sleger, K.J., *Symposium Secretary, 1985 IEEE GaAs IC Symposium*

Smardzewski, R.R., *Author, "Microprocessor Programming and Applications for Scientists and Engineers," Elsevier Science Publishing Co., Inc., New York*

Spielman, B.E., *Member, Steering Committee, 1984 IEEE Microwave & Millimeter-Wave Monolithic Circuit Symposium; Member, IEEE MTT-S Administrative Committee; Member, Technical Program Committee, IEEE International Microwave Symposium; Member, Program Committee, IEEE Microwave & MM-Wave Monolithic Symposium; Session Chairperson, IEEE Microwave & MM-Wave Monolithic Symposium; Navy Representative, 1985 DoD-NASA MM-Wave Workshop Organizing Committee*

Sprague, J.A., *Member, Program Committee, 1984 Electron Microscopy Society of America Annual Meeting*

Steele, L.E., *President, Federation of Materials Societies, 1984; Chairperson, Board of Directors, ASTM, 1984; Editor, "Light Water Reactor Structural Integrity" and "Radiation Embrittlement and Surveillance of Nuclear Reactor Pressure Vessels: An International Study"; Contributing Editor, "Radiation Embrittlement and Surveillance of Nuclear Reactor Pressure Vessels: An International Study"*

Steiger, D., *Chairperson, Technical Committee for Oceanic Engineering and Technology, IEEE Computer Society*

Taylor, H.F., *Elected Fellow, IEEE*

Turner, N.H., *President, ACS Chemical Society of Washington, D.C.*

Valenzuela, G.R., *U.S. Delegate, XXI General Assembly of International Union of Radio Science, Florence, Italy, 1984; Organizer, Advisor, and Member of Program Committee, Symposium on Wave Breaking, Turbulent Mixing, and Radio Probing of Ocean Surface, Sendai, Japan, 1984*

Van Buren, A.L., *Chairperson, Acoustical Society of America Working Group on Standards for Transducer Calibration*

Vittoria, C., *Elected Fellow, APS*

Vogt, P.R., *Coeditor, The Western North Atlantic Region Vol. M, Decade of North American Geology (D-NAG) series, Geological Society of America*

Wald, B., *Representative, ONR, Joint Directors of Laboratories Technology Panel for Strategic* 239

Computing; Member, Communications Advisory Committee, Electrical Engineering Department, University of Maryland; Member, Automatic Data Processing (ADP) Panel by Director of Naval Laboratories (DNL)

Wales, S.C., Member, NUSC/NORDA-sponsored Under-Ice Scattering Loss Model Committee

Wang, H.T., Member, Hydrodynamic Forces Committee, Offshore Mechanics and Arctic Engineering Division, American Society of Mechanical Engineers

Waynant, R.W., Editor, IEEE Circuits and Devices Magazine representing the IEEE Lasers and Electro-Optical Society; Member, Administrative Committee of IEEE Lasers and Electro-Optical Society (formerly Quantum Electronics and Applications Society)

Webb, D.C., Member, Program Committee, 1984 Ultrasonics Symposium; Member, Technical Committee on Ultrasonics; Member, IEEE Microwave Theory and Techniques Society;

Member, Technical Committee on High Frequency Properties of Magnetic Materials, IEEE Magnetics Society

Weinberg, D.L., Reviewer, "IEEE Transactions on Electron Devices"

White, J.D., Member, Technical Program Committee, Frequency Control Symposium

Willett, J.C., Member, Subcommission on the Global Circuit, International Association of Mercury Producers (IAMAP), International Union of Geodesy and Geophysics; Member, Committee on Atmospheric and Space Electricity, American Geophysical Union (AGU); Member, ad hoc Panel on Atmospheric Electricity, Geophysics Study Committee, National Research Council (NRC)

Williams, F.W., Vice Chairperson, Eastern Section of the Combustion Institute

Wolf, S.A., Elected Fellow, APS; Member, Electrical Magnetic and Optical Properties Committee, Metallurgical Society of America

ALAN BERMAN RESEARCH PUBLICATION AWARDS

The Annual Research Publication Awards Program was established in 1968 to recognize the authors of the best NRL publications each year. These awards not only honor individuals for superior scientific accomplishments in the field of naval research, but also seek to promote continued excellence in research and in its documentation. In 1982, the name of this program was changed to the Alan Berman Research Publication Awards in honor of its founder.

There were 122 separate publications in 1984 that were considered for recognition. Of those considered, 25 were selected. These selected publications represented 86 authors, who received awards. On March 8, 1984, the awards were presented to the authors at the Alan Berman Annual Research Publication Awards Dinner held at the Bolling Air Force Base Officers' Club. Each winner received a certificate, a bronze paperweight, and a booklet of the publications receiving special recognition.

The unclassified winning papers with their respective authors are listed below by their research units. Non-Laboratory coauthors are indicated by an asterisk.

Laboratory for Structure of Matter

Laser Dye Intermediates: Structures of 1,2,3,4-Tetrahydroquinolinium-7-sulfonate Monohydrate (I),
$C_9H_{11}NO_3S.H_2O$, and Twinned 1,2,3,4-Tetrahydro-1-methylquinolinium-7-sulfonate (II), $C_{10}H_{13}NO_3S$
Judith L. Flippen-Anderson and Richard D. Gilardi

Management Information Division

Multiple-Valued Negative Resistance Integrated Circuits
George R. Abraham

Space Science Division

The HEAO A-1 X-Ray Source Catalog
Kent S. Wood, John F. Meekins, Daryl J. Yentis, Herbert W. Smathers, Jr.,
Douglas P. McNutt, Richard D. Bleach, Edward T. Byram, Talbot A. Chubb,
Herbert Friedman, and Meir Meidav*

A Solar Spectral Line List Between 10 and 200 Å Modified for
Application to High Spectral Resolution X-Ray Astronomy
George A. Doschek and Robert D. Cowan*

Plasma Physics Division

Long-Pulse, High-Power Free-Electron Laser with No External Beam Focusing
John A. Pasour, Christos A. Kapetanakos, and Robert F. Lucey*

Theoretical Modeling of the Plasma Erosion Opening Switch
for Inductive Storage Applications
Paul F. Ottinger,* Shyke A. Goldstein,* and Robert A. Meger

Acoustics Division

A Preliminary Analysis of the NRL Airborne Gravimetry System
John M. Brozena, Jr.

Radar Division

Range Resolution of Targets
Gerard V. Trunk

Marine Technology Division

Calculation of the Wall-Pressure Field in a Turbulent Channel Flow
Robert A. Handler, Robert J. Hansen, Leonidas Sakell,
Steven A. Orszag,* and Edward Bullister*

Underwater Sound Reference Detachment

Measurement of Hydroacoustic Particle Motion by Hot-Film Anemometry
Pieter S. Dubbelday

Chemistry Division

*Simultaneous Determination of Hydrazine, Methylhydrazine, and
1,1-Dimethylhydrazine in Air by Derivatization/Gas Chromatography*
James R. Holtzclaw, Susan L. Rose, Jeffery R. Wyatt,
David P. Rounbehler,* and David H. Fine*

*Nuclear Magnetic Resonance Characterization of Graphite Intercalation
Compounds Containing AsF_6^- and AsF_6^- + AsF_3*
Michael J. Moran, Ronald A. DeMarco, Henry A. Resing, and Gerald Ray Miller*

Material Science and Technology Division

Crevice Corrosion of Passive Iron in Chloride Solutions
Edward McCafferty

Optical Sciences Division

Heavy Metal Fluoride Glasses and Fibers: A Review
Danh C. Tran, George H. Sigel, Jr., and Bernard Bendow*

*Use of Stimulated Raman Scattering for Reducing the
Divergence of Severely Aberrated Laser Beams*
Robert S. F. Chang, Robert H. Lehmberg,
Michael T. Duignan,* and Nicholas Djeu*

Condensed Matter and Radiation Sciences Division

Observation of Rayleigh-Taylor-like Structures in a Laser-Accelerated Foil
Robert R. Whitlock
Condenced Matter and Radiation Sciences Division

Mark H. Emery
Laboratory for Computational Physics

John A. Stamper, Edgar A. McLean, and Stephen P. Obenschain
Plasma Physics Division

Martin C. Peckerar
Electronics Technology Division

Energy-Dispersive X-Ray Diffraction with Synchrotron Radiation at Cryogenic Temperatures
Earl F. Skelton, Alan W. Webb, Joseph L. Feldman, Willian T. Elam,
Stuart A. Wolf, E. Roy Carpenter, Jr., Syed B. Qadri,*
Ronald C. Lacoe,* and Chao-Yen Y. Huang*

Electronics Technology Division

Novel Features of Quantum Hall Plateaus for Varying Interface Charge
John E. Furneaux and Thomas L. Reinecke

*Characteristics of the Material Improvement Process for Silicon on
Sapphire by Solid Phase Epitaxial Regrowth*
Daniel L. Richmond, Alvin R. Knudson, Tommy J. Magee,*
Harry A. Kawayoshi,* and Charles S. Leung*

Information Technology Division

*Improvement of the Narrowband Linear Predictive Coder
Part 2—Synthesis Improvements*
George S. Kang and Stephanie S. Everett

Multisignal Minimum-Cross-Entropy Spectrum Analysis with Weighted Initial Estimates
Rodney W. Johnson, John E. Shore, and John P. Burg*

Programs for professional development

One of the many programs
for professional development
is the Gifted and Talented
Internship Program. These
students are conducting an
experiment on weldments
under the supervision of
an NRL scientist.

PROFESSIONAL DEVELOPMENT

NRL has established many programs for the professional and personal development of its employees so that they may better serve the needs of the Navy. These programs develop and retain talented people and keep them abreast of advanced technology management skills. Graduate assistantships, fellowships, sabbatical study programs, cooperative education programs, individual college courses, and short courses for personal improvement contribute to professional development.

Programs are also available for non-NRL employees. These enhance the Laboratory research program by providing a means for non-NRL professionals to work at the Laboratory and thus improve the exchange of ideas, meet critical short-term technical requirements, and provide a source of new, dynamic scientists and engineers. The programs range from two-year graduate fellowships, faculty and professional interchanges, and undergraduate work to an introduction of gifted and talented high school students to the world of technology.

PROGRAMS FOR NRL PEOPLE

During 1984, NRL employees participated in 3112 individual training events. Many of these were presented as either video taped or on-site instructed courses on diverse technical subjects, management techniques, and enhancement of such personal skills as efficient use of time, speed reading, memory improvement, and interpersonal communications.

One common study procedure is for employees to work full time at the Laboratory while taking job-related scientific courses at universities and schools in the Washington area. The training ranges from a single course to full graduate and postgraduate programs. Tuition for training is paid by NRL. A description of the formal programs offered by NRL, along with a list of the 1984 participants of some of the larger programs, follows.

GRADUATE PROGRAMS

• The **Advanced Graduate Research Program** (formerly the Sabbatical Study Program) enables selected professional employees to devote full time to research or course work in their own or a related field for 1 academic year at an institution of their choice without the loss of regular salary, leave, or fringe benefits. NRL pays all education, travel, and moving expenses for the employee and dependents. Since the program began in 1964, 147 employees have participated. Criteria for eligibility include professional stature consistent with the applicant's opportunities and experience, a satisfactory program of study, and acceptance by the institution selected by the applicant. The program is open to paraprofessional (and above) employees who have completed 6 years of Federal Service, including 4 years at NRL.

NRL staff members who began their graduate programs in 1984 are listed below along with their respective divisions and the institutions where they studied.

Shannon L. Coffey (Space Systems), National Bureau of Standards, Gaithersburg, Maryland

Thomas L. Francavilla (Condensed Matter and Radiation Sciences), Catholic University of America, Washington, D.C.

Edward A. Metzbower (Material Science and Technology), The Welding Institute, Abington, England

Nelson S. Saks (Electronics Technology), Catholic University of Leuven, Heverlee, Belgium

• The **Edison Memorial Graduate Training Program** enables employees to pursue advanced studies in their fields at local universities. Eligible employees who are selected for participation in this program normally spend 24 hours of every workweek in their studies. The criteria for eligibility include a minimum of 1 year of service at NRL, a bachelor's or master's degree in an appropriate field, and professional standing in keeping with the candidate's opportunities and experience.

From 1963 through 1984, 154 employees studied under the Edison Program. In 1984, seven employees began work as Edison scholars: They are listed below.

Warren T. Beard (Electronics Technology), University of Maryland

Paul E. Denney (Material Science and Technology), George Washington University, Washington, D.C.

John V. Fritz (Space Systems), Catholic University of America, Washington, D.C.

Mark J. Lister (Space Systems), George Washington University, Washington, D.C.

George D. McNeal (Radar), Johns Hopkins University, Maryland

Susan L. Rose (Chemistry), Pennsylvania State University

Tab J. Smith (Plasma Physics), University of Maryland

• To be eligible for the **Select Graduate Student Program**, employees must have a college degree in an appropriate field and must have maintained at least a B average in undergraduate study. Accepted students devote a full academic year to graduate study. While attending school, they receive one half of their salary, and NRL pays for tuition, books, and laboratory expenses. During the summer, they work at the Laboratory and receive normal pay and fringe benefits. Thirty-four staff members have enrolled in the program since it began in 1967.

• Research conducted at NRL may be used as **thesis material for an advanced degree**. This original research is supervised by a qualified employee of NRL who is approved by the graduate school. The candidate should have completed the required course work and should have satisfied the language, residence, and other requirements of the graduate school from which the degree is sought. NRL provides space, research facilities, and supervision but leaves decisions on academic policy to the cooperating schools.

• The **Alfred P. Sloan Fellows Program** is designed for competent young executives whose job performance indicates senior management potential. The Sloan Fellows spend 1 year with the Massachusetts Institute of Technology faculty and with policymakers in industry and government. They study the theory and practice of effective and responsible management in a rapidly changing society.

• The **Education for Public Management Program** serves the training needs of individuals who are at midcareer and who have the talent to assume increasing responsibilities to direct agency programs and policies.

• The **Education Program for Federal Officials** exists for a small group of Federal employees who have demonstrated high competence and unusual promise. The Woodrow Wilson School of Princeton University has developed this program to enable selected midcareer officials to enlarge their knowledge in particular disciplines, to relate their fields of specialization to the broader concerns of government, and to sharpen their capacity for objective analysis of governmental problems.

• Federal Executive fellowships are available each year for employees to study in the **Brookings Institute Advanced Study Program**. In this program, the fellow is exposed to and participates in planning, developing, and conducting educational conferences on public policy issues for leaders in public and private life.

• The **Fellowship in Congressional Operations for Executives** provides an opportunity for some of the most promising young, technically oriented Federal executives to participate in a variety of assignments designed to develop their knowledge and understanding of Congressional operations. These fellows share activities with other members of the Congressional Fellowship Program who come mainly from journalism, law, and college teaching.

• The **Maxwell Midcareer Development Program** of the Maxwell Graduate School of Citizenship and Public Affairs, Syracuse, New York, increases the managerial knowledge, ability, and skills of experienced Government officials who have been identified by their agencies as having potential for advancement to positions demanding progressively greater managerial and executive responsibilities.

• The **Practicing Engineer Advanced Study Program** of the M.I.T. Center for Advanced Engineering, Cambridge, Massachusetts, enables experienced engineers and applied scientists to work in-depth in technological areas pertinent to their professions, preparing for continued leadership in an age of unparalleled technological change.

• The **Science and Technology Fellowship Program**, a subsidiary of the Commerce Science

248

Program, includes a variety of special events, lectures, seminars, visits, conferences, field trips, and interactions with key persons from both the public and private sectors. Participants spend 1 week on Capitol Hill in an intensive, congressional orientation; they spend 1 week with the Brookings Institute Science Policy Conference; and they take two week-long field trips for on-site inspection of scientific institutions and industrial complexes.

• The **Stanford-Sloan Program of the Graduate School of Business**, Stanford, California, gives exceptional young executives an opportunity to make an intensive study of new concepts in business, to develop a top management perspective, and to broaden their intellectual horizons.

• The **Naval Postgraduate School** (NPS) in Monterey, California, provides advanced graduate study for selected Federal civilian employees who meet NPS academic requirements for the program in which they are interested, and whose employing agency is willing to act as sponsor.

CONTINUING EDUCATION

• Local colleges and universities offer **undergraduate and graduate courses** at NRL for employees to improve their skills and keep abreast of current developments in their fields. These courses are also available at many other DoD installations in the Washington, D.C. area.

• The Employee Development Branch at NRL offers to all employees **short courses** in certain program areas which are not available at local schools; laboratory employees may attend these courses at nongovernment facilities as well. Interagency courses in management, personnel, finance, supervisory development, and clerical skills are also available.

For further information on any of the above programs, contact the Employee Development Branch (202) 767-2956.

TECHNOLOGY TRANSFER

• The **Navy Science Assistance Program** establishes an information loop between the Fleet and the R&D shore establishments to expedite technology transfer to the user. The program addresses operational problems, focuses resources to solve specific technical problems, and develops a nucleus of senior scientific personnel familiar with the impact of current research and system performance on military operations.

• The **Office of Research and Technology Applications Program** ensures the full use of the results of the Nation's Federal investment in research and development by transferring federally owned or originated technology to state and local governments and the private sector. Inquiries concerning technical information on NRL programs should be made through the contact below.

For these last two programs, Mr. Richard Fulper at (202) 767-3744 is the point of contact.

PROFESSIONAL DEVELOPMENT

NRL has several programs, professional society chapters, and informal clubs that enhance the professional growth of employees. Some of these are listed below.

• The **Career Counseling Center** helps employees to define short- and long-range career goals, to improve their job-seeking skills, and to deal with issues affecting job productivity. (Contact Dr. Diane Koslow at (202) 767-2956.)

• A chartered chapter of **Women in Science and Engineering** (WISE) was established at NRL in 1983. Informal monthly luncheons and seminars are scheduled to inform scientists and engineers of women's research at NRL and to provide an informal environment for members to practice their presentations. Recently, WISE initiated a quarterly colloquium series to feature outstanding women scientists. (Contact Dr. Marty Farmer at (202) 767-4301 or Dr. Cha-Mei Tang Hui at (202) 767-4148.)

Dr. Margaret Rossiter, of the Department of History of Science, Harvard University spoke on "What's Happened to Women Scientists Since 1940?" at the WISE (Women in Science and Engineering) Quarterly Colloquia Series. Dr. Rossiter's lecture was cosponsored by the Laboratory for Computational Physics and the Federal Women's Program.

Dr. Rita R. Colwell, Vice President of Academic Affairs and Professor of Microbiology at the University of Maryland, spoke at the WISE (Women in Science and Engineering) Quarterly Colloquia Series on October 29 on "Marine Biotechnology—An Exciting New Area of Interest to the Navy"

Dr. Xie Xide, president of Fudan University in Shanghai, China, was invited to visit the Electronics Technology Division on August 22. (Fudan University was one of the stops on President Reagan's recent visit to China.) Pictured (left to right) are Drs. Debra Rolison, Xie Xide, Steve Carhart, Martha Farmer, and Cha-Mei Tana Hui.

• **Sigma Xi**, the Scientific Research Society, encourages original investigation in pure and applied science. The society honors individuals who have demonstrated ability to perform original research by conferring membership and by conducting an active program in support of original research. The NRL chapter of approximately 450 members sponsors a series of monthly lectures (from September to June) on a wide range of pure and applied scientific topics of interest to both the scientific and government communities. During the 1984 season, Dr. Gerold Yonas, chief scientist of the Strategic Defense Initiative (SDI) "Star Wars" Program, spoke on the goals of that program. Each spring the chapter sponsors an Edison Day Memorial Lecture in honor of the founder of the Laboratory at which a distinguished scientist, usually a Nobel laureate, speaks on his or her research. Some of the past Edison Day speakers have been William Shockley, J. Robert Oppenheimer, Peter Debye, Theodore von Karman, Eugene Wigner, John Bardeen, Leo Esaki, Philip Anderson, and Nicolaas Bloembergen. The chapter also presents annual awards in pure and applied science to outstanding NRL staff members. (Contact Dr. John F. Reintjes at (202) 767-2175.)

• Any employee who is interested in developing effective self expression, listening, thinking, and leadership potential is invited to join either of two NRL chapters of **Toastmasters International**. Members of these clubs, who possess diverse career backgrounds and talents, meet three times a month where they learn to communicate not by rules but by doing in an atmosphere of understanding and helpful fellowship. (Contact Mrs. Kathleen Parrish at (202) 767-2782.)

• The **Federal Executive Professional Association** (FEPA) provides testimony, recommendations, and constructive criticism of the policies of the Executive Branch on existing proposed legislation and on regulatory actions. It also assists various advisory boards and commissions concerned with professional employee relations and benefits. The FEPA meets monthly for seminars given by NRL management. (Contact Dr. Louis Beach at (202) 767-5692.)

EQUAL EMPLOYMENT OPPORTUNITY (EEO) PROGRAMS

• Equal employment opportunity is a fundamental NRL policy for all persons, regardless or race, color, sex, religion, national origin, age, or physical/mental handicap. The EEO Office's major functions are: affirmative action employment; special emphasis programs (Federal Women's Program, Hispanic Employment Program, Handicap Program); discrimination complaint process; community outreach program; EEO training for supervisors, managers, and EEO collateral duty personnel; and advice and guidance to management on EEO policy.

Special programs are held during the year to promote an awareness of the contributions and capabilities of women and minorities. In addition to the programs described below, a commemorative program was held in January to honor the late Dr. Martin Luther King, Jr. A feature of this program was a talk entitled "Martin Luther King, Jr.—the Man and the Message" by Dr. Samuel L. Gandy, former Dean of the School of Divinity, Howard University.

A Black History Month Program was held in February. Dr. Elizabeth Clark-Lewis, Associate Professor of History, Northern Virginia Community College, spoke on "Black Americans in the Struggle for Excellence in Education in America." Other participants in the program included the Kankouran West African Dancers. Also, each year as part of the celebration, the Laboratory conducts an art and essay contest for students in nearby community schools. Awards are then presented at the Black History Month Program. The Program also sponsored a Christmas party for local schoolchildren.

• The **Federal Women's Program** (FWP) is a special emphasis program of the EEO Office which improves employment and advancement opportunities for women in the Federal Service. The FWP provides guidance and assistance to NRL managers and supervisors in their efforts to reduce underrepresentation of women in NRL's work force.

The FWP also sponsors awareness programs during the year to highlight concerns and issues   251
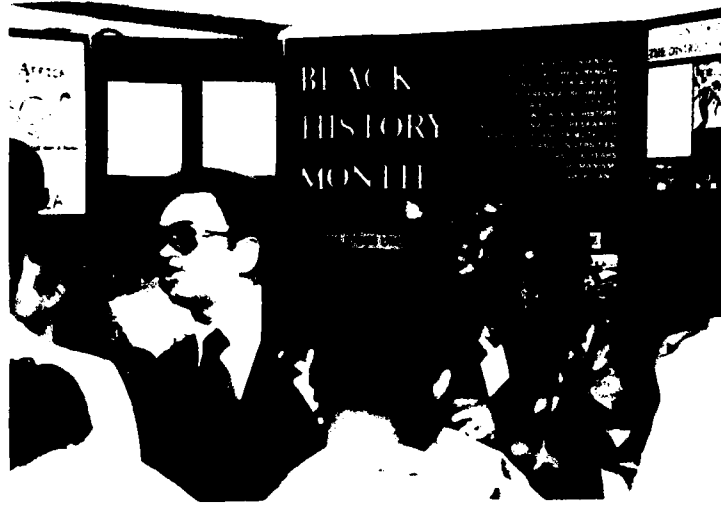
Visitors and employees gather for a reception held at an exhibit
focusing on education in black colleges and universities

Jean Martin, of Closet Assets, conducted a wardrobe-planning workshop
during Federal Women's Week, May 8 through 10

that affect women in the workplace. One highlight of the 1984 program was the observance of Federal Women's Week in May when many employees attended workshops on a variety of topics. Also, as part of the week's activities, Dr. Margaret Rossiter, author and guest lecturer at Harvard University, spoke on "What's Happened to Women Scientists Since 1940?" Her presentation was cosponsored by the FWP, the NRL chapter of Women in Science and Engineering, and the Laboratory for Computational Physics.

● The **Hispanic Employment Program** provides guidance and assistance on recruiting Hispanics and ensuring equal employment opportunity to Hispanic Americans. The program is involved with Hispanic community organizations, such as "El Ingeniero" (The Engineer) which encourages Hispanic youths to pursue a career in engineering.

● The **Handicap Program** provides technical assistance to management on recruiting

CAPT McMorris, answers questions posed about the Lab by members of El Ingeniero a group of Hispanic youths aspiring to be scientists and engineers. Sol Eaton, Deputy EEO Officer, looks on.

Allen Warner, an engineering aide with a hearing impairment, came to NRL as a result of the Laboratory's Handicap Program

Broadcaster Ed Walker of WMAL-Radio recalls obstacles facing a blind person aspiring to a broadcasting career on Handicap Awareness Day (November 8), at NRL. Linda Humphries signs for the hearing impaired members of the audience.

resources, training programs, removal of architectural barriers, and accommodations for handicapped employees, applicants, and disabled college and high school students in the paraprofessional and technical positions of engineering, physical sciences, and computer sciences. (Contact Ms. Sol del Ande Eaton, Deputy EEO Officer, at (202) 767-2486 for all EEO programs.)

● Other programs that enhance the development of NRL employees include computer clubs (Edison, Atari, Edison Commodore, and the NRL-IBM PC) and the Amateur Radio Club. The Recreation Club offers many facilities, such as a 25-yard, 6-lane indoor swimming pool; a gymnasium with basketball, volleyball, and bad-

minton courts; a weight room and exercise area; ping pong; meeting rooms; softball and basketball leagues; jacuzzi whirlpool; sauna; classes in karate, aerobics exercise, swimming, and swimnastics; and specialized sports clubs (running, skiing, biking, golfing). The Showboaters, a nonprofit drama group which presents live theater for the enjoyment of NRL and the community, performs in two major productions each year, in addition to occasional performances at Laboratory functions and benefits for local charities. Past productions have included "Fiddler on the Roof," "Brigadoon," and "Arsenic and Old Lace." Though based at NRL, membership in Showboaters is not limited to NRL employees.

PROGRAMS FOR NON-NRL PEOPLE

Several programs have been established for non-NRL professionals. These programs encourage and support the participation of visiting scientists and engineers in research of interest to the Laboratory. Some of the programs may serve as stepping-stones to federal careers in science and technology. Their objective is to enhance the quality of Laboratory research activities through working associations and interchanges with highly capable scientists and engineers and to provide opportunities for outside scientists and engineers to work in the Navy Laboratory environment. Along with enhancing Laboratory research, these programs acquaint participants with Navy capabilities and concerns.

RECENT Ph.D., FACULTY MEMBER, AND COLLEGE GRADUATE PROGRAMS

● The **National Research Council (NRC)/NRL Cooperative Research Associateship Program** selects associates who conduct research at NRL in their chosen fields in collaboration with NRL scientists and engineers. The tenure period is 2 years, and following their tenure, the Office of Naval Research offers the associate posttenure research grants tenable at an academic institution. The associates appointed in 1984 are listed below, along with their NRL divisions and degree-granting institutions.

Balla, R. Jeffrey (Chemistry), Pennsylvania State University

Beaver, Bruce D. (Chemistry), University of Massachusetts

Busse, Lynda E. (Optical Sciences), University of Illinois

Caras, Steve (Chemistry), University of Utah

Cook, Michael R. (Chemistry), Harvard University, Massachusetts

Dotson, Douglas A. (Chemistry), University of Maryland

Freas, Royal B. (Chemistry), University of Delaware

Fronko, Richard M. (Chemistry), University of Wisconsin

Gaskill, David K. (Chemistry), Oregon State University

Hodes, H. Daniel (Chemistry), Boston College, Massachusetts

Holtz, Ronald L. (Condensed Matter and Radiation Sciences), Boston College, Massachusetts

Hylden, Jeffrey L. (Electronics Technology), University of Minnesota

Lambrakos, Samuel G. (Laboratory of Computational Physics), Polytechnic Institute of New York

Laufer, Pinchus M. (Condensed Matter and Radiation Sciences), New York University

Lawrence, Steven H. (Material Sciences), Ohio State University

Leung, Michael (Electronics Technology), University of Maryland

Lill, James V., Jr. (Condensed Matter and Radiation Sciences), University of Illinois

Long, Treva D. (Chemistry), Carnegie-Mellon University, Pennsylvania

Miller, Joel B. (Chemistry), University of Delaware

Montague, Charles E. (Optical Sciences), Lehigh University, Pennsylvania

Mozurkewich, David (Space Sciences), University of Wyoming

Plant, Anne I. (Optical Sciences), Baylor College of Medicine, Texas

Rabinowitz, Martin J. (Chemistry), University of Texas

Sedney, Diana L. (Chemistry), Northeastern University, Massachusetts

Squire, David W. (Chemistry), Columbia University, New York

Thompson, Richard B. (Optical Sciences), University of Illinois

Thornhill, J. Ward (Plasma Physics), University of Michigan

Zabarnick, Steven S. (Chemistry), Pennsylvania State University

● The American Society for Engineering Education (ASEE) administers the **Office of** 255

Naval Technology (ONT) Postdoctoral Fellowship Program to increase the involvement of highly trained scientists and engineers in disciplines necessary to meet the evolving needs of naval technology. Appointments are for 1 year (renewable for a second and sometimes a third year). These competitive appointments are made jointly by ONT and ASEE.

● The American Society for Engineering Education also administers the Navy/ASEE **Summer Faculty Research Program** for university faculty members to work for 10 weeks with professional peers in participating Navy laboratories on research of mutual interest. NRL hosted 31 of these faculty participants in 1984; they are listed below, along with the participating NRL divisions and their home institutions.

Clifford A. Becker (Chemistry), Washburn University, Kansas

Iona N. Black (Condensed Matter and Radiation Sciences), Hampton Institute, Virginia

Kuldip P. Chopra (Space Sciences), Old Dominion University, Virginia

William G. Culbreth (Marine Technology), Naval Postgraduate School, Monterey, California

Charles H. Douglass (Chemistry), Trinity College, Washington, D.C.

John Eftis (Material Sciences), George Washington University, Washington, D.C.

James A. Ellison (Condensed Matter and Radiation Sciences), University of New Mexico

Tepper L. Gill (Condensed Matter and Radiation Sciences), Howard University, Washington, D.C.

Patrick R. Harrison (Information Technology), U.S. Naval Academy, Maryland

Irvin Heard (Electronics Technology), Lincoln University, Pennsylvania

Joseph Homeny (Material Sciences), University of Illinois

Craig M. Jensen (Space Sciences), University of Oklahoma

Yong H. Kim (Space Sciences), Saddleback College, California

Jay Liebowitz (Information Sciences), George Washington University, Washington, D.C.

Li Chung Ming (Condensed Matter and Radiation Sciences), University of Hawaii

Alan H. Nye (Space Sciences), Rochester Institute of Technology, New York

Robert N. Pangborn (Material Sciences), Pennsylvania State University

Vincent J. Parks (Marine Technology), Catholic University of America, Washington, D.C.

Keith E. Peterman (Chemistry), York College, Pennsylvania

Clarence E. Pfluger (Laboratory for Structure and Matter), Syracuse University, New York

George M. Reed (Information Technology), Ohio University

G. William Rollosson (Space Sciences), Menlo College, California

Donald Scarl (Optical Sciences), Polytechnic Institute of New York

William W. Schultz (Marine Technology), Rutgers University, New Jersey

James S. Shirk (Optical Sciences), Illinois Institute of Technology

Lawrence R. Sigur (Laboratory for Computational Physics), Southern University, Louisiana

Charles W. Sink (Chemistry), University of Pennsylvania

Gilbert R. Speich (Material Sciences), Illinois Institute of Technology

Vijai K. Tripathi (Electronics Technology), Oregon State University

Margaret A. Wechter (Chemistry), Southeastern Massachusetts University

Harold Weinstock (Electronics Technology), Illinois Institute of Technology

● The **NRL/United States Naval Academy (USNA) Cooperative Program for Scientific Interchange** allows faculty members of the U.S. Naval Academy to participate in NRL research. This collaboration benefits the Academy by providing the opportunity for USNA faculty members to work on research of a more practical

or applied nature. In turn, NRL's research program is strengthened by the available scientific and engineering expertise of the USNA faculty. Faculty members who participated in the 1984 program are listed below, along with the cooperating NRL divisions.

C. Elise Albert, Space Science
Gerald P. Calame, Optical Sciences
Graham T. Cheek, Chemistry
Francis D. Correll, Condensed Matter and Radiation Sciences
Robert DeMoyer, Jr., Electronics Technology
Mark L. Elert, Chemistry
John P. Ertel, Condensed Matter and Radiation Sciences
Anthony M. Gaglione, Radar
Murray S. Korman, Acoustics
Richard L. Martin, Electronics Technology
Anthony F. Norcio, Information Technology
Robert N. Shelby, Electronics Technology
L. L. Tankersley, Optical Sciences
Boyd A. Waite, Chemistry

● The **Office of Naval Research Graduate Fellowship Program** helps U.S. citizens obtain advanced training in disciplines of science and engineering critical to the U.S. Navy. The three-year program awards fellowships to recent outstanding graduates to support their study and research leading to doctoral degrees in specified disciplines such as electrical engineering, computer sciences, material sciences, applied physics, and ocean engineering. Award recipients are encouraged to continue their study and research in a Navy laboratory during the summer. Seven ONR graduate Fellows appointed in the 1984 program chose NRL for their summer work. They are listed below, along with the participating NRL divisions and their home institutions.

Brian K. Damkoger (Material Science and Technology), Colorado School of Mines
Terry J. Garino (Material Science and Technology), Massachusetts Institute of Technology
Ray G. Holt (Optical Sciences), University of Mississippi
Karl S. Keller (Information Sciences), University of Virginia

Richard I. Leighton (Marine Technology), University of Michigan
Thomas M. Parrill (Electronics Technology), Northwestern University, Illinois
Raymond L. Toy (Acoustics), Rensselaer Polytechnic Institute, New York

For further information about the above five programs, please contact Dr. Agda Cohen at (202) 767-2432.

● The **United States Naval Academy Ensign Program** assigns Naval Academy graduates to NRL to work in areas of their own choosing commensurate with their academic qualifications. These graduates provide a fruitful summer of research assistance, while gaining valuable experience in the Navy's R&D program. (Contact Lt. David Gates at (202) 767-2103.)

PROFESSIONAL APPOINTMENTS

● **Faculty Member Appointments** use the special skills and abilities of faculty members for periods of short duration to fill positions of a scientific, engineering, professional, or analytical nature.

● **Consultants and experts** are employed because they are outstanding in their fields of specialization, or because they possess ability of a rare nature and could not normally be employed as regular civil servants.

● **Intergovernmental Personnel Act Appointments** temporarily assign personnel from the state or local government or educational institution to the Federal Government (or vice versa) to improve public services rendered by all levels of government.

UNDERGRADUATE COLLEGE STUDENT PROGRAMS

Several programs are tailored to the undergraduate which provide employment and work experience in naval research. These are designed to attract applicants for student and full professional employment in the Laboratory's shortage category positions, such as engineers, physicists, **257**

mathematicians, and computer scientists. The student employment programs build an understanding of NRL job opportunities among students and educational personnel so that educators can provide students who will meet NRL's occupational needs. The employment programs for college students include the following.

• The **Cooperative Education Program** alternates periods of work and study for students pursuing bachelor degrees in engineering, computer science, or the physical sciences. Several universities participate in this program.

• The **Federal Junior Fellowship Program** hires students entering college to be assistants to scientific, professional, or technical employees.

• The **Summer Employment Program** employs students for the summer in paraprofessional and technician positions in engineering, physical sciences, and computer sciences.

• The **Student Volunteer Program** helps students gain valuable experience by allowing them to voluntarily perform educationally related work at NRL.

• The **1040-Hour Appointment** employs students on a halftime basis to assist in scientific work related to their academic program.

For additional information, contact Mrs. Cathy Downing at (202) 767-3030.

HIGH SCHOOL PROGRAMS

• The **Gifted and Talented Internship Program** provides a meaningful part-time employment experience for high school graduates who plan to pursue a bachelor's degree in engineering, computer science, or the physical sciences.

• The **Summer Research Apprentice Program** employs high school juniors and seniors to serve for 8 weeks as junior research associates. Under the direction of a mentor, students gain a better understanding of research, its opportunities, and challenges through participation in scientific programs. Criteria for eligibility are based on science and mathematics courses completed and grades achieved; scientific motivation, curiosity, and capacity for sustained hard work; a desire for a technical career; teacher recommendations; and ability and achievement test scores.

For additional information on these programs, please contact the Employee Development Branch at (202) 767-2956.
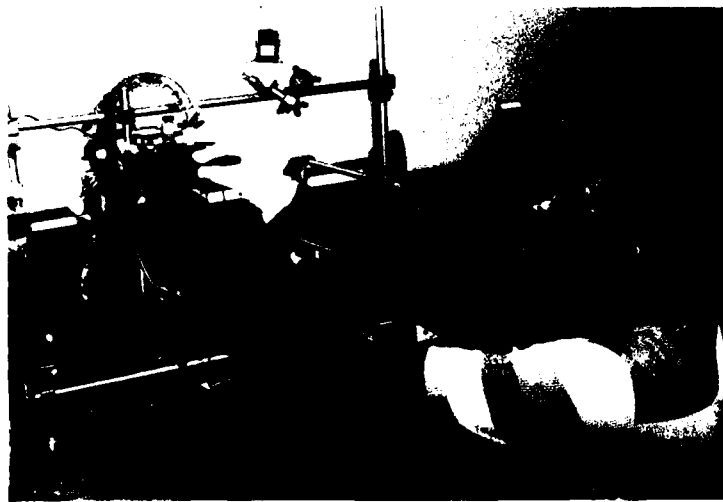
NRL apprentice Neicko Williams uses a solar simulator to measure the degradation in the electrical characteristics induced by radiation. Williams was one of several apprentices selected for the DoD Science and Engineering Summer Apprenticeship Program for high school students.

Papers, reports, and patents

The majority of NRL's 1984 product is ideas and hardware. This is represented by over 2000 books, patents, reports, papers in refereed journals, and oral presentations.

PAPERS, REPORTS, AND PATENTS

"From the beginning of the twentieth century, the Navy has been a pioneer in initiating new developments ... and a leader in their utilization in military operations. An objective of this document is to identify NRL's numerous scientific reports ... so that the detailed information these reports contain may be made readily accessible to those who may be involved with the subject matter in the future."

Louis A. Gebhard
Evolution of Naval Radio-Electronics
and Contributions of
The Naval Research Laboratory
1979

PAPERS IN JOURNALS, BOOKS, AND PROCEEDINGS OF MEETINGS

In several respects, NRL is like a factory — the input ingredients are the talents and ideas of the people and research funds, and the output product is information. This product is packaged in the form of reports; articles in science journals and books; papers presented to scientific societies and topical conferences; and patents.

This section lists a portion of NRL's output for 1984. The omitted parts are oral presentations (about 1450), reports that carry a military security classification, and letter reports to sponsors. In the following bibliography, an asterisk identifies a coauthor who is not a member of the NRL staff. In 62 years, NRL's pioneering research has led to 3039 patents. The table below summarizes the 1984 technical output.

Type of Contribution	Unclass.	Class.	Total
Papers in periodicals, books, and proceedings of meetings	775	0	775
NRL Reports	34	30	64
NRL Memorandum Reports	216	30	246
Books			2
Patents granted			36

ACOUSTICS

A Frequency-Domain Beamforming Algorithm for Wideband, Coherent Signal Processing, by Weber, M.E. and Heisler, R.,* *Journal of the Acoustical Society of America* 76:1132-1144

A Method for Measuring the Frequency Dispersion for Broadband Pulses Propagated to Long Ranges, by Yang, T.C., *Journal of the Acoustical Society of America* 76:253-261

A Study of Elastomer/Metal Bonds Applicable in Underwater Sonar Systems, by Ting, R.Y., *Adhesive Joints*, Plenum Publishing Corp., NY, pp. 555-564

Apparatus-Independent Acoustical-Material Characteristics Obtained from Panel-Test Measurements, by Rudgers, A.J. and Solvold, C.A., *Journal of the Acoustical Society of America* 76:926-934

Comments on "Distortion of Finite Amplitude Ultrasound in a Lossy Media," by M.E. Haran and B.D. Cool [J. Acoust. Soc. Am. 73, 774-779 (1983)], by Trivett, D.H.* and VanBuren, A.L., *Journal of the Acoustical Society of America* 76:1257-1258

Dispersion and Ranging of Transient Signals in the Arctic Ocean, by Yang, T.C., *Journal of the Acoustical Society of America* 76:262-273

Elements of a Geoacoustic Model of the Upper Crust, by Diachok, O.I., Dicus, R.L., and

261

Wales, S.C., *Journal of the Acoustical Society of America* 75:324-334

Interpretation of Sample Wave Speed Measured in an Impedance Tube, by Dubbelday, P.S. and Capps, R.N., *Journal of the Acoustical Society of America* 76:964-967

Nonlinear Scattering of Acoustic Waves by Vibrating Surfaces, by Piquette, J.C. and VanBuren, A.L., *Journal of the Acoustical Society of America* 76:880-889

Performance Characteristics of Biased Estimators, by Gerlach, A.A., *IEEE International Conference on Acoustics, Speech and Signal Processing*, Vol. 1, IEEE, NY, pp. 7.6.1-7.6.4

Polar Glass Ceramics for Sonar Transducers, by Ting, R.Y., Halliyal, A.G.,* and Bhalla, A.S.,* *Applied Physics Letters* 44:852-854

Transducers, by Bucaro, J.A., *McGraw-Hill Yearbook of Science & Technology*, McGraw-Hill Book Company, pp. 443-446

ARTIFICIAL INTELLIGENCE

An Expert System for Electronics Troubleshooting Based on Function and Connectivity, by Pipitone, F., *First Conference on Artificial Intelligence Applications*, IEEE, NY, pp. 133-138

An Intelligent Control Strategy for Computer Consultation, by Slagle J.R., Gaynor M.W.,* and Halpern E.J.,* *IEEE Transactions on Pattern Analysis and Machine Intelligence* PAMI-6:129-136

ATMOSPHERIC SCIENCES

Aerosol Size Distributions at a Site on the East Coast of the United States, by Hoppel, W.A., Larson, R., and Vietti, M.A., *Atmospheric Environment* 18:1613-1621

Atmospheric Radon Measurements in the Arctic, Fronts, Seasonal Observations, and Transport of Continental Air to Polar Regions, by Wilkniss, P.E.* and Larson, R.E., *Journal of the Atmospheric Sciences* 41:2347-2358

Equilibrium Size of Atmospheric Aerosol Particles as a Function of Relative Humidity: Calculations Based on Measured Aerosol Properties, by Fitzgerald, J.W. and Hoppel, W.A., *Hygroscopic Aerosols in*

the Planetary Boundary Layer, A. Deepak Publishing Co., Hampton, VA, pp. 21-34

Liquid Water Content of Fogs and Hazes from Visible Light Scattering, by Gerber, H., *Journal of Climate and Applied Meteorology* 23:1247-1252

NRL Artificial Aerosol Studies, by Gathman, S.G., *Smoke/Obscurants Symposium VIII, B-17*, p. 30

Navy Hygroscopic Aerosol Model, by Gathman, S.G., *Hygroscopic Aerosols in the Planetary Boundary Layer*, A. Deepak Publishing Co., Hampton, VA, pp. 93-115

Nonzonal Gravity Wave Breaking in the Winter Mesosphere, by Schoeberl, M.R.* and Strobel, D.F., *Dynamics of the Middle Atmosphere*, D. Reidel Publishing Co., Boston, MA

On the Relationships of the Dry Size Distribution of Hygroscopic Air to Electromagnetic Radiation Extinction, by Gathman, S.G., *Hygroscopic Aerosols in the Planetary Boundary Layer*, A. Deepak Publishing Co., Hampton, VA, pp. 339-348

Parameterization of IR Coding in a Middle Atmosphere Dynamics Model 2. Non-LTE Radiation Transfer and the Globally Averaged Temperature of the Mesophere and Lower Thermosphere, by Apruzese, J.P., Strobel, D.F., and Schoeberl, M.R.,* *Journal of Geophysical Research* 89:4917-4926

Reply, by Chang, S.W., *Monthly Weather Review* 112:1646-1647

The Effects of Meteorology on Marine Aerosol and Optical and IR Propagation, by Gathman, S.G., *AGARD Advisory Group for Aerospace Research and Development Conference Proceedings*, AGARD-CP-346, Chap. 7-1

BIOSCIENCES

Encapsulation of Hemoglobin Phospholipid Vesicles: Preparation and Properties of a Red Cell Surrogate, by Gaber, B.P. and Farmer, M.C., *The Red Cell: Sixth Ann Arbor Conference*, Alan R. Liss, Inc., NY, pp. 179-190

Physicians at Risk. Some Epidemiologic Considerations of Alcoholism, Drug Abuse, and Suicide, by Keeve, J.P., *Journal of Occupational Medicine* 26:505-508

Picosecond Relaxation Measurements in Biology, by Campillo, A.J. and Shapiro, S.L., *Ultra Short Light Pulses, Topics in Applied Physics*, Vol. 18 Springer-Verlag, NY, pp. 317-376

The Secondary Structure of Acetylcholine Receptor Reconstituted in a Single Lipid Component as Determined by Raman Spectroscopy, by Yager, P., Chang, E.L., Williams, R.W.,* and Dalziel, A.W., *Biophysical Journal* 45:26-28

CERAMICS, GLASSES AND PLASTICS

Anomalous Isotope-Mass Effect in Lithium Borate Glasses: Comparison with a Unified Relaxation Model, by Ngai, K.L., Rendell, R.W., and Jain, H.,* *Physical Review B* 30:2133-2139

Capabilities and Design Issues for Emerging Tough Ceramics, by Rice, R.W., *8th Annual Conference on Composites and Advanced Ceramic Materials in: American Ceramic Society Bulletin* 63:256-262

Ceramic Fracture Features, Observations, Mechanisms, and Uses, by Rice, R.W., *Fractography of Ceramic and Metal Failures*, ASTM STP 827, American Society for Testing and Materials, Philadelphia, PA, pp. 5-103

Effect of Impurities on the Vibrational Properties of ZrF_4-Based Glasses, by Strom, U., Freitas, J.A., Devaty, R.P., and Tran, D.C., *Infrared Optical Materials and Fibers III*, SPIE, Vol. 484, Society of Photo-Optical Instrumentation Engineers, Bellingham, WA, pp. 74-77

Electron Spin Resonance Studies of Trapped Hole Centers in Irradiated Alkali Silicate Glasses: A Critical Comment on Current Models for HC_1 and HC_2, by Griscom, D.L., *Journal of Non-Crystalline Solids* 64:229-247

Ferromagnetic Resonance of Precipitated Phases in Natural Glasses, by Griscom, D.L., *Journal of Non-Crystalline Solids* 67:81-118

Formation of Ceramic Composites and Coatings Utilizing Polymer Pyrolysis, by Coblenz, W.S., Wiseman, G.H., Davis, P.B., and Rice, R.W., *Emergent P. rcess Methods for High-Technology Ceramics*, Materials Science Research, Vol. 17, Plenum Press, NY, pp. 271-285

Fractographic Analysis of Biaxial Failure in Ceramics, by Mecholsky, J.J.* and Rice, R.W., *Fractography of Ceramic and Metal Failures*, ASTM STP 827, American Society for Testing and Materials, Philadelphia, PA, pp. 185-193

Future Needs in Ceramic Fractography and Failure Analysis. Panel Report, by Rice, R.W., *Fractography of Ceramic and Metal Failures*, ASTM STP 827, American Society for Testing and Materials, Philadelphia, PA, pp. 401-405

Heavy Metal Fluoride Glasses and Fibers: A Review, by Tran, D.C., Sigel, G.H., and Bendow, B.,* *Journal of Lightwave Technology* LT-2:566-586

Laser Processing of Ceramics, by Spann, J.R., Rice, R.W., Coblenz, W.S., and McDonough, W.J., *Emergent Process Method for High-Technology Ceramics*, Vol. 17, Plenum Publishing Corp., NY, pp. 473-503

On the Structure of Defect Centers in γ-Irradiated Alkali Silicate Glasses, by Cases, R.* and Griscom, D.L., *Proceedings of the 2nd International Conference on Radiation Effects in Insulators in: Nuclear Instruments and Methods in Physics Research* 229(B1):503-510

Processing of Advanced Ceramic Composites, by Rice, R.W., *Chemistry and Advanced Ceramics*, Materials Research Society Symposia Proceedings, Vol. 32, Elsevier, NY, pp. 337-345

Relaxation in Spin Glasses: Similarities with and Differences from Ordinary Glasses, by Ngai, K.L., Rajagopal, A.K.,* and Huang, C.Y.,* *Proceedings of the Twenty-Ninth Annual Conference on Magnetism & Magnetic Materials in: Journal of Applied Physics* 55:1714-1716

Static P-T-V Measurements in MgO: Comparison with Shock Wave Data, by Ming, L.C.,* Manghnani, M.H.,* Balogh, J.,* Qadri, S.B.,* Skelton, E.F., and Jamieson, J.C.,* *Shock Waves in Condensed Matter, Proceedings of the American Physical Society Topical Conference*, North-Holland, NY, pp. 57-60

Strength, Toughness and Fracture Initiation of Fluoride Glasses, by Wu, C.C.M., Lewis, D., and McKinney, K.R., *Infrared Optical Materials and Fibers III*, SPIE, Vol. 484, Society of Photo-Optical Instrumentation Engineers, Bellingham, WA, pp. 78-82

263

Tougher Ceramics Using Tetragonal ZrO_2 or HfO_2, by Rice, R.W., Bender, B.A., and Ingle, R.P., *Proceedings of Ultrastructure Processing of Ceramics, Glasses and Composites*, pp. 507-523

Transient Luminescence, Transport and Photoconductivity in Chalcogenide Glasses, by Ngai, K.L., *Polarons and Excitons in Polar Semiconductors and Ionic Crystals*, Plenum Publishing Corp., NY, pp. 383-418

CHEMISTRY

A Comprehensive Investigation of Residual Compounds of Br in HOPG and Graphite Fibers via X-Ray Absorption, by Feldman, J.L., Elam, W.T., Ehrlich, A.C., Skelton, E.F., Dominguez, D.D., Qadri, S.B.,* Chung, D.D.L.,* and Lytle, F.W.,* *EXAFS and Near Edge Structure III*, p. 464

A Nomenclature for Macrocyclic Compounds by Sequential Citation, by Fox, R.B., *Journal of Chemical Information and Computer Science* 24:266-271

An Assessment of Graphitized Carbon Fiber Use for Electrical Power Transmission, by Murday, J.S., Dominguez, D.D., Moran, J.A.,* Lee, W.D.,* and Eaton, R.,* *Synthetic Metals* 9:397-424

Analysis of Impregnated Charcoals by Desorption Ionization Mass Spectrometry, by Ross, M.M., Kidwell, D.A., and Campana, J.E., *Analytical Chemistry* 56: 2142-2145

Analysis of Middle Distillate Fuels by Flow Liquid Chromatography/Proton Nuclear Magnetic Resonance, by Hazlett, R.N., Dorn, H.L.,* and Glass, T.E.,* *Magnetic Resonance. Introduction, Advanced Topics and Applications to Fossil Energy*, D. Reidel Publishing Co., NY, pp. 709-720

Anisotropy Effects in the Linearly Polarized X-Ray Absorption Spectrum of Br_2 Intercalated Graphite Fibers and Highly Oriented Pyrolytic Graphite, by Feldman, J.L., Skelton, E.F., Ehrlich, A.C., Dominquez, D.D., Elam, W.T., Qadri, S.B.,* and Lytle, F.W.,* *Physical Review Letters* 49:1023-1026

Antistatic Agents, Lubricants, and Precision Bearing II. Conductive Electroactive Polymers, by Bernett, M.K., Ravner, H., and Weber, D.C., *38th Annual Meeting of the*

American Society for Lubrication Engineers in: Journal of the American Society of Lubrication Engineers 40:203-210

Applications of Ion-Implanted Covalent Polymers, by Weber, D.C., Bernett, M.K., and Ravner, H., *Ion Implantation and Ion Beam Processing of Materials*, Materials Research Society Symposia Proceedings, Vol. 27, North-Holland, NY, pp. 759-763

Autoxidation of Nitrogen Heterocycles. 1. Ultraviolet Spectra of Alkylpyrroles. Evidence for a Molecular Association Complex Between Oxygen and 2,5-Dimethylpyrrole in Non-polar Media, by Cooney, J.V. and Hazlett, R.N., *Heterocycles* 22:1513-1518

Book Review — Principles of Quantitative X-Ray Fluorescence Analysis by R. Tertian and F. Claisse, by Gilfrich, J.V., *Analytical Chemistry* 56:614A

Book Review — Introduction to Alpha Coefficients, by Gilfrich, J.V., *Applied Spectroscopy* 38:613

^{13}C NMR Determination of the In-Plane Carbon-Carbon Bond Length in Graphite Intercalation Compounds, by Miller, G.R.,* Poranski, C.F., and Resing, H.A., *Journal of Chemical Physics* 80:1708-1709

Chemical Ionization - Fast-Atom Bombardment Mass Spectrometry: a Novel Ionization Method, by Campana, J.E. and Freas, R.B., *Journal of the Chemical Society. Chemical Communications*, pp. 1414-1415

Chemical Kinetic-Fluid Dynamic Interactions in Detonations, by Oran, E., *The Chemistry of Combustion Processes*, ACS Symposium Series 249, American Chemical Society, Washington, D.C., pp. 151-173

Chemical and Physical Interactions in Covalent Polymers Implanted with Transition Metals, by Pehrsson, P.E.,* Weber, D.C., Koon, N., Campana, J.E., and Rose, S.L., *Ion Implantation and Ion Beam Processing of Materials*, Materials Research Society Symposia Proceedings, Vol. 27, North-Holland, NY, pp. 429-434

Chemically Modified Electrodes: A View and a Review, by Rolison, D.R., *Fundamental Aspects of Corrosion Protection by Surface Modification*, Electrochemical Society, Inc., Pennington, NJ, pp. 222-232

Chemically Suppressing Rusty-Bolt Intermodulation Interference, *by Cooper, J.C., Panayappan, R., and Stule, R.C.,* *IEEE 1984*

National Symposium on Electromagnetic Compatibility, IEEE, NY, pp. 233-240

Combined SIMS and Electron Spectroscopy Investigation of the Chemical State of Some Ion-Implanted Transition Metals and Steels, by Bone, W.M., Barlak, T.M., Singer, I.L., Jeffries, R.A., and Colton, R.J., *Secondary Ion Mass Spectrometry SIMS IV, Proceedings of the Fourth International Conference*, Springer-Verlag, NY, pp. 221-224

Comparative Study of Molecular Fragmentation in Sub-Initiated TATB Caused by Impact, UV, Heat and Electron Beams, by Sharma, J.,* Hoffsommer, J.C.,* Glover, D.J.,* Coffey, C.S.,* Santiago, F.,* Stolovy, A., and Yasuda, S.,* *Shock Waves in Condensed Matter - 1983*, North-Holland, NY, pp. 543-546

Complexes of Trialkylaluminum Compounds with Polyfunctional Ethers, by Shuler, R.L., De Marco, R.A., and Berry, A.D., *Inorganica Chimica Acta* 85:185-189

Computer Modeling of High Fluence Titanium Ion Implantation and Vacuum Carburization in Steel, by Farkas, D.,* Rangaswamy, M.,* and Singer, I.L., *Ion Implantation and Ion Beam Processing of Materials*, Materials Research Society Symposia Proceedings, Vol. 27, North-Holland, NY, pp. 609-614

Desorption Ionization Mass Spectrometry of Synthetic Porphyrins, by Kurlansik, L.,* Williams, T.J.,* Strong, J.M.,* Anderson, L.W.,* and Campana, J.E., *Biomedical Mass Spectrometry* 11:475-481

Determination of Ethylenediaminetetraacetic Acid in Boiler Water by Liquid Chromatography, by Venezky, D.L., and Rudzinski, W.E.,* *Analytical Chemistry* 56:315-317

Diode Laser Spectrum of Diacetylene Near 5 μm, by Pasternack, L. and McDonald, J.R., *Journal of Molecular Spectroscopy* 108:143-152

Direct Rotational Population Distributions of N_2 and N_2^+ in Pulsed Supersonic Beams, by Baronavski, A.P., Helvajian, H., and DeKoven, B.M., *Applications of Laser Chemistry and Diagnostics*, SPIE, Vol. 482, Society of Photo-Optical Instrumentation Engineers, Bellingham, WA, pp. 31-35

Electrically Conductive Polymer Composites of 7,7,8,8-Tetracyanoquinodimethane (TCNQ) Salt Dispersion: Influence of Charge-Transfer Interaction and Film Morphology, by Kim, O.K., *Polymers in Electronics*, ACS Symposium Series 242, American Chemical Society, Washington, D.C., pp. 515-531

Electrogenerated Coatings Containing Zeolites, by Murray, C.G., Nowak, R.J., and Rolison, D.R., *Journal of the Electrochemical Society* 164:205-210

Electron Affinities from Dissociations of Mixed Negative Ion Dimers, by Burinsky, D.J., Fukuda, E.K., and Campana, J.E., *Journal of the American Chemical Society* 106:2770-2771

Explicit Treatment of Correlation Within Density-Functional Theories that Use the Kinetic-Energy Operator, by Dunlap, B.I., *Physical Review A* 29:2902-2905

Factors Affecting Oxidation Stability of a Deuterated Ester, by Pande, S.G.,* Bolster, R.N., and Ravner, H., *ASLE-ASME Lubrication Conference in: ASLE Transactions* 27:352-358

Fast Atom Bombardment Mass Spectrometry of Phthalocyanines, by Freas, R.B. and Campana, J.E., *Inorganic Chemistry* 23:4654-4658

Formation of Tubules by a Polymerizable Surfactant, by Yager, P. and Schoen, P.E., *Molecular Crystals & Liquid Crystals* 106:371-381

Friction and Wear Behavior of a Cobalt-Based Alloy Implanted with Ti or N, by Dillich, S., Bolster, R.N., and Singer, I.L., *Ion Implantation and Ion Beam Processing*, Materials Research Society Symposia Proceedings, Vol. 27, 637-642

Friction, Wear and Deformation of Soft Steels Implanted with Ti and N, by Singer, I.L. and Jeffries, R.A.,* *Ion Implantation and Ion Beam Processing*, Materials Research Society Symposia Proceedings, Vol. 27, 667-672

Hardness as a Measure of Wear Resistance, by Oliver, W.C.,* Hutchings, R.,* Pethica, J.B.,* Singer, I.L., and Hubler, G.K., *Ion Implantation and Ion Beam Processing of Materials*, Materials Research Society, Vol. 27, North-Holland, NY, pp. 603-608

Imaging Biological Compounds Using the CARS Microscope, by Duncan, M.D., Reintjes, J., and Manuccia, T.J., *Applications of Laser Chemistry and Diagnostics*, SPIE, Vol. 482, Society of Photo-Optical Instrumentation Engineers, Bellingham, WA, pp. 46-52

Infrared Laser Probing of Combustion and Energetic Molecule Decomposition Reactions in Shock Waves, by Hsu, D.S.Y. and

Lin, M.C., *Applications of Laser Chemistry and Diagnostics*, SPIE, Vol. 482, Society of Photo-Optical Instrumentation Engineers, Bellingham, WA, pp. 79-88

Inhibition of Low Temperature Hot Corrosion by Zn,Na Mixed Sulfates, by Foggo, J.G., Nordman, D.B., and Jones, R.L., *Journal of the Electrochemical Society* 131:515-522

Kinetics and Mechanisms of the Reactions of CH and CD with H_2 and D_2, by Berman, M.R.* and Lin, M.C., *Journal of Chemical Physics* 81:5743-5752

Laser Techniques for the Production and Detection of Reactive Species of Importance in Combustion, by Nelson, H.H., Pasternack, L., and McDonald, J.R., *Applications of Laser Chemistry and Diagnostics*, SPIE, Vol. 482, Society of Photo-Optical Instrumentation Engineers, Bellingham, WA, pp. 58-65

Laser-Induced Fluorescence of $N_2(X^1\sigma g^+)$ and Electron-Impact Excited $N_2^+(x^2\sigma g^+)$ in a Pulsed Supersonic Beam: Rotational Distributions, by Helvajian, H.,* DeKoven, B.M., and Baronavski, A.P., *Chemical Physics* 90:175-183

Magnetic Properties of Iron Implanted Polymers and Graphite, by Koon, N.C., Weber, D., Pehrsson, P., and Schindler, A.I., *Ion Implantation and Ion Beam Processing of Materials*, Materials Research Symposia Proceedings, Vol. 27, North-Holland, NY, pp. 445-448

Mass Spectrometric Characterization of Desorbed Species from Weathered Activated Charcoals, by Ross, M.M., Campana, J.E., and Deitz, V.R., *Carbon* 22:98-99

Molecular Association and Monolayer Formation of Soluble Phthalocyanine Compounds, by Snow, A.W. and Jarvis, N.L., *Journal of the American Chemical Society* 106:4706-4711

Molecular Electronic Devices, Today's Dream, Tomorrow's Reality, by Carter, F.L., *Proceedings of Biotech '84*, USA, Vol. 2, Online Publications, Pinner, UK, p. 127

Molecular Electronics: An Opportunity for a Biotechnical Synergism, by Carter, F.L., *Nonlinear Electrodynamics in Biological Systems*, Plenum Publishing Corp., NY, pp. 243-273

$NHA^3\pi \rightarrow X^3\sigma^-$ Chemiluminescence from the $CHX^2\pi$ + NO Reaction, by Lichtin, D.A., Berman, M.R., and Lin, M.C., *Chemical Physics Letters* 108:18-24

Nitrogen 1s Binding Energy Shifts Detected from a Homologous Series of Cyanine Dyes, by Gold, L., and Giuliani, J.F., *Journal of the American Chemical Society* 106:2209-2210

NMR Imaging in Solids by Multiple-Quantum Resonance, by Garroway, A.N., Baum, J.,* Munowitz, M.G.,* and Pines, A.,* *Journal of Magnetic Resonance* 60:337-341

Nuclear Magnetic Resonance Characterization of Graphite Intercalation Compounds Containing AsF_6^- and AsF_6^- + AsF_3, by Moran, M.J., Miller, G.R., De Marco, R.A., and Resing, H.A., *Journal of Physical Chemistry* 88:1580-1584

On Spartina Alterniflora Litter and the Trace Metal Biogeochemistry of a Salt Marsh, by Pellenbarg, R.E., *Estuarine, Coastal and Shelf Science* 18:331-346

On the Development and Use of Fast Atom Beams for the SIMS Analysis of Polymers and Insulators, by Ross, M.M., Colton, R.J., Rose, S.L., Wyatt, J.R., DeCorpo, J.J., and Campana, J.E., *AVS National Symposium, 30th in: Journal of Vacuum Science and Technology* A 2:748-750

Optical Diagnostics of High Pressure Solid Propellant Flames, by Fleming, J.W., Barber, W.H.,* and Wilmont, G.B.,* *Applications of Laser Chemistry and Diagnostics*, SPIE, Vol. 482, Society of Photo-Optical Instrumentation Engineers, Bellingham, WA, pp. 74-78

Photochemical Separation of Xenon and Krypton, by Geosling, C.E. and Donohue, T., *Environmental Science and Technology* 18:262-264

Plasma-Polymerized Films of Vinylferrocene on Thermally-Oxidized Titanium and Single-Crystal Titanium Dioxide, by Rolison, D.R. and Murray, R.W.,* *Journal of the Electrochemical Society* 131:337-343

Poly(ethylene maleate)-Cyclopentadiene: A Model Reactive Polymer-Vapor System for Evaluation of a SAW Microsensor, by Snow, A. and Wohltjen, H., *Analytical Chemistry* 56:1411-1416

Polymers and Barnacles, by Griffith, J.R., *Journal of Chemical Education* 61:1090-1091

Processing Steels for Tribological Applications by Titanium Implantation, by Singer, I.L. and Jeffries, R.A.,* *Ion Implantation and Ion Beam Processing*, Materials Research Society

Symposia Proceedings, Vol. 27, 673-678

Prospects for Computation at the Molecular Size Level, by Carter, F.L., *COMPCON Spring '84 Intellectual Leverage. The Driving Technologies*, IEEE, NY, pp. 110-114

Pyrolysis of Organic Compounds Containing Long Unbranched Alkyl Groups, by Mushrush, G.W. and Hazlett, R.N., *I&EC Fundamentals* 23:288-294

Reissert Compounds and Their Open-Chain Analogs in Organic Synthesis, by Cooney, J.V., *Journal of Heterocyclic Chemistry* 823-837

Rotating Frame Cross-Polarization in Liquids, by Chingas, G.C., Garroway, A.N., and Moniz, W.B., *Topics in Carbon-13 NMR Spectroscopy*, Vol. 4, John Wiley & Sons, NY, pp. 159-177

Secondary Ion Mass Spectrometry (SIMS) of Metal Halides IV. The Envelopes of Secondary Cluster Ion Distributions, by Campana, J.E. and Dunlap, B.I., *International Journal of Mass Spectrometry and Ion Processes* 57:103-123

Sequencing of Peptides by SIMS from the C or N Terminus, by Kidwell, D.A., Ross, M.M., and Colton, R.J., *Secondary Ion Mass Spectrometry SIMS IV, Proceedings of the Fourth International Conference*, Springer-Verlag, NY, pp. 412-3414

Sequencing of Peptides by Secondary Ion Mass Spectrometry, by Kidwell, D.A., Ross, M.M., and Colton, R.J., *Journal of the American Chemical Society* 106:2219-2220

Simultaneous Determination of Hydrazine, Methylhydrazine, and 1,1-Dimethylhydrazine in Air by Derivatization/Gas Chromatography, by Holtzclaw, J.R., Rose, S.L., Wyatt, J.R., Rounbehler, D.P.,* and Fine, D.H.,* *Analytical Chemistry* 56:2952-2956

Site of Gas Phase Cation Attachment. The Protonation, Methylation and Ethylation of Morpholine, Thiomorpholine and 1,4-Thioxane, by Burinsky, D.J. and Campana, J.E., *Organic Mass Spectrometry* 19:539-544

Stop Wear the Hard Way, by Stern, K.H., *Chemtech* 749-751

Surface Analysis, Ion Implantation and Tribological Processes Affecting Steels, by Singer, I.L., *Applications of Surface Science* 18:28-62

Surface Analysis: X-Ray Photoelectron Spectroscopy, Auger Electron Spectroscopy, Secondary Ion Mass Spectrometry, by Turner, N.H., Dunlap, B.I., and Colton, R.J., *Analytical Chemistry* 56:373R-416R

Surface-Enhanced Raman Spectroscopy of Benzene Adsorbed on Vapor-Deposited Sodium. Chemical Contribution to the Enhancement Mechanism, by Lund, P.A.,* Tevault, D.E., and Smardzewski, R.R., *Journal of Physical Chemistry* 88:1731-1735

Synthesis and Characterization of Heteroatom-Bridged Metal-Free Phthalocyanine Network Polymers and Model Compounds, by Snow, A.W., Griffith, J.R., and Marullo, N.P.,* *Macromolecules* 17:1614-1624

The Relaxed Triplet State of the 1,2,4,5-Tetracyanobenzene-Benzene Complex. Triplet Energy Transfer Equilibration with Benzophenone, by Craig, B.B., Gorman, A.A.,* Hamblett, I.,* and Kerr, C.W.,* *Radiation Physics and Chemistry* 23:111-115

Thermal Decomposition of Hydroxylammonium Nitrate at Kilobar Pressures, by VanDijk, C.A. and Priest, R.G., *Combustion and Flame* 57:15-24

Tribomechanical Properties of Ion Implanted Metals, by Singer, I.L., *Ion Implantation and Ion Beam Processing, Materials Research Society Symposium Proceedings* 27:585-595

Ultra-high Mass Spectrometry, by Campana, J.E., Colton, R.J., Wyatt, J.R., Bateman, R.H.,* and Green, B.N.,* *Applied Spectroscopy* 38:430-432

Unicluster Dissociation of Large Alkali Iodide Cluster Ions, by Campana, J.E. and Green, B.N.,* *31st Annual Conference of Mass Spectroscopy and Allied Topics in: Journal of the American Chemical Society* 106:531-535

COMMUNICATIONS

An Architectural Framework for "Signal Flow", by Wu, Y.S. and Wu, L.J.,* *Digital Signal Processing-84*, North-Holland, NY, pp. 222-227

Designing Secure Message Systems: The Military Message Systems (MMS) Project, by Heitmeyer, C.L. and Landwehr, C.E., *Computer-Based Message Systems*, Elsevier Science Publishers B.V., NY, pp. 247-257

Improvement of the Narrowband LPC Synthesis, by Kang, G.S. and Everett, S.S., *IEEE International Conference on Acoustics,*

Speech and Signal Processing, Vol. 1, IEEE, NY, pp. 1.7.1-1.7.4

Multichannel Relative-Entropy Spectrum Analysis, by Johnson, R.W. and Musicus, B.R.,* *IEEE International Conference on Acoustics, Speech and Signal Processing*, Vol. 1, IEEE, NY, pp. 13.6.1-13.6.4

Parameter Selection for Isolated Word Recognition Using Vector Quantization, by Burton, D.K., Buck, J.T., and Shore, J.E., *IEEE International Conference on Acoustics, Speech and Signal Processing*, Vol. 1, IEEE, NY, pp. 9.4.1-9.4.4

Power Spectrum Estimation by Means of Relative-Entropy Minimization with Uncertain Constraints, by Johnson, R.W. and Shore, J.E., *IEEE International Conference on Acoustics, Speech and Signal Processing*, Vol. 1, IEEE, NY, pp. 13.8.1-13.8.4

Sources of Improved Signal Processing Performance, by Wald, B., *Digital Signal Processing-84*, North-Holland, NY, pp. 794-795

The Design and Simulation of a Mobile Radio Network with Distributed Control, by Baker, D.J., Ephremides, A., and Flynn, J., *IEEE Journal on Selected Areas in Communications* SAC-2:226-237

Vector Quantization Code Book Distortions as Features for Maximum Likelihood Classification of Isolated Words, by Buck, J.T., *GLOBECOM '84, IEEE Global Telecommunications Conference, Communications in the Information Age*, 1, IEEE, NY, pp. 260-264

Which is the Better Entropy Expression for Speech Processing: -S log S or log S?, by Johnson, R.W. and Shore, J.E., *IEEE Transactions on Acoustics, Speech and Signal Processing* ASSP-32:129-137

COMPUTER SCIENCES

A Formal Statement of the MMS Security Mode, by McLean, J., Landwehr, C.E., and Heitmeyer, C.L., *Proceedings of the 1984 Symposium on Security and Privacy*, IEEE, NY, pp. 188-194

A Security Model for Military Message Systems, by Landwehr, C.E., Heitmeyer, C.L., and McLean, J., *ACM Transactions on Computer Systems* 2:198-222

An Analytic Orbit Prediction Program Generator, by Coffey, S.L. and Alfriend, K.T.,

AIAA 21st Aerospace Science Meeting in: Journal of Guidance, Control, and Dynamics 7:575-581

Efficient Error Estimation for Gaussian Classifiers, by Flick, T.E. and Jones, L.K., *Seventh International Conference on Pattern Recognition Proceedings*, Vol. 2, IEEE, NY, pp. 1347-1350

Encoding Techniques for a Pictorial Database, by Yang, C.C. and Chang, S.K.,* *Statistical Signal Processing*, Marcel Dekker, Inc., NY, pp. 461-470

Hardware Requirements for Secure Computer Systems: A Framework, by Landwehr, C.E., and Carroll, J.M.,* *Proceedings of the 1984 Symposium on Security and Privacy*, IEEE, NY, pp. 34-40

Oceanographic Data Profile Analysis Using Interactive Computer Graphics Techniques, by Rosenblum, L.J., *Oceans '84 Conference Record*, Vol. 1, IEEE, NY, pp. 100-104

Picture Encoding Techniques for a Pictorial Database, by Yang, C.C., and Chang, S.K.,* *First International Conference on Computers and Applications*, IEEE, NY, pp. 777-786

The Modular Structure of Complex Systems, by Parnas, D.L., Clements, P.C., and Weiss, D.M., *7th International Conference on Software Engineering*, IEEE Computer Society Press, Los Angeles, CA, pp. 408-417

COSMIC RAYS

Cosmic-Ray Heavy Ions at and Above 40,000 Feet, by Tsao, C.H., Silberberg, R., and Letaw, J.R.,* *IEEE Transactions on Nuclear Science* NS-31:1066-1068

On the Abundance of Ultraheavy Cosmic Rays, by Letaw, J.R.,* Silberberg, R., and Tsao, C.H., *Astrophysical Journal* 279:144-150

Propagation of Heavy Cosmic Ray Nuclei, by Letaw, J.R.,* Silberberg, R., and Tsao, C.H., *Astrophysical Journal Supplement Series* 56:369

ELECTRONICS AND ELECTRICITY

An Active Circulator-Gyrotron Traveling-Wave Amplifier, by Lau, Y.Y., Barnett, L.R.,* and Baird, J.M.,* *IEEE Transactions on Electron Devices* ED-31:337-347

Coaxial EMI Feedthrough Filters Containing Ferrite Elements: Analysis and Test Results, by Krebs, J.J., Stauss, G.H., Maisch, W.G., and Rubinstein, M., *IEEE 1984 National Symposium on Electromagnetic Compatibility*, IEEE, NY, pp. 113-118

Collective-Interaction Klystron, by Lau, Y.Y., *Physical Review Letters* 53:395-398

Fast Passive Integrator, by Raleigh, M. and Pechacek, R.E., *Review of Scientific Instruments* 55:2022-2-26

InP Mixer Diodes with Etched Via Ohmic Contacts, by Christou, A., Davey, J.E., Tseng, W.F., and Bark, M.L., *Electronics Letters* 20:378-379

Inversion Theory for Almost Periodic Media, by Jaggard, D.L.,* and Jordan, A.K., *International Symposium on Electromagnetic Theory in: Radio Science* 19:1333-1341

Large-Signal Theory of a Two-Stage Wideband Gyro-TWT, by Ganguly, A.K. and Ahn, S., *IEEE Transactions on Electron Devices* ED-31:474-480

Multisignal Minimum-Cross-Entropy Spectrum Analysis with Weighted Initial Estimates, by Johnson, R.W., Shore, J.E., and Burg, J.P.,* *IEEE Transactions on Acoustics, Speech and Signal Processing* ASSP-32:531-539

Photodetector Approaches for Acousto-Optics Spectrum Analysis, by Anderson, G.W. and Spezio, A.E., *Optical Technology for Microwave Applications*, SPIE, Vol. 477, Society of Photo-Optical Instrumentation Engineers, Bellingham, WA, pp. 161-164

The Mutual Time-Frequency Content of Two Signals, by Szu, H.H. and Caulfield, H.J.,* *Proceedings of the IEEE* 72:902-908

Variable Radix Multistable Integrated Electronics, by Abraham, G., *Proceedings of the IEEE EASCON - 17th Annual Electronics and Aerospace Conference*, IEEE, NY, pp. 209-214

GEOSCIENCES

Earth Tides and Polar Motion, by Lanzano, P., *Journal of Geodynamics* 1:121-142

Reykjanes Ridge: Further Analysis of Crustal Subsidence and Time-Transgressive Basement Topography, by Johansen, B.,* Vogt, P.R., and Eldholm, O.,* *Earth and Planetary Science Letters* 68:249-258

Seasat Altimetry, the North Atlantic Geoid, and Evaluation by Shipborne Subsatellite Profiles, by Vogt, P.R., Zondek, B.,* Fell, P.W.,* Cherkis, N.Z., and Perry, R.K.,* *Journal of Geophysical Research* 89:9885-9903

The Geisha Guyots: Multibeam Bathymetry and Morphometric Interpretation, by Vogt, P.R. and Smoot, N.C.,* *Journal of Geophysical Research* 89:11085-11107

INSTRUMENTATION

An Inexpensive Heatable Sample Assembly and Transfer Mechanism, by Klebanoff, J., Ritz, V.H., and Thomas, R.E., *Journal of Vacuum Science and Technology* A2:1396-1397

Broadband High-Power, Millimeter-to-Centimeter Spectrometer, by Mako, F., Pasour, J.A., Roberson, C.W.,* and Lucey, R., *Review of Scientific Instruments* 54:712-715

Estimation of Detection Limits in X-ray Fluorescence Spectrometry, by Gilfrich, J.V. and Birks, L.S., *Analytical Chemistry* 56:77-79

Experimental Verification of the Three-Frequency Scatterometer Concept, by Schuler, D.L., Plant, W.J., and Miller, H.C.,* *Oceans '84 Conference Record*, Vol. 1, IEEE, NY, pp. 145-149

High Pressure Structural Data at 10,000-Times Faster Rates, by Skelton, E.R., *Naval Research Review* 36:3:20-30

Low Frequency Microwave Radiometer for NROSS, by Hollinger, J.P. and Lo, R.C., *Recent Advances in Civil Remote Sensing*, SPIE Vol. 481, Society of Photo-Optical Instrumentation Engineers, Bellingham, WA, pp. 199-207

The Evaluation of PVF$_2$ for Underwater Shock-Wave Sensor Application, by Meeks, S.W. and Ting, R.Y., *Journal of the Acoustical Society of America* 75:1010-1012

The Low Frequency Microwave Radiometer for N-ROSS, by Hollinger, J.P. and Lo, R.C., *Oceans '84 Conference Record*, IEEE, NY, pp. 167-174

The Mission Sensor Microwave Imager, Its Applications and Validation, by Lo, R.C. and Hollinger, J.P., *Oceans '84 Conference Record*, Vol. 1, IEEE, NY, pp. 162-166

LASER PHYSICS

A **High-Gain 35 GHz Free-Electron Laser Amplifier Experiment**, by Gold, S.H., Barnett, L.R.,* Granatstein, V.L.,* Hardesty, D.L., and Kinkead, A.K., *Proceedings of the International Conference on Plasma Physics*, Centre de Recherches en Physique des Plasmas, Lausanne, Switzerland, p. 393

A **High-Gain 35-GHz Free-Electron Laser-Amplifier Experiment**, by Gold, S.H., Hardesty, D.L., Kinkead, A.K., Barnett, L.R.,* and Granatstein, V.L.,* *Physical Review Letters* 52:1218-1221

Absolutely Uniform Illumination of Laser Fusion Pellets, by Schmitt, A.J., *Applied Physics Letters* 44:399-401

Active-Passive Mode Locking of a Nd: Phosphate Glass Laser Using #5 Saturable Dye, by Goldberg, L.S. and Schoen, P.E., *IEEE Journal of Quantum Electronics* QE-20:628-630

Basic Design Considerations for Free-Electron Lasers Driven by Electron Beams from rf Accelerators, by Gover, A., Freund, H., Granatstein, V.L., McAdoo, J.H., and Tang, C.M., *Infrared and Millimeter Waves*, Vol. 11, Academic Press, NY, pp. 292-365

Characteristics and Uses of X-radiation from Laser-Heated Plasmas, by Nagel, D.J., *X-Ray Lithography and Applications of Soft X-Rays to Technology*, SPIE, Vol. 448, Society of Photo-Optical Instrumentation Engineers, Bellingham, WA, pp. 17-24

Compact, Low-Cost Cryogenic Laser Head, by Eckardt, R.C.,* Storm, M.E.,* Linz, A.,* and Marquardt, C.L., *Review of Scientific Instruments* 55:1945-1947

Creation of Ultra High Pressure Shocks by the Collision of Laser Accelerated Disks: Experiment and Theory, by Rosen, M.D.,* Phillion, D.W.,* Price, R.H.,* Campbell, E.M.,* Obenschain, S.P., Whitlock, R.R., McLean, E.A., and Ripin, B.H., *Shock Waves in Condensed Matter - 1983, Proceedings of the American Physical Society Topical Conference*, North-Holland, NY, pp. 323-326

Demonstration of a Free Electron Laser with an Electromagnetic Wiggler, by Granatstein, V.L.,* Carmel, Y.,* and Gover, A.,* *Free-Electron Generators of Coherent Radiation*, SPIE, Vol. 453, Society of Photo-Optical

Instrumentation Engineers, Bellingham, WA, pp. 344-349

Efficiency Enhancement in Free-Electron Lasers Using a Tapered Axial Guide Field, by Freund, H.P.* and Gold, S.H., *Physical Review Letters* 52:926-929

Energy Transfer in Picosecond Laser Generated Compressional Shock Waves, by Campillo, A.J., Goldberg, L.S., and Schoen, P.E., *Ultrafast Phenomena IV*, Springer-Verlag, NY, pp. 289-291

Excimer Lasers, Their Applications, and New Frontiers in Lasers, ed. by Waynant, R.W., SPIE Vol. 476, Society of Photo-Optical Instrumentation Engineers, Bellingham, WA, 170 pp

Gain, Bandwidth, and Tunability of a High Power Millimeter-Wave Free-Electron Laser, by Gold, S.H., Black, W.M., Granatstein, V.L.,* Freund, H.P.,* and Kinkead, A.K., *Proceedings of the Fifth International Conference on High-Power Particle Beams*, Lawrence Livermore National Laboratory, Livermore, CA, pp. 612-616

Generation of mJ Pulses at 117 nm by Frequency Conversion of XeF Laser Radiation, by Dlabal, M.L., Reintjes, J.F., and Tankersly, L.L., *Excimer Lasers, Their Applications, and New Frontiers in Lasers*, SPIE, Vol. 476, Society of Photo-Optical Instrumentation Engineers, Bellingham, WA, pp. 65-71

High Gain XUV and X-Ray Free Electron Lasers, by Tang, C.M. and Sprangle, P., *Proceedings of the Topical Meeting on Free-Electron Generation of Extreme Ultraviolet Coherent Radiation*, AIP Conference 118, American Institute of Physics, NY, pp. 131-143

Instability of Relativistic-Electron Helical Trajectories in Combined Uniform Axial and Helical Wiggle Magnetic Fields, by Zachary, W.W., *Physical Review A* 29:3224-3233

Intermodal Injection Locking of Semiconductor Lasers, by Goldberg, L., Taylor, H.F., and Weller, J.F., *Electronics Letters* 20:809-810

Laser Photolysis of Nitroaromatics, by Craig, B.B. and Atherton, S.J.,* *Applications of Laser Chemistry and Diagnostics*, SPIE, Vol. 482, Society of Photo-Optical Instrumentation Engineers, Bellingham, WA, pp. 96-103

Laser Surface Modification Below a Liquid Layer, by Donohue, T., *Laser Processing and Diagnostics, Proceedings of an International Conference*, Springer Series in Chemical Physics 30, Springer-Verlag, NY, pp. 332-336

Liquid-Phase Laser Surface Modification, by Donohue, T., *Applications of Laser Chemistry and Diagnostics*, SPIE, Vol. 482, Society of Photo-Optical Instrumentation Engineers, Bellingham, WA, pp. 125-129

Long Pulse Free Electron Laser Driven by a Linear Induction Accelerator, by Pasour, J.A., Lucey, R.F.,* and Roberson, C.W.,* *Free-Electron Generators of Coherent Radiation*, SPIE, Vol. 453, Society of Photo-Optical Instrumentation Engineers, Bellingham, WA, pp. 328-335

Long-Pulse, High-Power Free-Electron Laser with No External Beam Focusing, by Pasour, J.A., Lucey, R.F.,* and Kapeta-nakos, C.A., *Physical Review Letters* 53:1728-1731

New Sources of High-Power Coherent Radiation, by Sprangle, P. and Coffey, T., *Physics Today* 37:44-51

Nonlinear Simulation of Raman Free-Electron Lasers with Axial Guide Fields, by Freund, H.P., *Free-Electron Generators of Coherent Radiation*, SPIE, Vol. 453, Society of Photo-Optical Instrumentation Engineers, Bellingham, WA, pp. 361-366

Numerical Studies of Laser-Induced Shock Structure in Condensed Materials, by Guirguis, R.H.* and Oran, E.S., *Shock Waves in Condensed Matter - 1983*, North-Holland, NY, pp. 351-352

Progress on the Scaling of the X-Ray Preionized Discharges Pumped XeCl Laser, by Champagne, L.F., Dudas, A.J.,* and Wexler, B.L., *Excimer Lasers - Their Applications and New Frontiers in Lasers*, SPIE, Vol. 476, Society of Photo-Optical Instrumentation Engineers, Bellingham, WA, pp. 2-5

Radiation Growth in a Millimeter-Wave Free-Electron Laser Operating in the Collective Regime, by Gold, S.H., Black, W.M., Freund, H.P.,* Granatstein, V.L.,* and Kinkead, A.K., *Physics of Fluids* 27:746-754

Reflective Probing of Laser Generated kbar Shocks in Water, by Campillo, A.J. and Schoen, P.E., *Shock Waves in Condensed Matter - 1983*, North-Holland, NY, pp. 347-350

Scaling of Collisionally Pumped 3s-3p Lasers in the Neon Isoelectronic Sequence, by Feldman, U., Seely, J.F., and Bhatia, A.K.,* *Journal of Applied Physics* 56:2475-2478

Semi-Analytical Formulation of the Two-Dimensional Pulse Propagation in the Free Electron Laser Oscillator, by Tang, C.M. and Sprangle, P., *Free-Electron Generators of Coherent Radiation*, SPIE, Vol. 453, Society of Photo-Optical Instrumentation Engineers, Bellingham, WA, pp. 11-24

Spectroscopy of X-Ray Lasers, by Dixon, R.H. and Elton, R.C., *Journal of the Optical Society* 1:232-238

Stable Active-Passive Mode Locking of a Nd:Phosphate Glass Laser Using #5 Saturable Dye, by Goldberg, L.S. and Schoen, P.E., *Ultrafast Phenomena IV*, Springer-Verlag, NY, pp. 87-89

Studies of Radiation Growth and Emission Spectrum of a Millimeter-Wave Free-Electron Laser Operating in the Collective Regime, by Gold, S.H., Black, W.M., Freunc, H.P.,* Granatstein, V.L.,* Efthimion, P.C.,* and Kinkead, A.K., *Free-Electron Generators of Coherent Radiation*, SPIE, Vol. 453, Society of Photo-Optical Instrumentation Engineers, Bellingham, WA, pp. 350-355

Thickness Variations in X-ray Filters and Laser Targets, by Whitlock, R.R. and Sprague, J.A., *Applied Physics Letters* 45:504-506

Transversely Excited N_2O Sequence Band Laser, by Hara, H.* and Whitney, W.T., *Applied Physics Letters* 44:155-156

Use of Stimulated Raman Scattering for Reducing the Divergence of Severely Aberrated Laser Beams, by Chang, R.S.F., Duignan, M.T.,* Lehmberg, R.H., and Djeu, N.,* *Excimer Lasers Their Applications and New Frontiers in Lasers*, SPIE, Vol. 476, Society of Photo-Optical Instrumentation Engineers, Bellingham, WA

MAGNETISM

Abstract: Interfacial Effects on Ferromagnetic Resonance: MBE Iron Films, by Vittoria, C., Rachford, F.J., Krebs, J.J., and Prinz, G.A., *29th Annual Conference on Magnetism and Magnetic Materials in: Journal of Applied Physics* 56:1247

Comment on "Time Decay of the Remanent Magnetization in Spin-Glasses", by Ngai, K.L. and Rajagopal, A.K.,* *Physical Review Letters* 53:1024

Magnetoelectric Susceptibility and Magnetic Symmetry of Magnetoelectrically Annealed $TbPO_4$, by Rado, G.T., Ferrari, J.M., and Maisch, W.G., *Physical Review B* 29:4041-4048

Microwave Properties of $GdFe_2:H_3$ Films, by Vittoria, C., Schelleng, J.H., Lubitz, P., and Forester, D.W., *Proceedings of the Twenty-Ninth Annual Conference on Magnetism and Magnetic Materials in: Journal of Applied Physics* 55:2450-2451

Surface Anisotropy Effects in the Spontaneous Magnetization of a Semi-Infinite Ferromagnet (Abstract), by Rado, G.T., *Proceedings of the Twenty-Ninth Annual Conference on Magnetism and Magnetic Materials in: Journal of Applied Physics* 55:2505

MATHEMATICS

A Nonlinear Implicit Code for Relativistic Electron Beam Tracking Studies, by Hui, B. and Lampe, M., *Journal of Computational Physics* 55:328

An Inverse Spectral Theory of Gel'fand-Levitan-Type for Higher Order Differential Operators, by Zachary, W.W., *Letters in Mathematical Physics* 8:403-411

Bistability, Basins of Attraction and Predictability in a Forced Mass-Reaction Model, by Schwartz, I.B., *Physics Letters* 106A:339-342,

Implementation of a Semianalytic Satellite Theory with Recovery of Short Period Terms, by Kaufman, B. and Harr, W.H., *33rd Congress of the International Astronautical Federation in: Acta Astronautica* 11:279-286

Inversion as Logical Inference - Theory and Applications of Maximum Entropy and Minimum Cross-Entropy, by Shore, J.E., *SIAM-AMS Proceedings* 14:139-149

Linear and Nonlinear Estimators for One- and Two-Dimensional Fourier Transforms, by Byrne, C.L. and Fitzgerald, R.M., *IEEE Transactions on Acoustics, Speech and Signal Processing* ASSP-32:914-916,

Modifications to Recursion Unfolding Algorithms to Find More Appropriate Neutron Spectra, by Lowry, K.A. and Johnson, T.L., *Health Physics* 47:587-593

Random Mixed Modes Due to Fluctuations in the Belousov-Zhabotinskii Reaction, by Schwartz, I.B., *Physics Letters* 102A:25-31

Rapid Poisson Series Evaluation, by Harr, W.H. and Kaufman, B., *1982 AIAA/AAS Astrodynamics Conference in: Journal of Guidance, Control, and Dynamics* 7:755-757

Spectral Estimators that Extend the Maximum Entropy and Maximum Likelihood Methods, by Byrne, C.L.,* and Fitzgerald, R.M., *SIAM Journal of Applied Mathematics* 44:425-442

Stochastic Propagation of the Mutual Coherence Function in the Deep Ocean, by Baer, R.N., Perkins, J.S., Wright, E.B., and McCoy, J.J.,* *Journal of the Acoustical Society of America* 75:1407-1414

Technique for Evaluating Indefinite Integrals Involving Products of Certain Special Functions, by Piquette, J.C. and Van Buren, A.L., *SIAM Journal of Mathematical Analysis* 15:845-855

MECHANICS

Calculation of the Wall-Pressure Field in a Turbulent Channel Flow, by Handler, R.A., Hansen, R.J., Sakell, L., Orszag, S.A.,* and Bullister, E.,* *Physics of Fluids* 27:579-582

Current-Induced Loads on Marine Structures Due to Vortex Shedding, by Griffin, O.M., *Ocean Structural Dynamics Symposium '84, Proceedings*, Oregon State University, Corvallis, OR, pp. 457-471

Effects of Constraint Variation on the Fatigue Growth of Surface Flaws, by Jolles, M. and Tortoriello, V.,* *Fracture Mechanics: Fifteenth Symposium*, ASTM STP 833, American Society for Testing and Materials, Philadelphia, PA, pp. 300-311

Effects of Rolled Plate Thickness on Anisotropy, with Application to Acoustic Stress Measurement, by Mignogna, R.B., Clark, A.V., Rath, B.B., and Vold, C.L., *Nondestructive Methods for Material Property Determination*, Plenum Publishing Corp., NY, pp. 339-351

Finite Element Modeling of Surface Waves in a Channel, by Keramidas, G.A., Ramberg,

S.E. and Griffin, O.M., *Applied Mathematical Modelling* 8:297-304

Finite Element Solutions for the High Pressure Shock Tube, by Miner, E.W. and Skop, R.A., *Fifth International Symposium on Finite Elements and Flow Problems,* University of Texas, Austin, TX, pp. 401-406

Geometry Variations During Fatigue Growth of Surface Flaws, by Jolles, M. and Tortoriello, V.,* *Fracture Mechanics: Fourteenth Symposium - Volume I: Theory and Analysis,,* ASTM STP 791, American Society for Testing and Materials, Philadelphia, PA, pp. I-297-I-307

Laboratory Studies of Steep and Breaking Deep Water Waves, by Ramberg, S.E. and Griffin, O.M., *Proceedings of the Fifth Engineering Mechanics Division Specialty Conference,* University of Wyoming, Laramie, WY, pp. 712-715

Laminar-to-Turbulent Transition on a Body of Revolution with an Extended Favorable Pressure Gradient Forebody, by Hansen, R.J. and Hoyt, J.G.,* *Journal of Fluids Engineering* 106:202-210

On the Stability of Vortex Motions in the Presence of Magnetic Fields, by Fung, Y.T., *Physics of Fluids* 27:838-847

Pseudospectral Solution of One- and Two-Dimensional Inviscid Flows with Shock Waves, by Sakell, L., *AIAA Journal* 22:929-934

The Turbulent Wake of a Flat Plate Near a Free Surface, by Swean, T.F. and Keramidas, G.A., *Proceedings of the Second International Conference on Computational Methods and Experimental Measurements,* pp. 1-3-1-17

Unified Finite Element Approach for Dynamic Thermal Stress Analysis, by Keramidas, G.A. and Ting, E.C., *Proceedings of the 2nd International Conference on Computational Methods and Experimental Measurements,* pp. 8-95-8-101

Vortex-Induced Strumming Vibrations of Marine Cable with Attached Masses, by Vandiver, J.K.,* and Griffin, O.M., *Proceedings of the Third International Offshore Mechanics and Arctic Engineering Symposium,* American Society of Mechanical Engineers, NY, pp. 300-309

Vortex-Induced Strumming Vibrations of Marine Cables with Attached Masses, by Griffin, O.M. and Vandiver, J.K., *Journal of Energy Resources Technology* 106:458-465

METALLURGY

Abrasive Wear with Fine Diamond Particles of Carbide-Containing Aluminum and Titanium Alloy Surfaces, by Ayers, J.D., and Bolster, R.N., *Wear,* 93:193-205

Characterization of Oxide Scales on Complex Alloys Using Multiple Microanalytical Techniques, by Sprague, J.A., Singer, I.L., and Gossett, C.R., *Proceedings of the 42nd Annual Meeting of the Electron Microscopy Society of America,* San Francisco Press Inc., San Francisco, CA, pp. 600-603

Composition of Metals Implanted to Very High Fluences, by Singer, I.L., *Vacuum* 34:853-859

Crack Propagation Under Creep and Fatigue, by Sadananda, K., *Nuclear Engineering and Design* 83:303-323

Creep and Fatigue Crack Growth in Several Cast Superalloys, by Sadananda, K., and Shahinian, P.,* *5th International Conference on Superalloys,* TMS-AIME Meeting, Superalloys 1984, pp. 741-750

Development of a Navy Standard Test Method for Fatigue Crack Growth Rates in Marine Environments, by Crooker, T.W., Gill, S.J., Yoder, G.R., and Bogar, F.D., *Environment-Sensitive Fracture: Evaluation and Comparison of Test Methods,* ASTM STP 821, American Society for Testing and Materials, Philadelphia, PA, pp. 415-425

Effect of Elastic Anisotropy on Brittle Fracture of a Polycrystalline Solid, by Pande, C.S., and Masumura, R.A., *Proceedings of the Sixth International Conference on Fracture,* pp. 857-861

Effect of Neutron Irradiation on Fatigue and Creep-Fatigue Crack Propagation in Alloy 718 at 427°C, by Michel, D.J. and Smith, H.H., *Proceedings of the Third Topical Meeting on Fusion Reactor Materials in: Journal of Nuclear Materials,* 122&123:153-158

Effect of Sequential Load or Potential Changes on Stress Corrosion Cracking Behavior of Steels, by Fujii, C.T., *Environment-Sensitive Fracture: Evaluation and Comparison of Test Methods,* ASTM STP 821, American Society for Testing and Materials, Philadelphia, PA, pp. 383-398

Effects of Constraint Variation on the Fatigue Growth of Surface Flaws, by Jolles, M., and Tortoriello, V.,* *Fracture Mechanics:*

273

Fifteenth Symposium, ASTM STP 833, American Society for Testing and Materials, Philadelphia, PA, pp. 300-311

Factors Governing Near-Threshold Fatigue Crack Growth, by Sadananda, K., *Second International Conference on Fatigue and Fatigue Thresholds, Fatigue 84*, Vol. 1, pp. 543-554

Fatigue Crack Growth Behavior of an Oxide Dispersion Strengthened MA 956 Alloy, by Sadananda, K., and Shahinian, P., *Metallurgical Transactions A*, 15A:527-539

Formation of Metal Carbide Powder by Spark Machining of Reactive Metals, by Ayers, J.D. and Moore, K., *Metallurgical Society Transactions A*, Vol. 15A:1117-1127

Four Days "On-Line" at Japan's Photon Factory, by Skelton, E.F., *ONR Far East Scientific Bulletin*, 9:2:102-112

Geometry Variations During Fatigue Growth of Surface Flaws, by Jolles, M. and Tortoriello, V.,* *Fracture Mechanics: Fourteenth Symposium - Volume I: Theory and Analysis*, ASTM STP 791, American Society for Test and Materials, Philadelphia, PA, pp. I-297-I-307

Grooving and Off-Center Crack Effects on Applied-Moment Double-Cantilever-Beam Tests, by Wu, C.C., McKinney, K.R., and Lewis, D., *Journal of the American Ceramic Society*, 67:C-166-C-168

High Dose Ion Implantation and Corrosion Behavior of Ferrous Metals, by Sartwell, R.D.,* Wheeler, N.S.,* Hubler, G.K., McCafferty, E., and Clayton, C.R.,* *Ion Mixing and Surface Layer Alloying*, Noyes Publications, Park Ridge, NJ, pp. 128-140

High Resolution Electron Microscopy of Superconductors, by Pande, C.S., *Bulletin of Materials Science*, 6:453-458

Influence of Helium on Fatigue Crack Propagation in Neutron Irradiated Type 316 Stainless Steel, by Michel, D.J., *Journal of Nuclear Materials* 120:113-114

Influences of Marine Environment and Electrochemical Potential on Fatigue Crack Closure in a High Strength Steel, by Gill, S.J., Jolles, M.I., Htun, K.M.,* and Crooker, T.W., *Embrittlement by the Localized Crack Environment*, Metallurgical Society of AIME, Warrendale, PA, pp. 471-483

Interfaces in Metal Matrix Composites, by Arsenault, R.J.,* and Pande, C.S., *Scripta Metallurgica*, 18:1131-1134

Ion Mixing of Cr Layers on Steel: Effect of Impurities During Ion Mixing, by Grabowski, K.S., Colton, R.J., Chan, W.K.,* and Clayton, C.R.,* *Ion Mixing and Surface Layer Alloying*, Noyes Publications, Park Ridge, NJ, pp. 108-117

Effect of Microstructure, Strength and Oxygen Content on Fatigue Crack Growth Rate of Ti-4.5Al-5.0Mo-1.5Cr (Corona 5), by Yoder, G.R., Froes, F.H.,* and Eylon, D.,* *Metallurgical Transactions A*, 15A:183-197

Mechanical Properties of Laser Beam Welds, by Metzbower, E.A., Denney, P.E., Fraser, F.W., and Moon, D.W., *64th AWS Annual Meeting in: Welding Journal*, 63:39-43

Microstructure of ASTM A-36 Steel Laser Beam Weldments, by Strychor, R., Moon, D.W., and Metzbower, E.A., *Journal of Metals*, 36:59-61

Microwave Properties of $(Fe_{0.82}B_{0.18})_{0.90}La_{0.05}R_{0.05}$ Amorphous Metal Alloys, by Vittoria, C., Koon, N.C., Lubitz, L., and Geohegan, J.A., *Journal of Applied Physics*, 55:1741-1742

On the Role of Microstructure in the Growth of Fatigue Cracks, by Yoder, G.R., Cooley, L.A., and Crooker, T.W., *Fatigue 84, Proceedings of the Second International Conference on Fatigue and Fatigue Thresholds*, Vol. 1, Engineering Materials Advisory Services, Ltd, West Midlands, UK, pp. 351-360

Proceedings of Topical Conference on Ferritic Alloys for Use in Nuclear Energy Technologies, ed. by Davis, J.W.* and Michel, D.J., Metallurgical Society of AIME, Warrendale, PA

Review of Vacuum Metallization Including PVD and CVD, by Kim, C., *Proceedings of the Science and Technology Symposium '84*, Korean Federation of Science and Technology, Seoul, Korea, pp. 537-543

The Surface Binding Energy for a Ternary Alloy Produced by Ion Implantation, *International Conference on Atomic Collisions in Solids in: Nuclear Instruments and Methods in Physics Research*, 230:804-808

Theoretical Aspects of Fatigue and Creep Crack Growth, by Sadananda, K., *6th International Fracture Conference*, Vol. 1, pp. 211-234

Wear Behavior of Carbide-Injected Titanium and Aluminum Alloys, by Ayers, J.D., *Wear*, 97:249-266

274

Wear Improvement in Ti-6Al-4V by Ion Implantation, by Vardiman, R.G., *Ion Implantation and Ion Beam Processing, Materials Research Society Symposium Proceedings*, 27:699-704

NUCLEAR SCIENCE

Pressure Vessel Steels Under Neutron Irradiation. IAEA Group Examines Steels for Nuclear Reactor Pressure Vessels, by Steele, L.E., *European Scientific Notes* ESN 38-4:191-193

OCEAN SCIENCE AND TECHNOLOGY

All-Weather Millimeter Wave Imaging in the Marginal Ice Zone, by Hollinger, J.P., Troy, B.E., and Hartman, M.F.,* *Radio Science* 19:862-870

Contamination of Conductivity Measurements by Waterborne Particles, by Okawa, B.S. and Dugan, J.P., *Ocean Engineering* 11:265-279

Laboratory Studies of Steep and Breaking Water Waves, by Ramberg, S.E. and Griffin, O.M., *Proceedings of the Fifth Engineering Mechanics Division Specialty Conference*, EM Division/ASCE, pp. 712-715

Mass Transfer Between Gulf Stream Rings, by Mied, R.P. and Lindemann, G.J., *Journal of Geophysical Research* 89:6365-6372

Microwave Emission from High Arctic Sea Ice During Freeze-up, by Hollinger, J.P., Troy, B.E., Ramsier, R.O.,* Asmus, K.W.,* Hartman, M.F.,* and Luther, C.A.,* *Journal of Geophysical Research* 89:8104-8122

Millimeter Wave Radiometric Images of the Marginal Ice Zone, by Hollinger, J.P., Keller, M.R., Luther, C.A.,* and Ramsirer, R.O.,* *1984 International Geoscience and Remote Sensing Symposium*, IGARSS 84, ESA SP-215, Vol. 1, European Space Agency, Paris, pp. 353-358

Remote Sensing in Belgium, by Valenzuela, G.R., *European Scientific Notes* ESN 38-2:92-93

Surface-Wave Expression of Bathymetry over a Sand Ridge, by Gordon, C., Greenewalt, D., and Witting, J., *Remote Sensing of Shelf Sea Hydrodynamics*, Elsevier Science Pub-

lishers, Amsterdam, pp. 159-185

The Modification of the Modulation Transfer Function by Sea Slicks Measured by L-Band Radar, by Huhnerfuss, H.,* Lange, P.,* Schlude, F.,* and Garrett, W.D., *Proceedings of the 1984 International Geoscience and Remote Sensing Symposium*, ESA-215, Vol. 2, European Space Agency, Paris, pp. 715-719

The Variation of Fine Structure Within a Gulf Stream Ring, by Mied, R.P. and Lindemann, G.J., *Journal of Geophysical Research* 89:3447-3456

OPTICAL SCIENCES

A High Performance Photo-Emitter Membrane Spatial Light Modulator, by Fisher, A.D., Ling, L.C., and Lee, J.N., *Spatial Light Modulators and Applications*, SPIE, Vol. 465, Society of Photo-Optical Instrumentation Engineers, Bellingham, WA, pp. 36-45

Aging Properties of Kodak Type 101 Emulsions, by Dohne, B., Feldman, U., and Neupert, W.,* *Applied Optics* 23:589-596

An Ultrahigh Vacuum Angular Encoder with Microradian Resolution, by Rife, J.C., *Third National Conference on Synchrotron Radiation Instrumentation in: Nuclear Instruments and Methods in Physics Research* 222:279-283

Attaching Single Mode Polarization Preserving Fiber to Single Mode Semiconductor Lasers, by Miles, R.W., Ceruzzi, A.,* and Marrone, M.J., *Applied Optics* 23:1096-1097

Bending Effects in Optical Fibers, by Taylor, H.F., *Journal of Lightwave Technology* LT-2:617-628

Bragg Diffraction of Light by Magnetostatic Waves as a Basis for Magneto-Optical Devices, by Fisher, A.D. and Lee, J.N., *International Magnetics Conference*, '84 Intermag Digest, North-Holland, NY, pp. FB-02

Characteristics of Compressional Shocks Resulting from Picosecond Heating of Confined Foils, by Schoen, P.E. and Campillo, A.J., *Applied Physics Letters* 45: 1049-1051

Characteristics of Ti-Indiffused Waveguides in MgO-Doped LiNbO₃, by Bulmer, C.H., *Electronics Letters* 20:902-904

Coherence Properties of Some Isotropic Planar Sources, by Carter, W.H., *Journal of the Optical Society of America A* 1:716-722

Detection Scheme in a Fiber-Optic Magnetic-Field Sensor Free from Ambiguity Due to Material Magnetic Hysteresis, by Koo, K.P. and Sigel, G.H., *Optics Letters* 9:257-259

Direct Problem of Image Processing, by Szu, H.H., *Journal of Mathematical Physics* 25:2773-2779

Effect of Low Dose Rate Irradiation on Doped Silica Core Optical Fibers, by Friebele, E.J., Askins, C.G., and Gingerich, M.E., *Applied Optics* 23:4202-4208

Effect of Relative Humidity on the Aerosol Backscattering Coefficient at 0.694- and 10.6-μm Wavelengths, by Fitzgerald, J.W., *Applied Optics* 23:411-418

Extended Precision in Video-Bandwidth Analogue/Digital Converters Using Optical Techniques, by Taylor, H.F., *Electronics Letters* 20:352-353

Factor Analysis of Raman Spectra of Polyethylene Under High Pressure, by Shih, L.B.,* and Priest, R.G., *Applied Spectroscopy* 38:687-692

Fiber and Integrated Optical Devices for Signal Processing, by Taylor, H.F., *New Directions in Guided Wave and Coherent Optics*, Vol. II, NATO Advanced Study Institute Series E, no. 79, Martinus Nijhoff Publishers, Boston, MA, pp. 437-448

Fiberoptic Gyroscopes, by Burns, W.K., *Laser Focus/Electro-Optics* 20:83-94

Fibre Optical Sensors, by Giallorenzi, T.G., *New Directions in Guided Wave and Coherent Optics*, Vol. I, NATO Advanced Studies Institute Series E, no. 78, Martinus Nijhoff Publishers, Boston, MA, pp. 225-245

Fibre-Optic Recirculating Analogue Delay Line, by Wang, C.C., Moeller, R.P., Burns, W.K., and Kaminow, I.P., *Electronic Letters* 20:486-488

Fields Generated by Homogeneous and by Quasi-Homogeneous Planar Secondary Sources, by Wolf, E.,* and Carter, W.H., *Optics Communications* 50:131-136

Focal Shift for a Gaussian Beam: An Experimental Study, by Sucha, G.D.,* and Carter, W.H., *Applied Optics* 23:4345-4347

Frequency Response of a Single-Mode Optical Fiber Phase Modulator Utilizing a Piezoelectric Plastic Jacket, by Jarzynski, J., *Journal of Applied Physics* 55:3243-3250

Grain Boundary Diffusion of Liquid Metal Coolants in Optical Materials for Use with High Power Synchrotron Radiation, by Hunter, W.R.,* and Williams, R.T., *Instrumentation for Synchrotron Radiation in: Nuclear Instruments and Methods in Physics Research* 222:359-363

Higher-Order Suppression in an On-Blaze, Plane-Grating Monochromator, by Hunter, W.R.,* and Rife, J.C., *Applied Optics* 23:293-299

Inverse Problem of Image Processing, by Szu, H.H., *Journal of Mathematical Physics* 25:2767-2772

Linear Interferometric Modulators in Ti:LiNbO$_3$, by Bulmer, C.H. and Burns, W.K., *Journal of Lightwave Technology* LT-2:512-521

Molecular Discrimination and Contrast Enhancement Using a Scanning Coherent Anti-Stokes Raman Microscope, by Duncan, M.D., *Optics Communications* 50:307-312

Nonlinear Optical Parametric Processes in Liquids and Gases, by Reintjes, J.F., Academic Press, NY

Object Identification from Images of Variable Scale, by Lahart, M.J., *Applications of Digital Image Processing VI*, SPIE, Vol. 432, Society of Photo-Optical Instrumentation Engineers, Bellingham, WA, pp.253-261

Object Identification from Images of Variable Scale, by Lahart, M.J.,* *Optical Engineering* 23:710-715

Optical Fiber Waveguides in Radiation Environments, II., by Friebele, E.J., Askins, C.G.,* Gingerich, M.E., and Long, K.J.,* *Proceedings of the 2nd International Conference on Radiation Effects in Insulators in: Nuclear Instruments & Methods in Physics Research* 229(b1):355-369

Optical Processing Using Outer-Product Concepts, by Athale, R.A. and Lee, J.N., *Proceedings of the IEEE* 72:931-941

Optical-Magnetostatic Wave Interaction for Spectrum Analysis, by Lee, J.N., and Fisher, A.D. *Optical Technology for Microwave Applications*, SPIE, Vol. 477, Society of Photo-Optical Instrumentation Engineers, Bellingham, WA, pp. 36-43

Picosecond Optical Control of Transferred-Electron Devices, by Carruthers, T.F., *Picosecond Optoelectronic Devices*, Academic

Press, NY, pp. 339-371

Polarization Properties of Birefringent Fibers with Stress Rods in the Cladding, by Marrone, M.J., Rashleigh, S.C., and Blaszyk, P.E.,* *Journal of Lightwave Technology* LT-3:155-160

Polarizer Requirements for Fiber Gyroscopes with High-Birefringence Fiber and Broad-Band Sources, by Burns, W.K. and Moeller, R.P., *Journal of Lightwave Technology* LT-2:430

Radiation Response Optical Fibers and Selfoc Microlenses at 1.3 μm, by Friebele, E.J., Long, K.J.,* Askins, C.G.,* and Gingerich, M.E., *Fiber Optics in Adverse Environments*, SPIE, Vol. 506, Society of Photo-Optical Instrumentation Engineers, Bellingham, WA, pp. 202-208

Readout Mechanisms for Focal Plane Arrays, by Milton, A.F., *Infrared Detectors*, SPIE, Vol. 443, Society of Photo-Optical Instrumentation Engineers, Bellingham, WA, pp. 112-119

Removal of Fe, Co, Ni, and Cu from Zr for 0.01-dB/km Fluoride Optical Fibers, by Klein, P.H., Nordquist, P.E.R., and Singer, A., *Infrared Optical Materials and Fibers III*, SPIE, Vol. 484, Society of Photo-Optical Instrumentation Engineers, Bellingham, WA, pp. 90-92

Simultaneous Image Processing and Feature Extraction for Two-Dimensional Non-Uniform Sensors, by Messner, R.A.,* and Szu, H.H., *Intelligent Robots: Third International Conference on Robot Vision and Sensory Control RoViSeC3, Part 2*, SPIE, Vol. 449, Society of Photo-Optical Instrumentation Engineers, Bellingham, WA, pp. 693-710

Technique for Elimination of Polarization Fading in Fibre Interferometers, by Frigo, N.J., Dandridge, A., and Tveten, A.B., *Electronics Letters* 20:319-320

The Fabry-Perot Etalon as an RF Frequency Channelizer, by Alexander, E.M. and Gammon, R.W.,* *Solid State Optical Control Devices*, SPIE, Vol. 464, Society of Photo-Optical Instrumentation Engineers, Bellingham, WA, pp. 45-52

Thermal Bleaching of X-Ray-Induced Defect Centers in High Purity Fused Silica by Diffusion of Radiolytic Molecular Hydrogen, by Griscom, D.L., *Journal of Non-Crystalline Solids* 68:301-325

Thermal Phase Compensation in Fiber-Optic Interferometers, by Dandridge, A. and Tveten, A.B., *Journal of Lightwave Technology* LT-2:73-75

Ultra-Low Loss Optical Fibers: An Overview, by Sigel, G.H., and Tran, D.C., *Infrared Optical Materials and Fibers III*, SPIE, Vol. 484, Society of Photo-Optical Instrumentation Engineers, Bellingham, WA, pp. 2-6

PLASMA PHYSICS

A Novel X-Ray Backlighting Method for Measuring Areal Densities of Rayleigh-Taylor Unstable, Ablatively Driven Targets, by Grun, J. and Kasenjar, S., *Applied Physics Letters* 44:497-499

A Unified Theory of the Diocotron, Cyclotron Maser and Negative-Mass Instabilities, by Lau, Y.Y., *IEEE Transactions on Electron Devices* ED-31:329-337

Analysis of Stability and Symmetry Implications for ICF, by Gardner, J.H., Bodner, S.E., Boris, J.P., Emery, M.H., Fritts, M.J., and Herbst, M.J., *Laser-Interaction and Related Plasma Phenomena*, Vol. 6, Plenum Press, NY, pp. 673-691

Axisymmetric Instabilities of Propagating Relativistic Electron Beams, by Joyce, G., Lampe, M., Hubbard, R.F., and Fernsler, R., *Beams '83, Fifth International Conference on High-Power Particle Beams*, Lawrence Livermore National Laboratory, Livermore, CA, p. 382

Beam Current Limitations Due to Instabilities in Modified and Conventional Betatrons, by Sprangle, P. and Chernin, D.,* *Particle Accelerators* 15:35-45

Characteristics of an Atmospheric Discharge Plasma as an RF Antenna, by Dwyer, T.,* Greig, J.R., Murphy, D.P.,* Perin, J.M.,* Pechacek, R.E., and Raleigh, M., *IEEE Transactions on Antennas and Propagation* AP-32:141-146

Collective Ion Acceleration by a Reflexing Electron Beam: Model and Scaling, by Mako, F. and Tajima, T.,* *Physics of Fluids* 27:1815-1820

Compact Toroid Created by Rotating Relativistic Electron Beams, by Sethian, J.D., Robson, A.E., Gerber, K.A., and DeSilva, A.W.,* *Journal of Applied Physics* 55:3280-3285

277

Comparison of Atomic Potentials and Eigen-values in Strongly Coupled Neon Plasmas, by Cauble, R.,* Blaha, M.,* and Davis, J., *Physical Review A* 29:3280-3287

Current Distribution in a Plasma Erosion Opening Switch, by Weber, B.V.,* Commisso, R.J., Meger, R.A., Neri, J.M., Oliphant, W.F., and Ottinger, P.F.,* *Applied Physics Letters* 45:1043-1045

Current Limitations Due to Instabilities in Modified and Conventional Betatrons, by Sprangle, P., *Beams '83, Fifth International Conference on High-Power Particle Beams,* Lawrence Livermore National Laboratory, Livermore, CA, p. 481

Dense Z-Pinch for Fusion, ed. by Sethian, J.D. and Gerber, K.A., *Dense Z-Pinch for Fusion Proceedings,* Naval Research Laboratory, Washington, D.C.

Density Measurement in a Vacuum-Spark-Discharge Microplasma from the Inner-Shell Excitation of Satellite Transitions, by Seely, J.F. and Lee, T.N., *Physical Review A* 29:411-414

Dynamics of a High-Current Electron Ring in a Conventional Betatron Accelerator, by Kapetanakos, C.A., Marsh, S.J.,* and Sprangle, P., *Particle Accelerator* 44:261-279

Electrostatic Ion-Cyclotron Waves in Magneto-spheric Plasmas: Nonlocal Aspects, by Ganguli, G.,* Bakshi, P.,* and Palmadesso, P., *Journal of Geophysical Research* 89:945-952

Emittance Growth in a Modified Betatron Crossing the Orbital-Turning-Point Transition, by Haber, I., Marsh, S.J.,* and Sprangle, P., *Beams '83, Fifth International Conference on High-Power Particle Beams,* Lawrence Livermore National Laboratory, Livermore, CA, p. 485

Excitation of the Plasma Waves in the Laser Beat Wave Accelerator, by Tang, C.M., Sprangle, P., and Sudan, R.N.,* *Applied Physics Letters* 45:375-377

External Injection into a High-Current Modified Betatron Accelerator, by Mako, F., Manheimer, W., Kapetanakos, C.A., Chernin, D.,* and Sandel, F.,* *Physics of Fluids* 27:2211-2214

Fast Collisionless Tearing in an Anisotropic Neutral Sheet, by Chen, J.,* Palmadesso, P.J., Fedder, J.A., and Lyon, J.G., *Geophysical Research Letters* 11:12-15

278 Finite Geometry Effects on the Stability of a

Charged Beam Propagating Through a Relativistic Annular Electron Beam, by Ganguli, G.* and Palmadesso, P., *Journal of Applied Physics* 55:2715-2720

General Model of Streamer Propagation, by Fernsler, R.F.,* *Physics of Fluids* 27:1005-1012

Generation of High Frequency Radiation by Quasi Optical Gyrotron at Harmonics of the Plasma Frequency, by Levush, B.,* and Manheimer, W.M., *IEEE Transactions on Microwave Theory and Techniques* MTT-32:1398

Generation of a Modulated Intense Relativistic Electron Beam with a Frequency Tunable by a Magnetic Field, by Friedman, M. and Serlin, V., *Review of Scientific Instruments* 55:1074-1076

Generation of a Monochromatic-High-Frequency (>100 mHz) Electrical Pulses with Peak Power $\sim 10^{10}$ Watts, by Friedman, M. and Serlin, V., *Proceedings of the 1984 Sixteenth Power Modulator Symposium,* IEEE, NY, pp. 172-181

High-Intensity Laser Absorption in Longer-Scalelength Plasmas, by Herbst, M.J., Young, F.C., Stamper, J.A., Kearney, K.J.,* Green, J.,* Gardner, J.H., Obenschain, S.P., McLean, E.A., and Ripin, B.H., *Radiation in Plasmas* 1, 1983, College of Plasma Physics, Trieste, World Scientific, Singapore, pp. 407-422

High-Power Electron-Beam Controlled Switches, by Commisso, R.J., Fernsler, R.F., Scherrer, V.E., and Vitkovitsky, I.M., *Review of Scientific Instruments* 55:1834-1840

Hydrodynamics Simulations of Light Ion Beam-Matter Interactions: Ablative Acceleration of Thin Foils, by DeVore, C.R., Gardner, J.H., Boris, J.P., and Mosher, D., *Laser and Particle Beams* 2:227-243

Influence of Lyman-Series Fine-Structure Opacity in the K-Shell Spectrum and Level Populations of Low-to-Medium-Z Plasmas, by Apruzese, J.P., Davis, J., Duston, D., and Clark, R.W., *Physical Review A* 29:246-253

Influence of Magnetic Shear on the Collisional Current-Driven Ion Cyclotron Instability, by Satyanarayana, S.,* Ganguli, G.,* and Ossakow, S.L., *Plasma Physics and Controlled Fusion* 26:1333-1342

Injection and Extraction of a Relativistic Electron Beam in a Modified Betatron, by Hui,

B. and Lau, Y.Y., *Physical Review Letters* 53:2024-2027

Interaction of a Modulated Intense Relativistic Electron Beam with a Cavity, by Friedman, M. and Serlin, V.,* *Applied Physics Letters* 44:394-395

Laser-Plasma Interaction Experiments and Diagnostics at NRL, by Ripin, B.H., Grun, J.,* Herbst, M.J., Kacenjar, S.T., McLean, E.A., Obenschain, S.P., Stamper, J.A., Whitlock, R.R., and Young, F.C., *Laser Interactions & Related Plasma Phenomena*, Vol. 6, Plenum Publishing Corp., NY, pp. 235-252

Long Wavelength Limit of the Current Convective Instability, by Huba, J.D., *Journal of Geophysical Research* 89:2931-2935

MHD Instabilities in Simple Plasma Configuration, by Manheimer, W.M. and Lashmore-Davies, C.,* Naval Research Laboratory, Washington, D.C.

Magnetic Field Measurements in Tokamak Plasmas, by Feldman, U., Seely, J.F., Sheeley, N.R., Suckewer, S.,* and Title, A.M.,* *Journal of Applied Physics* 56:2512-2518

NRL Capillary Z-Pinch Experiment, by Sethian, J.D., Gerber, K.A., DeSilva, A.W.,* and Robson, A.E., *Dense Z-Pinch for Fusion Proceedings*, Naval Research Laboratory, Washington, D.C., pp. 37-45

Nonlinear Mode Coupling Theory of the Lower-Hybrid-Drift Instability, by Drake, J.F.,* Guzdar, P.N.,* Hassam, A.B.,* and Huba, J.D., *Physics of Fluids* 27:1148-1159

Nonlinear Theory of the E × B Instability with an Inhomogeneous Electric Field, by Keskinen, M.J., *Journal of Geophysical Research* 89:3913-3920

Nonlocal Effects on the Convective Properties of the Electrostatic Current-Driven Ion-Cyclotron Instability, by Ganguli, G.,* Bakshi, P.,* and Palmadesso, P., *Physics of Fluids* 27:2039-2042

O^+ Acceleration Due to Resistive Momentum Transfer in the Auroral Field Line Plasma, by Mitchell, H.G.* and Palmadesso, P.J., *Journal of Geophysical Research* 89:7573-7576

Observation of Magnetic Fields in Laser-Produced Plasma Using the Zeeman Effect, by McLean, E.A., Stamper, J.A., Manka, C.K.,* Griem, H.R.,* Droemer, D.W.,* and Ripin, B.H., *Physics of Fluids* 27:1327-1335

Observation of Rayleigh-Taylor-like Structures

in a Laser-Accelerated Foil, by Whitlock, R.R., Emery, M.H., Stamper, J.A., McLean, E.A., Obenschain, S.P., and Peckerar, M.C., *Physical Review Letters* 52:819-822

Observation of the Rayleigh-Taylor Instability in Ablatively Accelerated Foils, by Grun, J., Emery, M.H., Kacenjar, S., Opal, C.B., McLean, E.A., Obenschain, S.P., Ripin, B.H., and Schmitt, A., *Physical Review Letters* 53:1352-1355

Plasma Current and Conductivity Effects on Hose Instability, by Lampe, M., Sharp, W.,* Hubbard, R.F.,* Lee, E.P.,* and Brigg, R.J.,* *Physics of Fluids* 27:2921-2936

Plasma Sources for X-Ray Lithography, by Nagel, D.J., *VLSI Electronics: Microstructure Science*, Vol. 8, Academic Press, NY, pp. 137-170

Quasi Steady State Multi-Plasma-Cloud Configurations in the F Region Ionosphere, by Chen, J.,* Satyanarayana, P.,* and Ossakow, S.L., *Journal of Geophysical Research* 89:6787-6792

Radiative Relaxation Rates for Individual 15-μ CO_2 Lines in the Upper Stratosphere and Lower Mesosphere, by Apruzese, J.P. and Strobel, D.F., *Journal of Geophysical Research* 89:7187-7194

Rayleigh-Taylor Growth Rate Scaling for Laser Ablated Plasmas, by Manheimer, W.M. and Colombant, D.G., *Physics of Fluids* 27:1927-1928

Rayleigh-Taylor Instability in the Presence of a Stratified Shear Layer, by Satyanarayana, P.,* Guzdar, P.N.,* Huba, J.D., and Ossakow, S.L., *Journal of Geophysical Research* 89:2945-2954

Relativistic Electron Beam Equilibrium in the Presence of a Gas Channel, by Hui, B. and Lampe, M., *Beams '83, Fifth International Conference on High-Power Particle Beams*, Lawrence Livermore National Laboratory, Livermore, CA, p. 374

Repetitively Pulsed-Plasma Soft X-Ray Source, by Nagel, D.J., Brown, C.M., Peckerar, M.C., Ginter, M.L.,* Robinson, J.A.,* McIlrath, T.J.,* and Carroll, P.K.,* *Applied Optics* 23:1428-1433

Resistive Instabilities of Propagating Electron Beams, by Lampe, M., Joyce, J., and Hubbard, R.F.,* *Beams '83, Fifth International Conference on High-Power Particle Beams*, Lawrence Livermore National Laboratory, Livermore, CA, p. 336

279

Rippled Wall Mode Converters for Circular Waveguides, by Levine, J.S., *International Journal of Infrared and Millimeter Waves* 5:937-952

Self-Modulation of an Intense Relativistic Electron Beam, by Friedman, M., Serlin, V., Drobot, A.,* and Seftor, L.,* *Journal of Applied Physics* 56:2459-2474

Slab Model for Rayleigh-Taylor Stabilization by Vortex Shedding, Compressibility, Thermal Conduction, and Ablation, by Manheimer, W.M. and Colombant, D.G., *Physics of Fluids* 27:983-993

Stability of Laminar Electron Layers, by Chernin, D.* and Lau, Y.Y., *Physics of Fluids* 27:2319-2331

Stabilization of the Negative Mass Instability in a Rotating Relativistic Electron Beam, by Lau, Y.Y. and Chernin, D.,* *Physical Review Letters* 52:1425-1428

Status of Light Ion Inertial Fusion Research at NRL, by Cooperstein, G., Ottinger, P.F.,* Goldstein, S.A.,* Barker, R.J.,* Colombant, D.G., Meger, R.A.,* Neri, J.M.,* Moshger, D., Sandel, F.L.,* Stephanakis, S.J., and Young, F.L., *Laser Interaction and Related Plasma Phenomena*, Vol. 6, Plenum Press, NY, pp. 957-979

Symmetry, Stability, and Efficiency in Direct Drive Laser Fusion, by Bodner, S., Emery, M., Gardner, J., Grun, J., Herbst, M., Kacenjar, S., Lehmberg, R., Manka, C., McLean, E., Obenschain, S., Ripin, B., Schmitt, A., Stamper, J., and Young, F., *Tenth International Conference on Plasma Physics and Controlled Nuclear Fusion*, IAEA-CN-44, International Atomic Energy Agency, p. 1

Tearing Instability in an Anisotropic Neutral Sheet, by Chen, J.* and Palmadesso, P., *Physics of Fluids* 27:1198-1206

Temporal Evolution of Whistler Growth in a Cold Plasma Injection Experiment, by Ganguli, G.,* Palmadesso, P., and Fedder, J., *Journal of Geophysical Research* 89:7351-7355

The Dense Z-Pinch as a Fusion Reactor, by Robson, A.E., *Dense Z-Pinch for Fusion*, pp. 2-12

The Role of Finite Parallel Length on the Stability of Barium Clouds, by Sperling, J.L.,* Drake, J.F.,* Zalesak, S.T., and Huba, J.D., *Journal of Geophysical Research* 89:10913-10919

Theoretical Modeling of the Plasma Erosion Opening Switch for Inductive Storage Applications, by Ottinger, P.F.,* Goldstein, S.A.,* and Meger, R.A., *Journal of Applied Physics* 56:774-784

Three-Dimensional, Nonlinear Evolution of the Rayleigh-Taylor Instability of a Thin Layer, by Colombant, D., Manheimer, W., and Ott, E.,* *Physical Review Letters* 53:446-449

Three-Dimensional, Nonlinear Evolution of the Rayleigh-Taylor Instability of a Thin Layer, by Manheimer, W., Colombant, D., and Ott, E.,* *Physics of Fluids* 27:2164-2175

Velocity Shear Stabilization of the Current Convective Instability, by Satyanarayana, P.* and Ossakow, S.L., *Journal of Geophysical Research* 89:3019-3022

Vortex Shedding Due to Laser Ablation, by Emery, M.H., Gardner, J.H., Boris, J.P., and Cooper, A.L., *Physics of Fluids* 27:1338-1340

RADAR

A Compact Flush-Mounting Antenna with Direction Finding and Steerable Cardioid Pattern Capability, by Coleman, H.P. and Wright, B.D., *IEEE Transactions on Antennas and Propagation* AP-32:412-414

A Comparative Study of Linear Array Synthesis Technique Using a Personal Computer, by Burns, M.A.,* Laxpati, S.R., and Shelton, J.P., *Proceedings of the 1983 Antenna Application Symposium*, Vol. II, RADC-TR-84-52, Rome Air Development Center, Griffiss AFB, NY, pp. 7-20

A Comparative Study of Linear Array Synthesis Technique Using a Personal Computer, by Burns, M.A.,* Laxpati, S.R.,* and Shelton, J.P.,* *IEEE Transactions on Antennas and Propagation* AP-32:884-887

A Technique for Estimating RMS Waveshift and Dominant Wave Period Using a Coherent Shipboard Radar, by Trizna, D.B. and Porter, D.L.,* *Oceans '84 Conference Record*, Vol. 1, IEEE, NY, pp. 134-137

Adaptive MTI and Doppler Filter Bank Clutter Processing, by Kretschmer, F.F., Lewis, B.L., and Lin, F.C., *Proceedings of the IEEE National Radar Conference*, IEEE, NY, pp. 69-73

An Improved Dual-Frequency Technique for the Remote Sensing of Ocean Currents and Wave Spectra, by Schuler, D.L. and Eng, W.P., *Proceedings of Commission F Symposium on Frontiers of Remote Sensing of the Oceans and Troposphere from Air and Space Platforms*, NASA Conference Publication 2303, NTIS, Alexandria, VA, pp. 199-214

Bicollimated Gregorian Reflector Antenna, by Rao, J.B.L., *IEEE Transactions on Antennas and Propagation* AP-32:147-154

Complex Frequency Poles of Radar Scattering from Coated Conducting Spheres, by Howell, W.E. and Uberall, H.,* *IEEE Transactions on Antennas and Propagation* AP-32:624-627

Electromagnetic Bias of 10-GHz Radar Altimeter Measurements of MSL, by Choy, L.W., Hammond, D.L.,* and Uliana, E.A., *Marine Geodesy* 8:297-312

End-fire Hybrid Array Antennas, by Kahn, W.K., *IEEE Transactions on Antennas and Propagation* AP-32:36-43

Normalized Relationship Among Errors and Sidelobe Levels, by Hsiao, J.K., *Radio Science* 19:292-302

On Eigenvalues, SINR, and Element Patterns in Adaptive Arrays, by Compton, R.T., *IEEE Transactions on Antennas and Propagation* AP-32:643-647

Performance of a Range-Ambiguous MTI and Doppler Filter System, by Hsiao, J.K., *Proceedings of the IEEE National Radar Conference*, IEEE, NY, pp. 95-99

Synthesis of Hexagonal and Square Arrays Using Discrete Convolution, by Shelton, J.P.* and Laxpati, S.R.,* *Radio Science* 19:1229-1237

The Dual-Frequency Scatterometer Re-examined, by Plant, W.J. and Reeves, A.B., *Proceedings of Commission F Symposium on Frontiers of Remote Sensing of the Oceans and Troposphere from Air and Space Platforms*, NASA Conference Publication 2303, NTIS, Alexandria, VA, pp. 193-198

RADIATION TECHNOLOGY

A High Energy Gamma Ray Calibration Source, by King, K.J. and Johnson, T.L., *Nuclear Instruments and Methods in Physics Research* 227:257-258

Advantages of Using a PMOS FET Dosimeter in High-Dose Radiation Effects Testing, by August, L.S. and Circle, R.R., *1984 Annual Conference on Nuclear and Space Radiation Effects in: IEEE Transactions on Nuclear Science* NS-31:1113-1115

Binary Collision Cascade Calculation of Sputtering from Cu-Ni Alloys by 90 keV Cu and Ni Ions, by Rosen, M. and Bassel, R.H., *Proceedings of the 10th International Conference on Atomic Collisions in Solids in: Nuclear Instruments and Methods in Physics Research* 230:592-595

Boltzmann Approach to Cascade Mixing, by Manning, I., *Ion Implantation and Ion Beam Processing, Materials Research Society Symposium Proceedings* 27:91-95

Comments on "Simple Explanation of a Well-Known Collision Experiment", by Piquette, J.C. and Wu, M.S.,* *American Journal of Physics* 52:83

Design Criteria for a High-Dose MOS Dosimeter for Use in Space, by August, L.S., *1983 IEEE Nuclear Science Symposium in: IEEE Transactions on Nuclear Science* NS-31:801-803

Effects of Large Angular Moments on the Fission Properties of Pt Isotopes, by Glagola, B.G., Back, B.B.,* and Betts, R.R.,* *Physical Review C* 29:486-497

Energy-Dispersive X-Ray Diffraction with Synchrotron Radiation at Cryogenic Temperatures, by Skelton, E.F., Webb, A.W., Qadri, S.G.,* Wolf, S.A., Lacoe, R.C.,* Feldman, J.L., Elam, W.T., Carpenter, E.R., and Huang, C.Y.,* *Review of Scientific Instruments* 55:849-855

Fragment Mass, Energy, and Angular Distributions for the 12C (^{4}He, Heavy Ion) Reaction Between 49 and 159 MeV, by Gokmen, A.,* Breuer, H.,* Mignerey, A.C.,* Glagola, B.G., Kwiatkowski, K.,* and Viola, V.E.,* *Physical Review C* 29:1595-1605

Low Level Tritium Detection Using Accelerator Mass Spectrometry, by Glagola, B.G., Phillips, G.W., Marlow, K.W., Myers, L.T.,* and Omohundro, R.J.,* *Third International Symposium on Accelerator Mass Spectrometry in: Nuclear Instruments in Methods in Physics Research* 233(B5):221-225

Predicting Single Event Upsets in the Earth's Proton Belts, by Bendel, W.L. and Petersen, E.L., *1984 Annual Conference on*

Nuclear and Space Radiation Effects in: IEEE Transactions on Nuclear Science NS-31:1201-1205

Production of a "Standard" Radiation Environment to Minimize Dosimetry Errors in Flash X-Ray Parts Testing, by Dozier, C.M. and Brown, D.B., *1984 Annual Conference on Nuclear and Space Radiation Effects in: IEEE Transactions on Nuclear Science* NE-31:1084-1088

Retention of Ions Implanted at Non-Normal Incidence, by Hartley, N.E.W.,[*] Grabowski, K.S., Gossett, C.R., and Manning, I., *Ion Implantation and Ion Beam Processing, Materials Research Society Symposium Proceedings* 27:615-620

Single Event Upset Rate Predictions for Complex Logic Systems, by Diehl-Hagle, S.E.,[*] Vinson, J.E.,[*] and Petersen, E.L., *1984 Annual Conference on Nuclear and Space Radiation Effects in: IEEE Transactions on Nuclear Science* NS-31:1132-1138

Statistical Analysis of Step Stress Measurements in Hardness Assurance, by Namenson, A.I., *Annual Conference on Nuclear and Space Radiation Effects in: IEEE Transactions on Nuclear Science* NS-32:1398-1401

The Total Dose Dependence of the Single Event Upset Sensitivity of IDT Static RAMs, by Campbell, A.B. and Stapor, W.J., *1984 Annual Conference on Nuclear and Space Radiation Effects in: IEEE Transactions on Nuclear Science* NS-31:1175-1177

Vibrational Enhancement of Total Breakup Cross Sections, by Haftel, M.I. and Lim, T.K.,[*] *Few Body Problems in Physics,* Vol. II, Contributed Papers, Elsevier Science Publishers, NY, pp. 329-330

SOLID STATE

A Eutectic Dislocation Etch for Gallium Arsenide, by Lessoff, H. and Gorman, R., *Journal of Electronic Materials* 13:733-739

A Statistical Study of Inclusions and Fracture in a Ferritic Steel, by Gilmore, C.M.,[*] Provenzano, V., Sprague, J.A., and Smidt, F.A., *Topical Conference on Ferritic Alloys for Use in Nuclear Energy Technologies Proceeding,* Metallurgical Society of AIME, Warrendale, PA, pp. 405-410

All Refractory, High T_c Josephson Device Technology, by Cukauskas, E.J., Nisenoff,

M., Jillie, D.W.,[*] Kroger, H.,[*] and Smith, L.R.,[*] *Advances in Cryogenic Engineering* 30:547-558

Amorphous Silicon Produced by Ion Implantation: Effects of Ion Mass and Thermal Annealing, by Waddell, C.N.,[*] Spitzer, W.G.,[*] Fredrickson, J.E.,[*] Hubler, G.K., and Kennedy, T.A., *Journal of Applied Physics* 55:4361-4366

Analytical Transmission Electron Microscopy of Multifilamentary V_3G Superconducting Wires, by Pande, C.S., Smith, S.,[*] Francavilla, T.L., and Gubser, D.U., *Proceedings of the 42nd Annual Meeting of the Electron Microscopy Society of America,* San Francisco Press, San Francisco, CA, pp. 494-495

Boundary Scattering Effects in High Field Transport in Submicron Structures, by Greene, R.F., Grubin, H.L.,[*] and Iafrate, G.J.,[*] *The Physics of Submicron Structures,* Plenum Press, NY, pp. 333-339

"Buffer-Layer" Technique for the Growth of Single Crystal SiC on Si, by Addamiano, A. and Sprague, J.A., *Applied Physics Letters* 44:525-527

Characteristics of the Material Improvement Process for Silicon on Sapphire by Solid Phase Epitaxial Regrowth, by Richmond, E.D., Knudson, A.R., Magee, T.,[*] Kawayoshi, H.,[*] and Leung, C.,[*] *American Vacuum Society 30th Meeting in: Journal of Vacuum Science and Technology A* 2:569-573

Characterization of Three E'-Center Variants in X- and γ-Irradiated High Purity a-SiO_2, by Griscom, D.L., *Proceedings of the 2nd International Conference on Radiation Effect in Insulators in: Nuclear Instruments & Methods in Physics Research* 229(B1):481-488

Charge Collection in Ge/As Test Structure, by McNulty, P.J.,[*] Abdel-Kader, W.,[*] Campbell, A.B., Knudson, A.R., Shapiro, P., Eison, F.,[*] and Roosild, S.,[*] *1984 Annual Conference on Nuclear and Space Radiation Effects in: IEEE Transactions on Nuclear Science* NS-31:1128-1131

Charge Collection in Multilayers, by Knudson, A.R., Campbell, A.B., Shapiro, P., Stapor, W.J., Wolicki, E.A., Petersen, E.L., Diehl-Nagle, S.E.,[*] Hauser, J.,[*] and Dressendorfer, P.V.,[*] *1984 Annual Conference on Nuclear and Space Radiation Effects in: IEEE Transactions on Nuclear Science* NS-31:1149-1154

Comparison of Heat-Pulse and Furnace Isothermal Anneals of Be Implanted InP, by Molnar, B., Kelner, G., Ramseyer, G.O., Morrison, G.H.,* and Shatas, S.C.,* *Ion Implantation and Ion Beam Processing of Materials*, Materials Research Society Symposia Proceedings, Vol. 27, North-Holland, NY, pp. 329-334

Comparison of Pulsed Laser and Furnace Annealing of Nitrogen Implanted Silicon, by Smith, T.P., Stiles, P.J.,* Augustyniak, W.M.,* Brown, W.L.,* Jacobson, D.C.,* and Kant, R.A., *Energy Beam-Solid Interactions and Transient Thermal Processing*, Materials Research Society Symposia Proceedings, Vol. 23, North-Holland, NY, pp. 453-458

Comparison of Pulsed Laser and Furnace Annealing of Nitrogen Implanted Silicon, by Smith, T.P.,* Stiles, P.J.,* Augustyniak, J.M.,* Brown, W.L.,* Jacobson, D.C.,* and Kant, R.A., *Energy Beam-Solid Interactions and Transient Thermal Processing*, Materials Research Society Symposia Proceedings, Vol. 23, North-Holland, NY, pp. 453-458

Competition Between Ferroelectricity and Ferroelasticity in $RbCdF_3$, by Flocken, J.W.,* Hardy, J.R.,* and Boyer, L.L., *Ferroelectrics* 55:125

Compound Semiconductor Digital Integrated Circuits, by Sleger, K., Mack, I., Scott, C., and Buot, F., *Proceedings of the IEEE EASCON — 17th Annual Electronics and Aerospace Conference*, IEEE, NY, pp. 91-98

Critical Properties of the Void Percolation Problem for Spheres, by Elam, W.T., Kerstein, A.R.,* and Rehr, J.J.,* *Physical Review Letters* 52:1516-1519

Crystallization of FeB Alloys with Rare Earths to Produce Hard Magnetic Materials (Invited), by Koon, N.C. and Das, B.N., *Proceedings of the Twenty-Ninth Annual Conference on Magnetism and Magnetic Materials in: Journal of Applied Physics* 55:2063-2066

Degradation in GaAs FETs Resulting from Alpha Particle Irradiation, by Anderson, W.T., Campbell, A.B., Knudson, A.R., Christou, A., and Wilkins, B.R., *1984 Annual Conference in Nuclear and Space Radiation Effects in: IEEE Transactions on Nuclear Science* NS-31:1124-1127

Device Isolation by Oxygen Implantation in n-type Indium Phosphide, by Thompson, P.E., Binari, S.C., Dietrich, H.B., and Henry, R.L., *Solid-State Electronics* 27:817-818

Effect of Coherent Multi-Ion Interference on Ionized-Impurity Scattering in Semiconductors, by Meyer, J.R. and Bartoli, F.J., *Physical Review B* 30:1026-1029

Effect of Cr^+ Implantation on the Thermal Oxidation of Ta, by Grabowski, K.S. and Gossett, C.R., *Ion Implantation and Ion Beam Processing*, Materials Research Society Symposium Proceedings 27:741-746

Effective Potentials for Kinetic Processes on Semiconductor Surfaces, by Ying, S.C.* and Reinecke, T.L., *Journal of Vacuum Science and Technology* B2:573-575

Effects of Bias on Radiation Induced Defects in MOS Oxides: an ESR Study, by Carlos, W.E., *Nuclear Instruments & Methods in Physics Research* 229(B1):383-386

Effects of Non-Normal Incidence on the Sputtering of Copper with Gold and Tantalum, by Malmberg, P.R., Allas, R.G., Lambert, J.M., Treado, P.A., and Reynolds, G.W., *International Conference on Atomic Collisions in Solids in: Nuclear Instruments and Methods in Physics Research* 230:679-683

Electric-Field-Modulated, Infrared Internal-Reflection Study of the Silicon-Electrolyte Interface, by Palik, E.D., Holm, R.T., and Stella, A.,* *Journal of Applied Physics* 56:843-849

Electron Energy Spectrum and de Haas-Van Alphen Effect in Ordered Cd_3Mg, by Khotkevich, V.V.,* Pluzhnikov, V.B.,* Svechkavev, I.V.,* Grechnev, G.E.,* Anderson, D.R.,* and Pickett, W.E., *Fizika Nizkikh Temperatur* 10:431-434

Electron Paramagnetic Resonance Identification of the Phosphorus Antisite in Electron-Irradiated InP, by Kennedy, T.A. and Wilsey, N.D., *Applied Physics Letters* 44:1089-1091

Electron Paramagnetic Resonance Spectroscopy of Fast Neutron-Generated Defects in GaAs, by Goltzene, A.,* Meyer, B.,* Schwab, C.,* Greenbaum, S.G.,* Wagner, R.J., and Kennedy, T.A., *Journal of Applied Physics* 56:3394-3398

Electron-Hole Liquid Condensation in Semiconductors, by Reinecke, T.L., *Polarons and Excitons in Polar Semiconductors and Ionic Crystals*, Plenum Publishing Corp., NY, pp. 343-382

Electron-Phonon Interaction in Transition 283

Metal Dihydrides, by Papaconstantopoulos, D.A., *LT-17 International Conference on Low Temperature Physics,* North Holland, NY, p. 129

Electron-Stimulated Desorption of Neutrals from Ionic Surfaces: OH from TiO_2, by Bermudez, V.M. and Hoffbauer, M.A., *Physical Review B* 30:1125-1128

Electronic Structure of the Ideal Silicon Vacancy by the Muffin-Tin Green's Function Method, by Pickett, W.E. and Klein, B.M., *Solid State Communications* 50:605-606

Ellipsometric-electrolyte Electroreflectance Study of the Si/SiO_2, by Glembocki, O.J., *Spectroscopic Characterization Techniques for Semiconductor Technology,* SPIE, Vol. 452, Society of Photo-Optical Instrumentation Engineers, Bellingham, WA, pp. 130-141

Extension of the Muffin-Tin Green's-Function Theory of Defects: Application to Defects in Aluminum, by Pickett, W.E. and Klein, B.M., *Physical Review B* 29:1588-1596

F-Center Formation in NaCl: Picosecond Spectroscopic Evidence for Halogen Diffusion on the Lowest Excitonic Potential Surface, by Williams, R.T., Craig, B.B., and Faust, W.L., *Physical Review Letters* 52:1709-1712

Ferromagnetic Echoes of Magnetostatic Surface Wave Modes in Ferrite Films, by Bucholtz, F., Webb, D.C., and Young, C.W., *Journal of Applied Physics* 56:1859-1865

GaAs MMICs: Manufacturing Trends and Issues, by Christou, A., *Proceedings of the IEEE Gallium Arsenide Integrated Circuit Symposium,* GaAs IC, IEEE, NY, pp. 149-153

Growth of Fe and $FeAs_2$ Films on GaAs by Organo-Metal Chemical Vapor Deposition Using Pentacarbonyl Iron and Arsine, by Walsh, F.J.* and Bottka, N., *Journal of the Electrochemical Society* 131:444-446

High-Density Cascade Effects in Ion Implanted Ag-Au Alloy, by Vozzo, F.S., *Ion Implantation and Ion Beam Processing of Materials,* Material Research Society Symposia Proceedings, Vol. 27, North-Holland, NY, pp. 181-186

High-Pressure Research with Synchrotron Radiation, by Skelton, E.F., *Physics Today* 37:2-10

284   Hydrogen in Amorphous Magnetic Rare Earth-

Transition Metal Alloys, by Forester, D.W., Lubitz, P., Schelleng, J.H., and Vittoria, C., *Journal of Non-Crystalline Solids* 61&62:685-690

Hydrogenation and Magnetic Properties of Amor- phous Rare-Earth-Iron (R-Fe) Alloys, by Schelleng, J.H., Forester, D.W., Lubitz, P., and Vittoria, C., *Proceedings of the Twenty-Ninth Annual Conference on Magnetism and Magnetic Matrials in: Journal of Applied Physics* 55:1805-1807

Hydrogenic Donors in Doping Superlattices: A Model Calculation, by Crowne, F.,* Reinecke, T.L., and Shanabrook, B.V., *Solid State Communications* 50:875-878

Infrared Properties of Heavily Implanted Silicon, Germanium and Gallium Arsenide, by Spitzer, W.G.,* Liou, L.,* Wang, K.W.,* Waddell, C.N.,* Hubler, G., and Kwun, S.I.,* *Advanced Semiconductor Processing and Characterization of Electronic and Optical Materials,* SPIE, Vol. 463, Society of Photo-Optical Instrumentation Engineers, Bellingham, WA, pp. 46-51

Interfacial Effects in Spin-Wave Resonance of Iron Films Grown by Molecular Beam Epitaxy, by Vittoria, C., Rachford, F.J., Krebs, J.J., and Prinz, G.A., *Physical Review B* 30:3903-3907

International Symposium on Solid State Physics Under Pressure: A Review, by Skelton, E.F., *ONR Far East Scientific Bulletin* 9:1:45-47

Interplay Between Superconductivity and Itinerant Ferromagnetism in Y_9Co_7 at High Pressure, by Huang, C.Y.,* Wolf, S.A., Olsen, C.E.,* Fuller, W.W., Huang, J.H., and Ting, C.S.,* *High Pressure in Science and Technology,* 9th AIRAPT International High Pressure Conference, Materials Research Society Symposia Proceedings, Vol. 22, North-Holland, N.Y., pp. 57-65

Intersubband Spectroscopy and Valley Degeneracy of Si(110) and Si(111) n-type Inversion Layers, by Cole, T.* and McCombe, B.D., *Physical Review B* 29:3180-3192

Investigation of the Structure and Compressibility of a Number of Chalcopyrite Compounds, by Qadri, S.B.,* Skelton, E.F., Webb, A.W., Wolf, S.A., Elam, W.T., and Rek, Z.,* *High Pressure in Science and Technology,* 9th AIRAPT International High

Pressure Conference, Materials Research Society Symposia Proceedings, Vol. 22, North-Holland, N.Y., pp. 25-29

Ion Implantation and Ion Beam Processing of Materials, ed. by Hubler, G.K., Holland, O.W.,* Clayton, C.R.,* and White, C.W., *Ion Implantation and Ion Beam Processing of Materials*, Materials Research Society Symposia Proceedings, Vol. 27, North-Holland, NY

Ion Implantation, by Butler, J.W., *Encyclopedia of Semiconductor Technology*, pp. 387-410

Ion-Beam Processing of Ion-Implanted Si, by Dietrich, H.B., Corazzi, R.J., and Tseng, W.F., *Ion Implantation and Ion Beam Processing of Materials*, Materials Research Society Symposia Proceedings 27:241-245

Laser Compressibility Studies of Selected Transition Metal Dichalcogenides, by Webb, A.W., Qadri, S.B.,* Skelton, E.F., Elam, W.T., Rek, Z.,* and Jaminson, W.E.,* *High Pressure in Science and Technology*, 9th AIRAPT International High Pressure Conference, Materials Research Society Symposia Proceedings, Vol. 22, North-Holland, N.Y., pp. 21-24

Line-Shape Anomaly in the Local Vibrational Modes of a Shallow Acceptro in GaAs, by Shanabrook, B.V., Moore, W.J., Kennedy, T.A., and Ruden, P.P., *Physical Review B* 30:3563-3565

Linear Compressibility Studies of Selected Transition Metal Dichalcogenides, by Webb, A.W., Qadri, S.B.,* Skelton, E.F., Elam, W.R., and Rek, Z., *High Pressure in Science and Technology*, 9th AIRAPT International High Pressure Conference, Materials Research Society Symposia Proceedings, Vol. 22, North-Holland, N.Y., pp. 21-24

Local Bonding Arrangements of Boron in Doped Hydrogenated Amorphous Silicon, by Greenbaum, S.G.,* Carlos, W.E., and Taylor, P.C.,* *Journal of Applied Physics* 56:1874-1877

Local-Density Approximation for Dynamical Correlation Corrections to Single-Particle Excitations in Insulators, by Pickett, W.E. and Wang, C.S.,* *Physical Review B* 30:4719-4733

Low-Frequency Relaxation in Condensed Matter and the Evolution of Entropy, by Rajagopal, A.K.,* Teitler, S., and Ngai, K.L., *Journal of Physics C: Solid State Physics* 17:6611-6622

Magnetic Properties of Iron-Implanted Graphite, by Koon, N.C., Weber, D., Pehrsson, P., and Schindler, A.I., *Proceedings of the Twenty-Ninth Annual Conference on Magnetism and Magnetic Materials in: Journal of Applied Physics* 55:2497-2499

Microwave Properties of GdFe$_2$,H$_3$ Films, by Vittoria, C., Schelleng, J.H., Lubitz, P., and Forester, D.W., *Journal of Applied Physics* 55:2450-2451

Muffin-Tin Green's Function Theory of Hydrogen Defects in Aluminum, by Klein, B.M. and Pickett, W.E., *Physical Review B* 29:1597-1605

Multiple-Valued Negative Resistance Integrated Circuits, by Abraham, G., *Computer Science and Multiple-Valued Logic Theory and Applications*, North Holland, NY, pp. 394-446

Nitride Offers 30K Transition, by Papaconstantopoulos, D.A., Pickett, W.E., Klein, B.M., and Boyer, L.L., *Nature* 308:494-495

Noise Properties of Granular NbN Josephson Microbridges, by Claassen, J.H., *Journal of Applied Physics* 55:3367-3370

Nondestructive Techniques for Solid State Devices: A General Survey, by Fatemi, M. and Green, R.E.,* *Review of Progress in Quantitative Nondestructive Evaluation* 3B: 871-878

Novel Features of Quantum Hall Plateaus for Varying Interface Charge, by Furneaux, J.E. and Reinecke, T.L., *Physical Review B* 29:4792-4795

Optical-pumping Study of Spin-dependent Recombination in GaAs, by Paget, D., *Physical Review B* 30:931-946

Parameter-Free Equation-of-State Calculations for CsCaF$_3$, by Boyer, L.L., *Journal of Physics C: Solid State Physics* 17:1825-1832

Penetration Depth in Proximity-Effect Superconductors, by Simon, R.W. Chaikin, P.M.,* *Physical Review B* 30:3750-3756

Phonon Transport in Photoexcited GaAs, by Culbertson, J.C., Strom, U., Klein, P.B., and Wolf, S.A., *Physical Review B* 29:7054-7057

Photoluminescence and Infrared Spectroscopy of Acceptors in GaAs, by Bishop, S.G., Shanabrook, B.V., and Moore, W.J., *Journal of Applied Physics* 56:1785-1790

Physical Properties of Two Metastable States of Amorphous Silicon, by Hubler, G.K., **285**

Waddell, C.N.,* Spitzer, W.G.,* Fredrickson, J.E.,* and Kennedy, T.A., *Ion Implantation and Ion Beam Processing of Materials*, Materials Research Society Symposia Proceedings, Vol. 27, North-Holland, NY, pp. 217-222

Planar Fully Ion Implanted InP Power Junction FET's, by Boos, J.B., Binari, S.C., Kelner, G., Thompson, P.E., Weng, T.H., Papanicolaou, N.A., and Henry, R.L., *IEEE Electron Device Letters* EDL-5:273-276

Physics and Modelling Considerations for VLSI Devices, by Grabin, H.L.,* Kreskovsky, J.P.,* Iafrate, G.J.,* Ferry, D.K.,* and Greene, R.F., *The Physics of Submicron Structures*, Plenum Press, NY, pp. 63-75

Retention of Ions Implanted at Non-Normal Incidence, by Grabowski, K.S., Hartley, N.E.W.,* Gossett, C.R., and Manning, I., *Ion Implantation and Ion Beam Processing of Materials*, Materials Research Society Symposia Proceedings, Vol. 27, North-Holland, NY, pp. 615-617

S Contacts Formed from Spun-on Metallo-Organic Solutions, by Pai, C.S.,* Scott, D.M.,* Lau, S.S.,* Bartur, M.,* and Tseng, W.F., *Thin Films and Interfaces II*, Materials Research Society Symposia Proceedings, Vol. 25, North-Holland, NY, pp. 639-644

Self-Consistent Band Structure Calculations of Titanium, Zirconium and Hafnium Dihydrides, by Papaconstantopoulos, D.A. and Switendick, A.C.,* *Proceedings of the International Symposium on the Properties and Applications of Metal Hydrides IV*, Part 2, Journal of the Less Common Metals 103:317-324

Site Distortion of the Beryllium Acceptor in Germanium, by Moore, W.J., *Physical Review B* 29:7062-7064

Slater-Koster Parametrization of the Band Structure of TiNi, by Papaconstantopoulos, D.A. and Shore, J.E., *Journal of Physics and Chemistry of Solids* 45:439

Slater-Koster Parametrization of the Band Structure of TiNi, by Shore, J.D. and Papaconstantopoulos, D.A., *Journal of Physics and Chemistry of Solids* 45:439-445

Specimen Preparation Techniques for Transmission Electron Microscope Study of Multifilamentary V_3Ga Superconducting Wires, by Pande, C.S., Smith, S.,* and Vardiman, R.G., *Journal of Material Sciences Letters* 3:495-498

Status of the NBS-NRL Determination of the Fine-Structure Constant Using the Quantized Hall Resistance Effect, by Cage, M.E.,* Dziuba, R.F.,* Field, B.F.,* Lavine, C.F.,* and Wagner, R.J., *Precision Measurement and Fundamental Constants II*, NBS Special Publication 617, Government Printing Office, Washington, D.C., pp. 539-541

Structural Studies at Elevated Pressures and Reduced Temperatures Using Synchrotron Radiation: Application to $Ce_{.8}La_{.1}Th_{.1}$, by Skelton, E.F., Webb, A.W., Elam, W.T., Wolf, S.A., Qadri, S.B.,* Huang, C.Y.,* Chaikin, P.M.,* Lacoe, R.C.,* and Gschneidner, K.A.,* *High Pressure in Science and Technology*, 9th AIRAPT International High Pressure Conference, Materials Research Society Symposia Proceedings, Vol. 22, North-Holland, NY, pp. 5-9

Study of the Effect of Ferromagnetism in the Kondo State: $Ce_{1-x}Gd_xAl_3$, by Edelstein, A.S. and Koon, N.C., *Proceedings of the Twenty-Ninth Annual Conference on Magnetism and Magnetic Materials in: Journal of Applied Physics* 55:1984-1986

Summary Abstract, Photoenhanced Oxidation of Gallium Arsenide, by Bermudez, V.M., *Journal of Vacuum Science and Technology A* 2:598-599

Summary Abstract: Basic Mechanisms of Metal/SiC Interface Formation, by Bermudez, V.M., *Journal of Vacuum Science and Technology A* 2:531-532

Superconductivity of VN Under Pressure, by Luo, H.L.,* Wolf, S.A., Fuller, W.W., Edelstein, A.S., and Huang, C.Y.,* *Physical Review B* 29:1443-1446

Surface Modification by Ion Beam Enhanced Deposition, by Kant, R.A. and Sartwell, B.D., *Ion Implantation and Ion Beam Processing of Materials*, Materials Research Society Symposia Proceedings, Vol. 27, North-Holland, NY, pp. 525-530

Surface Studies of Epitaxial β-SiC on Si(100), by Kaplan, R., *Journal of Applied Physics* 56:1636-1641

Surface Treatment of (1102) Sapphire for Silicon for Molecular Beam Epitaxial Growth, by Christou, A., Richmond, E.D., Wilkins, B.R., and Knudson, A.R., *Applied Physics Letters* 44:796-798

Temporal Development of Absorption Spectra in Alkali Halide Crystals Subsequent to

Band-Gap Excitation, by Faust, W.L., Williams, R.T., and Craig, B.B., *Ultrafast Phenomena IV*, Springer-Verlag, NY, pp. 173-175

The Effect of Interface Charges on the Quantum Hall Effect, by Furneaux, J.E. and Reinecke, T.L., *5th International Conference on Electronic Properties of Two-Dimensional Systems in: Surface Science* 142:186-188

The Electronic Activation by Barium and Oxygen of Different Tungsten Crystal Orientations, by Marrian, C.R.K. and Thomas, R.E., *Applications of Surface Science* 17:285-295

The Fermi Surface of Iron Under Pressure, by Johnson, W.B.,* Anderson, J.R.,* and Papaconstantopoulos, D.A., *Physical Review B* B29:5337-5348

The Role of Pressure in Understanding the Anomalous Superconductivity in $EuMo_6S_8$ and $(TMTSF)_2FSO_3$, by Wolf, S.A., Huang, C.Y.,* Chaikin, P.M.,* Fuller, W.W., Lacoe, R.C.,* Luo, H.L.,* and Weidl, F.,* *High Pressure in Science and Technology*, 9th AIRAPT International High Pressure Conference, Materials Research Society Symposia Proceedings, Vol. 22, North-Holland, N.Y., pp. 143-152

Intersubband Spectroscopy and Valley Degeneracy of Si(110) and Si(111) n-type Inversion Layers, by Cole, T.* and McCombe, B.D., *IX AIRAPT International High Pressure Conference*, Materials Research Society Symposia Proceedings, Vol. 22, North-Holland, NY, pp. 143-152

The Role of Thermal Expansion in the Melting and Superionicity of Alkali and Alkaline Earth Halides, by Boyer, L.L., *Thermal Expansion 8*, Plenum Publishing Corp., NY, pp. 21-30

Theoretical Lattice Constant of the Predicted High-T_c Compound: B1 Structure MoN, by Klein, B.M., Boyer, L.L., Krabauer, H.,* and Wang C.S.,* *Proceedings of the 17th International Conference on Low Temperature Physics*, p. 131

Theoretical Studies of Hydrogen Impurities in Palladium and Hydrogen Vacancies in PdH Using the Muffin Tin Green's Function Method, by Klein, B.M. and Pickett, W.E., *International Symposium on the Properties and Applications of Metal Hydrides IV in: Journal of the Less Common Metals* 103:185-201

Thermodynamics and Kinetics of Crystallization of Amorphous Si and Ge Produced by Ion Implantation, by Donovan. E.P.,* Spaepen, F.,* Turnbull, D.,* Poate, J.M.,* and Jacobson, D.C.,* *Ion Implantation and Ion Beam Processing of Materials*, Materials Research Society Symposia Proceedings, Vol. 27, North-Holland, NY, pp. 211-213

Time-Dependent Photoluminescence of InP:Fe, by Klein, P.B., Furneaux, J.E., and Henry, R.L., *Physical Review B* 29:1947-1961

Time-Resolved Photoluminescence and Phonon Transport in Amorphous Si:H Films, by Strom, U., Culbertson, J.C., Klein, P.B., and Wolf, S.A., *Phonon Scattering in Condensed Matter, Proceedings of the Fourth International Conference*, Springer-Verlag, NY, pp. 338-340

Tunneling $\alpha^2F(\omega)$, and Heat Capacity Measurements in High-T_c Nb_3Ge, by Kihlstrom, K.E., Mael, D.,* and Giballe, T.H.,* *Physical Review B* 29:150-158

V_3Ga Wire Fabricated by the Modified Jelly Roll Technique, by Gubser, D.U., Francavilla, T.L., Pande, C.S., Rath, B.B., and McDonald, W.K.,* *Journal of Applied Physics* 56:1051-1054

Wear Behavior of Flat and Graded Profile Boron-Implanted Beryllium, by Kumar, K.,* Newborn, N.,* and Kant, R., *Ion Implantation and Ion Beam Processing of Materials*, Materials Research Society Symposia Proceedings, Vol. 27, North-Holland, NY, pp. 649-654

X-Ray Spectra of B- and Be-Like Chromium in the 13-15 Å Region, by Burkhalter, P.G., Charatis, G.,* Rockett, P.C.,* and Newman, D.,* *Journal of the Optical Society of America B* 1:155-160

STRUCTURE RESEARCH

A General Rule and Many Formulas for the Evaluation of Triplet Phase Invariants from Isomorphous Replacement and Anomalous Dispersion Data, by Karle, J., *Acta Crystallographica* A40:374-379

Comments on: Polymorphism of Serine-Specific Transfer Ribonucleic Serine-Specific tRNA, by Hendrickson, W.A., Liljas, A., and Strandberg, B.E., *European Journal of Biochemistry* 141:237-238

Configurations of Antimalarials Derived from Quinghaosu: Dehydroquinghaosu. Artemether and Artesunic Acid. The Chemistry of Drugs. IV, by Flippen-Anderson, J.L. and Gilardi, R., *Helvetical Chimica Acta* 67:1515

Conformational Changes in Cyclic (D-Phe-Pro-Gly-D-Ala-Pro) Upon Complexation with Mg^{++}. A Crystal Structure Analysis, by Karle, I.L., *International Journal of Peptide and Protein Research* 23:32-38

Crystal Form II of Cycloamanide A, Cyclo (-L-Prolyl-L-valyl-L-phenylalanyl-L-phenylalanyl-L-alanyl-glycyl-)-Water-Ethanol (1/1/3), $C_{33}H_{42}N_6O_6-H_2O-3C_2H_6O$, Containing an Unusual β-Bend, by Karle, I.L. and Chiang, C.C.,* *Acta Crystallographica* C40: 1381-1386

Crystal Structure of (E)-5-Hydroxypyrrolizidin-3-one and (Z)-5-Thioketalpyrrolizidin-3-one, by Flippen-Anderson, J.L., D'Antonio, P., and Konnert, J.H., *Journal of Crystallographic and Spectroscopic Research* 14:565

Crystal Structures and EPR Spectra of Nitroguanidine Chloride and Nitroguanidine Nitrate, by Pace, M.D. and Flippen-Anderson, J.L., *Journal of Energetic Materials* 2:43-60

Direct Methods for Macromolecules, by Karle, J., *Methods and Applications in Crystallographic Computing*, Clarendon Press, Oxford, pp. 120-140

General and Special Techniques for Solving Equal Atom Structures Containing more than 200 Atoms per Asymmetric Unit, by Karle, I.L., *Methods and Applications in Crystallographic Computing*, Clarendon Press, Oxford, pp. 478-479

Investigation of the Structure and Compressibility of a Number of Chalcopyrite Compounds, by Qadri, S.B.,* Skelton, E.F., Webb, A.W., Wolf, S.A., Elam, W.T., and Rek, Z., *High Pressure in Science and Technology: Proceedings of the 9th AIRAPT Conference*, International High Pressure Conference, North-Holland, NY, pp. 25-29

Raman Spectroscopic Analysis of the Secondary Structure in Panulerus Interruptus Hemocyanin, by Williams, R.W. and Hendrickson, W.A., *FEBS Letters* 265:223-226

Rules for Estimating the Values of Triplet Phase Invariants in Multiwavelength Anomalous Dispersion Experiments, by Karle, J., *Acta Crystallographica* A40:366-373

Rules for Evaluating Triplet Phase Invariants by Use of Anomalous Dispersion Data, by Karle, J., *Acta Crystallographica* A40:4-11

Structure of 1,3,5,7-Tetranitroadamantane, $C_{10}H_{12}N_4O_8$, by George, C. and Gilardi, R., *Acta Crystallographica* C40:674-676

The Conformations of Five Tetra- and Pentamethoxylated Phenyl Derivatives: Weberine Analogs and Polymethoprims, by Karle, I.L., Flippen-Anderson, J.L., Chiang, J.F.,* and Lowrey, A.H., *Acta Crystallographica* B40:500-506

The Relative Scaling of Multiple-Wavelength Anomalous Dispersion Data, by Karle, J., *Acta Crystallographica* A40:1-4

Triplet Phase Invariants from an Exact Algebraic Analysis of Anomalous Dispersion, by Karle, J., *Acta Crystallographica* A40:526-531

SPACE SCIENCE AND TECHNOLOGY

3-10 keV and 0.1 to 2 MeV Observations of Four Gamma-Ray Bursts, by Laros, J.G.,* Evans, W.D.,* Fenimore, E.E.,* Klebesadel, R.W.,* Shulman, S.,* and Fritz, G.G., *High Energy Transients in Astrophysics, AIP Conference Proceedings No. 115*, American Institute of Physics, NY, p. 378

A 154-day Periodicity in the Occurrence of Hard Solar Flares?, by Rieger, E.,* Share, G.H., Forrest, D.J., Kanbach, G.,* Rippin, C.,* and Chupp, E.L.,* *Nature* 312:623-625

A Catalog of Selected Compact Radio Sources for Construction of an Extragalactic Radio/Optical Reference Frame, by Argue, A.N.,* deVegt, C.,* Elsmore, B.,* Fanselow, J., Harrington, R.,* Hemenway, P.,* Johnston, K.J., Kuhr, H.,* Kumkova, I.,* Niell, A.E.,* and Witzel, A.,* *Astronomy and Astrophysics* 130:191-199

A Far Ultraviolet Imagine Spectrograph for Shuttle , by Carruthers, G.R., *AIAA 22nd Aerospace Sciences Meeting*, AIAA-84-0294, AIAA, NY, 6pp

A Far-Infrared Survey of the Galactic Center, by Odenwald, S.F. and Fazio, G.G.,* *Astrophysical Journal* 283:601-614

A Search for Arcminute-Scale Radio Emission in BL Lacertae Objects, by Ulvestad, J.S.* and Johnston, K.J., *Astronomical Journal* 89:189-194

288

A Skylab Flare Associated with a Hard X-ray Burst, by Widing, K. and Hiei, E.,* *Astrophysical Journal* 281:426-434

A Solar Spectral Line List Between 10 and 200 Å Modified for Application to High Resolution X-Ray Astronomy, by Doschek, G.A. and Cowan, R.D.,* *Astrophysical Journal* 56:67-89

Ammonia Absorption Toward NGC 7538 IRS 1: Arc Second Observations in the (3,3) Line, by Henkel, C.,* Wilson, T.L.,* and Johnston, K.J., *Astrophysical Journal* 282: L93-L96

An X-Ray Survey of Clusters of Galaxies. Part IV. A Survey of Southern Clusters and Compilation of Upper Limits for Both Abell and Southern Clusters, by Kowalski, M.P., Ulmer, M.P.,* Cruddace, R.G., and Wood, K.S., *Astrophysical Journal* 56:403-506

Analysis of the Magnetic Field Configuration of a Filament-Associated Flare from X-Ray, UV and Optical Observations, by Cheng, C.C. and Pallavicini, R.,* *Solar Physics* 93:337-350

Arc Second Resolution Maps of the Compact Sources in Sagittarius B2 and G34.3+02, by Benson, J.M.* and Johnston, K.J., *Astrophysical Journal* 277:181-188

Are There Nuclear Contributions to Gamma Ray Burst Spectra?, by Matz, S.M.,* Chupp, E.L.,* Forrest, D.J.,* Share, G.H., Nolan, P.L., and Rieger, E.*, *High-Energy Transients in Astrophysics*, AIP Conference Proceedings 115, American Institute of Physics, NY, pp. 403-405

Associations Between Coronal Mass Ejections and Metric Type II Bursts, by Sheeley, N.R., Stewart, R.T.,*Robinson, R.D.,* Howard, R.A., Koomen, M.J.,* and Michels, D.J., *Astrophysical Journal* 279: 839-847

Beam-Return Current Systems in Solar Flares, by Spicer, D.S. and Sudan, R.N.,* *Astrophysical Journal* 280:448-456

Comment on "A Comparison of Control Techniques for Large Flexible Systems", by Lindberg, R.E., *Journal of Guidance, Control, and Dynamics* 7:635-637

Composite Equatorial Spread F Wave Number Spectra from Medium to Short Wavelengths, by Singh, M.* and Szuszczewicz, E.P., *Journal of Geophysical Research* 89:2313-2323

Contact Binary Stars. I. An X-Ray Survey, by Cruddace, R.G. and Dupree, A.K.,* *Astrophysical Journal* 277:263-273

Correlated Observations of Impulsive UV and Hard X-Ray Bursts in Solar Flares from the Solar Maximum Mission, by Cheng, C.C., Tandberg-Hanssen, E.,* and Orwig, L.E.,* *Astrophysical Journal* 278:853-862

Detailed Studies of the Dynamics and Energetics of Coronal Bullets, by Karpen, J.T.,* Oran, E.S., and Boris, J.P., *Astrophysical Journal* 287:396-403

Determination of Masses of Globular Cluster X-Ray Sources, by Grindlay, J.E.,* Hertz, P., Steiner, J.E.,* Murray, S.S.,* and Lightman, A.P.,* *Astrophysical Journal* 282:L13-L16

Direct Measurement of the Increase in Altitude of the Soft X-Ray Emission Region During a Solar Flare, by Seely, J.F. and Feldman, U., *Astrophysical Journal* 280:L59-L62

Discovery of Eclipses from the X-Ray Burst Source MXB 1659-29, by Cominsky, L.R.* and Wood, K.S., *High Energy Transients in Astrophysics*, AIP Conference Proceedings No. 115, American Institute of Physics, NY, p. 139

Discovery of a 7.1 Hour Period and Eclipses from MXB 1659-29, by Cominsky, L.H.* and Wood, K.S., *Astrophysical Journal* 283:765-773

Effects of Mass Motions on Solar Emission Measures Inferred from Transition Region Emission Lines, by Mariska, J.T., *Astrophysical Journal* 281:435-441

Erratic Variability in MXB 1916-05, by Hertz, P. and Wood, K.S., *High Energy Transients in Astrophysics*, AIP Conference Proceedings No. 115, American Institute of Physics, NY, p. 80

Far-Infrared Sources in the Vicinity of the Supernova Remanent W28, by Odenwald, S.F., Shivanandan, K., Fazio, G.G.,* Rengarajan, T.N.,* McBreen, B.,* Campbell, M.F.,* and Moseley, H.,* *Astrophysical Journal* 279:161-165

Frequency of Fast, Narrow Gamma-Ray Bursts, by Norris, J., Cline, T.L.,* Desai, U.D.,* and Teegarden, B.J.,* *Nature* 308:434-435

Further 11.1- and 3.7-cm Flux Density Variations of SS 433, by Johnston, K.J., Geldzahler, B.J., Spencer, J.H., Waltman, E.B., Klepczynski, W.J.,* Josties, F.J.,* Angerhofer, P.E.,* Florkowski, D.R.,* McCarthy, D.D.,* and Matsakis, D.N.,*

Astronomical Journal 89:509-514

HRTS Ultraviolet Images of the Solar Chromosphere and Transiting Zone, by Dere, K.P., Bartoe, J.D.F., and Brueckner, G.E., *Cool Stars, Stellar Systems, and the Sun*, Proceedings of the Third Cambridge Workshop, Lecture Notes in Physics **193**, Springer-Verlag, NY, pp. 180-185

Hard X-Ray and O V Emission in Solar Flares, by Poland A.I.,* Orwig, L.E.,* Mariska, J.T., Nakatsuka, R.,* and Auer, L.H.,* *Astrophysical Journal* 280:457-463

High Latitude Ionospheric Structure in Solar Terrestrial Physics: Present and Future, by Ossakow, S.L., Burke, W.,* Carlson,H.C.,* Gary, P.,* Heelis, R.,* Keskinen, M., Maynard, N.,* Meng, C.,* Szuszczewicz, E., and Vickrey, J.,* *A Report Based on the Solar Terrestrial Workshop, December 1982 to November 1983*, NASA Reference Publication 1120

High Resolution Observation of the Quasar 3C138, by Geldzahler, B.J., Fanti, C.,* Fanti, R.,* Schilizzi, R.T.,* Weiler, K.W.,* and Shaffer, D.B.,* *Astronomy and Astrophysica* 131:232-236

High Resolution Observations of the Steep Spectrum Source 2147+145, by Cotton, W.D.,* Owen, F.N.,* Geldzahler, B.J., Johnston, K., Booth, L.,* and Romney, J.,* *Astrophysical Journal* 277:L41-L44

High-Latitude Irregularities in the Lower F Region: Intensity and Scale Size Distributions, by Rodriguez, P. and Szuszczewicz, E.P., *Journal of Geophysical Research* 89:5575-5580

High-Resolution Far-Infrared Observations of the Extended W51 Complex, by Rengarajan, T.H.,* Cheung, L.H.,* Fazio, G.G.,* Shivanandan, K., and McBreen, A.,* *Astrophysical Journal* 286:573-577

High-Resolution Observations of Radio-Source Hot Spots at 329 MHz, by Linfield, R.* and Simon, R.S., *Astronomical Journal* 89:1799-1801

High-Resolution Telescope and Spectrograph Observations of the Quiet Solar Chromosphere and Transition Zone, by Dere, K.P., Bartoe, J.D.F., and Brueckner, G.E., *Astrophysical Journal* 281870-883

Infrared Emission from Accretion Disks: Detectability and Variability, by Beall, J.H.,* Knight, F.K., Smith, H.A., Wood, K.S., Lebofsky, M.,* and Rieke, G.,*

Infrared Emission from Accretion Disks: Detectability and Variability, by Beall, J.H.,* Knight, F.K.,* Smith, H.A., Wood, K.S.,* Lebofsky, M.,* and Rieke, G.,* *Astrophysical Journal* 284:745-750

Infrared Observations of Galactic Bulge X-Ray Sources, by Hertz, P. and Grindlay, J.E.,* *Astrophysical Journal* 282:118-124

Intense X-Ray Flares from Active Stellar Systems: EV Lacertae HD 8357, by Ambruster, C.,*Snyder, W.A.,* and Wood, K.S., *Astrophysical Journal* 284:270-277

Luminosities and Mass Loss Rates of OH/H$_2$O Maser Stars, by Bowers, P.F. and Hagen, W.,* *Astrophysical Journal* 285:637-647

Mg IX and Si XI Line Ratios in the Sun, by Keenan, F.P.,* Kingston, A.E.,* Dufton, P.L.,* Doyle, J.G.,* and Widing, K.G., *Solar Physics* 94:91-98

Microinstabilities Associated with a High Mach Number, Perpendicular Bow Shocks, by Wu, C.S., Winski, D., Zhou, Y.M., Tsai, S.T., Rodriguez, P., Tanaka, M., Papadopoulos, K., Akimoto, K., Lin, C.S., Leroy, M.M., and Goodrich, C.C., *Space Science Reviews* 37:63-109

Millisecond Variability of Cygnus X-1, by Meekins, J.F., Wood, K.S., Hedler, R.L., Byram, E.T., Yentis, D.J., Chubb, T.A., and Friedman, H., *Astrophysical Journal* 278:288-297

NGC 2024: Far-Infrared and Radio Molecular Observations, by Thronson, H.A.,* Lada, C.J.,* Schwartz, P.R., Smith, H.A., Smith, J., Glaccum, W.,* Harper, D.A.,* and Loewenstein, R.F.,* *Astrophysical Journal* 280:154-162

Neutron Generated Single-Event Upsets in the Atmosphere, by Silberberg, R., Tsao, C.H., and Letaw, J.R.,* *IEEE Transactions on Nuclear Science* NS-31:1183-1185

New Evidence on the Nature of the Neutron Star and Accretion Flow in Vela X-1 from Pulse Timing Observations, by Boynton, P.E.,* Deeter, J.E.,* Lamb, F.K.,* Zylstra, G.,* Pravdo, S.H.,* White, N.E.,* Wood, K.S., and Yentis, D.J., *Astrophysical Journal* 283:L53-L56

Numerical Simulations of Loops Heated to Solar Flare Temperatures III. Asymetrical Heating, by Cheng, C.C., Karpen, J.T.,* and Doschek, G.A., *Astrophysical Journal* 286:787-803

290

Observation of the Stellar Radiation Field at 975Å, by Opal, C.B. and Weller, C.S., *Astrophysical Journal* 282:445-451

OH Maser Emission as a Probe of Circumstellar Envelope Structure, by Bowers, P.F., *Cool Stars, Stellar Systems and the Sun*, Proceedings of the Third Cambridge Workshop, Lecture Notes in Physics 193, Springer-Verlag, NY, pp. 356-358

On the Number and Placement of Actuators for Independent Model Space Control, by Lindberg, R.E. and Longman, R.W., *1982 AIAA/AAS Astrodynamics Conference in: Journal of Guidance, Control and Dynamics* 7:215-221

On the Rate of Energy Input in Thermal Solar Flares, by Feldman, U., Doschek, G.A., and McKenzie, D.L.,* *Astrophysical Journal* 276:L53-L56

One to Eight Month X-ray Light Curves for 4 Active Extragalactic Objects, by Snyder, W.A.* and Wood, K.S., *X-ray and UV Emission from Active Galactic Nuclei*, MPE Report 184, 114 pp.

Opportunities for High Angular and Temporal Resolutions of Galactic Objects at Radio Frequencies, by Johnston, K.J., *Proceedings of Workshop on QUASAT*, ESA SP-213, pp. 187-189

Periodicities in Gamma Ray Bursts, by Wood, K.S., *High Energy Transients in Astrophysics*, AIP Conference Proceedings No. 115, American Institute of Physics, NY, p. 409

Phosphine Photochemistry in Saturn's Atmosphere, by Kaye, J.A. and Strobel, D.F., *Geophysical Research Letters* 10:957-960

Phosphine Photochemistry in the Atmosphere of Saturn, by Kaye, J.A. and Strobel, D.F., *Icarus* 59:314-335

Radiation Doses and LET Distributions of Cosmic Rays, by Silberberg, R., Tsao, C.H., Adams, J.H., and Letaw, J.R., *Radiation Research* 98:209-226

Radio Observations of the Jet in Fornax A, by Geldzahler, B.J. and Fomalont, E.B.,* *Astronomical Journal* 89:1650-1657

Rapid Radio Variations in the Flux Density of BL Lacertae, by Johnston, K.J., Geldzahler, B.J., Spencer, J.H., Waltman, E.B., Klepczynski, W.J.,* Josties, F.J.,* Angerhofer, P.E.,* Florkowski, D.R.,* McCarthy, D.D.* and Matsakis, D.N.,* *Astrophysical Journal* 277:L31-L34

Spectral Feature of 31 December 1981 γ-ray Burst not Confirmed, by Nolan, P.L., Share, G.H., Chupp, E.L.,* Forrest, D.J.,* and Matz, S.M.,* *Nature* 311:360-362

Star Formation in the M8E Region, by Cassar, L.,* Felli, M.,* Fischer, J., Massi, M.,* and Sanders, D.,* *Astrophysical Journal* 278:170-175

Stellar Ultraviolet Flux Distributions in the 900-1200 Å Wavelength Range, by Carruthers, G.R., Heckathorn, H.M., and Opal, C.B., *Future of Ultraviolet Astronomy Based on Six Years of IUE Research*, NASA Conference Publication 2349, NASA, Goddard Space Flight Center, Greenbelt, MD, pp. 534-535

The A-1 Survey of Fast X-Ray Transients, by Ambruster, C.* and Wood, K.S., *High Energy Transients in Astrophysics*, AIP Conference Proceedings No. 115, American Institute of Physics, NY, pp. 73-75

The Concentration of the Large-Scale Solar Magnetic Field by a Meridional Surface Flow, by DeVore, C.R., Sheeley, N.R., and Boris, J.P., *Solar Physics* 92:1-14

The Effects of Solar Flares on Single Event Upset Rates, by Adams, J.H. and Gelman, A., *IEEE Transactions on Nuclear Science* NS-31:1212-1216

The Effects of a Multidensity Plasma on Ultraviolet Spectroscopic Electron Density Diagnostics, by Doschek, G.A., *Astrophysical Journal* 279:446-452

The Energetics and Mass Structure of Regions of Star Formation: S201, by Thronson, H.A.,* Smith, H.A., Lada, C.J.,* Glaccum, W.,* Harper, D.A.,* Loewenstein, R.F.,* and Smith, J.,* *Monthly Notices of the Royal Astronomical Society* 207:659-670

The HEAO A-1 X-Ray Source Catalog, by Wood, K.S., Meekins, J.F., Yentis, D.J., Smathers, H.W., McNutt, D.P., Bleach, R.D., Byram, E.T.,* Chubb, T.A.,* Friedman, H., and Meiday, M.,* *Astrophysical Journal* 59:507-649

The Interaction of Relativistic Charged-Particle Beams with Interstellar Clouds, by Rose, W.K.,* Guillory, J.,* Beall, J.H., and Kainer, S.,* *Astrophysical Journal* 280:550-560

The Nature of AFGL 2591 and Its Associated Molecular Outflow: Infrared and Millimeter-Wave Observations, by Lada, C.J.,* Thronson, H.A.,* Smith, H.A.,

291

Schwartz, P.R., and Glaccum, W.,* *Astrophysical Journal* 286:302-309

The Possibility of Steady State Nonionization Equilibrium Conditions in Soft X-ray Flare Plasmas, by Doschek, G.A., *Astrophysical Journal* 233:404-412

The Radio Morphology of the X-Ray/Radio Sources near 0454-844 and 1803-784, by Johnston, K.J., Biermann, P.,* Eckart, A.,* Kuhr, H.,* Strittmatter, P.A.,* Strom, R.G.,* Witzel, A.,* and Zensus, A.,* *Astrophysical Journal* 280:542-546

The Relation of Electron Temperature to Emission Measure and Limits of Increase in Emission Measure in Soft X-Ray Flares, by Denton, R.E.* and Feldman, U., *Astrophysical Journal* 286:259-262

The S201 Far-Ultraviolet Imaging Survey III. A Field in Sagittarius, by Carruthers, G.R. and Page, T.,* *Astrophysical Journal Supplement Series* 55:101-125

The S201 Far-Ultraviolet Imaging Survey. II. A Field in Cygnus, by Carruthers, G.R. and Page, T.,* *Astrophysical Journal Supplement Series* 54:271-289

The S201 Far-Ultraviolet Imaging Survey: A Summary of Results and Implications for Future Survey, by Carruthers, G.K. and Page, T.,* *Publications of the Astronomical Society of the Pacific* 96:447-462

The Structure of OH Maser Clouds Associated with Late-Type Stars, by Bowers, P.F., Johnston, K.J., and Spencer, J.H., *VLBI &*

Compact Radio Sources, IAU Symposium No. 110, Reidel, Holland, pp. 327-328

The T Tauri Radio Source, by Schwartz, P.R., Simon, T.,*Zuckerman, B.,* and Howell, R.R.,* *Astrophysical Journal* 280:L23-L26

The Three-Dimensional Structure of a Circumstellar Maser, by Bowers, P.F. and Morris, M.,* *Astrophysical Journal* 276:646-652

Ultracompact Structure in the HII Region W49N, by Dreher, J.W.,* Johnston, K.J., Welch, W.J.,* and Walker, R.C.,* *Astrophysical Journal* 283:632-639

VLA Observations of 1612 and 1667 MHz OH Masers Associated with IRC+10420, by Bowers, P.F., *Astrophysical Journal* 279:350-357

VLA Observations of T Tauri Stars. II. A Luminosity-Limited Survey of Taurus-Aurgia, by Bieging, J.H.,* Cohen, M.,* and Schwartz, P.R., *Astrophysical Journal* 282:699-708

Very High Resolution Observations of Compact Sources in the Direction of Supernova Remanents: G74.87+1.22, by Geldzahler, B.J.,* Shaffer, D.B.,* and Kuhr, H., *Astrophysical Journal* 286:284:-288

W3 North: Far-Infrared and Radio Molecular Observations, by Thronson, H.A.,* Schwartz, P.R., Smith, H.A., Lada, C.L.,* Glaccum, W.,* and Harper, D.A.,* *Astrophysical Journal* 284:597-600

FORMAL REPORTS

ACOUSTICS

8721 **NRL Reverberation Model: A Computer Program for the Prediciton and Analysis of Medium- to Long-Range Boundary Reverberation,** by Franchi, E.R., Griffin, J.M., and King, B.J.

8792 **Vertical Coherence Along a Macroray Path in an Inhomogeneous Anisotropic Ocean,** by Perkins, J.S., Adams, B.B., and McCoy, J.J.*

8793 **Acoustic Propagation in a Wedge-Shaped Ocean with Perfectly Reflecting Boundaries,** by Buckingham, M.J.*

8820 **The Numerical Solution of Underwater Acoustic Propagation Problems Using Finite Difference and Finite Element Methods,** by Goldstein, C.I.*

8868 **Full Field Ambiguity Function Processing in a Complex Shallow-Water Environment,** by Heitmeyer, R.M.,* Fizell, R.G., and Moseley, W.B.

COMMUNICATIONS

8799 **Improvement of the Narrowband Linear Predictive Coder. Part 2—Synthesis Improvements,** by Kang, G.S. and Everett, S.S.

END

FILMED

DTIC

MICROCOPY RESOLUTION TEST CHART

NATIONAL BUREAU OF STANDARDS-1963-A

COMPUTER SCIENCES

ELECTRONICS AND ELECTRICITY

MECHANICS

OPTICAL SCIENCES

RADAR

SPACE SCIENCE AND TECHNOLOGY

293

BOOKS

Nonlinear Optical Parametric Processes in Liquids and Gases, by J.F. Reintjes (Academic Press, NY, 1984).

MHD Instabilities in Simple Plasma Configuration, by W.M. Manheimer and C. Lashmore-Davies (Naval Research Laboratory, Washington, DC, 1984).

PATENTS

4,426,268—Method for Forming High Superconducting T_c Niobium Nitride Film at Ambient Temperatures, January 17 to Edward T. Cukauskas

4,427,263—Pressure Insensitive Optical Fiber, January 24 to Nicholas Lagakos and Joseph A. Bucaro

4,430,170—Electrodeposition of Refractory Metal Carbides, February 7 to Kurt H. Stern

4,436,425—Signal Waveform Detector Using Synthetic FM Demodulation, March 13 to James H. Cole

4,438,203—Method and Apparatus for Determination of Lubricant Stability, March 20 to Henry Wohltjen, Paul J. Sniegoski, and Harold Ravner

4,439,269—Method for Making Josephson Junctions with Contamination-Free Interfaces Utilizing a ZnO Contact Insulator, March 27 to Edward J. Cukauskas

4,439,770—Cascaded Adaptive Loops, March 27 to Bernard L. Lewis and Frank F. Kretschmer, Jr.

4,440,498—Optical Fiber Gyroscope with (3 × 3) Directional Coupler, April 3 to Sang K. Sheem

4,441,237—Inhomogeneous Anisotropic Kinetic Energy Penetrators, April 10 to Chulho Kim and Raymond J. Weimer

4,442,350—Fiber Optic Sensor with Enhanced Immunity to Random Environmental Perturbations, April 10 to Scott C. Rashleigh

4,445,780—Fiber Optic Rotation-Sensing Gyroscope with (3 × 2) Coupler, May 1 to William K. Burns

4,447,272—Method for Fabricating MNOS Structures Utilizing Hydrogen Ion Implantation, May 8 to Nelson S. Saks

4,448,000—High Temperature Ultra-High Vacuum Infrared Window Seal, May 15 to Thomas J. Manuccia, John R. Peele, and Christine E. Geosling

4,449,105—Passive Maser Using Timesharing for Control of the Cavity and Control of the Oscillator on the Line of Stimulated Emission, May 15 to Alick H. Frank and Joseph D. White

4,452,533—External Cavity Diode Laser Sensor, June 5 to Ronald O. Miles, Thomas G. Giallorenzi, and Alan B. Tveten

4,452,624—Method for Bonding Insulator to Insulator, June 5 to Henry Wohltjen and John F. Guiliani

4,452,998—Fluorinated Diacrylic Esters, June 5 to James R. Griffith and Jacques G. O'Rear

4,453,238—Apparatus and Method for Determining the Phase Sensitivity of Hydrophones, June 5 to Arnie L. Van Buren

4,456,583—Preparation of Simple Nitronium Salts, June 26 to Ronald A. DeMarco and Michael J. Moran

4,456,889—Dual-Gate MESFET Variable Gain Constant Output Power Amplifier, June 26 to Mahesh Kumar

4,459,700—Adaptive MTI System, July 10 to Frank F. Kretschmer, Jr., Bernard L. Lewis, and James P. Hansen

4,463,678—Hybrid Shaped-Charge/Kinetic/Energy Penetrator, August 7 to Raymond J. Weimer and Chulho Kim

4,464,065—Fast Granular Superconducting Bolometer, August 7 to Stuart A. Wolf, Ulrich Strom, and Kurt Weiser

4,464,768—Adaptive Preprocessing System, August 7 to Bernard L. Lewis and Frank F. Kretschmer, Jr.

4,466,003—Compact Wideband Multiple Conductor Monopole Antenna, August 14 to Richard K. Royce

4,468,760—Directional Line-Hydrophone Array

Calibrator, August 28 to Joseph F. Zalesak and Peter H. Rogers

4,468,766—**Optical RF Downconverter**, August 28 to Anthony Spezio

4,468,794—**Digital Coherent Detector**, August 28 to William M. Waters and Bobby R. Jarrett

4,469,536—**Alloys and Method of Making**, September 4 to Donald W. Forester

4,469,977—**Superlattice Ultrasonic Wave Generator**, September 4 to John J. Quin, Ulrich Strom and Leroy L. Chang

4,471,219—**Amplitude Mode Magnetic Sensors**, September 11 to Thomas G. Giallorenzi

4,471,340—**Analog to Digital Converter**, September 11 to Bernard L. Lewis

4,471,359—**Dual Band, Low Sidelobe, High Efficiency Mirror Antenna**, September 11 to Dean D. Howard

4,489,320—**Interference Suppressor for Radar MTI**, December 18 to Bernard L. Lewis and Frank F. Kretschmer

4,489,392—**Orthogonalizer for Inphase and Quadrature Digital Data**, December 18 to Bernard L. Lewis

4,490,016—**Polarimetric Image Recorder**, December 25 to Irwin Schneider and Charles S. Guenzer

NRL FUNDING PROFILE

SOURCES OF FUNDS
FY 1984 (New Orders Received)

	$M
18.9% — Office of Naval Research (ONR)	70.6
10.8% — Naval Sea Systems Command (NAVSEA)	40.4
16.0% — Naval Electronic Systems Command (NAVELEX)	59.8
5.8% — Naval Air Systems Command (NAVAIR)	21.7
0.7% — Chief of Navy Material (CNM)	2.6
33.4% — Other Navy	124.8
14.4% — Other	53.9
Actual funding	373.8
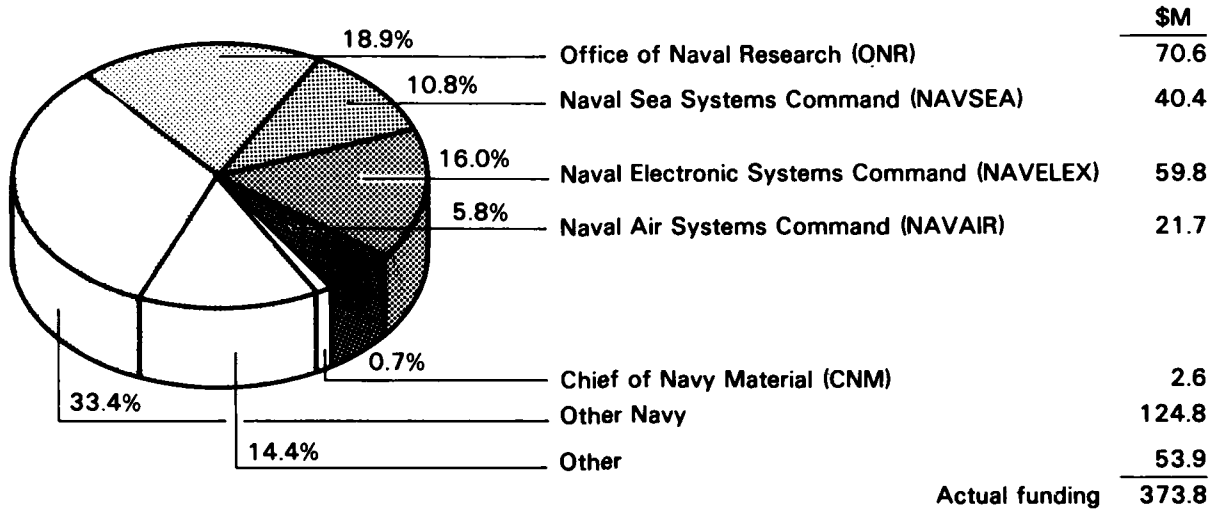
RDT&E NAVY FUNDS BY CATEGORY
FY 1985 PLAN (New Orders)

	$M
21.6% — 6.1 Research	64.3
20.6% — 6.2 Exploratory Development	61.5
6.6% — 6.3 Advanced Development	19.5
11.1% — 6.4 Engineering Development	33.2
1.2% — 6.5 Management and Support	3.5
38.9% — 6.6 Operational Systems Development	116.0
Total	298.0
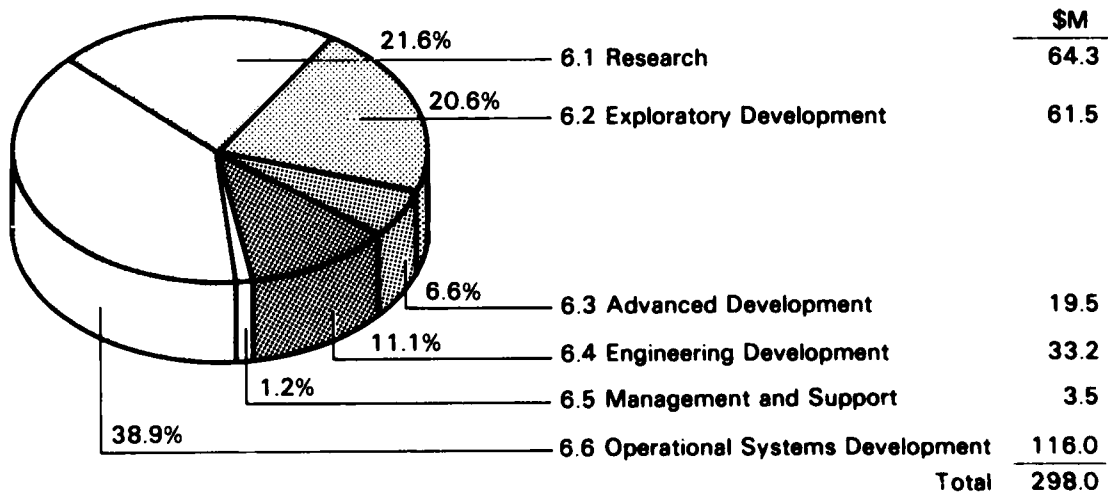
NRL WITHIN THE DEPARTMENT OF THE NAVY*

```
                        ┌──────────┐
                        │ SECNAV ╱ │
                        │      ╱ CNO│
                        └────┬─────┘
        ┌──────────┬────────┼────────┬──────────┬──────────┐
   ┌────┴────┐ ┌───┴───┐ ┌──┴────┐ ┌─┴──────┐ ┌─┴──────┐ ┌─┴──────┐
   │ CNR  ╱  │ │ NAVAIR│ │ NAVSEA│ │ SPACE &│ │ NAVSUP │ │ NAVFAC │
   │   ╱ OCNR│ │       │ │       │ │W'FARE SY│ │       │ │        │
   └─┬──────┬┘ └───────┘ └───────┘ └────────┘ └────────┘ └────────┘
     │      │                  │
  ┌──┴──┐ ┌─┴──┐          ┌────┴───┐
  │ ONR │ │ ONT│          │  DNL   │
  └──┬──┘ └────┘          └────┬───┘
     │      ┌──────┬───────┬───┼──────┬─────────┐
  ┌──┴──┐┌──┴──┐┌──┴──┐┌──┴──┐┌─┴───┐┌─┴───┐
  │ NRL ││ NADC││ NCSC││ NSWC││ NUSC││ NTEC│
  └──┬──┘└─────┘└──┬──┘└──┬──┘└──┬──┘└──┬──┘
  ┌──┴────┐   ┌────┴─┐┌───┴──┐┌──┴────┐┌─┴──┐
  │ NORDA │   │ NRPDC││ NOSC ││DTNSRDC││ NWC│
  └──┬────┘   └──────┘└──────┘└───────┘└────┘
  ┌──┴──┐
  │ NBL │
  └─────┘
```
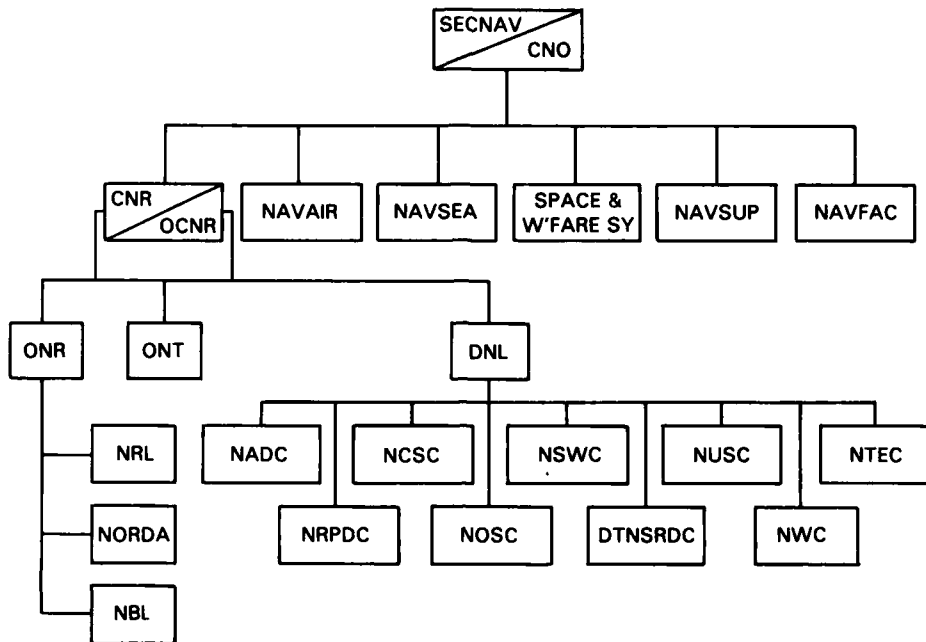
SECNAV/CNO   — Secretary of the Navy/Chief of Naval Operations
CNR/OCNR   — Chief of Naval Research/Officer of the Chief of Naval Research
NAVAIR   — Naval Air Systems Command
NAVSEA   — Naval Sea Systems Command
SPACE&W'FARE   — Space and Warfare Systems Command
NAVSUP   — Naval Supply Systems Command
NAVFAC   — Naval Facilities Systems Command
ONR   — Office of Naval Research
ONT   — Office of Naval Technology
DNL   — Director of Navy Laboratories
NORDA   — Naval Oceanographic Research and Development Activity
NBL   — Naval Biosciences Laboratory

*Approved by the Commanding Officer as of 2 July 1985

ORGANIZATIONAL CHART
DECEMBER 1984

COMMANDING OFFICER
Code 1000
CAPT J.P. O'Donovan, USN

DEPUTY EQUAL EMPLOYMENT OPPORTUNITY OFFICER
Code 1003
S. Eaton

DIRECTOR OF RESEARCH
Code 1001
Dr. T. Coffey

PUBLIC AFFAIRS OFFICER
Code 2610
J.W. Gately, Jr.

SCIENTIFIC CONSULTANT TO THE DIRECTOR OF RESEARCH
Code 1004
Dr. A.H. Aitken

OFFICE OF MANAGEMENT AND ADMINISTRATION
Code 1005
M. Oliver

OPERATIONS, SECURITY, AND CONTRACTS DIVISION
Code 1200
CAPT J.B. Morris, USN
● Operational Services
● Security
● Contracting
● Research Requirements & Applications
● NRL Flight Detachment

FINANCIAL MANAGEMENT DIVISION
Code 1300
R.W. Steinbeck
● Budget
● Accounting
● Disbursing

CIVILIAN PERSONNEL DIVISION
Code 1800
D.J. Blome
● Personnel Operations
● Employee Development
● Employee Relations

TECHNICAL SERVICES DIRECTORATE
Code 2000
J.D. Brown

GENERAL SCIENCE AND TECHNOLOGY DIRECTORATE
Code 4000
Dr. W.R. Ellis

SYSTEMS RESEARCH AND TECHNOLOGY DIRECTORATE
Code 5000
R.R. Rojas

MATERIAL SCIENCE AND COMPONENT TECHNOLOGY DIRECTORATE
Code 6000
Dr. A.I. Schindler

SPACE AND COMMUNICATIONS TECHNOLOGY DIRECTORATE
Code 7000
Dr. B. Wald

298

TECHNICAL SERVICES DIRECTORATE
Code 2000

ENGINEERING SERVICES DIVISION
Code 2300
LCDR M.L. Crouch, USN
- Mechanical Engineering & Manufacturing
- Electronic Engineering & Fabrication

SUPPLY DIVISION
Code 2400
LCDR T.R. Lippert, USN
- Purchasing/Requisition Control
- Receipt Control
- Material
- Automated Inventory Management
- Technical

PUBLIC WORKS DIVISION
Code 2500
CDR J.P. Collins USN
- Engineering
- Maintenance, Utilities, & Transportation
- Contract Administration
- Maintenance Control
- Administrative
- Planning

TECHNICAL INFORMATION DIVISION
Code 2600
E.E. Kirkbride
- Information Services
- Technical Library
- Publications
- Photographic/Illustration

CHESAPEAKE BAY DETACHMENT
Code 2700
CDR R.S. Holtz, USN
- Security
- Operations
- Maintenance & Support

RESEARCH COMPUTATION DIVISION
Code 2800
R.F. Saenger
- Software Systems & Support
- Operations
- Timesharing Computer
- Customer Planning & Support

GENERAL SCIENCE AND TECHNOLOGY DIRECTORATE
Code 4000

LABORATORY FOR COMPUTATIONAL PHYSICS
Code 4040
Dr. J.P. Boris

SPACE SCIENCE DIVISION
Code 4100
Dr. H. Gursky
- Atmospheric Physics
- X-Ray Astronomy
- Radio & IR Astronomy
- UV Measurements
- Gamma & Cosmic Ray Astrophysics
- Solar Physics
- Solar Terrestrial Relationships
- Ionospheric Effects
- E.O. Hulburt Center for Space Research

PLASMA PHYSICS DIVISION
Code 4700
Dr. S. Ossakow
- Plasma Radiation
- Laser Plasma
- High-Power Electromag. Radiation
- Experimental Plasma Physics
- Plasma Technology
- Geophysical & Plasma Dynamics
- Plasma Theory

SYSTEMS RESEARCH AND TECHNOLOGY DIRECTORATE
Code 5000

ACOUSTICS DIVISION
Code 5100
Mr. B.G. Hurdle*
- Acoustics Media Characterization
- Applied Ocean Acoustics
- Physical Acoustics
- Software Systems Development
- Large Aperture Acoustics

RADAR DIVISION
Code 5300
Dr. M.I. Skolnik
- Radar Analysis
- Radar Techniques
- Search Radar
- Target Characteristics
- Identification Systems
- Airborne Radar
- Electromagnetics
- Systems Control & Research

TACTICAL ELECTRONIC WARFARE DIVISION
Code 5700
Dr. J.A. Montgomery
- Offboard Countermeasures
- EW Support Measures
- Airborne EW Systems
- Ships EW Systems
- Advanced Techniques

MARINE TECHNOLOGY DIVISION
Code 5800
Dr. R.T. Swim
- Ocean Dynamics
- Marine Systems
- Structural Integrity
- Fluid Dynamics

UNDERWATER SOUND REFERENCE DETACHMENT
Code 5900
Dr. J.E. Blue
- Technical Services
- Acoustical Systems
- Transducer
- Measurements

CHART (Continued)

**S RESEARCH
HNOLOGY
RATE
9**

ACOUSTICS DIVISION
Code 5100
Mr B G Hurdle*
- Acoustics Media
  Characterization
- Applied Ocean Acoustics
- Physical Acoustics
- Software Systems
  Development
- Large Aperture Acoustics

RADAR DIVISION
Code 5300
Dr M I Skolnik
- Radar Analysis
- Radar Techniques
- Search Radar
- Target Characteristics
- Identification Systems
- Airborne Radar
- Electromagnetics
- Systems Control & Research

TACTICAL ELECTRONIC WARFARE DIVISION
Code 5700
Dr J A Montgomery
- Offboard Countermeasures
- EW Support Measures
- Airborne EW Systems
- Ships EW Systems
- Advanced Techniques

MARINE TECHNOLOGY DIVISION
Code 5800
Dr R T Swim
- Ocean Dynamics
- Marine Systems
- Structural Integrity
- Fluid Dynamics

UNDERWATER SOUND REFERENCE DETACHMENT
Code 5900
Dr J E Blue
- Technical Services
- Acoustical Systems
- Transducer
- Measurements

MATERIAL SCIENCE AND COMPONENT TECHNOLOGY DIRECTORATE
Code 6000

LABORATORY FOR STRUCTURE OF MATTER
Code 6030
Dr J Karle

CHEMISTRY DIVISION
Code 6100
Dr W M Tolles
- Chemical Kinetics
- Chemical Diagnostics
- Polymeric Materials
- Surface Chemistry
- Combustion & Fuels
- Biomolecular Engineering

MATERIAL SCIENCE AND TECHNOLOGY DIVISION
Code 6300
Dr B B Rath
- Environmental Effects
- Physical Metallurgy
- Ceramics
- Composite Materials
- Mechanics of Materials
- Thermostructural Materials

OPTICAL SCIENCES DIVISION
Code 6500
Dr T G Giallorenzi
- Optical Probes
- Advanced Concepts
- Applied Optics
- Laser Physics
- Electro optical Technology
- Optical Techniques

CONDENSED MATTER AND RADIATION SCIENCES DIVISION
Code 6600
Dr D J Nagel
- Radiation Survivability
- Metal Physics
- Radiation-Matter Interactions
- Materials Modification & Analysis
- Condensed Matter Physics

ELECTRONICS TECHNOLOGY DIVISION
Code 6800
Dr G M Borsuk
- Solid State Devices
- Electronic Material Technology
- Surface Physics
- Microwave & Millimeter
  Wave Tube Technology
- Microwave Technology
- Semiconductors

SPACE AND COMMUNICATIONS TECHNOLOGY DIRECTORATE
Code 7000

INFORMATION TECHNOLOGY DIVISION
Code 7500
Dr J R Davis
- Navy Center for
  Applied Research in
  Artificial Intelligence
- Communication System
  Engineering
- Transmission Technology
- Integrated Warfare Technology
- Computer Science & Systems

SPACE SYSTEMS AND TECHNOLOGY DIVISION
Code 7700
P G Wilhelm
- Electrical Systems &
  Spacecraft Integration
- Terrestrial Systems
- Mechanical Systems
- Systems Engineering
  & Analysis
- Digital Systems
- Radio Frequency
  & Optical
- Space Applications
- Space Sensing
  Applications

*ACTING

— — —ADDITIONAL DUTY

299

Code	Office	Key Personnel	Extension*

EXECUTIVE DIRECTORATE

Code	Office	Key Personnel	Extension*
1000	Commanding Officer	CAPT J.P. O'Donovan, USN	73403
1001	Director of Research	Dr. T. Coffey	73301
1003	DEEO Officer	Ms. S.A. Eaton	72486
1004	Scientific Consultant to the Dir. of Res.	Dr. A.H. Aitken	73724
1005	Head, Office of Management and Admin.	Ms. M. Oliver	73086
2610	Public Affairs Officer	Mr. J.W. Gately, Jr.†	72541
1200	Chief Staff Officer	CAPT J.B. Morris, USN	73621
1220	Head, Security Branch	Mr. M.B. Ferguson	73048
1300	Comptroller	Mr. R.W. Steinbeck	73405
1800	Head, Civ. Pers. Div.	Mr. D.J. Blome	73421
1810	Personnel Operations	Mr. D.J. Blome	73421

TECHNICAL SERVICES DIRECTORATE

Code	Office	Key Personnel	Extension*
2000	Assoc. Dir. Res. for Tech. Services	Mr. J.D. Brown	72879
2004	Patent Counsel	Dr. W.T. Ellis	73428
2010	Safety Officer	Mr. H.C. Kennedy, Jr.	72249
2020	Head, Administrative Services Office	Mrs. L.V. Dabney	73858
2300	Engineering Services Officer	LCDR M.L. Crouch	72300
2400	Supply Officer	LCDR T.R. Lippert	73446
2500	Public Works Officer	CDR J.P. Collins, USN	73371
2600	Head, Tech. Info. Div.	Mr. E.E. Kirkbride	73388
2700	Chesapeake Bay Detachment Officer	CDR R.S. Holtz, USN	301-257-4002
2800	Head, Research Computation Division	Mr. Rudi F. Saenger	72751

GENERAL SCIENCE AND TECHNOLOGY DIRECTORATE

Code	Office	Key Personnel	Extension*
4000	Assoc. Dir. Res. for General Sci. & Tech.	Dr. W.R. Ellis	73324
4040	Head, Lab. for Computational Physics	Dr. J.P. Boris	73055
4100	Supt., Space Science Div.	Dr. H. Gursky	76343
4700	Supt., Plasma Physics Div.	Dr. S. Ossakow	72723

SYSTEMS RESEARCH AND TECHNOLOGY DIRECTORATE

Code	Office	Key Personnel	Extension*
5000	Assoc. Dir. Res. for Systems Res. & Tech.	Mr. R.R. Rojas	73294
5100	Supt., Acoustics Div.	Mr. B.G. Hurdle**	73482
5300	Supt., Radar Div.	Dr. M.I. Skolnik	72936
5700	Supt., Tactical Elec. Warfare Div.	Dr. J.A. Montgomery	76278
5800	Supt., Marine Technology Div.	Dr. R.T. Swim	73314
5900	Supt., Underwater Sound Reference Det.	Dr. J.E. Blue	305-859-5120

MATERIAL SCIENCE AND COMPONENT TECHNOLOGY DIRECTORATE

Code	Office	Key Personnel	Extension*
6000	Assoc. Dir. Res. for Material Science & Component Tech.	Dr. A.I. Schindler	73566
6030	Head, Lab. for Structure of Matter	Dr. J. Karle	72665
6070	Head, Health Physics Staff	Mr. J.N. Stone	72232
6100	Supt., Chemistry Div.	Dr. W.M. Tolles	73026
6300	Supt., Mat. Sci. & Tech. Div.	Dr. B.B. Rath	72926
6500	Supt., Optical Sciences Div.	Dr. T.G. Giallorenzi	73171
6600	Supt., Condensed Matter & Radiation Sciences Div.	Dr. D.J. Nagel	72931
6800	Supt., Electronics Tech. Div.	Dr. G.M. Borsuk	73525

SPACE AND COMMUNICATIONS TECHNOLOGY DIRECTORATE

Code	Office	Key Personnel	Extension*
7000	Assoc. Dir. Res. for Space & Comm. Tech.	Dr. B. Wald	72964
7500	Supt., Information Technology Div.	Dr. J.R. Davis	72903
7700	Supt., Space Systems and Technology Div.	Mr. P.G. Wilhelm	76547

---

*Direct-in-Dialing (202) 76-; AUTOVON 29-
**Acting
†Additional duty

NRL REVIEW STAFF

The *NRL Reveiw* is a result of the collaboration of the scientific, engineering, and support staff with the Technical Information Division (TID). In addition to the scientists and engineers who provided material for the *Review*, the following have also contributed to its publication.

Senior Science Editor: Dr. Jack Kaiser   Senior TID Editor: Kathleen Parrish

Associated Science Editors: Dr. Phillip Mange, *General Science and Technology*

Dr. Felix Rosenthal, *Systems Research and Technology*

Mr. Richard Nekritz, *Material Science and Component Technology*

Dr. William Carter, *Space and Communications Technology*

Head, Technical Information Division: Earle E. Kirkbride

Covers and color page design: B. Zevgolis

Chapter title pages: T. Phillips

Interview: J. Kaiser, K. Parrish, B. Zevgolis

Photographic production: G. Blakes, D. Boyd, G. Gattis
H. Hill, B. Horton, A. Lancaster, A. MacDonald,
J. Marshall, C. Morrow, W. Nafey, M. Savell

Computerized composition production: D. Martin, D. Wilbanks

Editorial assistance: I. Barron, R. Baturin, P. Creech, G. Harrison-Rashin,
M. Long, D. Nelson

Computerized composition assistance: M. Bray, C. Cain, J. Craze, J. Hays, J. Kogok,
P. Lore, J. Mickelinc, D. Mitchell, K. Morin,
P. Newman, S. Schrock, C. Sims, C. Ward

Graphic services assistance: A. Green, L. Jackson, J. Milligan

Production coordination: T. Calderwood, P. Imhoff, M. Peevy

Valuable assistance in other matters was given by: J. Boris, H. Mitchell, E. Oran

EMPLOYMENT OPPORTUNITIES
FOR ENTRY-LEVEL AND
EXPERIENCED PERSONNEL

This *Review* illustrates some of the exciting science and engineering carried out at NRL as well as the potential for new personnel.

The Naval Research Laboratory offers a wide variety of challenging positions that involve the full range of work from basic and applied research to equipment development. The nature of the research and development conducted at NRL requires professionals with experience. Typically, there is a continuing need for electronics, mechanical aerospace, ceramic, and materials engineers; metallurgists with bachelor's and/or advanced degrees; and physical and computer scientists with Ph.D. degrees. Opportunities exist in the areas described below.

Ceramic and Materials Scientists/Engineers. These employees work on the mechanical properties, coating and materials processing, and materials research.

Electronics Engineers. These engineers work in the following areas: communication satellite design, analog and digital signal processing, information processing, strategic and tactical communication systems design, instrumentation, microcomputer design, satellite attitude-control systems, image processing, IR sensors, focal plane arrays, radar, inverse scattering phenomena, statistical communication theory, electrooptics, hardware/software interfacing, artificial intelligence, electromagnetic (EM) scattering, digital electronics, fiber optics, optical information processing, semiconductor device processing, microwave tubes, threat systems analysis, electroacoustic optics, RF measurement design, EM propagation, EM theory, HF radar propagation analysis, electronic warfare simulation, pulsed power technology, vacuum electronics, microwave technologies, networking techniques, speech processing, Navy C^3I, electronic countermeasure systems design, spacecraft attitude controls, and orbitology.

Mechanical and Aerospace Engineers. These employees may be assigned to satellite thermal design, structural design, propulsion, experimental fluid mechanics, experimental structural mechanics, solid mechanics, elastic/plastic fracture mechanics, materials characterization of composites, finite-element methods, nonde-

structive elevation, characterization of fracture resistance of structural alloys, and combustion.

Computer Science Graduates. Employees in this field are involved with artificial intelligence, software engineering, software systems specifications, computer design/architecture, systems analysis, and command information systems.

Chemists. Chemists are recruited to work in the areas of inorganic and organometallic synthesis, solution kinetics and mechanisms, surface analysis, organic chemistry, combustion, colloid/surface chemistry, fire suppression, and nuclear decay.

Physicists. Physics graduates may concentrate on such fields as electromagnetics, image processing, inverse scattering phenomena, acoustics, inversion theory, mathematical modeling of scattering processors, radar system development, electro-optics, focal plane arrays, signal processing, plasma physics, astrophysics, semiconductor technology, relativistic electronics, beam/wave interactions, low-temperature physics, superconductivity, physical/chemical vapor disposition of thin and thick coatings, wave propagation, ionospheric physics, computational hydrodynamics, computational atomic physics, and supersonic, gasdynamic numerical modeling.

FOR FOREIGN NATIONALS

U.S. citizenship is required for employment at NRL.

APPLICATION AND INFORMATION

Interested applicants should submit a résumé or a Federal Employment Application Form (OPM 1282), which can be obtained from local officers of the Office of Personnel Management and Personnel Offices of Federal agencies, to the address below.

Direct inquires to:

Naval Research Laboratory
Civilian Personnel Division, Code 1813 RV 84
Attn: Marguerite Luck
Washington, DC 20375-5000
202-767-3030

CONTRIBUTIONS BY DIVISIONS AND LABORATORIES

Laboratory For Computational Physics (4040)

Transition to Turbulence in Free Shear Flows, 53
The Structure of a Propagating Detonation, 215

Space Science Division (4100)

Solar Flare Effects in the Atmosphere, 133
Periodic Occurrence of Solar Flares?, 135
HEAO A-1 Discovers X-ray Eclipses, 137

Plasma Physics Division (4700)

Vibrational Energy Relaxation in Nitrogen, 177
Ionospheric Turbulence and Chaotic
   Fluid Behavior, 221

Acoustics Division (5100)

Modeling Long-range Arctic
   Acoustic Propagation, 107
Frequency Dependent Modal Excitation and
   Attenuation in Shallow Water, 108
Scattering from Rigid Bodies of Arbitrary Shape, 110
High-Precision Airborne Gravity
   System Demonstration, 208

Radar Division (5300)

Time-Domain Radar Interference Rejection, 123

Tactical Electronic Warfare Division (5700)

Full Engagement Decoy Simulator, 103
Modeling Radar Scattering from Ships, 124
Studies of Ship Infrared Signatures, 126

Marine Technology Division (5800)

Mixing Within an Ocean Front, 139
Acoustic Measurement of Ocean Water Velocities, 142
Imaging the Upper Ocean Temperature
   Variance Field, 144
Thermomechanical Response of Laser-Irradiated
   Composite Structural Elements, 188
Damage Predictions for Torpedo-Submarine
   Collisions, 195
Laboratory Studies of Steep and Breaking
   Deep Water Waves, 217
A Doubly Asymptotic Approximation for
   the Interaction of Water Waves and
   Ship Wake Currents, 219

Underwater Sound Reference Detachment (5900)

Porous Ceramic Loss Mechanism, 112
Glass Ceramics for Sonar Transducers, 113
Dynamic Bulk Modulus Measurement, 115
Extrapolation of Thick-Panel
   Reflection Measurements, 117

Laboratory for Structure of Matter (6030)

Structural Information from Regions
   6 to 20 Å in Diameter, 180

Chemistry Division (6100)

Fire! (Fire Suppression Research at NRL), 67
High Pressure Nervous Syndrome, 163
Synthetic Red Blood Cells, 165
Cure Monitoring of Polymeric Materials, 173
Advanced Mass Spectrometry of
   Complex Lubricants, 193

Material Science and Technology Division (6300)

Ceramics With Ordered Pore Structures, 167
The Mechanism of Void Formation and Ductile
   Fracture of Dispersion-Strengthened
   Copper-Aluminum Alloy, 170
Prediction of the Failure Behavior of
   Fiber-Reinforced Composites, 175
Fatigue Crack Growth Process, 190

Optical Sciences Division (6500)

Tunable High-Power, Color-Center Laser, 149
Fiber-Optic Gyroscope, 150
Optical Control of a Phased Laser Diode
   Array, 154

Condensed Matter and Radiation Sciences Division (6600)

NRL MOS Dosimeter for Space, 201

Electronics Technology Division (6800)

Structure Features in GaAs Substrates as Revealed
   by a Eutectic Chemical Etching, 183
Hydrogenic Donors in Quantum Wells, 185
Niobium Nitride for Josephson Tunnel
   Junctions, 202
The Gyroklystron — An Efficient, High-Gain,
   Fast-Wave Amplifier, 205

INDEX

307

LOCATION OF NRL IN THE CAPITAL AREA

END

FILMED

11-85

DTIC